Geochemical characteristics of carbonatite-related volcanism and sub-volcanic metasomatism at Oldoinyo Lengai, Tanzania

Laura Carmody

Department of Earth Sciences

A thesis submitted to University College London for the degree of

Doctor of Philosophy

2012

I, Laura Carmody, confirm that the work presented in this thesis is my own. Where information has been derived from other sources, I confirm that this has been indicated in the thesis.

Laura Carmody

Date

As a change I have included two opposing quotes for my thesis; the first is a statement by which many scientists live by known as Occam's razor. The second is a quote from one of my favourite authors H.G Wells from his science fiction work *The Time Machine*.

"Simpler explanations are, other things being equal, generally better than more complex ones"

Paraphrased from William of Ockham

"Very simple was my explanation, and plausible enough—as most wrong theories are!"

H.G. Wells, The Time Machine

Abstract

The eruption of xenolithic material during large explosive eruptions, at any volcano, supply vital samples of the sub-surface lithologies upon which it is built, which in turn provides an indication of the evolution of the volcanic complex, in particular the volcanic conduit, magma storage zones and crustal / mantle lithologies. This is particularly important at alkaline-carbonatite complexes which are known to have "exotic" chemistries and also cause extensive zones of alteration through fenitisation processes. As the only active carbonatite volcano on Earth and also the unusual nature of Oldoinyo Lengai, Tanzania, it is an excellent study site to better understand the generation and chemical influence of carbonate-rich melts and fluids from source to surface. This study has attempted to better constrain the sub-volcanic environment, the source of the carbon within the material and the processes which lead to the formation of such unique rocks.

Using geochemistry, isotopic studies and fluid inclusions, this thesis highlights the importance of fluid circulation within the volcanic system, both at the surface but also within the sub-volcanic mantle, leading to metasomatised material rich in carbon and alkali elements from which natrocarbonatite and potentially kimberlitic material could be derived. Almost all of the geochemical evidence and composition of fluid inclusions trapped within fenitised aureoles indicates a mantle derivation of carbonatitic material with isotopic signatures typical of the pre-defined "mantle-box". The nature of the fluids is also investigated using trace element modelling and argued to be both carbonatitic and siliceous in origin, which have been circulating within the mantle beneath the Gregory Rift since before the establishment of Oldoinyo Lengai.

These themes of research are discussed in terms of the genesis of natrocarbonatite, focussing upon the notion that it may be an evolutionary feature of Oldoinyo Lengai rather than a constant eruptive product.

Acknowledgments

I would first like to thank my supervisors Dr Adrian Jones and Dr Christopher Kilburn for their continual guidance throughout my time as their student. Both challenged me to achieve the best that I could out of my PhD and allowed me the freedom to work truly independently, devising my own research projects and collaborations. Dr Jones is also thanked for providing me with a number of opportunities during my time here at UCL, which have helped enhance my skill set.

Thanks must also be given to Dr Matthew Genge (Imperial College) for his encouragement in following this PhD in the first place.

This research project would not have been possible without the financial support of NERC, the Graduate School at UCL and The Geochemistry Group.

Thank you to Dr Andrew Steele and Dr Dina Bower (Geophysical Laboratory, Carnegie Institute) for their extensive help with micro-Raman analysis. Thanks are also given to all of Andrew's post docs for making me feel welcome during my visits to the GL.

Dr Ian Millar and the staff at British Geological Survey, Keyworth, for taking the time to help me with data collection and interpretation. Prof Peter J Treloar and Dr David Lawrence at Kingston for their time for fluid inclusion work at the very last minute. Dr Stanislav Strekopytov at NHM for helping with the geochemistry data and David Smith (curator of the NHM) for lending me thin sections for almost all of my PhD. Dr Sasha Verchovsky (OU) and Alexei Buikin (Verdansky Institute) are also thanked.

Dr Dorinda Ostermann (Bloomsbury Environmental Isotope Facility) and Dr Stuart Robinson (UCL) for their help with stable isotope work from such difficult material to work with and for the patience to try new methods of preparation when the first set of results were strange. Jim Davy (UCL) for his fantastic guidance in rock preparation, masterful skill of the temperamental SEM and putting up with me covering his lab in oil and methylated spirit.

Evans Munanga and William Masaai for their help organising the logistical nightmare that is field work at Oldoinyo Lengai, Tanzania. William's expertise proved vital during field work. The staff at Moivaro Lodge, Natron must also be thanked for their hospitality and friendly nature during our visit. The help of Abigail Church and all the staff at James Robertson Safari's for field work in Kenya and continual advice and support regarding field work and sample collection

and honey badger incidents. Thanks is also given to Jörg Keller (Uni Freiburg) for initial carbonatite samples.

Dr Sami Mikhail is thanked for being the first person who spoke to me when I first arrived at UCL and for every conversation since, which have always proven to be useful in one form or another. His passion for science is infectious and he has been the sounding block for a number of theories within this thesis.

I would like to acknowledge all of the academics I have spoken with during workshops and conferences for taking the time to discuss ideas which has always proved beneficial.

All of my PhD colleagues (present and past) – I wish I could thank you all individually. Collectively you have all helped me through the good times and the bad, offering advice, a break from writing and shoulders to cry on. A particular thanks to Lottie Davis for an amazing first set of field work in Kenya which we survived together. Also to Rick Wall for helping me keep my sanity via endless random conversations over coffee. For those of you who are still going, there is light at the end of the tunnel and for those who have already submitted, I finally see what you are all smiling about.

My house mates, Lucy Woodbine and Elinor Savage, also require a massive thank you for putting up with my ups and downs during this time in my life and the endless amount of field gear which fills the flat from time to time during field work seasons. My friends outside of my academic life must also be acknowledged for their support – I know my choice to study rocks seemed odd to most of you.

To my boyfriend Barry, we met in the most unlikely of circumstances and you have gotten to know me at the most stressful time of my life and yours, but have been a rock to me thus far. Thank you for keeping me sane and putting up with me when I am grouchy. I promise to do the same when you write up your thesis.

My final and biggest thank you goes to my parents, Lynn and Noel, and also to my sister Gemma. This thesis is for you. You have always supported me in whatever I decide to do without question and only the smallest amount of taunting. You have kept me focussed on the task at hand, supported me during the rough times and teary phone calls, helping to make my ambitions come true. In particular my mum who has made every attempt to learn all of the technical stuff, my dad for all the early morning airport runs and Gem for all the phone calls when things were not working out. I hope I have made you all proud.

Table of Contents

List of Figures

List of Tables

Chapter 1 –An introduction to the carbonatites of the East African Rift and Oldoinyo Lengai.

1.1. Carbon-rich igneous melts: Carbonatites

1.1.1.Subdivisions of carbonatites

Carbonatites are allocthonous igneous rock units. They can occur as intrusive, extrusive, hydrothermal or replacements bodies and contain more than 50%, by volume, primary igneous carbonate minerals derived from carbonate magma (Streckeisen, 1980, Le Maitre, 2002, Woolley, 1982). However, carbonatites have recently been redefined using a mineralogical-genetic classification, which resulted in their division into two groups: primary carbonatites, and carbothermal residua (Mitchell, 2005). Using this classification, primary carbonatites can be divided into groups of magmatic carbonatites that are associated with nephelinite, melilitite, kimberlite and other mantle-derived magmas, formed at different depths in the upper mantle by different degrees of partial melting. Carbothermal residua carbonatites, according to Mitchell (2005), are formed from low-temperature fluids derived from magma bodies, which are dominated by CO_2 but also contain H_2O and fluorine. The primary carbonatites are further subdivided into;

- calcio-carbonatites – sövites if coarse grained; alvikites if medium-to-fine grained;
- dolomite carbonatite – beforsite;
- ferrocarbonatite – formed primarily of iron-rich carbonate minerals;
- magnesiocarbonatites – main constituent is MgO
- natrocarbonatite – composed of sodium-potassium-calcium carbonate.

Until the observation of extrusive carbonate-rich lavas from Oldoinyo Lengai, Tanzania (Dawson, 1962a), carbonatites were not accepted as primary magmas but were instead thought to be the result of limestone syntexis (decomposition of limestone plateaus or country rock). This theory, however, had one major flaw in that field relationships of intrusive carbonatites from across the globe indicated that carbonatites were emplaced at temperatures well below that required to cause melting of pure calcium carbonate (temperature in excess of 1000°C), with a lack of thermal alteration of the country rocks into

which the carbonatite intruded. Only after subsequent investigations into the isotopic signatures and detailed petrographic studies was it confirmed that carbonatites could be derived from primary magmas (Dawson, 1962b, Dawson, 1962a).

1.1.2. Tectonic setting of carbonatites

Primarily, carbonatites are located within stable, intra-plate settings, over half of which are in Africa (Figure 1.1), often occurring in peripheral regions to orogenic belts showing an apparent link to orogenic events or plate separation (Bell, 1989, Veizer, 1992, Le Bas, 1987, Garson et al., 1984). A detailed account of African alkaline igneous provinces and carbonatites can be found within Woolley (2001). Carbonatite concentrations are generally associated with topographic swells which can be up to 1000 km across (Srivastava and Hall, 1995, Le Bas, 1971), with over half the African carbonatites spatially associated with the East African Rift (Woolley, 2001). The other carbonatite occurrences within Angola, Namibia and South Africa are thought to relate to major transform faults in the South Atlantic (Woolley, 1987). The apparent confinement of carbonatites to continental lithosphere led to the conclusion that the continental crust played a vital role within the genesis of carbonatite magmas (Bell and Blenkinsop, 1987b), since isotopic evidence suggests the derivation of these melts from asthenospheric depths (Nelson et al., 1988).

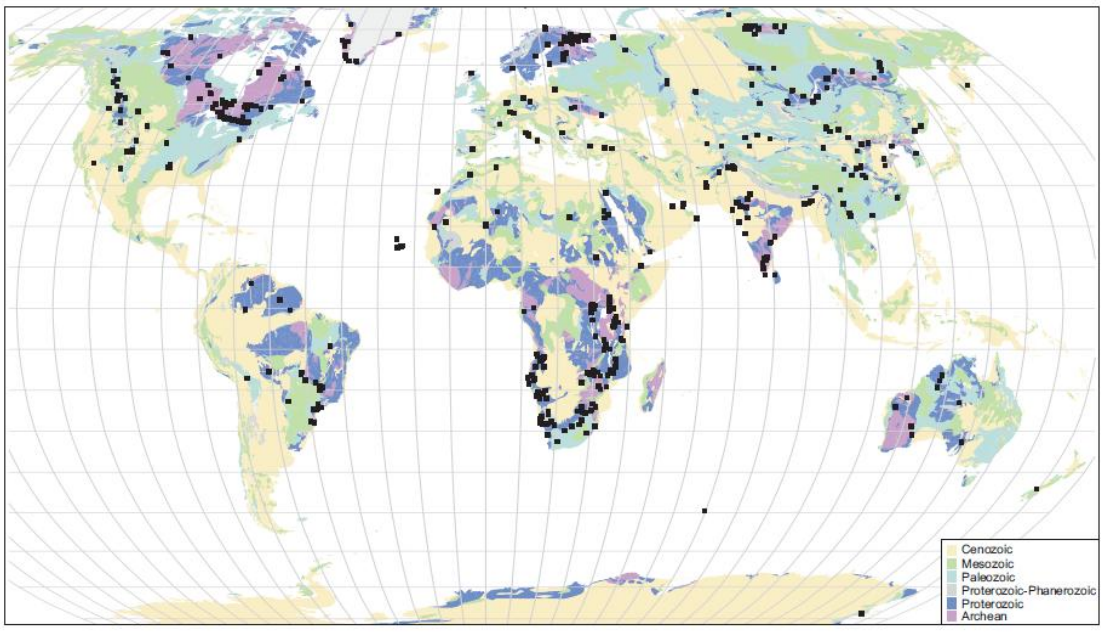

Figure 1.1: Global distribution of carbonatite complexes (Woolley and Kjarsgaard, 2008)

The only carbonatites noted to not occur above continental lithosphere are the Cape Verde exposures, which overlay oceanic lithosphere (Silva et al., 1981, Hoernle et al., 2002, Kogarko, 1993, Jørgensen and Holm, 2002). However, the discovery of carbonatite melt occurring as interstitial pockets within dunite xenoliths from the Kerguelen Archipelago (Moine et al., 2004), indicates that oceanic carbonatites may not be so rare and that the role of the continental crust in carbonatite generation is superficial. Areas of carbonatitic activity are often long lived and appear unrelated to the migration of mantle plumes, suggesting a direct relationship between the lithosphere and carbonatitic activity (Genge, 1994).

A more recent investigation into the role of the continental lithosphere, in particular Archaean cratons, into the formation of carbonatites suggests that repeated magmatism within cratons is the result of reactivation of lithosphere lesions during global plate movements and not related to fluctuating activity of mantle plumes (Woolley and Bailey, 2012). Using African carbonatite activity as a reference, Woolley and Bailey (2012) also corroborate spikes of carbonatite activity with tectonic events which affected the entire African plate, placing the entire anorogenic landmass under enormous stresses leading to brittle failure and the release of melts into the cratonic lithosphere. The apparent sparsity of large carbonatite complexes within oceanic areas is argued to be the result of a lack of thick crust which absorbs and conserves large amounts of CO_2 required for large scale production. This is also combined with a steeper geothermal gradient due to a thinner crust which hinders the liquid immiscbility processes (Woolley and Bailey, 2012).

1.1.3.Temporal distribution of carbonatite

Globally, there are around 527 carbonatite occurrences (Woolley and Church, 2005, Woolley and Kjarsgaard, 2008, Woolley, 2001), with 49 of these being extrusive carbonatites, ranging in age from Archean to present. The oldest dated carbonatite is approximately 3007 million years old, located in Tupertalik, Greenland (Downes et al., 2012). Of the 49 known extrusive carbonatites, 41 are calcio-carbonatites, 7 are dolomitic carbonatites and only one extrusive carbonatite is alkaline, i.e. natrocarbonatite (Woolley and Church 2005). However, recently It has been argued that carbonate-bearing lava flows are of relatively small abundance in comparison to carbonatite pyroclastics, which represent the majority of carbonatitic material, occurring as a matrix in between clasts of silicate glass which contain carbonate globules (Bailey and Kearns, 2012). With recognition of this particular form of carbonatite-silicate

volcanism, Bailey and Kearns (2012) argue that there are around 500 vents within Europe alone have not been included in Woolley and Church's (2005) review.

Carbonatites tend not to occur as single rock units but rather as part of a suite of alkaline igneous rocks, and so can be found in association with alkaline silicate rocks. A summary of the associated rock units from Woolley and Church (2005) clearly shows that nephelinite and melilitite are the most common associated extrusive silicate rocks. Yaxley and Brey (2004) argue that the relationship between carbonatite and silicate units could be due to the ascent of carbonatitic fluid through peridotitic wall rock, resulting in compositional deviation away from carbonatites and towards carbonated under-saturated silicate melts.

Despite the occurrence of carbonatites throughout the majority of geological periods since the Archean, there has been an apparent increase in frequency with episodic clusters of activity leading to the suggestion that conditions required for carbonatite formation needed to be established in the Archean and over time are becoming more widespread (Woolley 1989). This was argued to be the result of the growth of continental crust from small nuclei landmasses in the Early Archean towards a present day extent around 1.8 Ga, suggesting that if continental crust does play a role in generating carbonatite melts, the conditions required would have been established in the Paleoproterozoic (Veizer, 1992). A consequence of this is that there should not be an apparent increase in carbonatite formation over time from 1.8 Ga. Veizer et al (1992) argue that the apparent increase is a preservation artefact with crustal erosion and recycling of orogenic regions removing the topographic highs with which orogenic carbonatites are associated. The authors calculate a half life of carbonatite bodies and the host rocks they intrude into at ~445 Myr. All carbonatite units (orogenic and anorogenic) are easily weathered particularly in comparison to their associated silicate rocks. For this reason it is likely that carbonatite occurrences may appear to decrease the further back in geological history you go. This is even true for anorogenic occurrences which have multiple episodes of activity resulting in an incomplete geological record.

The extrusive carbonatites of Oldoinyo Lengai will be discussed within this thesis with some references made to Shombole carbonatite volcano and Kerimasi volcano. The three volcanoes are situated within the East African Rift, with Shombole being the northernmost and located on the border between Kenya and Tanzania, on the shores of Lake Natron. Kerimasi and Oldoinyo Lengai are situated within Tanzania with Kerimasi being the southernmost volcanic centre and often referred to as Oldoinyo Lengai's twin.

1.1.4.Genesis of carbonatites

The generation of carbonatite magma, especially that of natrocarbonatite, is a controversial and highly debated topic. The result of decades of research has resulted in three main theories of genesis;

1. Residual melts of fractionated carbonated nephelinite or melilitite (Gittins and Jago, 1998, Gittins, 1989).
2. Immiscible melt fractions of CO_2-saturated silicate melts (Kjarsgaard and Peterson, 1991, Lee and Wyllie, 1997, Kjarsgaard and Hamilton, 1988, Kjarsgaard and Hamilton, 1989, Brooker and Kjarsgaard, 2010, Brooker and Hamilton, 1990, Amundsen, 1987, Church and Jones, 1995, Freestone and Hamilton, 1980, Dawson, 1998, Moore, 2012).
3. Primary mantle melts generated through partial melting of CO_2-bearing peridotite (Harmer et al., 1998, Harmer and Gittins, 1998, Sweeney, 1994, Wallace and Green, 1988).

There are also a number of proponents for a combination of the above theories of genesis; for example the generation of carbonatite liquids at depth formed from carbonated eclogitic material, which infiltrates overlying mantle to generate silica-undersaturated carbonate-bearing liquids which may penetrate the crust and subsequently evolve or unmix (Yaxley and Brey, 2004). Bailey and Kearn (2012) also propose a petrogenesis theory for their new forms of abundant carbonatite-silicate volcanism which suggests they are primary magmas sourced from a depth of around 60 km due to the presence of dolomite but could potentially be from depths >90 km for those units which contain dolomite. A primary nature is invoked due to the transport of mantle material within these pyroclastic deposits and Mg# > 0.64 and so it is argued that these magmas have reached the surface, their final emplacement, from the mantle without modification (Bailey and Kearns, 2012). However the authors also acknowledge the evidence for liquid immiscibility in terms of the carbonate globules within the silicate glass clasts, suggesting that two possibilities must be considered; either immiscibility occurs during ascent or the source region is charactertised by the presence of unmixed conjugate melts, which then mingle prior to ascent. The presence of mulit-phase immiscibility documented at both Limagne, France and Kerimasi, Tanzania, further complicate the immiscibility method of formation (Guzmics et al., 2012, Bailey and Kearns, 2012).

A theory corresponding to primary carbonatite melts, but with a slight variation, was introduced in 2003, which suggested that the source of carbonatites is generated in the

lithospheric mantle by rising carbonatitic melts from an ascending mantle plume. When these melts reach higher levels they are stalled, due to a reduction in temperature, generating a carbonatite metasomatised horizon. As the much hotter centre of the plume approaches, melting is induced in the metasomatic horizon and results in generation of the carbonatite melts that are observed on the surface (Bizimis et al., 2003).

Although the above have emerged as the predominant methods of genesis, other processes have been discussed including anatexis of metasomatised basement (Morogan and Martin, 1985), incorporation of trona sediments [$Na_3(CO_3)(HCO_3).2H_2O$] and remobilisation of carbonate material already present on the volcano ((Church, 1995) and references therein). Each of these theories has received less support than the above and so has passed out of favour. In recent years a different theory for genesis has emerged which proposes natrocarbonatite, in particular, to be a cognate fluid condensate, i.e. a condensate of a co-magmatic fluid (Nielsen and Veksler, 2001, Nielsen and Veksler, 2002). This theory will be explored in more detail later in this chapter when reviewing Oldoinyo Lengai and natrocarbonatite.

An important factor in determining which of the above methods generates carbonatites, is characterising the parental unit from which they are derived and the pristine composition of the carbonatites prior to their eruption. The latter is often a controversial matter as carbonatites, like silicate melts, are subject to evolution through crystal fractionation and loss of elements due to fenitisation / metasomatism.

1.1.5. What is meant by fenitisation and metasomatism?

Metasomatism is defined as a metamorphic process by which the chemical composition of a rock or rock portion is altered in a pervasive manner. This can involve the introduction and/or removal of particular chemical components and is the result of the interaction of the rock with fluids. During metasomatism the rock remains in a solid state. Fenitisation is a particular form of metasomatism specifically related to the intrusion of alkaline igneous units such as nepheline syenites, carbonatites or ijolites (Zharikov et al., 2007).

It is at this point I feel it is necessary to define what is meant by a *fluid* in the context of this work. The term fluid can be ambiguous within the literature, with some authors using it to

describe volatiles in the system C-O-H-S-N (Navon et al., 1988); while others include non-solid phases such as dissolved oxides (Pearson et al., 2003). For the remainder of this work the term *fluid* shall be used to refer to a volatile-rich liquid also containing some dissolved solutes (oxides, sulfates, carbonates, nitrates or halides). It is important to emphasise that these fluids need not be aqueous liquids (H_2O-based) but may be carbonatitic liquids (CO_2-based).

The fenitisation process results in the alteration of the original country rocks to metasomatic units which are primarily composed of K-Na feldspars, nepheline, alkaline pyroxenes and alkaline amphiboles (Zharikov et al., 2007, Rubie and Gunter, 1983). The exact mineral assemblage of the resulting fenite is of course controlled by the composition of the intruding magma as well as the original composition of the country rocks (Le Bas, 1987). The process itself generates replacement aureoles of different grades of metasomatism and so different mineral assemblages. The outermost zones show the lowest degree of fenitisation and so often contain relict minerals, whilst the inner zones can be completely replaced and are often monomineralic. The products of fenitisation are thought to be determined by several important variables including temperature, pressure, CO_2 content and the K/Na ratio of the fluid (Rubie and Gunter, 1983). Importantly the fenite aureoles of carbonatites are recognisably different from those of ijolitic rocks, usually with extensive phlogopitisation, feldspathisation and amphibolisation associated with carbonatites (Richardson and Birkett, 1996).

There are a number of geological areas which epitomise the fenitisation process, including that of the carbonatite Fen complex, Norway, from which fenitisation derived its name (Andersen, 1988, Kresten and Morogan, 1986), however it is the early work on Alnö Island, Sweden, which provides us with the first recognition of the influence of carbonatite intrusions on the surrounding country rock (Eckermann, 1961, Eckermann, 1948). Eckermann (1948) observed that the composite berforsite-melilitite dykes on Alnö resulted in the generation of a red-coloured fenitic unit within the country granitic gneiss, that was adjacent to both the carbonatite and the silicate portion of the dyke suggesting the fenitisation process was not purely linked to the intrusion of the melilitite but also the berforsite magma.

1.2. The carbonatites of Oldoinyo Lengai, Tanzania

1.2.1.Geological context of the Gregory Rift and Oldoinyo Lengai

Oldoinyo Lengai sits in the East African Rift, part of the Afar extensional region. This divergent boundary is thought to be the result of the upwelling of asthenospheric mantle material generating new land through magmatism (Sun et al., 2007, Ni and Helmberger, 2003, Nyblade et al., 2000, Ritsema et al., 1999, Lithgow-Bertelloni and Silver, 1998). The number of plumes below the region is subject to debate; some scientists arguing for a single plume rising beneath the triple junction point of the triangle driving the separation of the Red Sea, Gulf of Aden and the East African Rift (Weeraratne et al., 2003). Opponents to this argue that there are multiple plumes generating volcanism across East Africa (Rogers et al., 2000, Pik et al., 2006, Furman, 2007).

The East African Rift Valley is around 3700 km long and varies in width from 48 to 80 km along its length, stretching from the Gulf of Aden through Ethiopia, Kenya and Tanzania. The vertical elevation of the rift can vary up to 3 km from the bottom of the valley and runs approximately North – South, with a divergence and eventual termination around Lake Victoria due to the fracture-resistant nature of the underlying Archaean Tanzania Craton (Dawson, 2008, Dawson, 2010). A detailed geological review of the Tanzanian Craton is beyond the scope of this thesis but in brief it is argued to comprise of six Neoarchean greenstone belts varying in age from 2823 Ma in the west to 2670 Ma in the northeast (Manya and Maboko, 2008). The greenstone belts consist of mafic-intermediate volcanic units which have subsequently been metamorphosed to greenschist / amphibolite facies. Due to its termination against the Tanzanian Craton, the southernmost section of the rift lacks distinct parallel rift features and so is in fact a half graben structure with no clear eastern boundary. This fracturing within the eastern branch of the rift, also known as the Gregory Rift, is accompanied by large amounts of volcanism, which began in Ethiopia ~30 Ma ago slowly progressing into Kenya and lastly Northern Tanzania ~8 Ma (Dawson, 2010).

1.2.2.Stratigraphy of Oldoinyo Lengai

Oldoinyo Lengai is the only site on Earth actively producing natrocarbonatite and so naturally has become a central focus for investigation into the formation of these exotic magmas. Located in the Gregory Rift, Tanzania (2°45S, 35°54E) approximately 16km south of Lake

Natron and rising to an altitude of 2960m, Oldoinyo Lengai forms an almost perfect stratovolcano comprising predominantly of nephelinite and phonolite with minor carbonatite material. The summit of the volcano contains two craters, north and south, separated by an east-west aligned ridge. Volcanic activity forming the Younger Extrusives of the Gregory Rift, is thought to have started after the generation of the major North-South fault approximately 1.2 Myrs ago, which now marks the western boundary of the rift valley (Dawson, 2010). The onset of activity has been poorly constrained with age measurements of the oldest pyroclastics (as determined by stratigraphic positioning) at 0.37 – 0.22 Ma (Bagdasaryan et al., 1973).

Richard (1942) and Dawson (1962) have written excellent summaries on the geology and historical activity of Oldoinyo Lengai. The geology of Oldoinyo Lengai was first described by Uhlig in 1907. Since then numerous authors have documented the volcano (Reck, 1923, Reck and Schulze, 1921, Dawson, 1962b, Dawson, 1962a, Goriatschev, 1968, Norton and Pinkerton, 1997, Richard, 1942). Stratigraphically Oldoinyo Lengai was first subdivided into the following units (oldest to youngest) by Dawson (1962):

1. Yellow palagonitized tuffs and agglomerates of phonolite and nephelinite with interbedded nephelinite / phonolite lavas.
2. Mica and pyroxene tuffs from parasitic cones and craters.
3. Black nephelinite tuffs, many of which are more than 200m thick.
4. Minor melanephelinite flows.
5. Variegated carbonatite flows.
6. Modern natrocarbonatite lavas.

Much of the oldest stratigraphic unit is thought to have originated from the now extinct southern crater and makes up 90% of the cone. All historic activity that has been recorded, shows eruptions only from the northern crater, which is separated into an active and inactive section, by an ash saddle. Later studies of the volcanic structure by Klaudius and Keller (2006) presented a more condensed stratigraphic subdivision of Lengai based upon Dawson's (1962) previous work and structural associations;

1. Lengai I – phonolite tuffs and phonolite lavas
2. Lengai II A – nephelinite tuffs and nephelinite lavas
3. Lengai II B – nephelinite tuffs, nepheline lavas, grey melilitite-bearing nephelinite tuffs and carbonatite tuffs and lavas of the active northern crater.

The relationship between each of these units is shown below in Figure 1.2 (Klaudius and Keller, 2006). The authors argue that Lengai is in fact a composite of two different cones formed in sequence after a major sector collapse around 10 ka ago (Klaudius and Keller, 2004b). The effect of this sector collapse will be discussed later in this review. The Lengai II formation is separated into A and B by a crater rim forming a visible unconformity indicating a change in eruptive product during the construction of this later section. Overall Klaudius and Keller (2004) estimate that Lengai I forms around 60% of the present day cone, Lengai II around 35% and the carbonatites constitute only 5%.

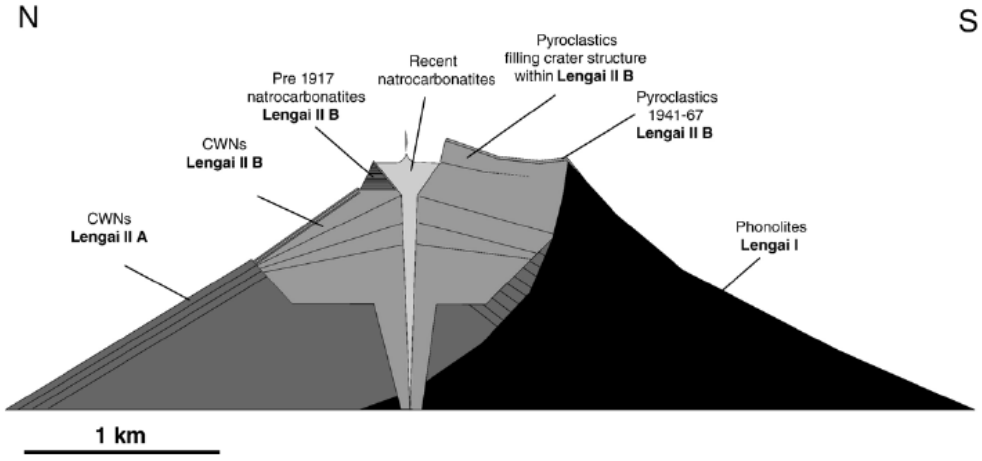

Figure 1.2: Cross section of Oldoinyo Lengai Upper cone showing geometry and stratigraphic relations of units (Klaudius and Keller, 2006).

1.2.3.Geometry of Oldoinyo Lengai from 1960 to 2007

Previous reports on Oldoinyo Lengai state the altitude of the volcano as 2086m (Nyamweru, 1988a). The eastern flank of the volcano has a deep amphitheatre-shaped collapse scar (discussed below) known as the Eastern Chasm (Kervyn et al., 2008a). This missing section must be taken into account when estimating the volume of the volcano and so adds uncertainty. Kervyn *et al* (2008) using remote sensing estimate the cone volume at 41±5 km^3 with the collapse scar resulting in no more than 0.3km^3 difference. This volume is intermediary to previous estimates of the volume ranging from 30km^3 (Donaldson et al., 1987) to 60km^3 (Brantley and Koepenick, 1995).

The geometry of the active northern crater has changed dramatically over time and eruptive cycles from a flat crater floor, with numerous hornito structures, to a deep crater after explosive activity, which is the present state. The northern crater has been observed by numerous geologists and reports of activity by Nyamweru (1988, 1990) are excellent summaries of the size and shape of the crater from 1960 to 1988. In the early 1960s the crater was estimated to be elliptical in shape with a diameter of 503m by 640m and a depth to the crater floor of 122m from the upper rim (Dawson, 1962a). At this point the volcano was in an effusive stage of activity generating natrocarbonatite material which was contained within the northern crater filling a previously created pit from prior explosive eruptions. Explosive activity once again occurred at Lengai in August – September 1966 generating "a small central pit below the ash slopes" (Nyamweru, 1990) with near vertical crater walls which drop sharply into the central pit. Nyamweru (1990) argues that the central pit only forms during the latter stages of the explosive activity caused by subsidence along ring faults after exhaustion of the magma column. After the explosive activity the crater remained in a dynamic, unstable state with numerous sites of slumping but without renewed effusive activity. The initiation of effusive activity in 1983 once again began to fill the crater with natrocarbonatite material raising the floor 30m from 1983 to 1988, a volume of 1.3 X 10^6 m^3 (Nyamweru, 1988a).

1.2.4.Eruption Style – effusive and explosive

The eruptive style of Oldoinyo Lengai is characterised by alternating periods (often months to years) of effusive activity, primarily contained within the northern crater and upper flanks, and explosive phases of Vulcanian / Plinian type volcanism lasting for shorter time periods of weeks to months. The effusive activity is predominantly carbonatitic material whilst explosive episodes can see the release of both alkaline silicate material and soda ash (Keller and Krafft, 1990). During its effusive phases Oldoinyo Lengai generates natrocarbonatite via lava fountains up to a few metres in height (Norton and Pinkerton, 1997, Keller and Krafft, 1990) from active spatter cones generating droplet lapilli. Lava flows from active vents are generally small (<100 m^3) with low effusion rates (~0.3 m^3s^{-1}) (Keller and Krafft, 1990). Interconnected lava lakes within the crater regularly overflow generating further lava flows which can top the crater rim and extend a few hundred metres down the upper flanks. Keller and Krafft (1990) report that during the 1988 activity the lava lake lost about 1000 m^3 during each overflow cycle.

Historically there have been ten reported explosive eruptions of the volcano since the 1880's. The activity up to 1955 is well documented by Dawson (1962) and references therein. In the last century Lengai has erupted explosively in 1917 which was large enough to remove the thick vegetation from the flanks of the volcano. Minor eruptions occurred in 1921 and 1926 followed by a major eruption in 1940 – 41 (Richard, 1942) and smaller eruptions in 1954 (Guest, 1956). In 1960 observations made by Dawson (1962) indicated the continuation of effusive activity in the northern crater. This activity was halted in 1966 - 67 with a major explosive eruption which cleared the northern crater floor, leaving an eruption pit (Goriatschev, 1968, Dawson et al., 1968). After this explosive eruption it is unclear whether effusive activity resumed resulting in a quiescent period until renewed activity in 1983 (Nyamweru, 1988b) with further explosive eruptions. Since the 1983 eruption it is argued that Lengai was then in continuous stage of effusive activity (Keller and Krafft 1990) until the most recent eruptions in 2006 – 07, which began with typical natrocarbonatitic effusive activity producing an unusually large volume lava flow down the western flank in April 2006 (Kervyn et al., 2008b). Effusive activity was continually monitored by satellite measurements of thermal activity up to June 2007 (Vaughan et al., 2008) and this period of unrest culminated in an eruption which was sub-plinian in character and generated an ash plume up to 5km in height on 4th September 2007. This period of explosive unrest at Oldoinyo Lengai continued from November 2007 until mid-February 2008 with low intensity ash emission and degassing. The final paroxysmal eruptions which generated eruption columns up to 15 km in height occurred at the end of February 2008 (Kervyn et al., 2010).

It is argued that the 2007 eruption may have been triggered by a magma-driven earthquake swarm which originated near the volcanic centre of Gelai (Baer et al., 2008). Thought to have been the result of normal slip on a deep-seated blind fault (A. Church pers comms), the volcanic swarm culminated in a magnitude 5.4 Earthquake, 2 days prior to the eruption of Lengai.

The explosive eruption is thought to have started with eruption of natrocarbonatite ash (Mitchell and Dawson, 2007) which rapidly changed to emission of silicate material. Mitchell and Dawson (2007) also argue that the material generated during this eruption is unlike any material present at Oldoinyo Lengai and is "unlikely to represent a simple differentiate of any of the magmas previously erupted..." Although the authors confirm a similar composition of material as indicated above, i.e. a combeite – wollastonite nephelinite lacking pyroxene, they suggest its origin to be that of a hybrid magma caused by desilication of nephelinite.

Desilication would be generated by the input of a large volume of natrocarbonatite, either that occupying the northern crater, added by thermal erosion and dissolution or magma stored within the chamber. Once the two magma types come into contact, decomposition and assimilation of the carbonatite occurs resulting in the addition of Na and Ca to the nephelinite changing the bulk rock composition with the replacement of pyroxene, which would now be meta-stable, to melilitite and combeite. Mitchell and Dawson (2007) question what causes the thermal erosion of the crater natrocarbonatite? This would require the presence of silicate lava close to the surface which should be degassed due to the reduction in pressure and so an explosive eruption would not occur. Later work has suggested that a lack of altered natrocarbonatite materials within the ash deposits indicates a lack of interaction with older natrocarbonatite material (Mattsson and Reusser, 2010).

1.2.5.Debris deposits on Oldoinyo Lengai

The 2006 deposit is minor in comparison to larger deposits present around the volcano. These deposits, termed Debris Avalanche Deposits (DADs), have been extensively investigated by Kervyn et al (2008). Hypothesised to be more mobile than non-volcanic landslides, DADs can travel up to 100 ms^{-1} and cover areas up to 1000 km^2. Recognised by their hummocky morphology and by use of remote sensing, Kervyn et al (2008) believe that three DADs emanate from Oldoinyo Lengai (Figure 1.3); labelled Zebra, Oryx and Cheetah DADs in Figure 1.5 (Klaudius and Keller, 2004a).

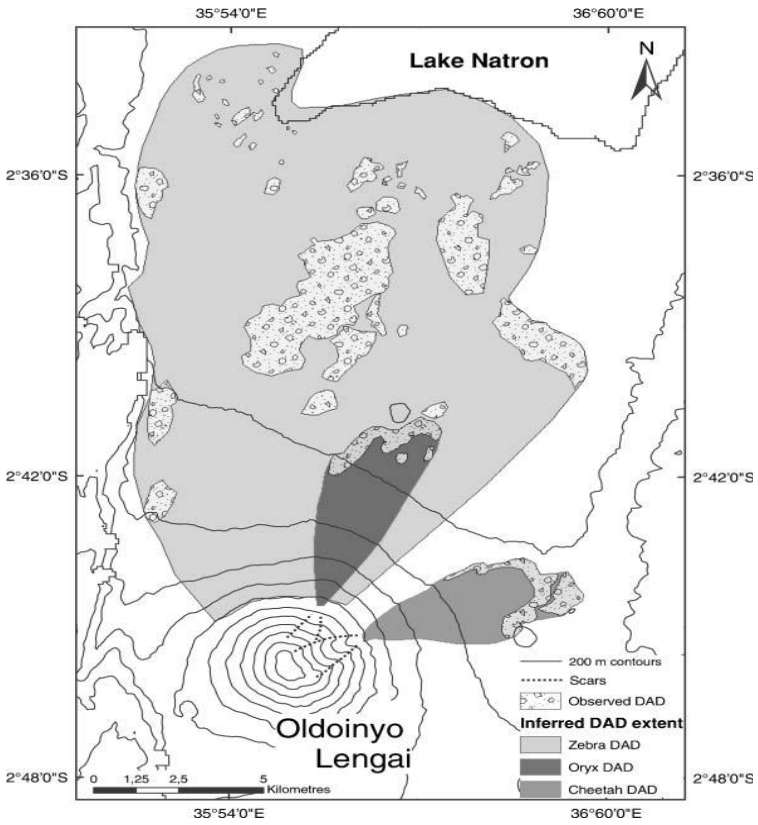

Figure 1.3: Mapped DAD flows emanating from Oldoinyo Lengai (Kervyn et al., 2008a).

The Zebra DAD is the largest of these deposits extending down to the shore of Lake Natron (~24 km in length) and relates to the sector collapse of Oldoinyo Lengai I (see above) due to the large amount of phonolite lava and pyroclastic blocks. As outlined in Table 1, the Zebra DAD is equivalent to the collapse of 12% of the current day cone. The smaller Oryx DAD contains predominantly combeite-wollastonite nephelinite lava clasts (Klaudius and Keller, 2004) indicative of origination from Lengai II formation (Kervyn et al, 2007). The Cheetah DAD, dated to ~2428 – 2960 years, contains rock units which are present in both Lengai I and Lengai II suggesting that this debris avalanche, which affected the eastern flank of the volcano, cut much deeper than that of the Oryx flow resulting in a deep amphitheatre shaped scar known as the Eastern Chasm. Remote sensing data also suggests the Cheetah DAD was likely to have been stopped en-masse by several scoria cones which exist at the base of Oldoinyo Lengai only reaching to half the height of the cones.

DAD	Area (km^2)	Max DAD Length (km)	Max DAD Width (km)	Average DAD Thickness (m)	Max Edge or Hummock Height (m)	Max Runout Distance (km)	Max Drop Height (m)	H/L	Volume (km^3)	%Volume*
Zebra	197.4	18.9	13.9	25	45	24.1	2600	0.108	4.9	12
Oryx	12.4	6.7	2.7	10	25	9.4	2100	0.223	0.1	0.3
Cheetah	11.5	6.2	2.9	20	40	8.5	1950	0.229	0.2	0.6
Kerimasi	33.1	8.9	4.8	30	60	10.8	1300	0.120	1.0	1-2

* Assuming recent OL and Kerimasi volume of 41 km^3 and 50-60 km^3, respectively

Table 1: Summary of estimates of sizes and volumes of DADs (Kervyn et al, 2008)

As shown above, Kerimasi also exhibits a scar indicative of a debris flow. Despite little field evidence of the material involved in the flow due to deposition of newer volcanic material, Kervyn et al (2008) uses remote sensing techniques and previous descriptions by (Siebert, 1984b) to estimate the characteristics of the Kerimasi flow. It can be seen in Table 1 that the Kerimasi flow is of the same order in terms of size as those currently seen at Oldoinyo Lengai. This suggests that processes that are currently active on Oldoinyo Lengai were most likely active on Kerimasi during its life cycle.

Triggering mechanisms for DADs have been discussed by Siebert (2004), who argues that an accumulation of volcanic material around a central vent will inevitably result in flank collapse, particularly if steep slopes are developed. Higher volcanoes are also more likely to fail (Kervyn et al, 2008 and references therein) with 30% of volcanoes over 2000 m experiencing flank collapse compared to 10% of volcanoes of 500 m. Other structural features must also be taken into account; the presence of competent lava flow layers between unconsolidated material, edifice construction, underlying geological structures, repetitive dyke intrusion events and hydrothermal weathering can all contribute to instability. Basement fault movement and explosive eruptions are also common factors causing flank collapse. It is known that the East African Rift region is subject to Earthquakes with Oldoinyo Lengai situated within the North Tanzanian Divergence (Baker et al., 1972), a region of high seismicity. Kervyn et al (2008) consider that earthquake-triggered collapse is possible for the generation of the Zebra and Cheetah DADs due to lack of magmatic intrusion, however they argue that the smaller Oryx DAD is most likely to have been caused by unstable growth of the upper flanks of Oldoinyo Lengai with narrow and shallow collapses leaving the V-shaped scar present on the cone today.

1.2.6.Mineralogy of natrocarbonatite from Oldoinyo Lengai

The petrology of Oldoinyo Lengai material has been extensively described by numerous authors (Dawson, 1962a, Peterson, 1990, Church, 1995, Church and Jones, 1994, Dawson, 1998, Dawson and Hill, 1998, Donaldson and Dawson, 1978, Keller and Krafft, 1990, Dawson et al., 1995). Natrocarbonatite from Oldoinyo Lengai is predominantly porphyritic in nature with phenocrysts (comprising about 50% of the rock) of platy nyerereite $(Na, K)_2Ca(CO_3)_2$ and more rounded gregoryite ($(Na,K)_2CaCO_3$) set in an aphyric groundmass of nyerereite and gregoryite, with sylvite–halite, fluorite, apatite-(CaF), alabandite and Mn-rich magnetite. Other accessory minerals in the natrocarbonatite include barite, khanneshite, sphalerite, pyrrhotite, galena, monticellite, neighborite and niocalite–cuspidine ((Zaitsev and Keller, 2006) and references therein). The phenocrysts occur in approximately equal proportions and both show twinning (Keller and Krafft, 1990). It is also noted that gregoryite commonly shows exsolution lamellae of nyerereite occurring in particular zones (Keller and Krafft 1990) and containing numerous mineral inclusions such as apatite.

An aphanitic variety of natrocarbonatite is also noted (Keller and Krafft, 1990, Gittins and Jago, 1998), consisting of the same constituents, which occurs as driblet cones, hornito-like structures and also as fluid flows leaking out from tops of lava flows. This aphanitic variety of natrocarbonatite is thought to be the result of filter pressing by the crystal mush of the porphyritic variety (Keller and Krafft 1990), termed ‘squeeze-ups’ by Gittins and Jago (1998).

1.2.6.1. Occurrence of melanophlogite at Oldoinyo Lengai

The above described mineralogy has been reported almost consistently since 1962 until the recent discovery of a different mineral within the mixed mineralogy of the 2006 lava flows known as melanophlogite (Beard et al., 2009). Melanophlogite is best described as a low temperature, late stage polymorph of SiO_2 with tetragonal habit and structure-stabilising guest organic molecules (e.g. CH_4, CO_2, SO_2, N_2, OH) trapped within a clathrate-type silicate framework. In the case of the occurrence at Oldoinyo Lengai the guest organic molecule is predominantly CO_2. It occurs as near perfect cubes between 50 to 80µm in size and electron microprobe analysis reveals well defined compositional zoning with variations in carbon content (Beard et al., 2009). Although this is not the first noted occurrence of melanophlogite worldwide, with a few occurrences in Italy (Adorni and Tateo, 2007) and Mount Hamilton,

California (Dunning and Cooper Jr, 2002), it is the first time it has been noted in lava flows at Oldoinyo Lengai and in a high temperature setting. This discovery raises numerous questions; has this rare mineral always existed within the magma of Oldoinyo Lengai? If not what physical processes cause crystallization of melanophlogite and how did the eruption of Oldoinyo Lengai in 2006 alter the magmatic system to allow its crystallization? Is it a primary mineral crystallised from the magma or is it a secondary mineral generated by some later process?

Interestingly descriptions of peralkaline nephelinitic units by Dawson (1998) suggest that electron microprobe analysis of combeite phenocrysts generate low overall totals which the author indicates could be "due to the presence of some unanalysed element such as O, H or C". Images of these crystals within the paper bear a resemblance to the morphology of melanophlogite with zoned sections and near cubic crystal form (Figure 1.4).

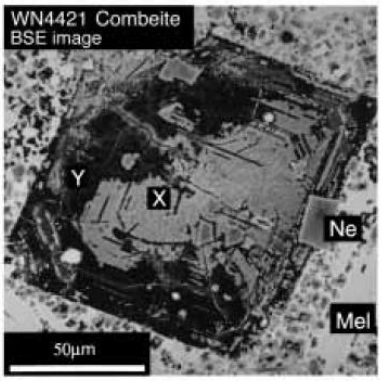

Figure 1.4: BSE image of altered combeite phenocryst from wollastonite nephelinite. Note inclusion of nepheline laths and zoning within crystal. (Dawson, 1998)

Melanophlogite was first discovered in Sicily, Italy and described as a silica polymorph containing films of organic matter which gave the mineral its slight brown colouration and upon heating turned black (Skinner and Appleman, 1963). Later studies using X-ray diffraction on the mineral resulted in the classification of melanophlogite as a clathrate - type mineral with polyhedral voids in which organic guest molecules are housed (Kamb, 1965, Zak, 1972). In the 1980s work on melanophlogite increased with the introduction of a new group of minerals known as clathrasils of which melanophlogite is a sub-group (Gies et al., 1982). Clathrasils are defined as porous tectosilicates which are distinct from zeolites. The guest molecules are argued to be non-exchangeable between cages due to the small size of the regions connecting cages.

The work by Gies et al (1982) demonstrated that melanophlogite could be synthesised from silica solutions at temperatures of around 170°C and pressures of 150 bar, but also revealed that synthetic melanophlogite has a cubic structure at room temperature whilst naturally occurring melanophlogite with the same guest molecules is tetragonal (Zak, 1972). Investigations into crystallisation conditions later revealed that synthetic melanophlogite can be generated by hydrolysis of tetramethyl orthosilicate ($Si(OCH_3)_4$) in 2M aqueous ethylenediamine ($C_2H_4(NH_2)$) in the presence of guest species but the absence of "help gases", i.e. atmospheric gases (Gunawardane et al., 1987). It was concluded that guest species act as templates during crystallization and the size and shape of cages within the tetrahedra is a function of the size and shape of the guest molecule. The presence of methylamine (CH_3NH_2) in the experiments crystallises melanophlogite at lower temperatures (160 - 200°C) irrespective of the presence of air but requires between 8 and 10 weeks for initial crystallisation, however like earlier work by Gies et al (1982) the synthetic melanophlogite is cubic. The change from tetragonal to cubic is argued to occur upon heating to temperatures around 338K (~65°C) (Gies, 1983) and further heating to temperatures of around 873K (~600°C) results in expansion of the cubic structure allowing guest molecules to escape (Liu et al., 1997). This change in crystal habit when at elevated temperatures may provide an explanation as to why the melanophlogite from Oldoinyo Lengai and synthetic melanophlogite is cubic rather than tetragonal.

The exact formation condition of melanophlogite in nature is not well defined with occurrences in different low temperature environments and as yet has not been identified to contain any H_2O within its cage structure. In the laboratory it has been shown that melanophlogite is unstable under hydrothermal conditions and the absence of molecular species at temperatures between 300 - 500°C and pressure up to 2kbar. In this situation the melanophlogite is often documented to revert to quartz. However under dry conditions metastability is possible up to 800°C ((Kolesov and Geiger, 2003) and references therein). Later work suggests that melanophlogite and other clathrasils are crystallization products of silica-rich colloids or gels, similar to that of cristobalite and chalcedony, and that the rarity of such minerals in nature is a result of the requirement of structure-directing agents such as CO_2, CH_4 and N_2 or more complex hydrocarbon chains for other clathrasils, which are just not as abundant in nature (Geiger and Dachs, 2008). Interestingly, clathrate formation is noted to take place at the smaller scale inside fluid inclusions. Mixed H_2O – NaCl – CO_2 inclusions are often difficult to study due to the presence of clathrate minerals (Shepherd et al., 1985). These

are argued to form upon cooling of fluid inclusions to temperatures of -28°C and are the result of strong interaction between the aqueous liquid, ice, solid CO_2, CO_2-rich liquid and CO_2-rich vapour.

1.2.7.Xenolith suites from Oldoinyo Lengai

The magmas at Oldoinyo Lengai have yielded numerous xenoliths of both plutonic (Dawson et al., 1995) and crustal origin which record the process of fenitisation beneath Lengai (Morogan and Martin, 1985), as well as indicating the petrology of the inner core of the volcano. Fenitisation is an alkaline metasomatic process, which characterises ijolitic and carbonatitic complexes causing a halo of alteration of the surrounding country rocks with production of hydrous alkali-rich minerals. The crustal fenitised xenoliths comprise of metagranitic and metagabbroic basement, which has undergone fenitisation resulting in rock units that contain sanidine, nepheline and aegirine-augite with evidence of melting at higher grades (Table 2). Thought to originate from either the Tanzanian Shield or Mozambique Orogenic Belt (Morogan and Martin 1985, and references therein) the presence of these xenoliths, along with other units such as nepheline syenites and biotite pyroxenites, seem to indicate the presence at depth of a widespread alkali metasomatic region beneath Oldoinyo Lengai.

	BD58	BD44	BD32	BD48	BD43	BD42	BD35	BD55
alkali feldspar	63		38	47	46	7	58	51
plagioclase	4	33					28	35
clinopyroxene	20	21	34	40	28	51	3	1
hornblende		34						
biotite	1	5						
quartz	1.5		2					
wollastonite	7		8	5	1		6*	8*
calcite	2.5	2	5	4			2	2
opaque phases	1	3			8	4		
apatite	tr	1	2	1	2	2		
titanite		1	1	3	3	6	1	tr
nepheline					5	30		
melanite							tr	1
glass					7	tr	2	2
number of points counted	1200	1000	1200	1000	400	700	600	500

BD58 low-grade fenite, granitic gneiss ancestor; BD44 low-grade fenite, metagabbro ancestor; BD32, BD48 medium-grade fenites, granitic gneiss ancestor; BD43 high-grade fenite, granitic gneiss ancestor; BD42 high-grade fenite, metagabbro ancestor; BD35, BD55 leucocratic contact fenites. * includes pectolite, tr trace. Results expressed in volume %.

Table 2: Modal compositions of crustal fenite xenoliths from Oldoinyo Lengai, (Morogan and Martin 1985)

Fenitisation occurs in grades and with increase in grade the relict mineralogy of original lithologies is replaced by nepheline, pyroxene and alkali feldspar through a series of reactions where minerals such as plagioclase and olivine are consumed in the production of nepheline or quartz. Plagioclase, K-feldspar, sillimanite and garnet are consumed due to the growth of sodium-rich feldspar, aegirine-augite, biotite, corundum and spinel (Robins, 1984, Bowden, 1985).

Nephelinisation: $CaAl_2Si_2O_8 + (Na,K)_2CO_3 = 2(Na,K)AlSiO_4 + CaCO_3$

OR

$4CaAl_2Si_2O_8 + 3NaAlSi_3O_8 + 2(Mg,Fe)_2SiO_4 + 4(Na,K)_2O = 11(Na,K)AlSiO_4 + 4Ca(Mg,Fe)Si_2O_6$

Feldspathisation: $2(Mg,Fe)_3Al_2(SiO_4)_3 + 7Al_2SiO_5 + 4(Na,K)^+ = 6(Mg,Fe)Al_2O_4 + 4(Na,K)AlSi_3O_8 + Al_2O_3 + Si^{4+}$

Phlogopitisation: $2(Mg,Fe)_3Al_2(SiO_4)_3 + Al_2SiO_5 + 4K^+ + 4H_2O = 4K(Mg,Fe)_3(AlSi_3O_{10})(OH)_2 + 3Al_2O_3 + Si^{4+}$

The grades of fenitisation enable the identification of five zones of fenitisation around ijolitic-carbonatitic complexes, which are as follows (Le Bas, 1977, Dawson et al., 1970);

1. Quartz still present, few sodic mafics.
2. No quartz, mainly feldspar, some sodic mafics
3. Feldspar and sodic pyroxene abundant
4. Feldspar, pyroxene and nepheline abundant
5. Little feldspar, mainly pyroxene and nepheline present

Compositionally the clinopyroxene within the fenites becomes less sodic as fenitisation grade increases resulting in a transition from aegirine to aegirine-augite (70%Ac to 20%Ac). The feldspars from all grades plot within the albite-orthoclase binary system with trends towards higher Or compositions with grade (Sanidine Or_{71} in highest grade fenites). An inversion of feldspars from monoclinic to triclinic habit sets a minimum temperature of formation of around 760°C and the absence of microcline (K-rich feldspar) limits fluid interaction of basement rocks to temperatures above 500°C, the limit of its stability (Morogan and Martin 1985).

Carbonatite metasomatism in particular, mainly results in feldspathisation caused by potassium-rich fluids. The resultant unit is composed almost entirely of potassium-rich orthoclase and a few iron-oxides between these feldspar crystals (Le Bas, 1977, Rubie and Gunter, 1983). Four other processes are thought to occur in relation to carbonatitic metasomatism, which is dictated by the chemistry of the carbonatite being intruded. Ferrocarbonatites can result in hematisation with the generation of hematite and magnetite. Carbonatisation is also a common process with existing silicate minerals retaining their textures but geochemically appear related to the late stage carbonatites. The generation of fluorite is argued to be the third metasomatic process. The final process of silicification of earlier carbonatitic intrusions could occur from the silica-rich solutions generated by previous metasomatic processes (Si^{4+} from above equations).

1.2.7.1. Previous work on xenoliths from Oldoinyo Lengai

A suite of plutonic xenoliths reported by Dawson et al (1995), consist of jacupirangite, pyroxenite, ijolite, nepheline syenite and wollastonitite all found within the pyroclastics of Oldoinyo Lengai, showing a mainly cumulate texture. The xenoliths consist of nepheline, clinopyroxene, Ti-andradite, spinel, apatite, perovskite, titanite, wollastonite, sulphides, mica, glass and K-rich feldspar. Some ijolites also contain megacrysts of olivine and mica. Olivine is often mantled with radiating pyroxene, magnetite, perovskite and mica minerals suggested to represent an early reaction corona (Dawson et al., 1995). Nepheline in specimens is either potassic or sodic with little variation betweens grains within samples. Individual grains however, show variation between core and rims with mostly more potassic rims of some crystals. Pyroxenes between xenoliths define a compositional trend from diopside to augite. Phenocrysts of pyroxene show variation in composition with zones and patches, which are distinct from one another differing in colour and/or inclusion content. The incorporation of pyroxene by ijolitic material is a common process which can be characterised in two ways; if the pyroxene material retains some of its primary characteristics, i.e. banding, they are considered to be pyroxenite xenoliths. If however the pyroxene becomes disaggregated the resultant rock unit is described as a meltiegite.

1.3. Uniqueness of Oldoinyo Lengai

As the only active carbonatite volcano on Earth, Lengai raises numerous questions about the mantle conditions beneath this part of the African continent and whether specific processes occur which do not occur or no longer occur elsewhere on the globe. Such conditions are thought to be rarely achieved and so the generation of natrocarbonatite is rare (Gittins, 1988). However Nielsen and Veksler (2002) suggest that fluid separation is a universal process that can occur from any carbonated alkalic body of magma, therefore natrocarbonatite volcanism could occur anywhere in the world that has such a body of magma. A similar argument is based upon the presence of alkali-rich fenitic aureoles around the majority of carbonatitic complexes, which suggests that almost all carbonatites at one point carried alkali elements in the same concentration as that of the natrocarbonatites at Oldoinyo Lengai (Woolley and Church, 2005). This leads to the question of how the carbonatite material at Lengai has managed to hold onto its alkalis? In the same paper Woolley and Church (2005) suggest that the alkali content of carbonatites is controlled by their formation process, with primary, deeper sourced carbonatite melts containing lower concentrations of alkalis than those formed from high level immiscibility and fractionation.

The unique nature of Lengai is argued to be the result of unique conditions, including the nature of the parent melt, structure of the subvolcanic system, the degassing process and the permeability of the cone, which optimise fluid separation. This idea is similar to that of previous authors who argue for an extreme or “freak” fractionation trend of the parental melts to natrocarbonatite enabling the production of this rare magma (Church, 1995). Church (2005) investigated the apparent difference between Oldoinyo Lengai and Kerimasi. These centres, both within the Gregory Rift and approximately 12 km apart, have similar parent magmas yet Kerimasi appears to have not produced natrocarbonatite. The proximity of the volcanoes appears to rule out sampling of a completely different mantle source, although small scale heterogeneities may result from metasomatic processes.

1.4. Formation of natrocarbonatite lava at Oldoinyo Lengai

The petrogenesis theories for natrocarbonatite are similar to those suggested for the formation of all carbonatites discussed above in section 1.2.4 and are best summarised in the diagram in Figure 1.5 below. Based on radioisotope data for rock units at Shombole volcano, Kenya, the models presented for calcite carbonatite production by Bell and Peterson (1991)

are applicable to theories of petrogenesis of carbonatite material at Lengai. All petrogenesis theories can be divided into two theories; either natrocarbonatite is a secondary magma generated by differentiation process from a parental silicate melt or they are primary magmas formed directly by evolution of mantle-derived carbonate melts.

Figure 1.5: Models of potential carbonatite formation processes for volcanoes of the East African Rift. (Bell and Peterson, 1991). CC = calcium carbonatite; N = Nephelinite; P = Phonolite; DC= Dolomite carbonatite; ON = Olivine nephelinite

Model one in Figure 1.5 focuses upon the generation of carbonatite through the process of liquid immiscibility from a carbonated, peralkaline silicate parent magma (whether that is an initial olivine nephelinite, a more evolved differentiated nephelinite or melilitite). The miscibility gap between carbonate and silicate melts with compositions akin to that of magma at Oldoinyo Lengai was first recognised experimentally in the early 1960's by Koster van Groos and Wyllie (1963) with later expansion by numerous authors (Peterson, 1989, Koster Van Groos and Wyllie, 1966, Visser and Koster Van Groos, 1977, Rankin and Le Bas, 1974, Kjarsgaard and Hamilton, 1989, Amundsen, 1987). A key paper by Freestone and Hamilton (1980) determined the miscibility gap to occur between 0.7 and 7.6 kbar at temperatures of between 900 and 1,250 °C and that natrocarbonatite at Oldoinyo Lengai was more likely to have separated from phonolitic magma than nephelinitic, based upon detailed ternary phase diagrams of the immiscible system (Figure 1.6). Extension of this work has been conducted over subsequent years with physical conditions of liquid immiscibility found to extend to pressures of 50 – 375 MPa (equivalent to 0.5 – 3.75 kbar) and temperatures of 700 – 850 °C (Kjarsgaard and Hamilton, 1989, Kjarsgaard et al., 1995, Brooker and Hamilton, 1990). Additional evidence for the liquid immiscibility model was provided upon the identification of silicate aggregates within natrocarbonatite units (Church and Jones, 1995, Mitchell, 2009), which were thought to represent the first identification of crystallisation of conjugate liquids within natural samples.

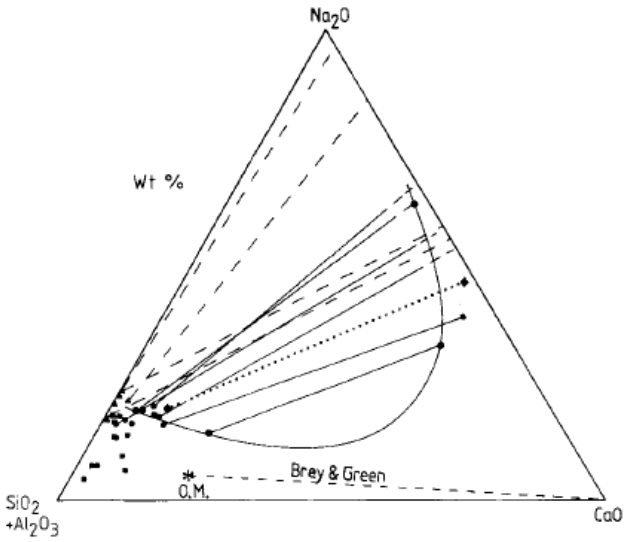

Figure 1.6: Ternary diagram illustrating process of liquid immiscibility and the composition of experimentally determined conjugate pairs of silicate and carbonatite melt. Solvus determined for pressure of 3 kbar. (Freestone and Hamilton, 1980)

A key counter-argument to the theory of derivation by liquid immiscibility invokes the difference in radiogenic isotope signatures from units which are proposed to be conjugate (Harmer and Gittins, 1998, Harmer et al., 1998). These conjugate melts should be in both chemical and isotopic equilibrium upon the point of separation, with differences indicating either modification through assimilation of country rock (which can be supported by higher Sr and Nd concentrations in the carbonatites) or that the melts are not related by immiscibility. The second model in Figure 1.5 is offered as an alternative genesis and illustrates the production of sodic, dolomitic carbonatite as a primary magma through partial melting of carbon-rich mantle material, from approximately the same source region as that of the silicate materials and by small degrees of partial melting causing the alkaline nature of the primary melts. This is then followed by fractionation to generate natrocarbonatite (Wallace and Green, 1988). Very little work on the application of this theory to Oldoinyo Lengai has been completed, but the application of this theory to other carbonatite complexes is detailed in Harmer and Gittins (1998) and Stoppa et al (2009). However work by Sweeney et al (1995) concluded that fractionated melts from the primary composition suggested by Wallace and Green (1998) were too sodic to be parental to Oldoinyo Lengai units and that reaction with mantle rocks would drive the compositions towards sövite rather than natrocarbonatite.

The final model presented by Bell and Peterson (1991) again depicts carbonatites as secondary magmas derived from a silicate parent melt and differentiated through contamination and

fractionation to produce the known forms of carbonatite including natrocarbonatite. Twyman and Gittins (1987) argue that natrocarbonatite is a late differentiate of an alkalic olivine sövite magma developed under low water fugacity, but should not to be considered parental to other carbonatite rock types but instead forms an extreme end-member of the differentiation process (Gittins and Jago, 1998, Twyman and Gittins, 1987). Later work by Gittins and Jago (1991) again highlighted the importance of fractional crystallisation for the production of natrocarbonatite, this time in the presence of fluorine which allows the thermal barrier generated by nyerereite to be broken so that differentiation can continue.

There is a fourth theory of formation which sees natrocarbonatite as a cognate fluid condensate which forms from a co-magmatic fluid phase generated during crystallisation of a parent silicate (Nielsen and Veksler, 2001, Nielsen and Veksler, 2002). In their work, Nielsen and Veksler (2002) conclude that the existing chemical data (in terms of both isotopes of conjugate melts and the difference between experimentally produced melts and natural melts) cannot be explained in terms of either immiscibility or fractional crystallisation. Instead the authors advocate the genesis of natrocarbonatite from a coexisting dense, alkali and CO_2-rich co-magmatic fluid. The volcanic cycle envisaged by Nielsen and Veksler (2002) is illustrated in Figure 1.7 below and indicates that natrocarbonatite production occurs upon heating of previously formed, alkali-rich metasomatic units upon introduction of new silicate material.

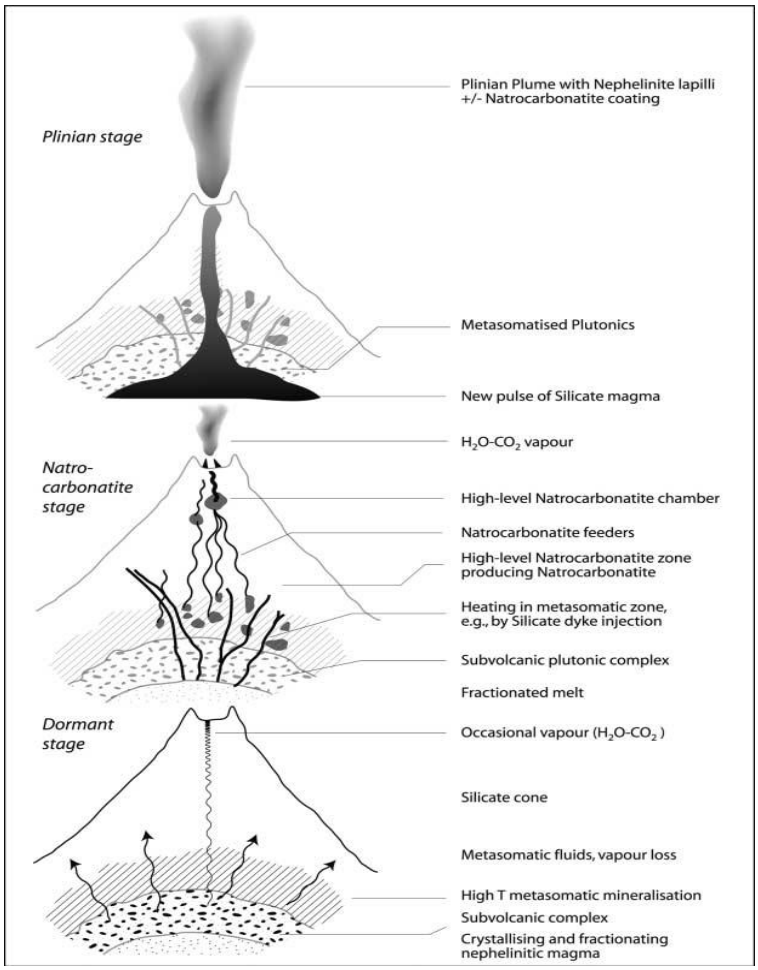

Figure 1.7: Schematic diagram illustrating the production of natrocarbonatite as a fluid condensate at Oldoinyo Lengai and the stages of activity observed. (Nielsen and Veksler, 2002)

1.5. Aims of this thesis

The first part of this thesis outlines the current physical state of the volcano post-eruption and also previous processes which have occurred to shape the volcano (chapter 3). This Chapter also investigates volcanic features throughout this region of the Gregory Rift to look at similarities and differences in volcanic processes between features. Following this a detailed description of the rock units present beneath Oldoinyo Lengai is presented based upon a suite of 20 xenoliths collected from the volcano (chapter 4). This chapter outlines the petrography, crystallisation histories and chemical variations of the crystal phases to hypothesis about magma source regions and processes occurring during crystallisation of the units.

In order to characterise Oldoinyo Lengai both chemically and physically, it is important to investigate the generation of such a unique lava type in terms of its mantle source and any

processes which occur during its emplacement. Therefore the next section of the thesis investigates the role of fluids that are generated during crystallisation of magma units in the upper mantle and crustal region (chapter 5). Here an outline of a number of fluid inclusion assemblages is discussed in terms of their composition and source. The presence of fenites or metasomites allows an investigation into the redistribution of carbon from original parent melts / fluids to country rocks. This is followed by geochemical modelling (chapter 6) to fully characterise the fluids and the metasomatic processes at work within the sub-continental mantle and crust, which also involves the use of radiogenic isotope signatures (chapter 7). Finally chemical redistribution of carbon is investigated using the alteration products of natrocarbonatite (chapter 8), which is important in resolving the uniqueness of natrocarbonatite by determining if there are any mineral indicators that are preserved, which may be observed at other carbonatite complexes.

The following chapter outlines the techniques used for the above investigations and also the results obtained.

Chapter 2: Methodology for all Analyses

The research included within this thesis has been accumulated using a number of techniques. An overview of these methods is provided below to give clarification to the reader when methods are discussed in the following chapters.

2.1. Sample preparation for thin sections

Thin sections were made of all rock samples collected during field work. Due to the hygroscopic nature of some of the samples, a number could not be made into sections using the standard techniques. Sections were therefore prepared either wet or dry.

2.1.1. Wet sample preparation

Xenolith samples and those which did not appear to contain natrocarbonatite were cut and polished under the presence of water. Samples were cut down into small sections using a diamond tipped bench circular saw and ground flat using a grinding wheel, both of which are lubricated with water. Specimens that were less consolidated were either surface or vacuum impregnated with epoxy resin. Surface impregnation involved applying a thin layer of epoxy resin to the surface of the sample and allowing it to soak into the upper few millimetres. Vacuum impregnation was applied to specimens which broke up easily. A thick MetPrep epoxy resin is mixed in 4 parts resin to 1 part hardener and poured over the samples within a disposable container. The samples were then placed within desiccators and pumped down to a vacuum. The epoxy resin is absorbed into gaps between grains of the sample and upon drying form a consolidated block of material.

The subsequent blocks of rock were then polished using polishing plates of carborundum powders of increasing grade from 320 to 1000. Once one face of the block had a reflective, smooth surface they were placed in the oven overnight at 50°C to dry the samples. Once dry, the samples were placed on a hot plate at 60°C and a mixture of epoxy resin was made in the ratio 3 parts resin to 1 part hardener by volume and coated over the surface of the samples. A clean glass slide was then placed over the sample and left to harden on the hot plate. Once the resin cured the glass slides were cleaned of any residual resin using a scalpel and placed on the vacuum holder of the Buhler PetroThin. Using the PetroThin the excess material is removed by

a diamond tipped blade so that the section was just over 100 microns thick. The grinding wheel of the PetroThin is then used to incrementally thin the samples to near 30 microns. Final adjustments to thickness were made using the polishing plates and sample thickness was gauged using birefringence colours of standard minerals such as nepheline or quartz. Samples which were required to be doubly polished were polished on all grades from 320 to 1000 and a final polish was achieved using a Lap Master polishing wheel with 1200 grade aluminium oxide power mixed with deionised water.

2.1.2.Dry sample preparation

A number of samples collected contained natrocarbonatite material or other hygroscopic material which could not be exposed to water during sample preparation. Large samples were cut into small blocks for thin sections using the same bench saw as above but prior to use the saw was drained off all water and thoroughly cleaned. Once dry the samples were cut under 3 in 1 oil, administered by hand during the cutting process. Samples were cleaned of excess oil by washing in methylated spirit. Smaller samples were cut dry using an angle grinder, mounted onto a bench mount, fitted with a diamond coated, 11.5cm diameter blade (Figure 2.1). Cutting samples this way was quick and generated straight cut samples for sections. Heat damage to the samples was minimal due to the amount of time taken to cut each sample.

Figure 2.1: Bench mounted angle grinder used to cut samples containing hygroscopic material. Blade diameter 11.5cm and diamond coated.

Samples were again ground flat using the bench mounted grinding wheel lubricated with 3 in 1 oil administered by hand. Polishing the surface to stick to the slide proved difficult. Initially samples were polished on the plates using the carborundum powder mixed with oil, but it was found that the oil was too thick and caused lubrication without polishing the rock face. Polishing was therefore achieved using Wet & Dry carborundum grit paper normally used in palaeontology. The wet & dry paper works in a similar way to the wet polishing plates with different grades from 120 – 1000 grit size. Samples were again thoroughly cleaned using methylated spirit and placed in the oven overnight to dry. The blocks were once again stuck to clean, dry glass slides using the same epoxy resin as above and left to cure on the heat. Once dry the samples could not be reduced in size using the PetroThin as this is lubricated and cooled using water. Dry samples were therefore reduced in size by sawing of as much of the excess block as was safely possible and the remainder was ground off using the bench mounted grinding wheel, again lubricated with 3 in 1 oil. This process obviously has the drawback that a large amount of sample is lost during the grinding process so repeat sections of the same block are not possible. Final adjustments to the thickness of the sections and polish were made using the Wet & Dry paper.

2.2. Scanning Electron Microscopy and Electron Microprobe

Elemental analysis and mineral determination of samples was completed using Scanning Electron Microscopy (SEM) at University College London using a Jeol JSM-6480LV high performance, variable pressure analytical scanning electron microscope with a high resolution of 3 nm. Energy dispersive X-ray spectroscopy (EDS) and electron backscatter diffraction analyses were also possible using the Oxford Link system. Samples were analysed as thin sections, coated in carbon and mounted using carbon tape. An acceleration voltage of 18kV and an acquisition time of 90 seconds was used for samples which do not volatilise easily, i.e. low in sodium, whilst the natrocarbonatite samples were analysed using an acceleration voltage of 10kV for only 20 seconds to reduce the loss of volatile elements. All samples were analysed at a working distance of 11 mm and a spot size of 65 µm. The EDS detector within the SEM has a resolution of between 70 to 130eV.

Highly volatile samples, such as natrocarbonatite, were analysed using repeated spot analysis for low count times, e.g. 5 repeats at 20s, to reduce the damage to the sample and loss of elemental data by volatilisation. Volatile loss during analysis cannot be completely avoided and

is thought to be the result of thermal activity breaking the Na – O bonds resulting in ionic diffusion. This process is normally evident from either a shift in alkali-metal count rate under constant beam voltage and current or low analytical totals (Spray and Rae, 1995). The decline in count rate varies over time with an initial steep decline in count rate for elements such as sodium with an eventual steady - state count rate achieved over longer acquisition times. It is therefore important to take into account the loss of alkalis metals when using EDS or WDS data for mineral calculations as the final concentrations are not truly representative of the sample. However, by tracking the shift in count rate during an analysis of nepheline, for example, it is possible to back calculate to the original sodium content. For each thin section analysed, initial measurements on nepheline crystals were made for 75-second acquisition times with a Na_2O value taken at 5 seconds and then every 10 seconds. The results of these are plotted below (Figure 2.2).

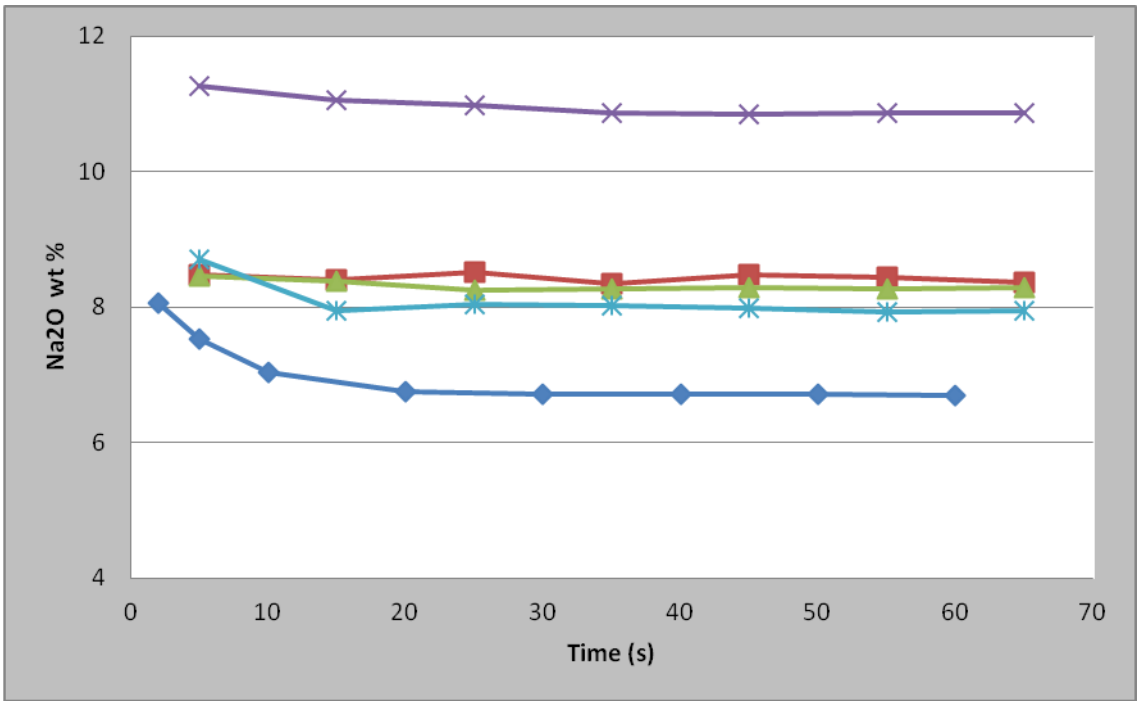

Figure 2.2: Graph to illustrate the Na volatilisation from sample OLX 17a over time under EDS beam conditions. Each line represents a different nepheline crystal.

The majority of analyses show the characteristic drop in Na_2O wt% with time, however some show very little decrease or even a slight increase. According to Spray (1995) this increase is due to electron accumulation at the surface of the mineral (know as a space-layer charge) in regions of thin conductive coating (in this case carbon coating), resulting in the attraction of Na

ions towards the surface. By extrapolation from these line graphs it is possible to determine the initial Na content of the minerals before excitation by the beam.

Samples of interest were also analysed using wavelength dispersive X-ray spectroscopy (WDS) which generates elemental data over a higher resolution than EDS, as the electron microprobe is set-up so that particular wavelengths are scanned and counted. This achieved by a precise set-up crystal spectrometers, which diffract the X-rays towards the detectors. WDS analysis was completed using a Jeol8100 Superprobe with Oxford Instrument INCA microanalytical system. The same carbon coated sections used on the SEM were used on the electron microprobe.

Some of the extremely hygroscopic material collected during field work was not suitable to be turned into thin sections and so SEM work was conducted upon grain mount stubs. SEM stubs with sticky carbon tape were dipped into sample bags containing grains of the material and then puffs of air were used to ensure the material was securely attached to the stub. These were then analysed using the same technical set up as above. Due to the inability to generate a polished surface on the grain material it must be expected that unfavourable scattering of the X-rays will occur and so analytical precision will decrease compared to measurements made upon polished sections. The results will only therefore be used as a guide to mineral chemistry.

2.3. Whole rock elemental analysis

To further investigate the genesis of some samples, in particular fenites and metasomatised units, bulk elemental data was required for major, minor and trace elements. This work was outsourced to the Natural History Museum and completed by Dr Stanislav Strekopytov using both Inductively Coupled Plasma Atomic Emission Spectroscopy (ICP-AES) and quadrapole Inductively Coupled Plasma Mass Spectroscopy (ICP-MS). The techniques were used to determine different elemental concentrations;

- ICP-AES
    - Al, Ca, Fe, K, Mg, Mn, Na, P and Ti (all measured in oxide weight percent (wt%))
    - Ba, Cr, S, Sr, V, Y and Zn (all measured in parts per million (ppm))
- ICP-MS

- Co, Cs, Ga, Li, Mo, Nb, Pb, Rb, Sb, Th, U, W, Zr and REE elements from La to Lu (all measured in ppm)

2.3.1.Sample preparation

Sample preparation for both methods was exactly the same. Slices of selected samples were cut using the diamond tipped angle grinder and then passed through a jaw crusher to produce centimetre sized chips of rock. The jaw crusher was thoroughly cleaned before use and between each sample to prevent contamination. Cleaning the equipment required removal of the crushing plates which were then scrubbed down with water and dried using acetone. The jaws and inside of the crushing were wiped down with a damp cloth and then vacuumed to remove any dust. The collection basket was also cleaned using a damp cloth and acetone to dry. The rock chips were then ground to a fine powder of 2 – 4 µm using a tungsten carbide Tema Mill set for 3 seconds. Again, the machinery was thoroughly cleaned prior to use and in between each sample, using water and acetone. Any large pieces of material were finished off by hand using an agate pestle and mortar.

2.3.2.Major and minor elemental analysis

For bulk concentrations of major and minor elements an aliquot of approximately 40 mg was taken of each sample, pre-treated with 1 ml concentrated HNO_3 and fused with 120 mg of $LiBO_2$ in a Pt/Au crucible (Hezel et al., 2011). The resulting material was then dissolved in 10% HNO_3 and run on the ICP-AES using a Varian Vista Pro-Axial. The ICP-AES technique works by using inductively coupled plasma to produce thermally excited atoms from a sample. Upon relaxation from this excited state the atoms emit electromagnetic radiation in the form of a photon of light which has a wavelength characteristic of the element. As a sample is formed of a mixture of elements simultaneous emission of a spectrum of wavelengths is produced which is then separated by a grating within the spectrometer and each emission is directed into a dedicated photomultiplier tube detector, which converts the electronic signal into concentration.

2.3.3.Trace element analysis

Trace element concentrations require the use of ICP-MS due to the lower abundance of these elements within a sample. The technique used is again that outlined in Hezel et al (2011). A 100 mg aliquot of each sample was pre-treated with concentrated HNO_3 and dissolved in a

mixture of 4 ml HF and 1ml $HClO_4$ at 100°C. The solution was then dried down at 150°C. The remaining residue was re-dissolved in 2 ml $HClO_4$ at 150°C. The solution was again dried down and then re-dissolved in a mixture of 1 ml concentrated HNO_3 and 1 ml H_2O and 0.5 ml H_2O_2 at 70°C. The solution was diluted up to 10 ml using deionised water. ICP-MS analysis works in a similar way to that of ICP-AES. The atoms of the elements are converted into ions by the plasma source and carried towards the mass spectrometer where they are separated and detection of ions is possible by their mass-to-charge ratio (M/Z). The detector within the mass spectrometer measures the number of ions striking the detector and translates this into an electrical signal which can be related to the number of atoms of the element.

2.3.4. Standards and calibration

All analyses for major, minor and trace elements were completed using certified reference materials;

- BCR – 1
- BHVO-1 (basalts)
- JG – 1 (granodiorite)
- JLS -1 (limestone)
- MAG – 1 (marine muds)

All the standards were run at the start of the analyses along with a blank to monitor the accuracy of the bulk elemental analysis. Laboratory control samples were also run after every batch of 10 samples to monitor the drift and precision of the machinery. All of these were found to be satisfactory for all elements.

2.4. Radio and stable isotope analysis

2.4.1.Radioisotope work

The following outlines the sample preparation and analysis for radiogenic isotope determination of both mica and pyroxene megacrysts as well as whole rock samples of carbonatite ash and fenitic units. The samples were primarily analysed for Rb and Sr, but some Sm and Nd analyses were also conducted using the NERC facilities at NIGL, BGS, Keyworth, UK.

2.4.1.1. Sample preparation

Initially mica minerals and pyroxene megacrysts were handpicked using tweezers and placed in disposable Petri dishes prior to crushing. The pre-crushed whole rock samples were measured out with a spatula and placed in glass capsules for weighing. The mica and pyroxenes were then crushed by hand using an agate pestle and mortar which was rinsed with deionised water between samples to prevent any contamination. The resulting powders were transferred to glass capsules for weighing. Sample weights were taken using a micro balance. The powders were placed into an acid cleaned plastic container with a small amount of Milli-Q (MQ) water to collect small flecks of powder attracted to container sides. A Zerostat anti-static gun was used to keep measurements as accurate as possible. The anti-static gun works by releasing a stream of positive ions when the trigger is squeezed and a stream of negative ions when the trigger is released, resulting in a neutrally charged surface. The majority of the samples weighed between 0.007g and 0.05g.

2.4.1.2. Chemical preparation

Mica samples were soaked in acetic acid for an hour to remove any carbonate material. All samples were spiked with Sr, Rb and Nd-Sm of known isotopic values for analysis. A pre-mixed Rb-Sr spike was used to reduce error on measurement due to small nature of natural concentrations in samples. Approximately 180 µl of mixed spike was added to each sample. Spike addition was achieved from dropper bottles which were weighed prior to administering and then after to find out how much had been added. Once spiked, samples were dissolved and evaporated in acid in a sequential way using nitric acid, hydrofluoric acid and hydrochloric acid until all impurities were removed and samples were reduced to small amounts of powder.

Ion exchange columns were removed from a bath of 6M HCl and rinsed with MQ water both inside and out. Any airlock present above the filter was removed by gently pressurising the top of the column with a thumb until the water drained freely. The columns were then filled with Sr Spec in H_2O (~ 9 drops) and cleaned using MQ water and 6M HCl (alternation about 5 times). The dried samples were dissolved in a small amount of acid and then placed into the columns using a pipette. The columns then go through Sr extraction procedure using HNO_3 of varying molarity (2 – 7M) to remove everything but Sr from the sample in the column. The "waste" products, which include the Rb, Sm-Nd and REE elements, are collected in a fresh beaker to be analysed later. The Sr is removed using 2 ml of 0.05M HNO_3 and collected in a beaker. Both beakers were then placed on the hot plate to evaporate.

The dried Sr forms a ball of material in the bottom of the beaker. This purified sample was loaded into the mass spectrometer using a carousel of single rhenium filaments. Each filament is loaded onto a current block, where 1 amp current is passed through to warm the filament. A small amount of Parafilm is placed on the sample 1/3 from either end to form a barrier to keep the sample from rolling off during placement. The Sr ball was dissolved in tantalum oxide and place onto the filament using a pipette. The sample was evaporated and then the current was slowly increased to 2amps causing the samples to glow for a few seconds. Samples are then loaded back onto the carousel and covered with metal plates. The carousel was then loaded into the Thermo-Electron Triton 1, thermal ionisation mass spectrometer (TIMS). This method of analysis works by generation of ions through thermal ionisation under a vacuum. These ions are then accelerated across an electric potential of around 10,000 volts and focused into a beam via slits and electro-statically charged plates. The ion beam is passed through a magnetic field and accelerated before it is separated into individual beams based upon the mass-to-charge ratio. These individual beams are then directed into faraday cup collectors where the beam charge is recorded as a voltage.

2.4.2.Stable isotope

Whole rock lava and volcanic ash samples from Oldoinyo Lengai were collected during field work for the purpose of stable isotope chemistry determination. All samples were kept in desiccant during transit from Africa to the UK to keep atmospheric alteration and so subsequent isotopic fractionation to a minimum. Upon return to UCL the samples were ground by hand using an agate pestle and mortar until a few microns in size (flour-like consistency).

2.4.2.1. *Carbon percentage analysis of samples*

Prior to isotopic analysis the powdered samples were analysed for total carbon using the ThermoFisher Scientific Flash EA 1112 NC analyser. Samples were weighed out into tin foil capsules using a micro-balance. The tin capsules were then carefully folded and rolled into small balls ensuring that all the air is removed from the capsule with no splitting of the container sides. The samples are then loaded into the autosampler along with 1 blank and 7 standard. The standards were positioned at the beginning, middle and end of the run to monitor the drift of the equipment during the analysis. The samples are dropped into a furnace with a pulse of oxygen and burned. The resultant gases are carried by helium carrier

gas through an oxidant to ensure complete burning. Chemical traps are in place to capture any sulphur or halogens that may be present. A copper reduction furnace is used to trap excess O_2 and convert any NO_x compounds to N_2 for analysis. A water trap, formed of a drying tube containing magnesium perchlorate, removes any excess water and a gas chromatography column separates the N_2 and CO_2. These gases then flow into the EA detector and finally through a CONFLO IV interface into the mass spectrometer.

2.4.2.2. *Isotopic determination procedure*

For isotopic analysis each sample was weighed out using micro-scales and platinum boats with sample weights ranging between 380 – 430 micrograms depending on their total carbon percentage previously measured. Multiple samples were weighed for repetition of measurements. Initially, samples were treated / washed with 10% H_2O_2 and left for 1.5hours. The mixture was then treated with acetone and placed in an oven at 50 degrees and left for 48 hours to dry. The samples were then placed in the run tray and flushed with helium to remove atmospheric gases from the vial prior to analysis. Whole rock and volcanic ash samples were analyzed at the Bloomsbury Environmental Isotope Facility (BEIF) at University College London on a ThermoFinnigan Delta^{PLUS} XP stable isotope mass spectrometer attached to a ThermoScientific Gas Bench II device. Standards and unknown sample rock and ash were loaded into glass vials, methanol rinsed, oven roasted at 200°C for 1 hour and kept overnight in a 70°C oven. For analysis, each vial was manually acidified with 100% Phosphoric acid (0.1 ml) using a syringe injection via the screw cap septa. Precision of all internal (BDH, IAEA & IFC) and external standards (NBS19) is ±0.03 for $\delta^{13}C$ and ±0.08 for $\delta^{18}O$. All values in later chapters are reported in the Vienna Pee Dee Bee notation (VPDB) relative to NBS19.

After the initial samples were analysed a number appeared to have large standard deviations between repeats which seemed anomalous and perhaps related to the preparation of the samples using hydrogen peroxide. A number of samples were therefore re-analysed using only roasting as the preparation to remove any organic molecules such as sulphur which may affect the performance of the mass spectrometer. The samples were re-weighed to approximately 600 micrograms with 3 repeats of each sample and the above method was repeated for analysis.

2.5. Micro Raman Spectroscopy

2.5.1. Theory and advantages of Raman Spectroscopy

Micro Raman techniques were used for non-destructive analysis of fluid inclusions located within nepheline, quartz and apatite grains. Raman spectroscopy is well suited for the study of fluid inclusions and petrographic studies due to the non-destructive nature and the rapidity of the measurements. Additionally, Raman spectroscopy can reveal the presence of numerous mineral phases within one spectrum at sub-micrometer resolution. This differs from electron beam elemental analysis which provides the bulk elemental make up of one or all the phases within the beam area. The technique is based upon the observations of Raman scattering caused by the excitation of molecules by irradiation from a light source of a specific wavelength. Photons from the source excite the molecules of the sample to a virtual excited energy state. When the molecule relaxes it returns to a different vibrational or rotational state and releases a photon whose frequency is shifted away from the excitation wavelength – known as the Stokes or Anti-Stokes Shift, depending on whether the photon has less or more energy, respectively, than the original photon (Keresztury, 2006, Burke, 2001). Only certain vibrational states are said to be "Raman Active" meaning that they are recognisable using this technique, which is ultimately dictated by the amount of deformation of the electron cloud and bonds of the molecule – the polarizability. For a vibration to be Raman active there must be a change in the size, shape or orientation of the polarizability ellipsoid during normal vibration, i.e. ground state vibration (Figure 2.3).

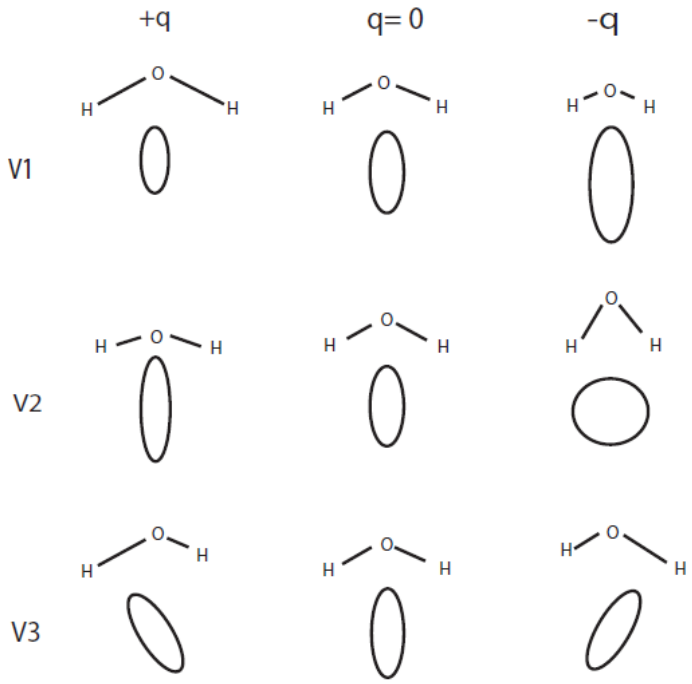

Figure 2.3: Example of Raman-active vibrations between two small displacements (+q and –q) within a water molecule (Ferraro and Nakamoto, 2003). V_1 represents a change in size; V_2 a change in shape and V_3 a change in orientation of the polarizability ellipsoid.

All of the Raman analysis was completed at The Carnegie Institution of Washington using non-cover slipped, doubly polished thin sections between 30 – 150 microns thick. Raman spectra were generated using a frequency-doubled solid-state YAG laser (532nm) operating between 0.3 and 1mW output. Imaging was performed using a Witec α-scanning near-field optical microscope (SNOM) which was customised to allow for confocal Raman spectroscopy imaging. The optical microscope was used with a 100x super long working distance (SLWD) objective and a 20x long working distance (LWD) objective. The lateral resolution of the instrument is approximately 460nm in air using the 100x SLWD objective or 810nm when using the 20x LWD objective. A 50µm optical fibre was used to act as the confocal pin hole and transmit the laser light and Raman signal. A Peltier-cooled Marconi 40-11 CCD chip was used to collect the spectra, after passing through a f/4 300mm focal length imaging spectrometer typically using 600 lines/mm grating (Steele et al., 2007). Raman spectroscopy calibration and laser tuning were achieved using both a pure silica standard and a type IIa diamond standard, with characteristic peaks at 520 cm^{-1} and 1332 cm^{-1} respectively.

2.5.2.Precautions for work on thin sections

A number of considerations must be taken when performing Raman spectroscopy on glass mounted thin sections. These will be outlined below but a full description of the precautions can be found in (Dieing et al., 2010). Firstly, thin section surfaces are often irregular and contain contamination from polishing material used during their production. Surface irregularities, such as pits or grooves, often cause scattering of the excitation beam and can contain abrasive grains of polishing powders. Surface spectra scans can often lead to the misinterpretation of the polishing material as a feature of the mineral. It is therefore advisable to check the scan area in reflective light prior to scanning to ensure the area is free of contaminant or to perform a scan below the surface of the mineral. Using the reflective light prior to scanning also enables the user to check they are focusing the upper surface of the thin section rather than the lower surface.

Secondly, the mounting resin used to stick the rock slice to the glass often permeates through cracks within the section, particularly for those made using the vacuum impregnation technique. The resin itself is a C-H based product and so generates peaks within the C-H stretch, higher wave number region of Raman spectra, as well as at lower wave numbers. It is advisable to take a reference spectrum (Figure 2.4) of the resin so that the peak combinations can be recognised and interpreted accordingly.

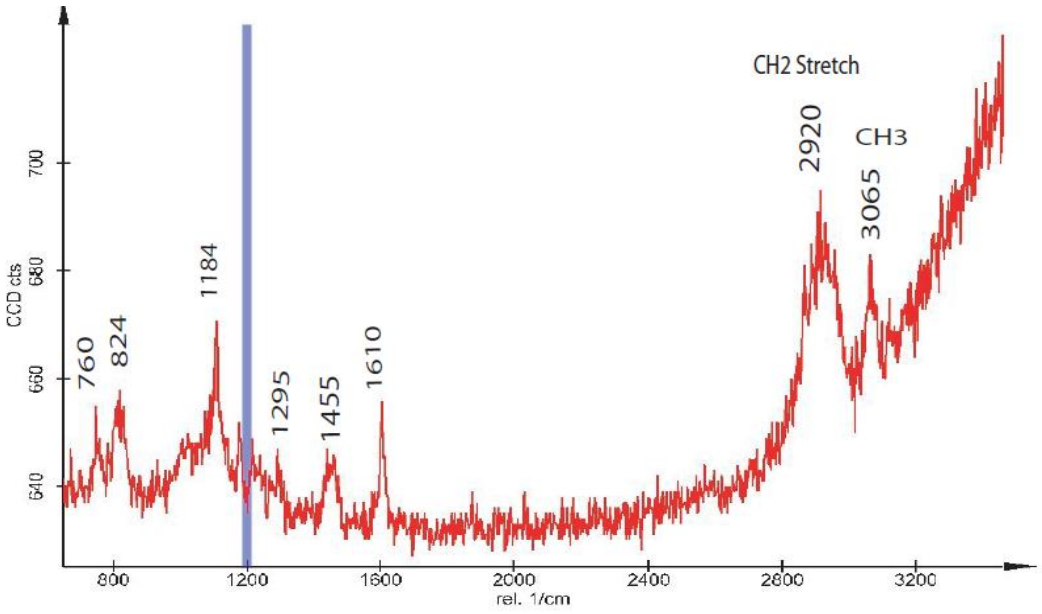

Figure 2.4: Raman spectra of thin section resin. Key identification peaks are marked. A number of these peaks correspond to mineral identifications peaks.

Thirdly, thin sections that have been studied using other techniques, for example electron microprobe or scanning electron microscopy, will have been previously carbon coated. This coating can be removed with extra polishing but removal is often imperfect and Raman spectroscopy is extremely sensitive to the presence of carbon. Any remaining coating will appear as laser-reflective material causing almost flat lined spectra. Imperfectly removed carbon coating produces a spectra similar to that of amorphous / glassy carbon (Dieing et al., 2010).

2.5.3. Setup for mineralogical imaging

Sections were loaded onto the microscope stage and viewed under a low magnification objective (20x). The site of interest was located and centred. The microscope can be used with either reflective or transmitted light at this stage. The surface of the section is brought into focus by raising or lowering the microscope stage and all co-ordinates were zeroed. The section was then viewed in transmitted light using a higher magnification objective (100x), which revealed the subsurface inclusions of interest (Figure 2.5).

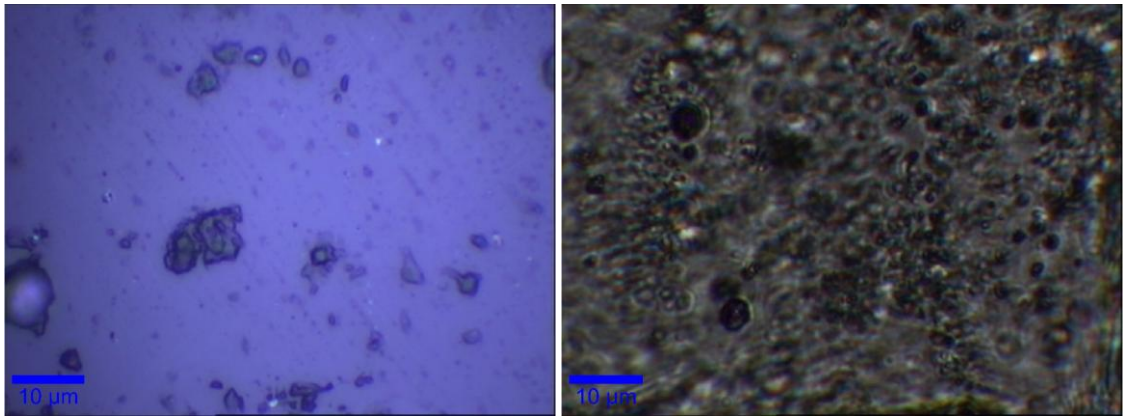

Figure 2.5: (a) Reflected light image of the surface of an inclusion rich mineral. Lineations visible at the surface are inclusion trails located a few microns below the surface; (b) Transmitted light image of the same site of interest taken 14.75 microns into the section. The sub-circular features are all fluid inclusions located at different focal depths within the section.

The microscope was then focused through the thin section until suitable inclusions were in focus. For CO_2-rich inclusions this was when a bright halo could be seen around the moving CO_2 bubble. At this point the z co-ordinate recorded the depth into the section that the laser would penetrate. As a confocal spectroscopy system the collection of light is constrained to a narrow band close to the selected focal plane. Any light from above or below this plane is

rejected at the confocal aperture and so data is collected for a thin slice of the section specific to the inclusion of interest. In theory several thin slices can be scanned of a single inclusion to build up a 3-dimensional image of the inclusion. Raman imaging was conducted by taking a Raman spectrum at each pixel within a manually defined scan area. Scan areas varied in size between 5x5μm^2 to larger area scans of 70x40 μm^2. For each scan the number of scan lines and points per line were defined according to the area size. For example, a scan of a region 5x5 µm would be set to scan 10 lines with 10 points per line, using the rule of thumb that number of lines and scan points should be at least double the maximum dimension of the scan area. Each point was scanned for an integration time of 3 or 6 seconds, depending on the resolution required. Larger area scans were primarily performed overnight, as scan run time (hours) = (number of lines * number of points * integration time) / 3600.

2.6. Microthermometry analysis of fluid inclusions

2.6.1. Sample preparation

Doubly polished thin section wafers were made at Kingston University from cut sections rock marked with areas of interest for fluid inclusion studies. The method of preparation is beyond the scope of this thesis and for a review of techniques see Shepherd et al (1985).

2.6.2. Heating and freezing stage

Microthermometry experiments were carried out at Kingston University, London using a Linkam TMS95 heating and freezing stage attached to a Nikon Optiphot microscope. The stage was regularly calibrated using a FLINC synthetic standard of H_2O fluid inclusions (pure H_2O critical point at +374.2 °C) as shown in Figure 2.6a. Standards and samples were loaded onto the microscope stage which is then sealed to create an isolated chamber. This chamber is heated to approximately 30°C and the chamber is purged of atmospheric gas by opening a one way valve. Purging of the chamber is an important process to ensure that condensation of air does not occur on the microscope and obscure the view of the inclusions. This is also achieved by flowing cold air over the surface of the glass window. Once purged the chamber is sealed by closing the valve and the temperature is lowered using liquid nitrogen.

If calibrating using the standards the inclusions are quickly cooled to -30°C at a rate of 100°C / min. Once this temperature is achieved the temperature is held for a few minutes to allow the development of solid material (ice crystals in the case of pure H_2O inclusions) before slowly heating the sample (1 - 10°C/min) and taking measurements for particular phase changes. It is important to make all measurements on the heating cycle rather than the cooling cycle due to the effect of super cooling. Fluid inclusions behave metastably during cooling with the development of new phases occurring reluctantly at lower temperatures than expected which varies with each cooling. The values are therefore meaningless. Upon heating the ice crystals are slowly lost back into the liquid of the fluid inclusion and homogenisation should take place around -0.2°C. Figure 2.6b shows the presence of ice crystals within the standard just prior to homogenisation with the final ice crystals located at the tips of the inclusion. In this instance the homogenisation occurred at 0.0°C which is 0.2°C higher than should be and so all results were corrected for this. A standard calibration was conducted first thing in the morning and before each new sample.

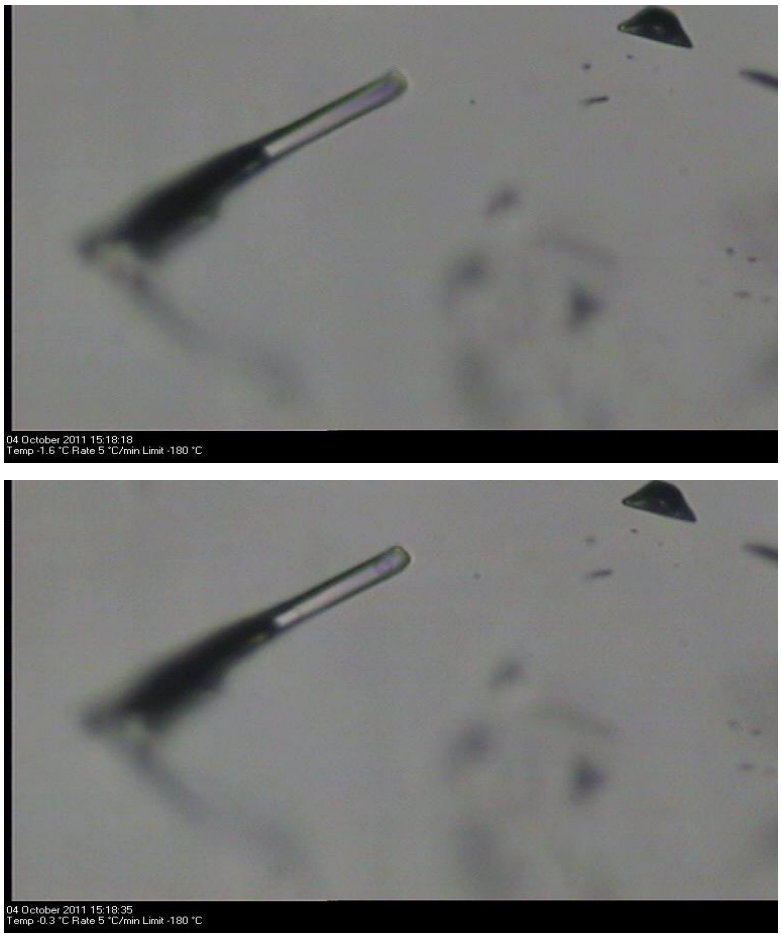

Figure 2.6: (a) FLINC pure H_2O fluid inclusion standard at -1.6°C; (b) The same fluid inclusion at -0.3°C with visible ice crystals, just prior to homogenisation, which took place between -0.2°C and +0.2°C.

Sample analysis occurs in much a similar way to that as the standard calibration with samples being quickly cooled to temperatures around -120°C or until solid material forms. In the case of CO_2 – rich inclusions this is a visible change with the generation of an inclusion that has a similar appearance to frog spawn (Figure 2.7).

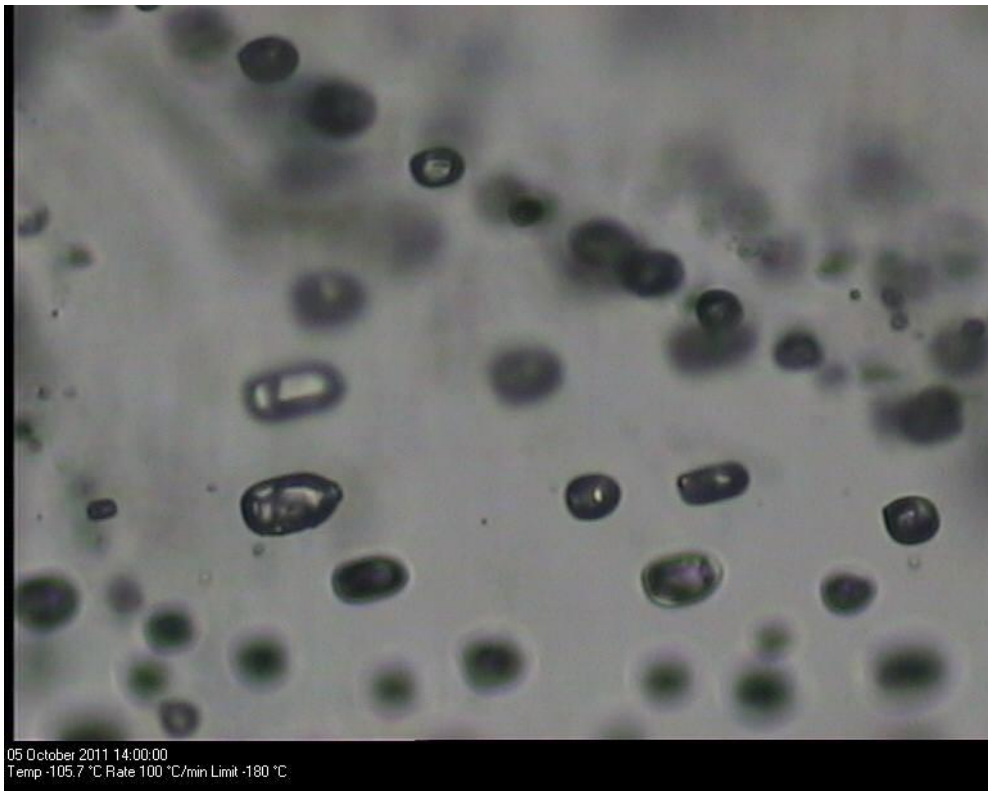

Figure 2.7: Solid-bearing fluid inclusions from sample OLX 3. Solids within the inclusion develop a pattern similar to that of frog spawn. Larger of inclusions ~ 20µm in length.

The sample is once again heated slowly and the measurements are made on the heating cycle. There are 2 important measurements to be made; firstly the melting temperature (T_m) which is the transformation of solid (S) + vapour (V) to liquid (L) + vapour (V) and secondly the homogenisation temperature (T_h) which is the change from liquid + vapour to liquid or vapour solely. It is important to note the type of homogenisation which occurs. The melting temperature provides an indication of the gas composition of the inclusion, with pure CO_2 inclusions melting between -56.6°C and -56.2°C. The presence of other gases will suppress this temperature to lower temperatures. The homogenisation temperature can then be used to calculate the density of the fluid within the inclusion.

When investigating aqueous inclusions a different set of measurements must be made during the heating cycle. For H_2O – Salt inclusions three measurements are made;

- First ice melting also known as eutectic (T_e) – which is the change from S + V to S + V + L and indicates the type of salt in solution i.e. NaCl, KCl.
- Last ice melting ($T_m$ice) – the change from S + V + L to V + L and an indication of the salinity
- Homogenisation temperature (T_h) – the final change from V + L to either V or L and can be used to determine the trapping pressure and temperature.

Immiscible H_2O – CO_2 – salt inclusions are slightly more complicated to investigate and require five main measurements;

- CO_2 melting (T_mCO2)
- First ice melting (T_m)
- Clathrate melting ($T_m$clath) – this is used as the proxy for salinity as essentially represents the last ice melting of the system and often occurs between – 6 and +12°C.
- Partial homogenisation (T_hCO2)
- Final homogenisation (T_h)

The reproducibility of the measurements was approximately ± 0.2 ºC below 30 ºC and ± 2 ºC above 30 °C. Analytical errors are insignificant in terms of geological interpretation.

2.7. Permeability measurement

The permeability of a rock sample was determined using a steady-state-flow permeameter. The permeameter and calculation of permeability is based upon Darcy's Law $Q = K A (\delta h/L)$, where Q is discharge through the sample, K is the hydraulic conductivity (permeability), A is the cross-sectional area of the core, δh is the difference in hydraulic head (pressure gradient) between the reservoirs and L which is the length of the core sample. The permeameter works by placing a small core of rock into rubber jacket and placing it into the sample assembly, through which water is passed from one reservoir at the top of the sample to another reservoir at the base. The sample itself is placed under a confining pressure and pore pressure using an oil confining medium which generates adequate pressure to seal the jacket on the sample and produce an effective pressure to simulate overburden during burial. Once the confining pressure is stabilised the reservoirs are filled with water so that one reservoir is full

and then other is near empty. The valves for the reservoirs are then opened so that flow through the sample can occur. The sample assembly contains numerous intensifiers which help generate the differential pressures at the sample ends encouraging flow. The servo controlled unit then monitors the flow rate both out of one reservoir and the flow rate into the other. From this a flow volume rate and subsequently discharge per unit area of the sample can be calculated and substituted into a rearranged version of Darcy's Law to determine the permeability of the sample.

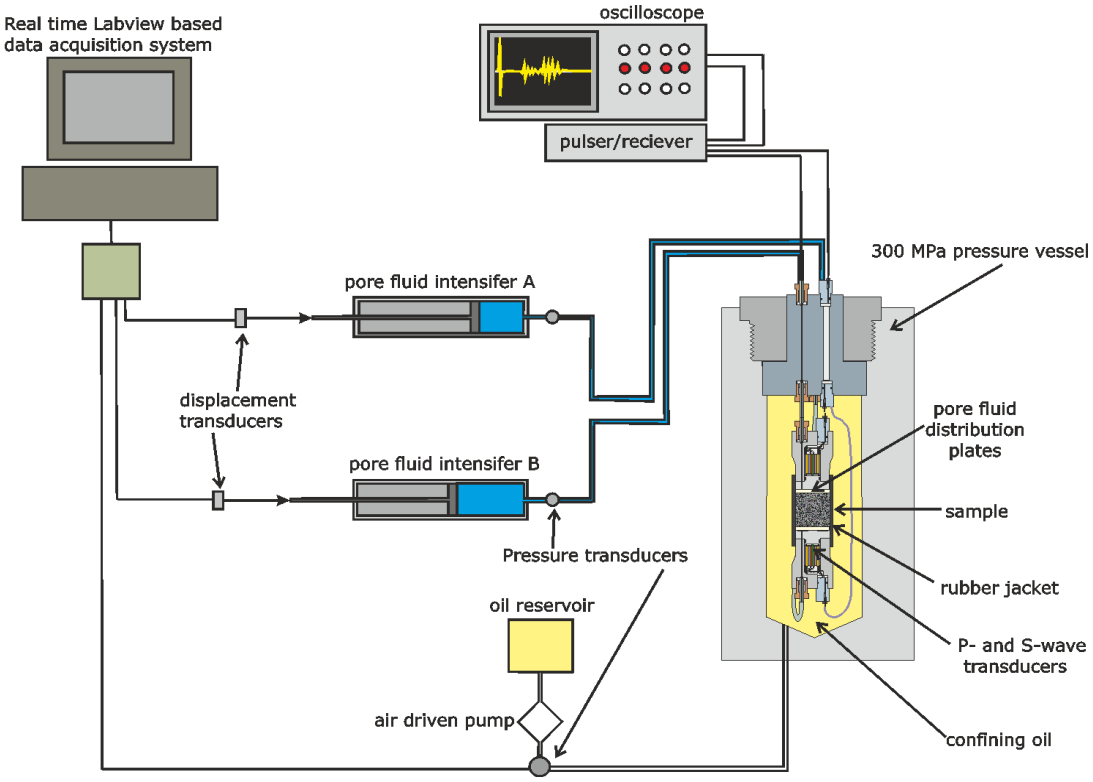

Figure 2.8: Inner sample assembly for the permeameter with sample jacket at centre. *Diagram courtesy of Liz Gaunt, Mike Heap and Steve Boon.*

2.7.1.1. Coring the natrocarbonatite

2.7.1. Core generation

Natrocarbonatite is extremely hygroscopic and so alters rapidly under the presence of water, for this reason a few adaptations to the procedure for generating cores were made. A core of

natrocarbonatite pavement lava was taken using a standard rock corer and a diamond tipped, 25 mm core drill bit. Water could not be used as the coolant and lubricant so was replaced with 3 in 1 oil. This was applied generously to the drill bit prior to coring. The core was then completed in small, incremental stages for the following reasons:

1. To prevent breakage or damage of the core unit
2. To keep the temperature of the drill bit to a minimum both to prolong the life of the drill bit and also to reduce the thermal damage to the sample.
3. Oil had to be administered to the sample and drill bit by hand using a distilled water bottle, so after small sections cored a generous amount of oil was applied for lubrication and cooling.

Normally cores are removed from the drill bit using a blast of water, so to remove the core a small amount of oil was passed around the inside of the bit and the core was gently pushed out using a steel rod to reduce damage to the surface of the core.

Grinding of the core was also completed by hand rather than using a Jones and Shipman grinding wheel, as the lubricant is water based in the machinery. The core was first ground by hand on dry polishing mats using the coarsest mat to speed up the process. Once the surfaces were flat, the top and base of the core were made perpendicular to the sides of the core by fixing the core into the jig normally used on the grinding wheel providing a flat, limiting surface to grind to, again using the dry polishing mats.

The core was kept in a sealed box with silica gel desiccant between uses to prevent alteration in atmospheric moisture. The core itself had an average diameter of 24.22 mm and average length of 25.20 mm. The sample mass was 25.10 g. The core was then placed within the permeameter assembly and fluid flow through the sample was monitored. The sample was left in the permeameter for just over 3 hours with one refill of the reservoir during this time.

Chapter 3: New Field Observations of Oldoinyo Lengai (post-eruption) and surrounding rift region

The aim of this chapter is to detail the observations made during a two-week field campaign to the Gregory Rift in May 2010. A number of volcanic features were visited and their exact GPS co-ordinates obtained (Appendix A). The primary aims of the observations were to document (1) the appearance of Oldoinyo Lengai after the 2007 eruption, and (2) the morphological features located on its flanks. The results were used to investigate the physical processes that have shaped the volcano and surrounding landscape and also, to compare the 2007 eruption with other historic eruptions to investigate the cyclicity of activity at the volcano.

3.1 New observations of Oldoinyo Lengai

3.1.1 Crater geometry and morphology

The process of crater filling discussed in Chapter 1 continued until the explosive activity in 2007, which again cleared the crater above the conduit and produced an irregular crater floor 172 m down from the rim of the ash cone (estimated maximum depth). The crater floor is enclosed by near-vertical lower walls, the upper rims of which are topped by inner slopes of the ash cone that dip inwards by about 45 ° (Figure 3.6). The crater is elliptical in shape with a N-S rim-to-rim distance of 262 m and an E-W, rim-to-rim distance of 289 m (measurements made using infrared rangefinder accurate to within 1 m). The crater floor is covered with rocky debris, including tilted broken lava plates (5-10 m scale) possibly from recent magma withdrawal, and collapse material from the locally unstable inner crater walls. Debris scars of about 30 m wide occur in the north-eastern and south-western sectors of the ash cone's rim indicating that some material appears to have fallen en masse into the crater whilst other sections have become disaggregated (Figure 3.4a and 3.4b).

The crater walls expose an upper series of lapilli-dominated ashes with white-to-ochre colours up to 30 m thick that mantle the topography of underlying grey-to-white carbonatite lava flows and lapilli tuff formed within the previous crater. A sub-vertical intrusion ~5 m wide with irregular boundaries was observed cutting most of the north wall of the crater. This may represent a vent or feeding conduit to previous hornitos that was plugged in the most recent (2007) activity (Figure 3.2). The head of this intrusion has caused deformation in the previous

sub-parallel deposits with upwards shearing at its margins. This appears to be the first recorded observation of dyke-like features within the crater walls of Lengai. Whether this feature represents a feeder system for one of the larger hornitos prior to the explosive eruption or a feeder system for the eruption itself is unknown. The composition of this feature is also unknown. Due to the instability of the overlying slopes it was not possible to collect rock samples. The lack of white alteration suggests that the dyke is comprised primarily of silicate rock rather than natrocarbonatite.

Close examination of the sub-parallel units within the tuff cone walls reveals some vertical offset between continuous layers of about 1 m, suggesting subsidence to the east of the crater possibly due to the intrusion of magma along a localised fault. Whether the fault was generated during or prior to magma intrusion is unknown. The distance of the observations unfortunately did not allow the identification of a chilled or baked margin associated with the body of magma.

The upper slopes and region between craters are littered with volcanic debris generated during the explosive activity. This debris consists mainly of 10 – 50 cm bombs coated in grey-to-ochre natrocarbonatite up to 1 cm thick (Figure 3.1). Once split open, the bombs revealed a number of lithologies related to the subsurface geology, which will be discussed in Chapter 4.

Figure 3.1: Surface of crater rim littered with volcanic bomb material. Average bomb size around 10 cm across. *Photo courtesy of Adrian Jones*

Numerous metre-scale white stalactites appended to overhangs indicate remobilisation of water-soluble carbonates from the white, lapilli-dominated ashes exposed on the rim of the crater. Such formations have previously been reported within caves exposed beneath inactive hornitos located on the crater floor prior to the explosive activity (McFarlane et al., 2004) but also appear on the recent lava flows associated with the overfilling of the northern crater prior to eruption (see section 3.1.3).

Figure 3.2: Close up of sub-vertical dyke-like feature located in the northern crater wall with deformation of the volcanic ash evident around the head of the intrusion. White-grey linear features are m-scale stalactites.

There were at least three visible sites of active degassing, two from fissures on the crater rim ash cone (Figure 3.3) and one from a vent on the crater floor. These plumes were white in colour and had a sulphurous smell suggesting the presence of hydrogen sulphide. The ash cone on the north-western approach to the crater showed up to knee-deep alteration to dark brown, yellow and black soil-like products with pockets of blue and green material accompanied by a distinctive sulphurous smell. Similar colourations could be seen on the precarious western crater wall just below the slope of ash. Rocky exposures of pyroclastic breccia on the upper north-western slopes of the volcano, immediately below the ash cone, have numerous expansion cracks and fissures suspected of recently releasing gas, as indicated by large numbers of dead insects. A gas haze in the same area suggests additional diffuse degassing from the upper flanks of the volcano. A full report on the degassing and plume of Lengai is included in Appendix C, which indicates the presence of aerosols from the diffuse emissions from the summit crater of the volcano.

Figure 3.3: Fracture located on the rim of the new ash cone of the northern crater, which showed degassing. A white effervescent coating can be seen around the fracture.

Observations of the crater suggest that the volcano is in a period of reduced activity following the explosive eruption in 2007 with no effusive lava production on the crater floor, although lava could be heard below the surface with assumed pockets of degassing lava, causing disturbances around cavities in the crater floor at intervals of 15 – 20 minutes. At least four open vents were observed on the crater floor appearing darker than their surroundings. A few of these cavities look to be the initiation of metre-scale hornito building, but are not yet well organised. Some areas near the crater wall appeared to have darker flow-like features from recent lava extrusion.

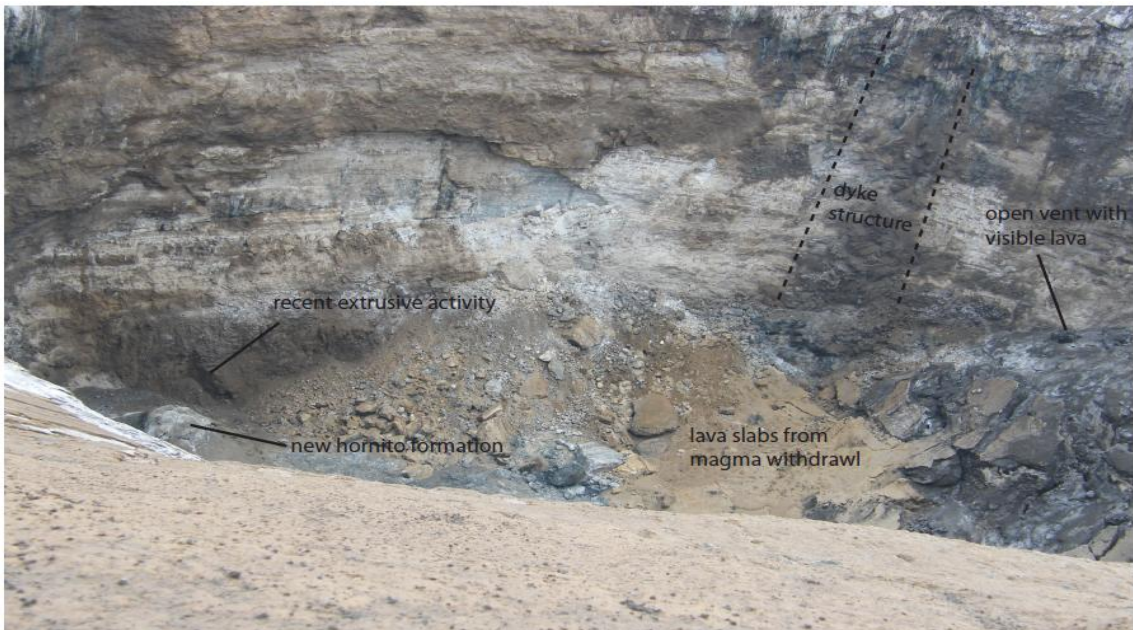

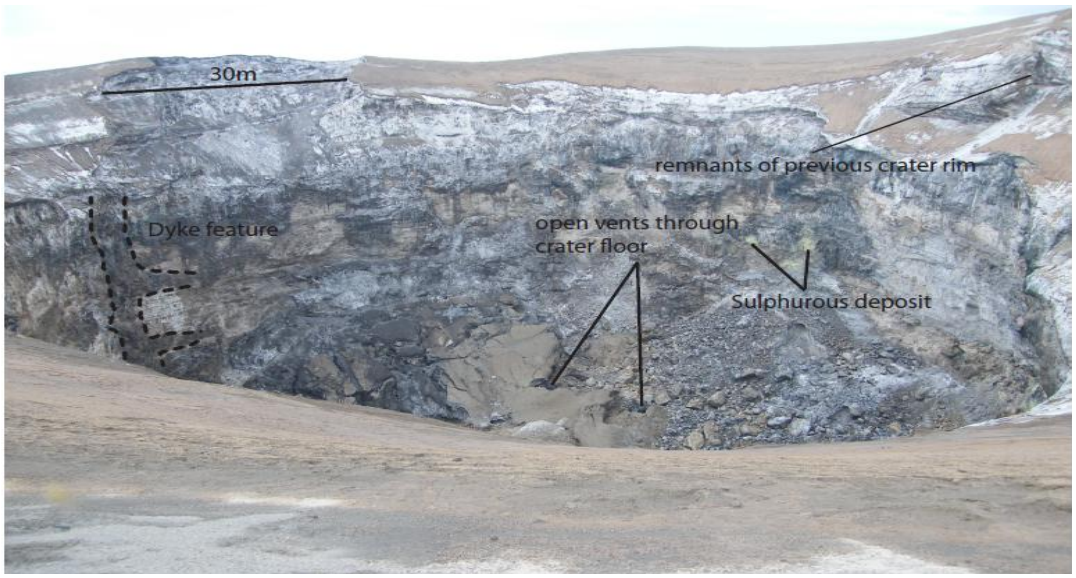

Figure 3.4: (a) Rim – to – rim view of the northern crater taken looking approximately East - West; (b) downward view into the crater from the western edge of crater rim.

The upper slopes of Oldoinyo Lengai are partly covered with indurated white- grey volcanic ash (2007), recently flushed with water from seasonal rains (Figure 3.5a). On the middle to lower slopes, the same white crust can be found on radial topographic highs. This indurated material breaks under foot to reveal dark water-saturated ash. The flanks vary in slope from 45 - 55° beyond the half way point and much of the recent ash had been removed, along deeply incised water-runoff gullies. A white effervescence of carbonate (Figure 3.5b), <1 mm in thickness, covers much of the upper slopes of the volcano and active erosion runoff channels extending down towards Lake Natron. This layer is thought to be the result of evaporation and crystallisation from carbonate saturated rainwater appearing similar to salt crystals.

Figure 3.5: (a) Upper slopes of Oldoinyo Lengai with large rock structures locally known as the "Pearly Gates". The photograph shows white covering of slopes representing weathered volcanic ash from the latest eruption; (b) close up of the carbonate effervescence present on the surfaces of the rain gullies on the upper slopes of the volcano. *Photo courtesy of Matt Genge.*

3.1.2 Estimation of solid carbonatite flux

By using the measurements of the crater, it is possible to estimate the volume of the crater itself. Previous estimates have been based on the crater being a nearly cylindrical shape (Nyamweru, 1990), which provides an upper limit to the crater volume. A lower limit for the volume can be estimated by approximating the crater to that of a cone. The drawback of this is that the cone top must be circular and so an average of the two distances must be used.

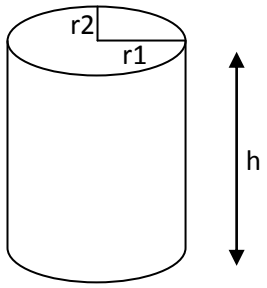

Volume of Cylinder (elliptical base):

$= \pi * r1 * r2 * h$

$= \pi * 144.475 * 131.215 * 172$

$= 1.02 \times 10^7 m^3$

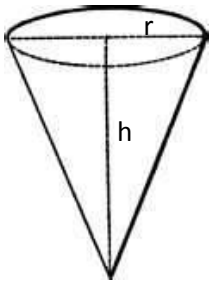

Volume of Cone:

$= 1/3 \pi r^2 * h$

$=1/3 \pi * (137.845)^2 * 172$

$= 3.42 \times 10^6 m^3$

If it is assumed that explosive eruptions, which excavate the crater, occur approximately every 40 years, a crude estimate for the average carbonate flux can be determined using the above calculated volumes;

Cylindrical - $1.02 \times 10^7 m^3$ / 40 years = 2.55×10^5 m^3/yr

Cone - $3.42 \times 10^6 m^3$ / 40 years = 8.55×10^4 m^3/yr

In the years before the explosive eruption of 2007, the crater overflowed with natrocarbonatite flows extending down the flanks from numerous sites. The breach of the crater rim on the north-western and eastern sides is thought to have occurred during extensive activity in 1998. The northern edge was topped in 2005 and the western rim in 2006. The volume of lava that has extended down the flanks of the volcano is not well documented

and so places an uncertainty on the carbonate flux from Oldoinyo Lengai. For example, observations of the 2006 flow suggest that 1.7 X 10^6 m^3 of natrocarbonatite material could have been emplaced on the slope (Kervyn et al., 2008b). Estimates of the volume of large lava flows, which have occurred on Oldoinyo Lengai in the last 25 years, are comparable to this flow rate. The Chaos Crag and Southern flow, which were emplaced in 1993, were documented to have a volume between of 0.15 X 10^7 m^3 and 1.3 X 10^7 m^3 (Dawson et al., 1994a, Venzke et al., 2002-). Dawson et al (1994) suggest that the flows were emplaced within 336 hours (~14 days) after almost 17 years of dormancy, showing that the crater filling occurs in sporadic events rather than as a continuous outpouring. The driving force of such large lava flows is little understood.

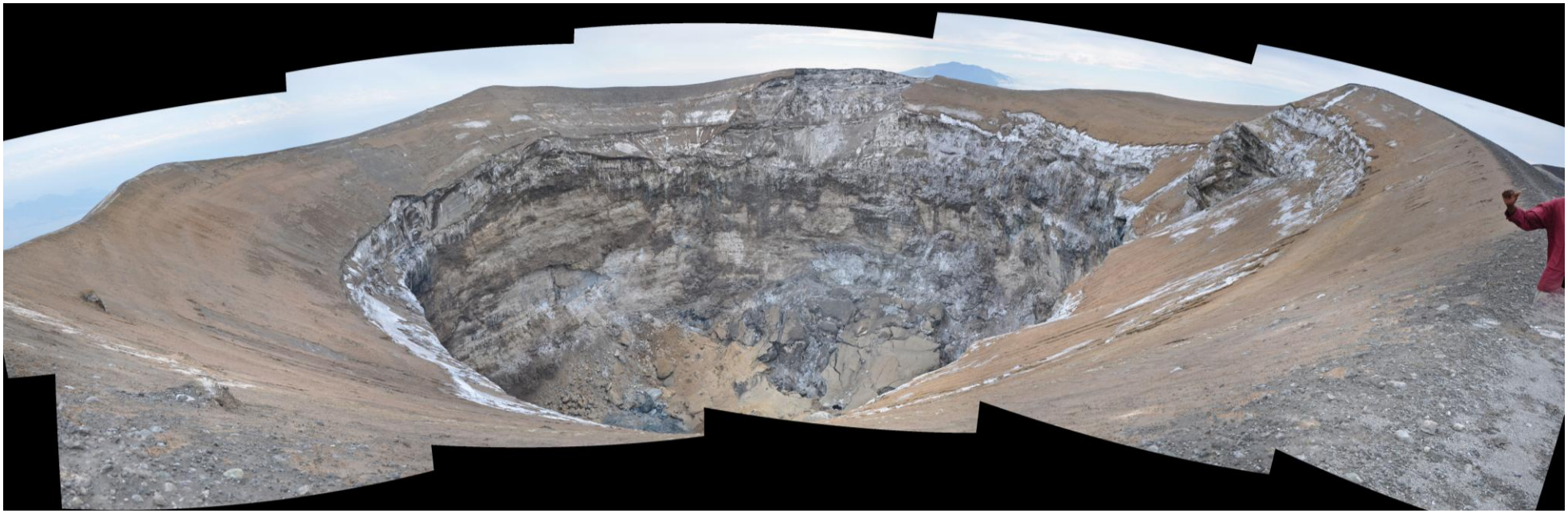

Figure 3.6: Stitched panoramic view of northern crater showing near vertical walls and steep upper slopes covered with lapilli ash from the 2007 eruption. The crater floor also shows collapse from the upper slopes and subsidence of the crater floor (brown slabs of rock). Remnants of the previous crater rim can be seen on the southern edge of the crater. Looking ~280° with Gelai peak just visible in the background.

3.1.3 Observations of 2006 Lava flow on the Western Flank

In the years before the 2007 explosion, Oldoinyo Lengai's activity was effusive and resulted in the production of two approximately 3 km long lava flow down the western flank of the volcano. According to local reports the flow was emplaced in less than 14 hours. At this time the northern crater was completely full with carbonatite material due to the outpouring of the central hornito. Small flows had already topped the crater rim to the north, northwest and east, but had extended no more than a few tens of metres down the flanks before cooling. The new lava flow on the western flank varies from rubbly pahoehoe to aa-like lava (Figure 3.7b). The central part of the flow (up to 15 m thick) is predominantly blocky lava with patches of pahoehoe lava, whilst towards the flow front (~2 m thick) the lava is predominantly pahoehoe with ropey textures within channels up to 15 cm in width. Previous estimates of the flow volume are in the range of 9.2 (±3.0)×10^5 m^3 (Vaughan et al., 2008, Kervyn et al., 2008c), yielding a mean effusive flow rate of 20 m^3s^{-1} or less. Over the 4 years since emplacement, exposure to the atmosphere has caused secondary alteration and turned the previously black-grey lava flow to white, so that it stands out against the upper grey slopes of the volcano (Figure 3.7a).

Figure 3.7: (a) Upslope view of 2006 lava flow showing contrast in colours between white altered natrocarbonatite and indurated slopes of Lengai of mixed carbonatite / silicate material; (b) Vertical section along eastern side of lava flow. Tape measure represents 5 m. *Photos courtesy of Adrian Jones.*

Alteration is restricted to the outer, exposed regions of the flow generating a white carapace a few centimetres thick. The carapace covers a brecciated flow top, as well as a basal breccia (Figure 3.8a). Just above this basal breccias are small (0.5 – 2 cm thick) layered flows of a browner coloured carbonate material (Figure 3.8c). These flows have distinct boundaries and appear to have been emplaced before the main flow. They may represent previous flows which are at a more advanced stage of alteration due to their colouration. The blocky type lava often contains pressure ridges and tumuli (Figure 3.8b), the largest of which is around 5 m tall (Mattsson and Vuorinen, 2009). The tumuli are generated by lava accumulating beneath a stronger crust and pushing the crust upward (Duncan et al., 2004, Guest et al., 1984). Mattson and Vuorinen (2009) indicate that two important conditions must be satisfied in order to generate these inflation features: firstly there must be a lateral barrier which prevents the flow from getting any wider and secondly there has to be a continual influx of material beneath the crust of the lava flow.

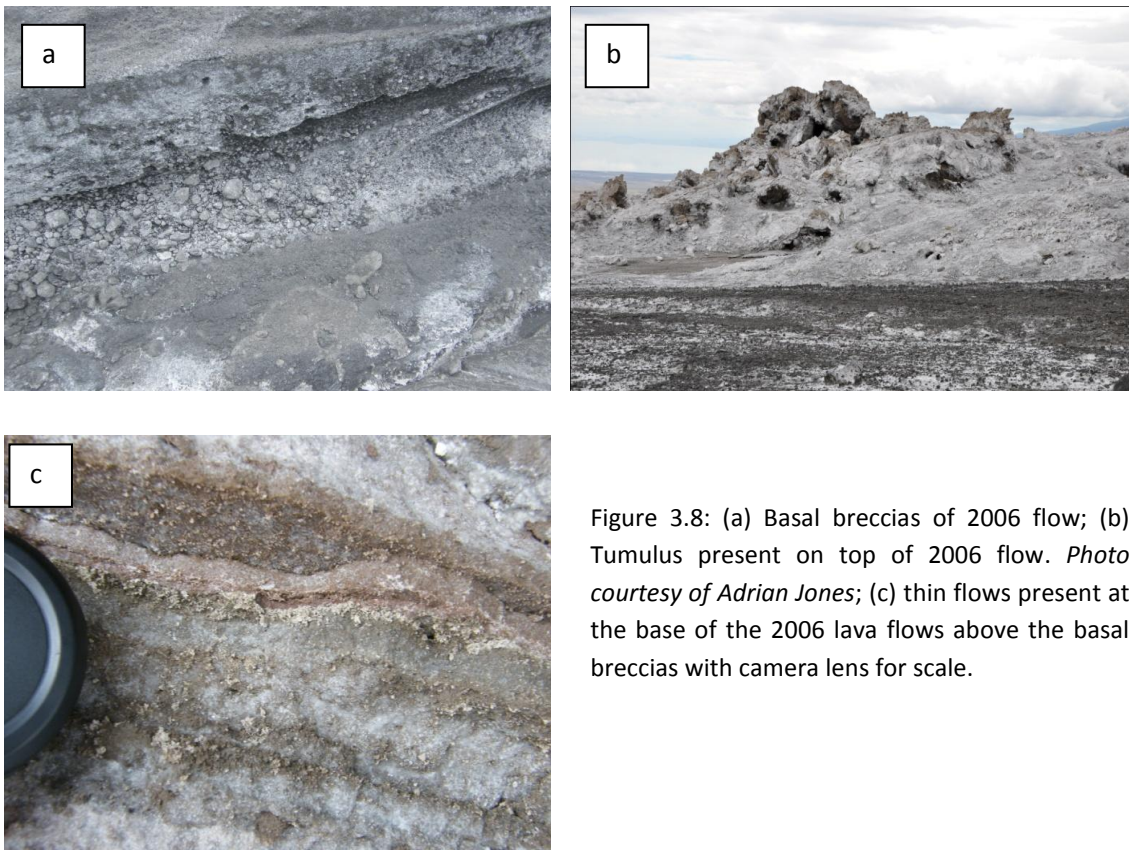

Figure 3.8: (a) Basal breccias of 2006 flow; (b) Tumulus present on top of 2006 flow. *Photo courtesy of Adrian Jones*; (c) thin flows present at the base of the 2006 lava flows above the basal breccias with camera lens for scale.

The interior of the main lava flow still appears fresh and maintains a predominantly black colour with some regions appear to have a brown colouration possibly due to localised weathering or a slightly different chemistry. The fresh natrocarbonatite is porphyritic with visible phenocrysts of nyerereite and gregoryite. Numerous xenoliths and volcanic bombs can be found within and on top of the lava flow. The clasts entrained within the flow are most likely to have been incorporated during its descent down the flanks of the volcano, whilst the xenoliths resting on the surface are volcanic bombs produced by subsequent explosive activity. The xenoliths and bombs vary in size from 5cm to 75cm but do not appear to have any chilled or baked margins.

Stalactites similar to those found on the crater walls, mentioned above, also extend from the underside of the 2006 lava flow (Figure 3.9a). They have maximum lengths of ~7 cm, and were seen with water droplets forming at their tips. The stalactites effervesce with the application of 10% HCl, indicating a carbonate mineralogy. Although the majority occur as vertical features, closer examination of the lava surface reveals horizontal tube-like structures formed of the same material (Figure 3.9b).

Figure 3.9: (a) Small stalactites hanging from lower surface of 2006 lava flow; (b) secondary alteration of lava flow generating horizontal tubes of material similar to that of the stalactites. GPS location 02°44.89S, 35°53.26E

The horizontal orientation may be due to wind blowing surface water down slope. Toward the side of the lava flow is an excavated gully, which runs parallel to the lava flow, most likely caused by rainwater and so winds are likely to be channelled along this gully. The insides of these stalactites, at their base, show sub-circular growth patterns with pore spaces, consistent with the addition, over time, of layers over an initial drop. Similar features were found inside the base of an inactive hornito before the explosive eruption and are argued to the be the result of precipitation from an alkaline brine generated by weathering of natrocarbonatite (Mitchell, 2006b, McFarlane et al., 2004). During weathering, highly soluble elements such as Na, K, Cl and F are concentrated in meteoric water, which then percolates through the lava at the roof of the hornito and precipitates minerals via evaporation. However, percolation through the lava body may not have been required to form the stalactites on the 2006 lava flow. In this case, it appears as though the meteoric water may simply flow over the surface and once it reaches the edge start to drip off and form the stalactites.

3.1.4 Interpretation of 2006 lava flow

The effusive activity in March – April 2006 is thought to represent the largest outpouring of natrocarbonatite in the historical record of Oldoinyo Lengai, even larger than that of the Chaos Crag flow in 1993. Nevertheless, similarities can be drawn between the events: both emplaced large volumes of crystal-rich, natrocarbonatite in short periods of time and were associated with contemporaneous or slightly delayed explosive activity. The 1993 event has been interpreted as an influx of silicate material into a magma chamber which was already crystallising nyerereite and gregoryite as a crystal mush, with residual aphyric natrocarbonatite

(Dawson et al., 1994a, Church, 1995). The addition of silicate lava, which was exsolving carbonate during its ascent, provided the driving force and additional material to generate a large lava flow (Dawson et al., 1994a).

Effusive behaviour is occasionally produced when the flank collapse of the hornito allows the escape of lava with elevated SiO_2 and crystal content. This was thought to be the case during the 1993 eruption and the 2006-07 eruptions (Kervyn, Ernst et al. 2008 and references therein). In 2006-07, the western flank lava flow, was emplaced in only 14 days at eruption rates of 3 – 12 m^3s^{-1} , which appear to be typical drainage of a shallow magma reservoir following hornito collapse. Kervyn et al (2008) interpret the 2006-07 flow to have resulted from the collapse of two central hornitos, forming a caldera-like pit crater and rapid drainage of the underlying lava lake. Petrographic analysis revealed a typical natrocarbonatite composition of nyerereite and gregoryite phenocrysts within a matrix of sylvite, nyerereite, gregoryite, fluorite and opaques. However the material also contained 3 – 7 vol% silicate spheroids, consisting of nepheline and pyroxene with minor Ti-andradite and wollastonite.

The 2006 effusion descended down the slope as two separate flows (Dawson, 2010, Mattsson and Vuorinen, 2009) with morphologies different from those normally seen for small volume breakouts (Mattsson and Vuorinen, 2009). In particular, MODIS thermal data show that the first flow descended the flank of Lengai on 25th March and the second on the 3rd April (Kervyn et al., 2008b). The driving force and mode of emplacement of such large flows are an important consideration for understanding the evolution of Oldoinyo Lengai and the magmatic processes beneath the summit crater. Mattsson and Vuorinen (2009) concluded that the flows were emplaced by overflowing the crater wall on the western rim and extending down the flank eroding a channel within which to flow, approximately 2.5 m deep and 5 m wide. The position of this channel is argued by Mattsson and Vuorinen (2009) to have been dictated by a pre-existing gully on the flank of the volcano. Pressure ridges and tumuli did not start to form until the flow reached the lower slopes of Lengai where the gradient is shallower and lateral barriers could develop.

Older lava flows contained solely within the crater, prior to all episodes of historical explosive activity, have been observed to issue from small hornitos and spatter vents or within small, open lava lakes (Keller and Krafft, 1990). In 1988 Keller and Krafft (1990) observed at least three crater lava lakes which were highly fluid and described as “vigorously boiling”. Periodically these lakes were observed to fill and overflow to feed lava flows up to 100 – 200m long and thought to be the result of a sudden upwelling of gas-rich, hotter lava. The authors

estimated each excursion of lava from these lakes to produce around 1000 m^3. Previous eruption rates of material produced by hornito collapse and drainage of a shallow reservoir have been estimated at 5 – 10 m^3 s^{-1} (Kervyn et al., 2008b) which are comparable to the estimate of eruption rates of the 2006 flows (3 – 12 m^3 s^{-1}) by the same authors. For this reason Kervyn et al (2008) argue that the western flank flow was the result of drainage of a shallow magma reservoir brought on by the collapse of hornitos due to destabilisation caused by an initial magma withdrawal. It is plausible that this initial magma withdrawal may have been the result of an influx of silicate material similar to that of the Chaos Crags. For this model to work it requires all of the hornitos to be interconnected to some larger magma reservoir located near the surface which can empty upon disturbance. A complete drainage of this shallow magma reservoir may explain the time required to refill the reservoir before activity can start again.

3.2 Field observations of hummocks

An important morphological feature found within the Gregory Rift on the flanks and surrounding plains of Oldoinyo Lengai and Kerimasi are large hummocks of debris material, which have previously been interpreted as Debris Avalanche Deposits (DADs) (Kervyn et al., 2008a).

Figure 3.10: Debris deposits (hummocks) located on the plains between Oldoinyo Lengai and Lake Natron. Photograph taken looking SE with Oldoinyo Lengai off to the right hand side of the photo. *Photograph courtesy of Adrian Jones.*

Previous work, outlined in chapter 1, concludes that the avalanches were provided by sector collapses of volcanic cones. The formation of the deposits is an important part of understanding the evolution and growth of the volcanic complex as well as the rift valley itself, particularly in terms of palaeoshores of Lake Natron. The following section outlines the features of the hummocks present on the current southern shore of Lake Natron.

As shown by the sketch map in Figure 1.5, the hummocks extend to the north and east from Oldoinyo Lengai. Some of the avalanches have run out distances over 20 km and are now located within the present southern shoreline of Lake Natron. Kervyn et al (2008) suggest that the debris material fanning out to the east of the volcano (referred to as the Cheetah DAD) is the result of a deep, v-shaped incision on the eastern slope of Oldoinyo Lengai, known as the Eastern Chasm. This collapse scar is shown in Figures 3.11a and b. The close up image of the scar shows the inner volcanic complex with layering of silicate and minor carbonatite material. The carbonatitic material occurs only in the top 10% of the volcano, owing to dissolution during weathering. Figure 3.11a clearly shows the feeding point and fan of material, which extends from the central region of the scar towards the plains.

Figure 3.11: (a) View of Eastern Chasm on Oldoinyo Lengai from the Serengeti road looking West; (b) Close up of the collapse scar with visible volcanic layers and black ash from recent eruption.

The hummocks themselves vary in size with the larger outcrops up to 200 m long, 10 m wide and 5 m high, whilst smaller outcrops are <20 m in length and 2 m in width or height. The hummocks show variation in size, mixing and lithology with distance from the source, which could be a result of mechanical sorting during transportation. The hummock at Location 10 was studied in depth and is located approximately 6 km northeast of the lower flanks of Oldoinyo Lengai. This hummock is around 20 m in length and 4 m in height (Figure 3.12). It is mainly clast-supported with clasts of nephelinite and wollastonite nephelinite ranging from ~3 cm to 1.5 m across, within a matrix of pulverised rock that contains remnant crystal fragments of nepheline and pyroxene. The larger clasts are more angular in shape and brecciated in a "jigsaw fit" fashion, whilst the smaller clasts are more rounded, but there is no apparent sorting of the deposits indicating turbulent movement and deposition, which can be characteristic of debris avalanche deposits (Siebert, 1984a). However, later work on landslides by Kilburn (2007) indicates that "jigsaw fit" blocks are not representative of turbulent flow, but merely signify the avalanche material was disaggregating during emplacement. The overall yellow appearance of the hummock and composition of the material is similar to that of the older, palagonitized units of Oldoinyo Lengai (Dawson, 1962a).

Figure 3.12: Small hummock on the flanks of Oldoinyo Lengai. *Photo courtesy of Adrian Jones*

Moving further away from Oldoinyo Lengai, the hummocks become more matrix-supported, with a coarse grained, welded matrix supporting sub-rounded blocks around 30 cm across. The matrix also contains some carbonate (which effervesces upon application of dilute hydrochloric acid). The large hummock on the shoreline of Natron seems to have crude layering of different flow units (Figure 3.13a): a lower grey-coloured unit containing polymict clasts of nephelinite, trachyte, phonolite and basement units of varying sizes, and an upper yellow unit with monogenetic clasts of phonolite, with large nepheline crystals up to 2cm across. The matrix is preferentially weathered in both layers resulting in the prominence of clasts. Composite bombs can also be found within the deposit, which appear to be formed of jacupirangite, urtite and nephelinite with fined grained, chilled margins. Location 14 represents a site on the deposit where a large, consolidated block of porphyritic lava has moved en masse towards the lakeshore, incorporating sediment into a wedge beneath the slab (Figure 3.13b). The observation of discrete flowing units or layers within the hummocks again counter the interpretation of turbulent flow, which requires the mixing of units from different levels (Kilburn, 2007).

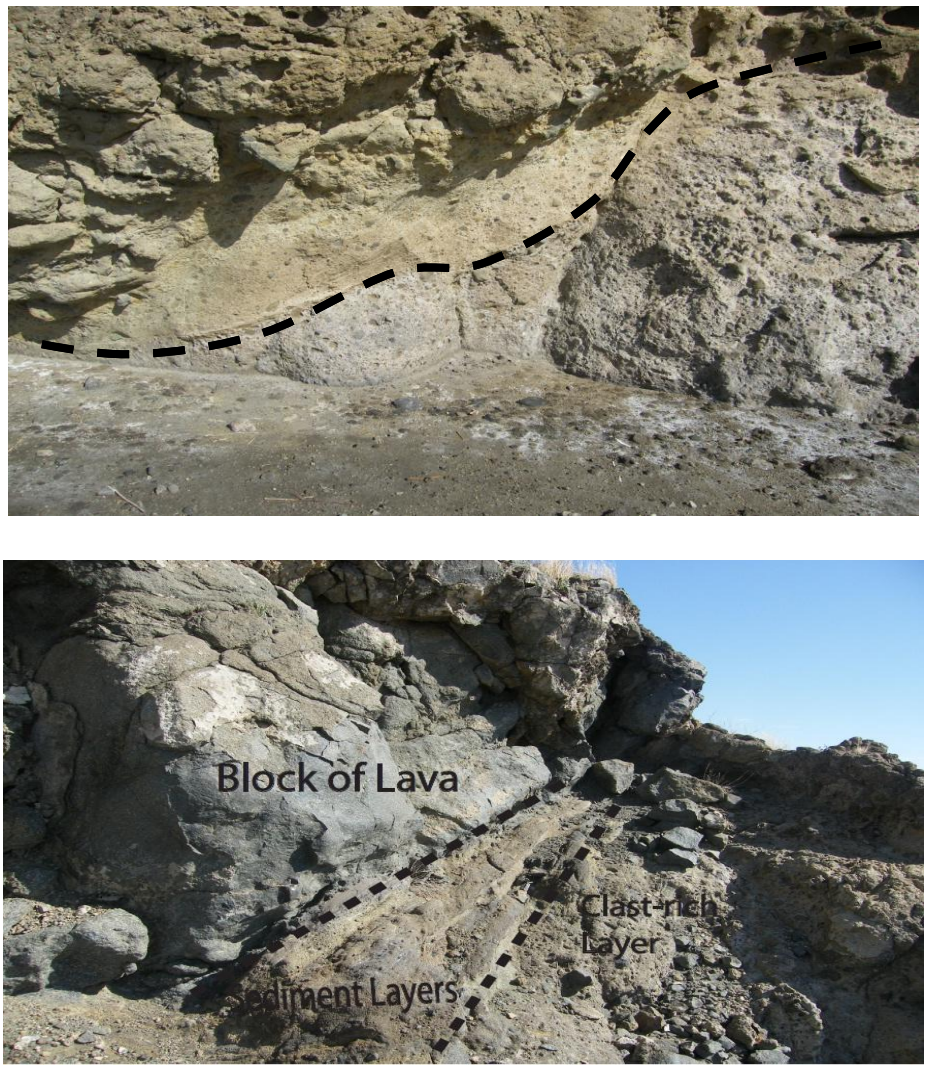

Figure 3.13: (a) Large hummock on shoreline of Lake Natron with apparent ramped flows discernible by colour; (b) Large slab of porphyritic lava with accumulated sediment. *Scale: 70cm at thickest end of sediment wedge*

The contact between the block of lava and sediment is undulate and discordant with a thin baked margin. The sediment wedge then grades into the grey clast - rich unit previously seen within the hummock. This grey unit could represent pyroclastic material previously deposited from explosive eruptions that have then been entrained by the debris avalanche flow. On the westward side of the hummock soft sediment deformation can be seen with folding of the yellow unit generating an east - west axial plane, suggesting a transport direction of north – south (Figure 3.14a). The sense of motion is also indicated by the presence of parallel laminations within the matrix of the hummocks, similar to those of shear planes (Figure 3.14b).

Figure 3.14: (a) Soft sediment deformation within one flow unit of the debris deposit; (b) Parallel laminations along shear planes

3.2.1 Volcanic activity during collapse

An interesting feature of the hummocks is that they do not appear to contain blocks of trona, a mineral readily precipitated from Lake Natron due to its alkaline chemistry, which in turn is thought to relate to the activity of Oldoinyo Lengai. A complex hydrothermal circulation system is thought to exist connecting the lake to the surrounding waters running off of Lengai. The water-soluble nature of the natrocarbonatite results in hydrothermal fluids saturated with alkalis (up to 30 X 10^3 ppm of dissolved solid sodium carbonate (Hillaire-Marcel et al., 1986, Hillaire-Marcel and Casanova, 1987)), which are introduced to the lake via hot springs found at numerous sites around the lake (Warren, 2006). The lack of trona within the debris deposits within the trapped sediment wedges suggests that the large, first sector collapse of Oldoinyo Lengai, from which the hummocks on the shoreline of Natron are thought to have originated, occurred during a time when the lake was not as alkaline as at present. The direct relation between the lake chemistry and the volcano's chemistry would thus further suggest that

Oldoinyo Lengai may not have been producing natrocarbonatite during the early stages of its growth and so the production of carbonatite is an evolutionary step rather than a consistent feature of this volcano. The presence of stromatolites at the distal end of some hummocks, as previously reported by Hillaire-Marcel et al (1987), Hillaire-Marcel and Casanova (1986) and Kervyn et al (2008) indicates that the lake level during this collapse would have been higher than present levels. A high stand is dated at ~10,000 years BP and so the debris deposits would have flowed into the lacustrine environment.

One of the most interesting consequences of the Zebra sector collapse, which occurred at Oldoinyo Lengai during its early stage of formation, is to cause the site of active lava production to shift from the southern crater to the now active northern crater. It is possible that the removal of a large percentage of material from the volcanic cone resulted in a change in the stress regime above the shallow magma chamber and ultimately caused the volcanic conduit to be moved northward. Migration of conduits has been documented at Las Cañadas caldera, in Tenerife, where overlapping calderas are thought to be the result of magma chamber migration due to the vertical collapse of a shallow chamber (Marti and Gudmundsson, 2000).

In a rifting regime, the principal stresses are oriented with a vertical maximum principal stress (σ_1) and horizontal minimum principal stress (σ_3). This allows horizontal extension which, in a volcanic situation, favours the propagation of dykes that open in the direction of σ_3. Gudmunsson (2000) argues that, after collapse of a volcanic edifice the maximum or intermediate principal stress can become horizontal due to a change in the overburden. Fractures can now not open laterally and so dyke formation is often arrested at depth. This results in fault propagation towards the region of higher overburden where the stress regime is under “normal”, pre-collapse conditions and results in the generation of a new magma chamber to the side of the previous, ultimately resulting in a movement of the conduit. A large time lag would occur between the collapse of the flank of the volcano and the onset of new volcanic activity as the conduit must be re-established.

3.3 Field observations of Kerimasi units

Kerimasi is an extinct volcano which lies approximately 12 km southeast of Oldoinyo Lengai and is thought to have been an earlier twin of Lengai, because both are comprised of nephelinitic and carbonatitic material. Kerimasi’s formation post-dates the Natron Basin

boundary fault. Its early activity was located close to the fault, building an edifice up alongside the escarpment, which it eventually overtopped and so the fault section is now buried beneath Kerimasi. The core of the volcano is formed of nephelinitic tuffs and agglomerates which are overlain by calcium carbonatite tuffs and agglomerates thought to represent the final activity of the volcano (Dawson, 2008, Church, 1995).

During the field campaign observations of the carbonatite material of Kerimasi were made in two locations: a gully section located between Kerimasi and Oldoinyo Lengai on the north-eastern slopes of Kerimasi and a ridge on the eastern flank of the volcano. The gully on the north-eastern slope cuts through the upper carbonatite carapace of Kerimasi consisting of a lower silicate agglomerate, approximately 1m thick with a pink colouration containing large clasts of alkaline units including ijolite, nepheline syenite, nephelinite and pyroxenite up to 20cm across (Figure 3.15a). Previous studies of similar units located on Kerimasi by Dawson (2008) also note the presence of more exotic clasts of amphibole meltiegite, melanite meltiegite, mica pyroxenite, urtite and uncompaghrite.

Figure 3.15: (a) ijolite clast within basal agglomerate; (b) accretionary lapilli tuff, clast supported with cored lapilli and proto lapilli in same formation. *Photos courtesy of Adrian Jones*

The agglomerate unit is overlain by a tapered, lenticular unit of welded calcium carbonate lapilli tuff approximately 8m thick at the centre and ~1 m at the edges with a complex stratigraphy. The base of the tuff is diffusively stratified with horizons rich in fine material intercalated with units of matrix-supported lapilli tuff. The lapilli vary in size from 0.5 cm to 2 cm and represent up to 35% of each stratification. The majority of the lapilli are sub-rounded to oblate and appear to have a fine-grained ash core lacking internal structure or to be proto-lapilli lacking any laminations.

Above this lies a massive clast supported accretionary lapilli tuff layer. Within this layer around 10% of the accretionary lapilli have mafic lithic cores and so are classified as cored accretionary lapilli (Brown et al., 2010). The unit shows little-to-no sub-parallel stratification and the lapilli constitute up to 65% of the unit. The lapilli can range in size from 0.5 cm to 5 cm and are sub-rounded in shape (Figure 3.15b). In some regions of this deposit there are indications of normal grading. Towards the tapered edge of the section are lenticular bodies of clast supported agglomerates with up to 80% clasts.

The welded tuff is capped by an ash aggregate layer typical of ash fallout. This unit (dark grey, draping lithology in Figure 3.16a) is approximately 2 – 2.5 m in thickness with well developed laminations, showing little variation along the length of the section and is comprised of clast-supported coated ash pellets, cored pellets and lastly ash pellets (normal grading visible from base to upper surface).

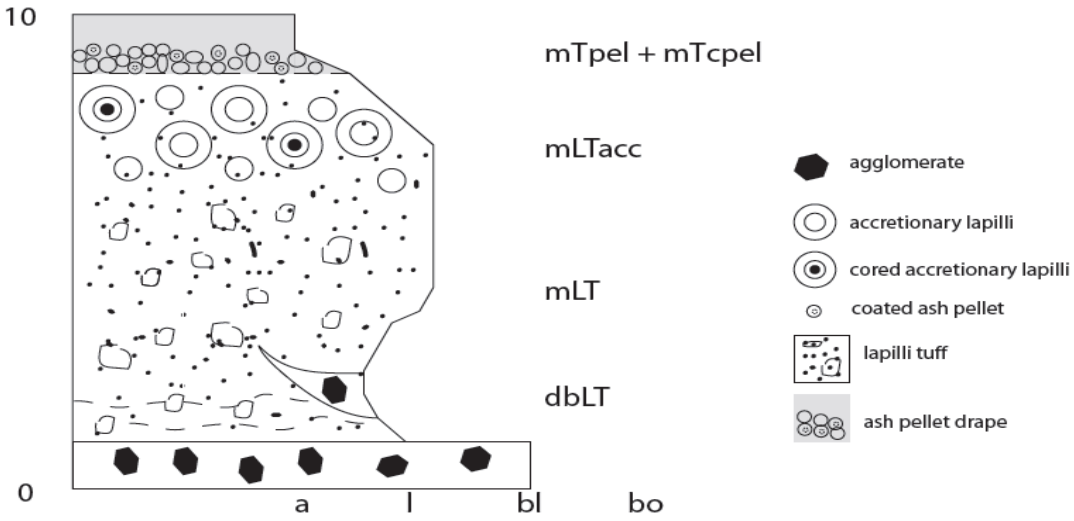

Figure 3.16: (a) Overview of tuff deposit located in gully between Kerimasi and Oldoinyo Lengai; (b) simplified stratigraphic log of tuff deposit; LT = lapilli tuff, Tacc = accretionary lapilli tuff, db = diffusively bedded, m = massive, pel = ash pellet, cpel = cored pellet, a = ash, l= lapilli, bl = block, bo=boulder *Photograph courtesy of Adrian Jones*

3.3.1 Interpretation of lapilli unit

At first glance the morphology of this deposit is typical of pyroclastic density current deposits. The pink coloured basal, unsorted agglomerates at this location represent either the initial stages of a pyroclastic flow after the initial basal surge deposits, which are not visible at this outcrop, or ballistic air fall deposits from the initial eruption column prior to the collapse and generation of the density current. The intermingling of both proto-lapilli and well developed accretionary lapilli could indicate that two different sources of material fed the same deposit. Ash aggregates and lapilli are common in deposits from both air fall and pyroclastic density currents. Accretionary lapilli, however, are thought to only form in turbulent regions from pellets or lithic fragments which are too large to be sustained within the rising plume (this could be the umbrella cloud of an explosive eruption or the lofted ash cloud of a density current) and so descend into the density current where ash accretes to the surfaces (Brown et al., 2010, Gilbert and Lane, 1994). It is therefore possible that during an explosive eruption the air fall deposit and a density current were depositing material in the same region which due to the heat of the density current becomes welded into one tuff unit. The ash fallout drape which caps the entire deposit records waning of the plume after the cessation of the pyroclastic density current and so normal grading occurs as successively smaller particles fall out of suspension.

3.4 Field observations of explosion craters and tuff cones

The younger volcanoes of the Tanzanian section of the East African Rift are typically highly explosive as can be witnessed with recent activity at Oldoinyo Lengai. This is also evident from the presence of minor volcanic features of explosion craters and tuff cones found within the Natron Basin on the plains between Kerimasi, Lengai and Gelai. The following section describes the morphology and petrology of some of these features from field observations.

3.4.1 Loolmurwak explosion crater

Loolmurwak explosion crater is a dry maar approximately circular in shape with a diameter of 915 m and a small tuff cone located at the southern edge. The southern wall of the crater contains a fault causing an estimated maximum offset of 30 m to the west. The orientation of this fault is similar to that of the larger scale faulting of the rift section and so are synthetic – antithetic faults. The outer slopes of the crater are gentle with an angle of no more than 20°, whilst the inner walls are near vertical and expose the strata through which the crater exploded (fig 3.18), argued to be Kerimasi pyroclastic material from previous work (Dawson and Powell, 1969). This material consists of fragmented urtite-meltiegite - ijolite tuff material which is cemented by calcite and occupies the lower stratigraphy of the crater. The upper 50 m of the crater walls are draped with a more mafic-rich ejecta material (visible in Figure 3.17a), the uppermost 5 m of which is a hydrated, palagonatised yellow tuff that contains abundant crystals of mica, pyroxene and olivine. The mica crystals occur as books up to 6 cm across and 2.5 cm in thickness whilst the pyroxenes are well formed crystals often appearing glassy (Figure 3.17b). The upper unit of Loolmurwak also contains numerous blocks of plutonic rocks; olivine – mica pyroxenite and mica pyroxenites. Dawson and Powell (1969) discuss the origin of these pyroxenites concluding that they are not consistent with the petrology of Kerimasi and so do not represent xenoliths entrained from Kerimasi material and ejected during the explosion which formed the craters. The authors also argue that these rocks do not represent metasomatic lithologies from the interaction of neighbouring carbonatite magmas.

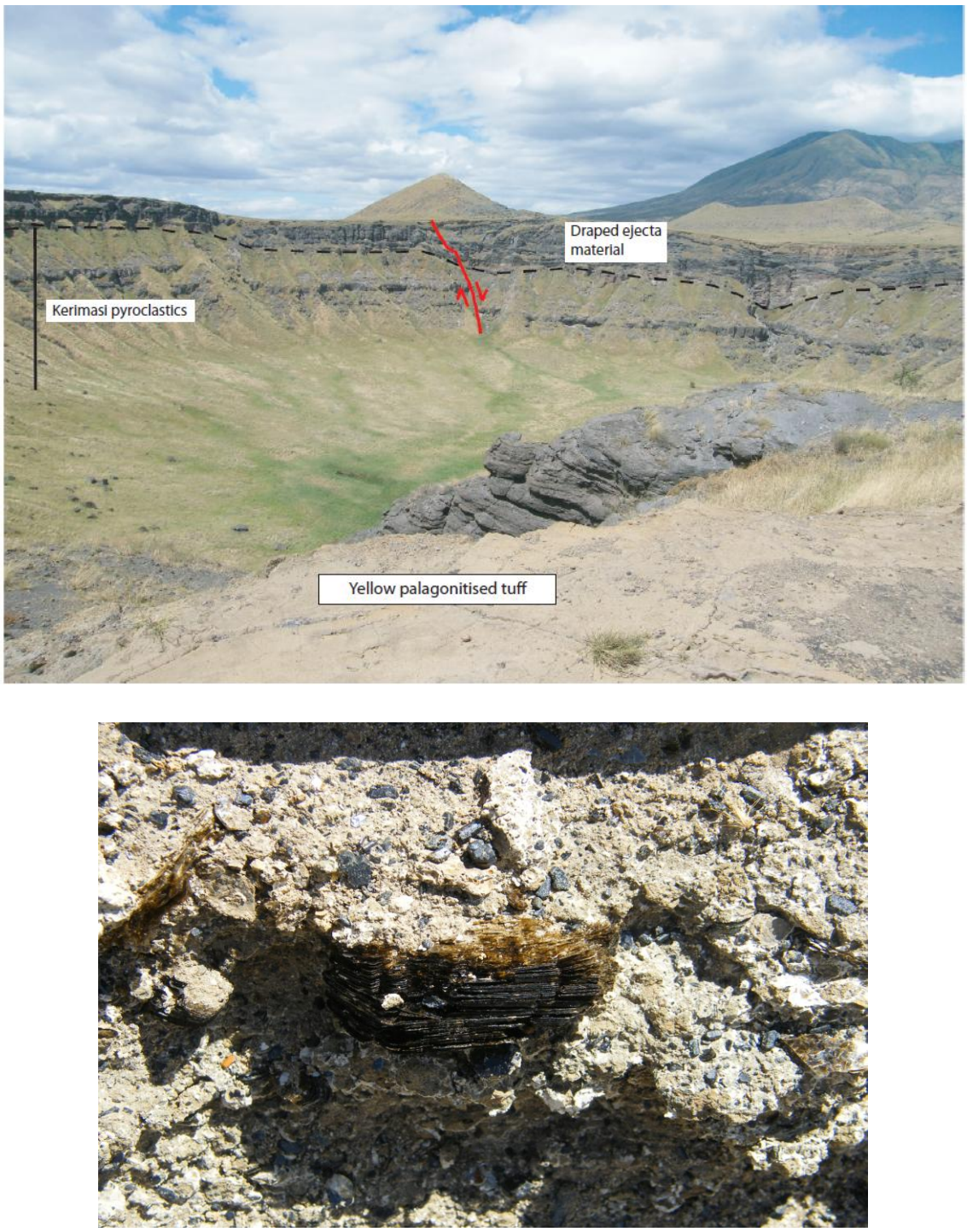

Figure 3.17: (a) Annotated photograph of Loolmurwak explosion crater with Kerimasi pyroclastics and upper ash drape / palagonitized unit. Back wall fault indicated in red, (b) close up of palagonitized unit of Loolmurwak with large mica book (6cm across) and pyroxene in matrix of hydrated carbonate cemented ash.

One key observation is that the draped material topping the explosion craters in this region is similar to that of the ash drape observed at the lapilli tuff outcrop within the gully between Kerimasi and Oldoinyo Lengai. Two explanations for the similarity are plausible. First the

explosion craters erupt on the slopes of Kerimasi display pyroclastic material in their vertical inner walls, so that the draped ejecta may represent material similar to the rock type through which the crater formed. Second, the eruption that produced the lapilli tuff deposit may have been sufficiently large to spread fine material (e.g. from a pyroclastic density current) around Kerimasi and so the ash drapes were formed in one single event. Which of these scenarios is correct has implications for the age of the craters in relation to that of Kerimasi and Lengai. If the first is correct, Loolmurwak and other explosion craters appear to have formed after the main explosive events of Kerimasi. However, if the second explanation is correct, then Kerimasi must still have been active during the formation of Loolmurwak. The presence of the yellow palagonitized unit at Loolmurwak provides a constraint since this unit is typical of the early volcanic sequence associated with Oldoinyo Lengai (Dawson, 1962a, Dawson, 2008). However yellow palagonitized units are also a common feature of hydrovolcanic features due to the alteration of magmatic glass to iron oxides and smectite clay.

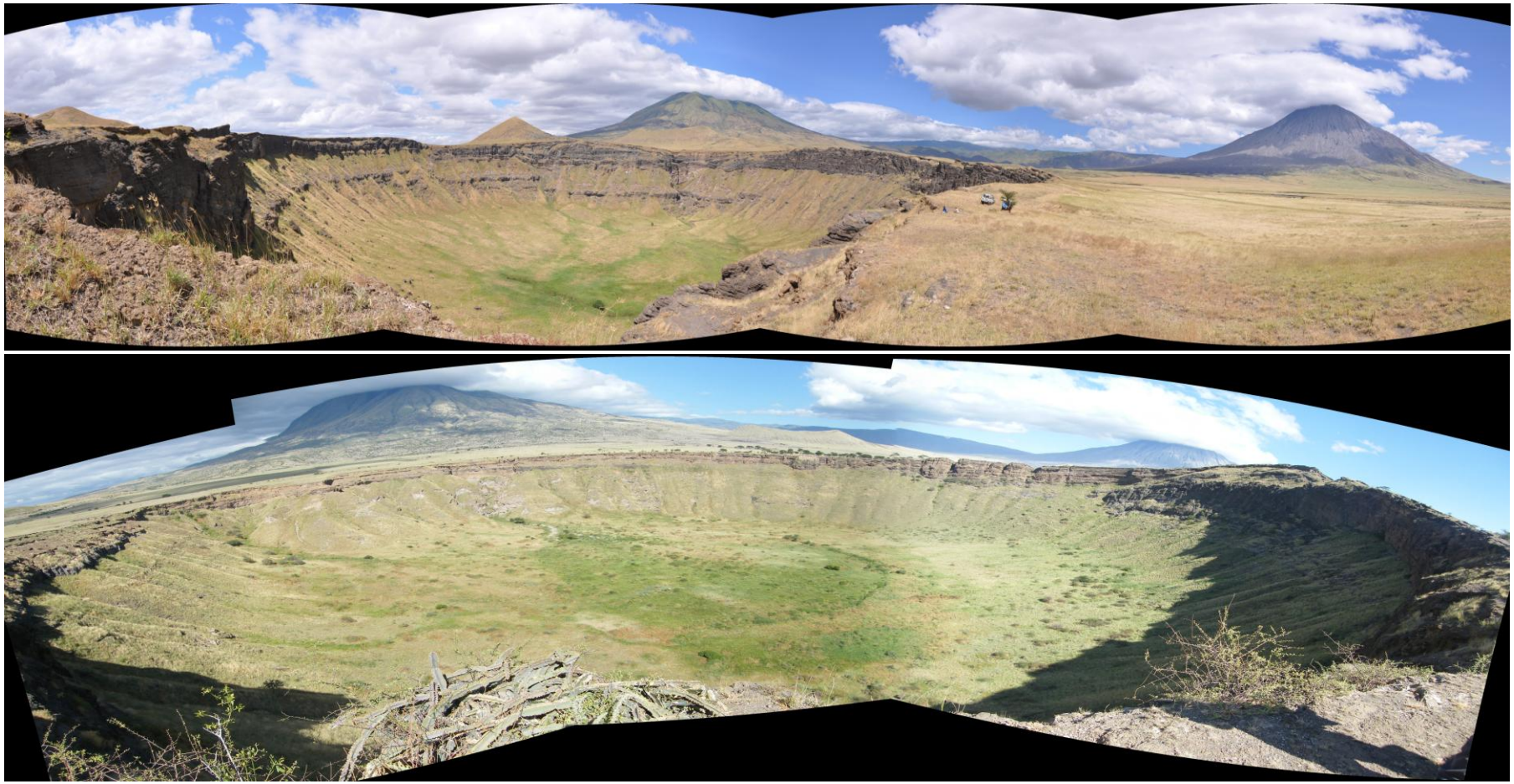

Figure 3.18: (a) Stitched panoramic of Loolmurwak explosion crater situated on the plain between Kerimasi (to the left) and Lengai (to the right), *Photograph courtesy of Adrian Jones and taken looking 250° with vehicle for scale*, (b) Panoramic of explosion crater locally named Kisetey located to the southeast of Loolmurwak, again with Kerimasi and Oldoinyo Lengai visible to the left and right respectively. *Photograph looking 267° Crater diameter ~ 600m (E-W* direction)

3.4.2 Tuff cones (Ubehebe type) – Loluni, Pello Hill and Deeti.

Ubehebe type tuff cones are those which stand above the surrounding plains with outer slopes up to 30° and more gently inclined inner slopes which lead to a bowl shaped crater. The outer slopes of the tuff cones found within the Gregory Rift are generally deeply incised by rainwater gullies generating a "ribbed" appearance (Figure 3.19).

Figure 3.19:(a) Loluni tuff cone exhibiting good parasol, "ribbed" weathering patterns and elongate morphology. Vertical height of slopes ~ 400 m. *Photograph taken looking west from Kisetey.*

During this field campaign three tuff cones were visited: Loluni located on the eastern flank of Kerimasi, Pello Hill located on the western flank of Gelai volcano and Deeti also on the eastern flank of Kerimasi. The lower slopes of Loluni tuff cone were visited to look for xenolithic material. The cone itself is primarily comprised of lapilli up to 3 cm in diameter, similar to that of Kerimasi and Loolmurwak, that contain large crystals of phlogopite and amphibole. The phlogopite crystals exist as loose mica books previously seen at other eruptive centres (up to 5 cm across) or as megacrysts within the tuff deposit itself. Deeti tuff cone also comprises of carbonate cemented, concentric lapilli and ejected bombs forming a 50 m high oval tuff cone with an eroded central crater. The megacryst suite at Deeti is formed of mica, amphibole and pyroxene. The concentric lapilli at this locality are often formed around a mica book. Previous work has suggested that the host lavas at Deeti are melilitites which are poor in olivine but rich in pyroxene (Johnson et al., 1997). This work also indicates the presence of ultramafic xenoliths at Deeti but these were not observed during this trip.

The Pello Hill tuff cone differs from both Deeti and Loluni in that it is not dominated by a lapilli tuff, but by ultramafic scoria. Pello Hill does have lapilli tuff deposits, but these are confined to

the lower sections of the cone with lapilli up to 3 mm in size showing glassy cores and cemented with carbonate material. Within the scoria, identified to be katungitic in composition (Dawson, 2008), resides a large number of xenoliths which vary in composition and can be up to 10 cm across. The most striking xenoliths are green peridotitic / pyroxenitic and cumulate blocks with visible chrome diopside pyroxene appearing apple green in colour. Around 40% of these green xenoliths contain mica-rich veins up to 5mm in width argued by this author and others (Church, 1995, Dawson and Smith, 1988) to be metasomatic alterations made to the original host unit. The veins cross cut in some regions which could be indicative of more than one metasomatic event. Pello Hill also contains a grey unknown xenolith with large phenocrysts of a red-brown and black mineral. The xenolith itself is fine grained and veined with a white mineral. It is possible this unit represents a block of the host katungite (kalsilite – leucite – olivine melilitite) with phenocrysts of melilite and olivine. Overall the xenoliths are heterogeneously distributed and constitute between 10 and 40% of the deposit.

3.4.3 Processes of formation of explosion craters and tuff cones

All of these minor volcanic features are typical formations caused by interaction between magma and water at different levels within the crust. The main factors that control the landform created during the interaction are;

1. Ratio of magma to water (typically 0.1 – 0.3 for efficient conversion of thermal energy to mechanical energy in basaltic systems (Sheridan and Wohletz, 1983))
2. Depth within the crust that the interaction takes place.

In general the closer to the surface the interaction occurs the more structurally-pronounced is the deposit generated. This is thought to be a result of a higher water-to-magma ratio, which causes the fragmentation process to be less efficient and produces water-saturated deposits that are able to build a cone with a slope steeper than the natural angle of repose at a short distance from the vent (Wohletz and Sheridan, 1983). Therefore, a maar or explosion crater such as Loolmurwak, which has very little surface expression, is the product of magma - water interaction at depth below the surface, usually attributed to magma encountering an aquifer. The resulting phreatic explosion excavates the observed crater and disperses relatively dry pyroclastics far from the vent at a low angle of deposition. Tuff cones, on the other hand, are the result of an interaction which has occurred at the surface when magma encounters a

shallow body of water to generate wet, cohesive ash that can build up steeper slopes (Sheridan and Wohletz, 1983, Wohletz and Sheridan, 1983). Thus tuff cones are associated with eruptions through standing water (such as a lake), whilst tuff rings and maars are associated with eruptions in initially dry conditions but where ground water (e.g. from an aquifer) or surface water is able to enter the vent. All the deposits contain material from pyroclastic surges dominated by lithic material, rather than juvenile material, with the presence of laminations and structures typical of laminar flow such as climbing dunes.

Field and geophysical data from maars and tuff cones in the Eifel region, Germany support the interpretation that large bodies of water at the surface prevent the formation of maars and deep diatremes and tend to result in the formation of tuff cone deposits (Lorenz, 1986). In particular Lorenz (1986) has argued that maar formation is related to a downward displacement of the hydrostatic pressure barrier which normally controls the depth at which explosive hydromagmatic eruptions can initiate. The periodic injection of groundwater as steam, in areas of limited groundwater supply, displaces this barrier downwards, allowing the root diatreme to extend to greater depths and ultimately results in a larger eruption and larger collapse features to form maars. However, if large amounts of water are available to replenish the volcanic system during the eruption the confining pressure zone is not lowered and the diatreme root does not penetrate further down than its starting depth, preventing maar formation. Conversely, in areas lacking water, maar-diatreme formation is also halted and the magma body is able to rise to the surface without interacting with the water to produce a lava lake or scoria cone. Lorenz (1986) therefore agrees with Sheridan and Wohletz (1983) that the formation of maars and tuff cones are favoured by critical magma: water rations of 3:1 and 1:1.

Understanding the formation of tuff cones and maars, is important for understanding their relative location to Oldoinyo Lengai and Kerimasi. The explosion craters appear to have occurred only on the plains between the large volcanic centres of this section of the Natron Basin, whereas the tuff cones are found on the lower slopes of the volcanoes. Dawson and Powell (1969) concluded that this spatial pattern reflected the amount of water which can accumulate on the plains and slopes of the volcanoes. They suggested that flat lying areas on the plains between the volcanoes were more likely to accumulate bodies of water during wet periods (or even due to a highstand of Lake Natron), resulting in phreatomagmatic eruptions forming maars. However, this interpretation does not explain the presence of hydromagmatic

tuff cones on the slopes of the large volcanic structures of Gelai and Kerimasi. It is also inconsistent with later experimental and observational data that indicate that large amounts of standing water are required to generate tuff cones (Wohletz and Sheridan, 1983, Sheridan and Wohletz, 1983, Lorenz, 1986).

The above explanation for maar formation does not correspond to the conclusion that explosion craters such as Loolmurwak and Emablulu were the result of magma interaction within swampy regions caused by a highstand of Lake Natron (Dawson and Powell, 1969). Evidence does exist which indicates that the shoreline of Lake Natron was substantially higher than present levels around 240,000 years B.P, 135,000 years B.P and more recently between 11,800 and 9,100 years B.P (Hilaire et al., 1987, Warren, 2006) but the exact extent of this lacustrine extension is unknown. The exposure of Kerimasi units within these explosion craters constrains their formation until after the main activity period of Kerimasi between 0.4 – 0.6 Ma (Church, 1995) with dating of phlogopite crystals from Loolmurwak between 140,000 to 570,000 years with an average of 350,000 years B.P (Macintyre et al., 1974) and so it is possible that their eruption coincided with a lake highstand. However, the amount of water available at the surface would have hindered the formation of maars and result in the formation of tuff cones. It seems more likely that the maars are the result of interaction with aquifers below the surface, located on the plains due to topographic driven flow. Pello Hill appears to have formed in a region lacking any ground water as evident by expression as a scoria cone and lack of palagonitisation. This may have implications for the timing of the eruption of Pello Hill and the extent of previous lake levels; either Pello Hill erupted before or long after an episode of lacustrine extension or the lake level never extended as far as Pello Hill.

The presence of tuff cones on the lower slopes of Kerimasi can be explained by shallow bodies of hydrothermally generated groundwater as a result of both topography driven fluid flow (flow system in which ground water flows from higher-elevation recharge areas, to lower-elevation discharge areas, where hydraulic head is lower) and thermally driven advection cells (Forster and Smith, 1989, Hurwitz et al., 2003).

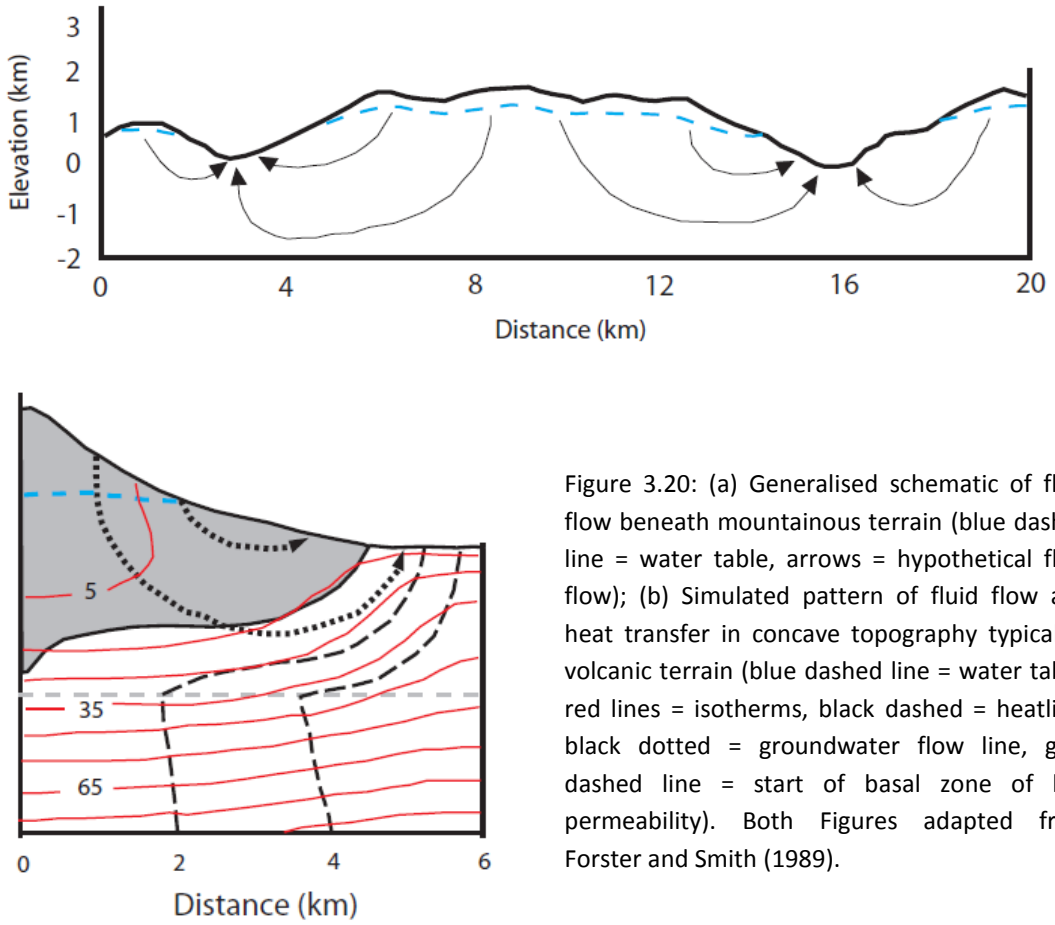

Figure 3.20: (a) Generalised schematic of fluid flow beneath mountainous terrain (blue dashed line = water table, arrows = hypothetical fluid flow); (b) Simulated pattern of fluid flow and heat transfer in concave topography typical of volcanic terrain (blue dashed line = water table, red lines = isotherms, black dashed = heatline, black dotted = groundwater flow line, grey dashed line = start of basal zone of low permeability). Both Figures adapted from Forster and Smith (1989).

Although beyond the scope of this thesis, computer models of hydrothermal circulation beneath volcanic edifices simulate topography driven flow vs. advection driven flow by setting fluid flow and thermal parameters including permeability, basal heat flow and thermal conductivity of the solid, liquid and vapour phases within a specified geometry (Hurwitz et al., 2003, Forster and Smith, 1989). Results of these simulations show that ascent of a hydrothermal plume can be facilitated by the presence of a heat source at depth, weak topography driven-flow, a flux of deep-sourced volatiles and a moderately permeable pathway through which the fluid can travel ($k \geq 10^{-16}$ m^2). All of these conditions are easily met at Kerimasi with the heat source provided by magma sourced at depth and volatile flux (primarily carbon dioxide and hydrogen sulphide) from numerous locations across the rift. However, eventually the water will be driven towards the lower slopes of the volcanic terrain and so thermal pools and springs can be found on the lower slopes of the volcanic edifice. Shallow bodies of water on the lower slopes of Kerimasi may also be the result of fault related fluid flow.

3.5 Concluding remarks - Interpretation of field observations

The above field observations, when combined with those previously made during different stages of Oldoinyo Lengai's eruptive cycle (Nyamweru, 1990, Nyamweru, 1988a, Dawson et al., 1994a, Keller and Krafft, 1990, Vaughan et al., 2008, Kervyn et al., 2008c, Kervyn et al., 2008b, Kervyn et al., 2008a), help to generate a broad-scale picture of how the magmatic system within the Gregory Rift has evolved since its first description in the early 1900's.

The eruptive cycle of Oldoinyo Lengai in 2006 - 07 appears to have continued in similar ways to previous eruptive cycles, suggesting a continuation of a deep seated processes this favours a cyclic activity at the volcano. The timing of the cycles has been investigated using isotope disequilibria and has been inferred to occur over periods of 7 – 18 years (Williams et al, 1986) or 20 – 81 years (Pyle et al, 1991). The nature of the eruptive cycle of Lengai has been addressed by Church (1995) who concludes that the cycle at Lengai can be summarised as;

1. An almost continuous rise of batches of natrocarbonatite lava during periods of effusive activity generating lava flows on the crater floor.

2. Occasionally a body of hotter, more volatile-rich, juvenile silicate magma will enter the volcanic system driving the release of CO_2 and causing explosive activity, the size of which depends on the size of the silicate magma body and the thermal contrast between the two magma types.

3. A period of repose then occurs as a result of drainage of the subvolcanic magma storage chamber. This repose ends when the residual silicate material fractionates and eventually reaches the threshold for liquid immiscibility to generate natrocarbonatite.

The observations of the 2006 – 07 activity in terms of the magma composition and eruptive behaviour of Oldoinyo Lengai (Kervyn et al., 2010, Keller et al., 2010), has led to more detailed evaluations of the volcanic activity of Lengai than that of Church (2006). The revised structure of the volcanic cycle can be summarised as follows;

1. A large explosive eruption excavates a large pit crater in the northern crater of the volcano.

2. An influx of new carbonated nephelinite (parental unit) enters the storage chamber.

3. Enrichment of CO_2 and alkalis occurs as the parental magma crystallises and fractionates resulting in the crossing of the liquid immiscibility solvus and natrocarbonatite is generated.

4. The immiscible natrocarbonatite rises to a shallow level reservoir where convective heat transfer and fluid motion causes the magma to rise within the conduit towards the surface where it can be observed as lava lakes or hornitos.

5. Thermal erosion of the bases of the hornito complexes by continual resurgence of natrocarbonatite lava results in the eventual collapse and effusion of large carbonatite flows like that of 2006.

6. The exhaustion of the shallow reservoir results in the system being recharged by silicate magma and so CO_2 and alkali enrichment continues in the upper part of the column generating a carbonated combeite-wollastonite-nephelinite which rises up the volcanic conduit due to the removal of the overlying carbonatite.

7. Ascent of this silicate magma leads to gas decompression which drives an explosive eruption of silicate material prior to production of natrocarbonatite.

It is clear that this region of Tanzania has undergone violent explosions from multiple centres. This has been witnessed in recent times at Oldoinyo Lengai with the eruptions in 1966 and 2007, but is also evident from other volcanic features in the vicinity. The presence of the lapilli tuffs on the flanks of Kerimasi provides evidence for high energy explosions during its active stage. These explosions would have been strong enough to generate a plinian eruption and pyroclastic density currents.

The explosion craters of the Natron basin are the result of magma interaction with bodies of water. It is concluded that the tuff cones and maars on the plains between Lengai and Kerimasi are not the result of magma interaction with standing surficial water, but rather due to the interaction of magma with aquifers, which are preferentially formed beneath the plains due to topography driven flow. It is proposed that these features are the result of magma rising in random pockets, potentially related to magma storage beneath the larger volcanoes Kerimasi, Lengai and Gelai, all of which have had batches of magma that miss the main storage zone and so erupt phreatomagmatically to produce parasitic cones. The composition of these parasitic cones raises some interesting questions. Are they chemically related to the magmas which

have been observed at the larger volcanic centres in particular Oldoinyo Lengai? Could they represent a juvenile magma composition from which the exotic magmas at Lengai could ultimately differentiate? Or do they represent precursory material before the eruption of natrocarbonatite?

The above observation-based model provides the first model of the eruption dynamics and cyclicity of Oldoinyo Lengai and so is a starting point from which future models can be postulated with increased observation of this unique volcano. In order to understand the processes which are at work at Lengai, it is important to combine physical observations, both of current activity and historical activity via deposits, with chemical and petrological observations of the volcanic complex as a whole.

Chapter 4: Petrology of a xenolith suite from Oldoinyo Lengai, post-2007 eruption.

4.1. Xenolith suite from 2007 – 2010

During a field campaign to Tanzania conducted during May 2010 a suite of rocks from volcanic centres within the Natron basin (Figure 4.1) were collected for further analysis upon return to the UK. The xenoliths amongst this suite are angular in shape and up to 9cm in length. The samples can be divided into two regions, those collected from the active volcano Oldoinyo Lengai and samples collected from the smaller volcanic centres located on the flanks and plains surrounding Lengai and neighbouring Kerimasi volcano.

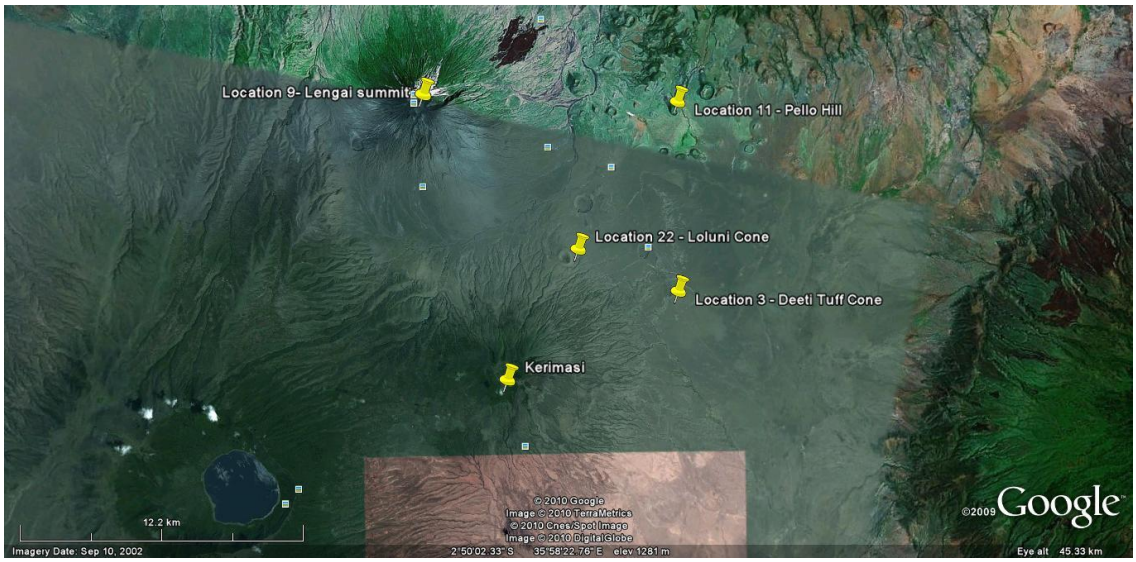

Figure 4.1: Satellite image of Natron basin region with sampling areas between Kerimasi and Oldoinyo Lengai indicated.

4.1.1.Lengai xenoliths

After the explosive activity in 2007 a suite of volcanic bombs containing xenoliths and ejected natrocarbonatite were collected from both the rim and upper flanks of the northern crater and the inactive southern crater of Oldoinyo Lengai. These xenoliths are comparable to those previously collected from Lengai by Dawson (1995), Dawson and Smith (1992) and Morogan and Martin (1985). The suite consists of 20 xenoliths of both volcanic and plutonic material whose mineralogy is summarised in table 3, along with that of a megacryst / xenocryst also collected from the rim of the active crater. The samples collected cover a range of lithologies

sampling different igneous environments and depths under the volcanic complex. All xenoliths are found as volcanic bombs (Figure 4.2) and so are coated in natrocarbonatite ash or nephelinite lava, which once hammered open, reveals different mineralogy.

Figure 4.2: View of summit at Oldoinyo Lengai with southern crater wall exposed on the right and the rim of the active northern crater to the left. Rubble on the ground consists of volcanic bombs containing xenolithic material.
Photos courtesy of Adrian Jones

4.1.2 Other samples

Further samples of xenolithic and megacrystic material were also collected from regions within the Natron – Engaruka horst block between Kerimasi and Oldoinyo Lengai to investigate the subsurface mineralogy of the region. This region between the two volcanic centres is dominated by small cones and craters belonging to the Younger Extrusive range of volcanic features (Dawson and Powell, 1969). The investigated sites include Loolmurwak explosive crater and Loluni and Pello Hill, which are both tuff cones, whose formation was discussed previously in chapter 3. A number of samples were also collected from the debris avalanche deposits on the shore of Lake Natron. Previous work on these debris flow deposits suggests that they originated from Oldoinyo Lengai and so samples should correspond to units already classified by Dawson (1962).

A full list of samples collected during the field campaign and also those donated for study by Abigail Chruch and Jörg Keller, can be found in Appendix B, along with the GPS co-ordinates of sample sites. For the remainder of the thesis samples will be referred to by their sample code, which can be summarised as;

OLX = Oldoinyo Lengai xenolith, OLC = Oldoinyo Lengai xenocryst, OLA = Oldoinyo Lengai ash, OL = Oldoinyo Lengai lava, DTC = Deeti megacryst, DTX = Deeti xenolith, PHX = Pello Hill

xenolith, PHC = Pello Hill megacryst, PH = Pello Hill material, LWX = Loolmurwak xenolith, LWC = Loolmurwak megacryst, HMK = Hummock material, NTR = Lake Natron material, KMS = Kerimasi material, LRX = Loluni xenolith and LRC = Loluni megacryst.

Sample Number	Neph	Alkali Feldspar	Pyroxene	Oliv	Carbonate	Titanite	Mica	Wol	Apatite	Gar	Fe Sulph	Other	Classification
Plutonic /volcanic xenoliths													
OLX 1	40		40 (au – hd)			15		5				<1 (Hauyne)	***Nephelinite***
OLX 2	45	5 (sd)	40 (dp – au)			1			1	2	1	<1 (Ti Mag)	***Ijolite / Meltiegite***
OLX 7					95				3		1	<1 (Fl)	***Natrocarbonatite***
OLX 10	5	25	30	15			25			5		<1 (Ti Mag)	***Olivine mica-ijolite***
OLX 16	40	5 (sd)	30										***Ijolite***
OLX 18	35		40			5		5	<1		2	10 (cmb)	***Nephelinite***
OLX 19	35		40			5			<1			15 (Cmb)	***Combeite Nephelinite***
OLX 20	45	10	25			5			10		5		***Ijolite***
OLC 2a	30	10	30	10			15					5 (Ilm)	***Mica ijolite with fenite vein***
OLC 2b	20		40			5	25		<1			5 (Ilm); 5 (pvs)	***Mica ijolite***
OLC 1							100						***Phlogopite megacryst***
OL 8	5		5		90								***Altered***

											Natrocarbonatite
OL 6	40	5	30		5	5		5		10	***Nephelinite***
Fenitic / altered xenoliths											
OLX 3	<1	80 (sd - an)	10	<1	5				4		***Contact Fenite***
OLX 4	35	20 (sd)	40 (au)						5		***High grade Fenite****
OLX 5	30	45 (sd – mc)	20 (ag-au)				2		3		***High grade Fenite†***
OLX 6	10	70 (sd)	10		2		1		5	2 (Quartz)	***Medium grade Fenite****
OLX 8	10	35	35 (au)		7				3		***High grade Fenite†***
OLX 13	10	40	30					5	10	5	***High grade Fenite†***
OLX 14	40	10 (mc - sd)	35 (au)		5		5	2	1	2 (Ag / Cu S)	***High grade Fenite****
OLX 15	20	25 (sd)	45 (hd – au)		2		1	5	2	1 (Ti Mag), 5 (amphi)	***Nepheline Syenite†***
OLX 17a	10	55 (sd)	30 (ag-au, dp)		1		1		1	2 (Ti-mag)	***High grade Fenite†***
OLX 17b		35 (sd)	30 (au)					10		25 (Quartz)	***Medium grade Fenite****

Table 3: Mineral assemblages of sample suite post-2007 eruption (modal %). (mc) = microcline, (sd) = sanidine, (an) = anorthoclase, (au) = augite, (hd) = hedenbergite, (dp) = diopside, (ag) = aegirine, (mag) = magnetite, (cmb) = combeite, (Ilm) = Ilmenite, (pvs) = perovskite, * = metagranitic protolith, † = metagabbroic protolith.

4.2. Petrography of Oldoinyo Lengai xenolithic material

4.2.1.Fenitised Pyroxenite

Xenolith OLX 15 consists of a sub-rounded, coarse-grained, equigranular, green inner unit coated in finer grained, porphyritic nephelinitic lava (Figure 4.3). The core unit appears similar to that of peridotite but its mineralogy is not consistent. Although approximately 45% of the unit is equant, subhedral pyroxene crystals showing zoning with lighter green cores and darker green rims, the remainder is alkali feldspar showing simple twinning and low order birefringence colours and smaller amounts of nepheline. All pyroxene crystals show pleochroism from brown to dark green indicative of aegirine-augite. The majority of the nepheline analysed was contained within the nephelinite coating of the xenolith. The inner unit also contains subordinate amounts of titanite, apatite, wollastonite and metal sulphides and oxides. A minor amount of alkaline amphibole occurs as pseudomorphs within the sample. The nephelinite coating on the sample consists of phenocrysts of nepheline and pyroxene within a groundmass of nepheline, pyroxene and minor titanite.

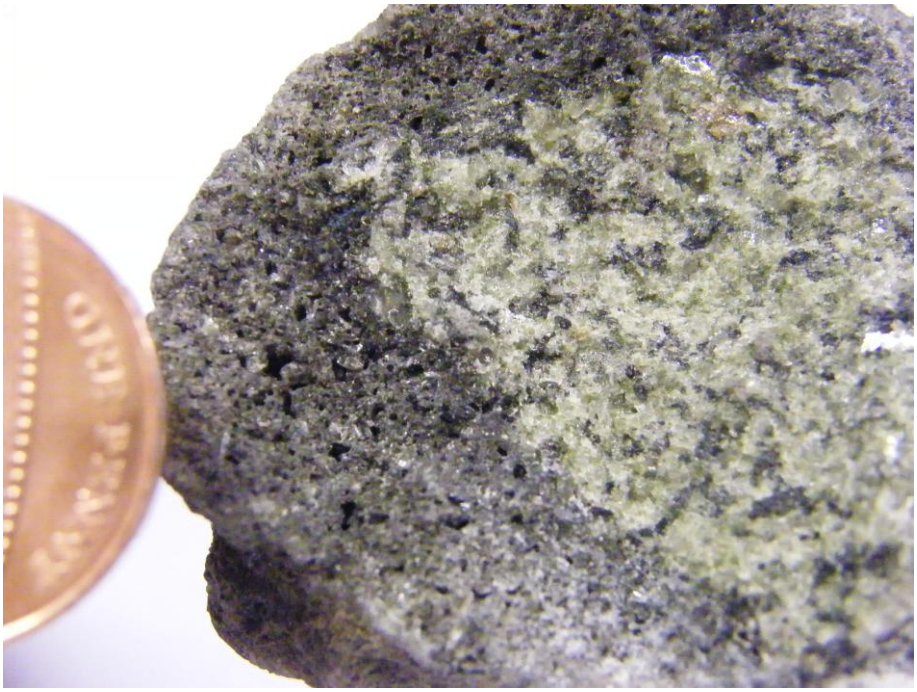

Figure 4.3: Hand specimen of OLX 15 showing cored xenolith with crystalline inner unit and finer grained nephelinitic lava outer selvedge. Dark flecks within inner unit represent metal oxide and sulphide grains.

The replacement textures and mineralogy of this xenolith indicate that it could represent a xenolith of fenitised ultra-mafic cumulate, which may have previously been a pyroxenite. There appears to be little evidence of olivine within the sample, which would suggest that it

has been completely replaced during metasomatism resulting in pseudomorphs of the olivine crystals. The formation of new minerals is indicative of modal metasomatism by infiltrating melts. Since the mineral compositions are typical of that associated with fenite alteration rocks, it would seem logical that this cumulate unit was also subject to alteration by melts / fluids associated with introduction of alkaline silicate or carbonatite melts.

4.2.2 Ijolite

A common rock unit beneath Oldoinyo Lengai is ijolite, which is a plutonic equivalent of nephelinite. It is primarily composed of nepheline and alkali pyroxene with accessory garnet, titanite, perovskite, apatite, iron sulphide and calcite. This mineral assemblage can be seen in sample OLX 2 which consists of a coarse grained (1- 3mm), euhedral nepheline and zoned glomeroporphyritic pyroxene, set within a matrix of finer grained material of the same phases (Figure 4.4a). Apatite crystals can be seen included within the nepheline as well as an interstitial phase. The garnet crystals in OLX 2 are melanite garnet and are well-formed crystals (Figure 4.4b). Zoning is common within the larger pyroxene crystals.

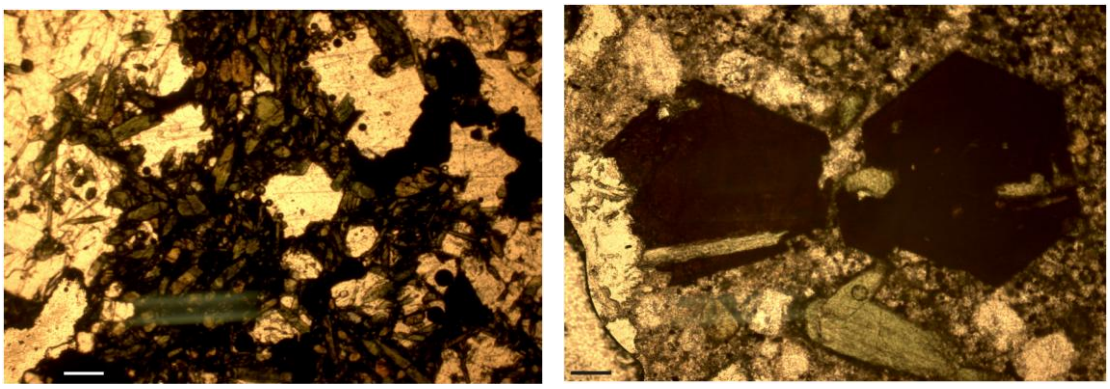

Figure 4.4: (a) Overview of OLX 2 showing well formed pyroxene and nepheline crystals. Needle-like inclusions within the nepheline are apatite. Scale bar = 150μm; (b) Melanite garnet crystals are common accessory minerals in ijolite. Scale bar = 66 μm.

Garnet crystals are also found within sample OLX 16 which is ijolitic / synenitic in composition with coarse grained, equigranular nepheline and alkali feldspar crystals with interstitial euhedral pyroxene. A number of nepheline crystals are poikilitic with small pyroxene inclusions as well as euhedral apatite crystals, many of which contain inclusions trails. Pyroxene crystals within OLX 16 are typically zoned with light green cores and dark green rims and also show slight pleochroism from brown to dark green. Pleochroic pyroxenes can also be

found within ijolite sample OLX 20, which appears similar in hand specimen to that of OLX 16, but in thin section shows some differences. It still consists of equigranular, euhedral nepheline crystals and elongate euhedral pyroxene which exhibit pleochroism in three different schemes; from pinky brown to yellow green, dark green to light green and straw yellow to lime green. This may represent different chemistries of pyroxene or different axial cuts of one type of pyroxene which has a pleochroic scheme.

A crystallisation sequence would involve initial generation of the large well-formed pyroxene and nepheline crystals, which grow at approximately the same time with some early apatite crystallisation coeval with the nepheline. Any apatite found within the interstitial, fine-grained matrix is most likely formed later. The presence of small (<0.5mm) rounded grains of iron sulphide within the pyroxene grains indicates early sulphide crystallisation similar to that seen in Dawson, Smith et al (1995). There appear to be no pseudomorphed mineral phases within this sample although previous publications on ijolitic material from Oldoinyo Lengai has exhibited microphenocrysts of pyroxene pseudomorphing olivine crystals (Dawson et al., 1995, Dawson and Smith, 1992a).

4.2.2.1 Olivine - mica bearing Ijolite

Xenolith OLX10 (Figure 4.5a) is similar in mineralogy to that of BD84 (Dawson et al., 1995) and can be classified as a olivine-mica-bearing ijolite. The xenoliths contain two types of xenocrysts; olivine and mica, both up to 3mm in size. Major element analysis of the mica reveals it is phlogopite with Fe content below 13 wt%. Interestingly the phlogopite exhibits kink banding (Figure 4.5c) indicative of pre-emplacement strain. This has previously been observed in olivine causing undulose extinction (Dawson and Smith, 1992a). The phlogopite crystals in OLX 10 are rimmed by Fe-rich biotite suggesting that the phlogopite is not in equilibrium with the surrounding rock unit. The olivine megacryst is also mantled by biotite (Figure 4.5b) indicating disequilibrium. Dawson et al (1995) observed the presence of Mn-rich pyroxene within the reaction rim around the olivine megacryst within BD84 however this is not seen in OLX 10. The megacrysts are contained within a groundmass of zoned pyroxene, alkali feldspar, mica and small amounts of euhedral melanite garnet phenocrysts, Ti-magnetite, titanite and ilmenite. The pyroxene within this unit often retains primary features such as zoning and so this rock type can be classified as an ijolite rather than a meltiegite, which has pyroxene showing no original features.

Figure 4.5: (a) Hand specimen of OLX10 with penny for scale; (b) PPL image of olivine xenocryst within OLX 10 (scale bar = 300µm); (c) PPL image of kinked mica within OLX 10 (scale bar = 150µm)

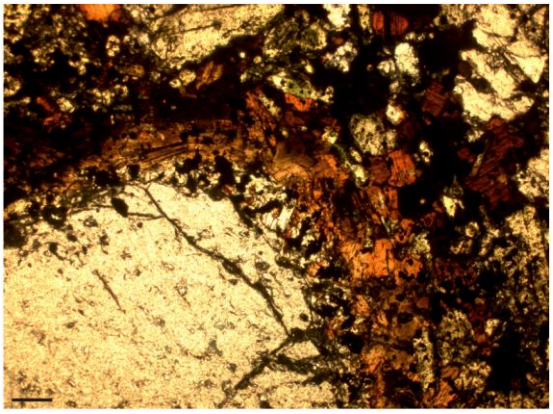

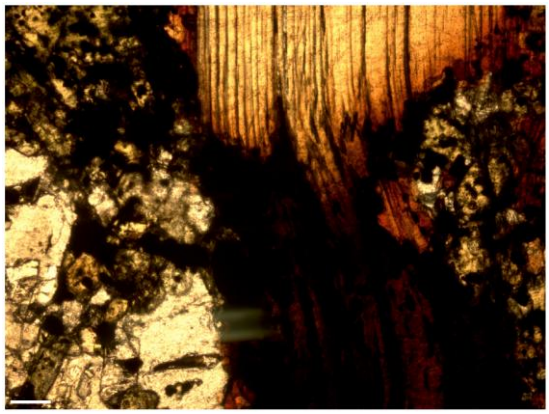

OLC 2 represents a similar sample to that of OLX 10 containing large megacrysts of olivine mantled by biotite mica. The host unit is ijolitic with euhedral nepheline and pyroxene crystals but contains up to 30% mica material which occur as phenocrysts up to 2 mm in length and visible within the thin section with the naked eye (Figure 4.6b). This sample also contains accessory perovskite which is not seen within sample OLX 10. An interesting feature of OLC 2 is a vein of alkali feldspar, nepheline and pyroxene, which is approximately 3 mm wide (Figure 4.6a). The mineralogy of this vein is similar to the mineralogy of fenitic units (discussed below).

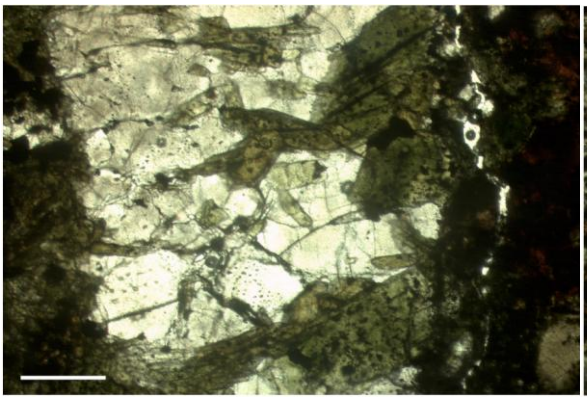

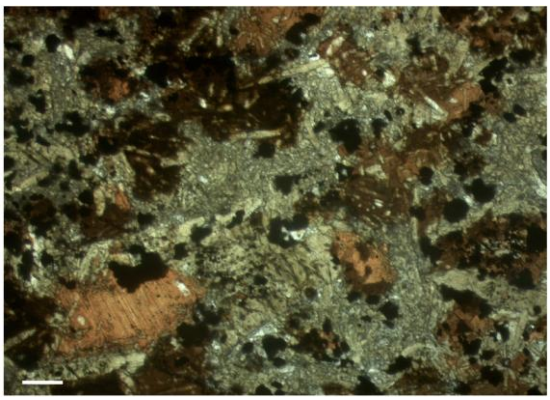

Figure 4.6: Ijolitic sample OLC 2; (a) Metasomatic vein consisting of alkali feldspar, nepheline and alkali pyroxene; (b) Overview of rock unit with abundant mica and ilmenite. Scale bars = 300µm

There appears to be no preferred orientation of the crystals within the vein, but rather the alkali feldspar and nepheline show triple junction suggesting recrystallisation of phases due to fluid flow. A number of the alkali feldspar crystals host fluid inclusion trails. It is thought that this vein represents a metasomatic vein caused by fluid alteration.

Crystallisation sequences of the ijolite units are similar to those quoted in Dawson, Smith et al (1995) with the large megacrysts of olivine and mica being incorporated into the host melt followed by crystallisation of pyroxene, alkali feldspar and garnet phenocrysts before final crystallisation of the groundmass matrix of pyroxene, feldspar, titanite, magnetite, ilmenite and mica.

4.2.3 Syenite

Specimen OLX 5 is classified as a syenite with the basic mineralogy of alkali feldspar, nepheline and pyroxene with accessory minerals of wollastonite ($CaSiO_3$), titanite and various iron sulphides. Interestingly the opaque iron sulphide minerals have a cuspate morphology (fig 4.10a). The alkali feldspar shows igneous crystallisation textures indicating that it is a primary mineral. The specimen show phenocrysts of pyroxene and alkali feldspar set within a finer grained matrix of the same mineralogy. Intragranular glass can be observed in specimen OLX 5.

The relationship between crystals within the syenitic units present at Oldoinyo Lengai suggests early crystallisation of the pyroxene and alkali feldspar phenocrysts. This is then followed by crystallisation of the accessory minerals of titanite, wollastonite and opaque minerals. A few of the titanite crystals appear to show a reaction rim when in close proximity to alkali pyroxene suggesting the phases are out of equilibrium. The groundmass phases and poikilitic alkali feldspar appear to be the final phases to form. This crystallisation sequence is in slight disagreement with that of Dawson et al (1995) who suggest that the alkali feldspar would be the last crystalline phase to form. The presence of cuspate opaque crystals and brown glass suggests that some regions were partially molten possibly due to localised re-melting of the unit during ejection or injection of residual melt prior to eruption.

4.2.4 Nephelinite

The associated silicate phases of Oldoinyo Lengai are nephelinite and phonolite, with the majority of the volcano being composed of these two rock units. It is therefore not surprising that a large number of xenoliths found at the summit of Lengai are nephelinitic, which have

essentially been plucked from the volcanic edifice upon eruption of magma. It is also thought that the explosive activity of the volcano was driven by eruption of volatile-rich silicate magma rather than carbonatite magma. This silicate magma would have been nephelinitic in composition after potential derivation via liquid immiscibility and fractionation from carbonated parent magma.

Samples OLX 1, OLC 6, OLX 18 and OLX 19 consist of euhedral nepheline phenocrysts of up to 3 mm across contained within a matrix of predominantly nepheline, pyroxene, wollastonite, titanite and metal sulphides. The wollastonite often contains nepheline inclusions suggesting coeval crystallisation. OLX 1 also contains a minor amount of the mineral hauyne. Pyroxene within the samples exhibit zoning from light, inclusion-bearing cores to dark, inclusion-free rims. OLC 6 appears more vesiculated than the other samples with plucking of minerals during thin section preparation and the presence of vesicles suggesting this sample of lava was more gas charged than other samples of nephelinite. The matrix of OLX 19 contains around 5% combeite ($Na_2Ca_2Si_3O_9$) crystals which appear as concentrically zoned microphenocrysts (Figure 4.7). Further investigation would be required to determine whether any of the combeite crystals have been altered to melanophlogite ($SiO_2 \bullet n(C,H,O,S)$) as has been previously suggested (Beard et al., In Prep).

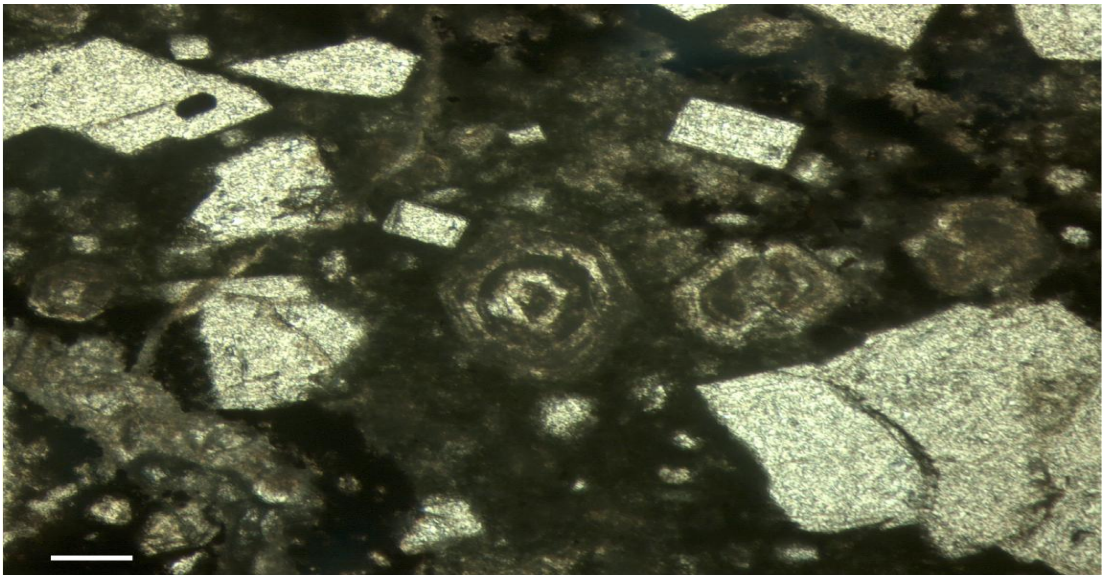

Figure 4.7: Concentrically zoned combeite crystals within the groundmass of sample OLX 19. Scale bar = 70µm

4.2.5 Fenite

A fenite is defined as a high temperature, quartzo-feldspathic rock that has been altered by alkali metasomatism at the contact of an alkaline - ultramafic magmatic complex, usually at the contact aureoles of nepheline syenites or ijolites. A fenite is mostly alkali feldspar (perthite, sanidine, microcline or anorthoclase), alkaline pyroxene (aegirine, aegirine – diopside, aegirine – augite), subordinate alkaline amphiboles and accessory sphene and apatite. Subordinate biotite – phlogopite micas, magnetite and ilmenite may also be present within fenite units (AGI, 1997, Zharikov et al., 2007). This definition of a metasomatic rock matches that of a number of samples collected from Oldoinyo Lengai, with the majority of xenoliths representing fenites; OLX 3, which is an inequigranular coarse grained porphyritic rock unit containing large alkali feldspar phenocrysts (Figure 4.8) up to 8mm across and 30mm in length. These phenocrysts are contained within a medium grained groundmass consisting of pyroxene and alkali feldspar with small amounts of titanite. The majority of alkali feldspar crystals show simple twinning with variations in birefringence colours. There appears to be no preferred orientation to the crystals. The mineralogy of sample OLX 3 is similar to that reported by Morogan and Martin (1985) of a contact fenite.

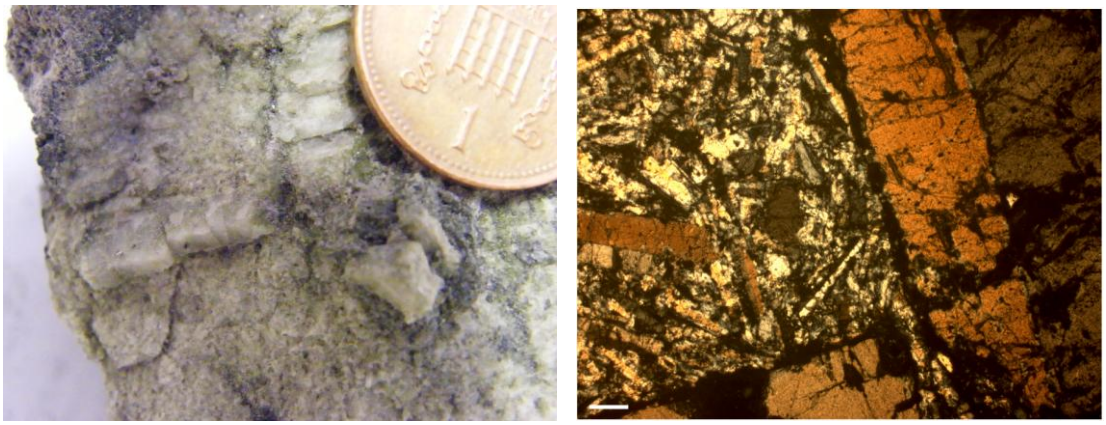

Figure 4.8: (a) Hand specimen of OLX3 with large alkali feldspar crystals. Slight green colouration to sample caused by presence of fine grained pyroxene; (b) Overview of OLX3 in section with large alkali feldspar showing twinning in groundmass of dominantly alkali feldspar. Scale bar = 300µm

OLX 4, OLX 8 and OLX 14 are similar fenitic units, both are fine-grained xenoliths made up of well-formed alkali feldspar and nepheline with interstitial glomerophyric, microphenocrysts of pyroxene, which appear as vein structures on the surface of OLX 4 and OLX 14. The pyroxene crystals within OLX 14 show no zoning but are weakly pleochroic in brown / dark green colour range. Green colouration indicates sodic pyroxene, possibly hedenbergite – aegirine crystals. OLX 14 also contains some unidentified metal-rich grains (Figure 4.9a). These were observed

using the SEM under back scattered electron mode and occur as small trails of 10 - 20µm metal rich blebs which are rich in Ag, Cu and U (fig 4.9b).

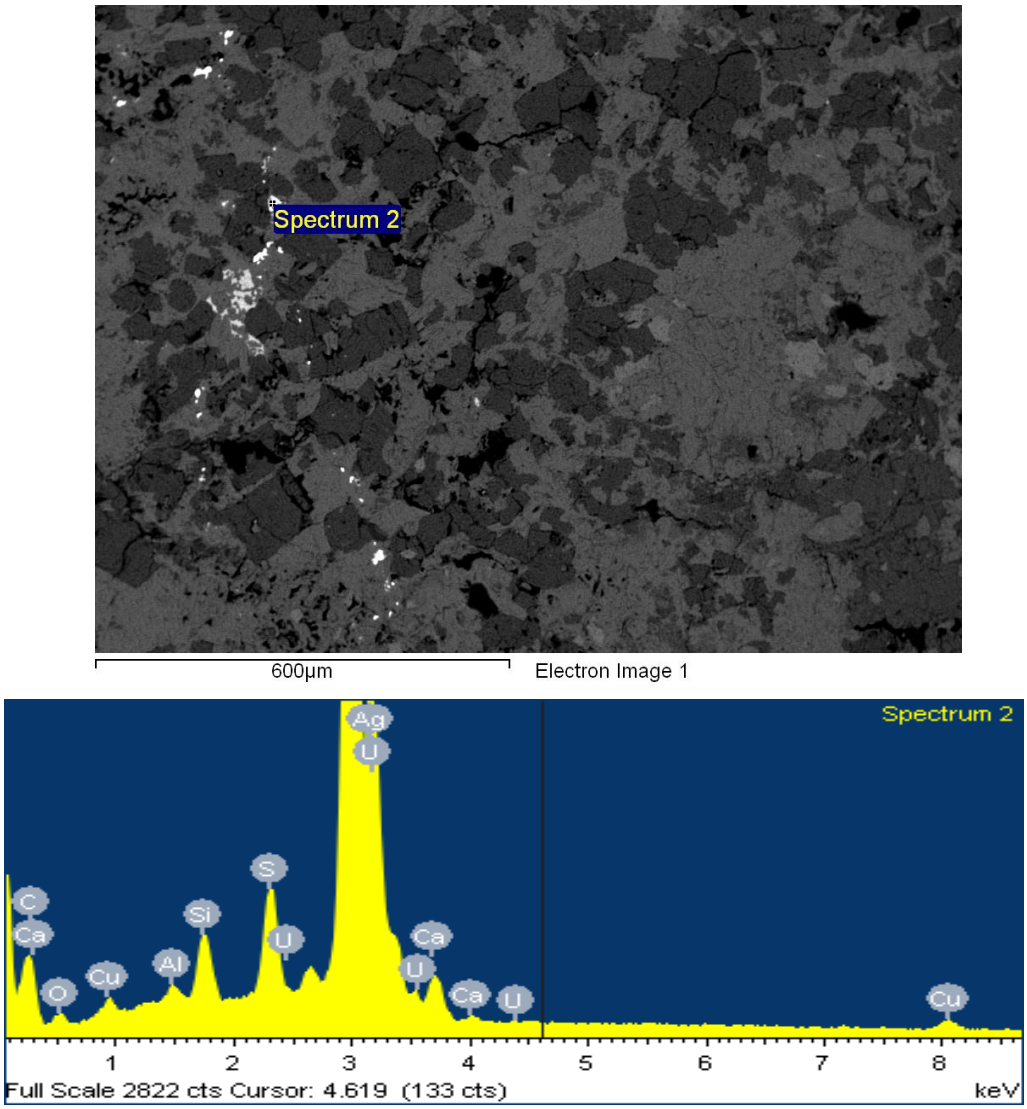

Figure 4.9: (a) SEM back scattered electron image of sample OLX 14 showing trail of metal rich grains within nephelinite (b) Associated SEM spectra showing presence of Ag (73.3 wt%), Cu (2.53 wt%) and U (2.9 wt%) in grain.

OLX 6 is a fine grained, leucocratic rock comprised primarily of alkali feldspar and pyroxene with minor nepheline, quartz, titanite, wollastonite and Fe sulphide. The rock texture is typical of re-crystallisation with small pockets of intergranular pyroxene crystals and radial feldspar (Figure 4.10b). A number of the Fe sulphide grains have cuspate shapes (Figure 4.10a) suggesting re-melting or mobilisation during generation of this unit. It is difficult to determine the protolith prior to fenitisation but the mineral assemblage indicates a high grade fenite generated from either metagranite or metagabbro (Morogan, 1994).

Figure 4.10: (a) Cuspate geometry of Iron sulphide within sample OLX 5 under plane-polarised light. Scale bar = 150µm; (b) Igneous feldspar (sanidine) crystallisation patterns within OLX6 under cross polars light. Scale bar = 150µm

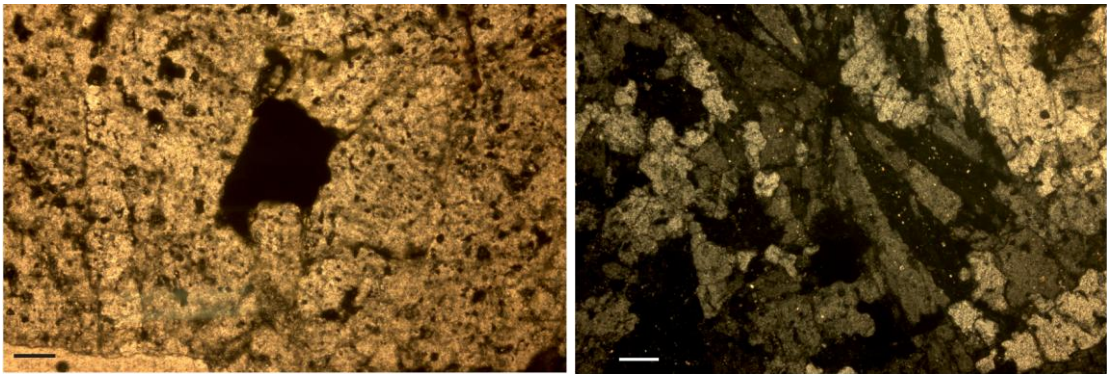

Samples OLX17a and OLX17b also represent fenites, which can be found at Oldoinyo Lengai. OLX 17a is a medium grained, highly veined rock-bearing some resemblance to gneissic textures (Figure 4.11a). The rock is equigranular and aphyric, composed of alkali feldspar and pyroxene with minor nepheline (~10%), titanite, wollastonite and Fe-sulphides and Ti-bearing magnetite. The majority of the alkali feldspar is concentrated along the veins, which do not appear to have any preferential alignment. The remaining rock consists of clusters of pyroxene with interstitial alkali feldspar and subordinate phases indicative of a mortar texture. Resorption and sieve textures are visible within prismatic pyroxene crystals when viewed on the SEM.

OLX 17b is a medium-to-coarse grained and slightly foliated fenite containing subhedral phenocrysts of alkali feldspar within a groundmass of feldspar, pyroxene, apatite and quartz. The xenoliths also contain a small amount of amphibole (Figure 4.11b). The quartz grains within this sample are thought to be relict minerals from the protolith from which this fenite was formed. Interestingly the pyroxene within this sample occurs as small (<1mm in length) oblate crystals, which occur within spaces left between grain boundaries of alkali feldspar.

A comparison of these xenoliths of fenite with those described previously by Morogan and Martin (1985) and Morogan (1994), it would seem that OLX 17b represents carbonatite fenitised metagranite / granite gneiss basement rocks which make up the Tanzanian shield whilst OLX 17a is formed from carbonatite-related fenitisation of a metagabbroic protolith.

Figure 4.11: (a) OLX 17a xenolith representing a high-grade fenite with feldspathic veins generating gneissic texture; (b) OLX 17b medium grade fenite with slight foliation fabric of feldspar and pyroxene

The fenites illustrated above have undergone both modal and cryptic metasomatism, which may provide some indication of their proximity to the unit causing the fenitisation. Those fenites which are obviously different from their protolith (OLX17a for example), with new mineralogy, have undergone modal metasomatism and so are likely to be more proximal to the intrusion. Samples such as OLX 17b, have retained some of the characteristics of the parent rock, have been subject to cryptic metasomatism which occurs at distances from the intruding magma.

4.2.6 Natrocarbonatite

A large block of carbonate-rich rock was also collected during the field campaign (xenolith OLX 7). This unit was collected from inside an ochre coloured volcanic bomb located in the southern inactive crater of the volcano. When hammered open it revealed a white and dark grey fine-grained rock about 20cm across. The outer surface of the xenolith is coated in a white powder consisting of secondary minerals associated with natrocarbonatite alteration upon exposure to the atmosphere. This is a result of the hygroscopic nature of the carbonatite material. The core of the block is still pristine with a slight purple colouration. Cavities also occur on the outside of the block which expose well formed crystals of secondary minerals (fig 4.12) and appear to have been formed by dissolution rather than as preservation of vesicle.

Figure 4.12: A cavity within the block of natrocarbonatite containing crystals of secondary minerals formed during alteration of the unit by meteoric water.

In thin section the xenolith consists of sodium-rich phases typical of natrocarbonatite; phenocrysts of both euhedral, lath-shaped crystals of nyerereite ($Na_2Ca(CO_3)_2$) and subhedral, rounded crystals of gregoryite ($(Na_2,K_2,Ca)CO_3$) within a groundmass of acicular nyerereite, gregoryite and smaller amounts of sylvite (KCl), fluorite, apatite and metal sulphide. The acicular nyerereite within the groundmass generates a texture similar to that of spinifex texture found within komatiites, which is indicative of quench crystallisation and has been referred to as "swallow-tailed" by previous authors (Keller and Krafft, 1990). Analysis of the sample using the SEM reveals the presence of small inclusions of silicate material within the carbonate minerals although the exact chemistry is difficult to resolve due to overlap with the host mineral.

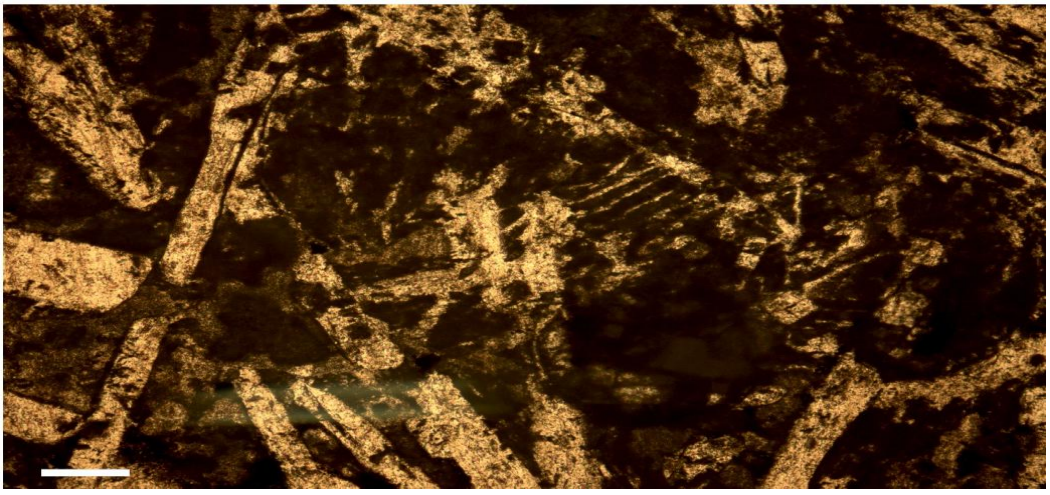

Figure 4.13: PPL view of OLX 7 showing lath-shaped nyerereite phenocrysts with acicular nyerereite in the groundmass showing quench crystallisation texture similar to that of spinifex. *Scale bar = 50µm*

Further samples of natrocarbonatite were also collected from the large flow on the western flank of the volcano. Sample OL 8 represents natrocarbonatite material after exposure to atmospheric conditions for four years and so is starting to show phases of alteration via hydration and removal of alkalis. In hand specimen the altering lava appears brown in colour. Under an optical microscope the sample consists of bladed nyerereite crystals and rounded gregoryite similar to that of the fresh samples with a similar spinifex crystallisation texture but a number of the crystals are pseudomorphed by new phases. Interestingly this sample also contains silicate minerals, which have been incorporated as xenocrysts during eruption. These xenocrysts include euhedral nepheline and pyroxene crystals, which have large, dark rims due to disequilibrium with surrounding material (Figure 4.14).

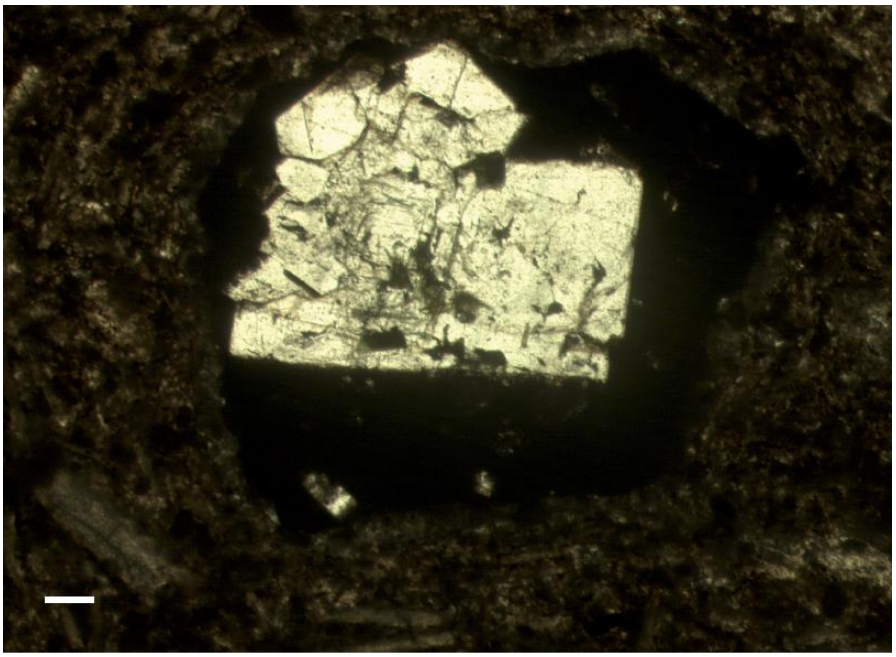

Figure 4.14: Nepheline xenocryst within natrocarbonatite lava from 2006 flow. Scale bar = 200µm.

The above descriptions of xenolithic material collected from Oldoinyo Lengai indicate that the explosive eruption in 2007 was large enough to sample the majority of units commonly associated with the volcanic complex. This in turn would suggest that the origin of magma body that caused the explosive eruption (most likely a gas-saturated silicate melt) must have been at depths capable of sampling all of these lithologies. The conduit utilised by this magma must also pass through these units in order to incorporate them. A closer look at the mineral phase chemistry should provide some depth and temperature constraints.

4.3. Phase chemistry

4.3.1.Olivine

The olivine megacrysts found within samples OLX 10 and OLC 2 are relatively homogeneous in terms of Fe /Mg content showing limited zoning from rim to core. Table 5 below summarises the chemistry of the olivine megacryst with no clear trend in the magnesium or iron content over the crystal, however the silica content of the crystal seems to increase from rim to core. The Mg # is fairly low for an olivine crystal that has been incorporated from depth with typical mantle olivine normally having an Mg # >0.90. However, previous observations of olivine chemistry indicate that low CaO values represent crystallisation at higher pressures (Adams and Bishop, 1982, Stormer Jr, 1973, Dalton and Lane, 1996).

Specimen	**1**	**2**	**3**	**4**	**5**	**6**	**7**	**8**	**9**
SiO2	40.2	37.4	39.7	35.6	37.40	37.42	38.56	33.36	41.11
TiO2	-	-	-	-	-	0.02	-	0.02	0.01
FeO	15.6	13.5	15.7	14.7	14.48	14.93	15.35	15.26	15.26
MnO	-	-	-	-	-	0.23	0.24	0.25	0.24
MgO	43.4	40.6	42.8	38.2	40.03	40.99	40.77	34.51	45.48
Cr2O3	-	-	-	-	-	0.02	0.003	-	0.009
CaO	-	-	-	0.3	-	0.24	0.22	0.22	0.25
NiO						0.10	0.03	0.20	0.06
Sum	99.0	91.5	98.2	88.8	91.91	93.95	95.17	83.82	102.5
Mg #	*0.83*	*0.84*	*0.83*	*0.82*	*0.83*	*0.83*	*0.83*	*0.80*	*0.84*
Position	*Core*	*Rim*	*Core*	*Rim*	*Rim*	*Rim*	*Core*	*Core*	*Core*

Table 4: 1-5 data collected from SEM of OLX10; 6-9 data collected from WDS EMPA of the same olivine megacryst

Comparison of the olivine megacryst from OLX 10 to that of olivine crystals within other rock types shows a similar chemistry. Figure 4.15 below illustrates the chemistry of the olivine from OLX 10 in comparison to that of common olivine reservoirs within the Earth's crust and mantle sampled by two different rock groups, kimberlites and peridotites. Chromium is often found within olivine as it substitutes for Fe and Mg within the crystal structure. It can be seen that the olivine from OLX 10 plots within the dunite, harzburgite and lherzolite field of this diagram, which could provide some indication of its source. The presence of the reaction rim around the olivine within OLX10 indicates that the mineral is not in equilibrium with the host unit. However the distinct lack of chemical variation between the rim and core of the olivine crystal is surprising.

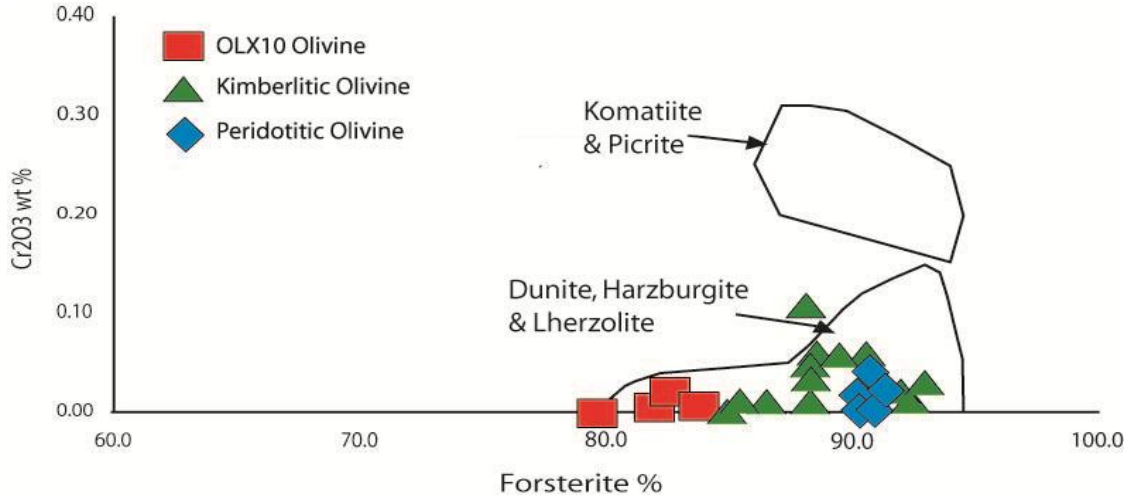

Figure 4.15: Mg # vs. Chromium oxide for olivine crystals within olivine – mica ijolite sample OLX 10. Kimberlitic olivine taken from olivine xenocrysts from Udachnaya (Kamenetsky et al., 2008); peridotitic olivine from xenoliths found within volcanic material and abyssal samples collected from MORB sites (Dawson et al., 1970, Arai et al., 2004, Niu, 2004)

4.4.2.Mica

Mica only occurs within a few of the xenolith units collected from the summit of Oldoinyo Lengai as shown by table 3. The mica within all the samples belongs to the phlogopite-biotite series with varying compositions. Table 5 below represents the composition of the phlogopite megacryst from sample OLX 10. This mica, as stated above, exists as large crystals within the xenoliths and is mantled by rim of mica with different birefringence colours, which is indicative of differing chemistry. The mica rim is biotitic and also occurs around the olivine megacryst in the same xenolith. The mantling of olivine crystals by mica can also be observed in sample OLC 2. The transition from phlogopite to biotite occurs at around 13wt% Fe_2O_3 as can be seen from the microprobe analyses in tables 5 and 6. Both mica phases are enriched in Ti, Al and Na in comparison to mica phases from other environments and neither shows any variation between core and rim of the crystals. The phlogopite megacryst shows higher MgO content than the biotite and consequently has *Mg* values which vary from 0.83 – 0.86, whilst the increased iron content of the biotite reduces the *Mg* value to 0.66 – 0.70. The higher *Mg* values are often indicative of more primitive material, which has been crystallised from mantle-derived melts.

Table 5: Mineral phase chemistry for phlogopite mica contained within sample OLX 10; Analysis 1 -4 from SEM for OLX 10; Analysis 5 – 10 from WDS Electron Microprobe for OLX 10;

	1	2	3	4	5	6	7	8	9	10
SiO_2	38.5	27.6	35.2	37.5	35.83	34.89	36.16	34.14	35.07	37.15
TiO_2	4.2	4.3	4.2	4.3	2.52	2.43	2.46	2.34	2.24	2.39
Al_2O_3	13.7	14.2	13.0	14.4	14.72	15.01	14.67	16.17	14.92	15.87
Cr_2O_3	0.7	-	-	0.8	0.52	0.53	0.52	0.51	0.51	0.55
FeO	6.2	6.4	5.9	7.0	6.39	6.14	6.16	5.90	6.45	6.41
MgO	21.3	20.0	18.3	20.3	18.36	18.76	18.20	18.09	17.67	19.20
Na_2O	-	-	0.6	0.6	0.69	0.69	0.76	0.56	0.66	0.56
K_2O	9.7	9.7	9.0	9.9	9.11	8.93	8.96	9.04	8.80	9.41
F	-	-	-	-	0.41	0.63	0.49	0.78	0.71	0.92
Cl	-	-	-	-	0.04	0.03	0.04	0.03	0.06	0.02
Sum	94.3	82.2	86.2	94.8	88.59	88.04	88.42	87.53	87.09	92.48
Mg #	*0.86*	*0.85*	*0.85*	*0.84*	*0.83*	*0.84*	*0.84*	*0.84*	*0.83*	*0.84*

Table 6: Biotite mica chemistry from rim of olivine and rims of phlogopite megacrysts in OLX 10 and biotite from OLC 2. Analysis 1 -3 from SEM; Analysis 4 – 9 from EDS Electron microprobe; 10 – 12 SEM analyses of OLC 2.

	1	2	3	4	5	6	7	8	9	10	11	12
SiO_2	29.1	34.7	36.2	36.54	35.79	35.37	36.96	37.10	36.49	37.9	38.4	31.8
TiO_2	1.7	2.4	2.9	2.44	4.28	2.66	2.16	3.33	3.08	3.4	4.2	3.2
Al_2O_3	8.4	10.1	11.0	12.22	14.03	14.71	12.27	14.37	14.23	11.0	11.1	9.8
Cr_2O_3	-	-	-	-	0.34	0.14	-	-	0.15	-	-	-
FeO	10.3	13.8	13.1	14.69	14.33	13.11	13.92	14.38	14.14	17.2	18.1	12.6
MgO	13.7	15.2	15.8	16.66	16.25	16.23	16.29	16.84	16.64	14.4	13.9	12.5
Na_2O	-	-	-	0.79	0.68	0.70	0.82	0.83	0.80	0.5	0.4	0.4
K_2O	7.3	8.5	9.2	9.71	9.68	9.28	9.81	9.52	9.10	8.9	9.4	7.6
Sum	70.5	84.7	88.2	93.05	95.38	92.2	94.93	96.37	94.63	93.3	95.5	77.9
Mg #	*0.70*	*0.66*	*0.68*	*0.67*	*0.66*	*0.68*	*0.67*	*0.67*	*0.68*	*0.59*	*0.58*	*0.64*

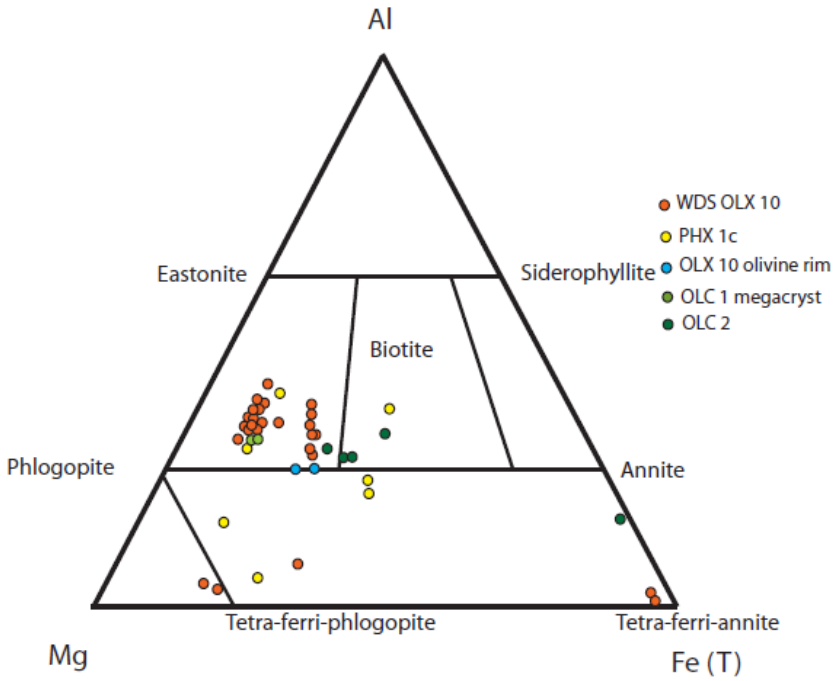

Figure 4.16: Ternary classification diagram for common mica minerals in terms of Al, Fe and Mg. All data plotted from xenoliths collected for this study. Adapted from Brod et al (2001)

A ternary plot (Figure 4.16) of the mica compositions determined from all mica-bearing samples collected during field work reveal a variation in chemistry between lithologies but also within a single sample. The majority of samples contain phlogopite mica which trends towards biotite with an increase in Fe. OLX 10 and PHX 1c (a mantle-derived xenolith from Pello Hill) also appear to contain some aluminium-poor but magnesium or iron-rich micas of the tetra – ferri phlogopite to tetra – ferri – annite series.

Figure 4.17 reveals that OLX 10 contains the most primitive phlogopite micas of all the samples. It is therefore important to look at how the mica material from OLX 10 compares to previous mica material collected during earlier studies of Lengai xenoliths, in particular in terms of the minor element composition to look for changes in the source region for these crystals. Figure 4.17 below compares the Cr and Ti of rock units akin to that of OLX 10. It can be seen that in terms of these elements the mica in OLX 10 is homogeneous and contains on average twice the amount of Cr than mica-bearing ijolites studied by Dawson et al (1995) or mica-bearing pyroxenites argued to be the result of metasomatism. This would seem to indicate that the source of the mica in this studies samples differs from that of those previously reported and so do not represent the result of metasomatism or co-magmatic phenocrysts resulting from polybaric crystalllisation during the early crystallisation stages of the host magma.

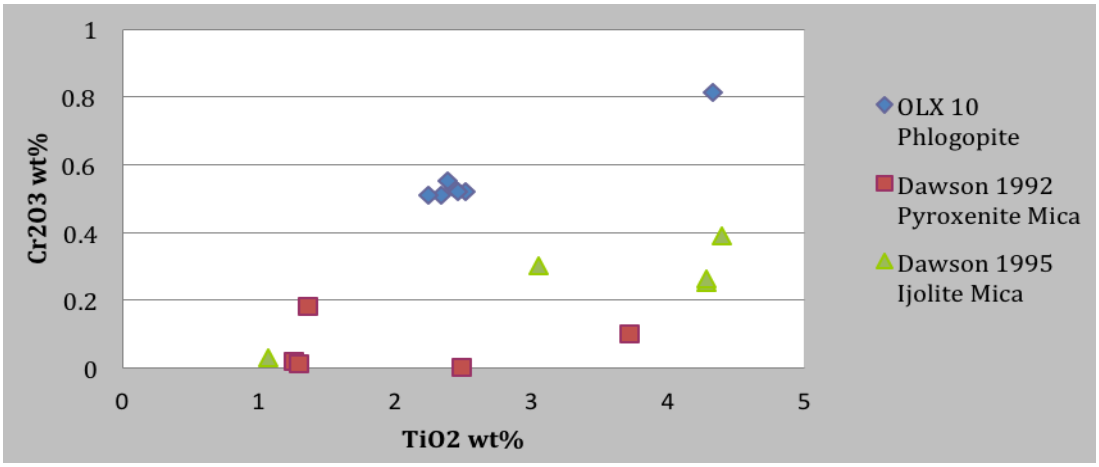

Figure 4.17: Graph comparing mica species from this study (OLX 10) and previous studies of xenolithic mica-bearing material from Oldoinyo Lengai. Data taken from Dawson and Smith (1992) and Dawson et al (1995).

Mica also occurs at Oldoinyo Lengai, at both the summit and along the flanks of the volcano, as mica xenocrysts, which can be found as mica books up to 1.5 cm thick, and 4cm across. This is not the first occurrence of these within the Natron Basin of the East African rift with samples previously collected from Deeti tuff cone approximately 13.5 km south east of Oldoinyo Lengai (Johnson et al., 1997). The mica books are also phlogopitic in composition with FeO < 13 wt% (table 7) and show Mg values similar to that of the phlogopite megacryst within sample OLX 10. The mica xenocryst again shows no zoning between rim and core of the sample.

Table 7: Chemistry of mica xenocryst (OLC1) collected from the summit of Oldoinyo Lengai. For comparison analysis 9 & 10 are mineral chemistries from Deeti (Johnson et al., 1997) All data collected using SEM.

	1	2	3	4	5	6	7	8	9	10
SiO_2	40.1	38.6	38.0	38.7	39.1	38.2	38.9	38.5	37.2	37.5
TiO_2	4.1	4.5	4.4	4.9	4.6	4.6	4.5	4.3	4.37	4.15
Al_2O_3	14.3	13.6	14.0	13.9	14.1	13.7	14.1	14.3	14.4	14.0
FeO	7.9	7.4	8.1	7.9	7.7	7.6	7.8	7.7	8.68	8.63
MgO	20.9	20.4	20.1	21.1	20.4	19.7	20.3	20.4	19.6	19.3
Na_2O	1.0	1.1	0.6	-	1.1	1.0	0.9	0.9	1.12	-
K_2O	9.2	8.8	10.1	9.4	9.3	9.0	9.4	9.5	9.07	10.4
Sum	97.5	94.4	95.3	95.9	96.3	93.8	95.9	95.6	94.44	93.98
Mg #	*0.83*	*0.83*	*0.82*	*0.83*	*0.83*	*0.82*	*0.82*	*0.82*	*0.80*	*0.80*
Position	core	core	rim	rim	core	core	rim	rim	-	-

There are some slight differences between the phlogopite phases present in the samples collected from Lengai. The xenocryst of phlogopite (OLC 1) appears to be more enriched in Na_2O and FeO than the megacrysts present within OLX 10 but more depleted in terms of Cr_2O_3.

When viewed in thin section the xenocrysts of phlogopite shows no crystal deformation as exhibited by that of OLX 10. However when the mineral chemistry of the mica book from Lengai is compared to that previously reported by Johnson et al (1997), it could be seen that they are similar.

4.4.3.Pyroxene

Pyroxene is an important mineral phase present within all xenoliths collected from Oldoinyo Lengai except the pure natrocarbonatite material. The majority of pyroxene crystals are Ca-rich clinopyroxene with compositions summarised in Figure 4.18. The remainder of analyses show pyroxenes, which vary in composition between lithologies, within a single unit and also within single crystals (chemical zoning). Table 8 summarises the pyroxene compositions.

	1	2	3	4	5	6	7	8	9
SiO2	51.9	51.5	50.9	53.7	50.3	51.5	46.7	50.9	54.5
TiO2	0.8	0.7	0.8	-	0.7	0.6	1.9	0.7	-
Al2O3	1.8	1.1	0.8	0.8	1.1	-	3.1	1.0	0.7
Fe2O3	8.2	5.6	6.3	0.7	7.7	6.9	0.2	0.7	1.0
FeO	2.7	5.8	11.1	10.5	9.7	11.1	5.3	4.8	9.4
MnO	-	-	-	-	-	-	-	-	-
MgO	11.5	11.1	7.3	11.1	7.8	6.9	12.3	13.0	11.9
CaO	22.2	23.3	20.1	22.0	20.5	19.3	22.0	23.2	22.7
Na2O	1.2	1.5	2.5	1.3	2.3	3.0	0.5	0.8	1.3
Sum	100.3	100.6	99.8	100.1	100.1	99.4	92.0	95.2	101.4
Mg/(Mg +Fe2+)	0.72	0.77	0.54	0.65	0.59	0.52	0.81	0.98	0.69
Fe3+/(Fe3+ Fe2+)	0.23	0.46	0.34	0.05	0.41	0.35	0.04	0.11	0.08
Position	Core	Core	Rim	Core	Core	Core	Core	Core	Core

Table 8: Selection of pyroxene chemistries from different rock units collected from Oldoinyo Lengai. All data collected using SEM. 1 – 6 = OLX 2 ijolite; 7 – 11 = OLC 2 olivine mica ijolite; 12 – 13 = OLX 1 nephelinite; 14 – 18 = OLX 5 nepheline syenite; 19 – 22 = OLX 15 metasomatised peridotite; 23 – 28 = OLX 17a fenite; 29 – 38 = OLX 17b fenite

	10	11	12	13	14	15	16	17	18	19	20	21	22	23	24	25	26	27
SiO2	53.3	52.2	40.7	45.1	46.4	48.3	47.6	46.5	51.4	47.1	46.0	51.2	50.6	50.7	45.6	48.3	43.8	46.0
TiO2	1.0	1.0	4.1	-	0.3	0.6	1.1	-	0.7	0.4	0.6	0.3	0.4	0.3	0.6	-	0.5	0.4
Al2O3	2.6	1.9	2.0	2.2	0.4	1.9	0.7	3.5	0.6	1.6	1.1	1.8	2.1	3.7	4.2	0.7	0.5	0.9
Fe2O3	1.4	1.5	20.6	24.4	20.6	18.8	17.6	13.8	9.1	7.0	7.1	9.2	7.4	8.6	6.8	3.3	3.4	1.9
FeO	4.6	4.4	1.9	4.0	12.0	10.6	11.1	13.2	18.0	13.3	11.3	9.4	9.7	10.9	10.2	8.0	10.0	8.4
MnO	-	-	-	-	-	-	-	-	-	0.5	0.5	0.3	0.5	0.4	0.4	1.1	1.3	0.4
MgO	14.2	13.8	4.9	8.0	4.4	4.1	4.8	4.1	3.4	4.0	5.3	6.0	6.3	5.6	5.3	9.2	5.8	9.5
CaO	23.8	23.8	26.0	15.8	14.7	12.4	15.8	15.3	14.1	14.9	15.2	13.7	14.4	13.6	13.6	19.3	19.7	19.8
Na2O	0.7	0.7	1.8	3.5	3.7	5.3	3.9	3.3	4.3	3.6	3.2	5.1	4.5	4.8	3.8	1.6	1.4	0.9
Sum	101.7	99.2	102.0	102.8	102.4	101.9	102.5	99.8	101.5	92.4	90.3	97.0	96.01	98.7	90.5	91.5	86.4	88.1
Mg/(Mg +Fe2+)	0.84	0.85	0.81	0.85	0.40	0.41	0.43	0.36	0.25	0.35	0.46	0.53	0.54	0.48	0.48	0.67	0.51	0.67
Fe3+/(Fe3+ Fe2+)	0.22	0.24	0.91	0.78	0.61	0.61	0.59	0.49	0.31	0.32	0.36	0.47	0.41	0.26	0.23	0.16	0.13	0.09
Position	Core	Rim	Rim	Core	Core	Core	Rim	Core	Core	Core	Rim	Core	Core	Rim	Rim	Core	Core	Core

	28	29	30	31	32	33	34	35	36	37	38
SiO2	44.9	44.9	51.3	43.6	48.8	48.0	47.5	46.3	47.1	46.8	51.93
TiO2	1.4	1.5	2.1	1.0	1.1	1.2	1.2	1.3	1.2	1.1	2.2
Al2O3	0.6	1.1	1.3	0.5	-	-	0.5	-	-	0.4	0.5
Fe2O3	3.34	5.9	8.7	6.8	7.1	8.2	7.6	6.3	8.3	7.1	8.3
FeO	5.4	11.9	9.7	9.7	9.5	9.4	8.9	9.3	8.3	9.5	7.3
MnO	0.4	-	0.3	0.4	-	-	0.4	-	0.4	-	0.5
MgO	9.9	4.9	4.9	5.2	6.5	5.7	6.1	5.9	6.1	5.5	6.8
CaO	18.0	10.2	7.2	10.9	11.9	10.6	11.4	11.3	11.0	10.3	10.1
Na2O	1.8	4.6	7.6	4.3	5.0	5.5	5.0	4.8	5.1	5.3	6.7
Sum	85.7	84.9	93.2	82.3	89.9	88.3	88.5	85.1	87.4	85.9	92.2
Mg/(Mg +Fe2+)	0.76	0.42	0.47	0.49	0.55	0.52	0.55	0.53	0.57	0.51	0.62
Fe3+/(Fe3+ Fe2+)	0.22	0.18	0.29	0.24	0.25	0.28	0.28	0.25	0.31	0.25	0.34
Position	Rim	Core	Rim	Core	Rim	Core	Rim	Core	Rim	Core	Rim

Table 8: cont'd

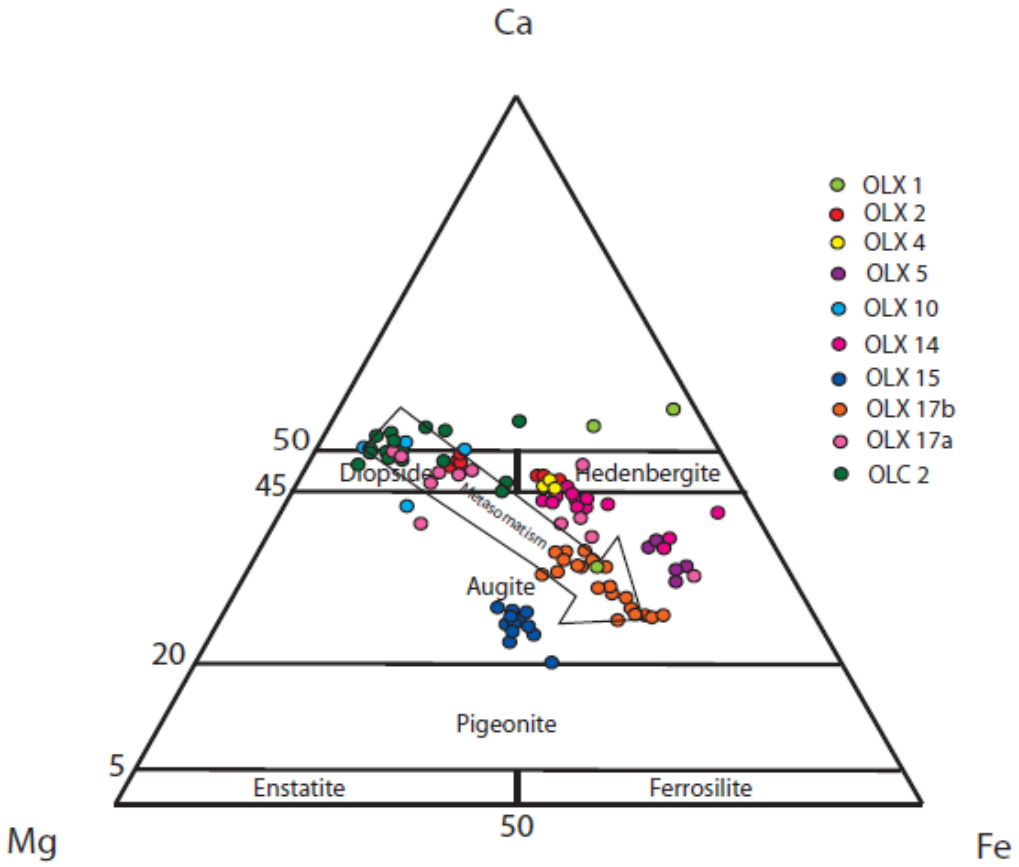

Figure 4.18: Ternary classification diagram for calcium, magnesium, and iron-bearing pyroxenes. Calcium end - member technically pyroxenoid Wollastonite. Arrow indicates the trend of composition caused by metasomatism.

4.4.3.1. Variations between lithologies

The above diagram illustrates that overall the pyroxenes analysed form a band extending from diopside to augite when plotted in Ca-Mg-Fe space (Figure 4.18). Similarly when plotted on a diopside-aegirine-hedenbergite ternary diagram, a trend from diopside to aegirine is observed (Figure 4.20).

Nephelinitic xenoliths (OLX 1 and OLX 18) contain hedenbergitic and augitic pyroxenes, which are amongst the most silica-rich (~50.7 wt%) and enriched in TiO_2 (1.36 wt%) of the different lithologies collected. In particular fenite sample OLX 14 contains no zoned crystals, but pyroxenes that are weakly pleochroic in brown / dark green colour range. A green colouration indicates sodic pyroxene, possibly hedenbergite – aegirine crystals. Nephelinite sample OLX 18 contains pyroxene crystals that exhibit two pleochroic schemes; the already noted brown to green pleochroism and also pink / green to yellow green.

Sample OLX 4 appears to only contain hedenbergite crystals although these plot close to the transition between hedenbergite and augite. The ijolitic units collected primarily contain diopsidic pyroxene although OLX 2 also contains pyroxenes with chemistry that plot within the hedenbergite field of the diagram. The pyroxene within the ijolite units appear to be the most primitive with Mg# ranging from 0.96 to 0.52 and MgO concentrations of 10.7 wt% on average. The ijolite pyroxenes also contain significantly more CaO than any of the other lithologies. Sample OLC 2 contains the most silica-rich pyroxene crystals with between 50.8 and 58.49 wt.% SiO_2 as well as 25 wt.% CaO. The pyroxenes within the ijolite units are all euhedral, bladed crystals often showing up to three pleochroic schemes; pink / brown to yellow / green, dark green to light green and straw yellow to lime green.

Fenitic units (OLX 6, OLX 17a, OLX 17b and OLX 15) consist mainly of sodic augite pyroxene with OLX 17a also containing some diopsidic pyroxene (Figure 4.19). When examined more closely on a Wo-Ag-Jd plot (Figure 4.21) the pyroxenes of these lithologies plot a linear trend from aegirine-augite towards wollastonititic compositions. OLX 3 shows pyroxenes, which appear as small, interstitial crystals of green weakly pleochroic pyroxene. The pyroxenes occur within micro-crystalline veins which are indicative of recrystallisation from alteration. This microcrystalline texture is also present within OLX 17a with light brown to dark green pleochroic pyroxenes, thought to be aegirine-augite. Some crystals show brownish green similar to that of augite.

Figure 4.19: Pyroxene crystals within fenitised cumulate (OLX 15) unit viewed under plane-polarised light. Pyroxene show two main colourations; green (which is pleochroic from light to dark) and brown. Scale bar = 70µm.

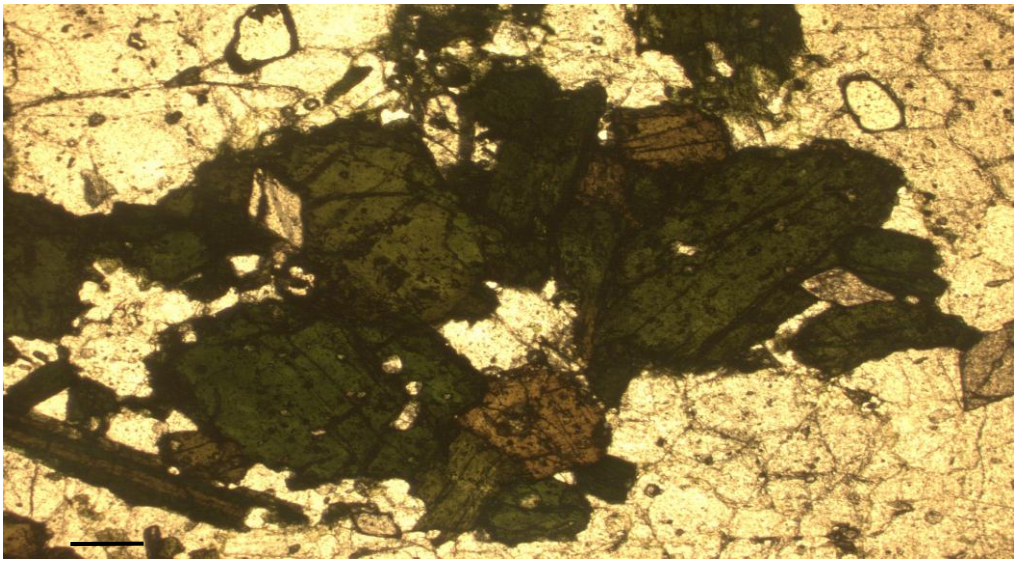

The syenitic sample (OLX 5) contains only aegirine - augite pyroxene appearing pleochroic in light brown to dark green but no zoning is observed. Pyroxene can been found as both groundmass minerals, phenocrysts and as inclusions within large nepheline crystals. Compositionally, on average the syenitic sample (OLX 5) contain the highest absolute concentrations of iron with Fe^{3+}/ (Fe^{3+} + Fe^{2+}) ratios varying between 0.31 and 0.61 and average FeO and Fe_2O_3 contents of 13.71 and 15.84 wt% respectively within the rims of the crystals which reflects the composition of the residual magma at the time of crystallisation.

It is useful to plot those pyroxene analyses that contain significant quantities of sodium and ferric iron on a separate ternary diagram in order to illustrate the proportion of diopside, aegirine and hedenbergite compositions and also to classify the sodium pyroxene crystals. It can be seen in Figure 4.21 that the pyroxene compositions from the xenoliths collected from Oldoinyo Lengai define a trend which extends from diopsidic pyroxene towards aegirine, similar to that shown in Figure 4.18. The pyroxene analyses from fenitic units contain mainly sodium pyroxene, typically aegirine – augite, as shown by Figure 4.21, which also define a trend from the Dp – Hd – Ag space towards more sodic aegirine – augite.

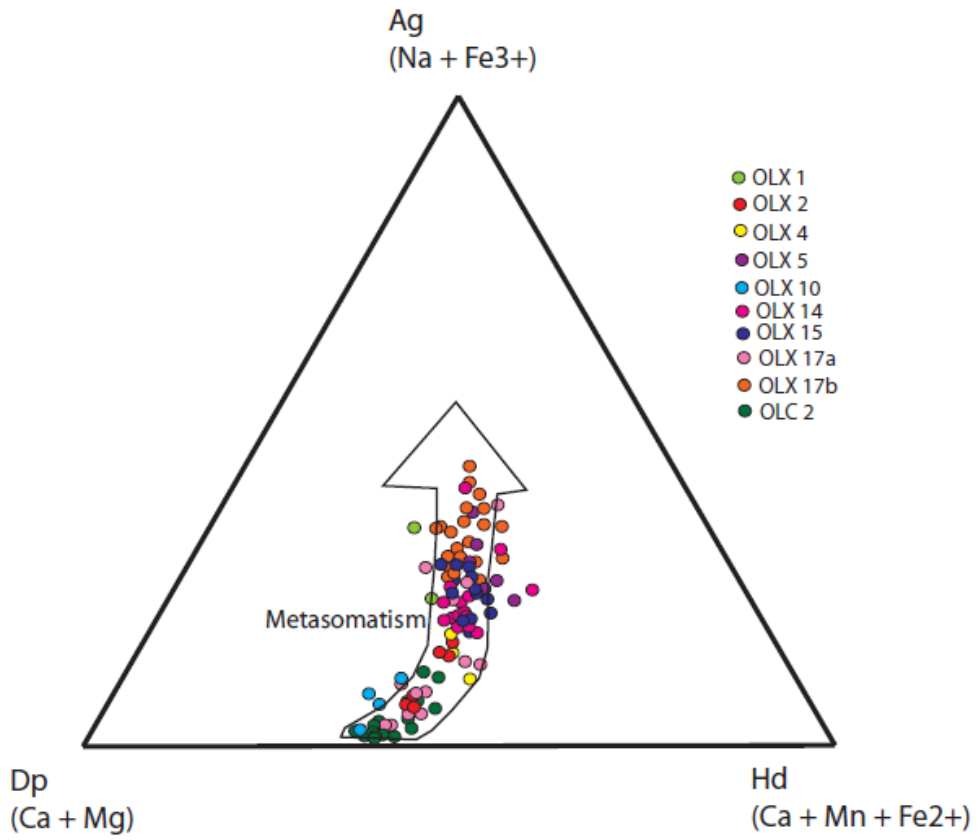

Figure 4.20: Diopside – hedebergite – aegirine plot for all Oldoinyo Lengai clinopyroxenes. Arrow indicates suggested trend within compositions caused by fluid metasomatism.

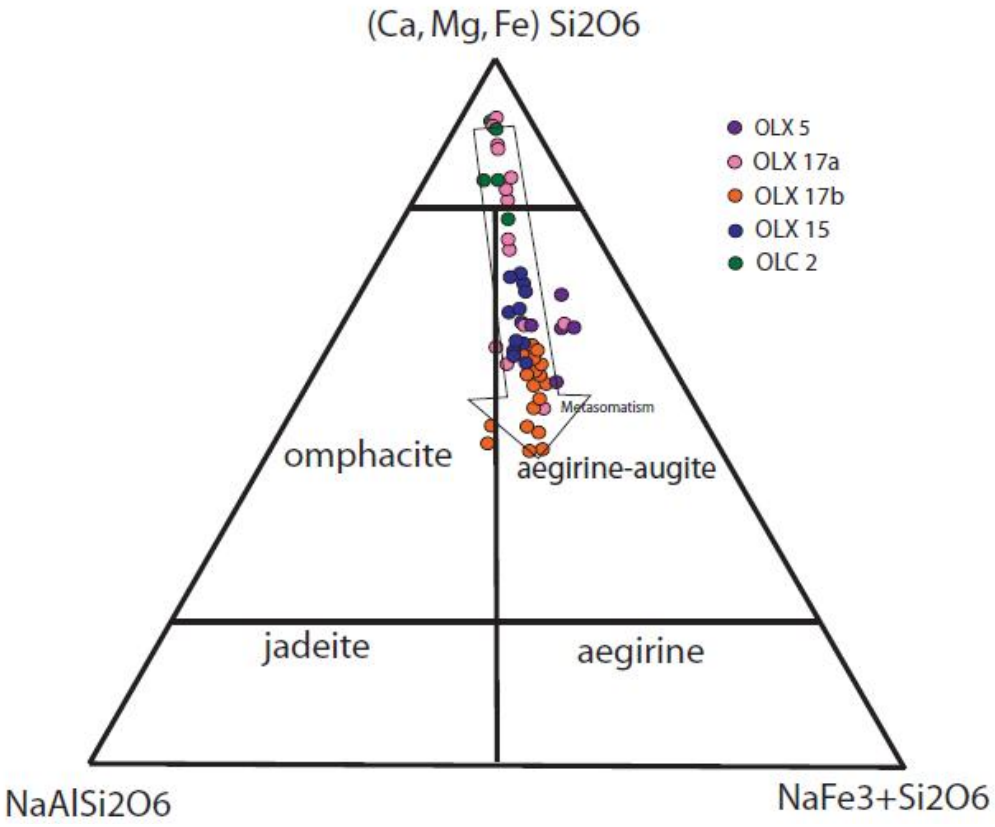

Figure 4.21: Ternary classification diagrams for sodium-bearing pyroxene for analyses of five of the metasomatised / fenitic units. Arrow indicates progression of metasomatic units.

4.4.3.2. Variation within individual grains

Chemical zoning within pyroxene is a common feature and is observed in a number of pyroxene grains within xenoliths (Figure 4.22). Within sample OLX 1 the majority of crystals are cored with zones of overgrowth often with resorption of core unit. The cores can be both pale green or light brown whilst the rims are green coloured. Some crystals contain dark green pleochroic cores. There are no crystals which show well defined multiple growth zones so appears to be more change in chemistry of magma rather than rhythmic recycling growth. Smaller interstitial brown coloured pyroxenes show weak pleochroism. Other nephelinite samples, for example OLX 18 and 19, also show zoned crystals with light green cores and dark green rims. A variation in the number of smaller mineral inclusions also occurs with inclusion-rich cores and inclusion-free rims (Figure 4.22b).

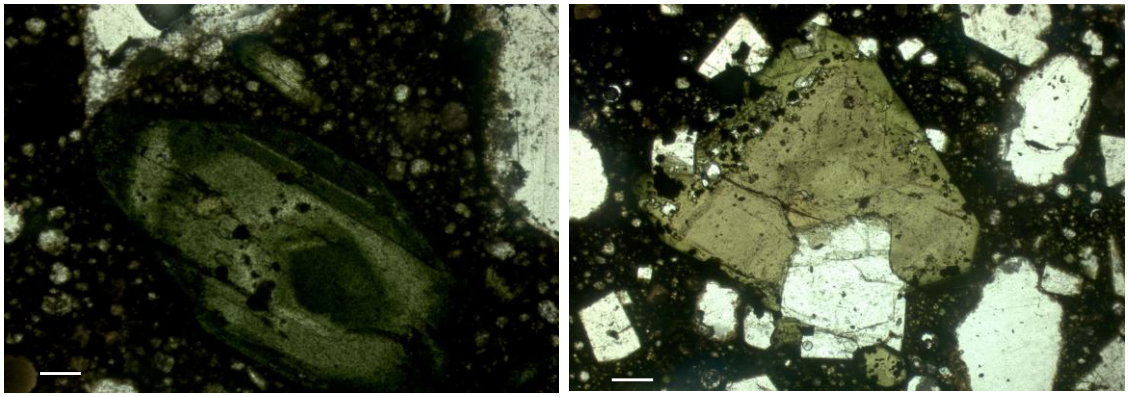

Figure 4.22: Zoned pyroxene crystals of OLX 18 nephelinite; (a) complex, oscillatory zoned crystal; Scale bar = 300µm; (b) subhedral pyroxene crystal showing large diopsidic core with inclusion-rich, sodic rim. Rim also shows preferential concentration of opaque minerals. Scale bar = 300µm.

Ijolitic units such as OLX 2 and OLX 10 contain pyroxenes that are chemically zoned. Zoning shows both dark cores with lighter rims and lighter cores with darker rims. Concentric zoning is also observed with darker green growth zones identified. Inclusion of small brown grains within the larger pyroxene crystals, indicative of co-crystallisation of different chemistries of pyroxene. The rims are often hedenbergite to aegirine – hedenbergite composition, Na and Fe-rich, whilst the cores are more diopsidic. Both zoned and patchy crystals are generally subhedral but some inner cores appear to be resorbed prior to overgrowth of new pyroxene (Figure 4.23).

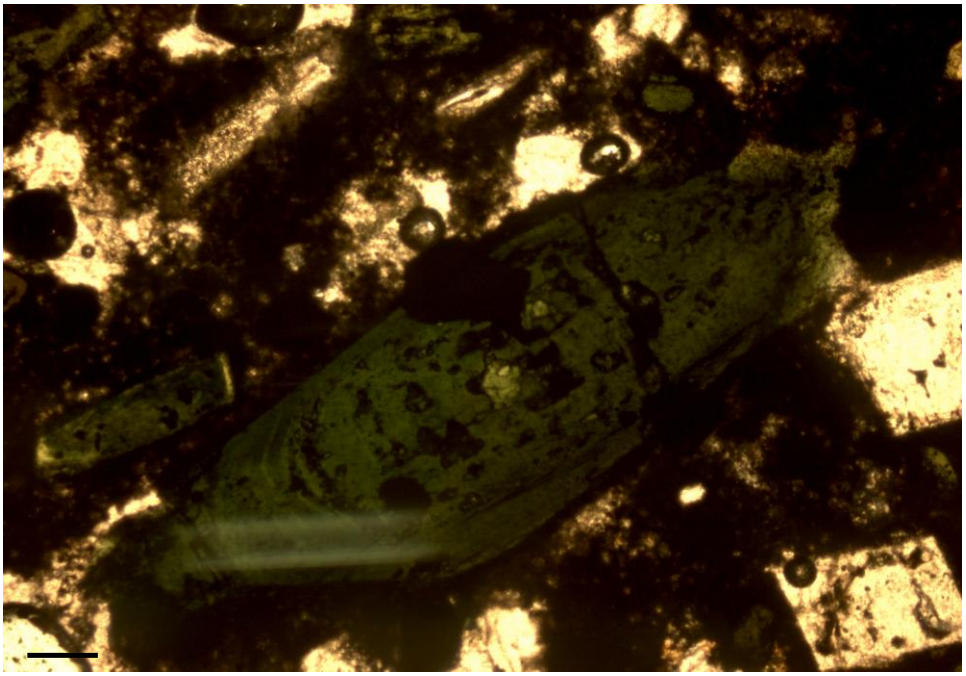

Figure 4.23: Oscillatory zoned pyroxene within ijolitic sample under plane-polarised light. At very core of crystal can see inclusion of different composition of pyroxene appearing as a lime green. Scale bar = 150µm

The fenitic units contain microcrystalline light brown to dark green pyroxene crystals which vary from diopsidic compositions at their cores to more sodium and Fe^{3+}-rich rims typically of aegirine - augite. Some crystals show brownish green similar to that of augite. This is argued to reflect the change in chemistry between the fluid from which crystallisation of the original pyroxene occurred generating the country rock and the subsequent throughflow of fluid during the fenitisation process. A number of the pyroxenes are completely altered to aegirine – augite with no cores of diopside preserved. This level of replacement is dependent on the grade of fenitisation involved with higher-grade fenites containing fewer relict crystals from the protolith.

4.4.4.Nepheline and alkali feldspar

Nepheline and alkali feldspar are two of the other constituent minerals which are found within xenoliths from Oldoinyo Lengai which are typical of peralkaline system. Nepheline is predominantly found as phenocrysts, microphenocrysts and as a groundmass mineral in almost all of the silicate rocks. The crystals are predominantly euhedral, indicating that they are one of the first phases to crystallise, except for those which can be found within the fenitic units. These units only contain minor nepheline which is subhedral to anhedral due to recrystallisation from an infiltrating fluid. As table 10 shows the nepheline compositions vary between lithologies as well as within the same lithology. Most analyses show that the nepheline within the samples contain significant amounts of Fe_2O_3 which is not uncommon for Lengai rocks (Dawson et al., 1995) which can be as much as 8.54 wt% but on average for the fenitic units (OLX 4 = 1.21 wt%, OLX 3 = 0.95 wt%, OLX 14 = 0.56 wt%, OLX 15 = 0.84 wt%, OLX 17a = 2.96 wt%), nephelinitic sample OLX 1 = 4.22 wt% and ijolitic units OLX 2 and OLC 2 contain 1.74 and 1.75 wt% respectively. The elevated iron content of the nephelinite sample would seem to suggest an evolved rock unit with concentration of Fe in the melt from which it crystallised. The fenitic units may have Fe contents which reflect the protolith from which the fenite was formed depending on the amount of recrystallisation for each grade of fenitisation.

The nepheline crystals within particular lithologies are consistently either potassic or sodic with little variation. In general the fenitic units appear to contain potassium-rich nepheline grains, whilst the nephelinitic sample contains sodic nepheline. This may be the result of the sodium being captured and contained within the sodic pyroxene crystals which occur alongside the nepheline within the fenite units. The Na / (Na + K) varies from 0.77 to 0.71 for ijolites, 0.84 – 0.69 for fenites and 0.84 – 0.75 for nephelinites. This results in the end member compositions (%) of the range between, nepheline = 74.1 – 57.8 for ijolites, 76.5 – 67.0 for

fenites and 85.2 – 71.4 for nephelinites, kalsilite = 39.2 – 20.6 for ijolites, 25.6 – 14.1 for fenites and 23.4 – 18.7 for nephelinites and quartz = 7.95 – 3.03 for ijolites, 13.4 – 2.71 for fenites and 6.83 – 0.17 for nephelinite. Individual grains of nepheline can show variation between cores and rims. Although not directly visible under optical microscopy, the SEM data reveals the presence of more potassic rims (analysis 12) to more sodic cores (analysis 13) within certain lithologies, whether this is the result of two different crystallisation episodes or a gradual change in magma composition due to fractional crystallisation is uncertain.

Nepheline is by far the most common feldspathoid mineral within the igneous rocks at Oldoinyo Lengai and so a large number of studies have been conducted to better understand its structure and paragenesis. An important observation is the apparent excess of silica within natural samples of nepheline which can act as an indicator of crystallisation and equilibration temperature of nepheline – alkali feldspar pairs (Hamilton, 1961, Powell and Powell, 1977, Watkinson and Wyllie, 1971). Using these principles it has been possible to plot the nepheline analyses from the suite of xenoliths in order to estimate crystallisation. The majority of the nepheline analysed crystallised between 800 to 1000°C.

Alkali feldspar crystals can also be found within almost all of the xenoliths collected from Lengai apart from the natrocarbonatites and nephelinite samples. In most units they are primarily found as microphenocrysts or a groundmass phase, except fenite sample OLX 3 where alkali feldspar constitutes 80% of the rock unit and occurs as large phenocrysts visible in hand specimen and as groundmass phase. The chemistry of the alkali feldspar crystals are similar throughout the collected lithologies with most containing sanidine (potassium-rich) feldspar, some of which are Fe-bearing. A number of alkali feldspar crystals within fenite units OLX 3 and OLX 15 also contain small amounts of BaO (0.73 – 1.24 wt%). Some variation in Na_2O, K_2O and Fe_2O_3 can be seen between lithologies as shown by table 9 below;

	Na_2O (wt%)	**K_2O (wt%)**	**Fe_2O_3 (wt%)**
Ijolite (OLX 10, OLX 2)	18.82 – 3.95	16.43 – 5.09	1.65 – 0.92
Syenite (OLX 5)	4.44 – 3.50	12.48 – 8.73	5.16 – 0.36
Fenite (OLX 3, 4, 6, 14, 15, 17a, 17b)	6.34 – 0.73	13.61 – 5.32	1.43 – 0.31

Table 9: Summary table illustrating variation in Na, K and Fe within alkali feldspar samples.

	1	2	3	4	5	6	7	8	9	10	11	12	13	14	15	16	17	18	19
SiO2	40.6	42.6	46.0	45.2	43.8	43.8	43.8	44.7	40.6	43.8	41.6	40.8	40.2	43.7	42.4	40.6	44.8	45.2	45.2
Al2O3	33.2	34.8	31.6	30.8	32.0	31.4	32.1	30.5	32.6	33.4	31.6	31.8	31.5	31.3	36.6	29.9	30.5	30.6	30.9
Fe2O3	1.2	1.2	1.0	1.9	1.5	1.8	1.2	2.3	4.5	0.6	4.4	5.9	8.5	2.4	1.00	6.6	2.5	2.0	1.9
MgO	-	-	-	-	-	-	-	-	-	-	-	-	-	-	-	-	-	-	-
CaO	-	-	-	-	-	-	-	-	0.7	0.5	-	0.5	-	1.4	0.3	0.7	-	-	-
Na2O	13.8	14.5	16.6	14.4	15.4	15.5	15.2	15.3	14.3	14.8	15.1	16.1	13.6	13.9	13.9	15.3	14.6	14.3	14.0
K2O	6.5	6.8	4.8	7.7	7.3	7.5	7.74	7.2	7.1	7.5	7.2	4.8	6.6	6.2	5.1	7.1	7.6	7.9	8.2
Sum	95.3	100.0	100.0	100.0	100.0	100.0	100.0	100.0	100.0	100.0	99.8	99.7	100.0	99.7	100.0	100.0	100.0	100.0	99.9
Na / (Na + K)	0.76	0.76	0.84	0.74	0.76	0.76	0.75	0.76	0.75	0.75	0.76	0.84	0.76	0.77	0.81	0.77	0.74	0.73	0.72
Ne	*74.9*	*74.9*	*76.5*	*57.8*	*72.6*	*72.2*	*71.0*	*71.2*	*77.2*	*71.4*	*76.2*	*85.2*	*79.8*	*73.2*	*79.8*	*78.5*	*69.5*	*67.7*	*67.0*
Ks	*22.4*	*22.4*	*14.1*	*39.2*	*21.6*	*21.8*	*23.0*	*20.8*	*22.3*	*23.4*	*21.3*	*14.4*	*20.0*	*20.0*	*18.7*	*20.1*	*22.2*	*23.2*	*24.1*
Qtz	*2.71*	*2.72*	*9.4*	*3.03*	*5.84*	*6.08*	*5.99*	*7.95*	*0.53*	*5.21*	*2.49*	*0.45*	*0.17*	*6.83*	*1.55*	*1.44*	*8.27*	*9.07*	*8.99*

	20	21	22	23	24	25	26	27	28	29	30	31	32	33	34	35	36	37	38
SiO2	44.9	44.3	46.89	46.6	44.5	47.0	48.0	39.3	36.3	36.5	38.5	41.8	42.6	41.3	40.6	37.1	46.7	44.4	44.2
Al2O3	29.0	30.0	30.61	30.3	28.2	31.2	30.3	29.9	27.2	27.0	26.0	32.7	34.8	32.7	32.4	28.6	37.7	34.7	34.4
Fe2O3	3.0	2.8	1.56	1.6	4.6	-	-	1.7	2.5	3.3	3.4	1.9	1.0	1.7	3.3	3.9	1.1	1.5	1.7
MgO	-	-	-	-	-	-	-	-	-	-	-	-	-	-	-	-	-	-	-
CaO	0.5	1.1	-	-	-	-	-	-	0.3	-	-	-	-	-	-	-	-	-	-
Na2O	15.1	13.6	13.76	14.7	13.5	14.2	15.7	11.7	11.0	11.1	11.6	13.0	14.6	12.4	13.1	10.9	14.7	12.9	14.1
K2O	7.5	8.2	7.16	6.8	9.2	7.5	6.1	6.2	6.2	6.7	6.5	6.5	6.6	7.1	6.7	6.8	7.4	6.7	6.3
Sum	100.0	100.0	99.9	99.9	99.9	99.96	100.02	88.7	84.6	850	86.0	96.0	99.7	95.3	96.4	87.2	107.5	100.2	100.5

Na / (Na + K)	0.75	0.71	0.75	0.76	0.70	0.69	0.80	0.74	0.73	0.72	0.73	0.75	0.77	0.73	0.75	0.71	0.75	0.75	0.77
Ne	*69.9*	*67.5*	*66.3*	*68.7*	*65.5*	*65.1*	*69.0*	*70.2*	*70.6*	*70.0*	*68.7*	*72.5*	*75.3*	*70.3*	*73.8*	*70.8*	*72.6*	*70.8*	*74.1*
Ks	*21.2*	*24.4*	*21.6*	*19.9*	*25.6*	*22.8*	*17.6*	*23.2*	*23.7*	*24.7*	*22.7*	*22.5*	*21.9*	*25.1*	*21.4*	*25.2*	*23.3*	*22.9*	*20.6*
Qtz	*8.93*	*8.03*	*12.1*	*11.4*	*8.97*	*12.1*	*13.4*	*6.57*	*5.63*	*5.37*	*8.66*	*5.04*	*2.86*	*4.56*	*4.78*	*4.02*	*4.20*	*6.39*	*5.33*

Table 10: Representative nepheline analyses for xenolithic material. Analyses 1 -2 = OLX 4; 3 = OLX 3; 4 – 8 = OLX 2; 9 – 16 = OLX 1; 17 – 21 = OLX 14; 22 – 26 = OLX 15; 27 – 32 = OLX 17a; 33 -38 = OLC 2

In a similar way to the nepheline analyses, it is possible to plot alkali feldspar chemistries on a $NaAlSi_3O_8$ – $KalSi_3O_8$ – SiO_2 ternary plot (Figure 4.24). Crystallisation of feldspars occurred at lower temperatures than that of the nepheline, which conforms with them being later crystal phases. Again there appears to be a trend from those rocks crystallised from a magma body and those which have experienced fenitisation processes resulting in the recrystallisation of alkali feldspar, with the former crystallising at the higher end of the temperature range than the latter.

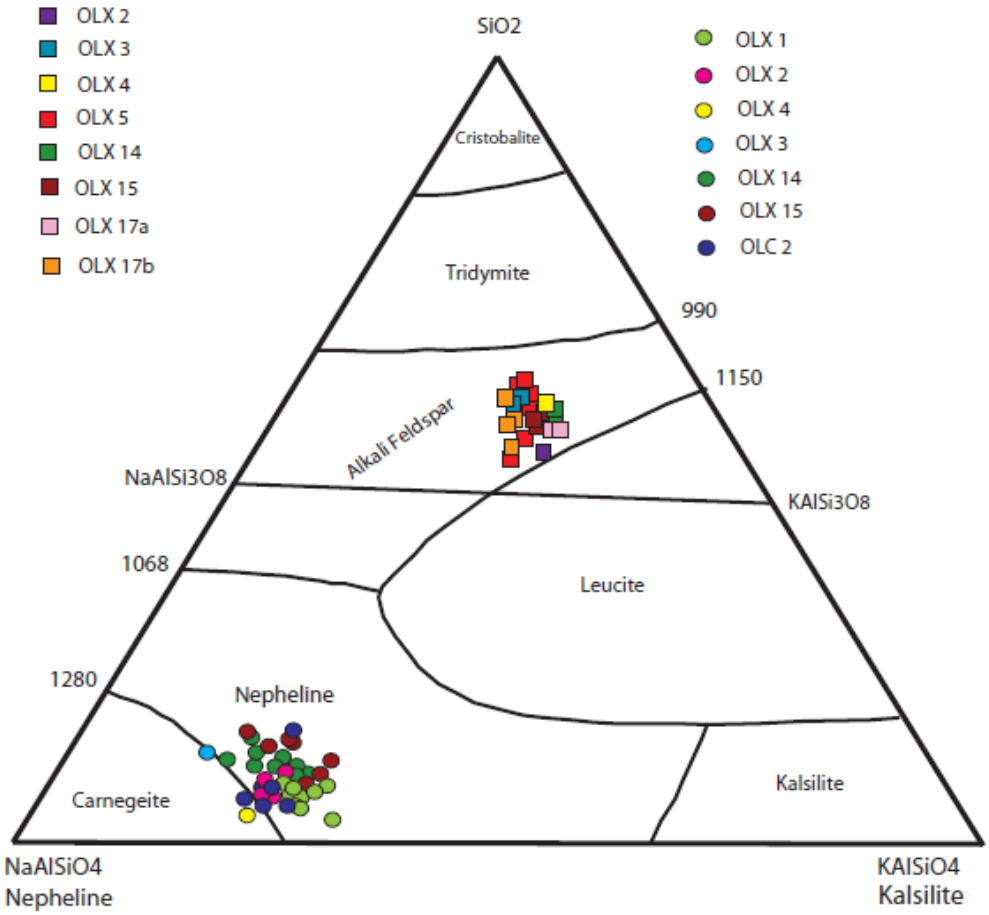

Figure 4.24: Ternary system quartz - nepheline – kalsilite. Nepheline analyses in coloured circles, alkali feldspar in coloured squares.. Adapted from (Hyndman, 1985).

4.4.5. Accessory mineral phases

4.4.5.1. *Perovskite*

Only one sample of those analysed from the xenolith suite contains perovskite ($CaTiO_3$) which was recognised initially by SEM analysis and later WDS EMP analysis in order to collect rare Earth element data. Ijolite OLC2 contains approximately 5% perovskite within the groundmass of the non-metasomatised part of the xenoliths, forming subhedral to anhedral crystals often enclosed by pyroxene and located next to other REE-bearing minerals such as titanite or apatite. Perovskite found at Lengai is rich in sodium in comparison with other occurrences of perovskite but contains less total REE than other carbonatite – silicate hosted perovskite. Those analysed in OLC 2 are also comparable to previous studies of perovskite at Lengai (Dawson et al., 1995) as shown by table 11 below and Figure 4.25. Perovskites are argued to be a late stage crystallisation feature.

	1	2	3	4	5	6	7	8	9	10	11
Na_2O	0.6	0.89	0.5	0.35	0.54	0.8	0.74	0.99	1.14	0.58	1.58
CaO	38	38.9	39.3	39.5	39.3	37.9	37.37	37.2	36.78	37.94	33.97
SiO_2	0	0	0.1	0.04	0.07	0	0.26	1.00	0.48	0.22	0.32
TiO_2	55.2	54.5	55.5	56	55.4	55.4	53.35	53.69	53.86	53.96	52.12
SrO	0.28	0.44	0.27	0.17	0.17	0.48	0	0.097	0.177	0	0.01
La_2O_3	0.71	1.01	0.27	0.27	0.32	0.53	0.99	1.10	1.12	1.20	1.54
Ce_2O_3	2.27	2.13	1.45	1.01	1.09	0.87	0.75	0.71	0.73	0.87	1.39
Nb_2O_5	1.36	1.48	0.55	0.29	0.3	1.13	0.365	1.19	1.47	0.275	1.758
Fe_2O_3	0.92	0.81	1.1	1.11	1.24	0.91	1.136	0.74	0.58	1.17	0.89
Sm_2O_3	0.09	0.11	0.04	0.03	0.04	0.06	0.029	0.05	0.07	0.01	0.05
Al_2O_3	0.1	0.08	0.1	0.14	0.17	0.09	0.046	0	0	0	0
Sum	99.53	100.4	99.18	98.91	98.64	98.17	95.02	96.81	96.45	96.23	93.69

Table11: Representative EMP WDS analyses of perovskite. OLC2 (7 – 11) compared with those collected by Dawson et al. (1995) (1 – 6). *NB La is calculated from peak and corrected background due to poor background position.*

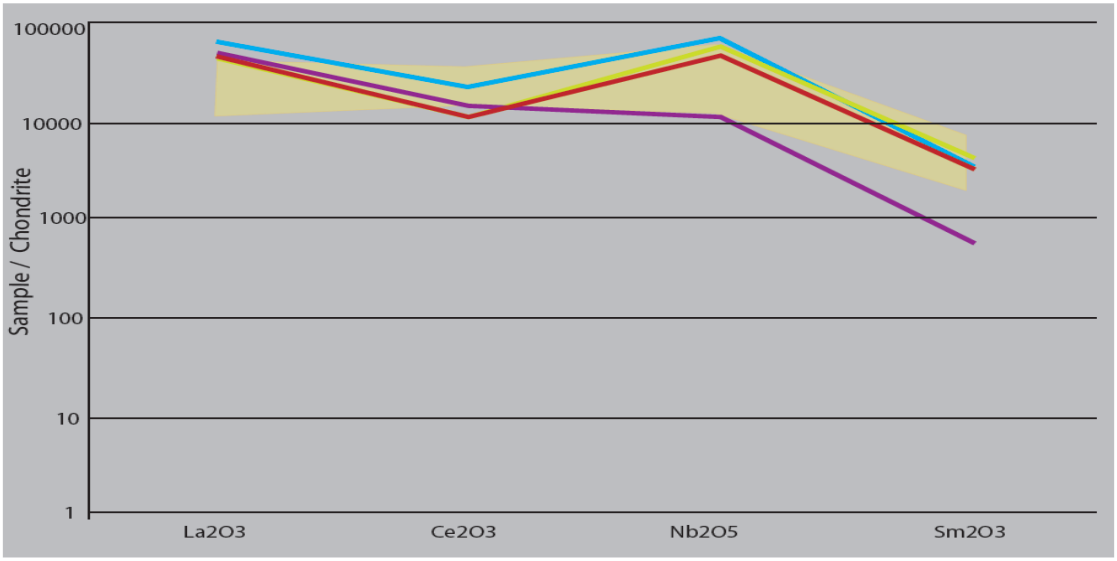

Figure 4.25: Chondrite-normalised rare Earth element concentration of perovskite from ijolitic sample OLC 2 with comparison to previous perovskite compositions (yellow shaded region) recorded by Dawson et al (1994b).

4.4.5.2. Wollastonite

Wollastonite occurs within five of the xenoliths, both as a major precipitating phase, which appears as elongate crystals, and a minor component as acicular intergranular groundmass, with no apparent difference in chemistry between these crystal habits. The average wollastonite analyses given in table 12 show, like other minerals found Lengai, enrichment in Na and Al along with being rich in FeO (up to 1.65 wt%). The wollastonite found within sample OLX 14 appears to contain the greatest enrichment in a number of oxide components along with Fe, including TiO_2 and Al.

	OLX 5 (n=2)	OLX6 (n=3)	OLX14 (n=5)	OLX15 (n=3)	OLX17a (n=5)
Na_2O	0.29	0.38		0.43	0.39
MgO	0.30		0.33		
Al_2O_3	2.09	0.68	1.33	0.8	0.91
SiO_2	46.75	58.15	45.39	50.62	44.04
SO_3	0.01	0.08			
K_2O	0.26	0.29			
CaO	49.93	46.09	40.03	43.53	39.69
TiO_2	0.03		0.52		
FeO	0.50		1.65	0.84	0.53
Sum	*100.16*	*105.67*	*89.25*	*98.22*	*85.56*

Table 12: Representative calculated average compositions of wollastonite from Lengai xenoliths. Data collected by EDS SEM.

4.4.5.3. Titanite

Titanite ($CaTiSiO_5$) is a common accessory mineral and so can be found within all types of xenoliths collected from Oldoinyo Lengai. It occurs as a groundmass mineral forming anhedral crystals indicative of late stage crystallisation. Titanite from Lengai contains significant quantities of sodium and aluminium, typical of an alkaline system. It can also be seen from table 13 that appreciable amounts of incompatible elements, in particular Nb, Sb, V, Zr and Sr, are also incorporated into the titanite mineral structure. This too is indicative of a late stage crystallisation phase which would take up any rare earths from the residual fluid and could be the reason the perovskite in sample OLC 2 appears to contain lower REE than expected with competition between the two minerals. Previous work has concluded that LREE partitioning is only slightly stronger in perovskite than titanite (Dawson et al., 1994b).

	OLX3 (n=1)	OLX4 (n=1)	OLX6 (n=3)	OLX14 (n=10)	OLX15 (n=4)	OLX17a (n=3)	OLC2 (n=6)
Na_2O	-	-	1.02	0.43	0.36	0.53	0.33
MgO	-	-	0.1	-	-	-	-
Al_2O_3	-	0.97	9.57	0.74	1.02	1.16	0.4
SiO_2	33.07	26.04	33.86	25.28	27.50	29.86	29.1
CaO	27.81	30.55	26.56	24.93	24.12	25.61	26.59
TiO2	35.57	40.14	33.15	33.23	33.35	36.84	36.84
Cr_2O_3	-	-	0.12	-	-	-	-
ZrO	-	-	-	-	-	-	1.06
FeO	1.13	1.26	-	2.90	1.29	1.39	1.68
Nb_2O_5	-	-	-	-	0.93	1.34	0.9
Sb_2O_3	1.95	-	-	1.04	-	1.18	1.64
V_2O_5	-	1.03	-	-	0.46	-	-
SrO	-	-	-	-	-	0.84	-
Sum	*99.53*	*99.99*	*104.38*	*88.55*	*89.03*	*98.75*	*98.54*

Table 13: Representative calculated average compositions of titanite. All analyses collected using SEM EDS.

The minerals themselves appear to be fairly homogeneous with little variation between core and rims. It is however interesting that of all the xenoliths collected, the most REE-rich titanite can be found within fenitic unit OLX 17a which contains over 2 wt% incompatible elements which includes 1.18 wt% antimony. This suggests that the fluid responsible for fenitisation was ricn in incompatible elements, which appears true for all samples which have experienced fenitisation or metasomatism suggesting the fluid is late-stage.

4.4.5.4. Amphiboles

Amphibole crystals can be found as a minor component of sample OLX 15 and are thought to be related to the metasomatic process which has altered this unit. The amphibole crystals form small microphenocrysts and interstitial groundmass phases which are subhedral in shape. Their chemistry shows slight variation between crystals but overall they are sodium calcium magnesium amphibole with minor amounts of Ti, Mn and Cl (~1 wt%, ~0.5 wt% and 0.3 wt% respectively). The normalised cation formula matches that of richterite - an amphibole often found within hydrothermally altered mafic igneous rocks belonging to the MARID suite (mica-amphibole – rutile – ilmenite – diopside) (Sweeney et al., 1993, Dawson and Smith, 1977). One analysis also shows the presence of potassic richterite with between 4.19 – 4.55 wt% K_2O.

4.4.5.5. Metal oxide grains

Metallic grains are common feature of xenoliths and different chemical compositions are observed in the suite of xenoliths. Magnetite ($Fe^{2+}Fe^{3+}{}_2O_4$) occurs in the ijolitic units from Lengai and occurs in minor amounts as opaque interstitial crystals. The crystals typically contain 66.83 – 83.82 wt% FeO. A number of impurities from the ideal magnetite formula can also be seen with the presence of up to 12 wt% TiO_2, 0.69 wt% Cr_2O_3, 0.55 wt% V_2O_5, 1.62 wt% MnO, 1.70 wt% MgO and ~3 wt% of an unidentified rare earth element..

Other samples contain abundant crystals (up to 10 %) of Fe-rich sulphide minerals again as interstitial groundmass phases, some often showing cuspate crystal shapes as mentioned previously. SEM analysis of the Fe-rich sulphide grains reveals that the majority contain 56 – 62 wt% FeO and 38 – 43 wt% S with minor amounts of Cr_2O_3 (<0.10 wt%). With an almost 1:1 relationship between Fe and S these sulphides are members of the pyrrhotite series approaching compositions of the troilite end member.

As mentioned above, sample OLX 14 also contains unidentified metallic grains which are enriched in Ag and Cu. Appearing as very small interstitial grains, often in trails, these metal-rich phases contain between 67.31 – 78.77 wt% Ag_2O and 2.39 – 3.17 wt% CuO. It appears that the grains are sulphur-bearing but not metallic sulphides as they only contain up to 9 wt% SO_3. Minor amounts of UO_3 were also detected with up to 3.49 wt% in some grains. Other minor chemical components include 1.18 – 3.54 wt % CaO, up to 5 wt% SiO_2, <1 wt% REE and Al_2O_3.

4.5. Thermobarometry of mineral phases from Oldoinyo Lengai

"Well-calibrated thermometers and barometers are essential tools if we are to fully appreciate the driving forces and inner workings of volcanic systems" – Keith Putirka

The compositions of coexisting minerals in equilibrium can be related by the thermodynamic properties of the minerals and the pressure and temperature conditions of equilibration. Thermometers are assemblages that form by reactions that are sensitive to temperature but not to pressure, whilst barometers are sensitive to pressure but not to temperature. The equations for calculation of both pressure and temperature have been collated by Putirka (1996, 2003, 2008). By comparing the mineral chemistry of each of these phases with the whole rock composition it is possible to generate a pressure and temperature estimate at which the rocks have formed / equilibrated and so provide an indication of the magmatic pathways leading to the crystallisation of the unit. This can be done from pressure estimates using the density of the rocks within the rift region and from temperature by use of geothermal gradient estimates. The derivation of the calculations for thermometers and barometers is beyond the scope of this thesis, but Putirka's review (2008) provides an excellent overview on the theoretical aspects of thermobarometry.

4.5.1. Thermobarometry equations

The xenolithic material from Oldoinyo Lengai contains numerous minerals which can be used to approximate the pressure and/or temperature of equilibrium using the following equations;

<u>Olivine-liquid equilibria (Putirka et al., 2007, Putirka and Tepley, 2008)</u>

Based upon; $MgO^{ol} + FeO^{liq} = MgO^{liq} + FeO^{ol}$

So that;

$$T(^{\circ}\mathrm{C}) = \{15294.6 + 1318.8P(\mathrm{GPa}) + 2.4834[P(\mathrm{GPa})]^2\} / \{8.048 + 2.8352 \ln D_{\mathrm{Mg}}^{ol/liq} + 2.097 \ln[1.5(C_{NM}^{L})] + 2.575 \ln[3(C_{\mathrm{SiO_2}}^{liq})] - 1.41NF + 0.222\mathrm{H_2O}^{liq} + 0.5P(\mathrm{GPa})\}$$

Where $C_{NM}^{liq} = X_{Mg}^{liq} + X_{Fe2+}^{liq} + X_{Ca}^{liq} + X_{Mn}^{liq}$; $C_{SiO2}^{liq} = X_{Si}^{liq}$; $NF = 7 / 2\ln(1 - X_{Al}^{liq}) + 7\ln(1 - X_{Ti}^{liq})$, where X_i^{liq} is the cation fraction of element *i* in the liquid phase and *P* is in GPa.

Clinopyroxene-liquid thermobarometers (Putirka et al., 1996, Putirka et al., 2003, Putirka and Tepley, 2008)

Original thermobarometers for pyroxene were based upon the equilibrium between clino-and orthopyroxene but the limited number of volcanic units which precipitated both pyroxenes led to the development of a thermobarometer for only clinopyroxene and its equilibrium with liquid or whole rock compositions. The thermobarometer is based upon the pressure and temperature dependence of jadeite, diopside and hedenbergite equilibrium with the liquid/whole rock. (Putirka et al., 1996, Putirka et al., 2003).

$$CaFmSi_2O_6^{px} + NaO_{1/2}^{liq} + AlO_{3/2}^{liq} = NaAlSi_2O_6^{px} + CaO^{liq} + FmO^{liq}$$

(where Fm =FeO + MgO)

From this Putirka et al (1996, 2003) derived the following equations for P and T estimates (Putirka et al., 1996);

$$P = -54.3 + 299*\frac{T}{10^4} + 36.4*\frac{T}{10^4}\ln\left[\frac{Jd^{px}}{[Si^{liq}]^2*Na^{liq}*Al^{liq}}\right] + 367*[Na^{liq}*Al^{liq}]$$

$$\frac{10^4}{T} = 6.73 - 0.26*\ln\left[\frac{Jd^{px}*Ca^{liq}*Fm^{liq}}{DiHd^{px}*Na^{liq}*Al^{liq}}\right] - 0.86*\ln\left[\frac{Mg^{liq}}{Mg^{liq}+Fe^{liq}}\right] + 0.52*\ln[Ca^{liq}]$$

Of course when using the thermobarometer the composition of the pyroxene phenocrysts must be subtracted from the composition of the whole rock being used for equilibrium and as most thermometers are P-sensitive, input of a nominal pressure of equilibration is also included.

Alkali feldspar-liquid thermobarometry (Putirka and Tepley, 2008)

Early models for feldspar thermobarometry were based for plagioclase-liquid equilibrium due to its common occurrence, however an extension to alkali feldspar-liquid thermobarometry is presented by Putirka et al (2008) which is based upon albite-liquid equilibrium in a hydrous environment, working best at temperatures < 1050°C;

$$\frac{10^4}{T(\mathrm{K})} = 17.3 - 1.03\ln\left(\frac{X_{Ab}^{afs}}{X_{\mathrm{NaO_{0.5}}}^{liq} X_{\mathrm{AlO_{1.5}}}^{liq} \left(X_{\mathrm{SiO_2}}^{liq}\right)^3}\right) - 200\left(X_{\mathrm{CaO}}^{liq}\right)$$
$$-2.42\left(X_{\mathrm{NaO_{0.5}}}^{liq}\right) - 29.8\left(X_{\mathrm{KO_{0.5}}}^{liq}\right) + 13500\left(X_{\mathrm{CaO}}^{liq} - 0.0037\right)^2$$
$$-550\left(X_{\mathrm{KO_{0.5}}}^{liq} - 0.056\right)\left(X_{\mathrm{NaO_{0.5}}}^{liq} - 0.089\right) - 0.078P(\mathrm{kbar})$$

$$\frac{10^4}{T(\mathrm{K})} = 14.6 + 0.055\left(\mathrm{H_2O(wt\%)}\right) - 0.06P(\mathrm{kbar}) - 99.6\left(X_{\mathrm{NaO_{0.5}}}^{liq} X_{\mathrm{AlO_{1.5}}}^{liq}\right)$$
$$-2313\left(X_{\mathrm{CaO}}^{liq} X_{\mathrm{AlO_{1.5}}}^{liq}\right) + 395\left(X_{\mathrm{KO_{0.5}}}^{liq} X_{\mathrm{AlO_{1.5}}}^{liq}\right) - 151\left(X_{\mathrm{KO_{0.5}}}^{liq} X_{\mathrm{SiO_2}}^{liq}\right)$$
$$+15037\left(X_{\mathrm{CaO}}^{liq}\right)^2$$

4.5.1.1. Sources of error

In his discussion of thermobarometry Putirka (2008) indicates two main sources of error when using experimentally calibrated geothermometers and geobarometers. Firstly there is an inherent error in the precision of the model based upon the ability to reproduce pressure and temperature in a laboratory setting, the attainment of equilibrium and errors related to measuring compositions. The second source of error is how closely the experimental model follows natural systems this is particularly important when deciding which "liquid" to use for equilibrium, i.e. is the whole rock a better representation of the equilibrated liquid or the glass. One method of testing is to determine the partition coefficients (K_D) of the mineral-liquid pair. These are normally based upon Fe-Mg exchange which is P and T independent (Putirka and Tepley, 2008) and can be compared to separately determined K_D values.

For the purpose of this thesis it is assumed that the model error is within acceptable limits and partition coefficients were calculated for all phases used in calculations.

4.5.2.Thermobarometry of mica – olivine ijolite

Ijolite sample OLX 10 contains a number of mineral phases which can be used for thermobarometric estimates including olivine, mica, pyroxene and feldspar. Due to its similarity to previous descriptions of olivine-mica ijolites, the whole rock and glass composition of this sample is assumed to be similar to that of ijolites described by Dawson and Smith (1995) and so these values were used in subsequent calculations. It is estimated that the depth of formation using the olivine mineral chemistry is between 57.8 and 64.3 km on average. However care must be taken using these values. As pointed out previously the olivine crystal

within OLX 10 is mantled by a significant rim of biotite indicative of a reaction rim and so disequilibria between the megacryst and the host unit. If the mineral is not in equilibrium or in fact not a crystallisation product of the host magma, the chemical comparison and subsequent depth estimation should be treated tentatively and possibly even disregarded.

It is therefore important to use mineral phases which have reached equilibrium with the host unit. In the case of sample OLX 10 this involves the thermobarometry of the clinopyroxene crystals. Again by comparing the crystal chemistries of the pyroxene phenocrysts with the glass, crystallisation temperatures were estimated at 900.4 – 1046.0°C ± 62.5°C and pressures between 7.4 and 8.1 kbar ± 0.55 kbar. By roughly equating the pressure to the density of continental crust (2833 g cm^{-3}) and the overlying thickness ($P = \rho gh$), a depth of 26.6 to 29.1 km is calculated. Pyroxene compositions from ijolitic sample OLC 2 were also compared with whole rock compositions resulting in crystallisation / equilibration estimates at pressures between 9.9 – 15.5 ± 0.6 kbar. This is equivalent to depths of between 37 and 59 km, which is in agreement with estimates for OLX 10. This indicates a region beneath the volcanic edifice where ijolitic material is abundant.

4.5.2.1. Evaluation of depth estimates

To a first approximation the depth estimates for the mica-olivine ijolite sample OLX 10 calculated above appear plausible, indicating that the ijolite crystallised near the middle to base of the crust rather than within the mantle region. The temperature and pressure estimates are also consistent with silicate mineral crystallisation of previously determined comparable silicate units - basanites (Figure 4.26). The estimates should be viewed in terms of how they relate to the stability of feldspar within ijolite, which is a low pressure crystallisation feature. From Figure 4.26 we can see that feldspar, such as plagioclase, requires pressures lower than 15 kbar for crystallisation to occur. This condition is met by sample OLX 10 but not by OLC 2. The depth estimate for sample OLC 2 is at mantle depths for this region and so seems unlikely.

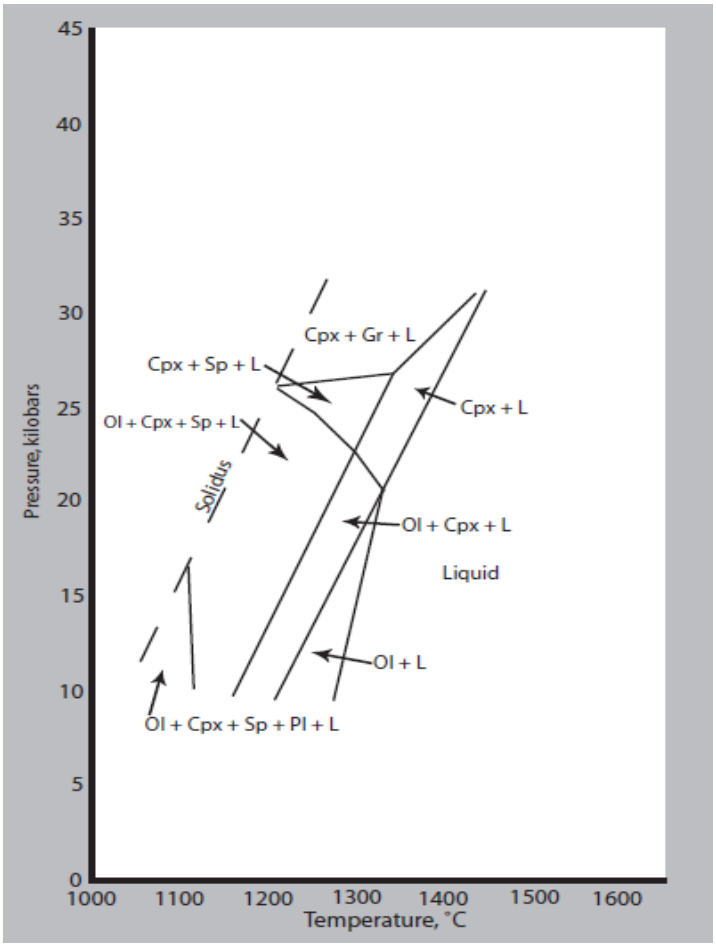

Figure 4.26:Pressure-temperature diagram for basanite crystallisation sequences to illustrate stability of mineral phases at particular P-T conditions (Arculus, 1975)

The erroneous estimates for sample OLC 2 can be attributed to some assumptions relating to the thermobarometry calculations; firstly the thermometers and barometers of Putirka (1996,2003, 2008) are calibrated using a basaltic composition and there is no way of compensating for the whole rock geochemical differences between ijolite and basalt. Secondly the oxidation state of the iron within the clinopyroxenes, with abundant Fe^{3+} rather than Fe^{2+}, will affect the calculations of the pyroxene end-members, along with the abundant Na content, which drives the pyroxene composition well away from jadeitic compositions. Re-calculation of the pyroxenes used in analysis should be completed, subtracting the acmite-aegirine composition in order to bring the compositions back into line with the model thermometers and barometers.

4.5.2. Thermobarometry of fenitic units

Previous studies of metasomatic units also indicates that the generation of a fenites requires the involvement of alkaline (pH >7) fluids at temperatures in excess of 650°C (Figure 4.27)

(Zharikov et al., 2007). This however does not agree with observations made by Le Bas (1987) which suggest carbonatitic fenitisation occurs at temperatures around 550°C and silicate fenitisation at temperatures in excess of 700°C. Additional to this is that if OLX 15 is similar to that of the MARID suite rocks, the presence of richterite restricts the depth to less than 100km (Dawson and Smith, 1977). This is also apparent from feldspar – liquid thermometry which indicates crystallisation / equilibration temperatures of between 606 and 578°C ± 6.1°C.

Temperature (°C)	Estimated Depth (km)
588.3	35.23
597.5	35.78
601.9	36.04
592.4	35.47
600.1	35.94
606.4	36.31
594.1	35.57
597.3	35.77
593.9	35.56
588.8	35.26
578.9	34.66
592.1	35.46
588.2	35.22
588.5	35.24
599.4	35.89
599.8	35.91
590.3	35.35
593.3	35.53
591.3	35.41

585.3	35.05
593.3	35.23
590.3	35.78
597.3	36.04

Table 14: Temperature and depth estimates for fenite sample OLX 17b based upon feldspar-liquid thermobarometry outlined by Putirka et al (2008). Depth calculated from temperature / geothermal gradient, which is estimated at 16.7°C per km (Wheildon et al., 1994, Lysak, 1992)

This result is also in line with seismic studies conducted in Northern Tanzania by the Tanzanian Broadband Seismic Experiment (TBSE) which concluded that the depth to Moho beneath the Mozambique Mobile belt is around 36 – 39 km and between 37 and 42 km under the craton itself ((Dawson 2010) and references therein).

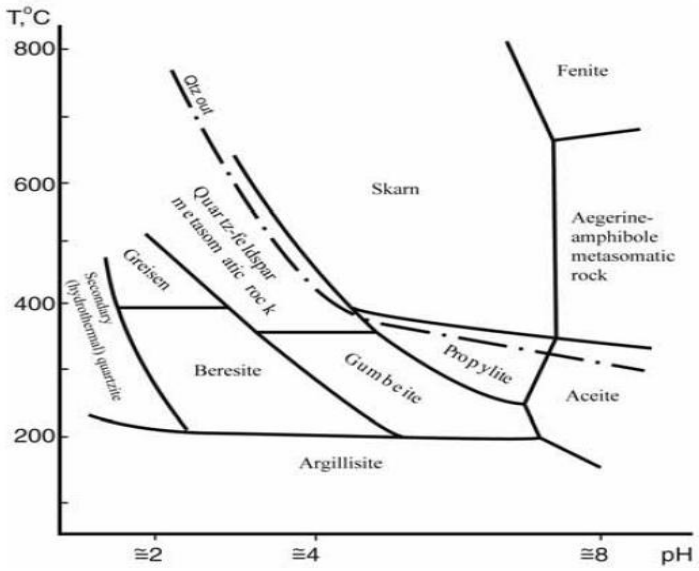

Figure 4.27: Diagram to illustrate the metasomatic families and qualitative T-pH fields for their formation and stability. (Zharikov et al., 2007)

4.6. Discussion - Interpretation of the xenolith suite

The xenolith suite produced from the 2007 eruption appears to cover a number of proposed subsurface environments, most of which are typical of carbonatitic complexes and have been previously documented (Peterson, 1989, Morogan and Martin, 1985, Martin and Morogan,

1988, Dawson et al., 1995, Klaudius and Keller, 2006, Church and Jones, 1995) and so will not be discussed in great length.

The xenolith suite can be crudely divided into two types of xenoliths; primary xenoliths, by which I mean rock units which are typical of the volcanic complex, crystallised from the parental magma and form the majority of the stratovolcano. This includes natrocarbonatite, nepheline, phonolite and ijolite and appears in descriptions of the volcanic stratigraphy by Klaudius and Keller (2006). The second group are lithologies which have been affected by fluid flow or secondary processes and classified as fenites or metasomatised units. It is evident that these metasomatised units have undergone both cryptic and modal metasomatism.

4.6.1. The "primary" xenolith group

The primary xenoliths from Lengai illustrate the ability to crystallise different units from parent magma through a number of physical processes. The formation of the peralkaline silicate material found at Lengai has been discussed in detail by numerous authors with many concluding that the different silicate units are the product of fractional crystallisation of a parent melt (Klaudius and Keller, 2006, Le Bas, 1987, Woolley, 2003, Bell, 1989). The silicate system at Oldoinyo Lengai is thought to behave like other silicate systems (i.e. sequence from basalt to rhyolite) with crystal fractionation and differentiation resulting in the formation of more evolved rock units (Figure 4.28). The parent unit for this process is beyond the scope of this thesis and has been discussed at length by (Klaudius and Keller, 2006, Keller et al., 2006). These authors argue that the parental unit to lithologies seen at Lengai is an olivine melilitite similar to material found at the parasitic cones on the slopes of the volcano.

Figure 4.28: Cartoon illustrating the relationship between silicate rocks associated with carbonatite units with differentiation series resulting in generation of different lithologies. Taken from Woolley (2003).

This process of differentiation and fractionation would leave behind an incompatible element rich residual melt from which groundmass / final stage melts are crystallised. The enrichment of REE's within residual melt with crystallisation and fractionation, results in a concentration of REE's in perovskite and other late stage minerals such as apatite and titanite which can be found in a number of the lithologies. This is typical of alkaline – carbonatite systems and also

has implications for ore deposit prospecting at other carbonatite complexes but not at Lengai (Jones et al., 1996, Bühn et al., 2002, Bühn et al., 2003, Ni et al., 2003, Rankin, 1975, Bühn and Rankin, 1999). Late stage REE – rich material can also be found as interstitial Ce – bearing carbonate within a number of xenoliths and is discussed later in chapter 5 with regards to melt inclusions.

4.6.2.Fenitic and metasomatic xenoliths

4.6.2.1. Evidence of mantle metasomatism

Evidence of metasomatism can be found throughout the Gregory Rift region with all explosive volcanic deposits containing crystals typical of metasomatism, including megacrysts of mica, pyroxene and amphibole (Dawson and Smith, 1988, Dawson and Smith, 1992a, Dawson and Smith, 1992b, Johnson et al., 1997, Dawson et al., 1970, Dawson and Powell, 1969, Rudnick et al., 1993, Koornneef et al., 2009, Aulbach and Rudnick, 2009, Bell and Tilton, 2001, Bell and Blenkinsop, 1987b, Kalt et al., 1997). Ultimately it is thought that the mantle beneath this section of the East African Rift is heterogeneous, containing both a depleted and a slightly enriched source. The cause and timing of this heterogeneity is unknown. Rudnick, McDonough et al (1993) argue it is the result of interaction between carbonate-rich melts / fluids and ultra basic depleted mantle material which has already been affected by melt removal, i.e. komatiite or large basaltic provinces typical of a rift setting, whilst Bell and Simonetti (1996) name the mixing reservoirs as that of EM1 and HIMU. This metasomatised mantle presented in Figure 4.28 and by previous studies is in keeping with the generation of the olivine melilitite which can be produced by partial melting of previously metasomatised mantle material ((Johnson et al., 1997) and references therein).

The evidence of mantle metasomatism, with subsequent fenitisation can be seen in sample OLX 15. This unit has mineral chemistries which place its equilibration at depths of around 50km (according to thermobarometric calculations) and so would have been part of the upper mantle just beneath the keel of the Tanzanian Craton. However, its mineralogy is no longer consistent with upper mantle material, i.e. spinel lherzolite / wehrlite indicating alteration by interaction with melt units generating a metasomatic pyroxenite, with further fenitisation by alkaline-carbonatitic fluids taking place in the lower-to-middle crust.

4.6.2.2. Mantle heterogeneities akin to kimberlites?

Some of the xenoliths collected are thought to provide information on subsurface lithologies and processes. The first of these is sample OLX 10 and the presence of large xenocrysts of olivine and mica which are not directly related to the host ijolite unit. Two lines of thoughts can be applied to the observations made for phlogopite and olivine;

1. **Syngenetic** mineral phases which are either juvenile or reworked lithic fragments.
2. **Xenocrystal** fragments from other rock units of essentially different ages, present within the vicinity of Oldoinyo Lengai.

When viewed in terms of the mineral chemistry it can be seen that these crystals are out of equilibrium with the host unit. I suggest that these crystals have been incorporated into the ijolite prior to crystallisation of the host rock from a lithology similar to that of a kimberlite.

This conclusion is based on the comparison of the mica and olivine xenocrysts with those previously reported for kimberlitic units, as well as the crystal deformation observed within the mica xenocryst. Mica is a dominant crystal found within kimberlite and often shows evidence of kink band deformation; indicative of pre-emplacement deformation in minerals which have undergone energetic processes, e.g. kimberlite eruption or shock (Figure 4.28).

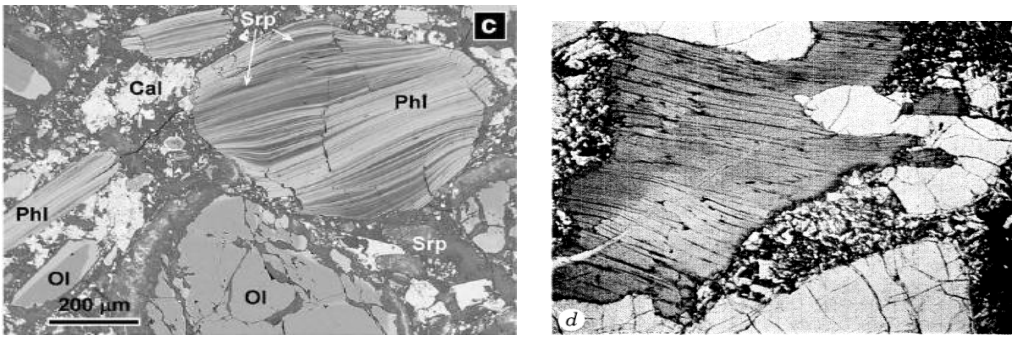

Figure 4.29: (c) Serpentinised phlogopite from Obnazhennaya Kimberlite, Russia (Reguir et al., 2009) (d) phlogopite from Lashaine, Tanzania, both with visible deformation of cleavage bands (Dawson and Andrews, 1972).

Comparison of the chemistry of phlogopite, shown in table 15, demonstrates similarities to kimberlitic material, which although not perfect is difficult to deny. The olivine, however, appears to have a predominantly mantle signature. The ability to crystallise olivine within kimberlitic melts has long been debated with many authors arguing that olivine within present day kimberlite units are xenocrysts incorporated from the source region (Brett et al., 2009,

Dawson and Andrews, 1972, Patterson et al., 2009, Matveev and Stachel, 2009). It is therefore unsurprising that the olivine megacryst within OXL 10 displays a chemistry out of equilibrium with its host unit and typical of mantle material albeit with potential overprinting. There is limited evidence of serpentinisation of the olivine, suggesting limited contact with aqueous fluids which would also indicate that the phlogopite is primary in nature rather than a secondary mineral.

	1	2	3	4	5	6	7	8	9
SiO_2	35.53	37.61	39.08	39.65	40.30	39.98	40.79	39.8	42.21
TiO_2	2.41	0.02	4.4	3.12	0.004	9.13	0	-	1.16
Al_2O_3	15.03	0.48	14.19	13.33	0.01	13.45	0.4	-	10.05
Cr_2O_3	0.78	0.01	-	1.04	0.04	0.71	0.04	-	0.20
FeO	6.22	15.20	7.54	3.24	10.76	3.57	8.32	15.2	6.50
MnO	0.04	0.24	-	0.04	0.17	0.04	0.13	0.32	0.03
MgO	19.95	40.44	20.41	23.14	48.31	18.73	49.45	44.5	24.08
CaO	-	0.23	-	0.06	0.07	-	0.02	-	0.03
Na_2O	0.62	-	1.06	0.16	-	0.06	-	-	0.13
K_2O	9.55	-	9.00	10.09	-	9.64	-	-	10.42
F	0.67		-	1.18	-	-	-	-	
Mg# (Fo%)	*85*	*83*	*82.5*	*92.7*	*88.9*	*90.3*	*91.3*	*84*	*87*

Table 15: Average composition of xenocrysts of phlogopite and olivine from OLX 10 determined by EDS / WDS analysis. (1) Phlogopite megacryst in Lengai sample OLX 10; (2) Olivine megacryst in Lengai sample OLX 10; (3) Mica xenocryst from Lengai slopes; (4) Average kimberlitic mica across globe (Reguir et al., 2009); (5) Average olivine composition from Udachnaya kimberlites (Kamenetsky et al., 2008),(Sobolev et al.); (6) Composition of mantle-derived mica material (Dawson and Andrews, 1972); (7) Composition of mantle-derived olivine (Arai et al., 2004); (8) Mica material from Deeti tuff cone Tanzania (Johnson et al., 1997); (9) Mica from MARID suite xenoliths (Dawson and Smith, 1977)

When plotted on a Ti vs. Cr plot (Figure 4.30) it can be seen that the xenocryst phlogopite from OLX 10 lies within a field similar to that of kimberlitic mica previously studied from the Wesselton Kimberlite, South Africa as well as overlapping with group II kimberlite – orangeites.

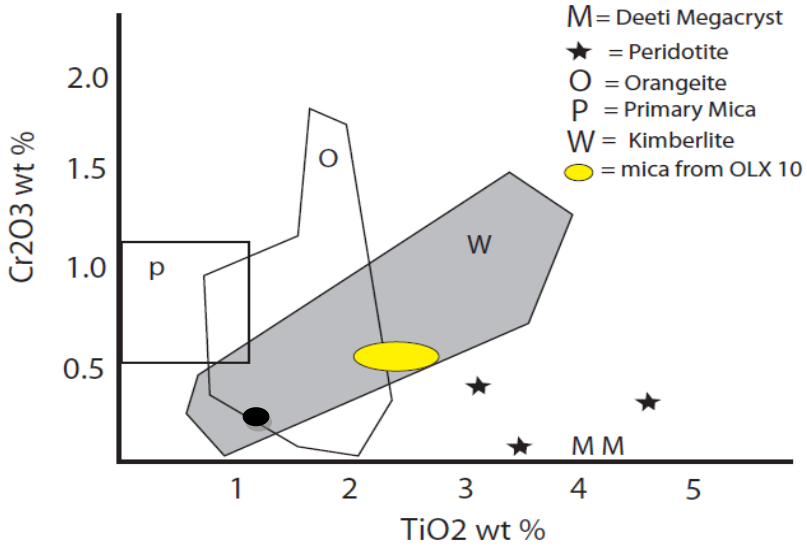

Figure 4.30: Ti vs. Cr plot of mica phases from mantle and kimberlitic units in comparison with that of Lengai sample OLX 10. Yellow are for OLX 10 sample is inclusive of analytical error. Black oval represents MARID suite mica. Adapted from (Johnson et al., 1997)

4.6.2.3. The relationship between kimberlites and carbonatites

A continuum between carbonatites and kimberlite has long been debated (Dalton and Presnall, 1998) and it seems there is no reason why there should not be kimberlite within the vicinity, especially with a diamond mine (Williamson mine) located within 400km of Lengai region. Kimberlite eruptions are extremely explosive caused by the rapid ascent of the magma from depth, often over 200 km down, from within the lithosphere. Recent research presented on the composition of kimberlite magmas shows that their buoyancy, related to their volatile content, can be problematic to achieve with the solubility of CO_2 in previously proposed proto-kimberlite, silicate melts deemed insufficient to drive such an eruption (Russell, 2011, Russell et al., 2012). However Russell (2012) suggests that the presence of carbonate melts would allow the presence of larger quantities of CO_2 with up to 40 wt% within sodium carbonate melts. With this in mind Russell (2012) controversially argues that kimberlites start as sodium carbonatitic material which then sample cratonic mantle, disaggregating peridotite so that the orthopyroxene is the first phase to be incorporated into the carbonatite melt resulting in almost immediate effervescence and providing a driving force for an eruption. This is also used to explain why kimberlite units at the surface appear not to contain orthopyroxene xenocrysts (Kamenetsky et al., 2009, Brett et al., 2009). A logical conclusion of this would seem to be that in a region such as Oldoinyo Lengai where sodium-rich carbonatite is in abundance, kimberlite magmas could be readily generated providing the mantle within this region contains enough orthopyroxene to satisfy the reaction.

However it is vital to point out that not all xenolithic material from kimberlites is devoid of orthopyroxene, with a number of kimberlites containing abundant pyroxene (Stachel et al., 1998, Eggler and Wendlandt, 1979, Garrison and Taylor, 1980, Arndt et al., 2010). It would therefore appear that this process can only be applied to kimberlites which show depletion in orthopyroxene and so is not a universal process.

The similarity of the phlogopite mica within sample OLX 10 to kimberlite can therefore be explained in two main ways; either by an involvement of this mineral in the formation of kimberlite. The incipient melting model favoured by Dawson (1972) requires the melting of a parental garnet peridotite which also contains titanium – rich phlogopite. Melting of this material result in enrichment in potassium, titanium and water as well as a source of mica if these units are broken up, this can then be incorporated as xenocrysts. The incipient melt according to this model will be kimberlitic in composition. However, as table 15 shows, the chemistry of OLX 10 phlogopite does not match that of the mica material from Lashaine volcano, which is argued by Dawson (1972) to be an example of parental mica material to kimberlites. The mica is also compared with that of the metasomatic units of the MARID suite which are suggested to be crystallized under oxidizing conditions from a magma, chemically similar to kimberlite (Dawson and Smith, 1977). Again we can see some similarities between the crystal compositions but the enrichment in Ti, Al and Cr of OLX 10 suggest it is not a sample of MARID mica either.

So an alternative is that the mica has been crystallised within the kimberlitic melt unit itself giving a composition that is kimberlitic. A key question which arises is then; if this mica is incorporated from a unit similar to a kimberlite, why did this unit not reach the surface and form a diatreme? Is it possible to have stalled or failed kimberlite which lack enough CO_2 and water during their ascent so that they no longer have the driving force to push through the craton and erupt at the surface, leaving a metasomatised region, potentially a feeder dyke / sill hypabyssal region, with kimberlitic overprinted minerals which can be incorporated as xenocrysts during ascent of later magma batches. Perhaps this is the result of an incomplete reaction in the model suggested by Russell (2012) due to a lack of available orthopyroxene, within the mantle material, depending on previous metasomatic processes, without which the "process would not be viable" (Russell et al., 2012). A number of questions are still to be answered relating to this model; why is the sub-cratonic mantle in these region opx-poor? Is this related to some earlier metasomatic event possibly the older volcanic systems within the

Rift? There is also no further development on the origin of the sodium-carbonatite melt precursor, which in Russell's model must be primary.

4.6.3.Crustal / plutonic metasomatic processes

Metasomatism and fenitisation are also prevalent within rock units erupted from Oldoinyo Lengai, with the presence of crustal fenitic units. These are primarily formed of K - Na rich minerals including sanidine feldspar, nepheline, alkali-rich pyroxene and amphibole, all of which are indicative of potassic - sodic fenitisation. The ternary diagrams for pyroxene classification presented earlier (Figures 4.18, 4.20 and 4.21) in this chapter are annotated with a suggested trend for the compositions expressed across the rock units from Oldoinyo Lengai. For each diagram it is seen that the pyroxenes appear to become more sodic in composition with progression away from primary rock units associated with the volcano – that is to say that phonolites, nephelinites and ijolites tend to have pyroxene of diopsidic composition whilst units identified as being affected by fluid flow are now dominated by aegirine – augite pyroxene. This type of trend is visible across all of the classification diagrams and matches that proposed by Dawson and Smith (1995).

The fenite units conform with Morgan's (1994) view of equilibration of the same fluid with a different protolith which causes the variation observed between each type of fenite and so subsequently sampling of different sections of the metasomatic aureole around the magma body must have occurred, from sample OLX 3 - a contact fenite which has been subject to numerous phases of fenitisation, a number of high grade fenites (OLX 4, 8, 13, 14 and 17a) which would occur at a slight distance from the intruding magma and finally medium grade fenites (OLX 6 and 17b) which occur further out still from the intrusion. The gradation in fenites is based upon the mineralogy present including phases such as wollastonite and sanidine, which according to Morogan (1994) only occur within high grade units. The presence of relict minerals is also only possible within low-to-medium grade units. These evaluations of grade of fenite also conform to earlier work which indicates that relict quartz and feldspar should occur in fenitic units which are around 250 – 450 m from the intrusion, corresponding to sample OLX 17b (Rubie and Gunter, 1983). The higher grade fenites (OLX 4, 8, 13, 14 and 17a) are thought to conform to Rubie & Gunter's zone III (90 – 160 m) with no relicts and abundant aegirine-augite whilst fenite OLX 3 samples a region of between 0 and 90 m from the intrusion.

This pattern of potassic and sodic fenitisation is thought to be the product of fluids from an intruding magma body at depths around 30 – 40km within the crust beneath the volcano, based upon the thermobarometry of samples. A depth of 30 – 40km is in agreement with previous work which argues that the presence of sodic fenites is more likely to occur at depths within the crust whilst potassic fenites are located at higher crustal levels (Woolley, 1982). This change in chemistry between sodic and potassic units is the result of alkali loss at a particular Na_2O : K_2O ratio determined by the ratio of these elements within the intruding magma body. Woolley (1982) argues that at higher ratios the first fenitised units will be rich in sodium and as the alkali-rich fluids from the intrusion percolate upwards the sodium content is gradually reduced until it becomes potassium-rich / sodium-free. It is therefore possible to estimate the depth of fenitisation based upon the dominant chemistry to a first approximation.

Previous work by Morogan (1994) argues that Oldoinyo Lengai units are only subject to carbonatite-related fenitisation rather than ijolitic, however previous work on metasomatism of mica pyroxenites by Dawson (1992) argued that it was not possible to determine the source of fenitisation in the absence of composite xenolithic blocks. Morgan's work also disagrees with previous work on fenitisation which argues that the lack of carbonate minerals around ijolites indicates that metasomatic solutions were unlikely to be carbonate-bearing (Le Bas, 1987). One important question becomes apparent from Le Bas (1987) in that he argues that the majority of carbonatite material generated by liquid immiscibility is natrocarbonatitic in nature and due to early alkali loss becomes sövitic and eventually dolomitic and ferrocarbonatitic with fractionation. The question remains as to even with fenitisation caused by fluids emanating from the natrocarbonatitic at Lengai, how does the lava produced in the active crater retain alkalis to still be classified as natrocarbonatitic rather than sövitic? (Figure 4.31)

Figure 4.31: Ternary classification diagram which schematically shows the trend from natrocarbonatite to sövite via loss of alkalis (Le Bas, 1981)

Therefore it seems important to distinguish which magma body and resultant fluids from crystallisation (silicate or carbonatite) cause the fenitisation of the surrounding country rocks and so this will be looked at in further detail in chapter 5 and 6 where a closer look at the fluids

trapped within inclusions will be undertaken and a geochemical model for fenitisation will be presented for the causes and differences seen in the fenitic units.

4.7. Conclusions

Understanding the petrography and petrogenesis of xenoliths produced during explosive eruptions is often the first step towards understanding how the volcanic system is working and evolving with time. It helps provide an initial evaluation of the rock units and highlight areas which require further investigation. It is hoped that this chapter has provided the preliminary grounding upon which geochemical and fluid flow investigations can be built in the subsequent chapters. The following conclusions can be drawn from the work presented in the above chapter on the petrography of the xenoliths suite from Oldoinyo Lengai;

- Variations in lithologies exist beneath Lengai and these are all sampled during large, vent-clearing explosive eruptions such as that of 1966 and 2007.

- The xenoliths collected after the 2007 eruption are generally similar to those that have previously been studied but a few contain new features, not previously documented.

- The presence of a fenitised pyroxenitic unit suggests a heterogeneous, metasomatised upper mantle beneath Oldoinyo Lengai and the Gregory Rift. This mantle was sampled by magma originating from depths with some residence time on its journey to the surface within a chamber located within the crust or volcanic edifice, during which fenitisation processes occurred resulting in a nepheline syenite composition.

- Phlogopite chemistry varies significantly from megacrysts erupted as mica books to xenocrysts incorporated in ijolite material. Xenocrystal mica shows an affinity to kimberlitic material perhaps indicating the presence of kimberlite metasomatised units beneath the Tanzanian craton which have been sampled during magma ascent. This has important implications for heterogeneities within the sub-cratonic mantle within this region of the rift and so the units available for melt production.

- Fenitic bodies provide evidence of extensive fluid flow within the craton, which is responsible for changes in country rock chemistry, forming a region between 30 and 50 km beneath the volcano.

- The presence of fenitic units which appear to be related to fluid loss from a carbonatitic body of magma indicating the presence of intrusive carbonatite beneath the volcanic edifice of Oldoinyo Lengai.

- Previous studies have indicated the fenitisation at Oldoinyo Lengai is the result of carbonatitic fluids. If correct this would suggest that during crystallisation and fluid loss the composition of the intruding magma is changed and so the composition of the magma sampled at the surface may not be the composition of the pristine carbonatite formed at depth.

Chapter 5: A first study on the fluid and melt inclusion occurrence within units of the Gregory Rift

The rock units of Oldoinyo Lengai are subject to interaction with numerous fluids both during magma generation and post-eruption. Characterising these fluids is an important step in deepening our understanding of the volcanic system. One way to characterise the agents causing alteration and also investigate the source of natrocarbonatite, is to use fluid inclusion chemistry. This has not previously been carried out using natrocarbonatite or other material from Oldoinyo Lengai, but should be possible by using fluid inclusions trapped within apatite or fluorite crystals (for fresh material) or calcite or nepheline for altered natrocarbonatite and associated silicate rocks.

5.1. Occurrence of inclusions within Lengai Rocks

It was assumed that all plutonic lithologies or porphyritic lithologies from Oldoinyo Lengai would contain some form of inclusions within the larger crystals, whether they be fluid or melt inclusions. A detailed study of all the lithologies within the xenolith suite collected was therefore conducted and the findings were as follows;

5.1.1.Plutonic and volcanic unit inclusions

The plutonic lithologies investigated for inclusions include ijolite, nephelinite, carbonatite and syenite with the lighter coloured minerals (nepheline, feldspar and apatite) being the main focus due to the ease of identification of inclusions. At low magnification it was determined that the inclusions within the plutonic units are predominantly melt inclusions with no definite identification of fluid inclusions within any crystals, but instead all inclusions appear glassy and crystallised (Figure 5.1). Occurring along growth zones within a number of crystals, these pockets of material are different to that of their host minerals, some with shapes similar to those expected of fluid inclusions.

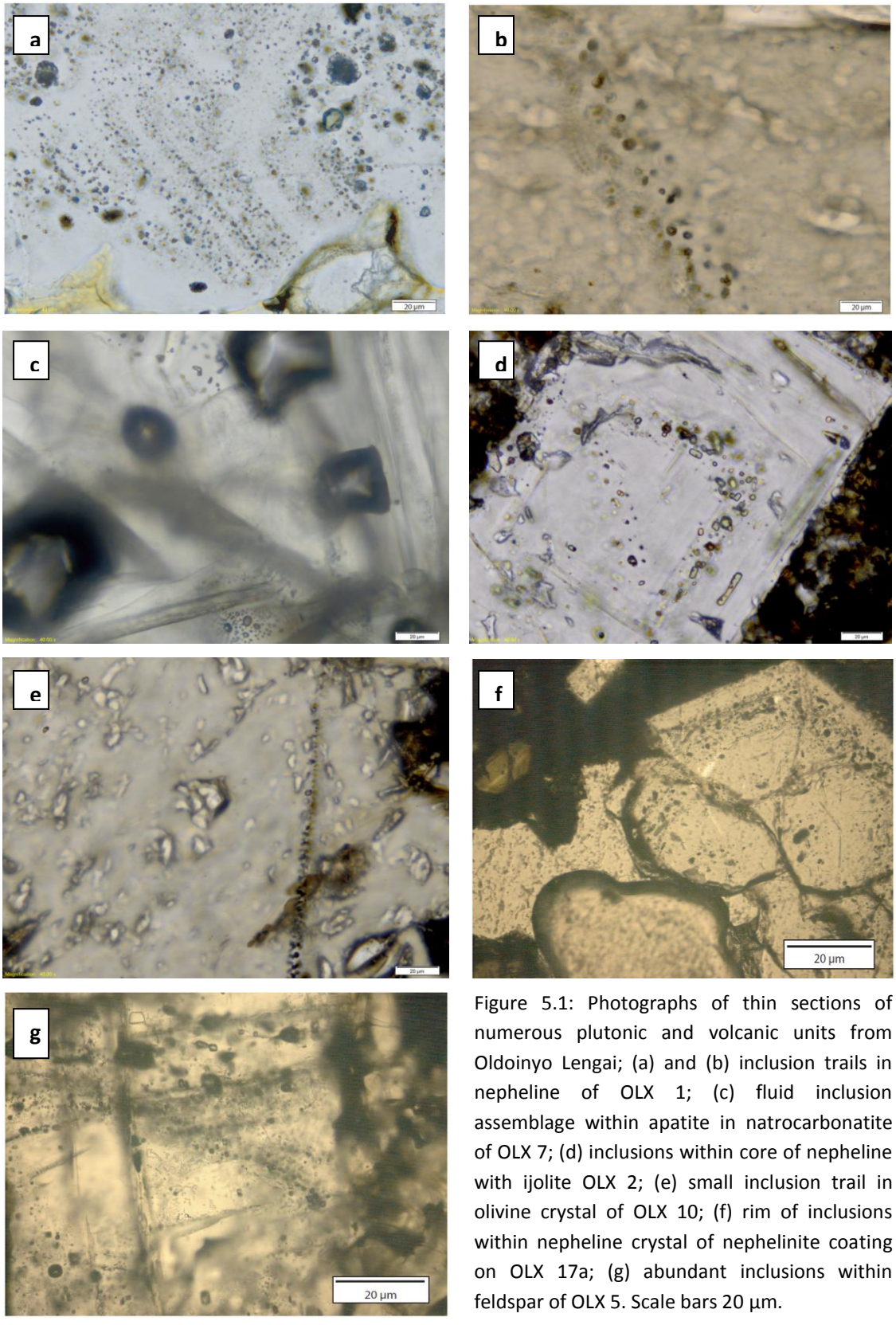

Figure 5.1: Photographs of thin sections of numerous plutonic and volcanic units from Oldoinyo Lengai; (a) and (b) inclusion trails in nepheline of OLX 1; (c) fluid inclusion assemblage within apatite in natrocarbonatite of OLX 7; (d) inclusions within core of nepheline with ijolite OLX 2; (e) small inclusion trail in olivine crystal of OLX 10; (f) rim of inclusions within nepheline crystal of nephelinite coating on OLX 17a; (g) abundant inclusions within feldspar of OLX 5. Scale bars 20 µm.

5.1.2.Fenitic unit inclusions

The xenoliths from fenitic lithologies from Oldoinyo Lengai host the best assemblages of fluid inclusions of the entire xenolith suite. Although appearing similar to those of the plutonic and volcanic units illustrated previously, the inclusions within minerals of the fenite lithologies are easily identifiable as fluid inclusions with extensive trails of inclusions containing visible vapour bubbles, many of which vibrate under the optical microscope (Figure 5.2).

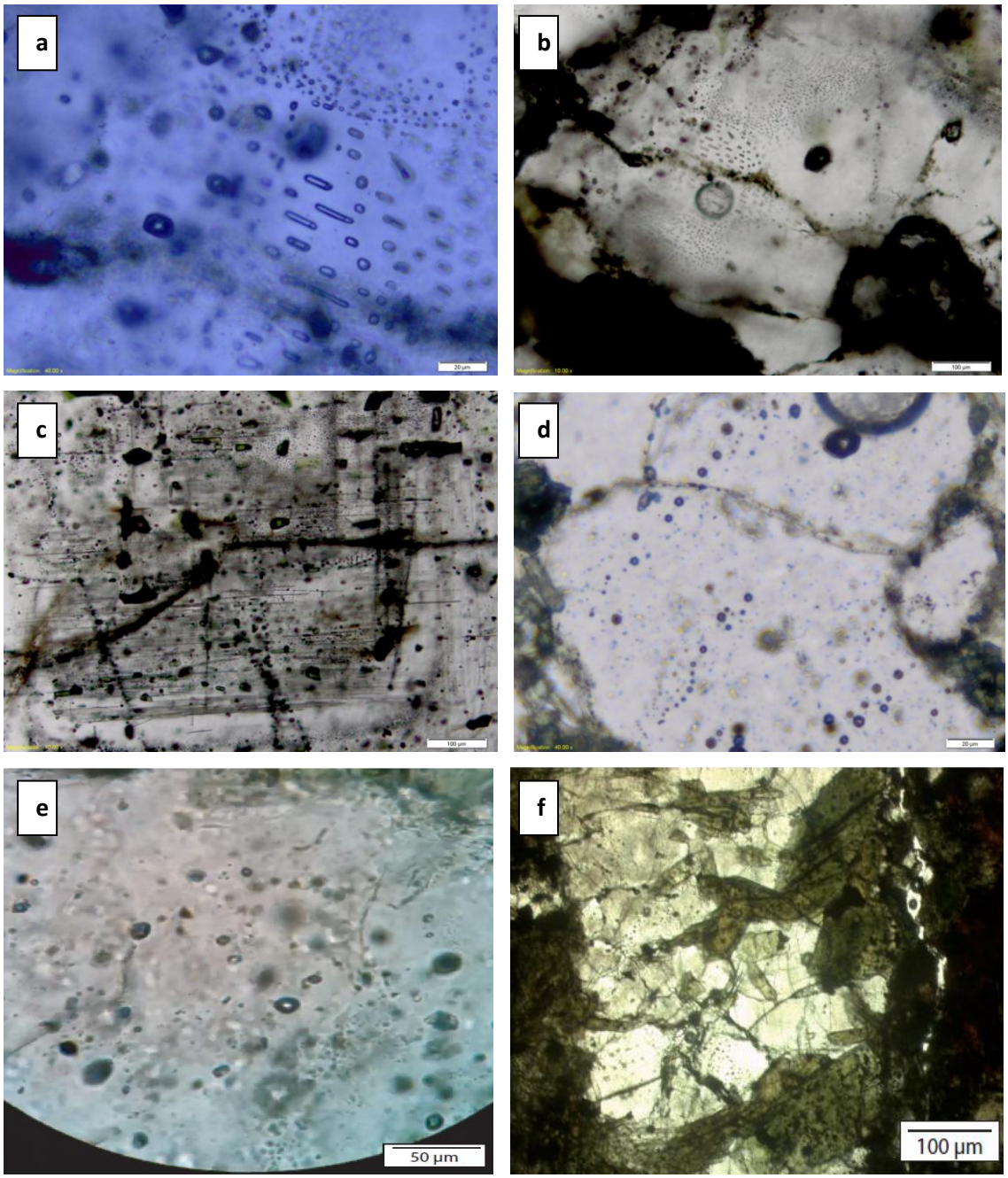

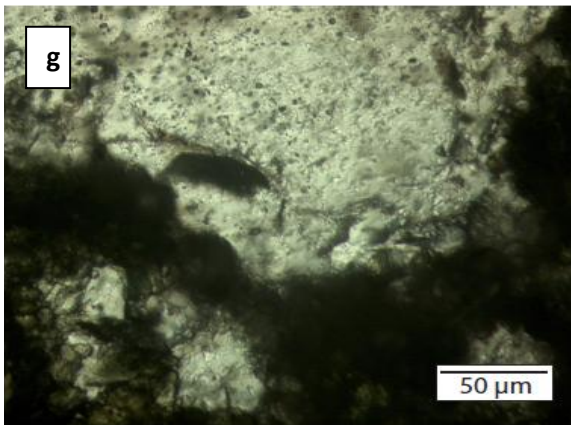

Figure 5.2: Photographs of thin sections of fenite units from Oldoinyo Lengai; (a) and (b) large fluid inclusion assemblage within feldspar of OLX 3 with visible vapour bubbles; (c) complicated pattern of fluid inclusions within nepheline from sample OLX 15; (d) and (e) fluid inclusions trails within relict quartz and feldspar of sample OLX 17b; (f) small inclusion trails in fenite vein of sample OLC 2; (g) trails within nepheline of OLX 8.

It is the fenitic units which form the main part of this study on fluid inclusions, although the plutonic and volcanic units have been subject to Laser Raman Spectroscopy to confirm their content. The remainder of this chapter is therefore mainly dedicated to the petrography and composition of the fluid inclusions within the fenite rocks, although some results from the non-fenitic units will also be presented.

5.2. Introduction to fluid inclusion analysis

During crystal growth from a fluid phase, small pockets of the fluid may become trapped within the crystal, which become isolated from the surroundings, recording the fluid composition and properties at the time of trapping. The best examples of this process are the inclusions found within natural diamonds, which can often be characteristic of the area or mine from which they were found.

Fluid inclusions can occur singularly or within trails, the latter of which are classified as primary, secondary and pseudosecondary depending on their spatial relationship to the crystal edge (Bodnar, 2003). Inclusions are generally caused by the trapping of fluid on surface imperfections, such as screw dislocations, resulting in growth spirals. Primary inclusions can be recognised as those which define growth zones of a crystal, i.e. occur parallel to crystal edges or in the cases where crystals only contain one large inclusion, this is also argued to be primary in origin. Secondary inclusions are the result of an annealed fracture after crystal growth has completed, often cross-cutting primary inclusions with trails that extend to the edge of a crystal. Pseudosecondary inclusion trails occur due to fracturing during periods of crystal growth resulting in a trail which cross-cuts primary inclusions but is eventually abutted by a set

of primary inclusions and so do not reach the edge of the crystal. This classification of inclusion trails is illustrated in Figure 5.3 below.

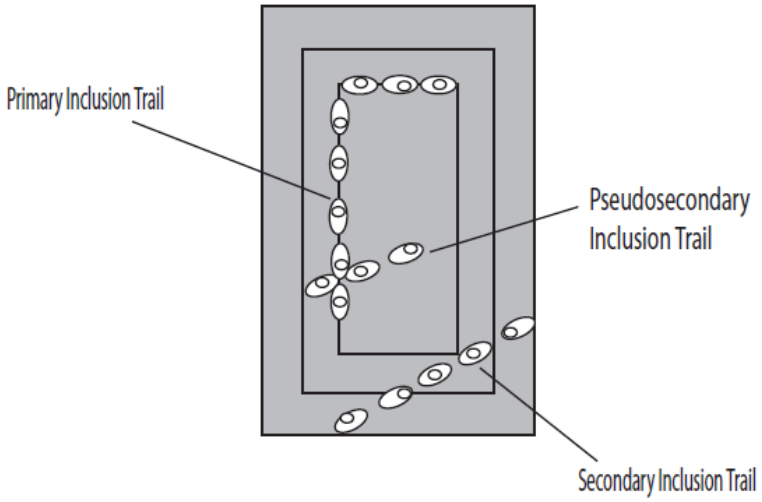

Figure 5.3: Fluid inclusion classification scheme based on position of trails within a crystal and growth zones. (Roedder, 1984)

Once the trails have been classified, it is important to describe the petrography of the inclusions for study in terms of their contents. Fluid inclusions can contain solid daughter minerals, liquid phases and vapour phases or a combination of all three (Figure 5.4). The inclusions within this work will be described as either mono-phase, bi-phase or multi-phase at room temperature. Mono-phase inclusions tend to be liquid-bearing, which can produce a vapour bubble upon heating, but can also be solely vapour-bearing inclusions. Bi-phase inclusions can be either liquid ± vapour or solid. The relative proportion of liquid and vapour determines whether bi-phase inclusions are classified as liquid-rich or vapour-rich. If a vapour bubble occupies <50% of the inclusion, it is liquid-rich and >50% is vapour-rich. Multi-phase inclusions contain liquid + solid + vapour, often with more than one daughter crystal (multi-solid inclusions).

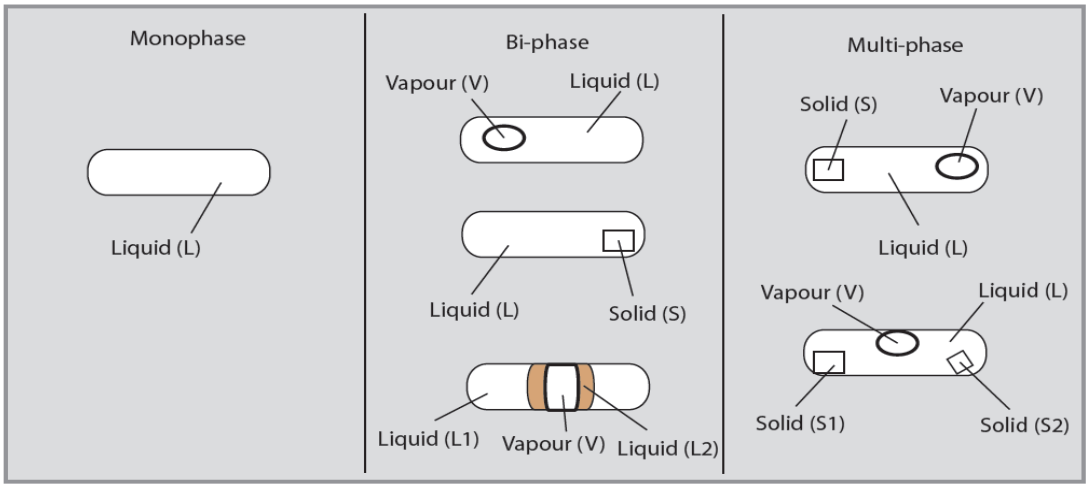

Figure 5.4: Cartoon illustrating the inclusion classification based upon phases present within the inclusions. Shapes and size of vapour bubbles and daughter crystals may vary significantly between inclusions. Liquid L2 represents an immiscible liquid for example hydrocarbon. Based upon Shepherd et al (1985) and Bodnar (2003).

The expected chemistry of fluid inclusions from a carbonatite region would be H_2O – CO_2 ± NaCl, which are in fact common within many geological environments. The presence of CO_2 within inclusions affects the phase equilibria and subsequently the pressure, volume and temperature of trapping (Azbej, 2006). Successful fluid inclusion studies have been completed on numerous carbonatite provinces providing evidence for mantle and magmatic processes, some of which may be applicable to Oldoinyo Lengai.

5.2.1. The CO_2 and CO_2-CH_4-N_2 systems of fluid inclusions

The most common fluids within magmatic systems are formed of combinations of H-O-C-N-S and fluid inclusions can be considered to be based on similar chemistry. The most applicable systems for this study are that of either pure CO_2 or CO_2 ± CH_4 ± N_2 and so a brief overview is provided here.

5.2.1.1. Pure CO_2 system

The CO_2 system is a relatively simple, unary system with three primary phases which can be present; solid, liquid or vapour. The majority of inclusions at room temperature are either mono-phase (L or V) or bi-phase (L +V), with the latter prevailing and easily identified by a CO_2 vapour bubble showing rapid movement around the inclusion (Shepherd et al., 1985). The system has univariant curves where S+L, S+V and L+V coexist, the last of which terminates at a

critical point of +31.1 °C. The invariant triple point for all primary phases for pure CO_2 occurs at -56.56 °C which is where all phases coexist (Figure 5.5).

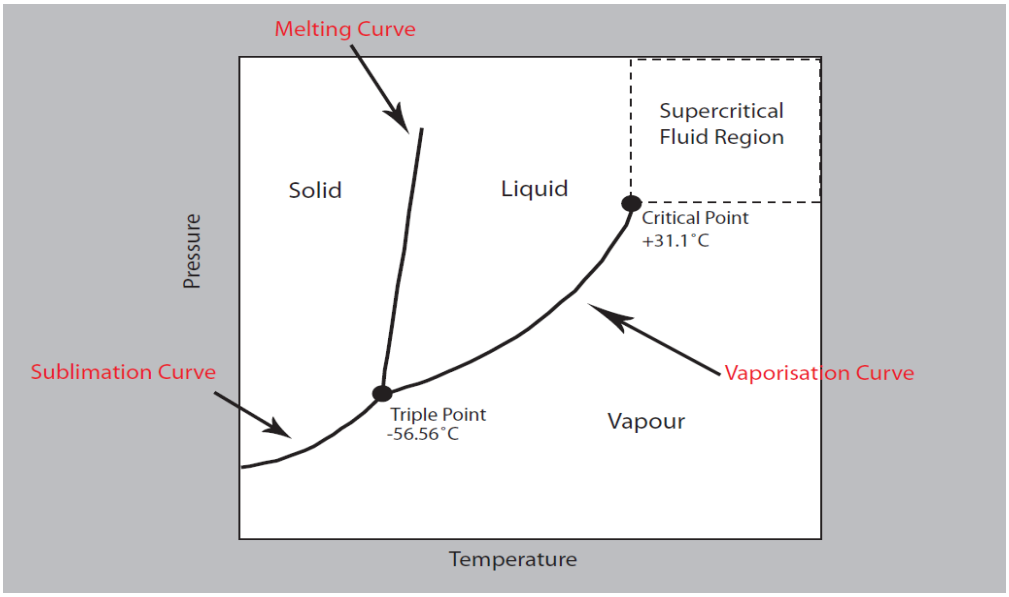

Figure 5.5: Schematic diagram illustrating phase changes and variant points for pure CO_2 system. Modified from (Shepherd et al., 1985).

5.2.1.2. $CO_2 – CH_4 – N_2$ inclusions

Mixed CO_2-CH_4 ± N_2 inclusions are common in natural samples but are almost indistinguishable from CO_2 inclusions at room temperature making their identification with optical microscopy near impossible. The addition of CH_4 results in a lowering of the triple point of the CO_2 phase system and also increases the temperature interval over which CO_2 solid melting takes place (Shepherd et al., 1985). Upon melting CH_4 is partitioned into the vapour phase and so does not contribute to the final bulk composition of the fluid. The addition of N_2 also results in a lowering of the triple point and also complicates the CO_2-CH_4 system and so caution must be applied if N_2 is present. Due to the complicated nature of this mixed system there are no phase diagrams which accurately represent the phase transitions between solid, liquid and vapour which ultimately indicate the density of the fluid inclusion or mole fraction of the vapour.

5.3. Fluid inclusions from carbonatite complexes

Fluid inclusions from Jacupiranga carbonatite-alkaline complex, Sao-Paulo Brazil, are hosted within apatite, calcite and pyrochlore and are present in four different forms; liquid-rich (two-phase), vapour-rich (two-phase), mono-phase (liquid or vapour) and multi-phase (solid or

multisolid) (Costanzo, Moore et al. 2006). Microthermometry of these inclusions was not possible as homogenisation temperatures exceeded the limits of the apparatus. However, Laser Raman Spectroscopy has revealed the presence of individual carbonate solid phases, most commonly sylvite and burbankite. Minor non-carbonate minerals were also present including apatite, pyrite, chalcopyrite and ilmenite. Raman spectroscopy of the liquid and vapour phases revealed the presence of H_2O but no CO_2. The chemistry of the solid phases indicates that carbon dioxide must have been present within the inclusion with subsequent leakage or complete sequestration into the solid phases (Costanzo et al., 2005, Costanzo et al., 2006).

Interestingly it was an abrupt change in chemistry of apatite crystals that provided the most information, with a decrease in REE concentration from core to rim relating to a decreasing number of fluid inclusions into which these elements partition. Costanzo et al (2006) argue that the lack of fluid inclusions in the rims of the apatite represents a lack of fluid in the carbonatite magma during final stages of crystallisation. A number of mechanisms may be employed to generate a loss of fluids from apatite crystals but the authors argue for the removal of the growing crystals from a fluid-rich magma to a fluid-poor magma region, essentially arguing for a stratified magma chamber. This study therefore allows some understanding of magma chamber processes.

The study of fluid inclusions in carbonatitic regimes can also be used to understand the composition of pristine carbonatite prior to element-loss during cooling and crystallisation. As stated previously the majority of carbonatites on Earth are Ca-Mg in composition, many with extensive fenitised zones showing Na-K metasomatism. It seems reasonable to suggest that the compositions of carbonatites exposed at the surface have experienced some deviation away from their original / pristine composition as a result of fluid loss which can be trapped and preserved as fluid inclusions in country rocks (Bühn and Rankin, 1999). Kalkfield carbonatite complex, Namibia, is sövitic in composition and shows a fenitised zone of country rocks along with autometasomatism causing enrichment in Fe. The majority of fluid inclusions within quartzite country rock are aqueous with solid daughter minerals / inclusions. Only 28% of inclusions are mixed $H_2O - CO_2 \pm$ solids and 2% represent pure CO_2 inclusions. Trapped carbonatitic fluid can be further divided into 3 components, as shown by Figure 5.6 (Bühn and Rankin 1999).

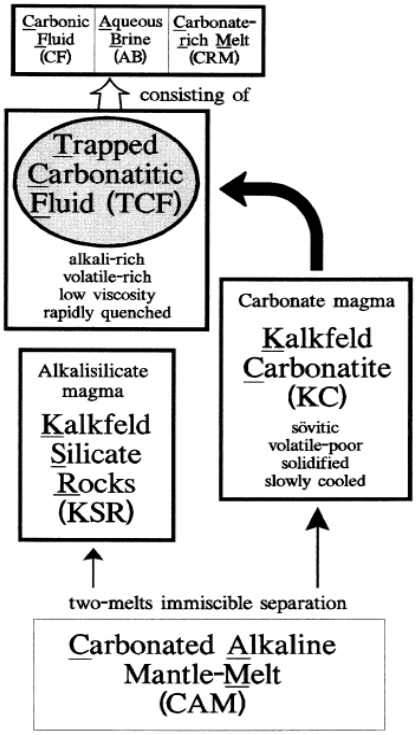

Figure 5.6: Proposed relationship and genesis of fluids found at Kalkfield, Namibia. (Bühn and Rankin, 1999)

The aqueous phase is argued to be Na-K-Ca brine with detectable chlorine present in similar compositions in all inclusions with an aqueous phase. The carbonic phase is predominantly CO_2 as revealed by microthermometry, but Laser Raman Spectroscopy also reveals the presence of CH_4. Identified solids within fluid inclusions from Kalkfield are listed in the table below in order of decreasing abundance. The presence of these minerals can determine the type of fluid trapped. In this instance a highly alkali, halogen and REE-rich carbonatitic fluid has been captured within fluid inclusions (Bühn and Rankin, 1999). This mineral assemblage is also similar to that of the work of Costanzo et al (2006) indicating that solid minerals within carbonatitic fluid inclusions are well constrained and fairly predictable.

Table 16: Identified solids in fluid inclusions of Kalkfield carbonatite complex. (Bühn and Rankin, 1999)

	Ideal formula	Elements detected by SEM-EDX	Elements detected by SXRF	Confirmed by Laser Raman	Mass ratios
Nahcolite	$NaHCO_3$	O, Na		*	
Halite	NaCl	Na, Cl, K			
Burbankite	$(Na,Ca)_3(Sr,REE,Ba)_3(CO_3)_5$	O,Na,Ca,Sr,Ba,LREE	REE,Sr,Ba,Y,Th,U	*	Na/Ca = 1.0 to 4.3
Sylvite	KCl	K,Cl,Na			
Fluorocarbonate (Rouvilleite ?)	$Na_3(Ca,Mn,Fe)_3(CO_3)_3F$	O,Na,Ca,F,Mn,Fe,Cl			Na/Ca = 0.3 to 2.5 Mn/Fe = 2 to 8 Ca/(Mn + Fe) = 2 to 7
Cryolite	Na_3AlF_6	Na,F,Al,Cl			
Mn–Fe–Calcite	$(Ca,Mn,Fe)CO_3$	O,Ca,Mn,Fe	Ca,Mn,Fe		Mn/Fe = 2 to 7, often 3 Ca/(Mn + Fe) = 1 to 7
Alkali–feldspar	$(Na,K)AlSi_3O_8$	O,Si,Na,K,Al			
Feldspathoid (Analcite ?)	$NaAlSi_2O_6$	O,Si,Na,K,Al			
Fluorite	CaF_2	Ca,F,Cl			
Fe–Cu–As–sulfide		S,Fe,Cu,As	Fe,Cu,As		
Fe–Zn–sulfide		S,Fe,Zn	Fe,Zn		
Phosphate (Fluorapatite ?)	$Ca_{10}(PO_4)_6F_2$	O,Ca,P,F,Mn			

The trapped carbonatitic fluid within the inclusions has two interpretations; firstly that it represents the pristine alkali-carbonatite which has evolved from carbonated alkaline mantle melt via immiscibility and is only slightly less alkaline than melts present at Oldoinyo Lengai (Bühn and Rankin, 1999). Crystallisation and cooling then result in the loss of alkalis via an aqueous phase and the Kalkfield carbonatite is the resultant carbonatite. If this was the case why is the expelled fluid not preserved as a fluid inclusion in other country rocks? Fluid inclusions representing expelled carbonatitic fluid from other carbonatite provinces in Namibia have been shown to carry up to 30 wt% $Na_2O + K_2O$ (Bühn et al., 2002).

Secondly, and the favoured interpretation by the authors, is that the fluid is a sample of metasomatic fluid expelled from the magma during its fractionation. This means that the "true" composition of carbonatite would lie somewhere between that of the Kalkfield carbonatite and the trapped carbonatitic fluid. Which of these processes is applicable to metasomatic provinces near Oldoinyo Lengai?

5.3.1. Fluid inclusions from mantle material

Investigation of mantle processes using fluid inclusions requires the study of mantle xenoliths. Inclusions in xenoliths from a region known to have experienced metasomatism, act as remnants of fluids present within the mantle at any one period of time. Like any magmatic centre, Oldoinyo Lengai also carries mantle debris to the surface, with recorded xenoliths including olivine – mica pyroxenites, mica pyroxenites and glimmerites (Dawson et al., 1995, Dawson and Smith, 1992a). Although these xenoliths have been studied in detail and are

thought to represent samples of metasomatised mantle, either directly or indirectly, no attempt to characterise the metasomatic fluid has been made.

Studies from other volcanic centres show that it is possible to obtain some information on metasomatic processes by viewing mantle xenoliths. Spinel harzburgite and lherzolite xenoliths from Tenerife, Canary Islands, contain three types of fluid inclusion; pure CO_2, mixed CO_2 – SO_2 and multi-phase inclusions dominated by silicate glass (Frezzotti et al., 2002). These fluids are thought to be the result of infiltration of a volatile-rich, siliceous, alkaline carbonatite melt into the upper mantle beneath Tenerife. During infiltration, processes of separation ensued resulting in the formation of each inclusion type. The first process resulted in generation of mixed CO_2 – H_2O –NaCl fluids and siliciocarbonatite melt. This melt evolved differently depending on its environment. Melt outside the inclusions (interstitial melt) reacted with wall rocks causing unmixing and the polyphase inclusions trapped in the carbonaceous silicate. During the early stages of the wall rock reactions consumption of the silicate portion of melt resulted in carbonate enrichment and formation of the mixed CO_2 – SO_2 inclusions. The mixed CO_2 – H_2O –NaCl fluid trapped inside inclusions then separated into pure CO_2 and H_2O – NaCl brine.

Microthermometric investigations of the CO_2-rich inclusions along with geothermometry of the mineral assemblages restricts the crystallisation of lherzolite to temperatures of 1000 - 1200°C and pressures of 0.7 – 1.7 GPa (Frezzotti et al., 2002). This therefore provides evidence for the metasomatism of the upper mantle in this region by a carbonatitic melt. A similar study conducted upon carbonatitic melt inclusions from xenoliths in Hungary concluded that xenoliths were generated at pressures of 2.2 – 3.8 GPa and that metasomatic carbonatitic fluids cannot be generated at depths shallower than 70 – 74km (Guzmics et al., 2008a). A corresponding TNT (Ti – Nb – Ta) anomaly is also argued to indicate the presence of either rutile or mica, which are thought to be phases characteristic of subducted material, which therefore provides some indication towards the origin of carbonated material.

The above review of fluid inclusion studies highlights a number of areas that could be investigated at Oldoinyo Lengai yielding different aspects of carbonatite generation and behaviour. A study of the fresh material may provide information regarding depth of formation of these melts. Mantle xenoliths and country rocks from the Lengai vicinity could provide information on two types of metasomatism; that which is occurring in the mantle generating a

possible carbonated source region and local metasomatism, which results from expulsion of fluids during crystallisation. The latter may also allow characterisation of pristine carbonatite material prior to crystallisation. The following work therefore focuses upon the identification and study of fluid inclusions within all of the xenolithic units collected during the field campaign.

5.4. Petrography of inclusions of Oldoinyo Lengai using Optical Microscopy

5.4.1.Paragenetic classification

The fluid inclusions present within the xenolith suite from Oldoinyo Lengai show primary, secondary and pseudosecondary inclusions, which are intrinsically linked to the formation of the host minerals. The plutonic and volcanic rock units typically contain primary and pseudosecondary inclusions which are indicative of the material from which they have formed. The primary inclusions are easily identified as they occur along the growth zones in minerals such as nepheline (Figure 5.1a, d, f). Interestingly, in Figure 5.1a and 5.1d not all of the growth zones are depicted by inclusions trails, with Figure 5.1d in particular only showing primary inclusion trails during the later stages of crystallisation. The presence of inclusions as large assemblages rather than as defined trails complicates the classification in terms of crystal growth and so are treated as primary if they occur towards the centre of the crystal but secondary or pseudosecondary if they are located near to the crystal edges.

The inclusions within the fenitic units are mainly pseudosecondary or secondary in origin if located within relict crystals from the original host rock, such as quartz (Figure 5.2d). Secondary fluid inclusions are generally not useful in fluid inclusions studies, for example in ore petrogenesis investigations, as they do not represent samples of the fluid from which the crystal formed. However in terms of fenitisation processes, secondary trails of inclusions in relict crystals are samples of the metasomatising fluid and so perfect for investigation. Primary inclusions in relict minerals would represent the original fluids involved in the metamorphism of the country rock. In newly precipitated crystals such as nepheline or sanidine feldspar, which have formed during the fenitisation process, the inclusions are primary or pseudosecondary. These again should contain fluids which characterise the fenitising fluid or perhaps different generations of fenitising fluids if pseudosecondary.

5.4.2.Mono-phase, bi-phase or multi-phase inclusions.

As stated previously, no vapour bubbles or daughter crystals are visible within the inclusions of the plutonic and volcanic units of the xenolith suite. They have therefore been classified as mono-phase inclusions until further analysis is completed.

Classification of the assemblages within the fenitic units are much simpler with both multi-phase and bi-phase inclusions present under higher magnification of an optical microscope. The majority of inclusions within the fenites appear at first glance to be liquid-rich, bi-phase inclusions, containing a vapour bubble which occupies <30% of the inclusion (Figure 5.7a). The inclusions are between 15 and 50 µm in length and often contain a thick, dark rim, which is indicative of carbon dioxide. The dark rim is a result of a contrast between the refractive index (RI) of carbon dioxide (1.18) and the host mineral (quartz for example has RI = 1.55) (Shepherd et al., 1985). The vapour bubble can be seen in rapid motion around the fluid inclusion due to the excitation caused by the light of the microscope. A number of the inclusions also seem to produce negative crystal features (Figure 5.7c).

Further analysis of the bi-phase inclusions reveals that a number of them also contain solid salt crystals (discussed in section 5.5 below) which are not visible during optical examination as they are obscured by the dark rim. However it is possible to see multiple solids in some inclusions where the dark rim is absent (Figure 5.7b). The multi-phase inclusions displayed in Figure 5.7b appear to contain up to 3 solid crystals, one of which is opaque and occupies the end of the inclusion. The remainder are colourless crystals of both square and needle-like shape, contained within a colourless liquid phase.

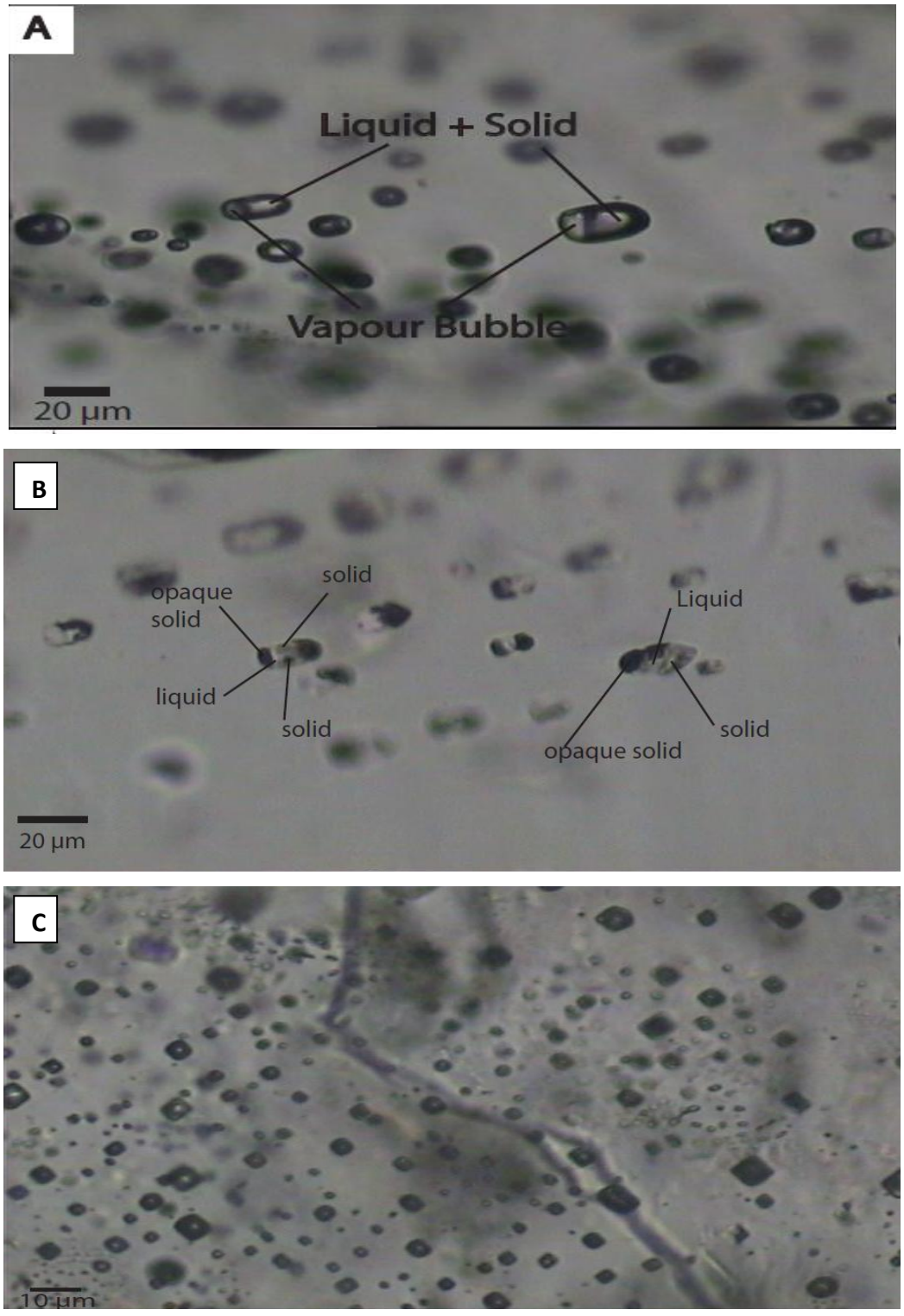

Figure 5.7: Photographs of inclusions from fenitic units illustrating phases present within samples: (a) Clear liquid-rich inclusion with vapour bubbles towards the end of the inclusion; (b) Multi-phase inclusions within fenite OLX 3 with different solid crystals within liquid inclusion; (c) large number of inclusions in assemblage of OLX 17b showing dark rims and negative crystal shapes. All appear as mono-phase inclusions

5.4.3.Trapping conditions

The manner in which the inclusions were trapped – homogeneously so that all inclusions represent samples of the same fluid and appear identical at first, or heterogeneously where variable compositions and phase ratios are trapped at the same time – is important in determining the timing of inclusion assemblage formation and characteristics of the solution at the time of trapping. Figure 5.8 below represents the different morphologies of inclusions that can be expected based upon the trapping conditions (Van den Kerkhof and Hein, 2001). For fluid inclusion analyses it is preferable to study assemblages of homogeneously trapped inclusions as they can provide multiple datasets for the same fluid.

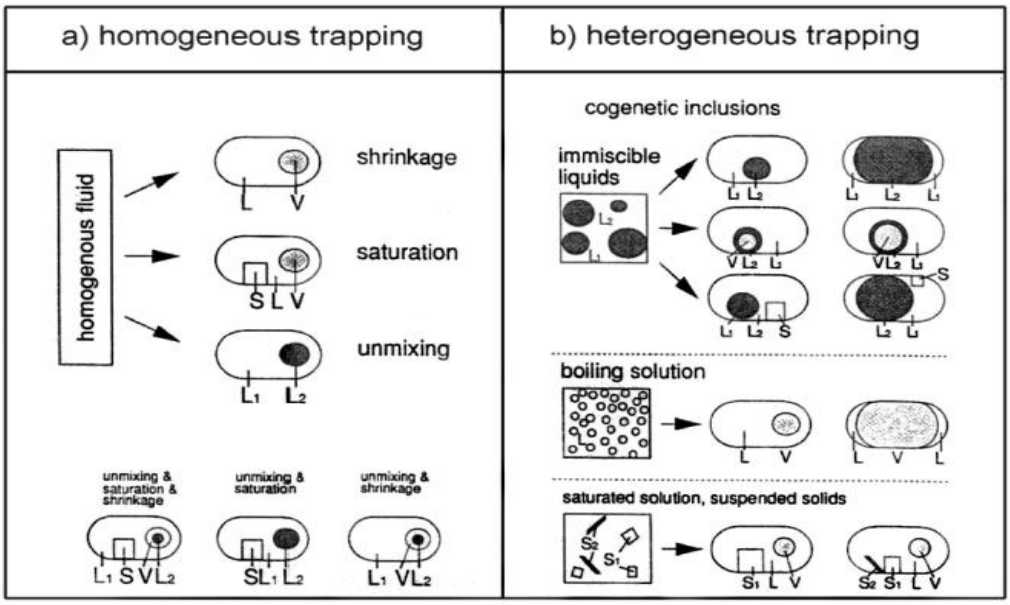

Figure 5.8: Illustration of inclusion morphologies depending on method of trapping. Homogeneous trapping results in inclusions which have similar phase ratios. Upon cooling vapour bubbles and solids may appear. Heterogeneous trapping results in inclusions with variable phase ratios. (Van den Kerkhof and Hein, 2001)

The inclusions analysed within this study appear to be mainly samples of homogeneous trapping with subsequent shrinkage and saturation, generating vapour bubbles and solid crystals. There are, however, examples of heterogeneously trapped fluids from a boiling solution which can be recognised by the presence of a meniscus between the vapour and liquid. It is possible that some of the crystals may be incorporated rather than precipitated, which is another indication of heterogeneous trapping, but it is difficult to determine the difference using optical microscopy (Shepherd et al., 1985).

With the inclusions now classified in terms of their timings of formation and phases present, the next step is to determine the chemical species within the inclusions. This can be completed using two different methods; the first discussed below in section 5.5, is non-destructive Laser Raman spectroscopy which can be used to determine all phases and their chemical composition. The second is microthermometry, which is a tool to determining the density of the inclusions, and shall be the focus of section 5.6.

5.5. Laser Raman Spectroscopy of fluid inclusions

Using the techniques outlined in chapter 2, several inclusion assemblages were analysed using Laser Raman Spectroscopy to investigate the chemical species present. Table 17 below outlines the full details of the inclusion suites analysed, but the main species are outlined below. It should be noted here that all identification peaks quoted below for chemical species are in accordance with published literature (Bühn et al., 2002, White, 1974, Frezzotti et al., 2012).

5.5.1. Solid species

5.5.1.1. Nahcolite

Nahcolite ($NaHCO_3$) is a common mineral within carbonatite regimes and has been identified in fluid inclusions from carbonatite complexes across the globe (Bühn et al., 2002, Bühn and Rankin, 1999, Ni et al., 2003, Rankin, 1975, Buhn et al., 1999). It is identified in Laser Raman Spectroscopy by peaks at 684, 1045 and 1268 cm^{-1}, of which the 1045 cm^{-1} is the most characteristic. During analysis for this study a slight shift in peaks resulted in the identification of nahcolite at wave numbers between 1033 and 1044 cm^{-1} as well as at 1268 cm^{-1}. The peaks associated with nahcolite were tall, narrow peaks indicative of single crystals of nahcolite up to 5 µm across (Figure 5.9a). Intensity maps easily identify anhedral, crystal-like features within inclusions (Figure 5.9b).

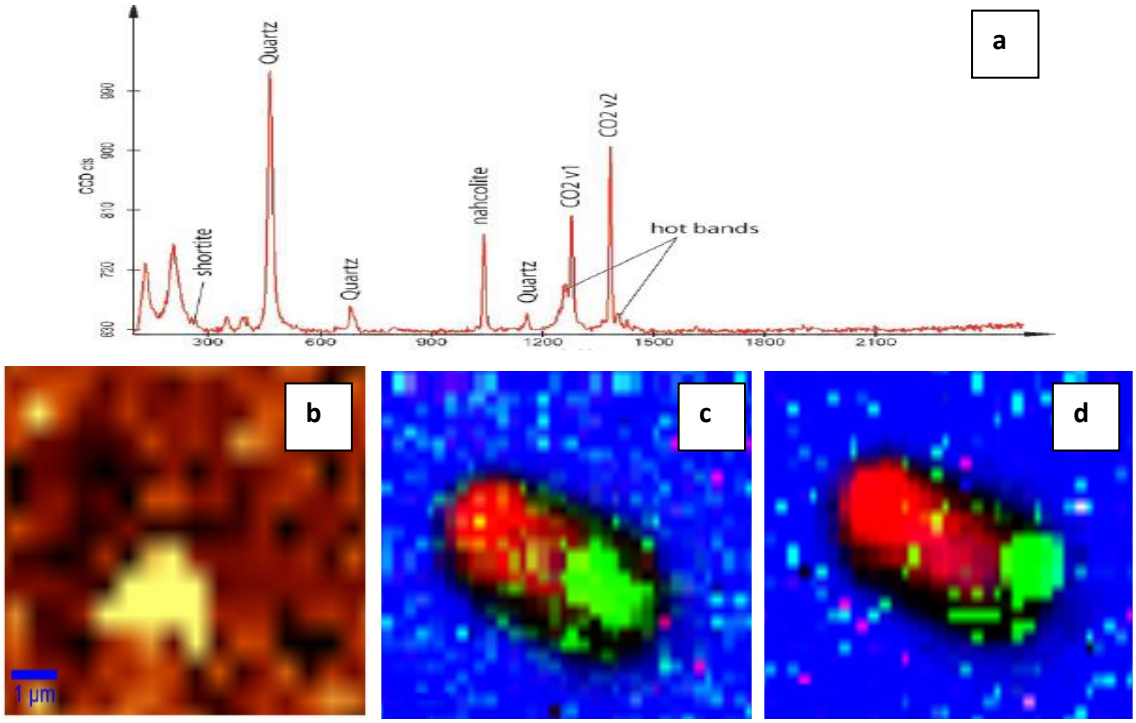

Figure 5.9: Raman Spectroscopy identification of nahcolite. (a) Raman spectra with identified peak at 1044 cm^{-1}; (b) intensity map for wave numbers between 1038 and 1050 cm^{-1} which shows outline of nahcolite crystal; (c) and (d) false colour composite images of inclusion from OLX 3 where blue = sanidine host mineral, red = vapour bubble and green = nahcolite crystal.

Interestingly the nahcolite crystals within inclusions are often not stationary but mobile around the inclusion. This was identified by repeated scans of the same inclusion which show a shift in the location of the 1044 cm^{-1} peak between scans. This is illustrated in the false colour images of Figure 5.9c and 5.9d which indicates the relative position of nahcolite during subsequent scans of the same inclusion. The nahcolite was also only found within inclusions of fenite samples.

5.5.1.2. Shortite and aphthitalite

Minor precipitates of the carbonate mineral shortite ($Na_2Ca_2(CO_3)_3$) were identified within the secondary and pseudosecondary inclusions from fenitic samples. The crystals of this mineral are not as large as those recorded for nahcolite but are still identifiable within the inclusions. The shortite is not mobile like the nahcolite and tends to form crystals which precipitate around the edges of the inclusions of around 1 – 2 µm in size. (Figure 5.10). Shortite has several characteristic peaks for identification including 1090, 1070, 269 and 137 cm^{-1}. A number of these peaks, for example 1070 cm^{-1}, correspond to numerous phases as they

represent C-O bonds and so are not specific to shortite. It was therefore identified using the 269 cm^{-1} peak in tandem with the other peaks present.

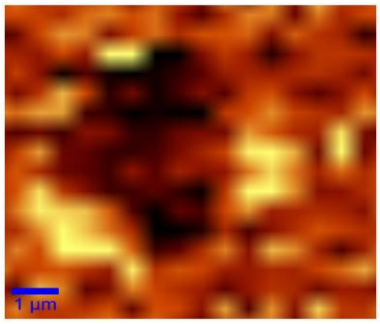

Figure 5.10: Raman intensity map for peak 269 cm^{-1} corresponding to precipitation of shortite around the inclusion edges.

A number of quartz-hosted inclusions within sample OLX 17b contain aphthiltalite ($K_3Na(SO_4)_2$), which is associated with the alteration products of natrocarbonatite. The Raman peaks for aphthiltalite are relatively small due to swamping by other precipitated minerals but clear peaks occur at 990 and 1182 cm^{-1} corresponding to SO_4^{2-} and SO_2 respectively (Burke, 2001). Again the crystals are relatively small and are likely to have precipitated directly from the fluid rather than being captured within the inclusions. The presence of the sulphate-bearing mineral therefore indicates a presence of sulphur within the fluid phase – albeit in small amounts.

5.5.1.3. Apatite

Another common mineral found within carbonatite-related inclusions is apatite ($Ca_5(PO_4)_3(F,Cl,OH)$) and within the inclusions analysed it occurs as either fluroapatite or carbonated apatite with large amounts of REEs in both resulting in high fluorescence in the higher wavenumber region. Care must be taken, however, as apatite can also be a host mineral for inclusions and so it is important to note which apatite signals belong to the inclusion as a daughter mineral and which correspond to host mineral. The characteristic and strongest peak for apatite occurs at approximately 960 cm^{-1} with a second strong peak at 1072 cm^{-1} if carbonated, i.e. contains CO_3. Unlike the minerals above, apatite is found within inclusions both of the fenitic units as well as in primary inclusions of volcanic / plutonic units. It is observed in inclusions as elongate, euhedral crystals approximately 3 µm in length.

5.5.1.4. Carbonate (CO_3) melt

Carbonate-rich melt is a predicted phase to occur within carbonatitic fluid inclusions by the aforementioned model by Buhn and Rankin (1999) in Figure 5.6. It occurs both within the inclusions of fenite units and inclusions within plutonic rock units, forming the main phase in the latter inclusions suggesting they are more likely to be melt inclusions than fluid inclusions.

Like shortite the carbonate melt tends to form a lining on the inclusion walls of a few microns in thickness. Importantly, since a number of expected carbonate salts also contain CO_3 it is important to distinguish between pure carbonate melt and carbonate-bearing minerals. The melt units should have a strong peak between 1075 and 1090 cm^{-1} with smaller peaks at lower wave numbers which provide some indication of the cation present. For example calcite can be identified by a strong peak at 1100 cm^{-1} and smaller peaks at 280 and 710 cm^{-1}.

Of the analysed inclusions a number contained calcitic and sodium-rich melts, as well as a carbonate melt with high concentrations of rare Earth elements causing fluorescence in the higher wavenumber region of the spectra (Figure 5.11b). It is proposed that these melts are likely to be burbankite ($(Na, Ca)_3(Sr, REE, Ba)_3(CO_3)_5$) or bastnäsite ($(Ce, La, Y)CO_3F$).

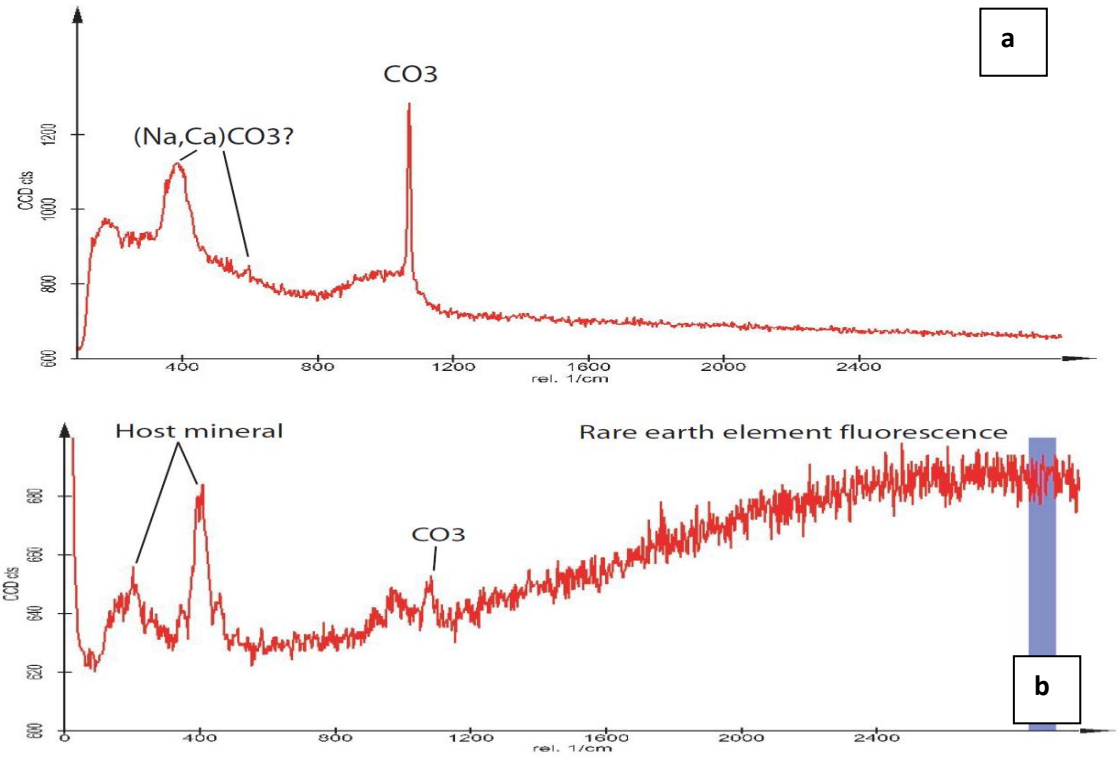

Figure 5.11: Raman spectroscopy spectra of carbonate melt within inclusions; (a) Spectra representing natrocarbonatite (sample OLX 7) with strong CO_3-related peak at 1072 cm^{-1}; (b) REE-bearing carbonate material with large fluorescence caused by REE. CO_3 peak still identifiable at 1075 cm^{-1}

5.5.1.5. Spinel and pyrite

It was noted previously that a number of inclusions contained opaque minerals which are not possible to identify from optical microscopy. Raman spectroscopy on a number of fluid and melt inclusions revealed that the crystals are predominantly spinel-group minerals either magnetite (Fe_3O_4) or chromite ($FeCr_2O_4$). This is evident from Figure 5.12 below which details a scan on a large olivine megacryst (Figure 5.12c) within sample OLX 10. The intensity map in Figure 5.12a reveals that the olivine crystal contains a 50 µm long trail of small inclusions. An intensity map of a peak located at 658 cm^{-1} is shown in Figure 5.12b and corresponds to a characteristic peak of spinel. Further investigation of the inclusion trail also indicated the presence of pyrite (FeS_2) crystallising alongside the spinel. Both minerals appear to form euhedral crystals of around 2 -3 µm in size.

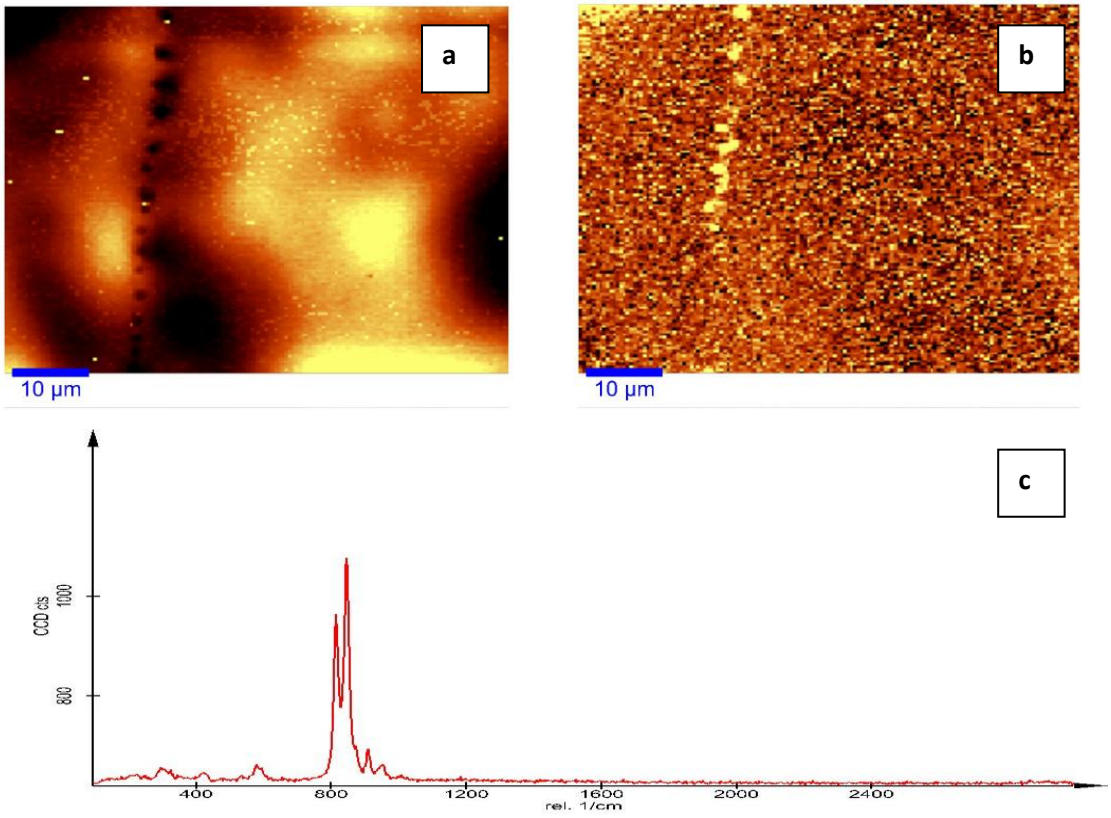

Figure 5.12: Raman intensity maps and spectra from sample OLX 10 olivine-mica ijolite; (a) intensity map for forsterite olivine showing trail of inclusions; (b) intensity map showing inclusions contain spinel (660cm^{-1} peak intensity); (c) Raman spectra for olivine showing characteristic split peak for forsterite at 820 and 850 cm^{-1}.

Spinel is not uncommon within fluid inclusions particularly those of mantle material (Andersen and Neumann, 2001), but is generally argued to be a captured mineral rather than a

precipitated phase. The fluid inclusions studied by Andersen and Neumann (2001) contained small platelets of spinel argued to be entrained from the spinel-harzburgite – the source rock for the mantle xenoliths. The presence of spinel within the suggested mantle-derived olivine of sample OLX 10 would seem to indicate that the source region of this olivine may be spinel-bearing. This would indicate a source within the uppermost mantle (<120 km), as at greater depths garnet becomes the stable Al-bearing phase (Robinson and Wood, 1998).

5.5.1.6. Melanophlogite

Crystals of different composition were also identified within the inclusions from the non-fenitic samples. At approximately 4-6 µm in size and forming what appear to be cubic crystals (Figure 5.13a), further Raman investigation suggests they may be melanophlogite ($C_2H_{17}O_5.Si_{46}O_{92}$). As discussed in Chapter 1 melanophlogite is a low temperature, late stage polymorph of SiO_2 with structure-stabilising guest organic molecules and occurs as a clathrate-type silicate framework (Skinner and Appleman, 1963, Nakagawa et al., 2001, Zak, 1972, Kamb, 1965, Gies et al., 1982), which has previously been reported to occur within the 2006 lava flow of Oldoinyo Lengai (Beard et al., 2009). Mineral separates of melanophlogite from the 2006 flow were also analysed using Raman Spectroscopy and a comparison with the material found within the inclusions is presented below (Figure 5.13c).

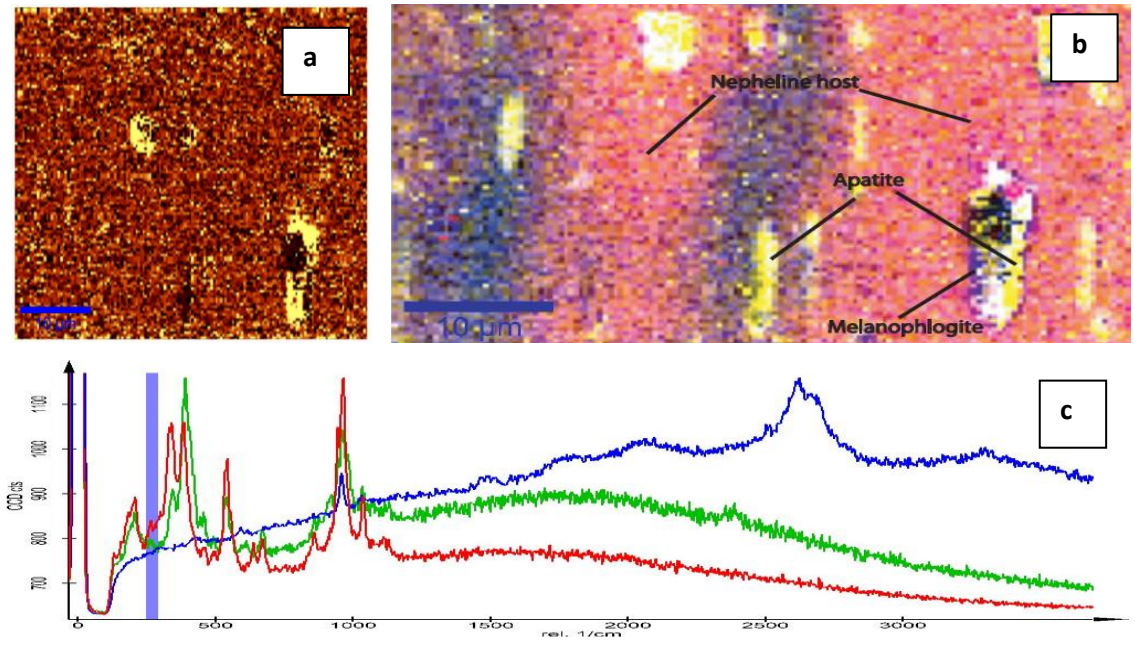

Figure 5.13: Raman spectroscopy investigation of melanophlogite within inclusions. (a) intensity map for peak 810 cm-1 showing location of melanophlogite within inclusions; (b) false colour composite image same elongate inclusions with host nepheline (red), apatite (yellow) and melanophlogite (blue); (c) Isolated Raman spectra of melanophlogite with mineral separates (red and green) compare to inclusion (blue).

Work on the Raman peaks for melanophlogite indicate peaks at 275, 350, 595 and 810 cm^{-1} with peaks at >1270 cm^{-1} indicative of the guest molecule present (Kolesov and Geiger, 2003). From the spectra above we can see that there is a match between the spectra from the mineral separates (red and green spectra lines) with that measured within a fluid inclusion (blue line), although it is not a perfect match. The peak around 810 cm^{-1} is the best matched peak, although it has undergone some shift and so it would seems plausible that fluid inclusions from Oldoinyo Lengai also contain this unusual clathrate. The peaks at higher wavenumbers may be the result of the guest molecule present or interference from other chemical species present within the inclusion. They do not correspond to any peaks identified by Kolesov and Geiger (2003) and so it seems more likely that they represent interference, in particular from the apatite which also precipitates within the inclusions.

Table 17: Summary table of all rock units studied using Raman Spectroscopy and the main chemical species found with listed identification Raman peaks. Inclusions are divided in the table according to the host mineral rather than standard classification. Additional notes provide some indication of inclusion density.

Sample	Host Mineral	Classification	Phases Present	Key Raman Peaks (cm^{-1})	Additional Notes
OLX 17b	Sanidine	Bi-phase (V+S) pseudosecondary	CO_2 (V), Apatite (S), CH_4 (V), N_2 (V), Trona (S) Some unknown phases	473 & 511 (sanidine) ; 1276 & 1384 (CO_2) ; 961 & 2106 (apatite) ; 1971, 2168 & 2563 (unk with apt) 754, 1004 & 1119 (unk) 3070 (methane hydrate)	• **Carbonated apatite or fluorapatite** • **CO_2 density = 0.19 – 1.02 gcm^{-3}**
	Nepheline	Bi-phase (V+S) pseudosecondary	CO_2 (V), Nahcolite (S), CO_3	1276 & 1384 (CO_2); 1044 &	• **CO_2 density = 0.42 – 0.82 gcm^{-3}**

			melt (S), Unknown	1268 (Nahcolite); 1075 (CO_3); 1207 (Unk)	
	Quartz	Bi-phase (V+S) secondary	CO_2 (V), Nahcolite (S), CO3 (S), Shortite (S), Gaylussite? (S), Unknown	466, 806 & 1160 (qtz); 1276 & 1384 (CO_2);1045 & 1268 (Nahcolite); 1075 (CO_3); 269 (Shortite); 1063, 1154 & 1224 (Unk)	• **Shortite precipitation around inclusion walls** • **CO_2 density = 0.10 - 0.94gcm^{-3}**
OLX 3	Sanidine	Bi-phase (V+S) primary inclusions	CO_2, nahcolite, CO_3, spinel	215, 405, 990 (Snd); 1268 (nahc); 1085 & 2569 (CO_3); 1276 & 1382 (CO_2); 676 (spl)	• **Elongate inclusions** • **CO_2 density = 0.21 – 1.21 gcm^{-3}** • **REE-rich CO_3 may be Bastnäsite or Burbankite**
OLX 5	Nepheline	Mono-phase (S) & melt inclusions	CO_3, nahcolite	290, 473 & 514 (neph); 1041 (nahc); 1080 (CO_3) 711 (calcite?)	• **No CO_2** • **REE-rich carbonate melt – bastnäsite / burbankite?**
OLX 10	Olivine	Mono-phase (S)	Spinel, pyrite	820 & 850 (olivine); 660 & 760 (spinel); 420, 594 & 1019 (pyrite)	• **Unsure of parent fluid from which these crystallised – fluid inclusion or melt inclusion?**
	Nepheline	Inclusion trail	Void (?)	-	• **Some REE fluorescence**

					with peaks 358 & 696. • **No definitive CO_3 peak**
OLX 15	Nepheline	Melt inclusions	CO_3	275, 405, 466 & 990 (neph); 1070 (CO_3); 290 & 354 (calcite?)	• **No clear way of identifying which type of CO_3.** • **Some REE fluorescence suggesting Bastnäsite?**
OLX 16	Apatite	Bi-phase primary inclusions?	CO_3	430 & 984 (apatite); 1073 (CO_3)	• **Elongate inclusions are at depth** • **REE fluorescence from carbonate material – bastnäsite / burbankite?**
OLX 1	Nepheline	Melt inclusions	CO_3	400, 473 & 990 (neph); 1075 (CO3); 655, 907 & 2420 (unk)	• **Potentially Melanophlogite showing peaks at 273 & 810 cm^{-1}**

5.5.2.Liquid and vapour species

5.5.2.1. Carbon dioxide

It is not surprising that in carbonatite-related rock units the major liquid and vapour phase within the fluid inclusions is carbon dioxide (CO_2), which is easily identified under optical microscope due to a vibration of the vapour bubble within the confines of the inclusion due to excitation by the light. When examined using Laser Raman Spectroscopy, CO_2 is identified by the presence of two well defined, narrow peaks at approximately 1285 and 1387 cm^{-1}. These peaks are known as the Fermi diad bands which correspond to two vibrational modes of the CO_2 molecule (Figure 5.14). The separation of the Fermi diad bands (Δ) is known as resonance

splitting and can be used to indicate the density of the carbon dioxide within the inclusion (see section 5.1.3 below). Another feature of the carbon dioxide peaks, are two shoulder peaks known as hot bands, which result from transitions to excited vibrational states due to the thermal energy of the molecule (Kawakami et al., 2003).

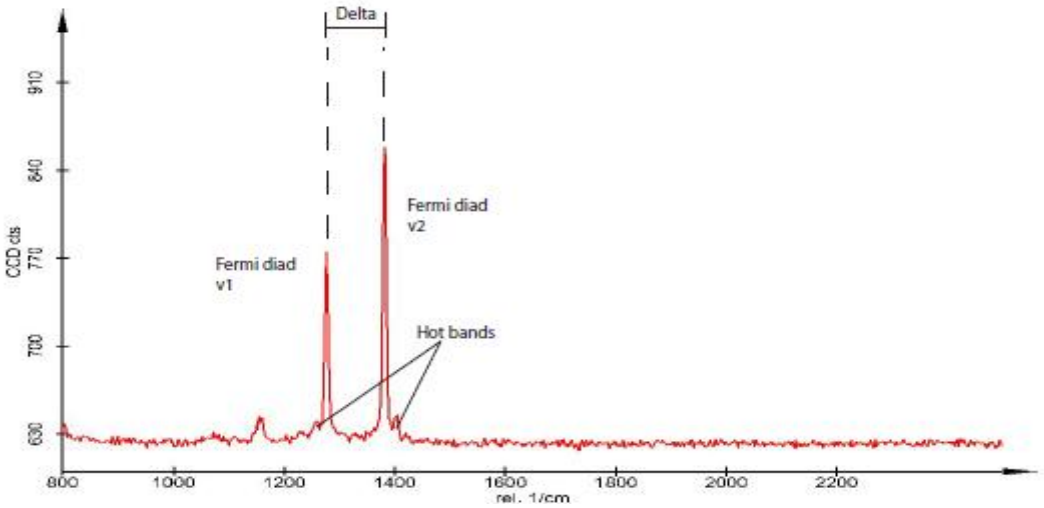

Figure 5.14: Raman spectra from inclusion within sample OLX 17b illustrating the identification peaks of carbon dioxide and position of hot bands

Carbon dioxide was identified within numerous inclusions both within the vapour bubble and in the liquid state of the inclusion, which appears to be a consequence of the density and pressure of the inclusion. Inclusions with a higher internal pressure contained liquid CO_2 whilst lower pressure inclusions were able to generate a vapour bubble of CO_2. Interestingly, carbon dioxide was only found within inclusions of the fenite units and even more surprisingly not within all of the units but only samples OLX 3, OLX 6 and OLX 17b but no carbon dioxide was recognized within the fenitised units of OLX 15 or OLX 17a.

It can be seen in Figure 5.15 that the vapour bubbles within the inclusions can be easily recognised and some have some interesting morphologies caused by the laser which pinches the bubble into oblate or arcuate shapes.

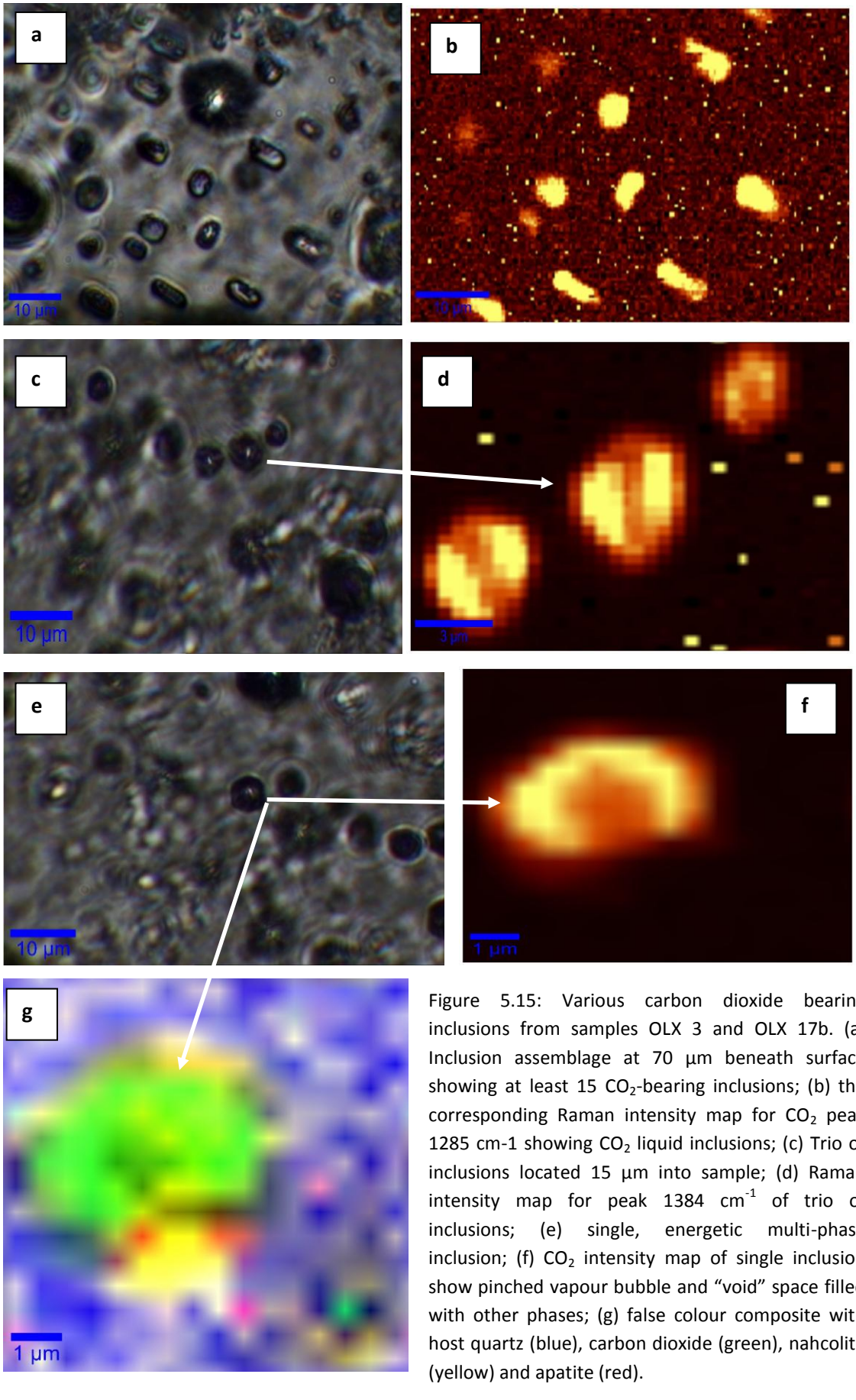

Figure 5.15: Various carbon dioxide bearing inclusions from samples OLX 3 and OLX 17b. (a) Inclusion assemblage at 70 µm beneath surface showing at least 15 CO_2-bearing inclusions; (b) the corresponding Raman intensity map for CO_2 peak 1285 cm-1 showing CO_2 liquid inclusions; (c) Trio of inclusions located 15 µm into sample; (d) Raman intensity map for peak 1384 cm^{-1} of trio of inclusions; (e) single, energetic multi-phase inclusion; (f) CO_2 intensity map of single inclusion show pinched vapour bubble and "void" space filled with other phases; (g) false colour composite with host quartz (blue), carbon dioxide (green), nahcolite (yellow) and apatite (red).

5.5.2.2. *Methane and nitrogen*

Carbon dioxide was not the only carbon-based species to be identified within the inclusions of OLX 3, 6 and 17b, with small amounts of methane (CH_4) also present, which is a common occurrence for carbonatite and alkaline igneous provinces (Williams-Jones and Palmer, 2002, Graser et al., 2008, Bühn et al., 2002, Konnerup-Madsen et al., 1985, Samson et al., 1995, Samson and Williams-Jones, 1991). Initially this was not identified using Raman Spectroscopy but became apparent during microthermometry analysis (See section 5.4) which indicated that 88 of the 124 inclusions studied were not pure CO_2 but a mixture of CO_2-CH_4-N_2. This prompted a re-analysis of the Raman spectra for the peaks characterising CH_4 and N_2, ~2917 and 2331 cm^{-1} respectively (Figure 5.16) (Burke, 2001, Shepherd et al., 1985, Wopenka et al., 1990). The N_2 peak is a relatively small peak and so requires magnification of the spectra by at least eight times in order to locate it, whilst the CH_4 peak is strong but due to its position it can be masked by REE fluorescence in the presence of apatite or REE-carbonate melt.

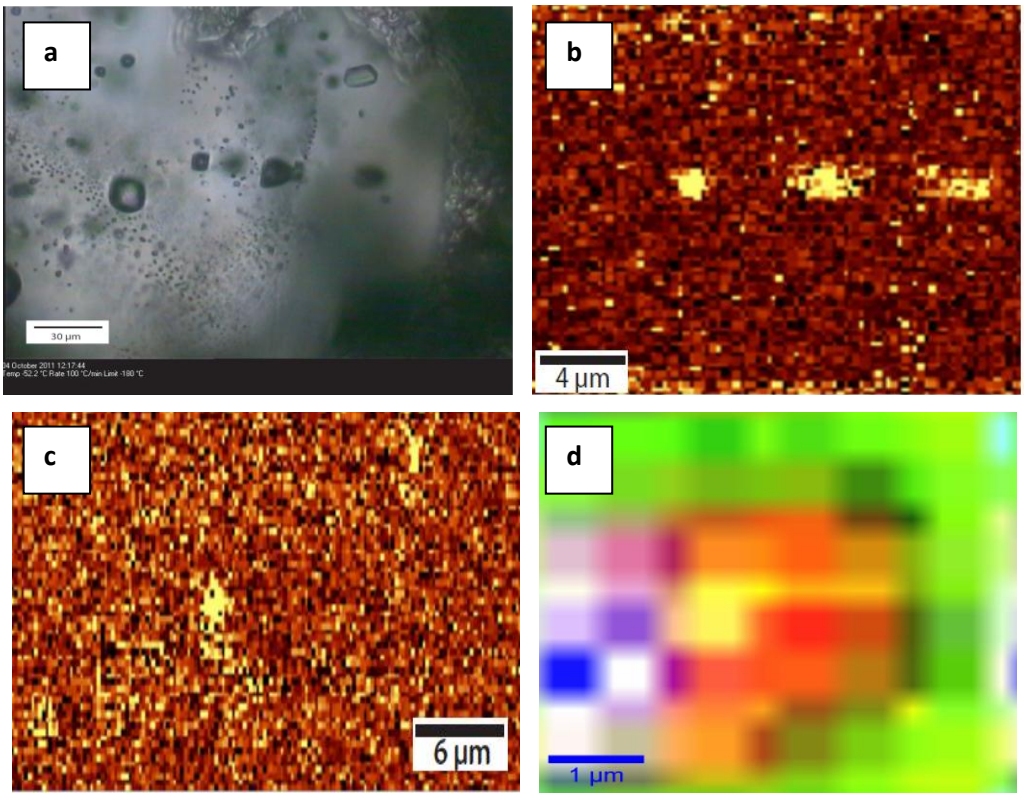

Figure 5.16: (a) photograph of inclusion trail and assemblage within sample OLX 17b; (b) Raman intensity map for N_2 peak 2331 cm^{-1} of trail of three inclusions from (a); (c) Raman intensity map from different inclusions for peak 2917 cm^{-1} for CH_4 mapping; (d) false colour composite map of single inclusion from OLX 17b with host mineral (green), CO_2 (red), CO_3 melt (blue), CH_4 hydrate (yellow)

Closer examination of the methane peak of five different fluid inclusions revealed the presence of a small shoulder peak at 3070 cm^{-1} which lies within the region expected for C-H stretch vibrational mode and previous work on CH_4 inclusions have concluded this corresponds to a gas hydrate structure of CH_4 when seen in association with the peak at 2917 cm^{-1} (Yoon et al., 2004, Sum et al., 1997). However later work has suggested that methane gas hydrate Raman signals should occur at 2905 and 2915 cm^{-1} (Lin, 2005). It is important to note that Lin (2005) highlights a change from a doublet peak for methane hydrate to a single peak when the hydrate stability is compromised and it decomposes to methane gas and so it is possible that the inclusions within the fenite units showing a small shoulder peak may well contain metastable hydrate. The intensity map and false colour composite of Figure 5.16 indicate the presence of a phase with characteristic peak at 3070 cm^{-1} but further work is required to confirm the existence with greater degree of certainty.

5.5.3.Missing H_2O

The most unusual result of the Raman Spectroscopy investigation was an apparent lack of spectra from any of the fluid inclusions (fenitic and plutonic) which indicate the presence of H_2O, either within the fluid phase of the inclusion or as hydrated carbonate minerals such as pirssonite ($Na_2Ca(CO_3)_2.2H_2O$), trona ($Na(HCO_3)(CO_3).2H_2O$) or thermonatrite ($Na_2CO_3.H_2O$). The presence of any of these within the inclusion would result in broad peaks within the region of 1581 and 1641 cm^{-1}, for O-H bend and 3219 and 3657 cm^{-1} for O-H stretch (Burke, 2001, Wopenka et al., 1990). As is evident from the Raman spectra, which have been included in this chapter thus far, no indication of these peaks is visible and so all the inclusions appear to be anhydrous. Proposed reasons for this anomaly will be discussed further in later sections.

5.5.4.Fluid inclusion density and isotopic composition using Raman spectra

A useful development in the study of CO_2-bearing inclusions is the determination of the density of the fluid inclusions based upon the separation of the Fermi diad bands. Early work on synthetic CO_2 inclusions observed that shifts in the bands were density-dependent, with the delta value (Δ) increasing with increasing density ((Yamamoto et al., 2007, Kawakami et al., 2003, Yamamoto and Kagi, 2006) and references therein). Therefore using the densimeter equation outlined by Yamamoto et al (2007) the density of the CO_2-bearing inclusions from

Oldoinyo Lengai vary between 1.22 gcm^{-3} to 0.09 gcm^{-3} for sample OLX 17b and between 1.21 gcm^{-3} and 0.18 gcm^{-3} for sample OLX 3.

Table 18 below illustrates the range in inclusion density for 29 inclusions within sample OLX 17b. Importantly inclusions within the same assemblage have the same densities which conforms to the earlier conclusion of homogeneous trapping of inclusions.

Table 18: Summary table illustrating the range of CO_2 densities based upon the separation of the Fermi diad bands (Δ) and isotopic composition based upon the position of the hot bands (v+ and v-)(Yamamoto et al., 2007, Irmer and Graupner, in press).

ID: OLX17b_	v1	v2	Δ	d (gcm^{-3})	v+ (1)	v- (1)	Isotope
1	1276.2	1381.3	105.1	1.045064	1259.6	1403.8	?
2	1275.2	1380.3	105.1	1.045064	1261.3	1404.1	$^{12}C^{16}O$
3	1280.0	1384.0	104.0	0.647163	1263.0	1403.1	$^{12}C^{16}O$
4	1275.4	1380.9	105.5	1.14132	1254.7	1403.5	$^{12}C^{16}O^{18}O$
5	1278.0	1383.4	105.4	1.120552	1262.2	1404.4	$^{12}C^{16}O$
6a	1278.0	1383.0	105.0	1.016156	1267.0	1410.0	$^{12}C^{16}O$
6b	1279.0	1384.0	105.0	1.016156	1265.0	1403.0	$^{12}C^{16}O$
7a	1278.0	1383.0	105.0	1.016156	1262.0	1404.0	$^{12}C^{16}O$
7b	1279.0	1384.0	105.0	1.016156	1260.0	1404.0	$^{12}C^{16}O$
8	1275.5	1380.3	104.8	0.953972	1260.6	1403.1	$^{12}C^{16}O$
9	1277.7	1382.5	104.8	0.953972	1262.2	1404.4	$^{12}C^{16}O$
10	1276.9	1381.7	104.8	0.953972	1250.3	1405.5	$^{12}C^{16}O^{18}O$
11	1277.6	1382.3	104.7	0.92093	1260.0	1403.0	$^{12}C^{16}O$
12	1278.2	1382.7	104.5	0.850937	1262.2	1404.4	$^{12}C^{16}O$
13	1277.8	1382.2	104.4	0.813772	1265.6	1408.2	$^{12}C^{16}O$
6c	1278.9	1383.3	104.4	0.813772	1260.3	1396.1	$^{12}C^{16}O$
14	1276.4	1380.6	104.2	0.734306	1249.9	1388.1	$^{13}C^{16}O$
15	1278.4	1382.4	104.0	0.647163	1262.2	1408.2	$^{12}C^{16}O$
7c	1278.0	1382.0	104.0	0.647163	1254.0	1403	$^{12}C^{16}O^{18}O$
16	1280.0	1383.8	103.8	0.552623	1260.1	1403.8	$^{12}C^{16}O$
6d	1279.5	1383.3	103.8	0.552623	1260.3	1396.1	$^{12}C^{16}O$
16a	1278.1	1381.8	103.7	0.503311	-	-	-
1a	1277.7	1381.3	103.6	0.45339	-	-	-
17	1279.8	1383.3	103.5	0.403643	1261.0	1402.2	$^{12}C^{16}O$
18	1280.1	1383.5	103.4	0.354995	1260.3	1405.6	$^{12}C^{16}O$
6e	1280.0	1383.0	103.0	0.189453	1260.0	1401.0	$^{12}C^{16}O$
7d	1279.0	1382.0	103.0	0.189453	1256.0	1404.0	$^{12}C^{16}O^{18}O$
19	1280.2	1382.9	102.7	0.097932	1256.6	1403.4	$^{12}C^{16}O$

Another use of the Raman spectra is the ability to indicate the isotopic composition of the inclusions (Irmer and Graupner, in press) by looking at the positions of the hot bands associated with the Fermi diad bands. This is more of a qualitative process than being able to provide quantitative isotopic ratios, but still has merits in understanding the nature of the fluid system, particularly in terms of whether it is degassed or not. Table 18 above outlines the hot band positions for the same fluid inclusions from sample OLX 17b and also the interpretation of the isotope system according to Irmer and Graupner.

It can be seen that the majority of inclusions belong to the light isotope system with ^{12}C and ^{16}O and again inclusions of the same assemblages tend to have the same isotope system. Four inclusions within sample OLX 17b appear to have a mixed oxygen isotope system with both ^{16}O and ^{18}O. This is thought to be the result of different isotopic compositions of the inclusion phases, for example and isotopically light vapour phase and heavier liquid or solid phase. The same technique was applied to the analyses of sample OLX 3 and again the majority of samples were isotopically light ($^{12}C^{16}O$).

5.5.4.1. Conversion to pressure and depth

With an estimate of the density of the fluid inclusions it is possible to derive an estimate for the pressure at which they formed and so subsequently the depth. By combining the temperature of fenitisation process stated in chapter 4 with a P-T diagram for CO_2 (Figure 5.17) a pressure can be determined (Pitzer and Sterner, 1994). Assuming that fenitising fluids have a temperature between 650 and 700 °C it can be seen that the fluid inclusion density range of 1.22 to 0.09 gcm^{-3} corresponds to pressures between 0.8 – 0.05 GPa for sample OLX 17b and OLX 3. This equates to a maximum depth of trapping at 28.79 km. It should be noted that CO_2-rich inclusions are prone to post-trapping modification during transport to the surface, resulting in decrepitation and leakage which can modify the internal pressure and density of the fluids. Therefore, the inclusions with extremely low densities can be interpreted as having some form of modification and the maximum density observed is likely to represent the minimum limit for trapping pressure.

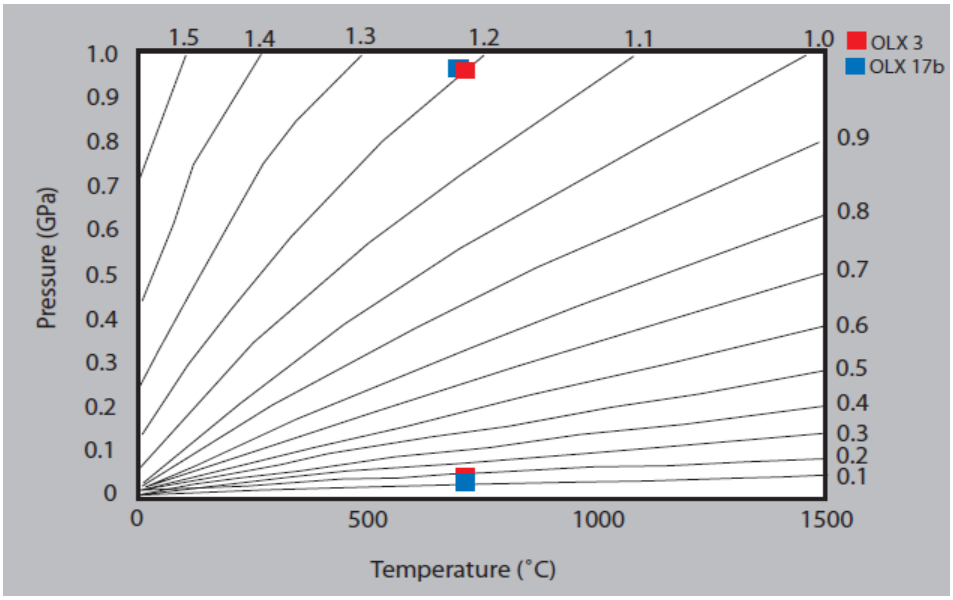

Figure 5.17: P-T diagram for CO_2 system with isochores and temperature estimated from thermobarometry (Yamamoto et al., 2007, Pitzer and Sterner, 1994)

5.6. Microthermometry of fluid inclusions

Microthermometry is one of the standard and most common techniques when studying fluid inclusions from all environments and can provide a wealth of information on the fluid inclusions suites. It is generally a non-destructive method of analysis, except in inevitable instances where rupturing of inclusions occurs. As outlined in chapter 2, CO_2-bearing inclusions require two measurements to be made on the heating cycle, the first when the first melting occurs (T_m) and the second when the inclusions homogenises (T_h) to either a vapour or a liquid (Figure 5.18). The homogenisation is often difficult to record since the inclusions have dark rims which obscure the vapour bubble.

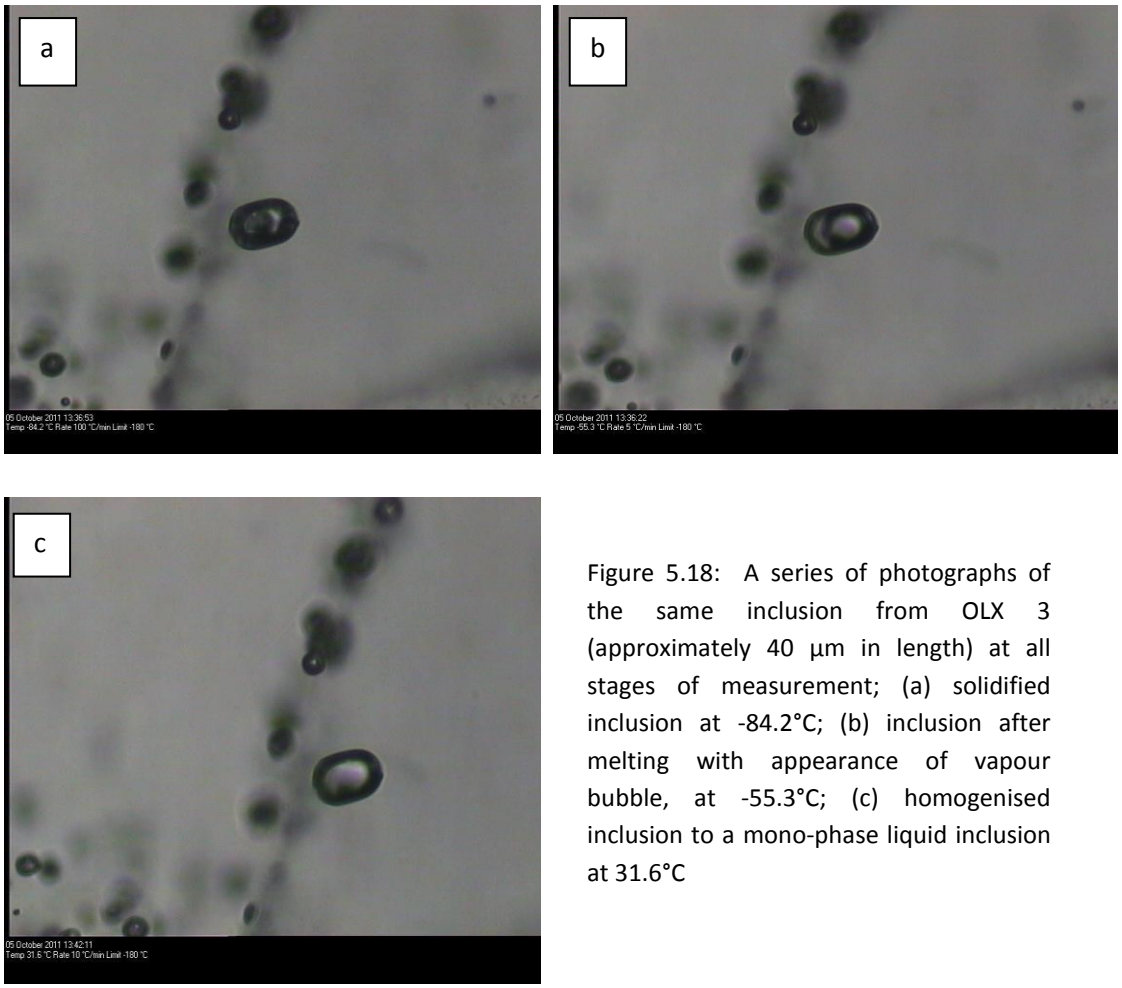

Figure 5.18: A series of photographs of the same inclusion from OLX 3 (approximately 40 µm in length) at all stages of measurement; (a) solidified inclusion at -84.2°C; (b) inclusion after melting with appearance of vapour bubble, at -55.3°C; (c) homogenised inclusion to a mono-phase liquid inclusion at 31.6°C

Only rock units known to contain large CO_2 inclusions were chosen for thermometric analysis to maximise the limited amount of time available on the equipment. This restricts the measurements to the fenitic units only and in particular OLX3, 6 and 17b. A wafer was also made of sample OLX 7 – natrocarbonatitic material but few viable inclusions were found for analysis. The work below will therefore detail the thermometric results of the fenitic units.

5.6.1.Melting temperature of inclusions

Inclusions of pure CO_2 are expected to melt at the triple point of -56.6°C and the depression of Tm to lower values is the result of other species present within the inclusion, in particular CH_4 and N_2. The graph below in Figure 5.19 illustrates the variation in T_m for all inclusions measured.

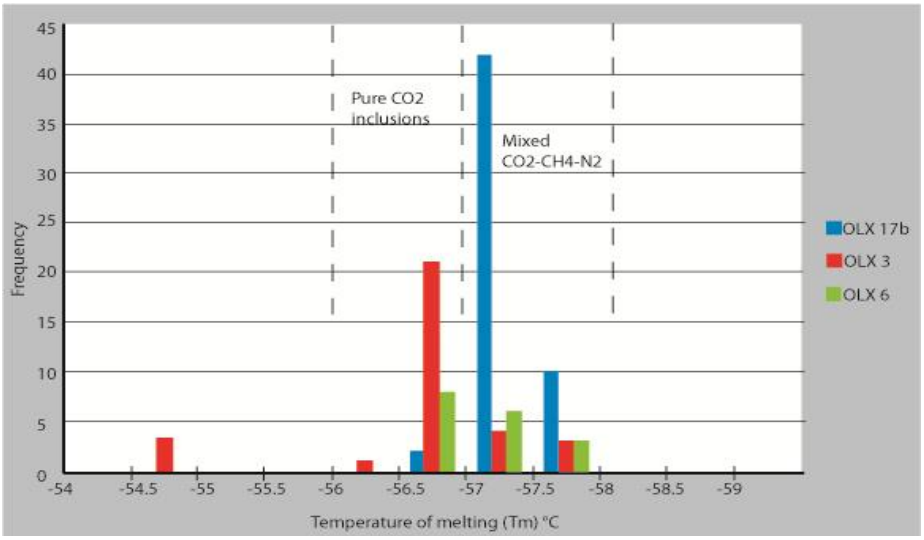

Figure 5.19: Histogram illustrating melting temperature variation of fenitic CO_2-bearing inclusions.

Just under half of the inclusions measured appear to be pure CO_2 inclusions with melting temperatures between -56.6 and -56.2°C, whilst the remainder appear to be inclusions with a mixture of gases, CO_2-CH_4-N_2 (Shepherd et al., 1985). Of the three samples analysed, OLX 3 hosts the majority of the pure CO_2 inclusions and OLX 17b the majority of mixed inclusions. OLX 6 has an even distribution of both inclusion types.

5.6.2.Homogenisation temperatures of inclusions

The next measurement to be made is that of homogenisation and the type of homogenisation which occurs – to liquid or to vapour. Again, the results for the variation in homogenisation temperature are displayed in the graph below (Figure 5.20). There are a number of observations that can be drawn from the graph; firstly the inclusions of OLX 3 homogenise both to liquid-rich inclusions and to vapour-rich inclusions, whilst the other samples only homogenise to liquid. Secondly, there appears to be three types of inclusion within the samples – those which homogenise early in the heating cycle (between -40 and -20°C), a second group which homogenise at an intermediary temperature (0 - 15°C) and the final group which homogenise at much higher temperatures of between 20 and 35°C.

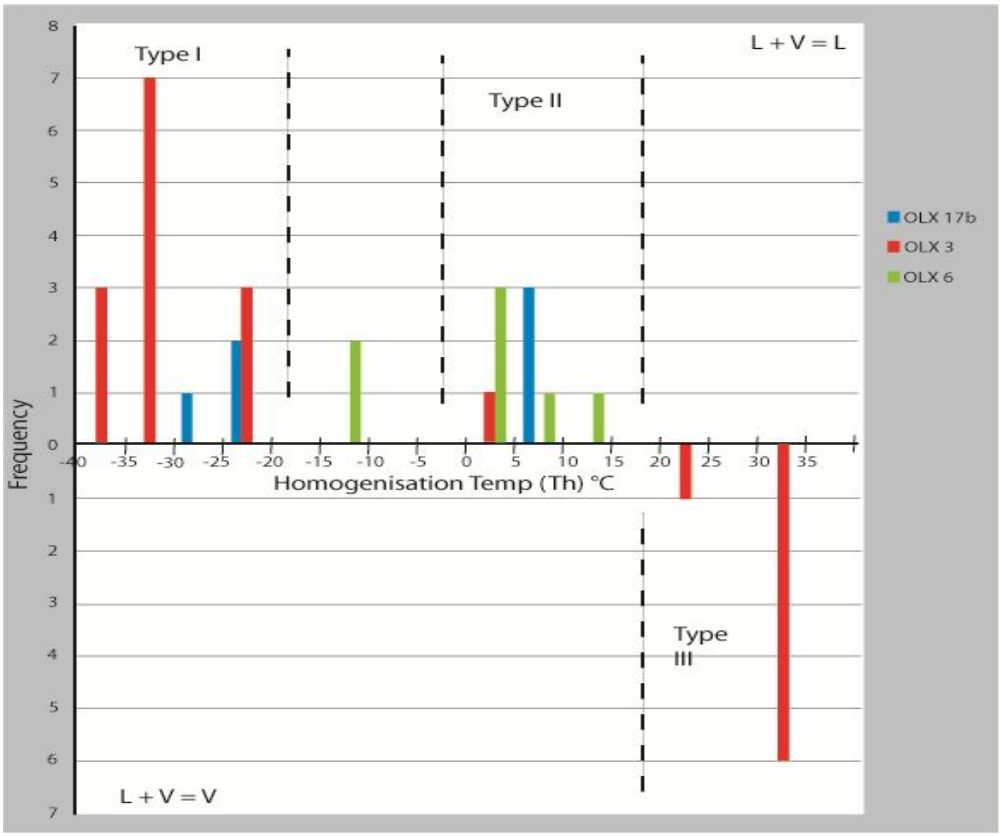

Figure 5.20: Histogram illustrating the variation in homogenisation temperature of inclusions studied. Highlighted are the three types of inclusions which can be observed within the study assemblage.

The homogenisation temperature of fluid inclusions is used as another guide to estimate the density of the inclusions and is achieved by plotting the results on the graph in Figure 5.21 below. It should be noted that this diagram is strictly for pure CO_2 inclusions and so will only be a guide for the mixed inclusions known to exist in the samples. Currently no density diagram is available for the CO_2-CH_4-N_2 system. There are diagrams for CO_2-CH_4 inclusions ((Shepherd et al., 1985) and references therein) but again these are not applicable to the mixed inclusions.

As the diagram illustrates, the mode of homogenisation is dictated by the inclusion density, with a critical value of 0.468 gcm^{-3}, above which all inclusions will homogenise into the liquid state. This provides some constraint for the type 3 inclusions above, which homogenise to vapour and so must have a density <0.468 gcm^{-3}.

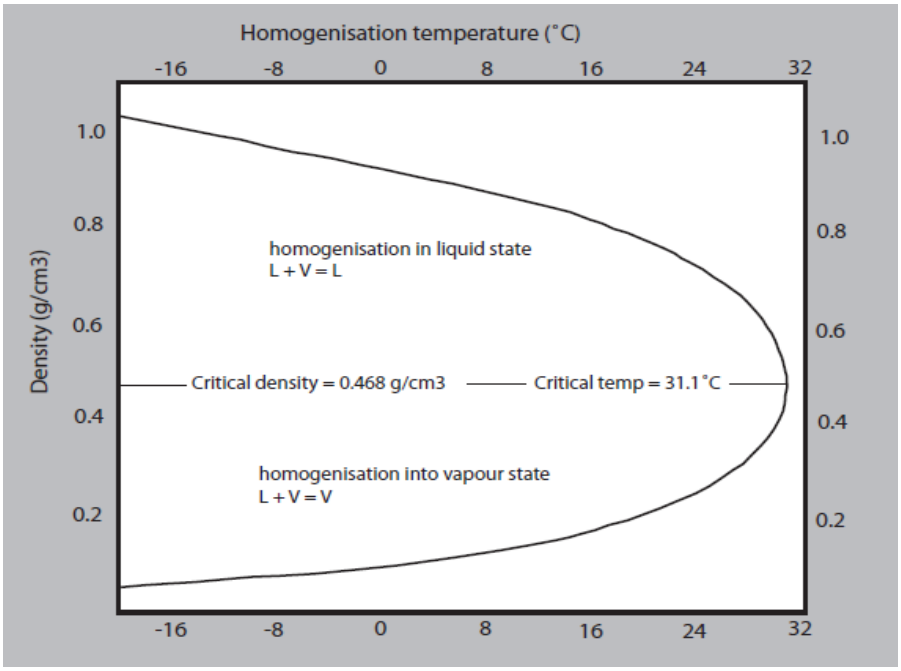

Figure 5.21: Graph of homogenisation temperature (Th) vs. Density for CO_2 fluid inclusions ((Shepherd et al., 1985) and references therein)

The type 2 inclusions have a density of between 0.8 – 0.91 gcm^{-3} which is in agreement with the previous density estimates from the Raman spectra in table 18. There are a number of inclusions which appear less dense than 0.8 gcm^{-3}, particularly from sample OLX17b, but it is possible that the homogenisation of these inclusions was not possible to measure due to the dark rim.

The homogenisation temperatures of the type 1 inclusions are too low to plot on Figure 5.21. This could be for two reasons; either the inclusions have densities much greater than 1.0 gcm^{-3} or the inclusions are mixed CO_2-CH_4-N_2 inclusions which are depressing the homogenisation temperature. Sample OLX 3 contained an assemblage of inclusions which are not plotted on the graph in Figure 5.19, with homogenisation temperatures of -57.2°C. This is thought to represent an inclusion which is extremely enriched in N_2, with previous work suggesting that a T_h of -58°C corresponds to 22 mol% of N_2 (Kooi et al., 1998). Such inclusions are often referred to as 'superdense' fluid inclusions (Andersen and Neumann, 2001).

5.7. Isotopic determination of fluid inclusions from fenites (Pilot study)

A small pilot study to quantitatively investigate the isotopic signature of the fluid inclusions was undertaken using a Finesse, multi-collector mass spectrometer with a mineral crushing device attached, the details of which can be found within Mikhail (2011). The analyses were conducted upon sanidine mineral separates from sample OLX 3, as these minerals are the easiest to obtain from the sample and the greatest in abundance compared to other samples. The mineral separates were crushed using a magnetic piston to break open the inclusions and the fluids (liquid and vapour) are drawn into a vacuum and passed through the Finesse.

Table 19: Summary of blank corrected data for fluid inclusion isotope analysis for carbon, nitrogen and argon from isotope crushing.

No. of Strokes	C (ng)	$\delta^{13}C$	N (ng)	$\delta^{15}N$	+/-	^{40} Ar (cc)	^{40}Ar / ^{36}Ar	He (cc)
50	215.0	-16.40	76.8	1.800	0.30	6.00e-07	391.0	7.00e-09
150	18.00	-28.40	4.20	-16.10	1.40	2.00e-08	-	-

Table 19 above outlines the measurements made after 50 and 150 strokes of the piston for both concentration and isotopic signature of carbon, nitrogen and argon. The release at 150 strokes is argued to be close to the blank level measurement of the machine (pers comms Mikhail 2011) and so all of the fluid from the inclusions is released during the initial 50 strokes. It can be seen that in terms of carbon the fluids are isotopically light (^{12}C-enriched) resulting in a negative $\delta^{13}C$, whilst the nitrogen is enriched in ^{15}N resulting in the positive $\delta^{15}N$. The light carbon isotope signature conforms to the qualitative assessment from the Raman spectra (section 5.54) and is also what is expected for a degassing magma, which would enrich light isotopes in the vapour phase whilst the heavy isotopes remain in the melt. Interestingly, the argon isotope signature appears to be atmospheric in that it is similar to atmospheric-saturated water (ASW) values at 295.5 (Mohapatra and Murty, 2000). It is not known at present whether this is indicative of contamination or evidence of a recycled component.

5.8. Discussion – Interpretation of fluid assemblages

This first look at the fluid inclusions from volcanic material from Oldoinyo Lengai aimed to shed light on magmatic evolution processes in terms of fluid generation and interaction with surrounding rock units, as well as to investigate the chemistry of fluids circulating within the sub-surface of this region of the Gregory Rift. The predominance of fluid inclusions within certain rock units, indicates that fluid phases were in abundance in the vicinity with any phases crystallising from a highly mobile fluid. Numerous observations have been made regarding the phases present and the relationship of the inclusions to one another and their host units, the interpretation of which shall now be discussed.

5.8.1.Fluid inclusion composition

The fluid inclusions of the fenitic units conform almost perfectly to the model of Bühn and Rankin (1999) illustrated in Figure 5.4, in terms of the components which make up fluid inclusions from carbonatitic regimes, specifically a carbonic fluid (CF), aqueous brine (AB) and carbonate-rich melt (CRM), all of which combine to generate an inclusion of trapped carbonatitic fluid (TCF). This TCF is typified as being alkali and volatile-rich and low viscosity (Bühn and Rankin, 1999) and represents homogeneous trapping of a supercritical fluid which varied in density. The authors specify that the TCF need not necessarily represent a fluid in the true sense of the word but can be viewed as a melt. This point may be particularly vital in understanding why there is a lack of aqueous brine (AB) within the inclusions of this study. This will be discussed further in section 5.8.2 below.

The alkali-rich nature of the fluid inclusions is exemplified by the precipitation of alkali-rich daughter minerals. The crystallisation of nahcolite, aphthitalite and shortite indicate that the fluid from which they crystallised was rich in Na^+ cations with lesser amounts of K^+, whilst the important anions within the inclusions are mainly CO_3^{2-} and lesser amounts of SO_4^{2-}. The nature of the fluid is as expected for fluids expelled from carbonatitic melts in particular alkali-rich ones as seen at Oldoinyo Lengai. The apparent lack of a brine phase appears to limit the chemical species, in particular anions, which are transported by the fluids. This is particularly noticeable due to a lack of halite which is common in inclusions from other carbonatite regimes (Rankin and Le Bas, 1973, Shepherd et al., 1985, Bühn et al., 2002, Bühn et al., 2003,

Ni et al., 2003, Rankin, 1975, Bühn and Rankin, 1999, Buhn et al., 1999, Frezzotti et al., 2002). The majority of the chemical species are carried within the carbonic phase, which in the fenitic units is either pure-CO_2 or a mixture of CO_2-CH_4-N_2, and it is from this that minerals are crystallised.

The absence of CO_2-rich inclusions within certain fenite samples, in particular OLX 17a, is argued to be a consequence of the type of fenitisation which has occurred, i.e. the magma body expelling fluids. As samples OLX 3,6 and 17b all contain CO_2-rich inclusions it would seem that they are all fenitised by the same type of igneous intrusion and one typified by a low H_2O/CO_2 ratio, which corresponds to carbonatite units. The other fenite units, which are devoid of CO_2 inclusions, are the product of fenitisation by a fluid of high H_2O/CO_2 ratio, which indicates an ijolitic source of fluids.

5.8.2.Missing water from inclusions

If the above interpretation of expected fluid inclusions based upon the magma body is correct, it is important to investigate the apparent lack of free H_2O within fluid inclusions from the xenolith suite. The following are proposed reasons as to why water may not be detected within the inclusions;

5.8.2.1. Difficulty in measuring

Despite H_2O-CO_2 inclusions being amongst the most common in all geological environments (Shepherd et al., 1985, Bodnar, 2003), water is often difficult to identify within inclusion suites from particular rock units, including mantle xenoliths (Andersen and Neumann, 2001). Optical microscopy is often unable to identify the presence of water within CO_2-H_2O inclusions due to the dark rim of carbon dioxide which can mask any aqueous regions of the inclusions or prevent the identification of ice crystals upon cooling. The use of Raman should be more sensitive to the bend and stretch of the O-H bond within water and so identification should be easier than using optical methods. Wopenka et al (1990) argue that Raman identification of water is easily achieved by understanding that the peak intensity is lower than other species, e.g. CO_2, due to the broadness of the peak and so may be less obvious within a spectra. With

this in mind it is possible that during this study the peak for O-H indicative of water was missed due to swamping by the intensities of the other peaks.

A solution would be to utilise the strong Infra-red absorption of water and investigate its presence using Fourier Transform Infra-red Spectroscopy (FTIR) which unfortunately was not available for this study.

5.8.2.2. Anhydrous regime

Perhaps the most obvious but also most difficult to prove explanation for the apparent lack of water, is that it was never present as the system is completely anhydrous. Previous studies of fluid inclusions from all tectonic settings appear to contain water in varying abundances, with xenoliths from active subduction zones appearing to contain fluid inclusions with the most H_2O within them ((Andersen and Neumann, 2001) and references therein). This of course is an expected correlation due to the subduction of hydrated oceanic crust which dehydrates upon descent, releasing fluids. In comparison, continental rift settings are relatively water-poor.

The presence of water within the entire Lengai volcanic system is a controversial topic in general. It is known that natrocarbonatite is hygroscopic and so is unlikely to carry large quantities of water within the melt. This is also confirmed by the lack of H_2O recorded within the volcanic plume, which instead is comprised almost completely of CO_2 with minor amounts of CO and SO_2 (Koepenick et al., 1996). Other measurements have suggested a greater contribution of H_2O to the volcanic plume (Teague et al., 2008, Oppenheimer et al., 2002), but have later concluded that these signals represent the release of water from re-melting of water-saturated magmas at the surface.

However, the presence of hydrous minerals, i.e. phlogopite and amphibole, within the volcanic system, both within fenitic units and the underlying sub-continental lithospheric mantle, indicate that free H_2O is available for reaction. Combined with the presence of H_2O-CO_2 inclusions from units of other carbonatite complexes (Rankin and Le Bas, 1973, Bühn et al., 2002, Rankin and Le Bas, 1974, Bühn et al., 2003, Ni et al., 2003, Rankin, 1975, Bühn and Rankin, 1999, Buhn et al., 1999) makes it unlikely that Oldoinyo Lengai is a completely anhydrous system.

5.8.2.3. Compositional re-equilibration

Much of the trapped H_2O in fluid inclusions can be lost by compositional re-equilibration which involves loss either by reaction to form hydrous minerals or through preferential leakage from the inclusion (Hansteen and Klugel, 2008, Bodnar, 2003). The first of these results in the formation of hydrous minerals around the inclusions walls (Roedder, 1984) with the pure-CO_2 actually forming the residual fluid from these reactions. Well known hydrous minerals such as amphiboles, phlogopite, hydroxylapatite and CO_2-clathrate (Andersen and Neumann, 2001) can be produced alongside minerals more specific to carbonatite regimes including trona, thermonatrite, gaylussite and pirssonite, all of which are hydrated carbonate minerals formed at Oldoinyo Lengai (Zaitsev and Keller, 2006).

The second form of re-equilibration relates to the modification of fluid inclusions during transit to the surface resulting in the loss of water through preferential leakage. This is argued to be the more important of the two processes and is a non-decripitative process which results in the leakage of water along dislocations and planar defects within a crystal (Bakker and Jansen, 1990, Hansteen and Klugel, 2008). As inclusions themselves form in imperfections of the crystal lattice they tend to act as sources of dislocations. The dislocations themselves are thought to be relatively small and so only enable the leakage of H_2O rather than CO_2. The result of this process is the appearance that the remaining fluid is CO_2 – CH_4 – N2-rich.

5.8.3.Clathrate and hydrate formation in inclusions

It was indicated above that the missing water may be bound up in the formation of gas hydrates, in particular that of CO_2-clathrate (Andersen and Neumann, 2001). The Raman analysis of the fluid inclusions within the units from Oldoinyo Lengai were argued above to potentially contain two types of clathrates: the first a gas-hydrate of CH_4 and also a silica based clathrate of melanophlogite. The presence of these units provides some additional information towards the physical and chemical conditions under which the inclusions were formed.

Gas hydrates (structural type I) form in inclusions due to the interaction between aqueous and non-aqueous phases (Shepherd et al., 1985), which results in the encasement of gas molecules in the cavities of a host crystal lattice made of water molecules (Collins, 1979). Clathrates in nature form in regions of low temperature or high pressure, for example on the sea bed at

depths of >300m (Hyndman and Davis, 1992), it would seem logical that the same physical constraints are required within fluid inclusions. Since trapping at low temperatures is unlikely for fenitic units, the clathrates within the samples must be the result of high internal pressures of the inclusions upon cooling. The formation of clathrate minerals indicate the presence of water within the inclusions. Interestingly, it is the presence of methane which is most unusual since this is a reduced form of carbon found within an inclusion with oxidised carbon phases. It can only be assumed that once encased within the clathrate structure the guest gas molecules do not interact with the free gas vapour within the inclusion. If oxidation occurs we would expect to find a graphite coating on the inner walls of the inclusion, which we do not.

Melanophlogite is a different type of clathrate mineral, but still structural type I, which consists of corner-sharing tetrahedra of SiO_4 with small guest molecules (CH_4, CO_2, N_2) within the vacant spaces between cages (Nakagawa et al., 2005, Navrotsky et al., 2003, Gies, 1983, Tribaudino et al., 2008, Gunawardane et al., 1987, Nakagawa et al., 2001, Xu et al., 2007, Gies et al., 1982). The exact formation conditions of this unusual mineral in nature is unknown but synthetic melanophlogite has been produced from silica solutions at temperatures of around 170°C and pressures of 15 MPa with 'help gases' (the guest molecules) which are thought to act as templates for formation and stability (Gunawardane et al., 1987). The presence of melanophlogite within non-fenitic inclusions i.e. carbon-poor / silica-rich inclusions, indicates some segregation of silica-rich melts and fluids, most likely due to immiscibility (Roedder, 1992). The pressure and temperature conditions indicated by synthetic production suggest that their natural formation within fluid inclusions occurs at shallow depths within the crust.

5.8.4.Similarity to mantle-derived fluids

The compositions of the inclusions studied show a resemblance to those previously reported for mantle-derived xenoliths from across the globe (Andersen et al., 1984, Andersen and Neumann, 2001, Frezzotti et al., 2002, Yamamoto et al., 2007, Yamamoto et al., 2002). The review by Andersen and Neumann (2001) concludes that upper mantle- derived units contain fluid inclusions of almost pure-CO_2 with some containing minor volatile species including N_2, SO_2, H_2O, noble gases and carbonate. All of these phases occur within the fluid inclusions from Oldoinyo Lengai and in similar proportions to those reported for mantle-derived units, which suggest a mantle origin for some of the fluids captured at Lengai.

The most interesting similarity of the reported mantle-derived inclusions and those at Lengai is the density of the inclusions. As Figure 5.22 shows mantle-derived inclusions have a density range between 0.47 and 1.18 gcm^{-3}, with some of the densest inclusions coming from the Hawaiian volcanic chain. Those at the upper end of the range are classified as 'superdense' inclusions and apart from Hawaii are only found within xenoliths from continental settings (Andersen et al., 1984).

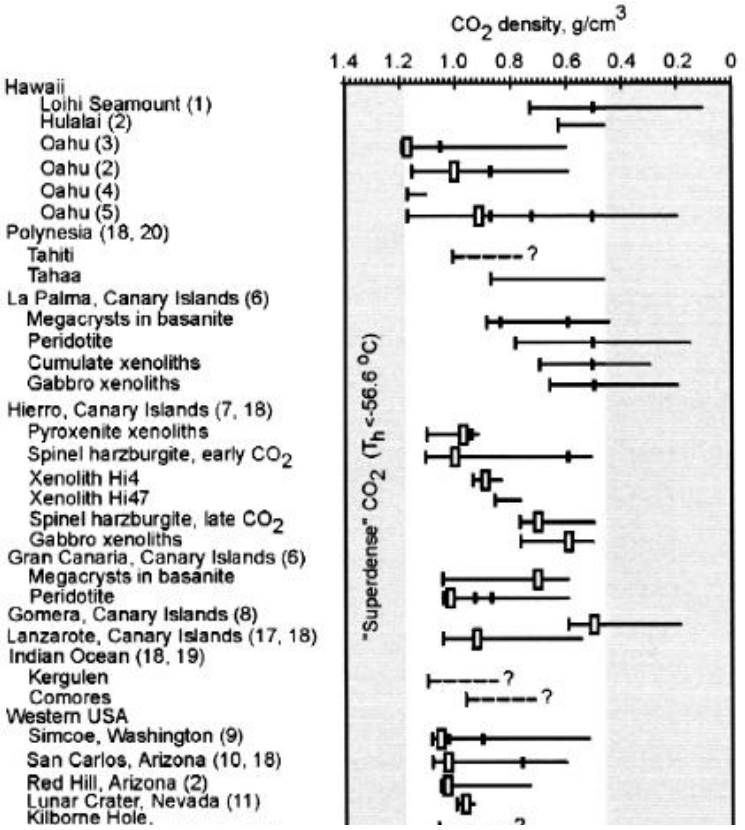

Figure 5.22: Excerpt of density data for pure-CO_2 mantle-derived fluid inclusions from across the globe from Andersen and Neumann review (2001).

The variation of the fluid inclusion densities of the fenitic units, between samples and also within single samples, suggests spatial and temporal evolution of the fluids. The presence of dense inclusions within sample OLX 3 can be expected as according to its mineralogy it represents a contact fenite and so occurs closest to the crystallising magma body. Units further from the intrusion (OLX 17b and OLX 6 for example) are likely to have less dense inclusions as lower density fluids will emanate further. It is however the bi-modal density of the inclusions within OLX 3 (Figure 5.20) which is puzzling and would suggest two processes; either the fluid inclusions of OLX 3 are more prone to post-trapping modification due to the host mineral being alkali feldspar, which is less ideal as a host for inclusions (Shepherd et al., 1985) or there

is some form of fluid stratification within the fenitic aureole. One other alternative is trapping of less dense fluid upon ascent through the eruption column, which results in some heterogeneous trapping of CO_2. Few of the inclusions appear to be 'necked-down' or stretched and so would appear to be intact since their formation.

5.8.5.Occurrence of fluid inclusions mainly in fenitic rock units

The presence of fluid inclusions within the altered crustal units is an important observation as it coincides with the levels where immiscibility is thought to take place. Even if carbonatites are primary in origin, it is likely that crustal depth is also the depth of crystallisation initiation, due to stagnation of melts and changes in pressure / temperature. The exsolution of carbon-rich fluids upon crystallisation results in fenitisation of the surrounding country rocks as these are the only rocks in contact with the igneous carbonate body. These units therefore host the majority of the fluid inclusions as it is consumed by the fenitisation process and so does not infiltrate the upper crust regions.

As the crystallisation process continues, a more fractionated melt is generated, which percolates upward through crustal rocks, driven by the exsolution of CO_2 and becomes trapped as melt inclusions within plutonic and volcanic rocks of the volcanic pile (non-fenitic units). Such inclusions have been the subject of studies within ijolite from other East African carbonatite complexes including western Kenya and eastern Uganda (Le Bas and Aspden, 1981, Rankin, 1975). The latter of these studies identified primary inclusions which contain carbonatitic fluid with a chemical composition comparative to that of natrocarbonatitic material (Figure 5.23). These are also comparable to melt inclusions within the 2007 xenolith suite.

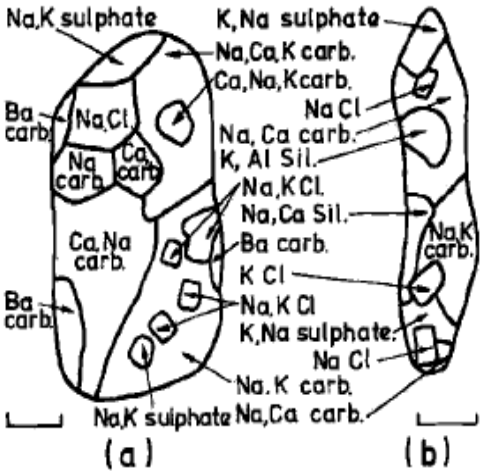

Figure 5.23: Diagrammatic illustration of the distribution of phases within inclusions from Usaki ijolite, western Kenya (Le Bas and Aspden, 1981)

Le Bas and Aspden (1981) argue that these inclusions represent droplets of immiscible carbonatite after separation from the parent melt. To a certain extent I agree with this conclusion but would also add that the material trapped has been subject to a precursory fluid loss event and then subsequent fractionation of the melt resulting in an increase in alkali and rare Earth elements.

5.8.6. Towards a pristine carbonatite composition

At the beginning of this chapter it was postulated that the compositions of carbonatites exposed at the surface have experienced some deviation away from their original / pristine composition as a result of fluid loss, which becomes trapped in surrounding rock units. The presence of fluid inclusions within the fenitic units supports this theory. If the fluids are interpreted as representing a direct sample of the highly evolved, alkali-carbonatitic fluid expelled from the fractionating and crystallising carbonatite (TCF in terms of Figure 5.4), then the composition of the original, pristine carbonatite lies somewhere between that of the fluid inclusions and the composition of natrocarbonatite sampled at the surface, which is the same conclusion of Bühn and Rankin (1999).

This off course does raise one conundrum; the fenitisation process is typified by a loss of alkalis to the surrounding rocks, how does the melt retain enough alkali to still be classified as sodium carbonatite? Was the initial carbonatite melt oversaturated in alkali elements?

One option is that the fenitised rocks also act as a source of alkalis in some form of autometasomatic process. What if over time the country rocks have become saturated with

alkalis and melting of them by an incoming batch of nephelinitic parent melts results in the production of alkali-rich carbonatite or what if the fenites are now “in equilibrium” with the arriving melts and fenitisation is now no longer so pronounced. Instead, when a new batch of magma arrives it gains alkalis from the fenite zone rather than losing them. A similar, small scale process was suggested by Rubie and Gunter (1983) to explain the chemistries of fenitic units around ijolites and carbonatites, concluding that feldspar minerals are subject to alkali exchange reactions and that the “high sodium content of carbonatitic fluids, compared with ijolitic fluids...could be the result of exchange reactions with feldspar”.

An autometasomatic process would require sustained carbonatite production since the early history of the volcano to generate a saturated metasomatic region beneath the Gregory Rift. However, the original carbonatite melts may not have erupted to the surface as natrocarbonatite, if they erupted at all. Instead they may have been consumed in fenitising processes, developing an alkali-rich region of rock units which could then generate alkali-rich carbonate upon re-melting in recent times. These still remain unanswered and requires further work on the chemistry of the melt and fluid inclusions to provide further constraints on the evolution of their composition from first genesis to surface. It does however show some consistency with the cognate condensate model of formation proposed by Nielsen and Veksler (2002).

5.9. Concluding remarks and future work

The study of fluid inclusions from rock units, in particular igneous units, provides samples of fluids which would not necessarily be otherwise seen, in particular fluids which circulate in the upper mantle. From the study of the inclusions found within the Lengai suite the following conclusions can be drawn:

- The fenitic rocks at Oldoinyo Lengai contain high density fluid inclusions rich in CO_2 with minor amounts of volatile species including CH_4 and N_2. They also contain solid species of apatite, nahcolite, shortite and carbonate melt (which often rims the inclusions). All phases are conducive with trapping and crystallisation of an alkali-rich, supercritical fluid of apparent upper mantle origin.

- An apparent lack of water indicates post-trapping modification of the inclusions as well as re-equilibration via generation of hydrous minerals and clathrates and preferential loss of water via inclusion leakage. Clathrate formation indicates trapping of supercritical fluids at high pressures.

- The fluid inclusion composition with the fenite units is a product of the magmatic body causing the fenitisation. Carbonatite-related fenitisation results in the trapping of CO_2-rich inclusions which reflects the high CO_2/H_2O ratio. Ijolitic-related fenitisation is thought to result in H_2O-rich inclusions as a result of the low CO_2/H_2O ratio, most of which have unfortunately lost their water.

- The inclusion assemblages represent samples of metasomatic fluid rather than pristine carbonatite.

- Melt inclusions within non-fenitic units represent trapped carbonate melt that has evolved from the original carbonatite which intruded / immiscibly separated in the crustal region. This late stage, evolved carbonate melt appears to be rich in rare earth elements due to fluorescence during Raman analysis.

The next stage to fully study the inclusion contents requires the opening of the inclusions (either through crushing or through laser ablation) to allow a complete characterisation of the solid species within both in terms of major/minor elements but also isotopic analysis of the solid carbonate salts and melt material.

This chapter has enabled us to look at the compositions of the fluids which have been captured during crystal growth and make some tentative assessments of the magma bodies from which the fluids have been expelled. The following chapters therefore look at the chemical effect these fluid have on the surrounding country rocks and further investigate the source of the fluids, both in terms of their magmatic derivation and in turn the source of the magmas within the Earth.

Chapter 6: Trace Element Geochemical Analysis of Erupted Material from Oldoinyo Lengai

6.1. Whole rock geochemical analysis

6.1.1. Previous work on bulk geochemistry for Lengai Units

6.1.1.1. Major element chemistry of carbonatite

Carbonatites, in general, are characterised by having high abundances of Sr, Ba, P and light rare Earth elements (LREEs), often more than 3 orders of magnitude higher than those of chondritic meteorites. The majority of carbonatites also show a large negative Zr and Hf anomaly (Nelson et al., 1988). Their chemical composition makes them useful rocks to study to understand the processes taking place within the upper mantle as the effects of crustal contamination on mantle signatures are reduced (Bell, 1994). An excellent overview of the average chemical composition for each sub-division of carbonatite can be found within Bell (1989). It is thought that concentrations of Si, Ti, Mn, Ba, Fe and F increase through the series of calciocarbonatites – magnesiocarbonatites – ferrocarbonatites whilst Al, Na, K, Sr and P are consistent throughout all of the carbonatite divisions, with the exception of natrocarbonatite which is dominated by Na_2O and K_2O (Woolley and Kempe, 1989).

Natrocarbonatite major element chemistry is characterised by enrichments in alkali elements with up to 41.5 wt% of Na_2O and K_2O but extremely low SiO_2, TiO_2 and Al_2O_3 (Zaitsev et al., 2009, Ridley and Dawson, 1975), along with high amounts of CaO and CO_2 and lesser amounts of BaO, SrO, P_2O_5, SO_3, Cl, F and MnO, but these are still in excess in comparison to silicate igneous rocks (Dawson et al., 1990, Church, 1995). Reported bulk chemistries from lava erupted in 1960, 1988 and 1992 all appear similar, suggesting that the natrocarbonatite bulk chemistry has not changed significantly in over 40 years and is thought to show a lack of fractionation of the carbonatite reservoir (Church, 1995). The associated olivine melilitites to Oldoinyo Lengai's carbonatite lavas are also higher in alkali elements than melilitites associated with other carbonatites globally.

6.1.1.2. Trace and rare Earth element chemistry of carbonatite

Rare-Earth element (REE) concentrations of a number of carbonatites and the Kaisersthul phonolite are shown below in Figure 6.1. It can be seen that carbonatites exhibit a steep, light rare-Earth element (LREE) enriched pattern when normalised to chondritic values.

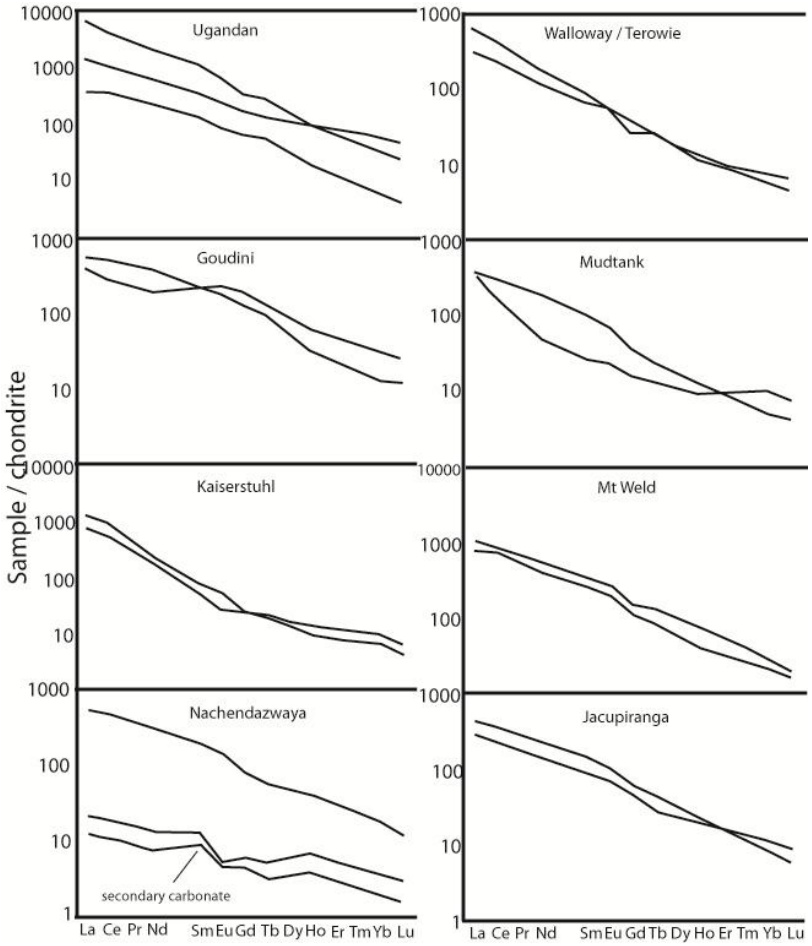

Figure 6.1: Typical chondrite normalized rare Earth patterns of carbonatitic material (Nelson et al., 1988)

The trace element and REE pattern for Oldoinyo Lengai natrocarbonatite is similar to that of other carbonatite varieties. In general, the lavas contain high concentrations of light rare Earth elements with La/Yb and U/Th ratios, being amongst the highest of all terrestrial magmas ((Dawson, 2008) and references therein). The 1993 natrocarbonatite lavas are particularly enriched in Ba, Cs, K, Mo, U and LREEs relative to primitive mantle (Simonetti et al., 1997) with slight variation between the lava types, i.e. spheroid-free or spheroid-bearing. Simonetti et al (1997) note other interesting features of natrocarbonatite chemistry; most samples have a Ba / Sr ratio of greater than 0.7 which is opposite to most primary calcite carbonatites. The Au

contents are also higher than those of continental crust. Distinct chemical varieties were also recognised by Keller and Krafft (1990) with aphyric, phenocryst-poor lavas having a more fractionated pattern with enrichments in Mn, Mg, Fe, V, Ba, Rb, Nb, Y and several volatile species in comparison to phenocryst – rich lavas.

Keller and Krafft (1990) also investigated the wetness of natrocarbonatite. A consistently low H_2O^+ value between 0.24 – 0.56% was noted, which shows the natrocarbonatite is extremely dry upon eruption. This of course has consequences for secondary water absorption leading to alteration, which will be discussed in chapter 8.

6.1.1.3. Bulk geochemistry of fenitic units

The bulk geochemistry of the fenitic units from Oldoinyo Lengai are more complex to characterise due to the influence of the original host rock from which they form. In general fenites are alkali-rich with abundant sodic and potassic pyroxene, amphibole and feldspar (Sutherland, 1969), but are heterogeneous in terms of SiO_2, Al_2O_3 and CaO (Kramm and Sindern, 1998). The fenite units from Kramm and Sindern (1998) continue to show variability in terms of their trace element patterns with no apparent systematic variation, except for Nb which is positively correlated with fenite grade.

The aim of this chapter is to further investigate the trace element chemistry of the fenite units erupted as xenoliths during the latest phase of activity of Lengai and compare them to the chemistry of the natrocarbonatite lava in an attempt to determine the source of the fenitising fluids circulating in the volcanic complex and shallow upper mantle. This in turn indicates the depth to which carbonatite melts exert a chemical influence.

6.2. Bulk Geochemistry of units from Lengai from 2006 / 07 eruption

6.2.1.Geochemistry of natrocarbonatitic units

Table 20 below contains the whole rock chemistry of a sample of the 2006 / 07 natrocarbonatitic flow, which descended the western slope of Oldoinyo Lengai prior to the explosive eruption, collected during the field campaign in May 2010. It is also compared with data from Keller et al (2010) for an average composition of natrocarbonatite material erupted in the active crater prior to the explosive eruption and a sample of the 2006 flow collected at

the end of August 2007. Therefore the data from this study and the data from Keller et al (2010) are similar except for the time difference between sample collection. This is evident from the trace element spider plot in (Figure 6.2).

Table 20: Whole rock chemistry of natrocarbonatite sample collected from the 2006 flow from the western slope of Oldoinyo Lengai during May 2010 field campaign. LoQ = limit of quantification; LOD = limit of detection.

1. Determined in this study by ICP – MS / AES.
2. Comparison data of material analysed by previous authors both prior to 2006 eruption and the 2006 material (Keller et al., 2010)

	OL3[1]	LoQ/LOD	Pre 2006[2]	Post 2006[2]
Al_2O_3	0.49	0.05	0.01	0.12
CaO	25.69	0.01	15.60	17.36
Fe_2O_3	1.35	0.001	0.45	0.53
K_2O	2.15	0.002	7.63	6.70
MgO	0.36	0.05	0.44	0.39
MnO	0.50	0.001	0.46	0.34
Na_2O	23.21	1	32.35	32.46
P_2O_5	1.18	0.05	0.89	1.05
TiO_2	0.05	0.01	0.01	0.05
ppm				
Ba	9838	1	11,485	9,124
Co	1.21	0.0019	0.5	-
Cr	<	40	5.3	-
Cs	2.69	0.0015	2.92	-
Ga	<2	0.151	-	-
Li	93.3	0.025	-	-
Mo	3.23	0.068	92	-
Nb	190	0.1	35	52
Pb	93.5	0.025	92	80
Rb	69.5	0.04	159	160
S	2713	90	-	-
Sb	0.592	0.004	2.35	-
Sr	13417	1	11,487	10,380
Th	15.3	0.014	4.2	1
U	10.5	0.0004	11	7
V	100	15	157	-
W	3.05	0.101	44	-
Y	24.7	3	7.0	-
Zn	242	5	122	-
Zr	14.3	0.220	0.82	-
ppm				
La	645	0.0008	543	412
Ce	806	0.0011	649	586

Pr	65.3	0.0007	44	-
Nd	176	0.0006	105	88
Sm	16.5	0.0005	7.09	-
Eu	3.64	0.0007	1.80	-
Gd	9.16	0.0008	3.87	-
Tb	0.867	0.0006	0.379	-
Dy	3.67	0.0008	1.41	-
Ho	0.572	0.0006	0.131	-
Er	1.32	0.0005	0.371	-
Tm	0.152	0.0006	0.034	-
Yb	0.918	0.0005	0.217	-
Lu	0.112	0.0006	0.028	-

The bulk chemistry of sample OL 3 is typical of natrocarbonatite which has been exposed to atmospheric conditions over a period of time. If we take the dataset from Keller et al (2010) to represent relatively fresh material, we can see that sample OL 3 is more enriched (up to 10 wt%) in Ca, Fe and Al, but is depleted in Na and K in comparison to the major elements of the other units. This is the result of mineral breakdown and secondary mineral precipitation which will be discussed in greater detail in chapter 8. All samples are enriched in particular trace elements (Ba, Sr, LREEs) as expected from previous work on carbonatites (Simonetti et al., 1997, Bell, 1989, Nelson et al., 1988). However OL 3 is also enriched in a number of elements which are generally fluid-mobile and so would have been introduced by the flow of atmospheric / meteoric water during alteration. A depletion in other fluid-mobile elements, such as Rb, has also occurred as these are stripped from the carbonatite during weathering. One enrichment that is unusual is the presence of over 2000 ppm of sulphur in sample OL 3 but not in Keller's datasets. This is thought to be the product of secondary mineralogy which occurs during alteration and the breakdown of the primary minerals nyerereite and gregoryite.

6.2.2. Bulk geochemistry of fenite units from Lengai (this study)

The fenitisation at Oldoinyo Lengai has previously been characterised as an equilibration of metagabbroic or metagranitic protoliths with an alkaline, CO_2-rich fluid (potentially even natrocarbonatite) within the temperature range of 700 to 800°C (Morogan, 1994). Towards the upper end of this temperature range Morogan (1994) argued that incipient melting occurs, recorded by silicate glass within high grade fenites – indicating that rheomorphism occurs during fenitisation. The author also argues that since equilibration occurs under the same conditions with the same fluid, any difference between fenitic units must be the product of a

different protolith. The work also shows that the fenite units previously studied from Lengai all have similar modal mineralogy but vary in their bulk geochemistry, which is again a product of the protolith involved.

In chapter 4 the petrography of fenitic units OLX 15, OLX 17a and OLX 17b was discussed in detail and argued to represent a fenitised pyroxenitic unit and two fenitised metagranitic or metagabbroic units, respectively. The determination of the protolith and degree of fenitisation for each unit has, at first approximation, been based on the mineralogy present in accordance with Morogan (1994). Using this method it is concluded that OLX 17a represents a high grade fenite from a metagabbroic protolith, whilst OLX 17b contains a mineral assemblage indicative of a medium grade fenite from a metagranitic unit. All three units appear to have been subject to carbonatitic rather than ijolitic fenitisation and the difference in grade between the samples accounts for the presence of relict quartz within OLX 17b, which if fenitised to a higher grade would have been fully incorporated.

A comparison of the bulk geochemistry of these samples is a logical progression in order to characterise their generation and so is the focus of the following sections.

6.2.2.1. Major element chemistry

The previous chapter highlighted that the fenitic units collected from Oldoinyo Lengai seem to be the only units which contain carbon dioxide-rich fluid inclusions. This observation would seem to suggest that the fenitic units are related to the carbonatitic material extruded from Oldoinyo Lengai. Previous work on fenites concluded that their bulk geochemistry shows a high concentration of calcium and an addition of Fe, Ti and P, but depletion of Si, if formed from a granitic ancestor. Those thought to have been produced from a gabbroic ancestor show a slight increase in Si but depletion in Al and Mg upon fenitisation (Morogan and Martin, 1985).

	OLX15[1]	OLX17a[1]	OLX17b[1]	LoQ/LOD	Meta-granite[2]	Pyroxenite[3]	Meta-gabbro[4]
Al_2O_3	11.0	18.1	12.8	0.05	16.24	5.63	13.60
CaO	13.25	20.09	2.55	0.01	3.806	12.13	13.11
Fe_2O_3	16.8	5.93	4.00	0.001	4.36	7.36	12.48
K_2O	2.50	3.26	4.83	0.002	1.868	3.48	0.50
MgO	3.64	1.92	1.35	0.05	2.452	16.97	8.74
MnO	0.42	0.44	0.09	0.001	0.05	0.26	0.20
Na_2O	9.39	9.85	6.92	1	4.57	0.87	1.86

P_2O_5	0.38	0.38	0.49	0.05	0.376	0.11	0.42
TiO_2	2.06	0.76	0.52	0.01	0.621	3.54	1.48
SiO2	40.7	39.3	66.5		65.66	41.06	47.40
$(Na_2O+K_2O)/Al_2O_3$	1.08	0.72	0.92				
ppm							
Ba	1036	792	1051	1	622.2	747.5	550.6
Co	28.3	9.93	8.03	0.0019	16.8	-	-
Cr	142	80.3	155	40	104	997	-
Cs	0.686	0.889	0.830	0.0015	-	-	-
Ga	24.0	30.6	12.1	0.151	-	-	-
Li	10.4	5.20	16.6	0.025	-	-	-
Mo	0.702	0.419	1.54	0.068	-	-	-
Nb	368	374	17.2	0.1	5.6	80.5	16.8
Pb	14.4	10.4	10.5	0.025	19.33	-	13.14
Rb	59.5	78.4	84.6	0.04	46.2	94.5	7.43
S	7347	2819	99.5	90	-	-	-
Sb	0.238	0.139	0.092	0.004	-	-	-
Sr	1074	1611	1032	1	504.6	381.5	726.7
Th	7.00	12.8	2.47	0.014	7.8	-	4.25
U	3.08	3.28	1.03	0.0004	2.1	-	1.8
V	606	126	85.2	15	75.2	235.5	-
W	0.574	0.556	0.798	0.101	-	-	-
Y	28.5	21.7	5.7	3	10.6	23.5	29
Zn	229	219	45.0	5	48	128	-
Zr	1125	95.0	38.3	0.220	139.2	222.5	121.4
ppm							
La	64.8	123	31.6	0.0008	31.7	86.6	27.8
Ce	131	234	47.6	0.0011	66.5	180.7	58.5
Pr	13.6	21.8	4.72	0.0007	7.982	22.1	9.1
Nd	49.7	67.8	16.3	0.0006	27.5	75.9	38.59
Sm	8.78	8.62	2.35	0.0005	4.9	13.4	8.96
Eu	2.66	2.21	0.529	0.0007	1.338	3.63	2.42
Gd	7.08	6.08	1.71	0.0008	3.34	10.4	9.43
Tb	0.961	0.733	0.218	0.0006	0.44	-	1.49
Dy	5.19	3.71	1.17	0.0008	2.08	5.63	8.94
Ho	0.920	0.641	0.211	0.0006	0.36	1.0	1.82
Er	2.48	1.61	0.557	0.0005	0.98	2.54	5.08
Tm	0.385	0.218	0.075	0.0006	-	-	-
Yb	3.03	1.42	0.493	0.0005	0.88	1.52	4.53
Lu	0.562	0.224	0.081	0.0006	0.132	0.21	0.65

Table 21: Major, minor and trace element data for fenitic units collected during field work.
LoQ = limit of quantification; LOD = limit of detection. OLX 15 – metasomatised peridotite; OLX 17a – fenite; OLX 17b – fenite. Green highlighted boxes represent elements gained during fenitisation, orange highlighted are elements lost during fenitisation.

1. Determined by ICP-AES / MS at the Natural History Museum for this study
2. Amphibolite country rock units from Tanzanian Craton. Data from (Manya and Maboko, 2008)
3. Average pyroxenite composition from samples BD93 and BD 867(Dawson and Smith, 1992a)
4. Metagabbroic country rock complied from (Johnson et al., 2007, Prochaska and Pohl, 1983, Nyamai et al., 1999)

In terms of major elements, all of the fenitic / metasomatised units have been subject to Na and K enrichment regardless of the protolith from which they were formed. However in agreement with Morogan and Martin (1985) particular changes to the major element chemistry can be seen depending on whether the unit was formed from a felsic or mafic protolith. All fenite samples show a loss in MgO content most likely as a result of breakdown and replacement of primary pyroxene or olivine depending on the protolith. This may also explain the apparent loss of total Fe from sample OLX 17a. The predicted Al depletion of samples formed from metagabbroic units is not apparent and unexplained at this point. Only sample OLX 15 appears to be peralkaline ($Na_2O + K_2O)/Al_2O_3$ >1).

Interestingly, sample OLX 17b appears to have only gained alkali elements and the remainder of the major elements show small loss or similarities to that of the metagranitic protolith. This is expected for a medium grade fenite with relict minerals, indicating the re-crystallisation has not completely destroyed the original chemistry of the rock. This is also indicated in the silica content of the unit which is almost exactly the same as the compared metagranitic unit (table 21).

The major element signatures of the fenite units above seem to agree with the proposed parent units but for a better understanding of the fluids causing the fenitisation the minor and trace elements must be investigated.

6.2.2.2. Minor and trace element chemistry

The minor and trace elements for any unit are best interpreted using chondrite-normalised spider diagrams as in Figure 6.2, which enable us to look at relative enrichments and depletions. Chondrite normalisation was completed using CI chondrite values outlined in Sun and McDonough (1989) and McDonough and Sun (1995). The first thing to notice is the similarity in the plots for samples OLX 15 and OLX 17a which is a result of the similarity of their protoliths – both derived from metasomatised mafic units.

OLX 15 exhibits gain of the heaviest REEs and is also the only metasomatised unit to have increased Zr concentration due to metasomatism. The elements gained for this unit are all typical elements for carbonatitic fluids with increases in Ba and Sr as well as REE which are abundant in carbonatites. The other enrichments are also of typical fluid-mobile elements, large ion lithophiles (LILEs) or high field strength elements (HFSEs) such as Rb, Nb and Y. Fenite

OLX 17a illustrates enrichment in fluid-mobile elements as well as LREEs. The HREEs are less enriched in this sample. This type of enrichment pattern has some similarities to both carbonatitic fluids and alkali-rich silicate fluids and so the source of fenitisation of OLX 17a is more complex.

The effect of carbonatitic fenitisation is best illustrated by the minor and trace elemental pattern of sample OLX 17b which only shows enrichments in Ba, Rb, Sr and V which are again elements associated with carbonatitic fluids either as elements which make regular substitutions within the carbonate minerals (Ba and Sr) or as fluid-mobile LILE's or HFSE's, which can be incorporated by interaction with the fluid. However the REE pattern in 6.2b shows that sample OLX 17b is depleted in REE's compared to all other fenitic units and table 21 shows that it is also depleted with respect to its parent unit – metagranite. I however suggest that the fenite is not depleted in REE but has not been subject to REE enrichment from fenitisation to the same extent as the other fenites. This is in keeping with the proposed proximity of this unit to the source of fenitising fluid. As a lower grade fenite than the other units, OLX 17b would not have been subject to the same level of fluid interaction as the other fenites and so the enrichment would not be as evident.

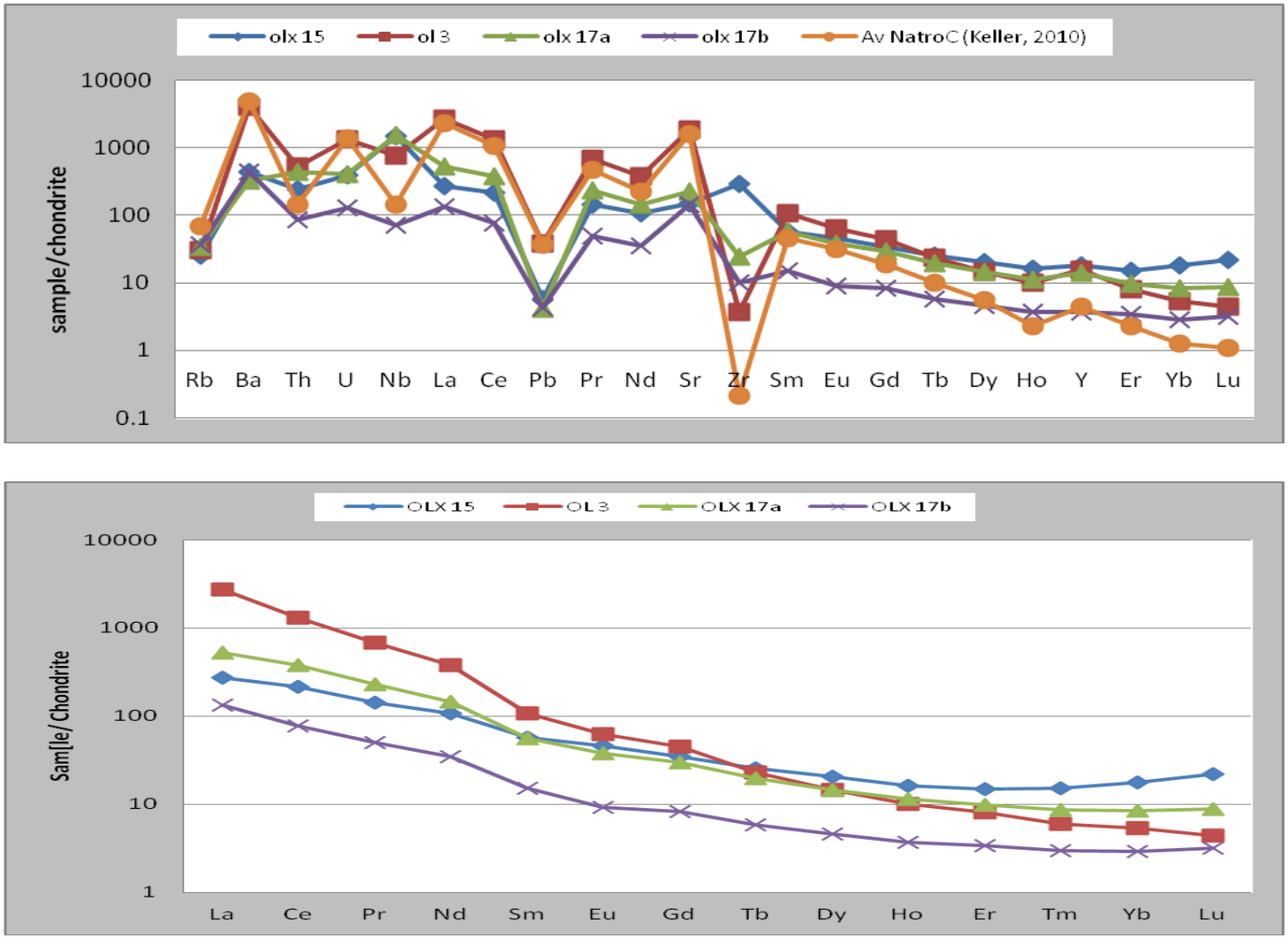

Figure 6.2: Minor and trace element plots of carbonatitic units and fenitic units from Oldoinyo Lengai. (a) Chondrite-normalised minor and trace element plot comparing all fenites with natrocarbonatitic material (OL 3); (b) REE plot of fenites and natrocarbonatite (OL 3) for closer look at mixing properties of the fenites with the carbonatite material. Chondrite normalised according to CI carbonaceous chondrite (McDonough and Sun, 1995, Sun and McDonough, 1989)

6.3. Geochemical modelling of trace element patterns of fenites

Primary magmas, once segregated from their source, are subject to processes which can alter their initial chemistry en route to the Earth's surface and also alter the chemistry of the units through which they pass. These processes take place both during transport and periods of storage in different parts of the Earth and are the reason for the diversity in rock units observed across the globe. The relation of metasomatism and magmatism can be viewed in two stages: the first is directly associated to the intrusion of the magma and the fluids which emanate from the intrusion and alter the surrounding solid host rocks. The second stage occurs after the intrusion and involves hydrothermal solutions either derived from the cooling magma or from external fluid sources which are heated due to the proximity of the intrusion, i.e. juvenile or meteoric water (Richardson and Birkett, 1996, Le Bas, 1981, Le Bas, 1987).

Normally restricted to discussion of contamination by crustal material to the ascending magma, the interaction between the upper mantle units and magmas are generally not discussed as contamination as the magmatic units are thought to be in equilibrium with the rocks since they have originally been derived from this material by partial melting. However, in the case of carbonatitic units this may not be the case. Despite derivation from a proposed carbonated peridotitic unit the melts are subject to non-steady state mass transfer and ultimately metasomatic processes, as indicated by the presence of sample OLX 15 within the xenolith suite. This alteration at high pressures and temperatures is thought to be the result of concentrated liquids which have properties between that of fluids and magmas. The mechanisms of alteration are not clear and ultimately this is referred to as mantle metasomatism (Zharikov et al., 2007).

The low viscosity and chemical composition of carbonatites makes them excellent metasomatic agents. Hammouda and Laporte (2000) argued that percolation of carbonatitic material through olivine occurs at a rate of several millimetres per hour by a process of dissolution-precipitation. The observed rates are several orders of magnitude higher than those previously found for basalt infiltration in mantle lithologies. However, it could be argued that such quick percolation may result in short residence times that do not enable chemical interaction and metasomatism to take place (Dalou et al., 2009). Carbonatite metasomatised units are however identifiable in the East African rift region resulting in fenitised units and glimmerite layers with abundant phlogopite, pyroxene and amphibole (Dawson and Smith, 1992b, Dawson et al., 1995, Dawson and Smith, 1988, Rhodes and Dawson, 1975), as well as across the globe (Stoppa et al., 2009, Stoppa et al., 2008, Rosatelli et al., 2007, Lev et al.,

1988). Could this metasomatism be the result of carbonatitic fluids derived from carbonatites or can carbonatites cause chemical changes during their rapid ascent?

Metasomatic processes are divided into two categories which depend on the nature of the mass transfer: either those caused by diffusion or those caused by infiltration (Korzhinskii, 1957). The latter is the result of material transfer by solution that infiltrates host rocks and is driven by the pressure and concentration gradients between the infiltrating fluid and the rock-pore fluids. Infiltration metasomatic units are of a greater volume and have an almost constant composition of minerals across the zone of alteration (Korzhinskii, 1968).

The presence of heterogeneities within the elemental patterns of certain rock units from Lengai can be interpreted as features produced by the interaction of rocks with infiltrating melts or fluids, generating metasomatic units. The metasomatism can either be the product of diffusion-controlled or percolation-controlled processes. These heterogeneities can also be seen at the microscopic scale with variations in mineral chemistry as documented in chapter 4.

The distribution of trace elements within magmatic units at a given time is predictable based upon the distribution coefficient of the element between the liquid and solid phases (DePaolo, 1981). Trace elements are ideal tools to investigate metasomatic process as they behave in similar ways during magmatic processes but have variation in their compatibility in fluids. Their concentration in trace amounts also means that subtle changes are often recorded. For this reason the bulk geochemistry of the fenitic units along with that of the natrocarbonatitic units were used for trace element modelling to determine the nature of the fenitisation beneath Oldoinyo Lengai.

It should be noted that the full derivation of the equations used for the geochemical models in the following sections is beyond the scope of this thesis and an outline of how these equations are generated can be found within Navon and Stopler (1987), Bodinier et al (1990) and Vasseur et al (1991).

6.3.1. Use of Assimilation – Fractionation – Crystallisation (AFC) model

6.3.1.1. The basics of the model

A first approximation, basic model, to determine the source of the fenitising fluid, is to view the system as one of assimilation. The study of the petrography of the samples in chapter 4 indicated that the parental units to the fenites are either metagabbroic or metagranitic

country rocks of the Tanzanian craton or the Mozambique mobile belt. If these units were subject to fluid flow by an infiltrating magma it can be imagined that assimilation may occur and subsequent crystallisation of the fenitic mineralogy. For any trace element the equation itself is as follows (DePaolo, 1981, Powell, 1984);

$$C_L = C_L^O f + (r / r\text{-}1+D) * C_* (1\text{-}f) \qquad (1)$$

Where $f = F^{-(r-1+D)/(r-1)}$, F = fraction of magma remaining (between 0.1 and 1), C_L = element concentration in the contaminated unit (fenite), C_L^O = element concentration in the parental rock unit (metagranite or metagabbro), C_* = element concentration in the contaminating fluid (natrocarbonatite or ijolite), r = ratio between assimilation and fractional crystallisation and D = the bulk distribution coefficient.

The trace element concentrations of the country rocks (C_L^O) are listed in table 21 above, along with the measured trace element concentrations of the fenites. The partition coefficient for each element was calculated based upon the mineral composition of the fenites and experimental data from numerous authors regarding the partitioning of elements between minerals and carbonatite / silicate melts (Klemme et al., 1995, Blundy and Dalton, 2000, Green, 1994, Dalton and Presnall, 1998, Sweeney et al., 1992, Irving and Wyllie, 1973, Dawson et al., 1994b, Dalou et al., 2009, Wilson, 1989), the limitations of which will be discussed below. The trace element concentration of the modelled fenite was then estimated for values of F between 0.1 and 1 for various values of r between 0 and 1. The actual trace element composition of the fenite was then superimposed on top of the range of concentrations for comparison and to decide which value of r and F were appropriate.

6.3.1.2. Results of the AFC modelling

The spider diagrams in Figure 6.3 below represent the modelled compositions of the 3 fenitic units (OLX 15, OLX 17a and OLX 17b) for which full elemental analysis was obtained by ICP-MS / AES. In all the diagrams the element concentrations are non-normalised units and so still contain the Oddo – Harkins effect of higher concentrations of even atomic number elements compared to that of odd numbers and so this must be taken into consideration.

The shaded area in all the spider diagrams represents the model results between F = 0.1 (black dashed line) and F = 0.9 or 1 (red dashed line) and the darker, solid line illustrates the actual measured composition of the fenitic unit. The colour ascribed to the shading also differs based

on the fenitising fluid modelled. The yellow shading represents the elemental signatures that would develop if the fenite were generated by the infiltration of ijolitic melt whereas the blue represents that of carbonatitic fenitisation. The model results below characterise what are judged to be the best fit results from all of the models generated using the AFC method. The best match was determined by those which have the most reasonable value for r and F and also produce trace element patterns with corresponding shapes to those actually measured.

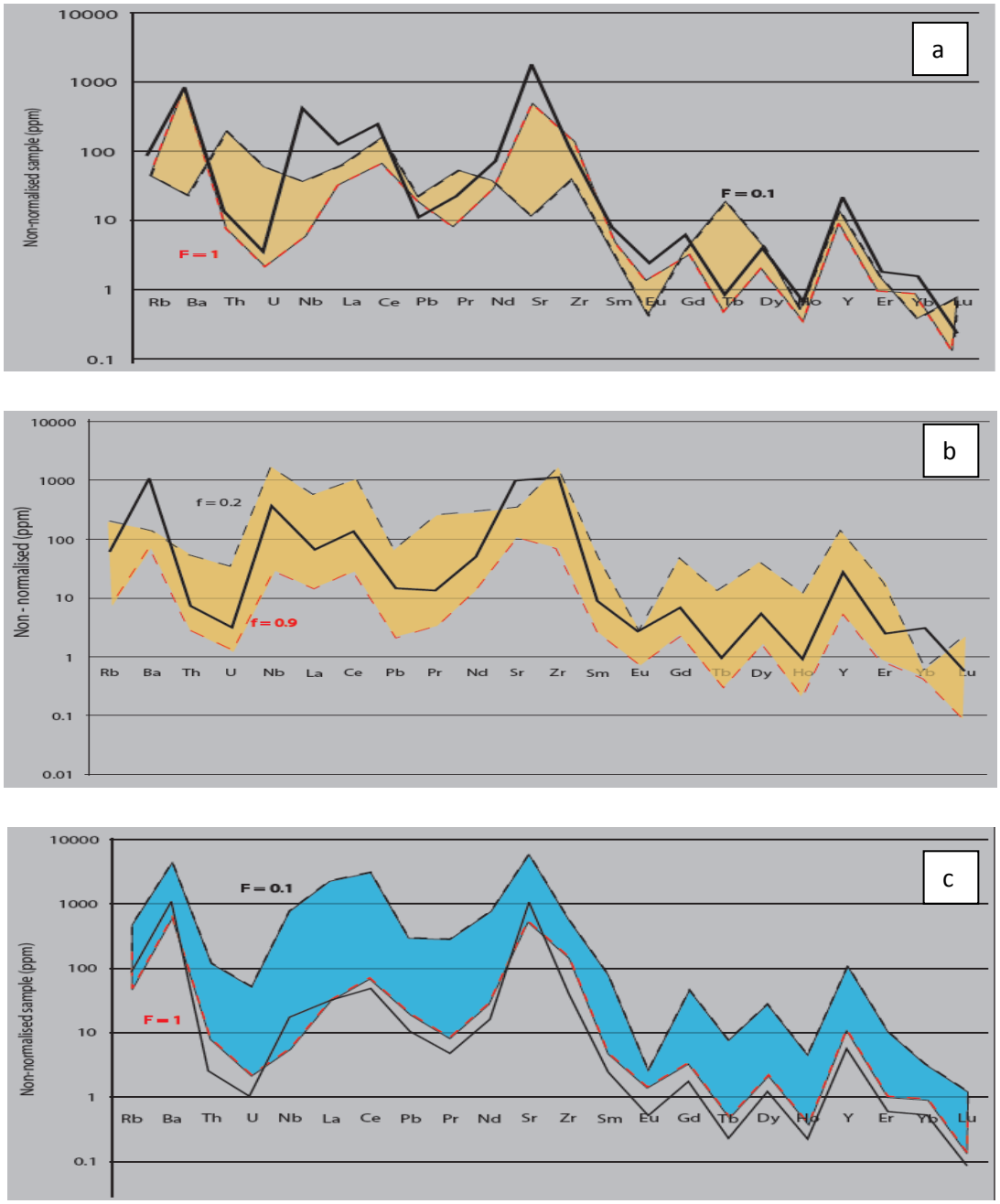

Figure 6.3: Spider diagrams of modelled trace element patterns after fenitisation; (a) Model for sample OLX 17a with ijolitic fenitisation at r = 0.7; (b) Model for sample OLX 15 with ijolitic fenitisation source at r = 2; (c) Model for sample OLX 17b at r = 0.3 with carbonatitic fenitising fluids.

At a first approximation, from the models above, it can be concluded that both ijolitic and carbonatitic fenitisation are taking place within the complex at Oldoinyo Lengai, which has previously been stated in chapter 4 as only being subject to carbonatitic fenitisation. Sample OLX 17a appears to correspond to the fenitisation of a meta-gabbroic host rock by an ijolite intrusion where the ratio between assimilation and crystallisation is ~0.7 and an infiltrating melt fraction of 80 – 90%.

Sample OLX 15 also appears to be the product of silicate melt metasomatism due to the lack of Nb and Zr depletion normally associated with carbonatite metasomatism (Downes, 2001). The model shows that the alteration of the mantle material to sample OLX 15 requires a ratio of 2 and a melt fraction of ~ 60%. This would again explain the similarity in the trace element patterns of OLX 17a and OLX 15 in Figure 6.2, as not only are their protolith similar in terms of mineralogy but also the fluid causing metasomatism is of similar chemistry.

Sample OLX 17b, however, appears to be the product of carbonatitic fenitisation occurring at different levels within the crust (as determined by thermobarometry from chapter 4). OLX 17b requires a ratio of 0.3 between assimilation and crystallisation and an apparent requirement of a melt fraction of around 90 – 95%. This seems unlikely to be accurate as it does not correspond with the petrographic interpretation that this unit represents only a medium grade fenite, due to the presence of relict quartz.

The above results do however conform with a number of observations made in the previous chapter and the presence of fluid inclusions within these fenitic samples. All three samples appear to contain fluid inclusions, but their composition is not uniform with sample OLX 17b containing abundant CO_2-rich inclusions. If the above models are accurate the observed differences in fluid inclusion content can be explained by the volatile content of the intruding magma and so subsequent emanating fluids. Ijolite magmas are known to be low in CO_2 but high in H_2O, whilst the opposite is true for carbonatitic fluids which are high in CO_2 and lower in H_2O.

6.3.1.3. Evaluation of using the AFC model

The AFC model provides us with a good starting place for modelling the trace element signatures of the fenitic units, but is a poor approximation at best due to a number of limiting factors:

1. The bulk D values used in the calculations are not all based upon carbonatite – mineral partitioning due to a lack of available data either from natural samples or those produced experimentally. This means that for some elements and minerals the models may not be a true representation of what is likely to happen in nature.

2. Partition coefficients are also not available for all minerals within the fenites and so it is possible that the modelled signature may be swamped by those minerals for which D is available.

3. Out of all the models produced, none were a perfect fit of the measured composition to model. The peaks and troughs appear to be in the correct places but some offset is always present for some elements suggesting an extra chemical source not taken into account.

4. There is an inability to truly model the systems based upon the unknown factor of r. At the moment r is estimated using my own judgement and so is purely subjective. Quantification of this ratio would improve the model.

5. The above improvements are likely to be universal for any geochemical model chosen to investigate the origin of the fenitisation in the Lengai region. However the main criticism of using the AFC model is that fundamentally the process of fenitisation implies a passage of fluid through a body of rock with an emerging fluid at the end of the process, i.e. ultimately an open system. The AFC model is a “closed” system rather than an open system, usually employed for the understanding of compositional changes of a magma contained within a chamber due to assimilation of the wall rocks of the chamber.

With the above criticisms in mind it can be seen that as a first approximation the AFC model does provide some useful, initial information but a more advanced model is required to better understand the metasomatic processes occurring. The next stage in the modelling is therefore to look into open system modelling such as that of the Chromatograph model which allows for an emerging liquid of some composition which is determined by the composition of the input melt and the matrix through which it flows. In the AFC model this expelled fluid may well be what is captured as inclusions in the other rock units within the volcanic complex.

6.3.2. A Chromatographic model for metasomatism

6.3.2.1. Theory of the Chromatograph model

The chromatograph model of metasomatism is based upon an infiltration method of metasomatism, proposed for melt percolation within the mantle (Navon and Stolper, 1987), with an ideal situation as follows; a column of porous rock that is uniform in composition, which contains interconnected pores accessible along grain boundaries. This column is infiltrated by a fluid which differs in chemistry from the original pore solution and displaces it in the direction of flow. The composition of the infiltrating fluid is argued to be constant and out of equilibrium at the origin of the column but is subject to continual reaction during percolation through the column and trends towards equilibrium with the matrix. Once this is achieved it is possible for the fluid introduced at the base of the column to pass through without interaction. The elements within the fluid and solid matrix behave differently during percolation and fractionation occurs according to the partition coefficients, the fluid fraction, column length, flow rate and diffusion coefficients of the fluid and matrix (Hofmann, 1972, Navon and Stolper, 1987, Korzhinskii, 1968, Vasseur et al., 1991, Bodinier et al., 1990).

In an ideal column the elemental exchange between the column matrix and incoming fluid is described by the conservation of mass (Navon and Stolper, 1987):

$$\partial/\partial t\,[\phi\rho_f C_{fi}] + \partial/\partial t[(1-\phi)\rho_s C_{si}] + V_f\,\mathrm{grad}[\phi\rho_f C_{fi}] + V_s\,\mathrm{grad}[(1-\phi)\rho_s C_{si}] - \mathrm{grad}\,[\phi\rho_f D_{fi}\mathrm{grad}C_{fi}] - \mathrm{grad}[1-\phi)\rho_s D_{si}\,\mathrm{grad}\,C_{si}] = 0 \quad (2)$$

Where t = time, ϕ = fluid fraction in the column, ρ = density of the fluid (f) or solid (s), C = trace element concentration in fluid or solid, V = melt velocity relative to the column, D = diffusivities in the fluid or solid.

Navon and Stopler (1987) resolve equation (2) to enable the determination of the concentration of trace elements within the solid matrix behind a concentration front, assuming that the concentration front is a sharp boundary and that the velocity of the incoming fluid is constant;

$$C_s(t) = K_d C_{fo} [\ 1 - (1 - \exp(-\alpha t) / \alpha t)] \quad (3)$$

$$\text{Where } \alpha = (4\pi D_s / a^2) \cdot ((1-\phi)/\phi) (\rho_s / \rho_f)) K_d \quad (4)$$

Where K_d = equilibrium partition coefficient between matrix and melt, C_{fo} = concentration in the fluid as it is introduced at the base of the column, a = radius of the grains in the column.

From the equations it can be seen that the chromatograph model contains a number of variable parameters, the values of which have primarily been determined from the literature and are listed in table 22 below.

Table 22: Input values for unknown parameters in chromatograph model determined from literature.

Parameter	Value	Reference
ρ_f	2.005 g /cm^3 for carbonatite; 2.4989 g/cm^3 for silicate	(Dobson et al., 1996, Wolff, 1994); (Bourgue and Richet, 2001)
ρ_s	3.363 g/cm^3 for mantle; 2.833 g/cm^3 for crust	(Christophe, 2006);(Christensen and Mooney, 1995)
D_s	10^{-12} cm^2 /s for mantle; 10^{-16} cm^2/s for crust	(Bodinier et al., 1990); (Korenaga and Kelemen, 1998)
K_d	Calculated for Bulk D	(Blundy and Dalton, 2000, Klemme et al., 1995, Sweeney et al., 1992, Green, 1994, Dawson et al., 1994b)
a	Modelled between 0.0125 cm and 0.075 cm	(Bodinier et al., 1990, Vasseur et al., 1991)

6.3.2.2. Results of Chromatograph model

All metasomatised units (OLX 15, OLX 17a and OLX 17b) were modelled for both ijolitic and carbonatitic metasomatism and between a fluid fraction (ϕ) of 0.001 and 0.2 and for a time period of 350 kyrs. This time period was chosen on a trial and error basis but fits in with the proposed age of volcanic units within the Gregory Rift of 0.37 Ma (Bagdasaryan et al., 1973) and also the proposed travel times indicated by Hammouda and Laporte (2000) to metasomatise a region of the scale of tens to hundreds of metres. Oldoinyo Lengai itself is argued to have been active from 22 ka (Dawson, 2008) and so it is hypothesised that metasomatism has been an ongoing process within the rift since its formation and not just related to the volcano. The results of the chromatograph modelling are illustrated below.

6.3.2.2.1. Chromatograph model for fenitised pyroxenite sample OLX 15

The modelling of the fenitised pyroxenite was completed using the same input compositions as in the AFC model above. Overall both the ijolitic and carbonatitic models show a good match to the measured composition of sample OLX 15, making it difficult to determine which metasomatising agent is responsible for the mineralogy seen. Both models result in a fluid fraction of around 0.02, which is similar to that of the mantle metasomatism modelled by Bodinier et al (1990) who assumed a fluid fraction of 0.03.

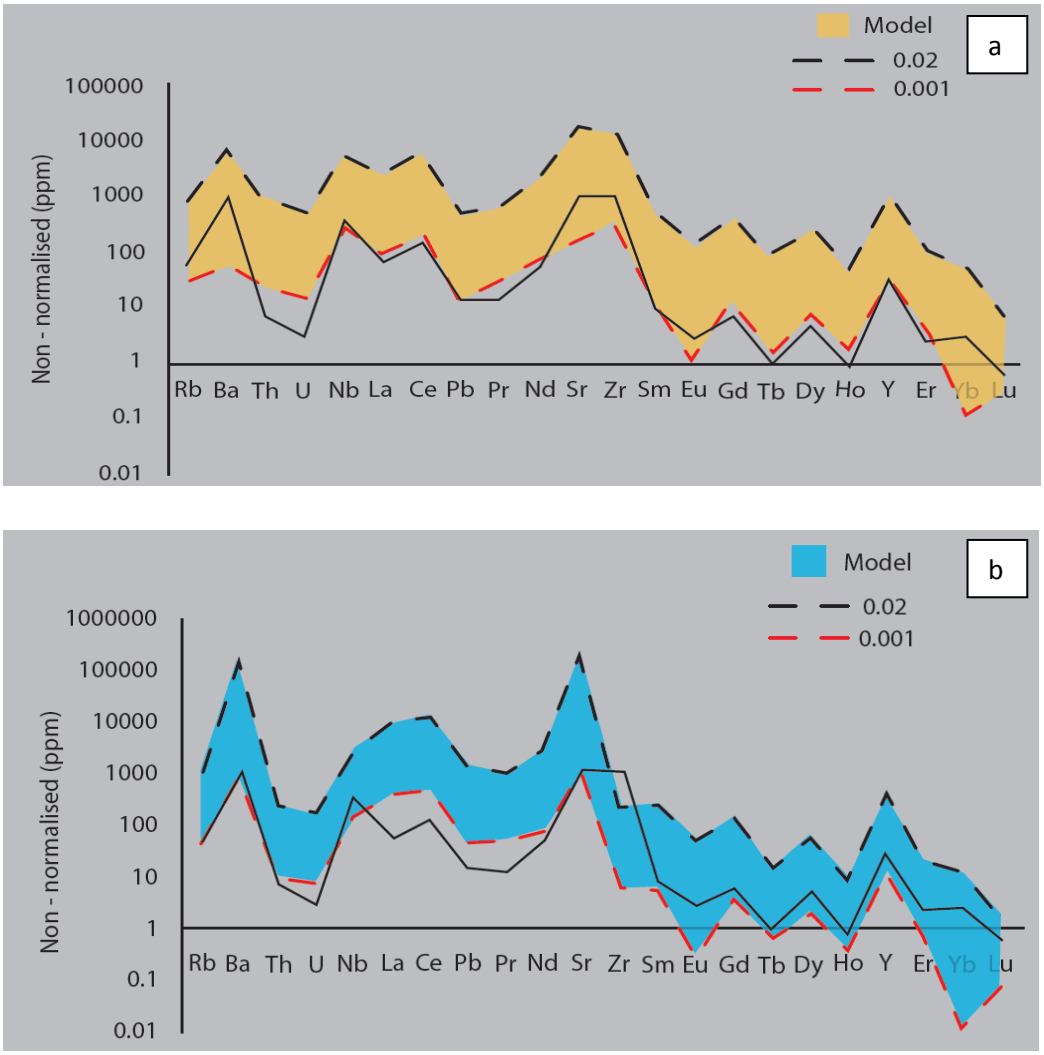

Figure 6.4: Results of chromatograph models for OLX 15; (a) Ijolitic / silicate metasomatism of mantle material over period of 350 kyrs; (b) Carbonatitic metasomatism model of same material over the same time period.

The sample is thought to have been subject to diffusion – controlled, modal metasomatism which results in the formation of new minerals, not normally associated with the mantle protolith. Diffusion – controlled metasomatism generally occurs at small distances to the

infiltrating magma body (for example as a vein network) whose composition is controlled by diffusion processes (Bodinier et al., 1990). The carbonatitic model (Figure 6.4b) predicts the concentration of the HREEs for this sample relatively well but less so for the LREEs and some trace elements. The reverse is true for the ijolitic / silicate model (Figure 6.4a) which models the trace elements and LREEs well, but less so for the HREEs with a minor offset between the model and measured concentrations. Based upon previous evidence from chapter 5 and enrichments of Zr and Nb not normally associated with carbonatitic metasomatism (Downes, 2001), the petrography of sample OLX 15 is argued to be the result of ijolite / silicate melt metasomatism.

6.3.2.2.2. Chromatograph model for crustal fenite OLX 17a

The similarity of the trace element signatures of samples OLX 15 and OLX 17a has previously been highlighted and was argued to be the result a similar chemistry of their protoliths (mantle pyroxenite and metagabbro). However it also appears to be the result of similar metasomatic histories of the units. The models below (Figure 6.5) inidicate that sample OLX 17a is most likely to be the result of ijolitic / silicate metasomatism via diffusion – controlled processes with a fluid fraction of 0.02 – 0.03. The change in mineral composition and the formation of new minerals again typify modal metasomatism, as does the flat chondrite-normalised REE pattern illustrated in Figure 6.2.

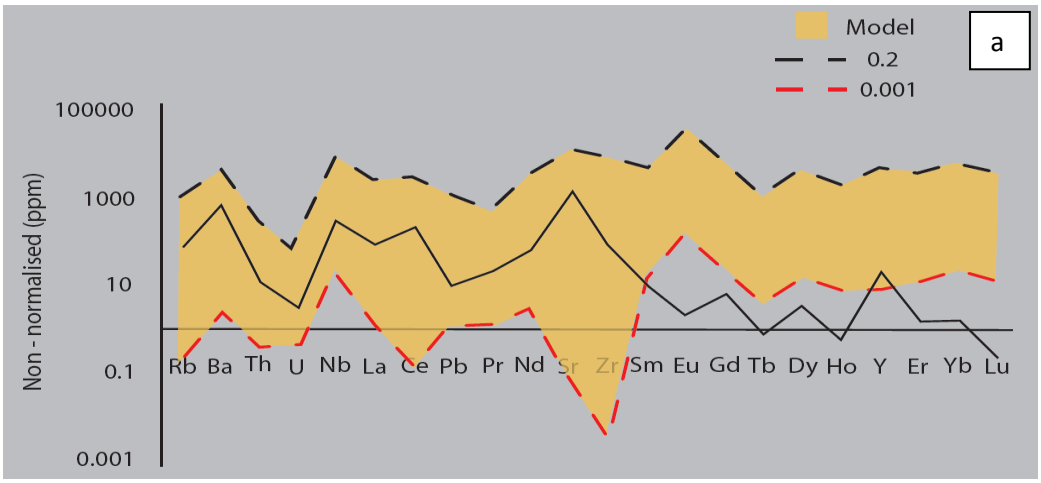

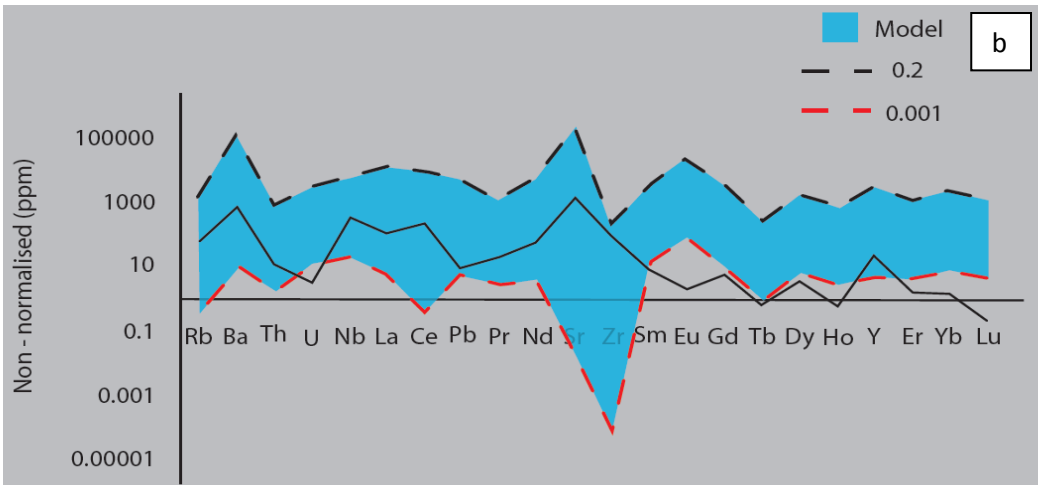

Figure 6.5: Results of chromatograph models for OLX 17a; (a) Ijolitic / silicate metasomatism of mantle material over period of 350 kyrs; (b) Carbonatitic metasomatism model of metagabbroic material over the same time period.

6.3.2.2.3. Chromatograph model for crustal fenite OLX 17b

A strongly fractionated REE pattern, as shown by sample OLX 17b in Figure 6.2, cannot be the result of diffusion-controlled metasomatism according to Bodinier et al (1990) but is the product of percolation-controlled metasomatism between the infiltrating melt and the host rock. This type of elemental exchange is the true interpretation of the chromatograph model and generates cryptic metasomatism within the crust, which changes the mineral compositions but does not result in the formation of new minerals. The presence of relict minerals within OLX 17b supports this and so this fenite is the product of percolation-controlled, cryptic metasomatism.

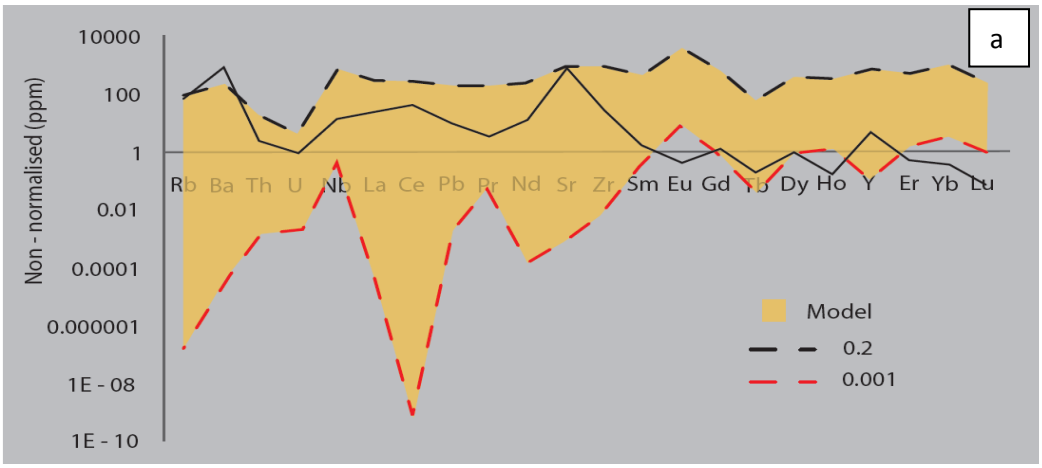

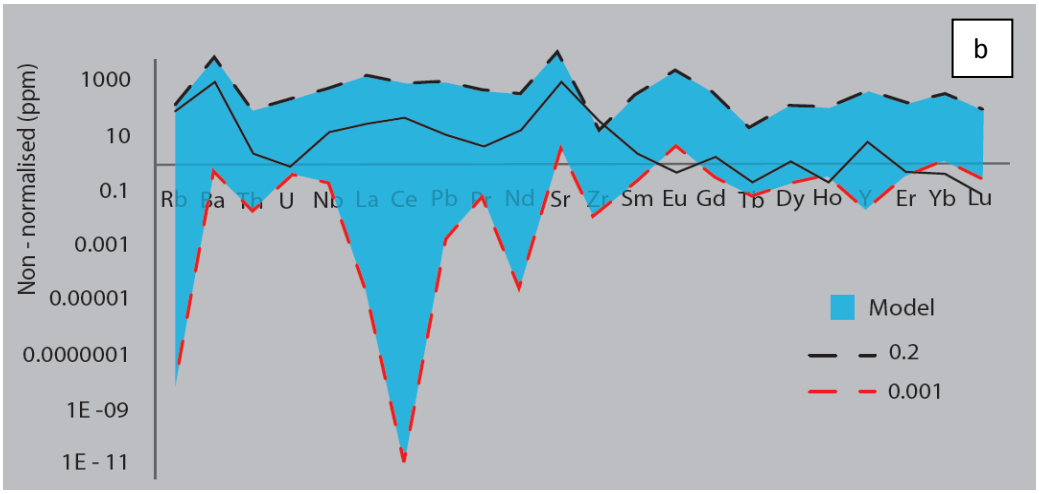

Figure 6.6: Results of chromatograph models for OLX 17b; (a) Ijolitic / silicate metasomatism of mantle material over period of 350 kyrs; (b) Carbonatitic metasomatism model of metagranitic host rock over the same time period.

Previous studies on the differences between modal and cryptic metasomatism have concluded that cryptic metasomatic fronts are found further from the network of infiltrating magma veins and may in fact be caused by the infiltration of CO_2-rich fluids which have partitioned from crystallising silicate melts (Menzies et al., 1985). Figure 6.6 illustrates the results of the chromatograph model for OLX 17b and also seems to support Menzies et al (1985). It can be seen that both the ijolitic and carbonatitic models provide a good estimation of the composition of the fenite unit with both models looking similar. However the match of the measured composition is slightly better with that of the carbonatitic fluid source and so is concluded to be a carbonatite metasomatised crustal unit. This conclusion is also supported by the presence of CO_2-rich fluid inclusions within minerals of OLX 17b (discussed in Chapter 5), which according to Menzies et al (1985) can be expected from the infiltration of a carbonatitic fluid. It is argued that sample OLX 3 discussed in chapters 4 and 5 also represents a cryptic carbonatite metasomatised unit.

6.3.2.3. Evaluation of the Chromatograph model

The chromatograph model has the slight drawback in that it is not known how the exchange process works with melts passing through a matrix of completely different composition, as it is normally used to model basaltic melts passing through mantle material from which they were originally derived. In theory so long as the infiltrating melt and the matrix are out of equilibrium chemical interaction and exchange should occur until an equilibrium is established

over time (Navon and Stolper, 1987). This process, however, introduces a second issue in that how can we be sure that the mantle / crustal column is not "used up" from fluid interaction so that any melt introduced at the base may now pass without interaction. The consequence of this notion is two-fold; firstly if the column has been re-equilibrated so that fluids pass through unaffected the process of zone refining above is obsolete as elemental exchange would no longer occur. Secondly if the column is still capable of imposing a chromatographic effect the modelled chemical composition of the input fluid (C_{fo}) maybe incorrect. The chemical compositions of carbonatite and ijolite were derived from the trace element signatures of the material once it is erupted at the surface either as lava or as xenolithic material. As stated previously, the fluid phase can be strongly affected by the chromatographic process and so these fluids may not represent C_{fo} but actually C_f (t).

The inability to generate a model which fits the natural data perfectly is likely to be the result of the variable nature of the parameters within the models. Each unknown parameter, i.e. ones which were not to be calculated or had not previously been measured, were based upon previous studies using chromatographic models and so although they offer a good approximation of nature they may not exactly characterise the physical properties of the sub-surface material of Lengai and the sub-continental lithospheric mantle of the East African Rift.

6.4. Zone-refining modelling of natrocarbonatite composition prior to percolation from source to eruption

6.4.1. Theory of zone – refining model

The chromatographic effect modelled above has significant implications for the process of zone refining as it is argued that the "geochemical signature of the fluid phase may be strongly affected by the interaction process" (Vasseur et al., 1991). The ascent of magmas from their mantle source is thought to occur via melt percolation and melting of the material in their path, depositing cumulates in their wake and can be thought of as a particular case of the AFC model where the r value is equal to 1, i.e. assimilation and crystallisation occur continuously (Wilson, 1989). It is not unreasonable to believe, therefore, that the compositions of carbonatites exposed at the surface have experienced some deviation away from their original / pristine composition as a result of fluid loss (studied in the previous chapter) and elemental exchange during percolation resulting in the gain and loss of elements according to

thermodynamic principles and partition coefficients. This is also commented on by Vasseur et al (1991) who observe the apparent change in composition of a modelled basaltic melt to that of a kimberlite.

Since we have established that carbonatite percolates / diffuses through certain rock units of known composition, is it possible to work backwards and determine the composition of the carbonatite prior to interaction with the wall rocks, crust and mantle? In order to look at this I have invoked the use of the Zone Refining model. Similar in concept to that of the Chromatograph model of metasomatism primary magmas and magmatic fluids, when segregated from their source pass through the mantle and crust via melting of the rocks in front of them, as they do this interactions between the fluids and the rocks occur and diffusion of incompatible elements either into or out of the fluid resulting in the generation of fenitic / metasomatised units of which we have sampled and know the trace element composition. This enrichment or depletion of incompatible elements is based upon the following model (Wilson, 1989):

$$\mathbf{C_L / C_{LO} = 1/D – [1/D\text{-}1]e^{-nD}} \qquad (5)$$

Where C_L is the composition of the "contaminated" magma, C_{LO} is the primary composition prior to exchange of elements, D is the bulk distribution coefficient between the minerals of the country rock and carbonatite fluids and n is the number of equivalent volumes of rock processed by the magma. When n is large the enrichment has a limiting value of 1/D. Equation 1 can be re-arranged so that C_{LO} can be estimated;

$$\mathbf{C_{LO} = C_L / (1/D – [1/D – 1]e^{-nD})} \qquad (6)$$

The use of the above model has been divided into two steps; the first is the back calculation from what is erupted at the surface after passing through the crustal unit residing underneath Oldoinyo Lengai and the second is the calculation of the composition of the carbonatite melt prior to its interaction with the mantle (Figure 6.7). It is assumed that this is a continuous process and so the maximum composition (where n = 100) from the crustal-refined model is used as the starting material for the mantle-refined model to provide a constraint on the composition.

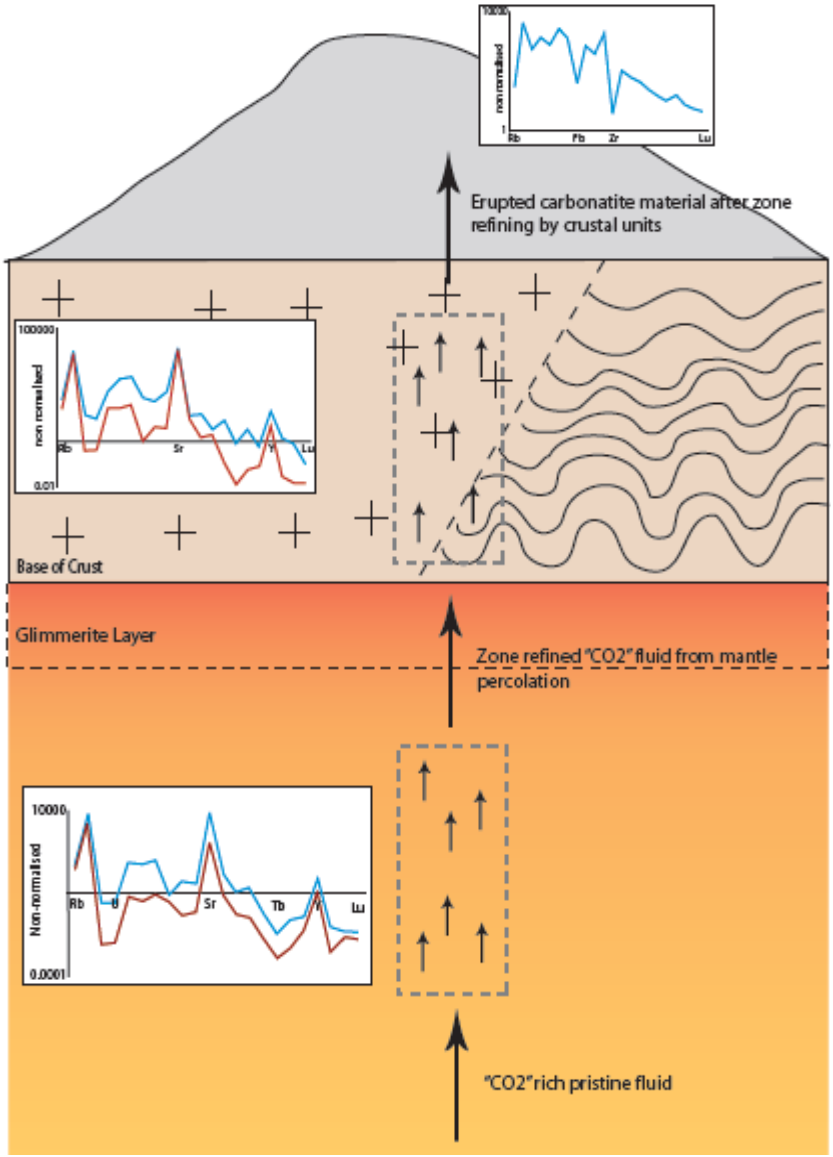

Figure 6.7: Schematic (not to scale) diagram to illustrate the process of zone refining and the modelled back calculated results for the initial carbonatite composition. The spider diagrams represent non-normalised trace element signatures. The spider diagram represtning erupted carbonatite is that of Figure 6.2. In the latter 2 diagrams the blue line represents n = 0.1 and the red represents n = 100

6.4.2. Zone refining through the crust

The composition of the carbonatite prior to interaction with crustal country rock has been based upon the dataset from OLX 17b. Comparison of this samples trace element signature with that of continental crust from Rudnick et al (2003) shows that OLX 17b still holds a signature indicative of its crustal origin (Figure 6.8) with the minor differences either a consequence of the fenitisation or of a slightly different mineralogy. Both the continental crust

and sample OLX 17b exhibit depletion in Pb which is likely to be due to the fluid-mobile nature of Pb indicating that the fenite sample has been subject to fluid flow. The relative enrichment of Sr compared to the continental crust is also thought to be indicative of carbonatite – related fenitisation.

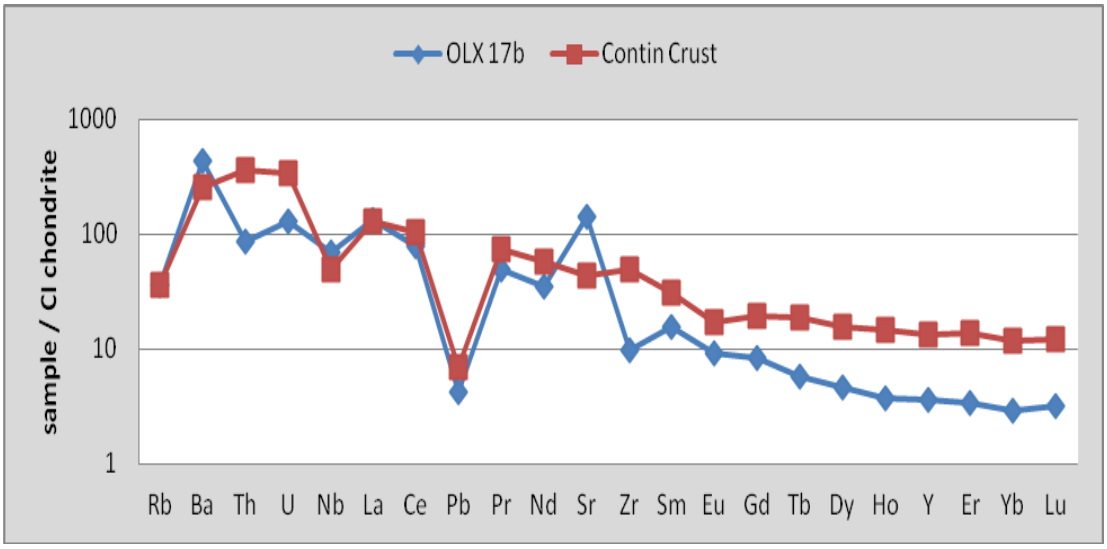

Figure 6.8: Trace element signatures for fenite OLX 17b and average continental crust (Rudnick and Gao, 2003) showing similarity of the samples and so the origin of OLX 17b as a metasomatised crustal unit.

For this first trial the country rock at crustal level is argued to be a granitic gneiss and so bulk D values were calculated from experimentally determined distribution coefficients (Blundy and Dalton, 2000, Sweeney et al., 1992, Green, 1994, Klemme et al., 1995, Tiepolo et al., 2002, Hammouda.T, 2008, Dasgupta et al., 2009, Dalou et al., 2009, Lemarchand et al., 1987, Brenan and Watson, 1991, Drake and Weill, 1975, Nielsen et al., 1992, Jones et al., 1995, Hammouda et al., 2010) between carbonatitic melt and the minerals which constitute the granitic gneiss and modelled for two different rock compositions with slightly differing mineralogy.

The input values for the composition of the liquid was that of the dataset for sample OL 3, natrocarbonatitic lava collected from the March 2006 flow on the western flank of Oldoinyo Lengai. The n value is unknown and so is varied between 0.1 and 100. Initially this was modelled between 0.1 and 10000 but at larger values n trended towards 1/D. This process can essentially be viewed as a “removal” of contamination from the melt.

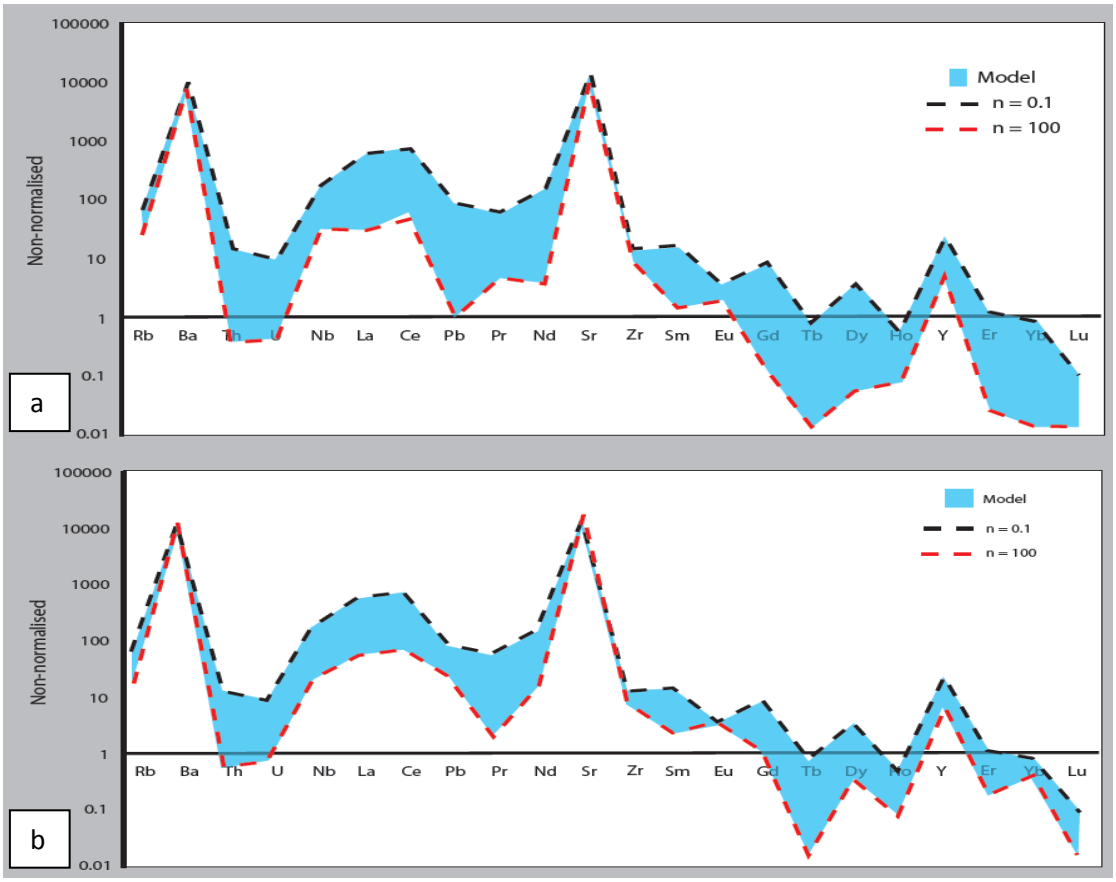

Fig 6.9: Zone refined models to calculate the composition of natrocarbonatite prior to interactions with country rocks. Country rocks assumed to be greenstone metagranitic units. The exact mineralogical composition of the country rock is unknown and so two different mineral abundances have been modelled; (a) amphibole (69%), ilmenite (2%), feldspar (19%), quartz (9%); (b) amphibole (31%), ilmenite (2%), feldspar (36%), pyroxene (30%).

It can be seen from Figure 6.9 that the refined carbonatite melt composition is quite strongly affected by the bulk mineralogy of the country rock modelled for, which can be expected due to the affinity of different minerals for elements via substitutions, for example the substitution of Eu within the feldspar crystal structure, Nb in Ilmenite, Yb in pyroxene or the substitution of LREE within amphibole (Mulrooney and Rivers, 2005). There is also no apparent effect on the concentrations of Sr and Ba with increasing volumes of country rock processed. This is thought to be a result of the high concentration of these elements within both carbonatite and the country rock, with crustal rock units enriched in the more incompatible LREE from the initial segregation of the continental crust (Rudnick and Gao, 2003). The effect of elemental exchange will not be so easily observed for a unit which is already enriched in a particular element as exchanges will represent a small percentage of the total, so although the distribution coefficient data suggests that both Sr and Ba should partition into feldspar over carbonatite (D ~3) the amount exchanged is too small to notice.

We can also identify the elements which are thought to be concentrated within the continental crust for example Th, U and Rb as these elements appear to become depleted once the crustal component is 'removed' from the carbonatite composition at higher values of n. The LREE are more incompatible and so during crustal formation they were originally concentrated into the continental crust (Rudnick and Gao, 2003). However the bulk distribution coefficients for these elements also enable them to form part of the carbonatite structure and so during percolation elemental exchange results in the enrichment of these elements within the carbonatite.

6.4.3. Zone refining through the mantle

There are two large assumptions made in order to use this model for mantle percolation; firstly that at mantle levels carbonatite exists as a melt, which is directly related to the melt which erupts and was sampled from the volcano. This argument is based upon the differences in isotopic ratios between carbonatites and the more evolved conjugate melts with which they are associated (Harmer and Gittins, 1998, Harmer et al., 1998). This lead Harmer et al (1998) to argue that some carbonatite complexes originate from carbonate melts which exist as discrete batches within the mantle. Later experimental work also indicated that primary carbonate-rich melts from partial melting of a carbonated peridotite are magnesio-carbonatites and that the generation of calcio-carbonatites can occur by the interaction of these primary melts with mantle harzburgites (Dalton and Wood, 1993). The next stage of the process requires the reaction of the calcio-carbonatite with fertile lherzolite to generate more sodic-rich melts akin to natrocarbonatite at low pressures (Sweeney, 1994). It is also assumed that recognisable chemical interactions take place which alter the chemistry of the host rock and the carbonatite.

The zone refined model for mantle rocks uses a typical peridotitic mineralogy composed of garnet, clinopyroxene, orthopyroxene, olivine and phlogopite in abundances dictated by peridotite xenoliths examined from other volcanic centres within the Gregory Rift (Dawson et al., 1970, Ridley and Dawson, 1975, Rhodes and Dawson, 1975, Aulbach and Rudnick, 2009, Rudnick et al., 1993). The bulk D values were again calculated for the experimentally determined partitioning of each trace element between a carbonatite melt and the minerals of peridotite. For this part of the model the input concentration of the carbonatite was derived from the model above for the crustal refinement on the basis that if this were a continuous

process the mantle refined melt would percolate into the crust and be subject to further refinement. The results of crustal refinement in Figure 6.9(a) at n = 100 were used in order to provide an end member value.

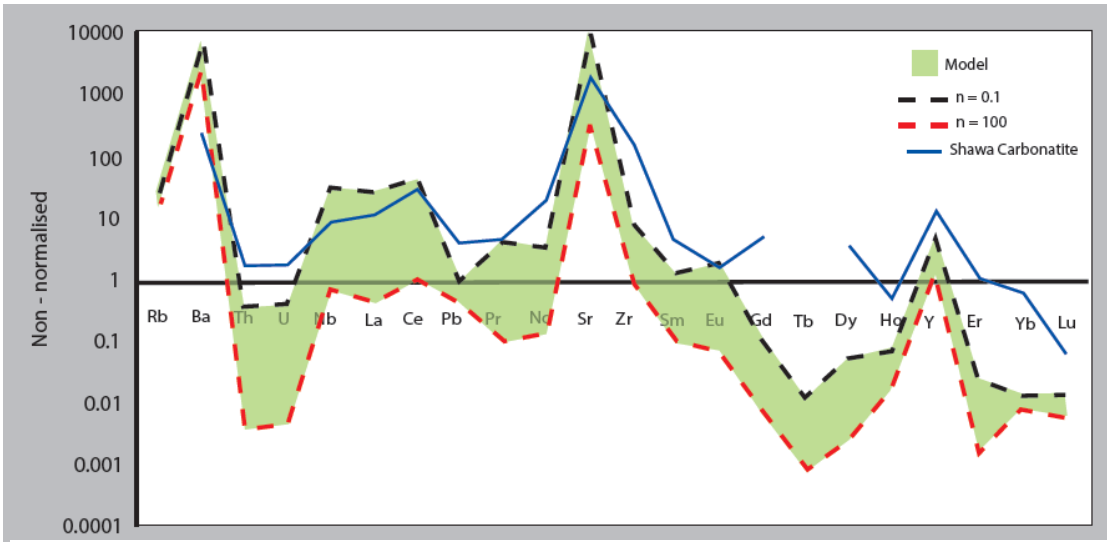

Figure 6.10: Trace element modelled data for pristine carbonatite melt composition prior to percolation through peridotitic mantle of garnet (5%), clinopyroxene (15%), orthopyroxene (15%), olivine (55%) and phlogopite (10%). Carbonatite starting composition is n=100 model of 6.3(a). "Shawa" line represents the trace element data from a suggested deep mantle carbonatite from Zimbabwe (Harmer et al., 1998).

The Shawa carbonatite complex is argued to be sourced predominantly from the depleted, sub-lithospheric mantle whilst the nephelinites of the same complex show a less radiogenic, enriched lithospheric mantle signature. The consequences of this are that the Shawa carbonatites exist as discrete carbonate magma at depths. They must also originate from depths which are below that of the source region for the nephelinites (Harmer et al., 1998, Harmer and Gittins, 1998). For this reason I have compared their composition with that of the modelled "pristine" carbonatite (Figure 6.10). The Shawa carbonatite composition lies close to the n = 0.1 modelled line which would match with proposed rapid ascent of carbonatites and so limited contact for elemental exchange with the mantle.

Similar to the crustal refined units there is little change to the concentration of Sr and Ba with percolation through the mantle which again is attributed to the elevated levels of these elements with carbonatites. Interestingly Tb and HREEs appear to be more depleted in the 'pristine' melt. According to Downes (2001) pyroxenes are the main hosts for REE and so interaction with pyroxene-rich units would result in the elemental exchange with enrichment

of REE within carbonatites with D values showing they are more likely to carry REE. This means that prior to percolation through the mantle the carbonatites are less enriched in REE. However carbonatite melts are thought to represent small degrees of partial melt of mantle peridotite and so would be expected to contain high levels of incompatible REEs. This is true for LREEs which are the most incompatible of the REE sequence and also for particular elements which have a propensity within the carbonatite melt structure, i.e. Sr, Ba and Y. However, if it is a garnet-rich mantle section then it can be expected that there will be very little change in the HREEs due to garnet retaining them and so if significant changes occur to the LREE concentration which makes the HREE end of the diagram appear more depleted when actually it is just not as enriched.

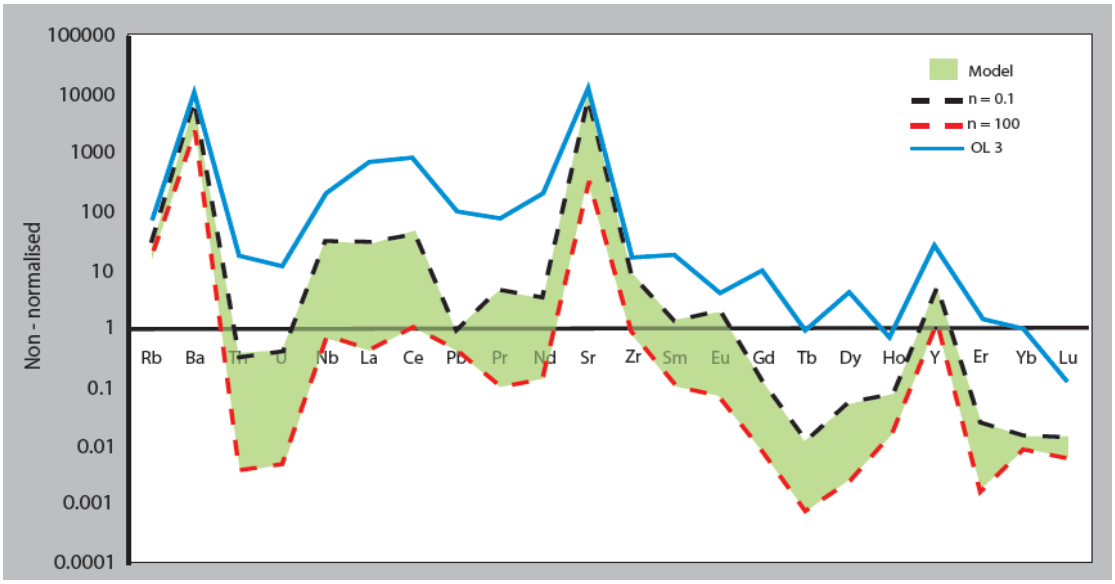

Figure 6.11: Comparison of erupted material collected from Oldoinyo Lengai (OL 3) with modelled dataset after crust and mantle refinement. This provides a maximum (black dashed) and minimum (red dashed) for the concentration of trace elements within a suggested original carbonatite unit.

When a comparison between the compositions of the collected natrocarbonatite is made with that of the final model product argued to be the 'pristine' composition, it can be seen that the erupted product is far more enriched than the original melt (Figure 6.11). The majority of the enriched elements can be explained through elemental exchange with the two host units modelled; elements which are typically enriched with the continental crust such as Th and Pb will be introduced into the carbonate melt upon percolation and so the original melt appears depleted. Similarly the HREE can also be exchanged with the carbonate melt during percolation through a garnet-bearing mantle which provides the source of these elements.

6.5. Oxygen fugacity of metasomatic fluids

A brief note on oxygen fugacity is also required to fully understand the petrogenesis of the samples as well as the long term evolution of the mantle beneath the East African Rift. It is not possible to determine the exact fO_2 of the samples collected, in particular that of the mantle unit, due to a lack of appropriate minerals such as orthopyroxene, spinel and olivine (Wood et al., 1990). However previous studies on mantle xenoliths indicate that those from continental regimes often show fO_2 of -1.5 to +1.5 log units relative to Fayalite – Magnetite – Quartz buffer (FMQ) (Wood et al., 1990). This is in agreement with earlier work which concluded that cryptic and modally metasomatised xenoliths are oxidized relative to non-metasomatised xenoliths, equilibrating near the FMQ buffer (Mattioli et al., 1989). The authors also noted a negative correlation between HREEs and log fO_2 which is thought to indicate that more depleted peridotite is more likely to be subject to metasomatism by oxidising fluids. This is also accompanied by an oxygen isotope shift from between $\delta^{18}O$ = +0.8 +1.4 to $\delta^{18}O$ = - 0.4 indicating the influx of an isotopically light (^{16}O enriched) fluid. The best candidate for metasomatism according to Mattioli et al (1989) is an oxidized $CO_2 – H_2O$ –rich fluid. The fO_2 for the crustal fenites at Lengai is likely to have been variable depending upon the metasomatising fluid. Those subject to ijolite fenitisation experience fO_2 conditions near the hematite – magnetite buffer (HM) whilst carbonatitic fenites display fO_2 nearer to the FMQ (Morogan, 1994).

6.6. Discussion of trace element modelling and carbonatite metasomatism processes

The use of trace element models within geochemistry provides important information which enable geologists to better understand the petrogenesis of igneous rocks by offering an explanation to fractionation patterns observed in natural samples, which can then be compared to expected outcomes from experimental or theoretical work. However like most attempts to model a natural system, no model provides a perfect explanation with limitations that must be considered. Ultimately it is important to remember that the metasomatised units, both mantle and crustal, have most likely been subject to long periods of melt / fluid interaction and so have gone through several phases of alteration resulting in significant overprinting of signals which are more difficult to model or interpret from modelling. The models also assume that the composition of input material has stayed the same over the active history of Lengai.

The zone refinement of the carbonate melt during mantle ascent, however, seems less probable as this process requires the rapid assimilation of mantle material which would require a vast amount of superheat. Refinement due to stagnation within the lower crust does seem plausible and is evident from fenite units which have been subject to carbonatitic fenitisation – whether this is from a melt or a high density fluid. This is likely to result in a significant difference in the composition of the carbonatite as illustrated by Figure 6.12 below. This has implications for future experiments which attempt to emulate the composition of natrocarbonatite for the purpose of determining its origin.

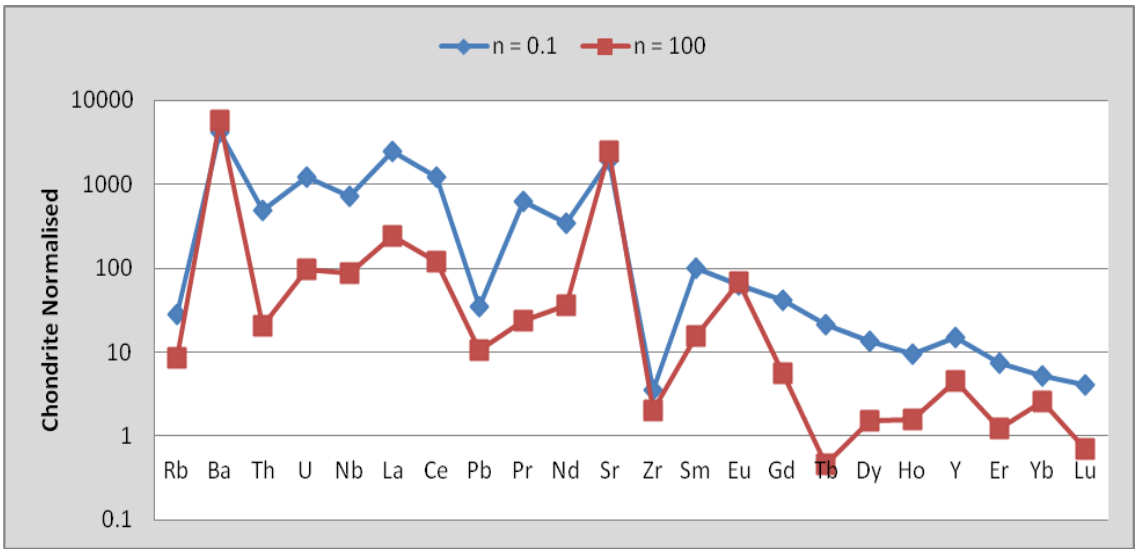

Figure 6.12: Chondrite-normalised spider diagram illustrating the maximum change to the trace element pattern of carbonatite prior to interaction and refinement by the continental crust. The upper blue line represents sample OL 3; lower red line modelled composition before refinement.

6.6.1. Mantle metasomatism by carbonatites

The presence of carbonate-rich melts at depth is still controversial despite the experimental evidence of carbonate stability within the lower mantle up to pressures of ~ 82 GPa, albeit with a new crystal structure (Oganov et al., 2008, Oganov et al., 2006, Biellmann et al., 1993, Bizimis et al., 2003) and also with the identification of carbonatitic inclusions within deep diamonds from Juina, Brazil (>670km), which are thought to indicate localised regions of carbonate stability at depth (Brenker and al, 2006, Brenker and al, 2007, Walter and al, 2008). Interestingly, further studies on the inclusions within the Juina diamonds also highlighted the presence of nyerereite and nahcolite (Kaminsky et al., 2009), two minerals which are typical of

natrocarbonatitic material. This would seem to indicate that primary carbonate material is found within the deep lithospheric mantle, perhaps even down to the transition zone, and plays a key role in the formation of diamonds.

There is evidence of carbonate-related metasomatic units within the East African rift as well as other carbonatite complexes across the globe (Andersen et al., 1984, Frezzotti et al., 2002, Dawson et al., 1970, Ionov and Hofmann, 1995, Ionov et al., 1993, Rudnick et al., 1993, Roden and Rama Murthy, 1985), with the presence of hydrous minerals including amphibole and phlogopite as well as anhydrous minerals which are rich in incompatible elements. In all likelihood it does seem plausible that carbonatitic fluids would generate significant elemental changes within the mantle rocks due to their wetting properties, despite a proposed rapid infiltration and ascent through the mantle (Hammouda and Laporte, 2000). This is likely to result in extreme fractionation of elements with similar partition coefficients within mantle material which in turn may be responsible for localised enriched regions within the uppermost mantle (Vasseur et al., 1991). However, there is no conclusive evidence of primary carbonatite melts at Oldoinyo Lengai from the trace element signatures of the metasomatised units collected.

The upper mantle pyroxenite sample OLX 15 appears to be the result of silicate metasomatism but it is possible that this silicate melt was carbonate – rich or OLX 15 simply represents a sample located within the metasomatic zone for silicates melts and carbonatite metasomatism only occurs in localised regions. A third alternative is that the trace element pattern for the unit is a mixture of both types of metasomatism. More conclusive evidence could be found in the form of melt inclusions which have not yet been studied for the rock suite but other mantle samples in Hungary and Australia which have provided evidence of carbonatite metasomatism in the upper mantle (Guzmics et al., 2008b, Yaxley et al., 1998). Interestingly, experimental work on the mantle rocks formed by the interaction of ijolite with peridotite at pressures below 17 kbar at 1000°C, shows the generation of amphibole – lherzolite and a CO_2-rich fluid (Meen, 1987), but only when the ijolite is used up in the reaction. This reaction seems to fit the observations of the fenitic units from Oldoinyo Lengai but does not require the full expenditure of the ijolitic melt which continues into the crust and metasomatises the country rocks to generate OLX 17a. This would result in the generation of an amphibole – lherzolite but without the CO_2 – rich fluid, in other words a lack of CO_2 fluid inclusions.

6.6.2. Comparison of fenitisation with other regions

Fenitisation by carbonatite – alkaline igneous melts should be fairly uniform across the globe with subtle differences in fenites being the result of the following variables (Le Bas, 1987);

i. Geochemistry of the intruding magma

ii. The nature of the fluids leaving the magma

iii. The depth at which fenitisation takes place

iv. The porosity and structure of the country rocks being fenitised

v. The geochemistry and mineralogy of the country rocks

vi. Water – rock interactions

Table 23 below compares the fenitic units studied from Oldoinyo Lengai with other well known examples of fenites across the globe, including the characteristic Fen complex, Norway from which the rock group inherited their name.

	Oldoinyo Lengai, Tanzania[1]	**Fen, Norway[2]**	**Alno, Norway[3]**	**Chipman Lake, Canada[4]**	**Pollen, Norway[5]**
Protolith	Metagranite/ metagabbro	Gneissic Granite	Migmatite	Granites / Metavolcanic greenstone	Gabbro
Extent	-	-	500 – 600 m	-	0.5 km^2
Temperature of Fenitisation	700 – 800 °C	500 – 650 °C / 500 – 700 °C	500 – 650 °C / 650 – 700 °C	-	-
Mineralogy	Quartz, feldspar, nepheline, calcite, alkaline pyroxene, titanite, apatite, iron oxides,	Quartz, feldspar, mica, amphibole, calcite, alkaline pyroxene, titanite, apatite, iron oxides,	Feldspar, calcite, alkaline pyroxene, titanite, apatite, amphibole, fluorite	Feldspar, alkaline pyroxene, mica, amphibole	Amphibole, mica, calcite, alkaline pyroxene, apatite,
Fluid Composition	CO_2 – rich, carbonatite melt	Ijolitic + sövitic	Ijolitic + sövitic /	Carbonatite melt (?)	CO_2 – rich / carbonatite melt
***f*O_2**	Low	Low for carbonatite; high for	Hm – Mt to FMQ (eastern	-	Low

	ijolite (FMQ)	sector); Hm – Mt (western sector)		
Presence of Fluorine		X		
Presence of H_2O	X	X	X (?)	X (?)

Table 23: A comparison of fenite units from Oldoinyo Lengai to other well known fenite complexes in terms of conditions of fenitisation and resulting mineralogy;

1. Information from this study and from Morogan (1994)
2. (Kresten and Morogan, 1986)
3. (Morogan and Woolley, 1988)
4. (Platt and Woolley, 1990)
5. (Robins, 1984, Robins and Tysseland, 1983)

It can be seen that in general the fenites from Lengai are similar to those of the other complexes with similar temperatures of formation and mineralogy for a specific protolith, i.e. mafic or intermediate. There are, however, some noteworthy differences; firstly the lack of amphibole or mica minerals within the Lengai crustal fenites (these are present within the mantle sample OLX 15) in comparison with the other units. Amphibole and mica minerals are typical of fluid interaction where XH_2O is high and so a lack of these minerals would suggest a fenitising fluid which has a low XH_2O and high XCO_2. The implication of this is that the melts associated with Oldoinyo Lengai (ijolite and natrocarbonatite) are likely to be under - saturated with regards to water. The presence of amphibole within the metasomatised mantle sample indicates that the melts may once have been saturated with H_2O but this is lost during the ascent, possibly in the formation of a glimmerite layer somewhere in the sub-continental mantle.

Secondly, Lengai units are the only ones that appear to contain nepheline, despite similarities within the protoliths of Lengai and Chipman Lake, Ontario or Fen complex, Norway. The explanation for this is unknown but could either be a result of the difference in chemistry of the carbonatitic units (natrocarbonatitic vs. sövitic) or a result of the temperature of fenitisation. Lengai units formed at slightly higher temperatures than those of the other complexes. This can be favourable to the formation of nepheline which becomes less stable at lower temperatures (400 – 500 °C) (Deer et al., 2006) and so may not have formed at the other complexes due to temperatures at the limit of its stability.

6.7. Conclusions

It has long been observed that the crustal rocks in the surrounding regions to alkaline – carbonatite complexes are subject to fluid flow and alteration. It is hoped that this chapter has provided some insight into the fluid alteration processes occurring at Lengai, how these correspond to the inclusions discussed in the previous chapter and how the fenitic units relate to the magmatic complex of the volcano. The following conclusions can be drawn from the above work;

- Natrocarbonatite collected from Lengai (OL 3) during the field campaign in 2010 is similar to that of units which were collected after the eruption in 2006 (Keller et al., 2010). The slight differences in composition are likely to be the result of alteration over time and will be discussed in the next chapter.

- The process of zone refinement during percolation through the crust could change the composition of natrocarbonatite from a pristine composition to that which we see at the surface. Potentially the concentration of elements such as Th, U, Tb, La and Ce could be up a factor of ten lower in the non-refined melt than that of surface natrocarbonatite.

- The sub-continental lithospheric mantle of the Gregory Rift exhibits heterogeneities caused by modal metasomatism from silicate melts.

- Two types of fenitisation occur in the continental crust of Oldoinyo Lengai – ijolitic and carbonatitic-related. Previous work by Morogan (1994) suggested that only carbonatitic fenitisation occurs at Lengai. A lack of hydrous minerals (amphibole or micas) within crustal fenites indicate a H_2O under-saturated fluid is responsible for fenitisation within the crust but a more H_2O – rich causes metasomatism at mantle depths.

- The fenitisation patterns agree with the fluid inclusion chemistries with carbonatite-related fenites containing high density, CO_2 - rich fluids and ijolite-related fenites being devoid of CO_2 inclusions.

- Carbonatite-related fenitisation provides evidence for an intrusive carbonatite body beneath Lengai which has not previously been reported. Fenitisation processes require a carbonatite body with a long residence time within the crustal regions in order to release fluids capable of altering the surrounding rock units.

6.8. Further Work

Future work to better understand the fenite units of Lengai requires a study of the stable isotopes, in particular of oxygen, to determine fluid interaction. This can be completed on both whole rock samples as well as mineral separates for example pyroxene or feldspar where fractionation during infiltration and replacement / precipitation should indicate the isotopic signature ($\delta^{18}O$) of the original fluid.

Chapter 7: Isotopic Analysis of Oldoinyo Lengai Material Part 1: Radiogenic signatures of natrocarbonatite and metasomatic units. Implications for petrogenesis.

A number of elements within nature have isotopes which are subject to radioactive decay, generating a daughter isotope by the spontaneous emission of either an alpha, beta or gamma particle. When a parent isotope is incorporated into a crystal structure it will continue to decay to its daughter isotope at a fixed rate, dictated by the isotope system half-life. The ratio of the parent to daughter isotopes therefore increases over time and is often used as a way of dating crystals and rock units. Only rocks which are unaffected by alteration provide reliable radiometric ages as the process of alteration can affect the isotope ratio. This is a result of the mobility of the isotopes in the radioisotope system; for example ^{87}Rb is fluid-mobile and so will be enriched in fluid-altered rocks, which in turn will be enriched in ^{87}Sr due to radioactive decay. This is not the case for the ^{147}Sm – ^{143}Nd system which are not readily remobilised by weathering or metamorphism. Melting events also cause fractionation of radioisotopes due to the differences in the compatibility of the parent and daughter isotopes. Rb is much more incompatible than Sr and so the melt is enriched in the parent relative to the daughter. The reverse is true for the Sm - Nd system where the daughter is enriched in the melt phase. However, if studying the process of fluid alteration the Rb – Sr system is advantageous due to the fluid-mobile nature of Rb. Rocks which are affected by metasomatism should exhibit a more radiogenic signature due to incorporation of Rb which will decay to Sr.

The aim of this chapter is to continue to look at the process of metasomatism of crustal and mantle units by carbonatitic fluids using radioisotopes to determine the extent of alteration. This is considered to be the next step having characterised the fluids and trace element compositions in the previous chapters.

7.1. Radioisotope signatures of carbonatites

As with most rock units, carbonatites can be described according to their radiogenic isotopes. Nelson et al (1988) provides a good overview of carbonatites, concluding that African complexes are time-integrated and depleted in LILE with respect to the bulk Earth isochron ($^{87}Sr/^{86}Sr$ = 0.7034 and $^{143}Nd/^{144}Nd$=0.511). The intersection of the Sr - Nd isochrons provides evidence of a depletion event around 3Ga, after which the source region of carbonatite

material remained essentially closed from isotopic exchange. Canadian carbonatite complexes show a similar depletion which has been argued to be global and so corresponds to a separation event of continental crust from mantle source, leading to the suggestion that the source of carbonatites resides in lithospheric mantle (Genge 1994, and references therein).

Interestingly Canadian complexes also show different phases of evolution when Pb isotope systematics are used; Young carbonatites (0-1100 Ma) plot within ranges of MORB and OIB below the Stacey Kramer lead evolution curve indicating derivation from a LILE-depleted reservoir. Carbonatites that plot to the right of this single stage isochron are thought to be the result of enrichment in ^{238}U relative to the bulk Earth (Stacey and Kramers, 1975). Carbonatites of 1900 Ma – 2.2 Ga have a different regression curve indicating an event between 1100 and 1900Ma. Two isotopic suites are also present; one representing enriched material and the other representing depleted material (clusters above and below the Stacey Kramer line) indicative of mixing of reservoirs, possibly asthenosphere and sub continental lithosphere (Genge 1994, and references therein). This suggests that there is no single source region for carbonatite and that mantle reservoir mixing is required for their formation.

Early work on carbonatites quoted their ^{87}Sr / ^{86}Sr as 0.7034 ± 0.0006 (Bell, 1989), which is less radiogenic than that of the continental crust and so thought to be consistent with a mantle origin. The range of isotope ratios for the different lithologies found at Oldoinyo Lengai are in table 24 below for comparison (Bell and Dawson, 1995, Cohen et al., 1984);

Table 24: Range of Sr and Nd isotope ratios for all rock units found at Oldoinyo Lengai ((Bell and Dawson, 1995) and references therein)

Rock Type	^{87}Sr / ^{86}Sr	^{143}Nd / ^{144}Nd
Carbonatite	0.70437 – 0.70445	0.51259 – 0.51263
Nephelinite	0.70414 – 0.70512	0.51249 – 0.51269
Phonolite	0.70418 – 0.70462	0.51250 – 0.51266
Jacupirangite	0.70378	0.51270
Ijolite	0.70412 – 0.70522	0.51249 – 0.51268
Pyroxenite	0.70529 – 0.70861	0.51174 – 0.51244
Nepheline Syenite	0.70418	0.51262

On an isotope ratio plot the data above form a linear arrangement extending from the upper left depleted quadrant to the lower right enriched quadrant with the majority of the rock units lying in the depleted quadrant. This linear array lies on the East African Carbonatite Line (EACL) (Bell and Blenkinsop, 1987b), which has often been thought to show binary mixing between the mantle reservoirs of HIMU (high ^{238}U / ^{204}Pb thought to be the results of recycled ancient, altered oceanic crust) and EM1 (enriched mantle 1, caused by the recycling of continental crust or lithosphere) (Kalt et al., 1997).

The remainder of this chapter will look at how the xenoliths collected during 2010 agree with the EACL and previous theories of mantle metasomatism.

7.2. Results - radiogenic signatures of 2010 xenolith suite

A pilot study was undertaken to complete the chemical understanding of samples/rocks found at Oldoinyo Lengai in terms of their radiogenic signatures and how this relates to fluid flow processes and metasomatism. The study involved the investigation of both whole rock material collected solely from Lengai and mineral separates collected from Lengai and other volcanic features mentioned in chapter 3. The pilot study was designed to look at the timing and extent of proposed metasomatic events within the Gregory Rift. In chapter 4 it was argued that xenocrystic mica within sample OLX 10 is kimberlitic in composition and so to test this hypothesis one aim of the pilot study was to determine the age of the mica using radioisotopes. If the mica is indeed kimberlitic, and so older, than the surrounding material, it should exhibit a more radiogenic signature.

7.2.1. Radioisotope ratio of natrocarbonatite

The natrocarbonatite samples used in this pilot study were collected by Jörg Keller shortly after the 2006 large effusive eruption which descended the western flank of the volcano (Kervyn et al., 2008b) and pyroclastic material from the active cone after the explosive eruption in 2007 (Keller et al., 2010). The full details of the samples can be found within these papers, but for the purpose of this study it is enough to know that OL BO6 – 6 represents pyroclastic material (ash and lapilli) collected from a stratigraphic section at the nearby Maasai Boma, the closest settlement to the volcano, after the explosive eruption. Sample OL 387 also represents carbonatitic lapilli but these were collected from the slopes of the active cone 6 months after

the 2007 eruption. OL S2 is a sample of the 2006 lava flow. Sample 801505 is of unknown origin but was analysed for comparison and potential identification.

Table 25: Radioisotope ratios for natrocarbonatitic lava and pyroclastic material associated with the latest phase of activity from Oldoinyo Lengai. Nd analysis was not completed multiple times unlike Sr and so is just assigned to the first of each lithology. All samples leached using 10% acetic acid.

Sample	Sub sample	Sr (ppm)	$^{87}Sr/^{86}Sr$	±2SE	$^{143}Nd/^{144}Nd$
0801505	Leachate	3661.71	0.704405	0.000006	0.512650
0801505	Leachate	3044.55	0.704416	0.000005	
0801505	Residue	1528.99	0.704377	0.000005	
OL B06-6a	Leachate	10846.19	0.704484	0.000006	0.512601
OL B06-6a	Leachate	7934.72	0.704387	0.000016	
OL B06-6a	Residue	6695.60	0.704481	0.000007	
OL B06-6b	Leachate	8019.85	0.704507	0.000007	
OL S2	Leachate	8962.15	0.704466	0.000005	0.512612
OL S2	Leachate	7454.99	0.704487	0.000007	
OL S2	Residue	4386.91	0.704403	0.000010	
OL 387	Leachate	8199.43	0.704437	0.000005	
OL 387	Leachate	356.58	0.704455	0.000005	
OL 387	Residue	12527.06	0.704475	0.000010	
OL B06-1	Leachate	9583.92	0.704455	0.000005	0.512615
OL B06-1	Leachate	8706.48	0.704468	0.000007	
OL B06-1	Residue	3128.90	0.704513	0.000005	

It can be seen from table 25 above that the radiogenic signature of the material are similar to those of the 1960 extrusions, reported by Bell and Dawson (1995), which in turn were also concluded to have a similar signature to samples of the 1988 extrusions (Keller and Krafft, 1990). The carbonatite samples are also similar to other carbonatitic material within the same volcanic province in particular that of the neighbouring volcano Kerimasi and also Homa Mountain volcano in Western Kenya, as shown by Figure 7.1. The samples of carbonatite from Lengai lie just above the EACL and close to the BE value for Nd vs. Sr, which is consistent with other studies of natrocarbonatite (Bell and Tilton, 2001, Bell and Blenkinsop, 1987b, Bell and Dawson, 1995, Bell and Simonetti, 1996, Bell and Blenkinsop, 1987a, Suwa et al., 1975)

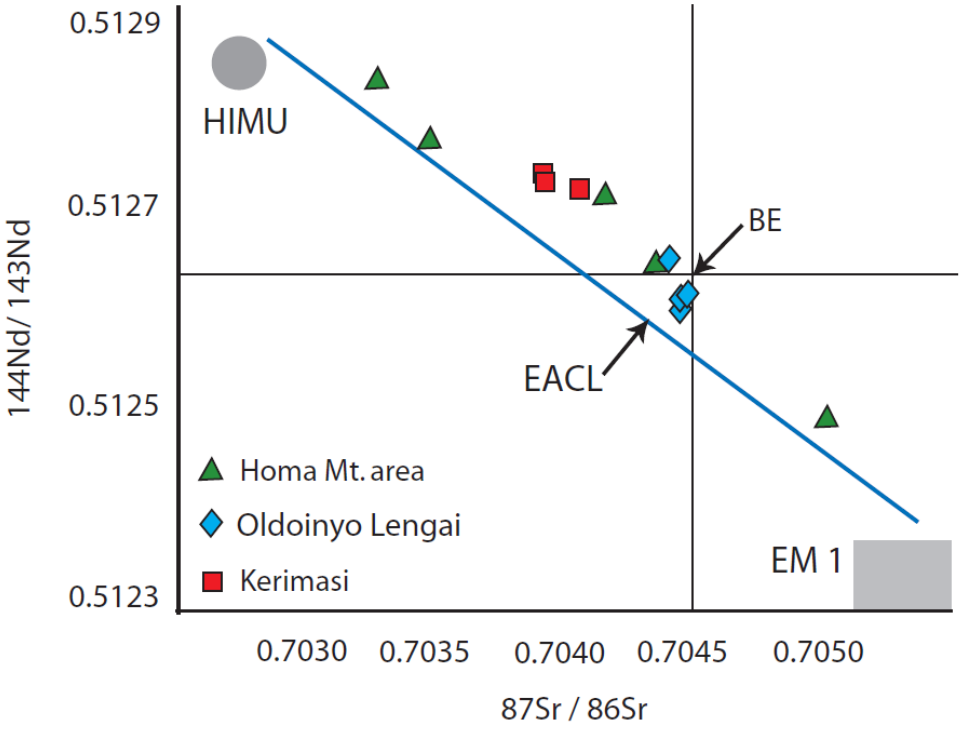

Figure 7.1: Diagram of Nd vs Sr showing the measured ratios of Oldoinyo Lengai carbonatite in comparison to carbonatite material from the neighbouring Kerimasi and Homa Mountain. The EACL of Bell and Blenkisop (1987) between EM1 and HIMU reservoirs. BE represents the Bulk Earth. Adapted from (Kalt et al., 1997). Note: Error bars for measurements are smaller than the symbols

7.2.2.Fenites and metasomatised units

The radiogenic signatures of the fenitic units from Oldoinyo Lengai have been less intensely studied in comparison to the natrocarbonatitic units. However an extensive study was completed by Kramm & Sindern (1998) and the results are listed in table 26 below along with the radiogenic signatures of the fenite units used in this pilot study.

Table 26: Sr ratios and concentrations for fenitic units. Data represents fenitic units from this study and published results from (Kramm and Sindern, 1998) for comparison. Samples were leached using 10% acetic acid.

Sample	Sub sample	Sr (ppm)	$^{87}Sr/^{86}Sr$	±2SE
OLx17a	Residue	1495.71	0.704441	0.000005
OLx17b	Residue	704.61	**0.706332**	0.000006
OLx15	Residue	906.46	0.704413	0.000006
Kramm & Sindern Samples				
OL 17/18 (granitic)	-	194	0.71429	0.00002

OL 17/6 (amphibolitic)	-	816	0.70846	0.00002
OL 17/16 (amphibolitic)	-	631	0.70943	0.00002
OL 18/3a (amphibolitic)	-	793	0.70711	0.00002
OL 18/3b (amphibolitic)	-	779	0.70674	0.00002
OL 16/2 (syenite)	-	348	0.71004	0.00002
OL16/2a (syenite)	-	313	0.70931	0.00002
OL 16/3 (syenite)	-	403	0.70669	0.00002
OL 16/4 (syenite)	-	1063	0.70632	0.00002
OL 17/19WR (syenite)	-	346	0.70740	0.00002

In general, fenitic units appear to be more radiogenic than magmatic products from Oldoinyo Lengai, with greater concentrations of Sr which is indicative of their fluid alteration. However, samples OLX 17a and OLX 15 are not as radiogenic as the amphibolitic units from Kramm & and Sindern (1998) which are thought to be the comparative units. Sample OLX 17b appears more radiogenic than the other two fenite samples, but again its $^{87}Sr/^{86}Sr$ is not as high as the granitic fenite reported by Kramm & Sindern (1998), despite the similarity in mineralogy. Metasomatised mantle xenoliths from other volcanic cones within the Gregory Rift have whole rock $^{87}Sr/^{86}Sr$ signatures of 0.703502 – 0.703875 (Rudnick et al., 1993). Sample OLX 15 therefore appears to be slightly more radiogenic than other mantle material perhaps indicating an earlier metasomatic event.

7.3. Radiogenic signatures of mineral separates

In order to investigate the extent of metasomatism within the Natron Basin section of the Gregory Rift, the Sr radiogenic signatures of mineral separates were also completed and the results can be found in table 27 below. The samples are primarily mica and pyroxene megacrysts collected from Oldoinyo Lengai and surrounding tuff cones or explosion craters described in chapters 3 and 4.

Table 27: Sr ratios and concentrations of mineral separates of mica and pyroxene from Oldoinyo Lengai (OL), Loluni tuff cone, Deeti tuff cone (DT) and Loolmurwak explosion crater (LWC).

Sample	Subsample	Sr (ppm)	$^{87}Sr/^{86}Sr$	±2SE
Loluni-1	mica	1022.52	0.704277	0.000005
Olx 10a	mica	374.45	0.703732	0.000006
OLC2	mica	534.26	0.704361	0.000009
DT1	mica	287.11	0.703504	0.000005

OLC3	mica	28.02	0.703563	0.000011
LWC1	mica	152.11	0.703675	0.000022
LWC2	mica	213.33	0.703515	0.000008
DTC4b	mica	80.54	**0.711661**	0.000021
OLC1	mica	276.10	0.703898	0.000007
Olx 10	mica	412.22	0.703875	0.000007
Olx 10	mica	412.18	0.703864	0.000012
DTC4	px	1153.95	0.703485	0.000006

The mineral separates from volcanic features within the Natron Basin all appear to have lower ^{87}Sr / ^{86}Sr ratios than that of the metasomatised mantle nodule (OLX 15) from table 26. The Sr ratio for the separates ranges from 0.703485 to 0.704361 for the majority of samples. However, the mica sample from Deeti tuff cone exhibits an extremely radiogenic ratio of 0.711661 ± 0.000021 despite having one of the lowest concentrations of Sr, at only 80.54 ppm. The ratios are comparable to other hydrous mineral megacrysts associated with metasomatised mantle material, which have isotopic signatures of 0.70323 – 0.70406 for diopside megacrysts and 0.70270 – 0.70408 for pargasite (Menzies and Murthy, 1980). Similar results were also found from mantle-derived material at Olmani Crater, a volcanic cone located on the lower slopes of Meru, Tanzania, which have radioisotope ratios of $^{87}Sr/^{86}Sr$ = 0.70340 – 0.703875 for clinopyroxene separates (Rudnick et al., 1993).

7.4. Discussion of radiogenic isotope signatures

7.4.1. Whole rock signatures and sources

Overall the results for the samples of natrocarbonatite from Oldoinyo Lengai agree with previous work and the recent extrusive samples continue to lie close to the EACL defined by Bell and Blenkisop (1987). This indicates that the source of these melts has remained consistent over time, with derivation of the melts from a slightly enriched source which appears to be the result of mixing between the mantle reservoirs of HIMU and EM1 (Kalt et al., 1997, Cohen et al., 1984).

The radiogenic signatures of the fenitic units, however, indicate that this group of rocks are isotopically heterogeneous and appear to be influenced by the original Sr signatures of the host rock from which they are formed. Sample OLX 17b, for example, is more radiogenic due to the original signature of the metagranitic rock units from which it as formed, in comparison

to pyroxenite and metagabbro of samples OLX 15 and OLX 17a respectively. This is a product of the mineralogy of the protoliths; the granitic host rock containing more minerals which host Rb, i.e. feldspar. Peridotite units are also depleted due to continental crust extraction early in the Earth's geological history. The process of fenitisation, which is element selective, is also argued to cause the heterogeneities within the samples (Kramm and Sindern, 1998). The authors suggest that the compositions of the fenites, with increased fluid flow, converge towards that of syenitic and ijolitic units with changes in the isotope compositions towards the signatures of that of the fenitising fluids – proposed to be an alkaline magma derived from mantle regions.

It is important to note that the $^{86}Sr/^{87}Sr$ ratio can be extremely variable in mafic – ultramafic units and so often can have values lower than that of the primitive mantle (Roden and Rama Murthy, 1985) depending on the mineralogy of the samples. For example Roden and Murthy (1985) argue that phlogopite-bearing mantle metasomites may have anomalously high Rb/Sr ratios due to the ability of phlogopite to retain Rb, but samples lacking phlogopite will have much lower ratios. This may explain why OLX 15 is not as radiogenic as expected due to a lack of phlogopite. The best system to use is Sm/Nd but this was not available during the pilot study unfortunately.

7.4.2. Radiogenic mantle signatures and metasomatism

The mineral separates show similar radioisotope signatures to that of other metasomatised mantle units and so are thought to represent disrupted vein material of metasomised regions. DTC 4b may, for example, represent part of glimmerite mica-rich vein region which is more radiogenic due to greater degrees of metasomatism, whilst remaining mica analyses represent interstitial mica from mica-pyroxenites or mica lherzolite nodules which have been subject to metasomatism by percolating melts. In order to look at this relationship fully Rb/Sr ratios for each mica unit is required. The metasomatic nature of these megacrysts has been reported previously and argued to be the result of carbonatite metasomatism (Rudnick et al., 1993, Johnson et al., 1997), with Rudnick et al (1993) arguing that the metasomatism took place with the Tertiary to Recent volcanism by melts of asthenospheric origin. Although dating of the metasomatic material in this study was not possible due to the lack of Sm – Nd data, previous work on the timing of metasomatism within the Gregory Rift supports Rudnick et al (1993), with suggested metasomatic ages of 10.4 Ma to 1.24 Ma, spanning the boundary between the

Tertiary and Quaternary periods and indicating that some metasomatism is relatively "young" (Koornneef et al., 2009).

Work by Johnson et al (1997) on the megacryst suite of Deeti tuff cone (similar to those within this study) concluded that megacrysts were not disaggregated xenoliths but products of metasomatism, with the large mica crystals originating from a pegamatoidal suite. Metasomatic veins that form in equilibrium with carbonated alkaline melts are thought to exhibit Rb/Sr ratios similar to that of the bulk Earth (Meen et al., 1989). The measured isotopes of the megacrysts conform to this hypothesis and so would seem to have formed in equilibrium with alkali-rich, carbonated melts at depths <70km, as shown by the phase relations of peridotite in the presence of H_2O and CO_2 (Figure 7.2).

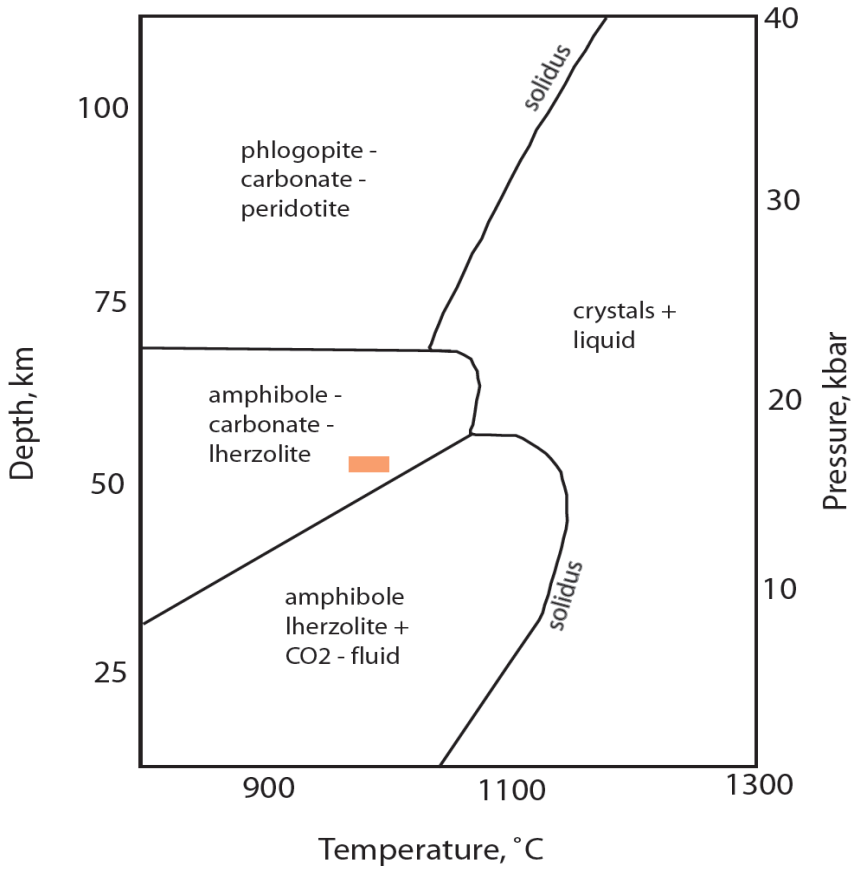

Figure 7.2: The predicted phase relationships of peridotite in the presence of H_2O and CO_2. When applied to metasomatic assemblages approximate depths of formation reveal that mica-rich material can only form at pressures >22 kbar. Adapted from (Olafsson and Eggler, 1983, Meen et al., 1989). Red box indicates approximate region of sample OLX 15 from mineralogy and thermobarometry.

The phase diagram above enables us to provide approximate pressure and depth ranges for the metasomatic material analysed in this study. According to Meen (1989) material of phlogopite – carbonate peridotite composition occur at pressures in excess of 22 kbar (70 km) whilst amphibole peridotite units appear at pressures of < 17 kbar (~50 km). This diagram also illustrates that the thermobarometry of the clinopyroxene within sample OLX 15 is accurate with a predicted temperature of formation between 900.4 – 1046.0°C ± 62.5°C and pressures between 7.4 and 15.5 kbar (from Chapter 4).

7.4.3. Kimberlitic mica within the mantle?

A key result from this pilot study is that the radioisotope data of the mica separates from sample OLX 10 do not appear to be kimberlitic due to a low radiogenic signature, which is not indicative of long time-integration and so older age. It is therefore still puzzling as to how the mica exhibits a chemistry which corresponds to that of other micaceous kimberlites (Reguir et al., 2009, Dawson and Andrews, 1972, Kelley and Wartho, 2000) and differs from other mica crystals within Lengai material or mica megacrysts. Could it have been formed from metasomatism by kimberlitic fluids which imprint the signature upon the mica? Or could it represent a relatively "young" kimberlite?

Young kimberlites in Tanzania are thought to be ~ 30 thousands years old (Brown, 2011). If such melts were present within the mantle but a lack or limited availability of mantle orthopyroxene (which reacts with olivine during metasomatism to form clinopyroxene (Johnson et al., 1997)), as required by Russell's (2012) model, meant that effervescence and rapid ascent were not possible, this could result in a stalled kimberlite which fails to penetrate to the surface and so remains within the sub-continental lithospheric mantle causing metasomatism (a kimberlite metasome) and crystallising kimberlitic minerals.

Kimberlites are water-rich, ultramafic melts and so may contribute to the formation of the mica-rich layers within the mantle, which can be sampled by later silicate melts. Metasomatism, in general, is thought to result from stalled asthenospheric melts which undergo thermal crisis due to the temperature decrease from the asthenosphere to the lithosphere (200 – 300 °C). This results in stagnation and fluid release (Haggerty, 1989). The fluid release is thought to be the first stage of the metasomatism process which generates phlogopite – K-richterite - peridotite units. Thermal reworking of the same unit by upwelling melts results in autometasomatism and the establishment of a metasome. According to Haggerty (1989) it is this metasome unit which is key in the generation of kimberlites, with

asthenospheric melts assimilating metasomatic material near the lithosphere – asthenosphere boundary (LAB) to generate proto-kimberlites. It would therefore seem logical to conclude that the mica within sample OLX 10 represents a portion of this metasome which has been overprinted by proto-kimberlite melts to generate a kimberlitic signature. The deformation of the micas mentioned in chapter 4 is the result of asthenospheric convection.

7.4.4.Evidence for carbonatite metasomatism

Using trace element modelling, it was concluded in the previous chapter that the pyroxenitic sample, OLX 15, was subject to metasomatism by an alkaline silicate similar to that of ijolite. This is also the view of Koornneef et al (2009) who argue that the late-stage, metasomatic patterns of Labait volcanic cone, Tanzania, are the product of a trace element enriched K-alkaline silicate melt that has a low LREE/HFSE ratio. However, as stated above, the megacryst suite and composition of the mantle-derived material lies within the amphibole - carbonate lherzolite section of the phase diagram. This requires a carbonate input during metasomatism.

One of the first studies which recognised the role of carbonatite melts in mantle metasomatism was based upon experimental and field observations from Mount Leura, Australia (Green and Wallace, 1988). Green & Wallace (1988) observed that small melt fractions in equilibrium with pargasite – lherzolite were capable of carrying significant quantities of large ion lithophiles, which would alter the material through which it percolated. Later petrological and chemical evidence by Rudnick et al (1993) presented several lines of evidence for carbonatite metasomatism at Olmani crater, which are as follows; low concentrations of Al and high Mg# of clinopyroxene from metasomatised material suggests a melt which is low in Al and Fe which does not correspond to silicate melts which generally enrich host rocks in Al and Fe. Crystallisation of REE-bearing apatite minerals are also indicative of a REE-rich melt most likely to be carbonatitic in composition and finally the F/Cl ratio of the apatite also requires precipitation from carbonatitic melts based upon measured and experimental partition coefficients between apatite and carbonatite melt (Baker and Wyllie, 1992, Dawson et al., 1994b, Hammouda et al., 2010).

7.4.5. Products of melting a metasomatised mantle

One of the key questions relating to the unusual magmatic system at Oldoinyo Lengai is what happens when a metasomatised mantle is melted - what magmas are produced? If we assume

that the majority of the mantle residing beneath the Tanzanian Craton has mineralogy and chemistry similar to that of sample OLX 15, two different melt products are predicted to form; melting of a carbonated amphibole lherzolite at temperatures of 1000 – 1100 °C is argued to generate a carbonatite or carbonated – alkaline melt with a CO_2 : H_2O ratio and trace element signature similar to that of the metasomatic agent (Meen et al., 1989). However Meen et al (1989) also conclude that if the mantle is not carbonated, melting of the amphibole – lherzolite at 1000 – 1100 °C results in non-carbonated alkaline magmas.

In order to generate the lithologies found at Oldoinyo Lengai the mantle beneath must be carbon - bearing so that melting produces carbonatitic magma. This suggests the presence of some form of "deep" carbon not sourced from within the lithosphere, but potentially asthenosphere, to cause the metasomatism. This is also the view of Haggerty (1989) who argues that rock units such as kimberlites and carbonatites cannot be generated by realistic melting (i.e. more than 1%) of primitive / pristine peridotite, but requires melting of a metasomatised mantle. The melting of the metasomatised mantle material may result in some form of autometasomatic process which perpetuates a cycle of carbonatite production.

7.5. A deep-carbon reservoir?

Overall, the generation of carbonatitic and perhaps even kimberlitic melts rely on the existence of metasomatised regions within the lithosphere. The mantle beneath the Gregory Rift is thought to be extensively metasomatised with evidence erupted at the surface over an area of at least 60 km^2. It is, however, still unknown as to what the composition of the original metasomatic agent actually was – carbonatitic or silicate? And from where was this sourced – could it be primordial?

7.5.1. Identification of deep carbon

The recognition of deep-seated carbon reservoirs within the Earth is not a recent idea with the study of inclusions within diamonds, fluid and melt inclusions within olivine mantle-nodules and carbonatite melts themselves, which are all argued to be samples of deep carbon (Deines and Gold, 1973, van Achterbergh et al., 2002, Achterbergh et al., 2003, Mohapatra and Honda, 2006, Berg, 1986). Of these representations of "mantle – derived" carbon, diamonds and the inclusions within are the most greatly studied due to the ability of diamond to preserve inclusions in a closed system from source to surface. The study of the inclusions within

diamonds from Juina, Brazil, indicated the presence of carbonate, in the form of calcite (Brenker and al, 2007, Walter and al, 2008), as shown by the Raman spectra in Figure 7.3. The carbonate is not solely restricted to calcite compositions with the identification of nyerereite ($Na_2Ca(CO_3)_2$) and nahcolite ($NaHCO_3$) within diamonds from the same pipe in Brazil (Kaminsky et al., 2009).

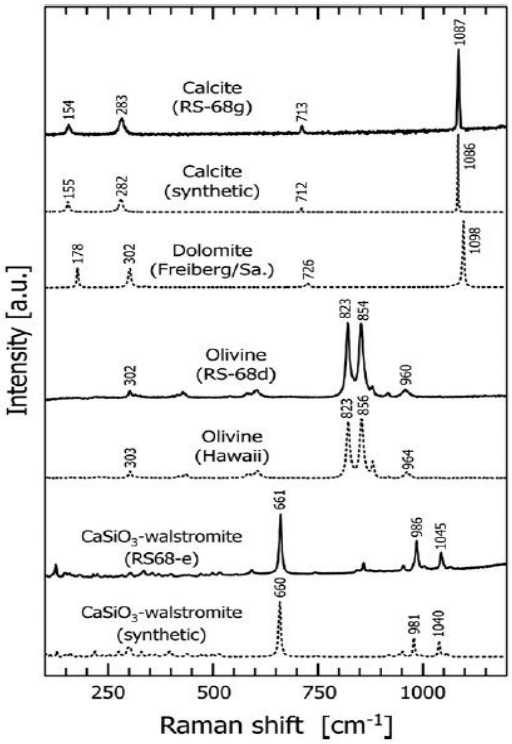

Figure 7.3: Typical Raman spectra from inclusions within diamonds from Juina, Brazil. (a) Calcite carbonate inclusions. Solid lines represent measured spectra whilst dashed lines are reference spectra. (Brenker and al, 2007); (b) Calcite and nahcolite inclusions. (Kaminsky et al., 2009)

The identification of a deep carbon reservoir is not only concluded from carbonate inclusions within deep diamond, but also through geophysical and experimental data. A laboratory study of the electrical conductivity of the deep mantle concluded that small volumes of interconnected carbonate melt may result in the observed enhanced electrical conductivity of the asthenosphere (Evans, 2008). This observation is combined with experimental results which aim to determine the stability and so "survivability" of carbonate material within the deep mantle (Oganov et al., 2008, Oganov et al., 2006, Biellmann et al., 1993, Hammouda, 2003, Pal'yanov et al., 2002, Sweeney, 1994, Yaxley and Brey, 2004, Yaxley and Green, 1994). Of these numerous publications early work by Beillmann et al (1993) indicated the stability of carbonate material to depths of 1500 km and pressures of 20 to 50 GPa as magnesite.

Table 28: Summary of carbonate high-pressure phases from experimental and theoretical work by Oganov et al (2008).

		Pressure increases →						
		$(CO3)^{2-}$ triangles			$(C_3O_9)^{6-}$ rings of tetrahedra		Chains of CO_4-tetrahedra	
		Calcite CN(M)=6	Aragonite CN(M)=9	Post-aragonite CN(M)=12	Phase II CN(M)= 8 and 10	Phase III CN(M) = 8 and 10	$Pna2_1$-20 CN(M)=9	$C222_1$ CN(M)=10
Cation radius increases ↓	$MgCO_3$	0–82 GPa	–	–	82–138 GPa	138–160 GPa	>160 GPa	?
	$CaCO_3$	0–2 GPa	2–42 GPa	42–137 GPa	–	–	–	>137 GPa
	$SrCO_3$	–	0–10 GPa	>10 GPa	–	–	–	?
	$BaCO_3$	–	0–8 GPa	>8 GPa	–	–	–	–

This later work by Oganov et al (2008) confirmed the experimental work of Beillmann et al (1993) and also extended it to experimental pressures of 82 GPa and theoretical pressures of 150 GPa. Oganov et al (2008) concluded that carbonate is indeed stable at lower mantle pressures but exists as a new crystallographic structure, changing from CO_3^{2-} triangles to rings of $C_3O_9^{6-}$ tetrahedra, as shown by table 28 above.

7.6. Conclusions

The above brief pilot study of radiogenic signatures of material from Oldoinyo Lengai and tuff cones from the Natron Basin has highlighted a number of important chemical processes which all contribute to the understanding of the chemical environment of the sub-continental mantle beneath the East African Rift. In summary these are as follows;

- The source of the natrocarbonatite magma at Oldoinyo Lengai appears to have been consistent over historical activity with little variation in the radioisotope signature of the newest material from 2006 / 07. This would indicate a well established cycle of production from a slightly enriched source.

- The carbonatites of East Africa all show similar sources which define the EACL (Bell & Blenkisop, 1987), to which the latest eruption material also conforms.

- The aureole of Oldoinyo Lengai intrusive rocks contains fenites with a radiogenic signature which is controlled by both the original radioisotope ratio of the protolith as well as the ratio of the fenitising fluid. It is also thought that the highest grade fenites start to exhibit radioisotope ratios similar to that fenitising fluid alone.

- Megacrysts suites from the tuff cones within the Natron Basin are derived from highly metasomatised mantle material, most likely metasomatised by the onset of Tertiary volcanism up until the present.

- Sample OLX 15 also records the metasomatic process with equilibration with a H_2O – CO_2 – bearing alkaline magma at a depth of <70km. The melting of a pyroxenitic mantle which is typified by sample OLX 15 results in the generation of carbonatitic melts or carbonated alkaline melts which may be the precursors to the natrocarbonatite of Lengai.

- The boundary between the lithosphere and asthenosphere beneath Lengai is thought to be glimmeritic in composition with abundant mica material which has been chemically over printed by kimberlitic or proto-kimberlitic melts to generate deformed micas with high Ti and Cr concentrations.

- The establishment of this glimmeritic layer is argued to require a flux of carbon from the asthenosphere and so points to the presence of a deep seated carbon reservoir which is not isolated from the remaining mantle.

Chapter 8: Isotopic Analysis of Oldoinyo Lengai Material Part 2: Stable isotope variation with alteration.

Isotopic geochemical analyses are an essential tool in petrogenetic studies and interpretations of igneous rocks. Stable isotopes such as carbon, oxygen, hydrogen and sulphur are extremely useful at monitoring geological processes due to a large proportional difference in atomic mass between isotopes, which results in isotopic fractionation. Ultimately the difference in the properties of the isotopes leads to a different vibrational frequency of the atoms which can affect the bond strength. Lighter isotopes vibrate with higher frequencies and so tend to form less strong bonds to other atoms in comparison to the heavier isotope. This difference in bond strength is only noticeable when there are large relative differences in the masses of the isotopes. The difference in vibrational frequencies is also less pronounced at higher temperatures and so isotopic fractionation is also less pronounced.

The causes of isotopic fractionation can be categorised into three different mechanisms (Krauskopf and Bird, 1995);

1. Physical processes such as evaporation, precipitation or diffusion. Due to the strength of bonds between light isotopes and other atoms, during evaporation the vapour phase becomes enriched in light isotopes (e.g. ^{16}O) whilst the liquid is enriched in heavy isotopes (e.g. ^{18}O). During precipitation the solid will become enriched in the heavier isotope compared to the solution.
2. Equilibrium exchange reactions will result in isotopic equilibrium between two substances if each contains only light or heavy isotopes. For example:

$$8H_2{}^{16}O + KAlSi_3{}^{18}O_8 \quad \Longleftrightarrow \quad 8H_2{}^{18}O + KAlSi_3{}^{16}O_8$$

3. Isotope fractionation as a result of reaction kinetics dictated by the equation;

$$k = Ae^{-Ea/RT}$$

Where k is the rate constant, A is a constant specific to each reaction, Ea the activation energy, R the gas constant and T the absolute temperature. The rate of isotope reactions can vary greatly and at lower reaction temperatures the rates can be so slow that equilibrium isotope fractionation is not achieved. This results in the generation of light isotope enriched products and is particularly noticeable in biologically catalyzed reactions.

The distribution of isotopes between minerals which form at the same time can therefore be a measure of geologic temperatures or characteristic of certain geologic environments and so

may provide information on sources of minerals or fluids. It is for these reasons that stable isotope analysis has become an important step in understanding the petrogenesis of rock units, in particular carbonatites. Variations of stable isotope ratios can therefore be attributed to three main processes (Deines, 1989);

i. Compositional differences in source regions

ii. Fractionation processes during the evolution of the carbonatite melt

iii. Post-magmatic alteration of units at shallow levels.

It is the aim of this chapter to investigate which of these processes are taking place at Oldoinyo Lengai and how these affect the stable isotope signatures ($\delta^{18}O$ and $\delta^{13}C$) of the carbonatite.

8.1. Previous work on stable isotopes from Lengai

The stable isotope signatures of primary, unaltered natrocarbonatite from Oldoinyo Lengai are argued to fall within the "Lengai box" which indicate their mantle source (Keller and Hoefs, 1995, Zaitsev and Keller, 2006). This "Lengai box" is characterised by $\delta^{13}C$ of -6.3 to -7.1 and $\delta^{18}O$ of +5.8 to +6.7. The authors argue that isotope signatures outside of this range are representative of alteration under atmospheric conditions and so deviate away from the primary signal to that of heavier isotopes, in particular heavier $\delta^{18}O$ according to the processes listed above by Deines (1989). The mantle range for oxygen isotopes, as determined from the study of chondrites, mantle xenoliths and basalts, is relatively restricted to between 5 and 6‰ (Deines, 1989). According to Deines (1989) the isotopic composition of mantle-derived carbonatites can be determine by their fractionation with the minerals which constitute mantle peridotite (olivine, ortho – and clinopyroxene and garnet) and lies between 7 and 8‰.

The carbon isotope signature of the mantle is more difficult to determine due to it being a trace element within the mantle. There is a large amount of variability in the isotopic compositions of meteorites, xenoliths and basalts with respect to carbon, but carbonatites seem to have a relatively restricted range with a mode around -5‰ (Deines 1989). This value is higher (more positive) than that of diamond or meteoritic isotope signatures and according to Deines, is thought to be the result of some enrichment mechanism during melt formation from an isotopically averaged source region.

8.2. Secondary deposits and minerals at Oldoinyo Lengai

The minerals which make up natrocarbonatite are extremely hygroscopic and so are unstable under atmospheric conditions resulting in the formation of secondary mineral assemblages. These minerals can be formed by the escape of hot gases during cooling, atmospheric alteration by hydration of certain minerals or by reaction with fumarolic gases (Genge et al., 2001, Zaitsev and Keller, 2006). The alteration of primary natrocarbonatite magma is a rapid process which can be seen in real time during rain storms where the black, fresh lava preserves rain droplet marks as white pits.

Stalactites, shown in Figure 8.1a and 8.1b, found appended to the underside of the 2006 lava flow were carefully collected and kept in desiccant to be analysed back in the UK. These delicate features are extremely brittle during handling and so were placed into epoxy resin blocks for ease of handling. Interestingly, when the resin blocks containing the stalactites were sawn in half, with the aim of making thin sections, the stalactites had a moist, gelatinous texture suggesting a reaction had occurred between the resin and the minerals of the precipitates.

Along with the stalactites, another precipitate was found near the 2006 natrocarbonatite flow. The walls of the gully between the flow and the flank of the volcano were covered with yellow / orange micro-crystalline material (Figure 8.1c and 8.1d). Both formations are thought to represent precipitates of leached material from the natrocarbonatite. For this reason it was decided that a closer look at their mineralogy and stable isotope signature would help provide an insight into the alteration and mobilisation of material in the Lengai system.

Figure 8.1: (a) & (b) Stalactite formations appended to the underside of the 2006 natrocarbonatite lava flow on the western flank of Lengai. The tip of stalactite in (a) shows a water droplet indicating formation via precipitation. Stalactites approximately 5 – 8cm in length; (c) Yellow precipitate also found as a coating on lava flows on Lengai; (d) hand specimen of yellow precipitate illustrating that it is micro-crystalline and bulbous in structure. The core of this specimen appears to be carbonatitic lava.

Due to the inability to generate thin sections of the stalactite material, chemical analysis was carried out using EDS SEM analysis of both the white stalactites and the yellow precipitates, which revealed that they are both made of secondary alteration minerals from the breakdown of primarily gregoryite and minor amounts of nyerereite. This has previously been documented by numerous authors (Mitchell, 2006b, Mitchell, 2006a, Zaitsev et al., 2008, Zaitsev and Keller, 2006, Dawson, 1993, Genge et al., 2001, Gilbert and Williams-Jones, 2008, McFarlane et al., 2004). Table 29 below outlines the secondary minerals found after alteration and also categorises them according to the mechanism of formation (Zaitsev and Keller, 2006). Later work also generated an alteration sequence from nyerereite to pirssonite to calcite to shortite dependent upon the partial pressures of H_2O and CO_2 (Zaitsev et al., 2008).

Minerals	Minerals formed due to		
	Lava degassing during cooling	Atmospheric alteration and hydration by meteoric waters	Reaction with fumarole gases
Nahcolite $NaHCO_3$	+++	+++	
Trona $Na_3H(CO_3)_2{\cdot}2H_2O$	+++	+++	
Thermonatrite $Na_2CO_3{\cdot}H_2O$	+++	+++	
Halite NaCl	+++		
Sylvite KCl	+++		
Aphthitalite $K_3Na(SO_4)_2$	++	+	
Kalicinite $KHCO_3$	+		
Villiaumite NaF	+		
Pirssonite $Na_2Ca(CO_3)_2{\cdot}2H_2O$		+++	
Gaylussite $Na_2Ca(CO_3)_2{\cdot}5H_2O$		+++	
Shortite $Na_2Ca_2(CO_3)_3$		+++	
Kogarkoite $Na_3(SO_4)F$		+	
Calcite $CaCO_3$		+++	+++
Sulphur S			+++
Gypsum $Ca(SO_4){\cdot}2H_2O$			+++
Anhydrite $CaSO_4$			++
Monohydrocalcite $Ca(CO_3){\cdot}H_2O$			++
Fluorite CaF_2		+	++
Barite $BaSO_4$			++
Celestine $SrSO_4$			+

+++ major minerals, ++ minor minerals, + accessory minerals.

Table 29: Secondary minerals found at Oldoinyo Lengai (Zaitsev and Keller, 2006)

Both the white stalactites and yellow precipitate appear to contain nahcolite, aphthitalite and an ephemeral pentasodium phosphate carbonate, which has not yet been described in relation to the stalactitic material from Lengai, but has been noted within altered natrocarbonatite lapilli (Mitchell, 2006a). The aphthitalite can form euhedral, hexagonal crystals which have apparent layers within them (Figure 8.2a). Analysis of the different layers reveals a transition from pentasodium phosphate carbonate (grey layer) to aphthitalite (white layer). The pentasodium phosphate carbonate forms euhedral octahedral crystals. In addition to these the white stalactites also contain quantities of sylvite and thermonatrite. The yellow precipitate also contains trona, halite, kogarkoite and schairerite. This precipitate is richer in sulphate-bearing minerals which is responsible for the yellow colouration of the deposit.

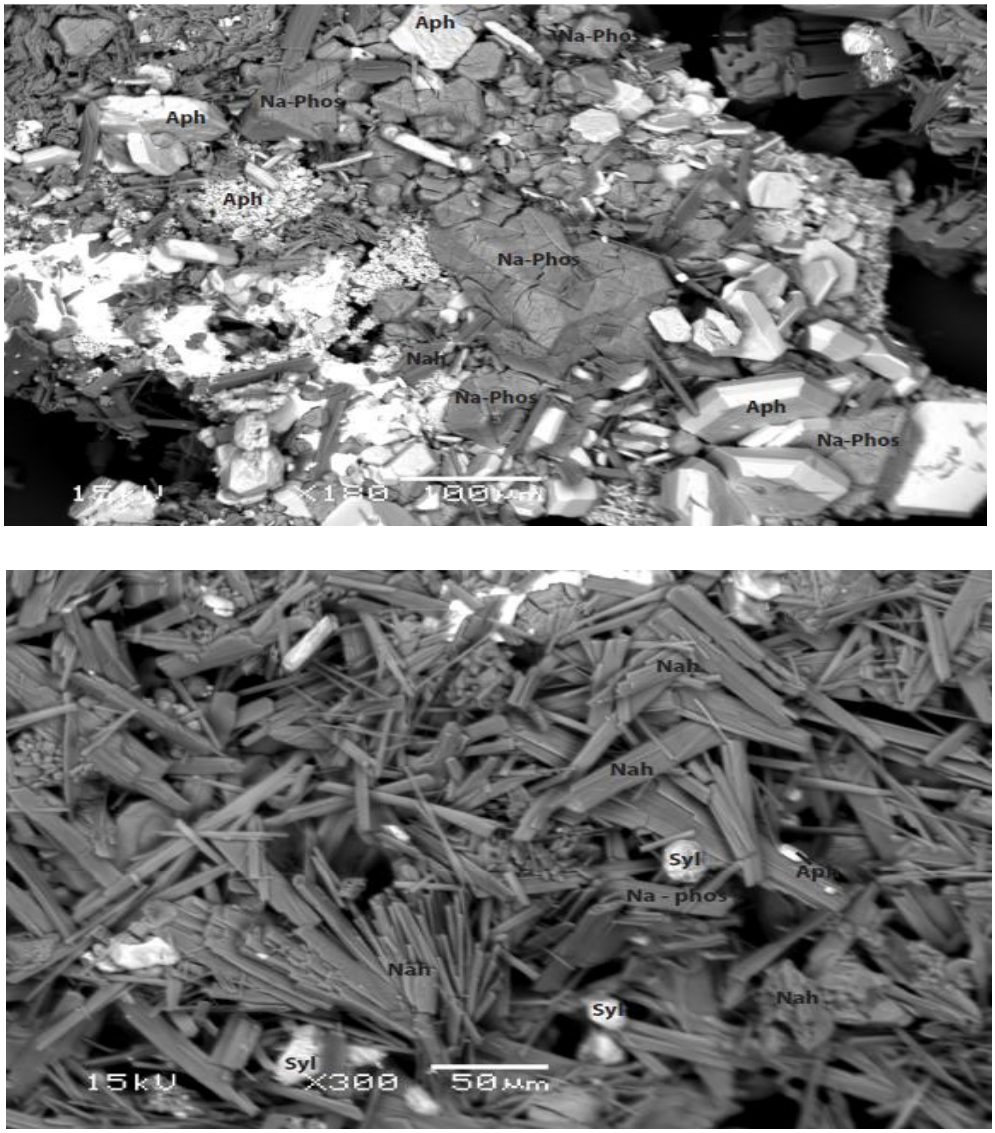

Figure 8.2: Backscattered electron SEM images of sample OL 9 white stalactite (a) white stalactite material showing well formed crystals of aphthitalite (Aph), pentasodium phosphate carbonate (Na-Phos); (b) image of nahcolite (Nah) crystals present in the white precipitated stalactites from the 2007 flow. Nahcolite forms long bladed crystals, the white rounder crystals are aphthitalite (Aph) and sodian sylvite (Syl).

Alteration of primary natrocarbonatite results in a rapid loss of K, followed by a more gradual loss of Na, Cl and S. An increase in H_2O, Ca, Sr, Ba, F and Mn is also noted. Zaitsev and Keller (2006) argue that two stages of alteration occur; the first producing pirssonite carbonatites with relict fluorite which are rich in Na and Ca but depleted in K, whilst the second stage results in calcite carbonatites which are Ca-rich and Na-K-poor. This alteration from sodium carbonatite to calcium carbonatite was originally noted by Dawson (1993). Previous to this it had been argued that this calcium-rich material represented a primary sövite present at Oldoinyo Lengai (Harmer and Gittins, 1998), affecting petrogenesis arguments by suggesting that natrocarbonatite is formed by the fractionation of sövite from a parent melt which was mixed alkali-calcium carbonate. Chemical comparisons, however, reveal the similarity in the materials, with analysed samples of the sövite dyke showing higher absolute concentrations of REEs than in natrocarbonatite lavas but overall the normalised patterns (Figure 8.3) are very similar.

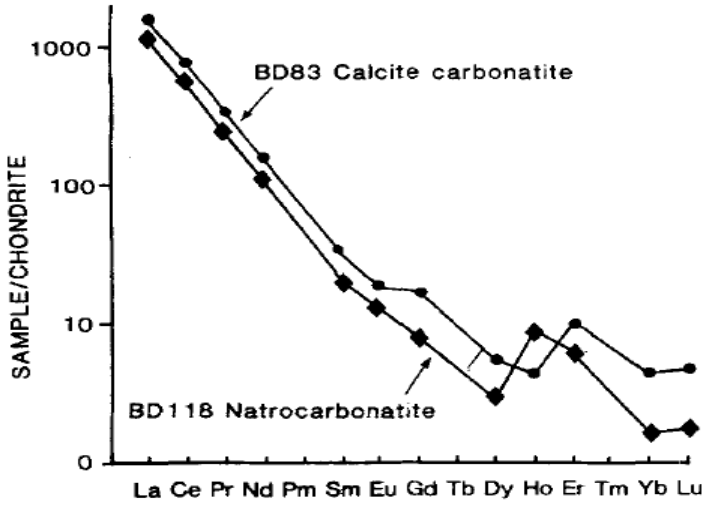

Figure 8.3 (*left):* REE patterns for natrocarbonatite and calcium carbonatite from Oldoinyo Lengai (Dawson, 1993).

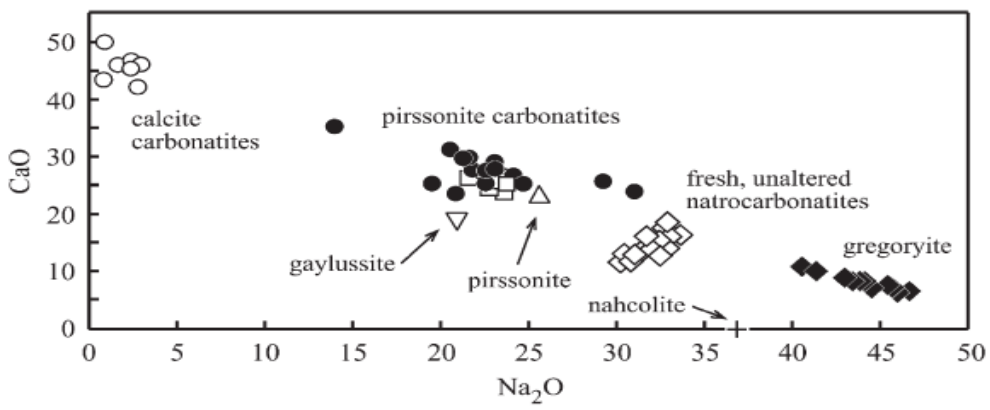

Figure 8.4 *(below):* Ca vs. Na plot for mineral separates and whole rock samples from altered material on Oldoinyo Lengai (Zaitsev and Keller, 2006)

The supposed sövite at Oldoinyo Lengai is enriched in REE, Y, Zr, Th, Nb and Pb but depleted in Rb, Cs, Ba, Cl and S (Keller and Zaitsev, 2006). It can be seen from Figure 8.4 that there appears to be a compositional trend from gregoryite and fresh natrocarbonatite. The authors in fact argue that only "*stable isotope ratios are independent criteria indicating extensive alteration and secondary exchange*"

8.3. Stable isotope variation of natrocarbonatite with alteration

As mentioned previously it is assumed that fresh natrocarbonatite stable isotope signatures are indicative of mantle derivation with $\delta^{13}C$ between -5 and -8‰. Figure 8.5 (Carmody et al., 2009) outlines the stable isotope signatures determined for fresh Lengai material (red box), mantle (blue box), primary sövite material (green box), the calcium carbonatite dyke (star) and altered material from Oldoinyo Lengai (orange box). The trends present on the graph attempt to model isotopic mixing trends which would generate the observed signatures.

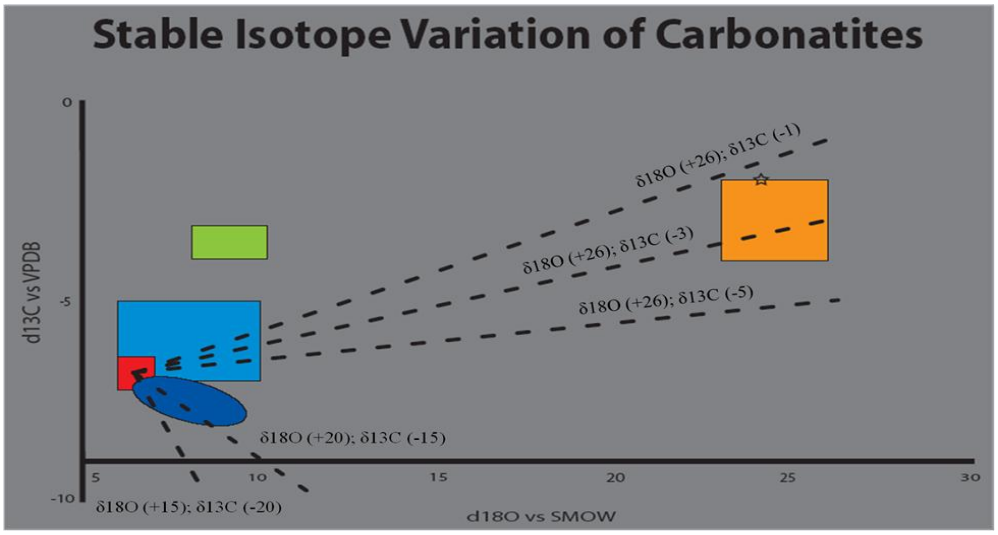

Figure 8.5: Stable isotope signatures of various carbonatitic materials associated with Oldoinyo Lengai. Colours explained in text. (Carmody et al., 2009). Each dash along the mixing line represents 5% increments of mixing between original compositions (red box) and indicated fluid composition.

It can be seen that the characterisation of the fluids causing alteration is needed as the trend lines shows that the oxygen isotopes of altered samples are vastly different from those of primary Lengai material (from $\delta^{18}O$ +6.5 to +26 vs. SMOW), whilst the carbon isotopes remain relatively unchanged (from $\delta^{13}C$ -6.8 to -2 vs. VPDB). Interestingly the blue oval represents altered material from the 2006 lava flow. It can be seen that this material does not support the hypothesis that Lengai material alters to eventually resemble that of calcium carbonatite

material. Could this be the result of different mineral chemistry of the lava itself or due to interaction from a different fluid source?

Deines (1989) review of stable isotopes within carbonatites provides some insight into why you may see enrichment of ^{18}O, beyond the expected upper value of 9.5‰ of mantle-derived material. For massive carbonatite bodies he outlines 5 ways of causing enrichment;

1. Loss of fluids during emplacement due to pressure reduction
2. An exchange of heavier oxygen with magmatic fluids of high ^{18}O content
3. A retrograde exchange with magmatic waters
4. Exchange with ^{18}O-rich hydrothermal fluids
5. Low temperature exchanges with meteoric waters which influx post-emplacement.

The final of these proposed ideas is thought to cause the isotopic shift illustrated above from primary carbonatite material to more isotopically evolved material upon eruption to the surface. The only problem with such a process is the temperature at which this exchange is taking place. Meteoric waters, in particular those derived directly from precipitation within the Natron basin, are thought to have an isotopic value of approximately $\delta^{18}O$= -4‰ (Hillaire-Marcel and Casanova, 1987). In order to cause enrichment in ^{18}O or a positive shift in $\delta^{18}O$ the isotopic exchange must take place at a temperature below 250°C. If the exchange were to take place at elevated temperatures a further depletion of ^{18}O would occur. Heavier waters (0‰) are capable of generating an isotopic enrichment up to 25‰ at temperatures of around 40°C, but at similar temperatures isotopically lighter waters can only produce enrichment up to 19‰. Deines (1989) however suggests that some carbonatites do not appear to show significant shifts in their isotopic composition despite long periods of time being exposed to atmospheric conditions. This may be true for calcium carbonatite material but natrocarbonatite is known to alter significantly after short periods of time at the surface.

8.3.1.Stable isotope signatures of altered lavas, ash and secondary precipitates

During the field campaign a variety of carbonate – bearing material was collected for the purpose of stable isotope analysis with two main aims; to look for a time-integrated signature for variation with alteration and also to look for a spatial relation for the ash material generated during the 2007 eruption to determine if there is some form of fractionation during dispersal.

Sample	δ13C (VPDB)	δ18O (SMOW)	% carbonate	Sample label
Lengai Summit ash	-3.62	23.75	9.76	OLA 4
Lengai Slope ash	-5.58	24.31	15.16	OLA 2
Gully on plain ash	-3.28	22.36	36.42	OLA 1
Trona 300m from shore	-1.94	26.78	42.51	NTR 4
Trona 500m from shore	-2.46	29.17	48.75	NTR 5
Natrocarbonatite Block	-5.41	11.02	55.82	OL 3
Stalactite	-8.00	16.11	56.16	OL 9
Yellow Precipitate	-7.52	21.79	69.10	OL 7
2007 Ash	-3.95	23.84	69.76	OLA 3
Trona from hot spring	+3.91	33.67	75.83	NTR 1
Altered 2006 lava	-5.55	12.39	96.34	OL 5
Brown 2006 lava	-5.80	18.39	100.42	OL 8

Table 30: Stable isotope values for material collected from Oldoinyo Lengai and Lake Natron during 2010 field campaign. Also shows % carbonate within the sample.

The data above (table 30) shows that the majority of the carbonate – bearing material lies within the mantle range (-5 to -8‰) for $\delta^{13}C$ with the trona and ash samples having a slightly more enriched $\delta^{13}C$ signal. The oxygen isotope signature is however a lot more variable and not representative of primary, mantle material (+6 to +10‰), except for that of OL 3, a natrocarbonatitic block. A comparison of this data from altered sources to that of primary carbonatite material is shown in Figure 8.6 below and the following section attempts to explain these isotopic shifts between different materials.

The trona samples will not be discussed in terms of alteration and fluid percolation as these rock units are not largely affected by fractionation due to low temperature exchange with meteoric water. The isotope signature of trona samples is the result of dissolution, evaporation and precipitation from a hypersaline lake (Lake Natron). The process of evaporation enriches products in heavier isotopes ((O'Neil and Hay, 1973) and references therein).

8.3.2. Modelling of isotope exchange during brine percolation

8.3.2.1. Background to stable isotope model

The data of ash and lava samples from Lengai (Figure 8.6) show some form of mixing with a different isotopic source – so far labelled as a brine phase but may be as simple as meteoric water. Whether this is a simple two part, binary mixing or more complicated three part mixing

is unknown, so for now the samples are modelled as though there are only subject to binary mixing with one water source. The isotopic signatures of the infiltrating waters are given below in table 32.

The first approximation model itself is constructed by incremental mixing of the two sources; the original mantle signature for carbonatite material (taken as an average value from data set, $\delta^{18}O$ = 5.27 and $\delta^{13}C$ = -7.62) and the signature for the infiltrating liquid, i.e. meteoric water. The incremental mixing is between 100% and 0% for each component, for example if the resulting isotope composition were the result of mixing 90% of the original carbonatite with 10% meteoric water. This is evaluated for both carbon and oxygen. As the isotopic signature is known for the carbonatite material this remains constant during modelling but the fluid signature is unknown and so is modelled for different combinations of $\delta^{13}C$ and $\delta^{18}O$. An excerpt of the model used is displayed in table 31 below.

Table 31: Small section of stable isotope model for the mixing of Oldoinyo Lengai material and meteoric water of different isotopes ratios.

		OL	**5.27**	**5.27**	**5.27**
δ18O		Meteoric	-4	-3	-2
%Mantle	%meteoric	0	5.27	5.27	5.27
95	5	5	4.8065	4.8565	4.9065
90	10	10	4.343	4.443	4.543
85	15	15	3.8795	4.0295	4.1795
80	20	20	3.416	3.616	3.816
75	25	25	2.9525	3.2025	3.4525
70	30	30	2.489	2.789	3.089
65	35	35	2.0255	2.3755	2.7255
60	40	40	1.562	1.962	2.362
55	45	45	1.0985	1.5485	1.9985
50	50	50	0.635	1.135	1.635

8.4. Results and discussion of isotope modelling

The results of the isotope modelling are displayed graphically in Figure 8.6 below. Each marker along the lines represents 5% incremental mixing away from the original, mantle values towards the modelled end member. The exchange from primary carbonatite magma to the more isotopically enriched lavas, which have been exposed to the atmosphere for approximately 4 years prior to sampling and analysis, is clearly illustrated. The main trend line through the samples appears to show variation from primary magma over time, but is also a function of surface area:volume. Since the ash particles have a smaller surface area:volume

ratio, they show greater isotopic equilibration with any fluid over the same amount of time as the exposure of the lava to the same fluid. This trend line also shows minimal exchange of carbon during the weathering process with carbon values of all the measured material within the mantle range.

The minimal change in carbon isotope signature is most noticeable within the precipitates. The oxygen however shows isotopic exchange with a more enriched ($\delta^{18}O$ >1) source under certain temperature conditions. At first glance the modelling appears to require an interaction of a fluid with $\delta^{18}O$ of 26‰ and $\delta^{13}C$ of -7‰ with between 50 and 80% mixing. It is known from previous work that there is a fractionation of oxygen between calcite and water resulting in a fractionation factor $1000\ln\alpha$ = ~ 28‰ at 25°C (Sharma and Clayton, 1965, Bottinga, 1968). When this is taken into consideration it can be seen that the fluid required for the formation of the precipitates (yellow oval) has a $\delta^{18}O$ of approximately -2‰. Comparison of this with known isotopic signatures of common water sources listed in table 32 below reveals that it is most likely the result of isotopic exchange with meteoric water.

Table 32: Stable isotope signature of fluids associated with alteration of the natrocarbonatite and responsible for the formation of the secondary precipitates. (Warren, 2006, Goff and McMurtry, 2000, Hilaire et al., 1987)

Fluid Source	$\delta^{18}O$	$\delta^{13}C$
Magmatic (Juvenile)	+5 to +9‰	-4.3‰
Meteoric (at 2000m altitude)	-4.37‰	+1‰
Interstitial Brines	+8‰	+1‰
Hydrothermal	-12 to -6.5‰	-4.3 - +0.7‰

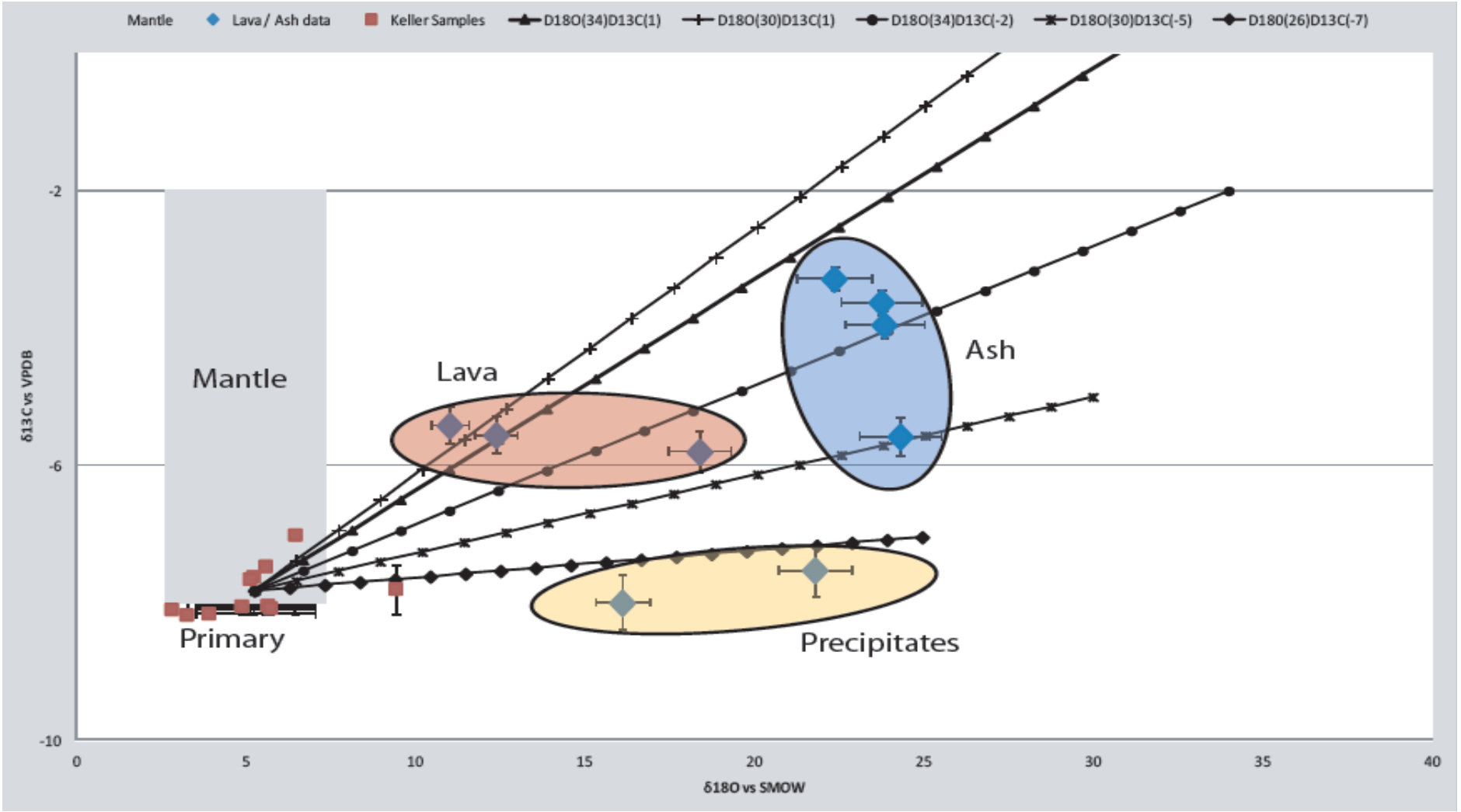

Figure 8.6: Graph illustrating stable isotope variation of lava and ash samples associated with Oldoinyo Lengai and Lake Natron. These are compared to stable isotopes of erupted carbonatite material from the 2006 flow prior to alteration. The analyses can be grouped by material type; red oval = altered lava from 2006 flow collected in 2010; blue oval = samples of ash from summit and slopes; yellow oval = secondary precipitates.

The fluids compositions responsible for the alteration of the lava and ash samples are slightly more complex. From the model results it can be seen that the lava samples require ~30% mixing of a fluid that has a $\delta^{18}O$ of between 30 – 34‰ and a $\delta^{13}C$ of between -2 and +1‰. When the fractionation factor listed above is taken into account the fluid $\delta^{18}O$ is actually between +2 and +6‰, which appears to indicate the role of magmatic water as the cause of alteration. However this isotopic range does not match that of the published magmatic water isotopic signature and so I believe that the altering fluid for the lava samples is a mixture of both magmatic and meteoric waters. Table 33 below outlines the overall isotopic signature for mixtures of magmatic and meteoric water and it can be seen that a mixture of 45% meteoric and 55% magmatic water results in an isotope signature of $\delta^{18}O$ of +2.05‰. This mixture also has a $\delta^{13}C$ of -1.915‰ which could generate the isotopic shift in $\delta^{13}C$ observed during lava alteration.

Table 33: Modelled isotope signatures resulting from the incremental mixing of magmatic with meteoric waters during alteration of natrocarbonatitic material.

			$\delta^{18}O$	$\delta^{13}C$
		Meteoric	-4	1
		Magmatic	7	-4.3
%Meteoric	%Magmatic	0	-4	1
95	5	5	-3.45	0.735
90	10	10	-2.9	0.47
85	15	15	-2.35	0.205
80	20	20	-1.8	-0.06
75	25	25	-1.25	-0.325
70	30	30	-0.7	-0.59
65	35	35	-0.15	-0.855
60	40	40	0.4	-1.12
55	45	45	0.95	-1.385
50	50	50	1.5	-1.65
45	55	55	2.05	-1.915
40	60	60	2.6	-2.18
35	65	65	3.15	-2.445
30	70	70	3.7	-2.71

25	75	75	4.25	-2.975
20	80	80	4.8	-3.24
15	85	85	5.35	-3.505
10	90	90	5.9	-3.77
5	95	95	6.45	-4.035
0	100	100	7	-4.3

The alteration of the ash products from Lengai appear to be more complex than the lava samples. Figure 8.6 shows alteration by 65% mixing of a fluid with $\delta^{18}O$ and $\delta^{13}C$ similar to that required by the lava material. Although the percentage of mixing is plausible the interaction of the ash units with magmatic water is less likely, unless alteration begins in the eruption column and so reacts with "steam". Magmatic water interaction may also be possible for ash which was collected from the summit of the volcano due to condensation of gas from the active crater. It is, however, expected that the main fluid source altering the ash would be meteoric / atmospheric water during its journey in the eruption column, umbrella cloud and settling onto the surrounding plain. However the isotope signature for meteoric water presented in table 33 does not result in the isotopic shift when modelled.

Hillaire-Marcel, et al (1987) present data for atmospheric water (i.e. precipitation) at different altitudes which may account for the isotopic signatures of the ash. The data (illustrated in Figure 8.7) show that the $\delta^{18}O$ isotope value is heavier at lower altitudes within the Natron Basin.

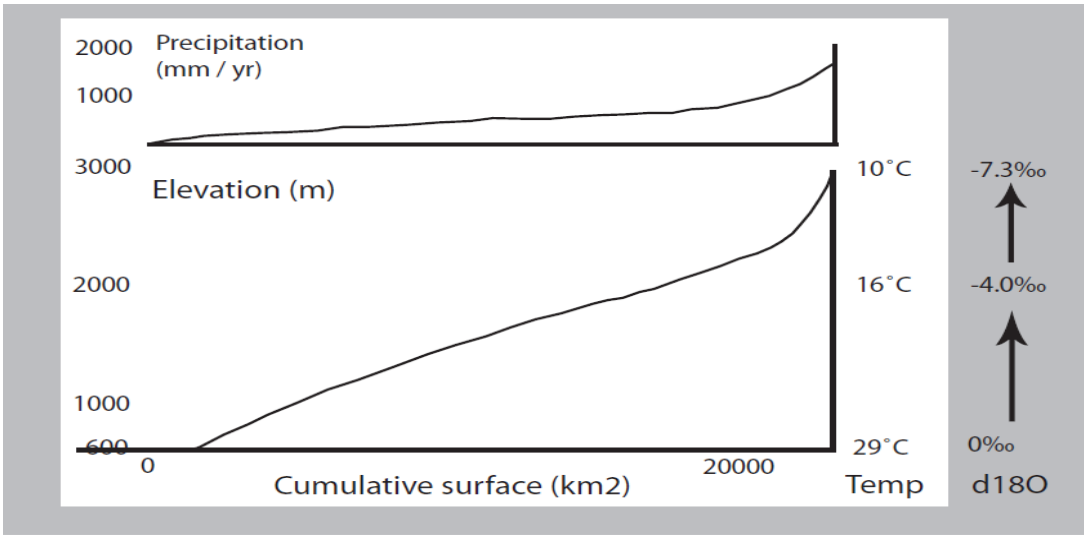

Figure 8.7: Variation in basin elevation, precipitation and $\delta^{18}O$ within the Natron Basin. (Hillaire-Marcel and Casanova, 1987)

With the above variations in $\delta^{18}O$ in mind it can be argued that the ash collected show isotopic variation which is the result of their altitude. The ash collected from the plains around Lengai are at roughly 650 m in altitude and so from Hillaire – Marcel et al (1987) would be expected to equilibrate with precipitation of $\delta^{18}O$ of 0‰. When the fractionation factor at 25°C is taken into account ($\ln 1000\alpha = 28‰$) this fluid could generate the isotopic shift measured. The slight shift in carbon isotopes of the ash samples is proposed to be the result of isotopic exchange with atmospheric CO_2 during transport in the eruption column.

8.5. Whole rock alteration and formation of precipitates

The result of the alteration is to turn lava flows from black solid bodies of lava into white / brown, unconsolidated sandy masses which may contain relict material within its core, destroying all primary magmatic textures exposed at the surface. Re-equilibration under atmospheric conditions occurs immediately after solidification with continued alteration in the presence of meteoric water (Zaitsev and Keller, 2006). Lava flows are cut by networks of cracks which become infilled with polymineralic encrustations. Genge et al (2001) described such encrustations as transient salt fringes and tubes consisting of more than 70% thermonatrite. Aphthitalite, halite and sylvite are also present within the fringes with specific growth patterns indicating a sequence of precipitation.

The formation of these subsolidius minerals requires the input of an external water source for a minimum amount of time. However the determination of the exact water source requires further investigation. Genge et al (2001) suggest that the salt fringes and tubes result from sublimation from steam-dominated fumaroles caused by the extrusion of new natrocarbonatite over older flows which have become water saturated with time. The chemistry of the encrustations is therefore governed by the changes in temperature of the gases and by the chemical composition of leached fluids from the cooling lava with alkalis and halides being sourced from the neighbouring natrocarbonatite, in particular from gregoryite and sylvite. A magmatic gas input is also required according to Genge et al (2001). The presence of CO_2 and H_2S carrying alkalis provides the necessary components for the crystallisation of aphthiltalite, in particular sulphur which does not appear to have been sourced from nearby natrocarbonatite. Further investigation into the encrustations present at Oldoinyo Lengai resulted in their classification into two groups; REE-rich and REE-poor

hypothesised to have formed by different processes as shown by their relative REE patterns (Gilbert and Williams-Jones, 2008).

REE-rich encrustations located in close proximity to the hornitos are formed from exsolved high temperature gas and are essentially sublimates. REE-poor encrustations consist of minerals which are only stable at lower temperatures i.e. <50°C and are likely to be formed by precipitation from steam generated by the interaction of water with hot rock, supporting the conclusion made by Genge et al (2001). Their lower REE content is argued to be the result of reduced mobility of these elements during weathering by low temperature fluids. The formation of REE-rich encrustations by high temperature, low density vapours requires that these vapours also carry significant amounts of REE elements by solvation and complexation with anions such as chloride, fluoride or carbonate (Gilbert and Williams-Jones, 2008).

The pentasodium phosphate carbonate is thought to derive its composition from gregoryite as it does not occur in material where the primary mineral is present (Mitchell, 2006a). The author therefore argues that this new mineral represent a sublimate of volcanic gas, which is concentrated in Na, CO_2 and F, combined with the decomposition of gregoryite. Mitchell (2006b) argues that the stalactites represent precipitation from alkali-rich brine formed during the passage of meteoric water through natrocarbonatitic units. This also takes into account the breakdown of fluorite to generate the free F for binding into new minerals, claiming this requires pH of greater than 12.4, which seems unlikely in the Lengai system. Confirmation of this requires collection of the fluid which is dripping from the stalactites.

8.5.1. Permeability of natrocarbonatite

A key parameter that requires a brief discussion is the rate at which fluid-percolation takes place, which in turn is related to the permeability of the rock units themselves. Permeability is of course the measured ability of a rock unit to transmit fluids and so is a measure of the connectedness of the pores of a rock. This physical property can be a time limiting factor as it dictates how quickly fluid can pass through the natrocarbonatite over time. Measurement of permeability of natrocarbonatite has not previously been completed, but inferred (Mattsson and Vuorinen, 2009, Pinkerton et al., 1995), largely due to the difficult nature of generating samples for measurements which normally requires the use of water during coring. The production of samples for this study is outlined in Chapter 2.

Overall a decrease in permeability was observed under an effective pressure of 5 MPa. This decrease in permeability is about 1 order of magnitude over 11000 seconds (~3 hours) from 6.98 x 10^{-13} to 5.73 x10^{-14} m^2 as shown by table 34. This implies that in nature, over time, less water is able to flow through the rock unit, so alteration becomes slower over time and therefore precipitation of secondary mineral structures, i.e. stalactites, is a quick process.

Table 34: Summary of results from permeability measurements between two selected time periods.

Confining Pressure (MPa)	Effective Pressure (MPa)	Time (min)	flow volume (m3)	volume flow rate(m3/sec)	Q (vol flow rate(m3/sec)/area of sample(m2))	Permeability K= Q η/ (dP/dx)
10	5	31.67086333	3.84345E-06	7.69635E-09	1.56789E-08	**6.9771E-13**
10	5	215.020155	6.319E-07	6.32043E-10	1.28759E-09	**5.72976E-14**

The decrease in permeability is argued to be the result of pore collapse due to the alteration of the primary minerals of natrocarbonatite which ultimately destroys primary structure. Photographs taken after the core was removed from the permeameter and 24 hours later provide some indication as to why the permeability drops. The core sample during fluid flow appears to have broken in 2 possibly as a result of material removal due to the hygroscopic nature of the natrocarbonatite. When left after removal from the permeameter the samples appears to have altered to a brown, sand like unit which is unconsolidated (Figure 8.8). This is typical of natural samples which are exposed to atmospheric conditions resulting in the alteration of the natrocarbonatite to secondary minerals. The pores which were once able to contain fluids are infilled with broken down material which prevents the flow of fluids through the sample.

Figure 8.8: Photographs of the natrocarbonatite core sample used for permeability tests. (a) Directly after removal from the permeameter where sample has broken in half with alteration occurring; (b) 24 hours after the permeability test sample has dried to brown, unconsolidated, altered unit.

8.5.2. Water / rock ratio during alteration

By using the stable isotopes measured in this study it is possible to estimate the fluid / rock ratio required for the alteration of the natrocarbonatite. This is described by the equation (Krauskopf and Bird, 1995, Taylor, 1974):

$$W/R = \ln ((\delta_{rf} - \delta_{ri} / -\delta_{rf} + \delta_{wi} - \Delta) + 1) * (C_r/C_w) \quad (1)$$

Where $$\Delta = ((2.68 \times 10^6) / T^2) + 3.53 \quad (2)$$

Where the subscripts are as follows; r = rock, w = water, f = final, i = initial, T = temperature at which alteration occurs, C = concentration of oxygen. For this study the concentration ratio of oxygen between the fluid and rock is assumed to be 0.5 and the temperature is varied between 25°C and 100°C. The initial $\delta^{18}O$ is that of the fresh lava and the final $\delta^{18}O$ is that of the altered units which show the large shifts in isotope signatures. The initial $\delta^{18}O$ of the fluid is that of standard meteoric water (-4‰). This calculation was also completed for lava and ash separately for 25°C and only for the lava at 100°C.

	Lava	Ash
W/R at 25°C	0.0012	0.0021
W/R at 100°C	0.018	-

Table 35: Results of W/ R interaction ratios based upon isotopic values determined of altered ash and lavas.

The calculations of W/R ratio (table 35) show that it does not require large influxes of fluid in order to cause the alteration observed and the shifts in isotopic signatures. This may indicate how dissolution and precipitation of the secondary features can take place before the decrease in permeability hinders fluid flow.

8.6. Conclusions of stable isotope study of Lengai material

The alteration of natrocarbonatite material has been documented by numerous authors since the first observations of Oldointo Lengai began, with the description of “white flows” within

the active crater and descending the slopes of the volcano. The use of stable isotope studies of the material from Lengai has generated the following conclusions:

- Exposure of the lava to the atmosphere results in rapid alteration which destroys primary structures and minerals both on the surface and within the cores of the lava flows. This alteration can result in an isotope shift of +15 to +20‰ for ^{18}O and +4‰ for ^{13}C.

- The dissolution of the primary minerals generates a "brine" phase which upon evaportation crystallises secondary minerals of apthitalite, halite, sylvite, nahcolite and a pentasodium phosphate carbonate on the surface of lava flows, similar to previous studies. The "brine" is composed of meteoric water, either from rainfall or atmospheric vapour.

- The stable isotope signature of the precipitated material only shows a shift of the oxygen isotopes. This is a result of involvement of purely meteoric water, which contains little carbon for isotopic exchange.

- Precipitation of these secondary minerals is a rapid process, requiring small amounts of water interacting with the rocks, which takes place before the permeability of the natrocarbonatite is decreased due to pore collapse and infill.

- The lava itself also shows alteration with the generation of an unconsolidated, brown / white unit. There is a shift in both the oxygen and carbon isotope signuture of this material which indicates the involvement of other fluid sources than just meteoric. A mixture of magmatic and meteoric water is invoked to result in the alteration of the lava. Magmatic water refers to water contained within the lavas themselves as well as condensates from "steam" emitted by the lava. Genge et al (2001) argue for the formation of steam from heated water-saturated lava flows which may also be plausible.

- Ash samples from Lengai show greater degrees of alteration in terms of the shift in stable isotope signatures which is the result of the surface area : volume ratio. They too demonstrate alteration due to atmospheric / meteoric water as a result of injection into the atmosphere. The isotope signature of the fluid with which the ash exchanges oxygen is dictated by the altitude at which the ash alters.

Chapter 9 – Carbonatite-related volcanism and sub-volcanic metasomatism of Oldoinyo Lengai; Conclusions and discussion

9.1. Introduction

The main aims of this thesis were to better understand the sub-volcanic environment of this unique volcano in an attempt to generate an improved model cross-section and determine how the interplay of the rock units within the environment may contribute to the unusual lavas produced from Oldoinyo Lengai. In doing so it was also an aim to estimate the carbon flux from this volcano in terms of the input, storage and output of all chemical forms of carbon. From the numerous studies which have been conducted the following conclusions can be drawn:

i. The 2007 eruption of Lengai appears to have been fed and sustained by a silicate dyke-feature which is now visible in the crater wall. The eruption punctuated the end of regular, well documented volcanic cycle which alternates between effusive and explosive behaviour (Chapter 3).

ii. The solid flux of carbon during effusive episodes is between 85,500 m^3 per year and 255,000 m^3 per year (Chapter 3).

iii. A lack of trona within early volcanic debris avalanche deposits which entered Lake Natron during transport indicates a lack of alkaline carbonatite production during the early part of Lengai's history, suggesting that the production of natrocarbonatite is an evolutionary process (Chapter 3).

iv. Fluid inclusions and fenite compositions indicate the presence of both ijolitic and carbonatitic crystallising magmas within crustal regions; the first indication of an intrusive carbonatite body or substantial carbonatite reservoir beneath the volcano (Chapter 4,5).

v. Fluids circulating within the crust are mantle-derived (Chapter 5).

vi. The composition of carbonatite at Oldoinyo Lengai is constantly evolving from when it is generated to its alteration at the surface. This is a result of refining by the rock units through which it infiltrates and the loss of fluids upon crystallisation (Chapter 6).

vii. A significant metasomatised region lies in the sub-lithospheric mantle which is glimmeritic in composition and due to its radiogenic nature appears to have been established for a long period of time (Chapter 7).

viii. A failed kimberlite, which resulted in a kimberlite metasomite, is a potential mantle heterogeneity beneath Oldoinyo Lengai (Chapter 7).

ix. The presence of highly alkaline fenitic regions within the crust of Lengai contribute to the alkali nature of the natrocarbonatite magma through an autometasomatic process (Chapter 5).

The remainder of this chapter will expand upon the above conclusions and attempt to interpret how the interaction of the rock units contributes to the evolution of the volcanic complex at Oldoinyo Lengai.

9.2. A closer look at the sub-volcanic environment

The sub-volcanic environment of any volcano is likely to be complex and it is argued that Oldoinyo Lengai is of no exception to this. The best indication geologists have of the sub-volcanic lithologies is through the study of volcanic debris from large explosive eruptions in the form of xenolithic material. Xenoliths from Oldoinyo Lengai have been a constant source of information of the past three decades with relatively consistent suites of rocks generated during each explosive episode. This in itself indicates that the magmatic source and pathway for explosive eruptions during historical times has remained regular, with previous estimates of natrocarbonatite formation and eruption, based upon Ra-Th disequilibria, ranging from 20 to 81 years (Pyle et al., 1991). However with the presence of large quantities of mica material now present on the flanks of the volcano, in the form of megacrysts, which have not previously been reported, it would appear that the depth tapped during the latest explosive activity was deeper into the mantle

9.2.1. A model cross-section of Oldoinyo Lengai

The study of the xenoliths generated during the 2007 eruption has enabled me to generate an improved cross-section of Oldoinyo Lengai which is presented in Figure 9.1 below. The sketch cross-section illustrates the expected positions of the different rock units within the volcanic

complex using the xenoliths as examples of each rock type. The depth estimations are based upon thermobarometry and stability of minerals identified within the xenoliths.

From the cross-section it can be seen that it is proposed that within the crustal region exists both an ijolitic intrusive body and a carbonatite intrusive body, similar to models previously envisaged by Le Bas (1977) for carbonatite complexes in general. Of course it should be noted that the shape and dimensions of the bodies are not known. Extending from the intrusive bodies are fenitic aureoles of different grades and it is from here that the fenite samples of this study have been derived. It is important to emphasise the different locations of the fenites in terms of the aureole region which they sample, with OLX 3 and 17b sampling carbonatitic fenitised units and form at different locations within the aureole, whilst OLX 17a is associated with ijolitic fenitisation.

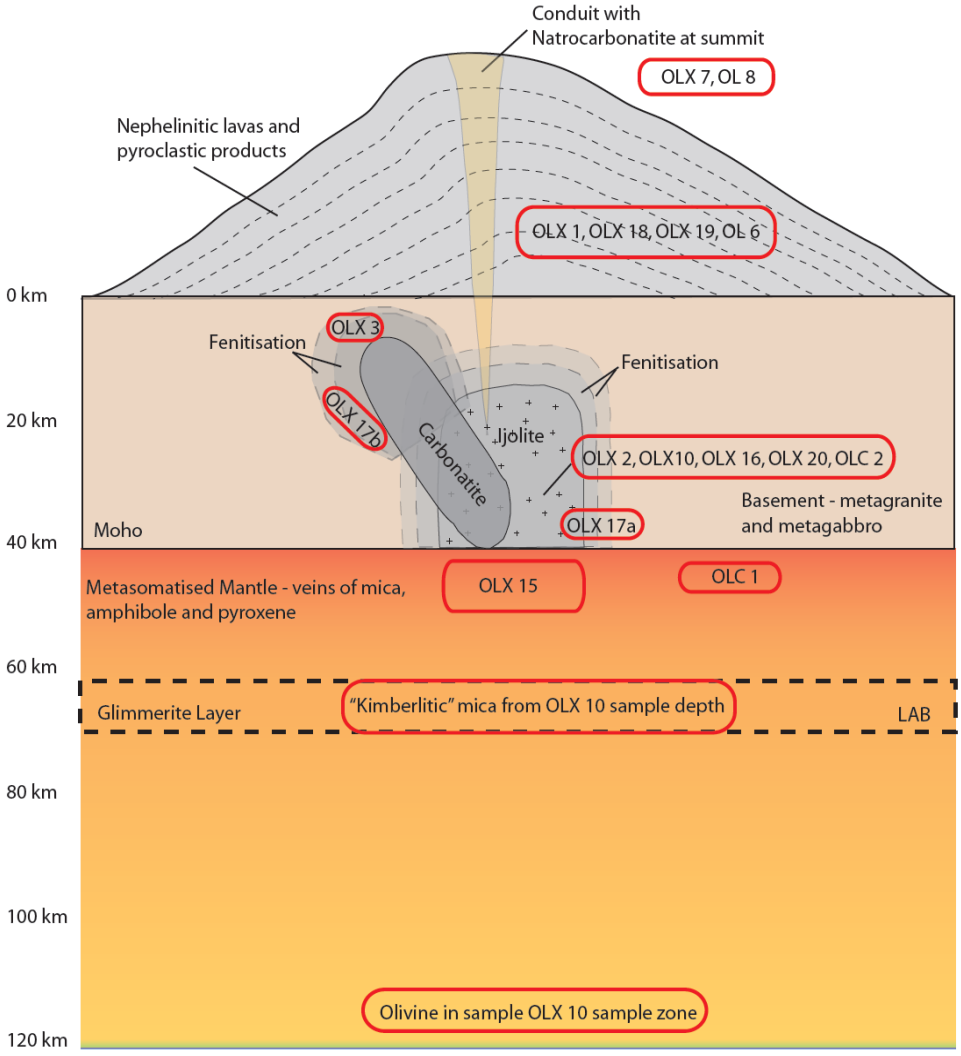

Figure 9.1: Diagrammatic cross-section of Oldoinyo Lengai showing sub-volcanic lithologies and zones of mineral derivation and metasomatism. Sample which typify each region are labelled. LAB = lithosphere–asthenosphere boundary

The sub-continental mantle beneath East and South Africa has been envisaged to be heterogeneous by numerous authors (Johnson et al., 1997, Sweeney et al., 1993, Aoki, 1975, Kjarsgaard and Peterson, 1991, Bell and Blenkinsop, 1987b, Dawson and Smith, 1988, Hawkesworth et al., 1990, Rudnick et al., 1993) and so the proposed existence of metasomatised regions beneath Lengai is of no surprise, however, the proposed chemistry of these metasomites may appear controversial. Here it is suggested that the uppermost mantle directly beneath the crust is highly metasomatised due to the infiltration of both silicate and carbonate material resulting in a heterogeneous layer, rich in veined pyroxenites with abundant amphibole and alkali pyroxene (typified by sample OLX 15) and other mantle-derived units observed at nearby volcanic features (Johnson et al., 1997).

Located beneath this metasomatised upper mantle region, at a depth of between 60 and 70 km, is argued to be a glimmeritic layer with a kimberlitic chemical composition which is the result of a failed kimberlitic melt which originated or traversed from depths of around 120 km. This glimmeritic region yields deformed mica crystals with high Ti and Cr contents consistent with other kimberlitic mica material (Dawson et al., 1970, Kelley and Wartho, 2000, Graham et al., 2004, Reguir et al., 2009, Edwards and Howkins, 1966, Dawson and Andrews, 1972, Kjarsgaard, 2011).

The presence of olivine megacrysts within samples from Oldoinyo Lengai, which are thought to have a depth of origin from between 80 and 120 km, indicates that the source region for alkaline magmas must be of similar depths. Upon their ascent they incorporate olivine crystals of a composition different to that of the host magma and so disequilibrium, reaction rims form. The point of incorporation of these olivine crystals is not known, whether at the start after formation or upon ascent and interaction with the “kimberlitic” layer. Olivine crystals within kimberlite melts are a controversial issue as it is not certain whether this mineral can crystallise from kimberlite melts or simply represent incorporated crystals (Brett et al., 2009, Kamenetsky et al., 2008). The harzburgitic composition of the olivine within sample OLX 10 would suggest that the latter is more likely.

9.3. The importance of metasomatic regions

The main theme throughout this thesis has been the existence and role of fluid-related metasomatism of the sub-surface lithologies of Oldoinyo Lengai and how the chemistry of these regions affects the overall chemistry of the eruption products found post-2007. It

therefore seems that these metasomatic regions play an important role in magma genesis and evolution both within the mantle and also the crust.

Unlike Morogan and Martin (1985) it has been shown that both silicate and carbonate-related fenitisation / metasomatism is present within the crustal units of Oldoinyo Lengai and so it is possible that these melts also cause metasomatism within mantle regions - whether as individual magmas or as one carbonated silicate parent melt. As discussed within chapter 7, section 7.4.5, the production of melt products seen at Oldoinyo Lengai requires the presence of metasomatised mantle, in particular the presence of carbon within the mantle to generate carbon-bearing magmas upon melting. This therefore requires a long time-integrated process of metasomatism to have occurred before or contemporaneously with establishment of Oldoinyo Lengai.

The current melt products located at Oldoinyo Lengai are not the only evidence for requirement of metasomatised material, but also the existence of kimberlitic minerals. As discussed previously, Russell et al (2012) argue that the production of kimberlite requires the reaction of sodium carbonatite precursor melt with orthopyroxene resulting in exsolution of CO_2 and the propulsion of kimberlite to the surface. The authors also argue that without significant orthopyroxene this process is not viable, which I conclude to result in failed kimberlites within the mantle. Fertile mantle of course contains abundant orthopyroxene and so some precursory metasomatism must have occurred to remove or decrease the abundance of opx from the mantle beneath Lengai. The type of metasomatism at this point is still unknown and so requires further work, however since orthopyroxene is the most silica-saturated phase, Russell et al (2012) argue that it is preferentially assimilated over other phases.

9.3.1. *The timing of metasomatic events*

Unfortunately it has not been possible to date the metasomatic units to provide an indication of when such fluid influx events have occurred. However the presence of radiogenic units and mineral separates suggest that they have been subject to long time-integrated radioactive decay and so the metasomatic events are likely to be relatively old. However, confirmation using Rb/Sr ratios is required. Such events elsewhere in Tanzania have been estimated to have occurred between 610 and 650 Ma (Koornneef et al., 2009).

9.4. The source region of carbon

All lines of research throughout this thesis have indicated that the source of both the silicate and the carbonatite units at Oldoinyo Lengai is from within the metasomatised region of the mantle, which in terms of the diagram above represents the upper 250 km.

The radiogenic isotope ratios are similar to those previously reported for carbonatites and natrocarbonatite at Oldoinyo Lengai conforms to the EACL, thought to represent mixing between HIMU and EM1 heterogeneities within the mantle (Bell and Tilton, 2001, Bell and Blenkinsop, 1987b, Bell and Dawson, 1995, Bell and Peterson, 1991). The stable isotope measurements of primary, unaltered material also conform to an accepted "mantle box" with $\delta^{13}C$ = -5 to -8‰ (Keller and Hoefs, 1995, Deines, 1989, Hoefs, 2009).

In part the fluid inclusions studied within this thesis also agree with the upper mantle origin of the carbonatite units with the presence of high density, alkali-rich and CO_2-bearing fluid inclusions. A number of the inclusions exhibiting densities >1 gcm^{-3}. There are, however, some lines of evidence from the inclusion studies which could indicate a slightly deeper origin of the fluid inclusions. The first of these is the presence of other gases including N_2 and CH_4, both of which are minor components within the upper mantle. At a first glance the presence of a reduced from of carbon requires derivation from a region of the mantle which is not oxidised, otherwise the carbon would be present purely as CO_2. From Figure 9.2 below we can see that it is estimated that a change in oxygen fugacity occurs around a depth of 250 km which sees a change from oxidised carbon species above and reduced and neutral forms below (Mikhail, 2011, Rohrbach et al., 2007, Deines, 2002). This suggests that the CH_4 has been incorporated from depths of >250 km within the mantle. A different view may be that there is a methane reservoir within the crustal units themselves or a reducing environment within the fenitic aureole zone. However, this would only be plausible if the fluid inclusions were not a mixture of both reduced and oxidised phases.

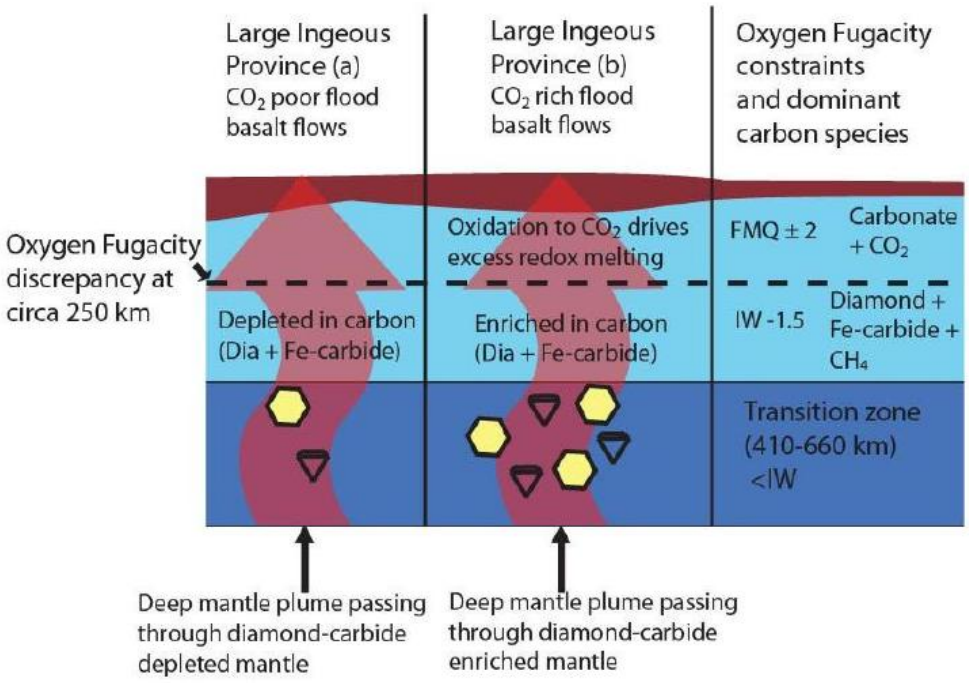

Figure 9.2: Cartoon to illustrate the potential for transport via plumes of reduced / neutral carbon phases towards the upper mantle. (Mikhail, 2011)

However it may be erroneous to assume that a heterogenetic upper mantle, in terms of chemical composition, is homogeneous in terms of its oxygen fugacity. With this in mind it could be possible that there are regions within the upper 220 km of the mantle which are reducing enough to enable CH_4-bearing fluids to be stable, as studies of the South African sub-cratonic mantle have shown (Woodland and Koch, 2003). Other cratonic mantle regions across the globe have also been shown to be reducing, i.e. $\Delta \log fO2$ [FMQ] = -1.5 to -4.5 (McCammon and Kopylova, 2004, McCammon, 2005). The authors argue that the cratonic mantle is primarily buffered by the exchange of Fe^{2+} and Fe^{3+} between accessory spinel and garnet and so there is a change in oxygen fugacity with the disappearance of spinel. There are, however, some implications to this that in such reducing environments beneath the craton carbonate melts should not be stable and so this idea is not agreement with metasomatism through carbonatitic fluid infiltration.

There is a third method of generating CH_4-bearing fluids which is a product of chemical reactions between oxidised forms of carbon and hydrogen known as Fischer – Tropsch synthesis, defined by equation 1 below;

$$nCO_2 + (3n + 1)H_2 \longrightarrow C_nH_{2n+2} + 2nH_2O \qquad (1)$$

This process has been known to occur within fluid inclusions resulting in the formation of secondary trails of CH_4-domainted or H_2O-dominated inclusions generated from previously CO_2-rich inclusions (Potter et al., 2004) with H_2 derived from serpentinisation processes (McCollom and Seewald, 2001) or via complex hydrothermal reactions which alter nepheline, augite and Ti-magnetite to magnetite, biotite, aegirine and zeolites (Potter et al., 1998).

A lack of pure CH_4-bearing fluid inclusions suggests that Fischer-Tropsch synthesis is unlikely, although the mixed nature of the inclusions may represent incomplete reactions due to a lack of available reactants. The exact depth of the carbon source is therefore unknown and further analysis would be required to better characterise the fluids and so determine their source, although it is clear that they are mantle-derived. The carbon isotope ratio for example may shed light on the generation of carbon fluids.

9.4.1.The carbon isotope ratios

As stated previously whole rock samples of natrocarbonatite have a carbon isotope signature of between -5 to -8 ‰ indicating mantle derivation. However the carbon isotope signature determined from the pilot study of the fluid inclusions indicates a $\delta^{13}C$ of -16 ‰ (chapter 5). The light nature (enrichment in ^{12}C) is usually indicative of two processes; degassing or isotopic exchange with organic material. Both processes result in a fixing of light carbon within the vapour phase for degassing and from organic material.

This result can therefore be interpreted in two ways; either the fluid inclusions represent trapping of fluid condensate from a degassing magma body or they are samples of mantle material which has had some isotopic exchange with organic matter generating a bimodal carbon isotope signature for mantle rocks. The latter idea is not a new idea with numerous authors arguing that the mantle is bimodal in its carbon isotope signature with a mode at -5‰ and also at -25‰, as illustrated by Figure 9.3 (Deines, 2002). The more negative of the two modes is thought to originate from the incorporation of organic material re-introduced into the mantle via subduction.

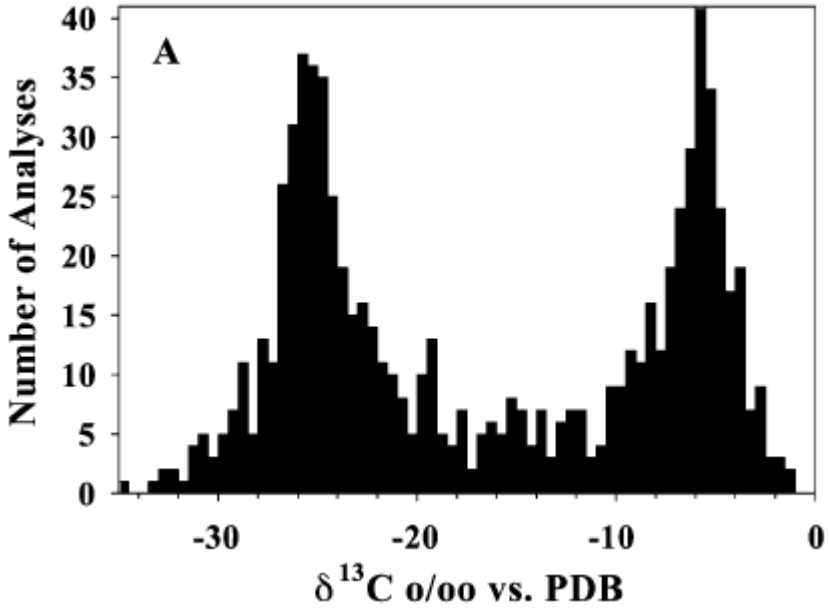

Figure 9.3: Histogram of carbon isotope ratios for mantle xenoliths collected across the globe from different geological and tectonic environments. Illustrates the bimodality of the mantle. ((Deines, 2002) and reference therein).

In the case of crustal units though, it is not clear whether the light isotope signature is a product of organic material within the mantle or whether it is the result of isotopic exchange with organic material within the crust. An added complication is also the presence of air-like noble gas signatures within the fluid inclusions which would seem to suggest contamination, although studies have shown that air-like noble gas signatures can be preserved within the mantle from subducted material (Mohapatra and Honda, 2006, Mohapatra and Murty, 2000).

9.4.2.Primary or secondary nature of natrocarbonatite

One of the key questions when understanding the production of natrocarbonatite is whether the magma is primary or secondary in origin, by which it is meant as to whether the carbonatite exists as an individual melt within the mantle or whether it is the result of an secondary process such as separation via liquid immiscibility. The latter is by far the most popular within the literature with early work on carbonate-silicate immiscibility beginning in the 1960's (Koster Van Groos and Wyllie, 1966, Visser and Koster Van Groos, 1977, Van Groos and Wyllie, 1963). However a number of theories and conclusions within this thesis, in particular the generation of kimberlitic material, require natrocarbonatite to be a primary magma derived from depth within the mantle. This is not to say that it exists throughout the

mantle as sodium-potassium-rich carbonatite akin to that which we see at the surface, but rather as some precursory carbonatitic fluid which ultimately evolves to natrocarbonatite as it nears the surface. The existence of primary, deep carbonatite material has been discussed previously in this thesis with evidence from carbonatitic inclusions within diamonds (Walter and al, 2008, Brenker and al, 2007), geochemical evidence (Harmer et al., 1998) and geochemical modelling of the stability of carbonate down to pressures of 137 GPa within the mantle (Oganov et al., 2008, Oganov et al., 2006).

The highly alkaline nature of natrocarbonatite indicates that it is extremely fractionated and likely to be the end member melt of a fractionation series. This is also the view of Gittins and Jago (1998) who concluded that the "progressive differentiation affects an already evolved magma and drives it to the very highly evolved aphyric types" occurring in discrete magma chambers within the volcanic complex.

Early work by Wallace and Green (1988) introduced the expected carbonatite compositions which are able to coexist with amphibole lherzolite between 21 – 31 kbar, concluding it is a sodic dolomitic carbonatite. From this composition they also calculated the crystal fractionation pathway which was required to generate magmas similar to that of Oldoinyo Lengai. It is important to note that within their work Wallace and Green (1988) highlighted that the highly reactive nature of the "primary" carbonatite would result in significant metasomatism within the upper mantle.

Later work on the derivation of natrocarbonatite from Wallace and Green's primary composition concluded that the late-stage residual melts were too sodic to be parental to that of natrocarbonatite at Oldoinyo Lengai (Sweeney et al., 1995). Sweeney et al (1995) allow for the formation of natrocarbonatite upon 59 wt% crystallisation and adjustment of the original composition of the peridotite from which the carbonatite melt is derived, requiring a more Mg-rich / Fe-poor mantle than that of the Hawaiian Pyrolite used by Wallace and Green (1988).

I would, however, like to suggest that the extremely sodic composition predicted by Wallace and Green's model (1988) is in agreement with that of natrocarbonatite seen at Oldoinyo Lengai, but represents the melt before the release of fenitising fluids, which results in a significant loss of alkalis to the surrounding country rocks. In addition to this the composition of the carbonatite at the surface is not the same as that which enters the upper mantle. This

carbonatite unit is refined by infiltration processes through both the upper mantle and the continental crust, as well as due to fluid loss and so both processes should be taken into account.

9.4.3. A preliminary model for natrocarbonatite generation

There are two observations from this thesis which are important for a model of natrocarbonatite formation; that the production is an evolutionary feature and was not always present at Lengai and that the fenitic aureoles beneath Oldoinyo Lengai contain large quantities of alkalis and carbon. With these and other observations in mind I present the following preliminary process of natrocarbonatite genesis;

a) An early metasomatic event prior to the establishment of Oldoinyo Lengai changes the sub-cratonic mantle mineralogy, depleting the rock units in orthopyroxene. This metasomatic event may be linked to the Older Volcanic units of the Gregory Rift, which are typified by large basaltic – phonolitic volcanoes.

b) Early in Lengai's history, primary carbonatitic material rises into the lithospheric mantle (potentially as a mantle plume) and is consumed by metasomatic processes, either in the formation of proto-kimberlites or mica-pyroxenitic mantle material, due to the reactive nature of carbonatites. The consequence of this is that the melts do not make it to the surface.

c) Over time the mantle region and carbonatite units establish an equilibrium and carbonatitic material ascends further into the crustal regions causing fenitisation, so once again consumed and importantly still unable to penetrate the crust to erupt at the surface. This carbonatitic material which ascends into the crust can be of two forms; either the primary melt which rises from deeper mantle regions or products of melting the metasomatised regions created previously. If the latter is true the carbonatitic material may occur either as an individual melt or as a carbonated silicate unit which then unmixes.

d) Extensive fenitised zones are produced and the arrival of new batches of silicate magma result in the re-melting of this fenitic material, generating an alkali-rich carbonatitc melt which passes through the crustal regions (which are now in equilibrium with the melt) and to the surface where it erupts as natrocarbonatite. By this method the natrocarbonatite is autometasomatised by its own fenitic units and is

an evolutionary feature of the volcano which requires the establishment of these enriched regions.

This model appears similar to the conclusions of both Bizimis et al (2003) and Nielsen and Veksler (2002). It also agrees with to ideas of chromatographic zone-refinement of the carbonatite unit during its passage through the mantle and crust discussed in chapter 6. However, the radiogenic isotope signatures do not agree with derivation of carbonatite from re-melting or incorportation of crustal material, with a much greater Sr concentration and $^{86}Sr/^{87}Sr$ expected.

9.5. Mantle fluid variation – a continuum in compositions

The evidence for fluid circulation within the mantle is easily identified via the generation of metasomites and other heterogeneities. However, it is important to consider whether the fluids and the metasomatic units they produce are linked in a continuum through fluid pathways – that is to question if there is a connectivity between metasomites, such as MARID suite rocks, kimberlites, carbonatites (both mantle and crustal) and diamond-forming fluids, which are often argued to be carbonatitic in composition (Brenker and al, 2007, Cartigny et al., 1998, Matveev and Stachel, 2009, Navon et al., 1988, Pearson et al., 2003, Schrauder and Navon, 1993, Tappert et al., 2005, Tomlinson et al., 2005, Walter and al, 2008, Weiss et al., 2009, Tomlinson et al., 2006, Tomlinson et al., 2009).

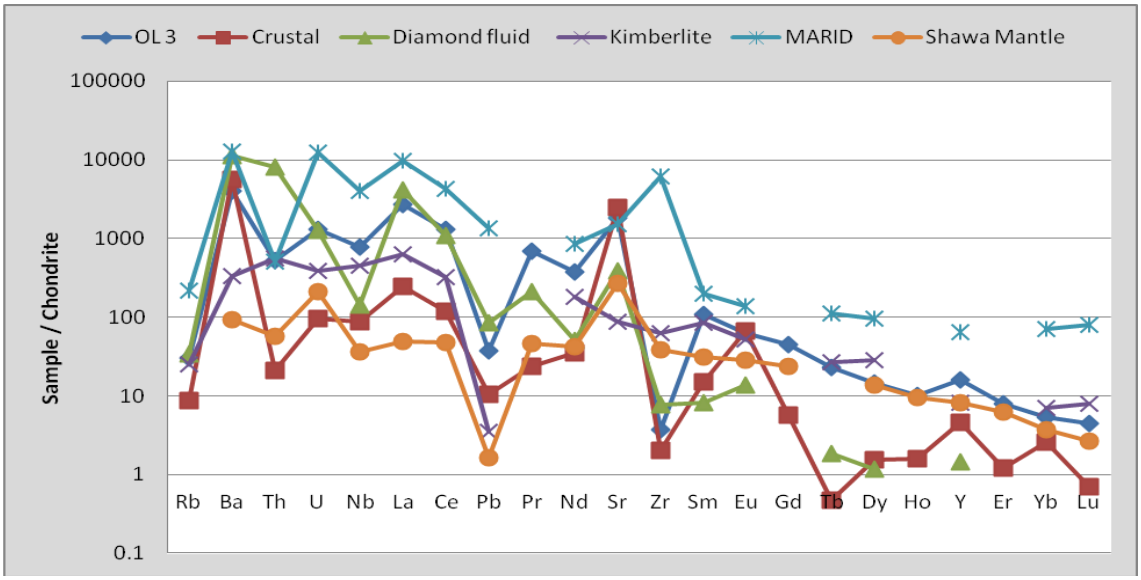

Figure 9.4: Comparison of erupted natrocarbonatite and lower crust carbonatite with other mantle - derived fluids or rock units. OL 3 = erupted carbonatite (this study), Crustal carbonatite = from refinement modelling (this study), Diamond fluid = fluid inclusions from Panda diamonds (Tomlinson et al., 2009), Kimberlite = global average (Wedepohl and Muramatsu, 1979), MARID = (Jones and Ekambaram, 1985, Jones et al., 1982); Shawa mantle = deep mantle carbonatite (Harmer et al., 1998)

When normalised to chondrite material and plotted on a trace element spider diagram (as in Figure 9.4) it can be seen that mantle-derived, fluid-associated units occupy a relatively narrow chemical composition range, with MARID suite rocks representing the most enriched in trace elements, whilst mantle carbonatite (both deep and shallow) are less enriched in trace elements. In order to fully understand the possible connectivity between fluids it is vital to look at the spatial distribution of the above units (Figure 9.5).

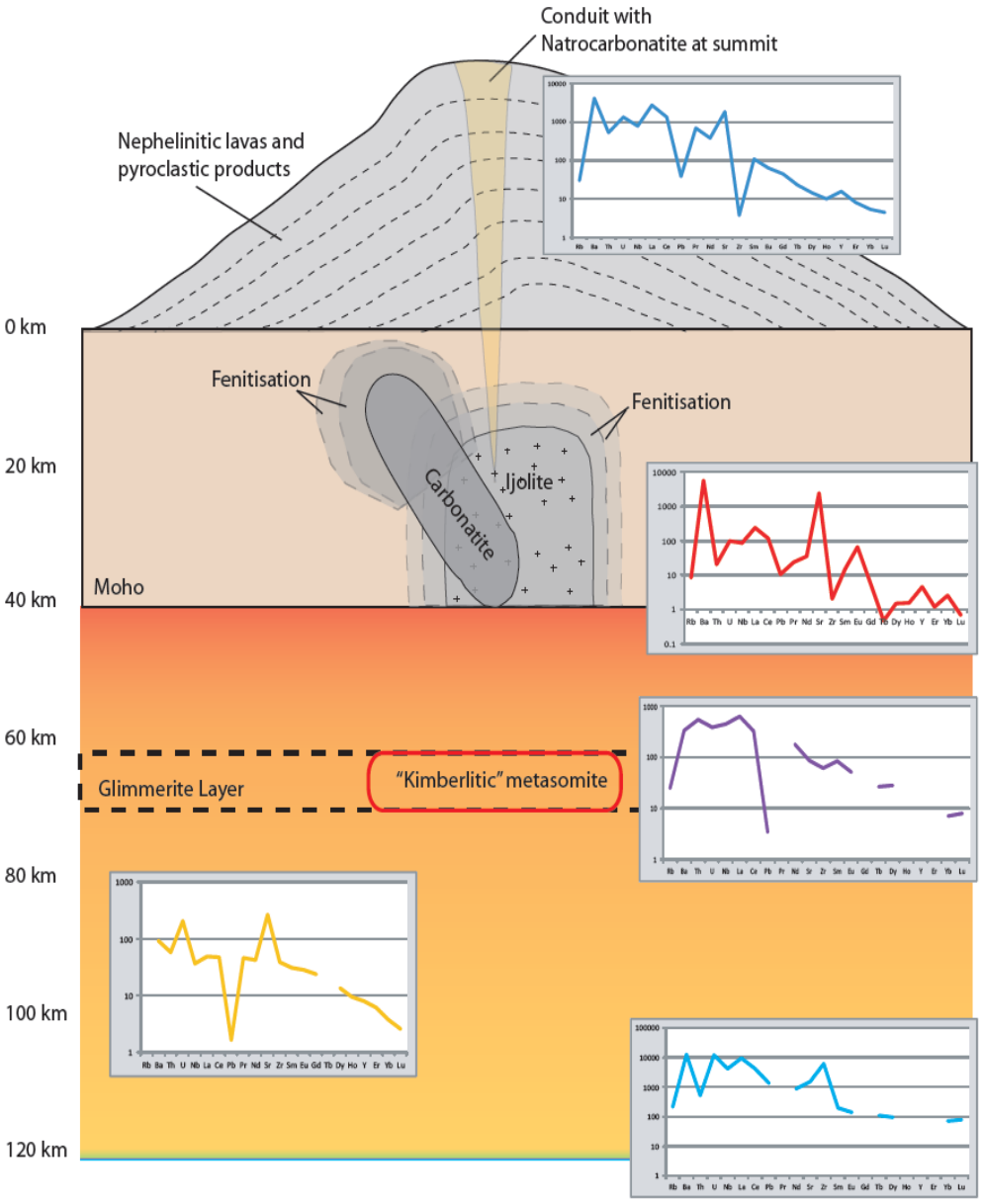

Figure 9.5: Schematic illustrating the spatial relation of metasomatic units and fluids within the sub-continental mantle. From erupted natrocarbonatite to MARID suite rocks. Line colours same as legend in Figure 9.4.

I argue, it is possible to present a hypothesised connectivity between these units based upon the evolution of the metasomatic agent during ascent; this begins with the infiltration of a pristine, enriched metasomatic fluid (potentially even carbonatitic in composition similar to that of the deep carbonatites from Shawa) which causes metasomatism and produces the MARID suite of rocks, explaining their more enriched nature. The lack of carbonate and Pb anomaly within MARID suite rocks indicates that none of the metasomatic fluid is retained during alteration but continues as a mobile fluid leaving behind a region of "restite" or residual melt left by emplacement and alteration (Mazzone and Haggerty, 1989).

The alteration continues until a local equilibrium is established (the time taken for this to occur is not constrained), likely to be caused by lining of fluid pathways by new minerals which reduces the efficiency of chemical diffusion (Navon and Stolper, 1987, Foley, 1992). Continued ascent of the metasomatising agent results in chemical reaction with the upper mantle wall rock material, ultimately resulting in the production of a slightly less enriched metasomite than MARID, which could potentially be kimberlitic if the conditions satisfy those proposed by Russell et al (2012). The chemical reactions result in the decrease in trace elements such as Ti, Y and Zr depending upon which minerals are present within the "wall rocks" and residual carbonatitic fluids which can be trapped in minerals, for instance (Tomlinson et al., 2009). Finally the metasomatic agent continues to rise through crust, refined en route, and erupts at the surface as the carbonatites we sample.

For this connectivity it is suggested that the original melt is a primitive carbonatite, of composition not seen erupted at the surface, which evolves upon ascent. The exact composition is, however, not known. The requirement for primitive carbonatite is primarily based upon the exceptional wetting properties and subsequent reduction in solidus of surrounding material facilitating metasomatic alteration and the production of enriched metasomites.

9.6. Carbon storage and flux

The global carbon cycle above ground is a well constrained cycle, but the sub-surface aspect and the depth to which it extends is relatively unknown. The cycling of carbon within the Earth's mantle and subsequent release from volcanoes plays an important part in controlling the Earth's atmosphere and so the storage and flux within volcanoes such as Oldoinyo Lengai are essential to understand. Figure 9.6 below is the same model cross-section as before but this time highlights the reservoirs of carbon that have been identified, some with flux values.

The flux of carbon at Lengai can be divided into two forms; gaseous and solid material. Work on the carbon gas flux from Lengai has been completed by previous studies and suggested to be circa 7,200 tonnes per day of CO_2 (Koepenick et al., 1996, Brantley and Koepenick, 1995). The visible solid carbonatite flux was calculated earlier in chapter 3 and is estimated to be approximately 255,000 m^3 per year if the conduit is assumed to be cylindrical in shape and fill over 40 years between eruptions.

As Figure 9.6 also illustrates there are a number of storage areas within the volcanic complex which contain carbon which also form part of the volcanic flux. The largest of these is likely to be the intrusive carbonatite bodies and magma chambers located within the crust and volcanic cone. Pyle et al (1991) estimated that a magma chamber beneath Lengai would contain up to 1.5 X 10^7 m^3 which reside there for up to 81 years.

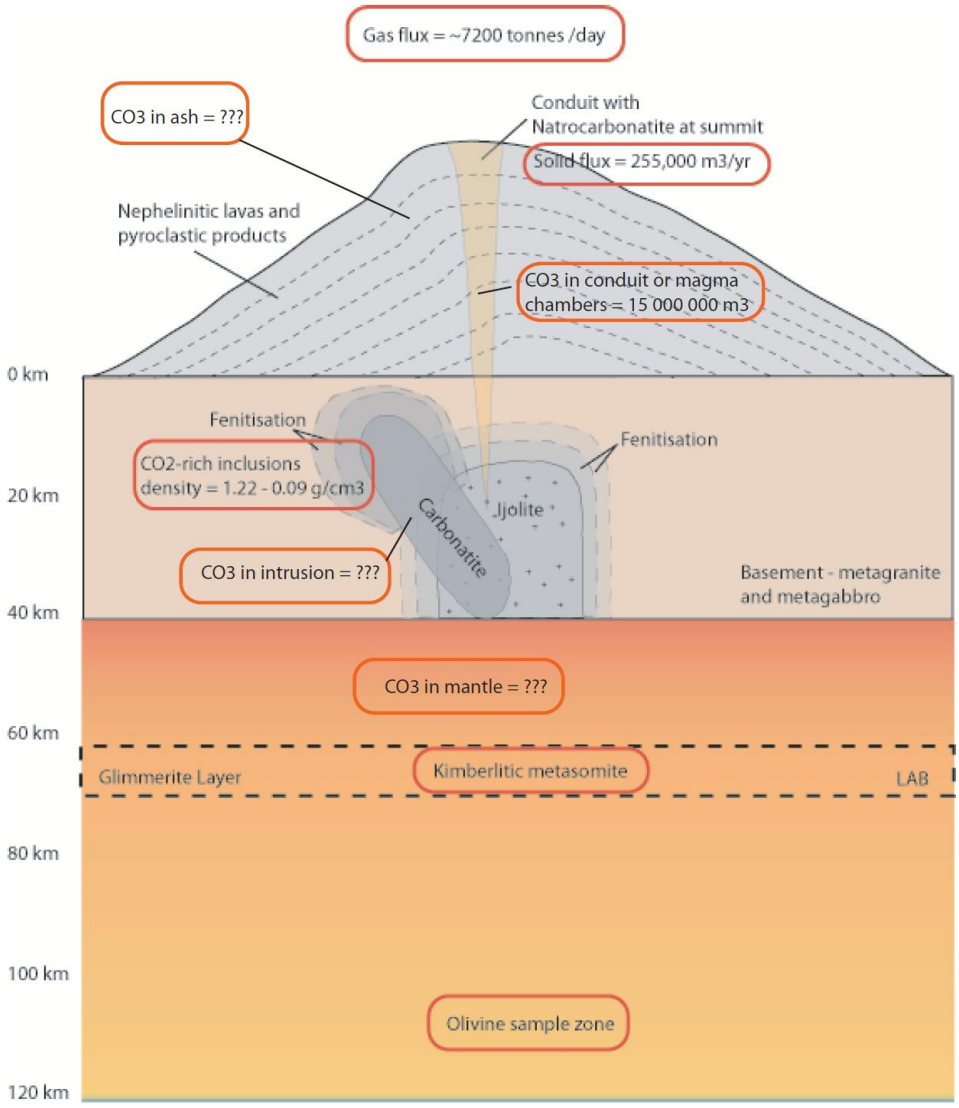

Figure 9.6: Model cross-section illustrating carbon storage and flux at Oldoinyo Lengai from identified carbon reservoirs. Gas flux from Brantley et al (1995), magma chamber volume estimated by Pyle et al (1991).

Carbon is also stored within the fenitic aureoles as fluid inclusions rich in CO_2 and carbonate minerals. As we can see the maximum CO_2 density of the inclusions is 1.22 g/cm^3. If at a first approximation we assume each inclusion of 100 µm in radius has a volume of 0.005 cm^3, each would contain up to 0.0061 g of CO_2. If we assume that there are 10 million inclusions within the fenitic aureoles of this size, then collectively they would contain 61 kg of CO_2.

There are two final unknown aspects of the carbon storage and flux shown in Figure 9.6; the first is the amount of carbon stored within the mantle beneath Lengai. At the very start of this thesis it was stated that carbon is trace element within the mantle, and although this is still true for the sub-cratonic mantle of this section of the Gregory Rift, from previous discussions it seems logical that the carbon concentration beneath Lengai may be significantly greater than that the global average for mantle carbon (circa 500 ppm) due to metasomatic heterogeneities. Further study of carbon concentrations within mantle xenoliths from this region is required to determine the carbon storage in the mantle.

The second large uncertainty is the flux of carbon related to the volcanic ash layers of the volcano. Formed during explosive eruptions, the volcanic ash from Lengai tends to be a mixture of both silicate and carbonatite material (Kervyn et al., 2008b, Keller et al., 2010, Kervyn et al., 2010, Mattsson and Reusser, 2010). Table 31 in chapter 8 shows that the ash samples from Lengai can vary in carbon content from 9 to 70% depending on the silicate / carbonate ratio. Although it was determined that the isotopic value of the ash varies only slightly with alteration, it is unknown how the overall concentration of carbon varies with exposure to the atmosphere.

9.7. Further Work

The investigations within this thesis have highlighted a number of topics which require further work either to deepen our understanding of the volcanic system at Lengai or to clarify some of the conclusions made. These are as follows:

i. Fluid and melt inclusion studies

The fluid inclusion study within this thesis represents the first study on Lengai units in terms of understanding the fluid alteration processes by examining inclusions. Melt inclusions are a common investigative tool (van Achterbergh et al., 2002, Church and Jones, 1995, Heinrich et

al., 2003, Stoppa et al., 2009, van Achterbergh et al., 2003, Guzmics et al., 2008b, Rosatelli et al., 2007), but further work on both is required to fully characterise the different fluid species circulating within the volcanic complex. Firstly it is important to establish whether the presence of fluid inclusions is solely confined to the fenitic units or whether other lithologies within the complex also contain fluid inclusions and subsequently how the phase compositions between lithologies compares.

Both melt and fluid inclusion analysis would benefit from LA-ICP-MS to accurately determine the major and minor element composition of the solid material. This would be a straightforward process for the melt inclusions which may highlight heterogeneities within the melts or how the trapped melt compares with that of the surface carbonatites. The fluid inclusions can be ablated as they are within the unit or after the inclusion can be broken, revealing the solid material, although loss of phases may occur with the pressure reduction from opening inclusions. A better understanding of the chemical changes which occur as a result of fenitisation would be gained by a complete chemical composition of all phases within fluid inclusions as well as start the back-calculations towards pristine carbonatite composition prior to fluid loss.

ii. Isotopic work – radiogenic and stable

The incorporation and fractionation of different isotopes within minerals is a useful tool in assessing the petrogenesis of igneous units. Thus far the isotopic signatures of the rock units presented here indicate a mantle derivation of the units but use of a second radiogenic system, i.e. Sm /Nd would enable a timing to be placed on metasomatic events within the mantle and crustal units. Stable isotope signatures of the metasomatised units may also provide an indication on the characteristics of the fluids causing alteration.

An expansion of the stable isotope investigation of the fluid inclusions should also be carried out to determine the characteristics of the fluids involved and how they compare to isotope signature of the whole rocks. This would further explore the bi-modality of mantle-derived fluids.

iii. Sampling of water from stalactites

The secondary mineral deposits on Lengai are agreed by all authors to be the result of exposure of natrocarbonatite to the atmosphere and the precipitation from fluid or brine (McFarlane et al., 2004, Zaitsev et al., 2008, Zaitsev and Keller, 2006, Genge et al., 2001,

Mitchell, 2006b). However there is no agreement upon the fluid source in terms of whether it is purely meteoric or a mixture of meteoric and magmatic. Stalactites observed during the field campaign were seen to have water dripping from their tips, and hindsight now suggests that collection of the water would enable chemical and isotopic analysis to determine its source.

iv. Experimental work on metasomatism

One of the key questions which has arisen from this thesis is what type of metasomatism would preferentially remove orthopyroxene from the upper mantle and so disabling the ability of natrocarbonatite to fully evolve into kimberlite. Experimental work could focus on simulating metasomatic events at upper mantle temperatures (900 – 1100 °C) and pressures (<4 GPa) to investigate the chemical reactions between an infiltrating melt and peridotitic mantle which results in the resorption and removal of orthopyroxene.

v. Metasomatism across the Gregory Rift

Mineral indicators for metasomatism have been identified at numerous volcanic features within the Gregory Rift (Johnson et al., 1997, Dawson et al., 1970, Dawson and Powell, 1969, Dawson and Smith, 1988, Dawson and Smith, 1977, Rhodes and Dawson, 1975) but the extent of the metasomatism is unknown; are there pockets of metasomatic material related to the rise of discrete batches of magma or is the metasomatism a laterally extensive layer?

Investigation of the type of metasomatism of other volcanic features in the Gregory Rift may provide answers as to why Oldoinyo Lengai appears to be unique in its production of natrocarbonatite, when the next closest volcano, Kerimasi, has not produced it despite potentially sampling the same sub-lithospheric mantle. Is there something “missing” in the Kerimasi volcanic system?

Appendix A – Field Diary

Fieldwork was undertaken in the Gregory Rift region during May 2010 (14th – 28th May). The primary aims of this field campaign were;

1. Observe the present state of Oldoinyo Lengai after the explosive eruption in 2007 in terms of volcanic edifice geometry and activity within the newly excavated pit crater.
2. Collect samples of erupted material; xenoliths, ash samples from different locations on the volcano and surrounding area and lava samples (ideally fresh and altered).
3. Observations and measurements of the 2006 natrocarbonatite flow on the western flank of the volcano.
4. Determine sights of carbon dioxide degassing both on Oldoinyo Lengai and within the Gregory Rift, in particular hot springs and collect gas samples for analysis.
5. Investigate collapse features from both Oldoinyo Lengai and Kerimasi in terms of run out distance and composition.
6. Collection of xenolithic material from volcanic centres located on the flanks of Oldoinyo Lengai. This material should include mantle xenoliths and megacrysts of mafic minerals and mica.
7. Take aerosol optical thickness (AOT) measurements using the Microtops Sunphotometer.

Field Localities and brief descriptions

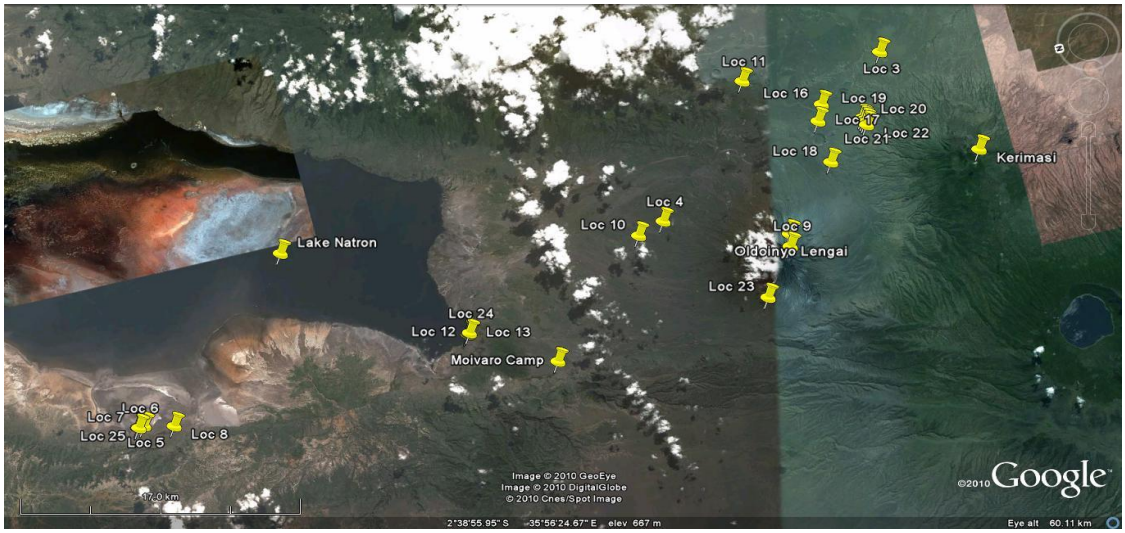

Figure A1: (a) Plan view of area covered during fieldwork. Google Earth image is taken looking east

Day 1 – Drive from Nairobi to Arusha. A short stop was taken at unnamed cone located approximately 40km outside of Arusha (GR 3°06.72S, 36°42.14E, WGS84 Datum). The unnamed cone consisted of glassy mafic scoria and mafic blocky units with pahoehoe flow tops. The lower unit of the cone appeared to be formed of palagonatised alkaline pyroclastics.

Day 2 – Drive from Arusha to Natron area and Moivaro camp ~ 6km southwest of Lake Natron. Route taken over rift walls and then along the rift valley floor passing Kitumbeine and eventually Gelai. Rift valley walls consist of relatively well - bedded basalt / phonolite complexes. Some units are not laterally continuous and abut against other flows. Location 2 (GR 03°05.74S, 36°01.04E, WGS84 Datum) was stop on small ridge to get view of rift valley to the north. The ridge itself was composed of basalt with large feldspar crystals (up to 2mm). Continued our journey northwards towards Lake Natron with a brief stop at Deeti tuff cone on the slopes of Kerimasi (GR 02°50.64S, 36°00.94E, WGS84 Datum). Deeti tuff cone shows mica rich sands with large lapilli tuff blocks containing grey, cored lapilli up to 2cm in diameter. Large mafic megacrysts (~4cm in length) can also be found at Deeti with mica books, amphiboles and pyroxene crystals (Figure A2).

Figure A2: Large single crystal of pyroxene contained within the lapilli at Deeti tuff cone. Camera lens for scale.

Location 4 (GR 02°42.26S, 35°56.80E, WG84 Datum) was large dry river channel south west of Oldoinyo Lengai consisting of dark grey epiclastic material most likely sourced from Oldoinyo Lengai with interbedded white, altered ash indicating a carbonate phase. The epiclastic layer contains clasts varying from 2 – 20cm across, which appear to be nephelinite and amphibole megacrysts. The white ash layers are fine grained and form an approximately 2cm layer. Botryoidal shapes also occur within the ash layers indicative of carbonate saturation and

subsequent evaporation. This type of deposit is common amongst all river channels leading from Oldoinyo Lengai.

Day 3 – Location 5 (GR 02°23.64S, 35°53.86E) and location 6 (GR 02°23.62S, 35°53.86E, WGS84 Datum) were hot alkaline springs located on the western shore of Lake Natron approximately 24km from base camp. Microtops AOT readings were taken at each hot spring. Location 7 (GR 02°23.61S, 35°53.87E, WGS84 Datum) lies about 250m north of the hot spring. Location 8 (GR 02°24.79S, 35°53.64E, WGS84 Datum) was purely to take a background AOT reading away from visibly degassing springs to generate reference value.

Day 4 – The main focus of the day was working on the summit of Oldoinyo Lengai. Climb to summit started at 2.30am and northern crater rim was reached by 9.30am, location 9 (GR 02°45.87S, 35°54.96E, WGS84 Datum). Climbing conditions were difficult with indurated surfaces and small gullies to walk in. Slope of the volcano's flanks vary from 30° at its base to ~55° at Pearly gates and newly deposited ash cone. Ash cone itself consisted of very soft saturated ash. After 2 hours working at the summit, observations of crater (see Chapter 3) and microtops measurements, group descended using the same path as ascent.

Day 5 – The morning of 19th May was spent taking microtops AOT readings from base camp as background measurements. In the afternoon group drove out to Location 10 (GR 02°41.67S, 35°56.52E, WGS84 Datum) a debris flow mound thought to have originated from early collapses of Oldoinyo Lengai. Location 11 (GR 02°45.99S, 36°01.03E, WGS84 Datum) is Pello Hill cone approximately 8.5km east of Oldoinyo Lengai where group collected xenoliths (see Appendix B).

Day 6 – Southern shore of Lake Natron investigating debris flow deposits. Locations 12 – 15 (GR 02°35.08S, 35°54.49E to 02°35.02S, 35°54.47E, WGS84 Datum) represent one large hummock investigated. Microtops AOT measurements made and samples of debris deposit clasts collected (see Appendix B).

Day 7 – The main aims of the day were to visit and sample the other volcanic centres in the region and so consisted of 7 localities;

- Location 16 - (GR 02°48.33S, 35°59.60E). An unnamed cone on the flanks of Kerimasi with most mafic units within the rift valley. Cone consists of black slab-like lavas known to be rich in magnesium and classified as olivine nephelinite.

- Location 17 – (GR 02°48.07S, 35°59.03E). Loolmurwak explosion crater for collection of xenoliths and megacryst material (see Appendix B).
- Location 18 – (GR 02°48.10S, 35°57.52E). Locality in between flanks of Kerimasi and Oldoinyo Lengai containing large carbonate lapilli tuffs and agglomerates.
- Location 19 – (GR 02°49.47S, 35°58.79E). Kerimasi debris flow unit.
- Location 20 – (GR 02°49.50S, 35°58.71E). Kerimasi related deposits with more agglomerates of lapilli.
- Location 21 – (GR 02°49.53S, 35°58.62E). Agglomerate deposit at the base of Kerimasi and Loluni cone where local Masaai chief suggest site of gas release. Again none emitted during time spent there.
- Location 22 – (GR 02°49.55S, 35°58.52E). Loluni tuff cone located on the slopes of Kerimasi.

Day 8 – Group returned to Oldoinyo Lengai in the morning to study the large lava flow generated prior to the explosive activity in 2007. Location 23 (GR 02°44.90S, 35°53.36E) is accessible point to the flow located in deep gully approximately half way up the slopes of Lengai. In the afternoon we returned to the hummocks on the shoreline, location 24 (GR 02°35.08S, 35°54.49E) for further observations.

Day 9 – Return to hot spring on western shore of Lake Natron for further sampling of the gases from the hot springs, location 24 (GR 02°23.64S, 35°53.86E). Temperature and pH readings similar to those measured previously. A rough calculation of flow rate based on filling time of flasks was ~10 litres/s.

Appendix B: Sample Catalogue

Volcanic Feature	Sample Label	Description	GPS (if known)	Source	Referred to in thesis
Lengai	OLX 1	Xenolith	N. Crater	Abigail Church	X
	OLX 2	Xenolith	"	"	X
	OLX 3	Xenolith	"	"	X
	OLX 4	Xenolith	"	"	X
	OLX 5	Xenolith	"	"	X
	OLX 6	Xenolith	"	"	X
	OLX 7	Xenolith	S. Crater	"	X
	OLX 8	Xenolith	N. Crater	"	
	OLX 9	Xenolith	"	"	
	OLX 10	Xenolith	"	"	
	OLX 11	Xenolith	"	"	
	OLX 12	Xenolith	N.Crater	"	
	OLX 13	Xenolith	02°45.874S, 35°54.957E	Field Campaign	
	OLX 14	Xenolith	"	"	X
	OLX 15	Xenolith	"	"	X
	OLX 16	Xenolith	"	"	X
	OLX 17a	Xenolith	"	"	X
	OLX 17b	Xenolith	"	"	X
	OLX 18	Xenolith	"	"	X
	OLX 19	Xenolith	"	"	X
	OLX 20	Xenolith	"	"	X
	OLC 1	Mica Xenocryst	N.Crater	Abigail Church	
	OLC 2	Mica Xenocryst	02°45.874S, 35°54.957E	Field Campaign	X
	OLC 3	Mica Xenocryst	"	"	X
	OLC 4	Mica Xenocryst	"	"	X
	OLC 5	Amphi Xenocryst	02°42.26S, 35°56.80E	"	
	OLC 6	Spinel Xenocryst	"	"	
	OLA 1	Gully Ash	"	"	X
	OLA 2	Slope Ash	Upper western flank	"	X
	OLA 3	2007 Ash	02°44.896S, 35°53.361E	"	X
	OLA 4	Summit Ash	02°45.874S, 35°54.957E	"	X
	OL 3	Carbonatite block	"	"	X

	OL 5	Altered 2006 lava	02°44.896S, 35°53.361E	“	X
	OL 6	2006 lava	“	“	X
	OL 7	Yellow precipitate	“	“	X
	OL 8	Brown 2006 lava	“	“	X
	OL 9	Stalactite	“	“	X
	OL B06-1	Pyroclastic material	-	J.Keller	X
	OL B06-6a	Pyrocalstic material	-	“	X
	OL B06-6b	Pyroclastic material	-	“	X
	OL S2	2006 lava	-	“	X
	OL 387	Carbonate lapilli	-	“	X
	0801505	-	-	“	X
Deeti	DTC 1	Mica megacryst	02°50.64S, 36°00.94E	Field campaign	X
	DTC 2	Mica megacryst	“	“	
	DTC 3	Mica megacryst	“	“	
	DTC 4	Pyroxene megacryst	“	“	X
	DTC 4b	Mica megacryst	“	“	X
	DTC 6	Mica megacryst	“	“	
	DTC 7	Mica megacryst	“	“	
	DTC 8	Mica megacryst	“	“	
Loolmurwak	LWX 1	Xenolith	02°48.066S, 35°59.034E	“	
	LWX 2	Xenolith	“	“	
	LWC 1	Mica megacryst	“	“	X
	LWC 2	Mica megacryst	“	“	X
	LWC 3	Mica megacryst	“	“	
Loluni	LRC 1	Mica megacryst	02°49.553S, 35°58.515E	“	X
	LRC 2	Mica megacryst	“	“	
Kerimasi	KMS 1	Magnetite sövite	02°49.466S, 35°58.791E	“	
	KMS 2	Lapilli block	“	“	
	KMS 3	Lapilli block	02°48.099S, 35°57.517E	“	
Lake Natron	NTR 1	Trona block	02°23.64S, 35°53.86E	“	X
	NTR 4	Trona from 300m on shore	-	“	X
	NTR 5	Trona from 500m on shore	-	“	X
Debris	HMK 1	Clast	02°41.366S,	“	

Hummock			35°56.517E		
	HMK 2	Clast	02°35.081S, 35°54.492E	“	
	HMK 3	Matrix	“	“	
	HMK 4	Clast	“	“	
	HMK 5	Clast	02°35.074S, 35°54.481E	“	
	HMK 6	Clast	“	“	
Pello Hill	PH 1	Mica megacryst	02°45.993S, 36°01.030E	“	X
	PHX 1	Xenolith	“	“	X
	PHX 2	Xenolith	“	“	X
	PHX 3	Xenolith	“	“	X

Appendix C: A brief report on field gas and optical aerosol thickness measurements at Oldoinyo Lengai and the Gregory Rift Region

Volcanic gases are generated both during volcanic eruptions and passive degassing during quiescent, inter-eruptive phases. A study of 12 volcanoes across the globe, within different tectonic settings indicated that over 95% of the gases released from volcanoes are derivatives of C, O, H and S (Giggenbach, 1975). The generation of these gases conforms to thermodynamic theory which suggests that under the temperature, pressure and oxygen fugacity conditions typical of magmatic environments, the above elements combine to form predominantly H_2O, CO_2 and SO_2. The addition of significant quantities of gas (CO_2, H_2O, SO_x, NO_x, He, HF, HCl) to the atmosphere during both phases of activity can often have negative consequences. A topical debate in the current scientific community is the impact of increasing CO_2 within our atmosphere. As a major greenhouse gas it is surprising that little attention has been paid to direct observations of the volcanic contribution over the long term and also during past volcanic cycles. In addressing this issue it is important to consider all phases of volcanic gas emission; passively degassing volcanoes, short lived eruptions of volcanoes in different tectonic settings and volcanoes which are essentially continuously erupting (Williams et al., 1992).

I. Gas Emissions from Oldoinyo Lengai

Oldoinyo Lengai is an example of a volcanic centre which passively degasses large amounts of carbon dioxide (6000 – 7200 tonnes per day (Brantley and Koepenick, 1995)). Its alkaline nature, along with other centres such as Mt Erebus, Antarctica and Nyiragongo, Democratic Republic of Congo, is thought to result in the production of 1 – 2 orders of magnitude more carbon dioxide than other sub-aerial volcanoes (Koepenick et al., 1996). The measurement of carbon dioxide emission can be completed in two ways; firstly through infrared spectroscopy (airborne) of the gas column or secondly through C/S ratios collected from fumaroles. Koepenick et al (1996) concluded that 75% of carbon dioxide emitted from Oldoinyo Lengai originated from seven vents within the active northern crater, with the remainder coming from lower temperature vents around the crater rim. Other emissions stem from faults near the crater edge and some emissions emanating from the uppermost flanks (recognised from increased soil concentrations). This spatial pattern of degassing is unusual compared to other CO_2 producing volcanoes e.g. Mt Etna, which can have up to 50% of carbon dioxide being

emitted from the flanks of the volcano as a result of migration along faults (Allard and al, 1991, Giammanco and Bonfanti, 2008). The restriction of Lengai's gaseous emissions to an area of roughly 2km in diameter is argued to show that no magma chamber or shallow magma network exists below Oldoinyo Lengai (Koepenick et al., 1996). The diffuse emissions associated with Mt Etna represent degassing of a magma body approximately 15km wide at a depth of 20km (Allard and al, 1991). It is suggested that magma rises intermittently at Oldoinyo Lengai in batches resulting in eruptions / effusive activity as previously discussed in Chapters 1 and 3.

Previous fumarole analysis at Oldoinyo Lengai revealed that gases are predominantly made up of CO_2 with lesser amounts of H_2O, 64 – 74% and 24 – 34% respectively. Other gases emitted include ~1% H_2, 0.1 – 0.4% CO and <0.1% H_2S, HCl, HF and CH_4 (Koepenick et al., 1996). Isotopic analysis of collected samples was carried out, with the two hottest vents generating $\delta^{13}C$ values of -7.37 to -4.46‰. Soil gases were also analysed generating $\delta^{13}C$ signatures of +0.3 to -2.7‰ showing enrichment in carbon-13. Similar enriched $\delta^{13}C$ signatures of -2.36 to -4.01‰ were measured in crater emissions during a new eruptive sequence in 2005 (Fischer et al., 2009). The gases sampled in this study were collected from a body of degassing silicate magma. The same gases were also analysed for $\delta^{15}N$ generating values of -4.0 to -5.1‰. Observations using Fourier transform spectroscopy absorption spectra of the lava lakes, plume and fumaroles concluded that water was the predominant gas, exceeding 60 – 75 mol% (Oppenheimer et al., 2002). However the authors realise that this may not necessarily represent only magmatic water but rather water contained within old, hydrated natrocarbonatitic material, which is subsequently re-melted upon injection of fresh magma batches.

ii. Gas collection in Gregory Rift

The Gregory Rift is degassing not only from the active volcano of Oldoinyo Lengai, but also from other regions within the rift. Identified as hot, bubbling springs around the shores of Lake Natron or as dry vents where local Masaai have heard gas rushing from cracks within rock units, the rift itself is releasing significant quantities of gas from the upwelling magma generating the rifting. Collection of some of this gas was an aim of the field campaign to Tanzania with crude methods being deployed since degassing at Oldoinyo Lengai and within the rift is a more diffuse process than previous sampling campaigns, which targeted active fumaroles within the crater of Lengai (Teague et al., 2008, Fischer et al., 2009).

Sampling of gases being released from the hot springs on the shore of Lake Natron involved the displacement filling of 250ml polypropylene Erlenmeyer flasks. Each flask was submerged in the spring until full with water and then turned upside down over the regions where springs were bubbling.

Figure B1: pH reading being taken at hot spring on the western shore of Lake Natron with ripples caused by escaping gas. *Photo courtesy of Adrian Jones.*

As the gas enters the flask it pushes the water out and after approximately 25 minutes the flask was 80% full of headspace gas. The screw caps were fitted to the flasks whilst still submerged and screwed tightly. Around 20% spring water was left within the flasks to act as a seal preventing gas escape. Once dry, the neck of each bottle was sealed using two-way stretching, self-sealing Nescofilm©. This film provides an almost vacuum seal to the tops of the bottles and is moisture-proof, resistant to air, gases, alcohol and common acids and has a more general use in biological context to prevent contamination of samples. Temperature and pH readings were taken in both pools, with the larger pool temperature at 49.6°C and pH 9.96. The smaller of the pools at location 6 had a temperature of 48.9°C and pH of 10.08. Both springs had numerous sites where gas was bubbling through the sediment and water in convection cells.

iii. Sun Photometer (Microtops) Data Collection

The Microtops II sun photometer borrowed from NERC Field Spectroscopy Facility (FSF) is a multi-band sun photometer, which uses the sun to measure aerosol optical thickness (AOT), and derives the column water vapour content. The Microtops II contains five aligned optical collimators, which collectively have a field of view of 2.5°. The channels cover the optical wavelengths of 440, 675, 870, 936 and 1020nm. The channels' peak wavelength precision is ±1.5 nm. Each has a narrow-band interference filter and photodiode particular to each wavelength. The Microtops II also has a sun target and pointing display attached to the block that is laser aligned to obtain accurate alignment with all the optical channels. During use the sun photometer is pointed directly at the sun until the image of the sun is centred in the bull's eye display and must remain so during each scan. At this point it is known that the channels will be oriented directly at the solar disk. Keeping the Microtops pointed directly towards the sun so that the target is always centred is often difficult due to natural unsteadiness of the operator's hands or due to windy or cold weather, which is common at the summits of volcanoes. To combat this effect the data collection was conducted sitting down whilst leaning against a supporting structure i.e. boulder or another member of the field party to keep the user as still as possible. The equipment also contains an algorithm that uses a series of repeated measurements from three of the channels and only those with the highest signal strength and so best sun positioning are used for further processing.

Figure B: Microtops II sunphotometer with sun target and GPS attachment. *Photograph courtesy of NERC Field Spectroscopy Facility.*

During a scan radiation captured by the collimators and filters are focused onto the photodiodes, which generate an electrical current proportional to the radiant power. Internal processing of the signal amplifies the electrical signals and then converts them into a digital signal using an A/D converter. The assembly contains an internal pressure sensor, which is

required for determination of the Rayleigh scattering. Calculation of the AOT and water vapour is based upon the Bouger-Lambert-Beer law, which states that there is a logarithmic dependence between the transmission of light through a medium and the product of the absorption coefficient of that medium and the path length of the light ($A = a_\lambda \times b \times c$, where A is measured absorbance, a_λ is wavelength-dependent absorptivity coefficient, b is path length and c is concentration).

$$I = I_0 e^{-\alpha\mu\Omega - m\beta P/Po}$$

I = intensity; $\mathbf{I_o}$ = intensity of light of particular wavelength before it passes through atmosphere; **Ω** = amount of ozone; **α** = ozone absorption coefficient at specific wavelength; **μ** = ratio of actual and vertical path lengths; **P** = pressure of atmosphere; **Po** = standard pressure of 1013.25 mB; **m** = optical airmass; **β** = Rayleigh scattering coefficient.

The calculation of AOT relies on the subtraction of the optical depth due to Rayleigh scattering from the total optical depth. The precipitable water column is calculated through measurement of the water absorption peak at 940nm and measurement of either the 870 or 1020nm peak, which show no absorption by water vapour in the atmosphere.

The initial calibration of the sun photometer was carried in the University College London quad prior to the field campaign to Tanzania in order to check the calibration constants. These calibration constants are in place from manufacture and relate the electrical signals to the physical processes (irradiance, aerosol optical thickness, water vapour and pressure) being measured via the analogue / digital converter. Once in the field a set of Langley calibrations were also performed as recommended to maintain the accurate calibration (Schmid and Wehrli, 1995, Slusser et al., 2000). This involves making preliminary measurements at different solar elevation angles or air masses and the plotting of the natural log of the signal output against the relative air mass.

III. Sun photometer results and interpretation

The table below shows the compilation of sun photometer readings taken during the field campaign to Tanzania. It can be seen that a number of areas were investigated and fall into the categories of hot springs on the shores of Lake Natron, the degassing plume at the summit of Oldoinyo Lengai and a dry spring also on the shore of Lake Natron. A number of out of plume,

background readings were also taken from the Moivaro Camp and on the plains between Oldoinyo Lengai and Kerimasi, which provide a true background reading. The most important features of this dataset are represented on the graph below (Figure B3) which illustrates the aerosol optical thickness of the measured airmass in the 440nm wavelength channel over the time period of measurements.

The scans show that the aerosol optical thickness (AOT) at the summit of Lengai is greater than that of the background value for the rift. At its maximum the inferred summit plume has an AOT over an order of magnitude higher than that of the background in the rift. This can also be seen to vary over the time scale of the measurements made with an increase from ~4 to 7 T_{AOT} over a 5 minute period. The weather conditions during this measurement were changeable as the summit of Lengai is often subject to cloud cover during the early hours of the morning and so may result in an increased optical thickness. However comparison of the total water vapour within the measured column between the background values and the summit measurements reveals that the measurements at Lengai were taken under lower water vapour conditions and so this is not the cause of the elevated optical thickness. A background measurement within the rift was also taken during a dust storm to indicate how the optical thickness changes with dust particulate material from the volcanic plain. This is highlighted in Figure B3 and again we can see that although a dust storm significantly elevates the AOT in comparison to the background AOT, the summit degassing plume from Lengai still shows a higher AOT than that observed during the dust storm.

TIME	LAT	LONG	ALT	PRES	SZA	AM	AOT440	AOT675	AOT870	AOT936	AOT1020	T_{AOT} 440	T_{AOT} 675	T_{AOT} 870	T_{AOT} 936	T_{AOT} 1020
8:14:59	-2.394	35.898	599	946	28.94	1.142	0.275	0.161	0.132	0.139	0.147					
8:23:09	-2.394	35.898	605	947	27.65	1.128	0.311	0.186	0.15	0.151	0.152					
8:23:53	-2.394	35.898	603	946	27.54	1.127	0.309	0.179	0.143	0.145	0.146					
8:26:32	-2.394	35.898	607	946	27.15	1.123	0.291	0.161	0.128	0.127	0.127					
8:27:20	-2.394	35.898	609	945	27.03	1.122	0.288	0.172	0.133	0.133	0.133					
9:10:30	-2.394	35.898	608	949	22.41	1.081	0.258	0.135	0.107	0.095	0.083					
9:11:25	-2.394	35.898	606	948	22.36	1.081	0.251	0.141	0.11	0.1	0.09					
9:45:01	-2.413	35.894	613	944	21.96	1.078	1.734	1.805	1.851	1.848	1.846	1.562	1.686	1.752	1.739	1.727
9:46:05	-2.413	35.894	613	944	22	1.078	1.703	1.74	1.812	1.824	1.836	1.531	1.621	1.713	1.715	1.717
9:46:18	-2.413	35.894	612	944	22.01	1.078	1.712	1.758	1.828	1.842	1.856	1.54	1.639	1.729	1.733	1.737
8:37:36	-2.761	35.913	2877	728	26.11	1.113	4.374	4.696	4.932	5.012	5.091	4.202	4.577	4.833	4.903	4.972
8:40:38	-2.761	35.913	2888	728	25.73	1.109	6.973	7.001	7.068	7.045	7.022	6.801	6.882	6.969	6.936	6.903
8:40:58	-2.761	35.913	2888	728	25.69	1.109	7.179	7.235	7.332	7.294	7.256	7.007	7.116	7.233	7.185	7.137
7:11:48	-2.628	35.88	688	938	41.24	1.329	0.169	0.127	0.104	0.114	0.124					
7:12:25	-2.628	35.88	677	938	41.12	1.326	0.175	0.111	0.094	0.104	0.114					
6:25:30	-2.585	35.908	603	948	51.18	1.593	0.189	0.161	0.152	0.162	0.173					

6:26:44	-2.585	35.908	602	948	50.91	1.584	0.181	0.157	0.143	0.153	0.162					
6:34:51	-2.584	35.908	600	946	49.14	1.526	0.197	0.175	0.16	0.168	0.176					
7:08:55	-2.584	35.907	602	946	41.9	1.342	0.158	0.127	0.11	0.116	0.123					
10:45:10	-2.628	35.88	602	935	28.73	1.14	0.219	0.186	0.176	0.183	0.189					
10:09:25	-2.803	35.964	1072	897	24.71	1.1	3.108	3.42	3.629	3.692	3.755	2.936	3.301	3.53	3.583	3.636
10:10:23	-2.803	35.964	1070	897	24.79	1.101	0.377	0.341	0.342	0.35	0.357					
8:03:32	-2.394	35.898	600	946	31.78	1.176	1.679	1.76	1.824	1.82	1.815	1.507	1.641	1.725	1.711	1.696
8:03:52	-2.394	35.898	601	946	31.72	1.175	1.619	1.684	1.758	1.754	1.749	1.447	1.565	1.659	1.645	1.63

Table B1: Data output table from sun photometer for measurement of Aerosol Optical Thickness (AOLT). Lat = Latitude; Long = Longitude; Alt = Altitude; Pres = Pressure; SZA = Solar zenith angle; Am = Optical Airmass; Temp = Temperature of optical block in degrees Celsius; AOT = Aerosol optical thickness from specified channels; Water = total water vapour in the column in cm; T_{AOT} = total aerosol optical thickness ($T_{AOT} = T_{\lambda} - T_{background}$

Yellow = Hot, wet Springs on western shore of Lake Natron; Red = Summit of Oldoinyo Lengai; Blue = Moivaro Camp; Green = Dry spring on southern shore of Lake Natron near hummocks; Orange = Valley between Lengai and Kerimasi;

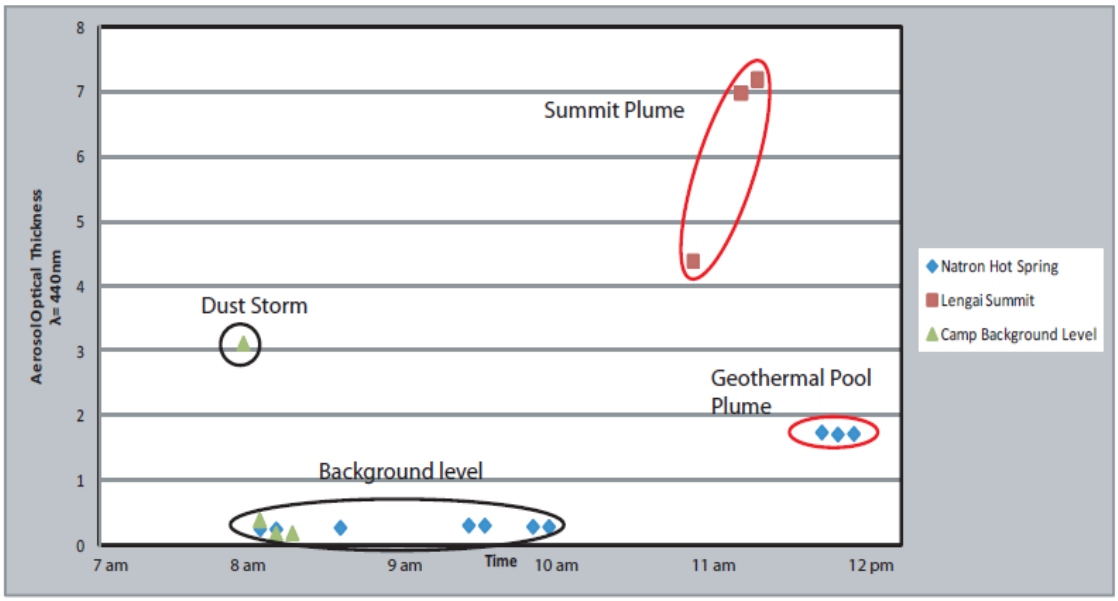

Figure B3: A plot of AOT from the 440nm optical channel vs. time (minutes) of the two main degassing sites. Circled in black are the reference / background measurements taken out of the plume; in red are the measurements taken within the inferred gas plumes.

Figure B3 also shows the probable presence of aerosols within the inferred plumes degassing from the floor of the Gregory rift at the hot springs around Lake Natron. The measurements made at this field location were completed over a two day period (non consecutive) with the first set of measurements conducted over a time period of 90 minutes from two different positions; one near the larger of the two geothermal pools and the other between the two geothermal pools. The second day of measurements was five days later taken over a 30 minute period, from the same position in near the larger of the geothermal pools. The data shows an increase from background levels of around 0.3 to 1.7 between these two days, resulting in a total AOT of between 1.5 and 1.7.

There are three possible interpretations for this result; the first is that there was a general increase in the background AOT level of the rift valley; secondly a difference in the type of cloud cover during the measurements resulting in an increase in AOT or thirdly measurements were conducted within an inferred degassing plume which occurs intermittently either due to natural variations in the degassing of the underlying geothermal system or due to variation in the wind direction. A difference in cloud cover does not seem to provide an explanation for the change in AOT as both days were subject to similar weather conditions, with low level stratocumulus cloud cover and a similar level of atmospheric water vapour ~ 3.2 – 3.5 cm. A variation in the background level of AOT in the rift region may be the cause behind the

increase between measurements and may ultimately be linked to a variation in the degassing regime of the underlying geothermal system. More measurements over a longer period of time would be required to accurately determine the cause of this change in levels.

IV. Problems and Future Considerations for Analysis

A number of obstacles were encountered during the field campaign in terms of achieving the aim to quantify the amount and rate of degassing from Oldoinyo Lengai, post eruption as well as other sites within the Gregory Rift. The first and most important of these is the lack of safe access to fumaroles or places of visible degassing at the summit of Oldoinyo Lengai. As stated earlier previous measurements of the gas flux from Lengai were made from the hornito structures located on the crater floor or around the crater rim. These features no longer exist and sites of degassing are limited to a few open vents on the inaccessible crater floor and fractures along the unstable ash cone.

The implication of this is that direct sampling of the gases being emitted is near impossible with specialist climbing and sampling equipment. Ultimately this results in a long period in time after large explosive eruptions in which the degassing of the volcano is unmeasured and so unknown. It is however this phase in the volcanoes activity which may prove to be important in terms of the source of the degassing, in particular with the onset of natrocarbonatite effusion after the repose period. An important and unanswered question is whether there is a change in the stable isotope signature over the eruptive cycle of volcanoes such as Oldoinyo Lengai. If large explosive eruptions clear the crater as well as the volcanic conduit, it is plausible that the isotopic signature may reflect that of a primary, mantle-derived degassing magma body, potentially that of the new batch of natrocarbonatite or parental melt from which the natrocarbonatite segregates. If a change does occur it would also imply that previous isotopic measurements reflect generation via reworking of the carbonatite material which resides under the hornito structures.

Gas samples were successfully collected from the springs near the shores of Lake Natron however upon return to the UK it became clear that the samples required analysis as soon as possible to prevent degradation and exchange with air, but due to a lack of appropriate equipment this was not possible. Gas samples, as stated above, were collected in polypropylene Erlenmeyer flasks but were not collected under vacuum conditions and so the gas is non-pressurised within the flasks. This causes problems removing the head space gas for

analysis as bottles would need to be drilled and then gas extracted using a syringe before any can be lost to the surroundings. This process is normally not required if caps for the flasks contain a one way septa through which a syringe needle can pass without allowing any gas loss. The flasks used unfortunately do not have a standard one way septa cap in manufacture and so this was not possible.

Appendix D: Data Tables

D1 -Electron Micropobe EDS: Sample OLX 10

Phase	F	Na	Mg	Al	Si	K	Ca	Ti	Cr	Mn	Fe	Total	
Small Mica													
	0.000	0.863	18.208	15.257	38.062	10.180	0.053	4.274	0.464	0.280	11.166	98.809	
Large Mica													
	0.000	0.946	18.585	14.450	35.107	9.540	0.061	4.286	0.419	0.005	6.917	90.316	
	0.000	0.775	17.212	16.107	33.299	9.345	0.027	4.373	0.584	0.010	6.532	88.265	
	0.000	0.972	15.426	14.462	31.054	9.051	-0.057	3.873	0.318	0.104	6.142	81.345	
	0.000	0.878	18.260	14.689	36.174	9.590	-0.005	4.257	0.571	0.025	6.614	91.056	
	0.000	0.731	20.877	16.185	38.503	10.163	0.090	4.223	0.732	-0.042	6.974	98.436	
	0.000	0.895	20.915	16.120	39.579	10.472	-0.039	3.891	0.649	0.163	8.694	101.339	
				15.324				4.151	0.546		6.979		
Mica Megacryst	**F**	**Na**	**Mg**	**Al**	**Si**	**K**	**Ca**	**Ti**	**Cr**	**Mn**	**Fe**	**Ni**	**Total**
	0.000	0.794	16.668	12.222	36.540	9.707	-0.024	2.448	-0.189	0.294	14.692	-0.181	92.971
	0.000	0.700	19.234	15.040	36.770	9.835	0.134	4.050	0.604	0.122	6.598	-0.152	92.937
	0.000	0.916	16.927	17.554	32.147	9.093	-0.065	3.996	0.250	0.111	6.120	0.238	87.287
	0.000	1.079	19.838	14.413	36.973	9.764	-0.078	4.248	0.737	0.014	6.749	0.122	93.859
	0.000	0.760	19.010	14.941	36.747	9.715	0.039	3.704	0.621	-0.156	6.420	-0.135	91.664
	0.000	0.922	20.728	15.619	38.520	10.153	0.127	3.975	0.698	0.021	6.710	0.541	98.015
	0.000	0.675	18.730	14.377	35.098	9.815	-0.136	4.367	0.528	0.343	6.309	0.166	90.273
	0.000	0.806	18.967	14.235	35.554	9.952	-0.076	4.028	0.701	-0.124	7.081	0.198	91.321
	0.000	0.995	18.963	14.657	35.702	10.331	0.135	4.099	0.568	-0.097	6.647	0.419	92.420
	0.000	0.670	17.179	14.200	36.484	10.208	-0.046	4.169	0.312	0.269	9.175	0.115	92.735
	0.000	0.521	17.761	13.218	34.457	9.535	-0.044	4.170	0.669	0.110	6.863	0.281	87.542

	0.000	0.667	20.383	14.677	38.079	10.238	-0.117	4.057	0.784	0.103	6.804	-0.041	95.632
	0.000	0.923	18.517	15.877	35.768	9.352	-0.010	4.308	0.664	0.147	6.645	0.256	92.447
	0.000	0.741	21.181	16.499	39.093	10.050	-0.253	4.192	0.618	-0.014	6.488	0.344	98.939
	0.000	0.749	18.160	16.369	35.056	9.598	0.139	4.250	0.434	-0.031	6.897	-0.004	91.616
	0.000	0.801	21.256	15.258	38.655	9.753	-0.086	4.174	0.706	-0.070	6.562	0.033	97.043
	0.000	0.772	19.988	14.975	37.463	9.928	0.047	3.694	0.550	0.074	6.559	0.356	94.406
	0.000	0.808	20.099	15.683	37.005	10.239	0.048	3.960	0.538	0.225	6.549	-0.215	94.939
	0.000	0.748	19.977	15.423	38.341	9.934	-0.133	3.917	0.618	-0.027	7.768	0.272	96.838
	0.000	0.670	18.813	14.743	35.792	9.849	0.083	3.957	0.430	0.160	7.661	0.123	92.280
	0.000	1.435	9.408	1.550	42.261	0.059	18.805	0.499	0.083	0.139	8.662	-0.118	82.782
	0.000	0.626	12.843	12.605	28.945	7.773	-0.009	2.875	0.449	0.164	10.251	0.567	77.091
	0.000	0.763	14.578	15.468	32.513	8.465	0.099	3.189	0.000	0.225	11.457	0.214	86.971
	0.000	0.683	16.254	14.040	35.797	9.682	-0.023	4.288	0.344	0.501	14.337	0.136	96.038
	0.000	0.701	16.235	14.717	35.374	9.288	0.048	2.670	0.150	0.426	13.112	-0.054	92.668
	0.000	0.826	16.293	12.279	36.970	9.814	-0.051	2.169	-0.056	0.429	13.925	-0.044	92.553
	0.000	1.295	15.258	1.062	56.316	0.223	24.591	0.627	0.011	0.160	5.907	0.203	105.652
	0.000	1.184	15.408	0.825	56.611	0.134	24.483	0.576	0.202	0.148	7.110	0.020	106.700
	0.000	12.016	0.141	23.973	31.089	4.929	0.149	-0.010	-0.116	0.048	1.549	-0.003	73.764
	0.000	11.528	0.126	24.223	29.503	5.457	0.130	0.068	0.092	-0.063	1.310	-0.280	72.094
	0.000	16.060	0.211	37.704	42.067	6.925	0.121	0.257	0.044	-0.042	0.871	0.219	104.436
	0.000	15.045	0.126	34.236	41.416	7.135	0.056	0.110	-0.125	0.032	1.539	-0.067	99.502
	0.000	0.344	1.381	1.684	0.169	0.001	0.081	8.632	0.475	1.267	83.954	0.247	98.235
	0.000	0.325	1.398	0.751	0.294	-0.015	-0.066	8.879	0.257	1.186	85.439	0.178	98.624
	0.000	0.834	16.844	14.374	37.107	9.527	-0.028	3.332	0.003	0.458	14.381	0.048	96.880
	0.000	0.808	16.646	14.237	36.495	9.108	0.042	3.080	0.158	0.563	14.146	-0.095	95.188
	0.000	12.664	0.240	29.212	36.777	6.757	0.221	-0.023	-0.192	0.052	1.735	0.375	87.818
	0.000	16.626	0.122	34.876	42.235	6.978	0.239	-0.133	0.083	0.055	1.320	-0.142	102.260
olivine clast	F	Na	Mg	Al	Si	K	Ca	Ti	Cr	Mn	Fe	Ni	Total
	0.000	0.000	40.546	4.449	37.607	0.199	0.295	0.280	-0.127	0.274	15.613	-0.100	99.406

0.000	0.000	42.711	2.871	38.990	-0.040	0.278	0.041	-0.072	0.155	16.459	0.034	101.723
0.000	0.000	46.448	0.843	42.631	0.122	0.242	-0.059	-0.001	0.333	16.182	-0.203	106.897
0.000	0.000	46.021	0.726	42.859	0.052	0.309	-0.036	0.053	0.199	16.433	-0.057	106.874

D2 - Electron Microprobe WDS: Sample OLX 10

Olivine

F	Cl	Na2O	K2O	Al2O3	CaO	SiO2	FeO	MgO	TiO2	Cr2O3	MnO	SrO	P2O5	Total
0.031	0.017	0.049	0.051	0.897	0.243	37.423	14.928	40.992	0.024	0.022	0.232	0	0	94.892
0.015	0.006	0	0.007	0.567	0.216	38.557	15.352	40.773	0.003	0.003	0.241	0	0.003	95.736
0	0.006	0.022	0.017	0.266	0.218	33.358	15.261	34.511	0.022	0	0.245	0	0	83.925
0	0.028	0.065	0.067	0.176	0.247	41.107	15.261	45.477	0.014	0.009	0.236	0	0	102.681

Mica

F	Cl	Na2O	K2O	Al2O3	CaO	SiO2	FeO	MgO	TiO2	Cr2O3	MnO	SrO	P2O5	Total
0.419	0.041	0.695	9.111	14.724	0.01	35.83	6.397	18.362	2.522	0.523	0.025	0	0.011	88.485
0.504	0.041	0.726	8.812	15.71	0.043	34.817	6.113	18.101	2.688	0.545	0.033	0	0.013	87.925
0.639	0.031	0.695	8.931	15.005	0.014	34.896	6.141	18.761	2.437	0.535	0.033	0	0.014	87.856
0.544	0.052	0.747	8.865	14.771	0.025	35.801	6.104	18.65	2.336	0.561	0.046	0	0	88.261
0.493	0.041	0.76	8.966	14.671	0.043	36.166	6.166	18.201	2.466	0.523	0.044	0	0.014	88.337
0.591	0.033	0.571	8.931	14.139	0.034	35.57	6.161	17.863	2.416	0.518	0.022	0	0	86.593
0.784	0.033	0.562	9.049	16.178	0.017	34.143	5.902	18.094	2.344	0.517	0.035	0	0.01	87.331
0.867	0.045	0.602	9.059	14.763	0.01	35.904	6.17	18.896	2.273	0.522	0.029	0	0	88.765
0.719	0.066	0.669	8.801	14.921	0.025	35.075	6.452	17.677	2.247	0.516	0.068	0	0.015	86.933
0.812	0.027	0.524	9.485	14.526	0	35.503	6.441	18.628	2.406	0.543	0.06	0	0	88.607
0.929	0.029	0.565	9.412	15.875	0.007	37.162	6.413	19.2	2.395	0.552	0.074	0	0	92.215

D3 - Flash EA Total Organic Carbon (TOC) Analysis: Lava and Ash Samples

Sample Name		Sample Weight			Nitrogen %	Carbon %	Carbonate Content
Standard1	STD	10.458	6.3	1	0.510999978	4.59100008	
Standard2	STD	19.833	6.3	1	0.510999978	4.59100008	
Standard3	STD	30.092	6.3	1	0.510999978	4.59100008	
MGD1	UNK	9.947	6.3	1	0	0.242160976	2.139088621
NTR1	UNK	10.034	6.3	1	0	10.90632725	96.33922402
NTR5	UNK	9.837	6.3	1	0.161874369	4.812688828	42.51208464
NTR4	UNK	10.107	6.3	1	0	5.96971035	52.73244143
OL5	UNK	10.211	6.3	1	0	11.36818981	100.41901
OLA1	UNK	10.458	6.3	1	0	4.123461723	36.42391189
Standard4	UNK	14.051	6.3	1	0.506949186	4.775036335	
Standard5	UNK	19.684	6.3	1	0.504570246	4.743005276	
OLA3	UNK	9.868	6.3	1	0	6.319192886	55.81953716
OL8	UNK	10.104	6.3	1	0	7.823007107	69.10322944
OL3	UNK	10.099	6.3	1	0	8.584431648	75.82914623
OLA2	UNK	10.046	6.3	1	0	1.689630389	14.92506844
OLA 4	UNK	9.768	6.3	1	0	1.49857378	13.23740172
Standard6	UNK	15.875	6.3	1	0.538866997	4.692002773	
Standard7	UNK	21.235	6.3	1	0.534059346	4.622047424	
					SDEV carbon STD	*0.06674078*	

Sample Name		Sample Weight			Nitrogen %	Carbon %	% Carbonate
Standard1	STD	10.294	6.3	1	0.510999978	4.59100008	
Standard2	STD	20.137	6.3	1	0.510999978	4.59100008	
Standard3	STD	30.004	6.3	1	0.510999978	4.59100008	
MGD1	UNK	51.213	6.3	1	0	0.271036357	2.394154484
MGD1	UNK	95.406	6.3	1	0.011834	0.290868908	2.569342022
NTR5	UNK	11.551	6.3	1	0.192490757	5.478847027	48.39648207
NTR5	UNK	10.289	6.3	1	0.169977441	5.10652256	45.10761595
OLA2	UNK	21.099	6.3	1	0	1.802632689	15.92325542
OLA2	UNK	29.321	6.3	1	0	1.655413985	14.62282354
Standard4	UNK	17.53	6.3	1	0.510824919	4.667862892	
Standard5	UNK	26.739	6.3	1	0.509461462	4.619635105	
OLA4	UNK	20.244	6.3	1	0	0.855495811	7.556879659
OLA4	UNK	29.144	6.3	1	0	0.96100086	8.488840928
OL7	UNK	10.19	6.3	1	0.240445867	7.961428165	70.32594879
OL7	UNK	21.153	6.3	1	0.224878713	7.832751751	69.18930713
OL9	UNK	11.183	6.3	1	0	7.220984459	63.78536272
OL9	UNK	24.012	6.3	1	0	5.494285583	48.53285599
Standard6	UNK	15.375	6.3	1	0.590218186	5.000579834	
Standard7	UNK	28.122	6.3	1	0.521719277	4.558966637	

D4 - Stable Isotope Analysis: Keller Samples (fresh) and Lava / ash samples (secondary)

	d13C	d18O	d18OSMOW
OL B06-1	-7.0	-22.8	+7.46
OL B06-6a	-7.5	-22.2	+8.01
OL B06-6b	-7.5	-22.2	+8.05
OL S2	-7.8	-20.9	+9.42
OL 387 (2006)	-7.0	-23.7	+6.46
0801505 (837)	-8.2	-22.9	+7.27

Sample Name	d13C	d18O (SMOW)
Magadi Ash	*0.58*	*29.29858248*
Summit Ash	-3.62	23.75432114
Slope Ash	-5.58	24.30976048
Gully Ash	-3.28	22.35869936
300m trona	-1.94	26.78467814
500m trona	-2.46	29.16735538
Natro Block	-5.41	11.01902953
Stalactite	-8.00	16.1087262
Yellow Stuff	-7.52	21.79166506
2007 Ash	-3.95	23.83699134
Trona spring	3.91	33.67178319
older lava	-5.5545667	12.3898225
brown lava	-5.798773	18.39417838

D5 - Radioisotope - Mica material, Keller Samples and Fenites

Sample	Subsample	Sr ppm	±2SE	87Sr/86Sr_tr	±2SE	84Sr/86Sr	±2SE	85Rb/86Sr	±2SE	TotalSr	TotalSr_2se
Loluni-1	mica	1022.52	0.10	0.704277	0.000005	0.089084	0.000034	0.000009	0.000002	10.4	0.1
Olx 10a	mica	374.45	0.03	0.703732	0.000006	0.133218	0.000083	0.000002	0.000002	10.6	0.1
OLL1	mica										
OLC2	mica	534.26	0.05	0.704361	0.000009	0.122700	0.000017	0.000017	0.000005	5.0	0.1
OLC6	mica										
DT1	mica	287.11	0.01	0.703504	0.000005	0.193524	0.000071	0.000001	0.000002	12.4	0.1
OLC3	mica	28.02	0.00	0.703563	0.000011	1.864044	0.003269	-0.000006	0.000005	9.2	0.7
LWC1	mica	152.11	0.01	0.703675	0.000022	1.635090	0.000703	0.000002	0.000009	2.9	0.3
LWC2	mica	213.33	0.00	0.703515	0.000008	0.657449	0.000236	0.000002	0.000003	8.0	0.2
DTC4b	mica	80.54	0.01	0.711661	0.000021	0.545802	0.000600	0.000012	0.000008	3.6	0.1
OLC1	mica	276.10	0.01	0.703898	0.000007	0.481596	0.000152	0.000005	0.000003	11.0	0.2
Olx 10	mica	412.22	0.02	0.703875	0.000007	0.193442	0.000062	0.000001	0.000002	7.7	0.1
Olx 10	mica	412.18	0.03	0.703864	0.000012	0.193578	0.000072	0.000009	0.000007	3.0	0.1
DTC4	px	1153.95	0.16	0.703485	0.000006	0.083081	0.000019	-0.000005	0.000002	10.5	0.1
0801505	Leachate	3661.71	1.29	0.704405	0.000006	0.063477	0.000005	-0.000001	0.000003	10.1	0.2
0801505	Leachate	3044.55	4.27	0.704416	0.000005	0.057099	0.000015	0.000020	0.000003	9.6	0.2
0801505	Residue	1528.99	1.01	0.704377	0.000005	0.059503	0.000021	0.000006	0.000003	10.7	0.9
OL B06-6a	Leachate	10846.19	6.66	0.704484	0.000006	0.060661	0.000013	0.000002	0.000003	10.3	0.2
OL B06-6a	Leachate	7934.72	85.65	0.704387	0.000016	0.057476	0.000122	0.000070	0.000022	23.3	2.4
OL B06-6a	Residue	6695.60	52.30	0.704481	0.000007	0.055525	0.000052	-0.000004	0.000004	9.3	0.6

OL B06-6b	Leachate	8019.85	6.37	0.704507	0.000007	0.059109	0.000016	-0.000003	0.000002	11.7	0.1
OL S2	Leachate	8962.15	2.06	0.704466	0.000005	0.068463	0.000007	-0.000003	0.000002	11.2	0.2
OL S2	Leachate	7454.99	26.13	0.704487	0.000007	0.055717	0.000008	-0.000003	0.000004	7.1	0.2
OL S2	Residue	4386.91	21.04	0.704403	0.000010	0.057363	0.000127	0.000000	0.000003	9.5	1.5
OL 387	Leachate	8199.43	0.48	0.704437	0.000005	0.116476	0.000016	-0.000005	0.000002	13.0	0.2
OL 387	Leachate	356.58	0.08	0.704455	0.000005	0.067549	0.000020	-0.000006	0.000002	10.1	0.2
OL 387	Residue	12527.06	83.97	0.704475	0.000010	0.055454	0.000043	0.000010	0.000003	7.7	0.6
OL B06-1	Leachate	9583.92	3.07	0.704455	0.000005	0.064834	0.000008	-0.000001	0.000002	11.1	0.4
OL B06-1	Leachate	8706.48	44.08	0.704468	0.000007	0.055710	0.000036	0.001226	0.000080	11.2	0.9
OL B06-1	Residue	3128.90	4.20	0.704513	0.000005	0.056805	0.000014	0.000000	0.000002	11.6	1.1
OLx17a	Leachate	1495.71	0.15	0.704441	0.000005	0.092246	0.000017	0.000007	0.000002	10.2	0.1
OLx17b	Leachate	704.61	0.03	0.706332	0.000006	0.147695	0.000024	-0.000003	0.000002	10.1	0.1
OLx15	Leachate	906.46	0.09	0.704413	0.000006	0.091545	0.000013	0.000000	0.000002	12.9	0.1

Sample	**Subsample**	**Sm ppm**	**±2SE**	**Nd ppm**	**ppm_2se**	**143Nd/144Nd**	**±2SE**	**150Nd/144Nd**	**±2SE**	**147Sm/144Nd**	**±2SE**
OL B06-1	Leachate	0.61	0.00	5.85	0.00	0.512615	0.000006	0.820560	0.000182	-0.000001	0.000001
OL S2	Leachate	0.16	0.00	1.92	0.00	0.512612	0.000023	2.309255	0.000560	-0.000003	0.000005
0801505	Leachate	2.81	0.00	29.12	0.00	0.512650	0.000007	0.357053	0.000070	-0.000001	0.000001
OL B06-6a	Leachate	0.19	0.00	2.51	0.00	0.512601	0.000008	1.639791	0.000691	-0.000002	0.000002

D6 - Fluid Inclusion: Microthermometry

OLX 17b

	Tm	Th
	-57.5	
	-57.5	
	-57.6	
	-57.4	
Assemblage 1	-57.2	
	-57.2	
	-57.3	
	-57.6	
	-57.4	
	-57.4	
	-57.2	
	-57.2	
	-57.3	
	-57.3	
	-57.3	
	-57.3	
	-57.1	
	-57.1	
Assemblage 2	-57.1	
	-57.1	
	-57.1	
	-57.1	
	-57.1	
	-57.1	
	-57	
	-57.2	
	-57.2	
	-57.1	
	-57.1	
	-57.3	
Assemblage 3	-57.3	-28.8
	-57.7	
	-57.7	
	-57.5	
Assemblage 4	-57.4	
Assemblage 5	-57.6	
	-57.6	
	-57.5	
	Tm	**Th**
	-57.4	
	-57.4	
	-57.4	
	-57.4	
Assemblage 4	-57.3	
	-57.4	
	-57.4	
	-57.4	
	-57.4	
	-57.4	
	-57.4	
	-56.9	
	-56.9	
	-57	5.8
Assemblage 5	-57	5.8
	-57	5.8

OLX 3

	Tm	Th
		-32.6
		-23.1
Assemblage 1		-36.8
		-35.1
		-30.6
		-30.7
	-57.5	-37.7
		-30.4

		-33.8
	-57.6	
	-57.7	
Assemblage 2	-54.5	
	-54.5	
	-54.5	
Assemblage 3	-56.9	
	-56.9	
Assemblage 5	-56.7	
	-56.9	-20.4
	-56.9	3
	-57	-20.4
		-34.1
	-56.7	-34.3
	-57.1	
	-57.1	
	-57.1	

		-57.2
Assemblage 1		19.7
Assemblage 2	-57.1	32.1
	-57.1	32.1
	-57.1	32.1
	-57.1	32.1
Assemblage 3	-57.1	
	-57.1	
	-57.1	
	-57.1	
	-57.1	
	-57.1	
	-57.1	
	-57.1	
	-57.1	

Assemblage 4	-57	31.3
Assemblage 5	-56.9	
Assemblage 6	-57	30.9

OLX 6	**Tm**	**Th**
	-57.2	
	-57.3	
	-57.4	8.1
Assemblage 1	-57.1	13
		4.4
	57.3	4.2
Assemblage 2	-57.7	4.2
	-57.2	
	-56.8	
	-56.8	
Assemblage 3	-56.8	-11.3
	-56.8	-11.3
	-56.8	
	-56.8	
	-57.9	
	-56.8	
	-56.8	

ACHTERBERGH, E. S., GRIFFIN, W. L., S.Y;, O. R., RYAN, C. G., PEARSON, N. J., KIVI, K. & DOYLE, B. J. (2003) Melt inclusions from the deep slave lithosphere: Constraints on the origin and evolution of mantle-derived carbonatite and kimberlite. *8th International Kimberlite Conference.* Victoria, Canada.

ADAMS, G. E. & BISHOP, F. C. (1982) Experimental investigation of CaMg exchange between olivine, orthopyroxene, and clinopyroxene: potential for geobarometry. *Earth and Planetary Science Letters,* 57, 241-250.

ADORNI, F. & TATEO, F. (2007) A new Melanophlogite Occurrence from The Case Montanini Quarry, Parma, Northern Appennines, Italy. . *Axis,* 3, 1 - 12.

AGI (1997) Fenite. *Dictionary of Mining, Mineral, and Related Terms.* Virginia, Springer.

ALLARD, P. & AL, E. (1991) Eruptive and diffuse emissions of CO_2 from Mount Etna. *Nature,* 351, 387 - 391.

AMUNDSEN, H. E. F. (1987) Evidence of liquid immiscibility in the upper mantle. *Nature,* 327, 692 - 695.

ANDERSEN, T. (1988) Origin and significance of fluid inclusions in matrix minerals in carbonatites, a case study from the Fen carbonatite complex, Norway. *Fluid inclusions*, 25-36.

ANDERSEN, T. & NEUMANN, E.-R. (2001) Fluid inclusions in mantle xenoliths. *Lithos,* 55, 301-320.

ANDERSEN, T., O'REILLY, S. Y. & GRIFFIN, W. L. (1984) The trapped fluid phase in upper mantle xenoliths from Victoria, Australia: implications for mantle metasomatism. *Contributions to Mineralogy and Petrology,* 88, 72-85.

AOKI, K.-I. (1975) Origin of phlogopite and potassic richterite bearing peridotite xenoliths from South Africa. *Contributions to Mineralogy and Petrology,* 53, 145-156.

ARAI, S., TAKADA, S., MICHIBAYASHI, K. & KIDA, M. (2004) Petrology of Peridotite Xenoliths from Iraya Volcano, Philippines, and its Implication for Dynamic Mantle-Wedge Processes. *J. Petrology,* 45, 369-389.

ARCULUS, R. J. (1975) Melting behaviour of two basanites in the range 10 to 35 kbar and the effect of TiO_2 on the olivine-diopside reactions at high pressures. *Carnegie Inst. Washington Yearb,* 74, 512 - 515.

ARNDT, N. T., GUITREAU, M., BOULLIER, A.-M., LE ROEX, A., TOMMASI, A., CORDIER, P. & SOBOLEV, A. (2010) Olivine, and the Origin of Kimberlite. *Journal of Petrology,* 51, 573-602.

AULBACH, S. & RUDNICK, R. L. (2009) Origins of non-equilibrium lithium isotopic fractionation in xenolithic peridotite minerals: Examples from Tanzania. *Chemical Geology,* 258, 17-27.

AZBEJ, T. (2006) The Role of Fluids in Geological Processes. *Earth Science.* Blacksburg, Virginia Polytechnic Institute and State University

BAER, G., HAMIEL, Y., SHAMIR, G. & NOF, R. (2008) Evolution of a magma-driven earthquake swarm and triggering of the nearby Oldoinyo Lengai eruption, as resolved by InSAR, ground observations and elastic modeling, East African Rift, 2007. *Earth and Planetary Science Letters,* 272, 339-352.

BAGDASARYAN, G. P., GERASIMOVSKIY, V. I., POLYAKOV, A. I., GUKASYAN, R. K. & VERNADSKIY, V. I. (1973) Age of volcanic rocks in the rift zones of East Africa. *Geochemistry International,* 10, 66 - 71.

BAILEY, D. K. & KEARNS, S. (2012) New forms of abundant carbonatite-silicate volcanism: recognition criteria and further target locations. *Mineralogical Magazine,* 76, 271-284.

BAKER, B. H., MOHR, P. A. & WILLIAMS, L. A. J. (1972) Geology of the eastern rift system of Africa. *Geol Soc Am Spec Pap,* 136, 1 - 67.

BAKER, M. B. & WYLLIE, P. J. (1992) High-pressure apatite solubility in carbonate-rich liquids: Implications for mantle metasomatism. *Geochimica et Cosmochimica Acta,* 56, 3409-3422.

BAKKER, R. J. & JANSEN, J. B. H. (1990) Preferential water leakage from fluid inclusions by means of mobile dislocations. *Nature,* 345, 58-60.

BEARD, A., HOWARD, K. & JONES, A. (2009) Melanophlogite: A new occurrence from a recent eruption of Oldoinyo Lengai, Tanzania. *Volcanic and Magmatic Studies Group.* Bournemouth.

BEARD, A. D., HOWARD, K., CARMODY, L. & JONES, A. P. (In Prep) The origin of melanophlogite, a clathrate mineral, in natrocarbonatite lava at Oldoinyo Lengai.

BELL, K. (1989) *Carbonatites: Genesis and Evolution,* London, Unwin Hyman.

BELL, K. (1994) Carbonatites and mantle evolution: a review. *Goldschmidt.* Edinburgh.

BELL, K. & BLENKINSOP, J. (1987a) Archean depleted mantle: Evidence from Nd and Sr initial isotopic ratios of carbonatites. *Geochimica et Cosmochimica Acta,* 51, 291-298.

BELL, K. & BLENKINSOP, J. (1987b) Nd and Sr isotopic compositions of East African carbonatites: Implications for mantle heterogeneity. *Geology,* 15, 99-102.

BELL, K. & DAWSON, J. B. (1995) Nd and Sr Isotope Systematics of the Active Carbonatite Volcano, Oldoinyo Lengai. IN BELL, K. & KELLER, J. (Eds.) *Carbonatite Volcanism: Oldoinyo Lengai and the Petrogenesis of Natrocarbonatites.* Berlin, Spinger - Verlag.

BELL, K. & PETERSON, T. (1991) Nd and Sr isotope systematics of Shombole volcano, East Africa, and the links between nephelinites, phonolites, and carbonatites. *Geology,* 19, 582-585.

BELL, K. & SIMONETTI, A. (1996) Carbonatite Magmatism and Plume Activity: Implications from the Nd, Pb and Sr Isotope Systematics of Oldoinyo Lengai. *J. Petrology,* 37, 1321-1339.

BELL, K. & TILTON, G. R. (2001) Nd, Pb and Sr Isotopic Compositions of East African Carbonatites: Evidence for Mantle Mixing and Plume Inhomogeneity. *Journal of Petrology,* 42, 1927 - 1945.

BERG, G. W. (1986) Evidence for carbonate in the mantle. *Nature,* 324, 50 - 51.

BIELLMANN, C., GILLET, P., GUYOT, F. O., PEYRONNEAU, J. & REYNARD, B. (1993) Experimental evidence for carbonate stability in the Earth's lower mantle. *Earth and Planetary Science Letters,* 118, 31-41.

BIZIMIS, M., SALTERS, V. J. M. & DAWSON, J. B. (2003) The brevity of carbonatite sources in the mantle: evidence from Hf isotopes. *Contrib. Mineral. Petrol,* 145, 281 - 300.

BLUNDY, J. & DALTON, J. (2000) Experimental comparison of trace element partitioning between clinopyroxene and melt in carbonate and silicate systems, and implications for mantle metasomatism. *Contributions to Mineralogy and Petrology,* 139, 356-371.

BODINIER, J. L., VASSEUR, G., VERNIERES, J., DUPUY, C. & FABRIES, J. (1990) Mechanisms of Mantle Metasomatism: Geochemical Evidence from the Lherz Orogenic Peridotite. *Journal of Petrology,* 31, 597-628.

BODNAR, R. J. (2003) Introduction to fluid inclusions. IN SAMSON, I., ANDERSON, A. & MARSHALL, D. (Eds.) *Fluid Inclusions: Analysis and Interpretation.* Mineralogical Society of Canada, Short Course.

BOTTINGA, Y. (1968) Calculation of fractionation factors for carbon and oxygen isotopic exchange in the system calcite-carbon dioxide-water. *The Journal of Physical Chemistry,* 72, 800-808.

BOURGUE, E. & RICHET, P. (2001) The effects of dissolved CO2 on the density and viscosity of silicate melts: a preliminary study. *Earth and Planetary Science Letters,* 193, 57-68.

BOWDEN, P. (1985) The geochemistry and mineralization of alkaline ring complexes in Africa (a review). *Journal of African Earth Sciences (1983),* 3, 17-39.

BRANTLEY, S. L. & KOEPENICK, K. W. (1995) Measured Carbon-Dioxide Emissions from Oldoinyo-Lengai and the Skewed Distribution of Passive Volcanic Fluxes. *Geology,* 23, 933-936.

BRENAN, J. M. & WATSON, E. B. (1991) Partitioning of trace elements between carbonate melt and clinopyroxene and olivine at mantle P-T conditions. *Geochimica et Cosmochimica Acta,* 55, 2203-2214.

BRENKER, F. E. & AL, E. (2006) CO_2 - recycling to the deep convecting mantle. *Goldschmidt*

BRENKER, F. E. & AL, E. (2007) Carbonates from the lower part of the transition zone or even the lower mantle. *Earth and Planetary Science Letters,* 260, 1 - 9.

BRETT, R. C., RUSSELL, J. K. & MOSS, S. (2009) Origin of olivine in kimberlite: Phenocryst or impostor? *Lithos,* 112, Supplement 1, 201-212.

BROOKER, R. A. & HAMILTON, D. L. (1990) Three-liquid immiscibility and the origin of carbonatites. *Nature,* 346, 459 - 462.

BROOKER, R. A. & KJARSGAARD, B. A. (2010) Silicate–Carbonate Liquid Immiscibility and Phase Relations in the System SiO2–Na2O–Al2O3–CaO–CO2 at 0·1–2·5 GPa with Applications to Carbonatite Genesis *Journal of Petrology*.

BROWN, R. J. (2011) The Holocene eruptions of the Igwisi Hills Volcanoes, Tanzania. *IUGG General Assembly.* Melbourne, Australia.

BROWN, R. J., BRANNEY, M. J., MAHER, C. & DAVILA-HARRIS, P. (2010) Origin of accretionary lapilli within ground-hugging density currents: Evidence from pyroclastic couplets on Tenerife. *Geological Society of America Bulletin,* 122, 305-320.

BÜHN, B. & RANKIN, A. H. (1999) Composition of natural, volatile-rich Na-Ca-REE-Sr carbonatitic fluids trapped in fluid inclusions. *Geochimica et Cosmochimica Acta,* 63, 3781-3797.

BUHN, B., RANKIN, A. H., RADTKE, M., HALLER, M. & KNOÌˆCHEL, A. (1999) Burbankite, a (Sr,REE,Na,Ca)-carbonate in fluid inclusions from carbonatite-derived fluids: Identification and characterization using Laser Raman spectroscopy, SEM-EDX, and synchrotron micro-XRF analysis. *American Mineralogist,* 84, 1117-1125.

BÜHN, B., RANKIN, A. H., SCHNEIDER, J. & DULSKI, P. (2002) The nature of orthomagmatic, carbonatitic fluids precipitating REE,Sr-rich fluorite: fluid-inclusion evidence from the Okorusu fluorite deposit, Namibia. *Chemical Geology,* 186, 75-98.

BÜHN, B., SCHNEIDER, J., DULSKI, P. & RANKIN, A. H. (2003) Fluid-rock interaction during progressive migration of carbonatitic fluids, derived from small-scale trace element and Sr, Pb isotope distribution in hydrothermal fluorite. *Geochimica et Cosmochimica Acta,* 67, 4577-4595.

BURKE, E. A. J. (2001) Raman microspectrometry of fluid inclusions. *Lithos,* 55, 139-158.

CARMODY, L., JONES, A., ROBINSON, S., KELLER, J., LENG, M. & STOPPA, F. (2009) Precursory study into variation in Oxygen and Carbon in the Oldoinyo Lengai volcanic system. *General Assembly of European Geophysics Union.* Vienna, Austria.

CARTIGNY, P., HARRIS, J. W. & JAVOY, M. (1998) Eclogitic Diamond Formation at Jwaneng: No Room for a Recycled Component. *Science,* 280, 1421 - 1424.

CHRISTENSEN, N. I. & MOONEY, W. D. (1995) Seismic velocity structure and composition of the continental crust: A global view. *J. Geophys. Res.,* 100, 9761-9788.

CHRISTOPHE, P. (2006) On the role of heat flow, lithosphere thickness and lithosphere density on gravitational potential stresses. *Tectonophysics,* 425, 83-99.

CHURCH, A. A. (1995) The petrology of the Kerimasi carbonatite volcano and the carbonatites of Oldoinyo Lengai, with a review of other occurrences of extrusive carbonatites. *Earth Sciences.* London, University College London.

CHURCH, A. A. & JONES, A. P. (1994) Hollow natrocarbonatite lapilli from the 1992 eruption of Oldoinyo Lengai, Tanzania. *Journal of the Geological Society,* 151, 59-63.

CHURCH, A. A. & JONES, A. P. (1995) Silicate-Carbonate Immiscibility at Oldoinyo-Lengai. ***Journal of Petrology,*** **36, 869-889.**

COHEN, R. S., O'NIONS, R. K. & DAWSON, J. B. (1984) Isotope geochemistry of xenoliths from East Africa: Implications for development of mantle reservoirs and their interaction. ***Earth and Planetary Science Letters,*** **68, 209-220.**

COLLINS, P. L. F. (1979) Gas hydrates in CO 2 -bearing fluid inclusions and the use of freezing data for estimation of salinity. ***Economic Geology,*** **74, 1435-1444.**

COSTANZO, A., FEELY, M. & MOORE, K. (2005) The application of laser raman spectroscopy to fluid inclusion studies: a case study from Pocos de Caldas Alkaline Massif, Sao Paulo State, Brazil ***Proceedings of SPIE - The International Society for Optical Engineering.***

COSTANZO, A., MOORE, K. R., WALL, F. & FEELY, M. (2006) Fluid inclusions in apatite from Jacupiranga calcite carbonatites: Evidence for a fluid-stratified carbonatite magma chamber. ***Lithos,*** **91, 208-228.**

DALOU, C., KOGA, K. T., HAMMOUDA, T. & POITRASSON, F. (2009) Trace element partitioning between carbonatitic melts and mantle transition zone minerals: Implications for the source of carbonatites. ***Geochimica et Cosmochimica Acta,*** **73, 239-255.**

DALTON, J. A. & LANE, S. J. (1996) Electron microprobe analysis of Ca in olivine close to grain boundaries; the problem of secondary X-ray fluorescence. ***American Mineralogist,*** **81, 194-201.**

DALTON, J. A. & PRESNALL, D. C. (1998) The Continuum of Primary Carbonatitic-Kimberlitic Melt Compositions in Equilibrium with Lherzolite: Data from the System CaO-MgO-Al2O3-SiO2-CO2 at 6 GPa. ***J. Petrology,*** **39, 1953-1964.**

DALTON, J. A. & WOOD, B. J. (1993) The compositions of primary carbonate melts and their evolution through wallrock reaction in the mantle. ***Earth and Planetary Science Letters,*** **119, 511-525.**

DASGUPTA, R., HIRSCHMANN, M. M., MCDONOUGH, W. F., SPIEGELMAN, M. & WITHERS, A. C. (2009) Trace element partitioning between garnet lherzolite and carbonatite at 6.6 and 8.6 GPa with applications to the geochemistry of the mantle and of mantle-derived melts. ***Chemical Geology,*** **262, 57-77.**

DAWSON, J. & POWELL, D. (1969) The Natron-Engaruka explosion crater area, northern Tanzania. ***Bulletin of Volcanology,*** **33, 791-817.**

DAWSON, J. B. (1962a) The geology of Oldoinyo Lengai. ***Bulletin of Volcanology,*** **24, 349 - 387.**

DAWSON, J. B. (1962b) Sodium carbonate lavas from Oldoinyo Lengai, Tanganyika. ***Nature,*** **195, 1075 - 1076.**

DAWSON, J. B. (1993) A supposed sövite from Oldoinyo Lengai, Tanzania: result of extreme alteration of alkali carbonatite lava. ***Mineralogical Magazine,*** **57, 93 - 101.**

DAWSON, J. B. (1998) Peralkaline Nephelinite-Natrocarbonatite Relationships at Oldoinyo Lengai, Tanzania. ***J. Petrology,*** **39, 2077-2094.**

DAWSON, J. B. (2008) ***The Gregory Rift Valley and Neogene-Recent Volcanoes of Northern Tanzania,*** **London, Geological Society London.**

DAWSON, J. B. (2010) Aspects of Rift Valley faulting and volcanicity in North Tanzania: report of a Geologists' Association Field Meeting in 2008. ***Proceedings of the Geologists' Association,*** **121, 342-349.**

DAWSON, J. B. & ANDREWS, J. R. (1972) Kimberlites and their Relation to the Mantle [and Discussion]. ***Philosophical Transactions of the Royal Society of London. Series A, Mathematical and Physical Sciences,*** **271, 297-311.**

DAWSON, J. B., BOWDEN, P. & CLARK, G. C. (1968) Activity of the carbonatite volcano Oldoinyo Lengai 1966. ***Geol Rundschau,*** **57, 865-879.**

DAWSON, J. B. & HILL, P. G. (1998) Mineral chemistry of a peralkaline combeite-lamprophyllite nephelinite from Oldoinyo Lengai, Tanzania. ***Mineral Mag,*** **62, 179-196.**

DAWSON, J. B., PINKERTON, H., NORTON, G. E. & PYLE, D. M. (1990) Physicochemical properties of alkali carbonatite lavas:Data from the 1988 eruption of Oldoinyo Lengai, Tanzania. ***Geology,*** **18, 260-263.**

DAWSON, J. B., PINKERTON, H., PYLE, D. M. & NYAMWERU, C. (1994a) June 1993 eruption of Oldoinyo Lengai, Tanzania: Exceptionally viscous and large carbonatite lava flows and evidence for coexisting silicate and carbonate magmas. ***Geology,*** **22, 799-802.**

DAWSON, J. B., POWELL, D. G. & REID, A. M. (1970) Ultrabasic Xenoliths and Lava from the Lashaine Volcano, Northern Tanzania. ***J. Petrology,*** **11, 519-548.**

DAWSON, J. B. & SMITH, J. V. (1977) The MARID (mica-amphibole-rutile-ilmenite-diopside) suite of xenoliths in kimberlite. ***Geochimica et Cosmochimica Acta,*** **41, 309-323.**

DAWSON, J. B. & SMITH, J. V. (1988) Metasomatised and veined upper-mantle xenoliths from Pello Hill, Tanzania: evidence for anomalously-light mantle beneath the Tanzanian sector of the East African Rift Valley. ***Contributions to Mineralogy and Petrology,*** **100, 510-527.**

DAWSON, J. B. & SMITH, J. V. (1992a) Olivine-mica pyroxenite xenoliths from northern Tanzania: metasomatic products of upper-mantle peridotite. ***Journal of Volcanology and Geothermal Research,*** **50, 131-142.**

DAWSON, J. B. & SMITH, J. V. (1992b) Potassium loss during metasomatic alteration of mica pyroxenite from Oldoinyo Lengai, northern Tanzania: contrasts with fenitization. ***Contributions to Mineralogy and Petrology,*** **112, 254-260.**

DAWSON, J. B., SMITH, J. V. & STEELE, I. M. (1994b) Trace-element distribution between coexisting perovskite, apatite and titanite from Oldoinyo Lengai, Tanzania. ***Chemical Geology,*** **117, 285-290.**

DAWSON, J. B., SMITH, J. V. & STEELE, I. M. (1995) Petrology and Mineral Chemistry of Plutonic Igneous Xenoliths from the Carbonatite Volcano, Oldoinyo Lengai, Tanzania. ***J. Petrology,*** **36, 797-826.**

DEER, W. A., HOWIE, R. A., WISE, W. S. & ZUSSMAN, J. (2006) Framework Silicates - Nepheline - Kalsilite Group. ***Rock - Forming Minerals, Vol 4B: Framework Siliacates - Silica Minerals, Feldspathoids and Zeolites.*** **London, Geological Socieity of London.**

DEINES, P. (1989) Stable isotope variations in Carbonatites. IN BELL, K. (Ed.) ***Carbonatites: Genesis and Evolution.*** **London, Unwin Hyman.**

DEINES, P. (2002) The carbon isotope geochemistry of mantle xenoliths. ***Earth-Science Reviews,*** **58, 247-278.**

DEINES, P. & GOLD, D. P. (1973) The isotopic composition of carbonatite and kimberlite carbonates and their bearing on the isotopic composition of deep-seated carbon. ***Geochimica et Cosmochimica Acta,*** **37, 1709-1733.**

DEPAOLO, D. J. (1981) Trace element and isotopic effects of combined wallrock assimilation and fractional crystallization. ***Earth and Planetary Science Letters,*** **53, 189-202.**

DIEING, T., HOLLRICHER, O., TOPORSKI, J., FRIES, M. & STEELE, A. (2010) Raman Spectroscopy and Confocal Raman Imaging in Mineralogy and Petrography. ***Confocal Raman Microscopy.*** **Springer Berlin / Heidelberg.**

DOBSON, D. P., JONES, A. P., RABE, R., SEKINE, T., KURITA, K., TANIGUCHI, T., KONDO, T., KATO, T., SHIMOMURA, O. & URAKAWA, S. (1996) In-situ measurement of viscosity and density of carbonate melts at high pressure. ***Earth and Planetary Science Letters,*** **143, 207-215.**

DONALDSON, C. H. & DAWSON, J. B. (1978) Skeletal crystallization and residual glass compositions in a cellular alkalic pyroxenite nodule from Oldoinyo Lengai. *Contributions to Mineralogy and Petrology,* 67, 139-149.

DONALDSON, C. H., DAWSON, J. B., KANARIS-SOTIRIOU, R., BATCHELOR, R. A. & WALSH, J. N. (1987) The silicate lavas of Oldoinyo Lengai, Tanzania. *Neues Jahrbuch fur Mineralogie,* 156, 247 - 279.

DOWNES, H. (2001) Formation and Modification of the Shallow Sub-continental Lithospheric Mantle: a Review of Geochemical Evidence from Ultramafic Xenolith Suites and Tectonically Emplaced Ultramafic Massifs of Western and Central Europe. *Journal of Petrology,* 42, 233-250.

DOWNES, H., WALL, F., DEMENY, A. & CS., S. (2012) Continuing the Carbonatite Controversy. *Mineralogical Magazine,* 76, 255-257.

DRAKE, M. J. & WEILL, D. F. (1975) Partition of Sr, Ba, Ca, Y, Eu2+, Eu3+, and other REE between plagioclase feldspar and magmatic liquid: an experimental study. *Geochimica et Cosmochimica Acta,* 39, 689-712.

DUNCAN, A. M., GUEST, J. E., STOFAN, E. R., ANDERSON, S. W., PINKERTON, H. & CALVARI, S. (2004) Development of tumuli in the medial portion of the 1983 aa flow-field, Mount Etna, Sicily. *Journal of Volcanology and Geothermal Research,* 132, 173-187.

DUNNING, G. E. & COOPER JR, J. F. (2002) Pseudomorphic Melanophlogites from California. *Mineralogical Record,* 33, 237-242.

ECKERMANN, H. V. (1948) The alkaline district of Alno Island. *Sver. Geol. Undersokning,,* Ser C, 175.

ECKERMANN, H. V. (1961) The petrogenesis of the Alnö alkaline rocks. *Bull. Geol. Inst. Univ. Uppsala,* 40, 25 - 36.

EDWARDS, C. B. & HOWKINS, J. B. (1966) Kimberlites in Tanganyika with special reference to the Mwadui occurrence. *Economic Geology,* 61, 537-554.

EGGLER, D. H. & WENDLANDT, R. F. (1979) Experimental studies on the relationship between kimberlite magmas and partial melting of peridotite. *Kimberlites, Diatremes, and Diamonds: Their Geology, Petrology, and Geochemistry.* Washington, DC, AGU.

EVANS, R. L. (2008) Carbon in Charge. *Science,* 322, 1338-1340.

FERRARO, J. R. & NAKAMOTO, K. (2003) *Introductory Raman Spectroscopy,* San Diego, Elsevier.

FISCHER, T. P., BURNARD, P., MARTY, B., HILTON, D. R., FURI, E., PALHOL, F., SHARP, Z. D. & MANGASINI, F. (2009) Upper-mantle volatile chemistry at Oldoinyo Lengai volcano and the origin of carbonatites. *Nature,* 459, 77-80.

FOLEY, S. F. (1992) Vein-plus-wall-rock melting mechanisms in the lithosphere and the origin of potassic alkaline magmas. *Lithos,* 28, 435-453.

FORSTER, C. & SMITH, L. (1989) The Influence of Groundwater Flow on Thermal Regimes in Mountainous Terrain: A Model Study. *J. Geophys. Res.,* 94, 9439-9451.

FREESTONE, I. C. & HAMILTON, D. L. (1980) The role of liquid immiscibility in the genesis of carbonatites — An experimental study. *Contributions to Mineralogy and Petrology,* 73, 105-117.

FREZZOTTI, M. L., ANDERSEN, T., NEUMANN, E. R. & SIMONSEN, S. L. (2002) Carbonatite melt-CO2 fluid inclusions in mantle xenoliths from Tenerife, Canary Islands: A story of trapping, immiscibility and fluid-rock interaction in the upper mantle. *Lithos,* 64, 77-96.

FREZZOTTI, M. L., TECCE, F. & CASAGLI, A. (2012) Raman spectroscopy for fluid inclusion analysis. *Journal of Geochemical Exploration,* 112, 1-20.

FURMAN, T. (2007) Geochemistry of East African Rift Basalts: An overview. *Journal of African Earth Science,* 48, 147 - 160.

GARRISON, J. R. & TAYLOR, L. A. (1980) Megacrysts and xenoliths in kimberlite, Elliott County, Kentucky: A mantle sample from beneath the Permian Appalachian Plateau. *Contributions to Mineralogy and Petrology,* 75, 27-42.

GARSON, M. S., COATS, J. S., ROCK, N. M. S. & DEANS, T. (1984) Fenites, breccia dykes, albitites, and carbonatitic veins near the Great Glen Fault, Inverness, Scotland. *Journal of the Geological Society,* 141, 711-732.

GEIGER, C. A. & DACHS, E. (2008) Stability and Occurrence of the Molecule-Containing SiO2 Clathrate Melanophlogite: Metastable Crystallization from a Colloid or Gel? *American Geophysical Union Fall Meeting.* San Francisco, AGU.

GENGE, M. J. (1994) The structure of carbonate melts and implications for the petrogenesis of carbonatite magmas *Earth Sciences.* London, University College London.

GENGE, M. J., BALME, M. & JONES, A. P. (2001) Salt-bearing fumarole deposits in the summit crater of Oldoinyo Lengai, Northern Tanzania: interactions between natrocarbonatite lava and meteoric water. *Journal of Volcanology and Geothermal Research,* 106, 111 - 122.

GIAMMANCO, S. & BONFANTI, P. (2008) Cluster analysis of soil CO_2 data from Mt. Etna (Italy) reveals volcanic influences on temproal and spatial patterns of degassing. *Bull. Volcanol.*

GIES, H. (1983) Studies on clathrasils. III. *Zeitschrift für Kristallographie,* 164, 247 - 257.

GIES, H., GERKE, H. & LIEBAU, F. (1982) Chemical composition and synthesis of melanophlogite, a clathrate compound of silica. *Neues Jahrbuch fur Mineralogie, Monatshefte*, 119-124.

GIGGENBACH, W. F. (1975) A Simple for the Collection and Analysis of Volcano Gas Samples. *Bulletin of Volcanology,* 39, 132 - 145.

GILBERT, C. D. & WILLIAMS-JONES, A. E. (2008) Vapour transport of rare earth elements (REE) in volcanic gas: Evidence from encrustations at Oldoinyo Lengai. *Journal of Volcanology and Geothermal Research,* 176, 519-528.

GILBERT, J. S. & LANE, S. J. (1994) The origin of accretionary lapilli. *Bulletin of Volcanology,* 56, 398-411.

GITTINS, J. (1988) Partial melting of fenitized crustal xenoliths in the Oldoinyo Lengai carbonatitic volcano, Tanzania: Discussion. *American Mineralogist,* 73, 1465-1467.

GITTINS, J. (1989) The origin and evolution of carbonatite magmas. IN BELL, K. (Ed.) *Carbonatites: genesis and evolution.* London, Unwin Hyman.

GITTINS, J. & JAGO, B. C. (1998) Differentiation of natrocarbonatite magma at Oldoinyo Lengai volcano, Tanzania. *Mineralogical Magazine,* 62, 759-768.

GOFF, F. & MCMURTRY, G. M. (2000) Tritium and stable isotopes of magmatic waters. *Journal of Volcanology and Geothermal Research,* 97, 347-396.

GORIATSCHEV, A. B. (1968) Isverschenie Oldoinio Lengai (Eruption of Oldoinyo Lengai). *Priroda*, 88 - 92.

GRAHAM, S., LAMBERT, D. & SHEE, S. (2004) The petrogenesis of carbonatite, melnoite and kimberlite from the Eastern Goldfields Province, Yilgarn Craton. *Lithos,* 76, 519-533.

GRASER, G., POTTER, J., KÖHLER, J. & MARKL, G. (2008) Isotope, major, minor and trace element geochemistry of late-magmatic fluids in the peralkaline Ilímaussaq intrusion, South Greenland. *Lithos,* 106, 207-221.

GREEN, D. H. & WALLACE, M. E. (1988) Mantle metasomatism by ephemeral carbonatite melts *Nature,* 336, 459 - 462.

GREEN, T. H. (1994) Experimental studies of trace-element partitioning applicable to igneous petrogenesis -- Sedona 16 years later. *Chemical Geology,* 117, 1-36.

GUEST, J. E., WOOD, C. & GREELEY, R. (1984) Lava tubes, terraces and megatumuli on the 1614–24 pahoehoe lava flow field, Mount Etna, sicily. *Bulletin of Volcanology,* 47, 635-648.

GUEST, N. J. (1956) The volcanic activity of Oldoinyo Lengai, 1954. *Geol Survey Tanganyika Records,* 4, 56 - 59.

GUNAWARDANE, R. P., GIES, H. & LIEBAU, F. (1987) The Effect of "Help Gases" on the Formation and Stability of Clatrasils. *Z. anorg. allg.Chem,* 546, 189 - 198

GUZMICS, T., MITCHELL, R., SZABÓ, C., BERKESI, M., MILKE, R. & RATTER, K. (2012) Liquid immiscibility between silicate, carbonate and sulfide melts in melt inclusions hosted in co-precipitated minerals from Kerimasi volcano (Tanzania): evolution of carbonated nephelinitic magma. *Contributions to Mineralogy and Petrology*, 1-22.

GUZMICS, T., ZAJACZ, Z., KODOLÃ¡NYI, J., HALTER, W. & SZABÃ³, C. (2008a) LA-ICP-MS study of apatite- and K feldspar-hosted primary carbonatite melt inclusions in clinopyroxenite xenoliths from lamprophyres, Hungary: Implications for significance of carbonatite melts in the Earth's mantle. *Geochimica et Cosmochimica Acta,* 72, 1864-1886.

GUZMICS, T., ZAJACZ, Z., KODOLANYI, J., HALTER, W. & SZABO, C. (2008b) LA-ICP-MS study of apatite- and K feldspar-hosted primary carbonatite melt inclusions in clinopyroxenite xenoliths from lamprophyres, Hungary: Implications for significance of carbonatite melts in the Earth's mantle. *Geochimica et Cosmochimica Acta,* 72, 1864-1886.

HAGGERTY, S. E. (1989) Mantle metasomes and the kinship between carbonatites and kimberlites. IN BELL, K. (Ed.) *Carbonatites: Genesis and Evolution.* London, Unwin Hyman.

HAMILTON, D. L. (1961) Nephelines as Crystallization Temperature Indicators. *The Journal of Geology,* 69, 321-329.

HAMMOUDA, T. (2003) High-pressure melting of carbonated eclogite and experimental constraints on carbon recycling and storage in the mantle. *Earth and Planetary Science Letters,* 214, 357 - 368.

HAMMOUDA, T., CHANTEL, J. & DEVIDAL, J.-L. (2010) Apatite solubility in carbonatitic liquids and trace element partitioning between apatite and carbonatite at high pressure. *Geochimica et Cosmochimica Acta,* 74, 7220-7235.

HAMMOUDA, T. & LAPORTE, D. (2000) Ultrafast mantle impregnation by carbonatite melts. *Geology,* 28, 283-285.

HAMMOUDA.T (2008) Trace element partitioning during partial melting of carbonated eclogites. *Physics of the Earth and Planetary Interiors,* 174, 60-69.

HANSTEEN, T. H. & KLUGEL, A. (2008) Fluid Inclusion Thermobarometry as a Tracer for Magmatic Processes. *Reviews in Mineralogy and Geochemistry,* 69, 143-177.

HARMER, R. E. & GITTINS, J. (1998) The Case for Primary, Mantle-derived Carbonatite Magma. *Journal of Petrology,* 39, 1895-1903.

HARMER, R. E., LEE, C. A. & EGLINGTON, B. M. (1998) A deep mantle source for carbonatite magmatism; evidence from the nephelinites and carbonatites of the Buhera district, SE Zimbabwe. *Earth and Planetary Science Letters,* 158, 131 - 142.

HAWKESWORTH, C. J., ERLANK, A. J., KEMPTON, P. D. & WATERS, F. G. (1990) Mantle metasomatism: Isotope and trace-element trends in xenoliths from Kimberley, South Africa. *Chemical Geology,* 85, 19-34.

HEINRICH, C. A., PETTKE, T., HALTER, W. E., AIGNER-TORRES, M., AUDETAT, A., GUNTHER, D., HATTENDORF, B., BLEINER, D., GUILLONG, M. & HORN, I. (2003) Quantitative multi-element analysis of minerals, fluid and melt inclusions by laser-ablation inductively-

coupled-plasma mass-spectrometry. *Geochimica et Cosmochimica Acta,* 67, 3473-3496.

HEZEL, D. C., SCHLÜTER, J., KALLWEIT, H., JULL, A. J. T., AL FAKEER, O. Y., AL SHAMSI, M. & STREKOPYTOV, S. (2011) Meteorites from the United Arab Emirates: Description, weathering, and terrestrial ages. Blackwell Publishing Ltd.

HILAIRE, C., CASANOVA, J. & TAIEB, M. (1987) Isotopic Age and Lacustrine Environments during Late Quaternary in the Tanzanian Rift (Lake Natron). IN RAMPINO, M. R., SANDERS, J. E., NEWMAN, W. S. & KÖNIGSSON, L. K. (Eds.) *Climate: History, Periodicity and Predictability.* New York, Van Nostrand Reinhold.

HILLAIRE-MARCEL, C., CARRO, O. & CASANOVA, J. (1986) 14C and Th/U dating of Pleistocene and Holocene stromatolites from East African paleolakes. *Quaternary Research,* 25, 312-329.

HILLAIRE-MARCEL, C. & CASANOVA, J. (1987) Isotopic hydrology and paleohydrology of the Madagi (Kenya)-Natron (Tanzania) basin during the late quaternary. *Palaeogeography, Palaeoclimatology, Palaeoecology,* 58, 155-181.

HOEFS, J. (2009) *Stable Isotope Geochemistry*, Springer

HOERNLE, K., TILTON, G., LE BAS, M., DUGGEN, S. & GARBE-SCHÖNBERG, D. (2002) Geochemistry of oceanic carbonatites compared with continental carbonatites: mantle recycling of oceanic crustal carbonate. *Contributions to Mineralogy and Petrology,* 142, 520-542.

HOFMANN, A. (1972) Chromatographic theory of infiltration metasomatism and its application to feldspars. *American Journal of Science,* 272, 69 - 90.

HURWITZ, S., KIPP, K. L., INGEBRITSEN, S. E. & REID, M. E. (2003) Groundwater flow, heat transport, and water table position within volcanic edifices: Implications for volcanic processes in the Cascade Range. *J. Geophys. Res.,* 108, 2557.

HYNDMAN, D. W. (1985) *Petrology of igneous and metamorphic rocks,* New York, McGraw - Hill.

HYNDMAN, R. D. & DAVIS, E. E. (1992) A Mechanism for the Formation of Methane Hydrate and Seafloor Bottom-Simulating Reflectors by Vertical Fluid Expulsion. *J. Geophys. Res.,* 97, 7025-7041.

IONOV, D. A., DUPUY, C., O'REILLY, S. Y., KOPYLOVA, M. G. & GENSHAFT, Y. S. (1993) Carbonated peridotite xenoliths from Spitsbergen: implications for trace element signature of mantle carbonate metasomatism. *Earth and Planetary Science Letters,* 119, 283-297.

IONOV, D. A. & HOFMANN, A. W. (1995) Nb---Ta-rich mantle amphiboles and micas: Implications for subduction-related metasomatic trace element fractionations. *Earth and Planetary Science Letters,* 131, 341-356.

IRMER, G. & GRAUPNER, T. (in press) Isotopes of C and O in CO_2: a Raman study using gas standards and natural fluid inclusions. Freiburg, TU Bergakademie.

IRVING, A. J. & WYLLIE, P. J. (1973) Melting relationships in CaO-CO2 and MgO-CO2 to 36 kilobars with comments on CO2 in the mantle. *Earth and Planetary Science Letters,* 20, 220-225.

JOHNSON, L. H., JONES, A. P., CHURCH, A. A. & TAYLOR, W. R. (1997) Ultramafic xenoliths and megacrysts from a melilitite tuff cone, Deeti, northern Tanzania. *Journal of African Earth Sciences,* 25, 29-42.

JOHNSON, S. P., DE WAELE, B., TEMBO, F., KATONGO, C., TANI, K., CHANG, Q., IIZUKA, T. & DUNKLEY, D. (2007) Geochemistry, Geochronology and Isotopic Evolution of the Chewore-Rufunsa Terrane, Southern Irumide Belt: a Mesoproterozoic Continental Margin Arc. *Journal of Petrology,* 48, 1411-1441.

JONES, A. P. & EKAMBARAM, V. (1985) New INAA analysis of a mantlederived titanate mineral of the crichtonite series, with particular reference to the rare earth elements. ***Am Mineral,*** **70, 414 - 418.**

JONES, A. P., SMITH, J. V. & DAWSON, J. B. (1982) Mantle metasomatism in 14 veined peridotites from the Bultfontein mine, South Africa. ***J Geology,*** **90, 435 - 453.**

JONES, A. P., WALL, F. & WILLIAMS, C. T. (1996) ***Rare Earth Minerals: Chemistry, origin and ore deposits,*** **London, Chapman & Hall.**

JONES, J. H., WALKER, D., PICKETT, D. A., MURRELL, M. T. & BEATTIE, P. (1995) Experimental investigations of the partitioning of Nb, Mo, Ba, Ce, Pb, Ra, Th, Pa, and U between immiscible carbonate and silicate liquids. ***Geochimica et Cosmochimica Acta,*** **59, 1307-1320.**

JØRGENSEN, J. Ø. & HOLM, P. M. (2002) Temporal variation and carbonatite contamination in primitive ocean island volcanics from Sao Vicente, Cape Verde Islands. ***Chemical Geology,*** **192, 249-267.**

KALT, A., HEGNER, E. & SATIR, M. (1997) Nd, Sr, and Pb isotopic evidence for diverse lithospheric mantle sources of East African Rift carbonatites. ***Tectonophysics,*** **278, 31-45.**

KAMB, B. (1965) A clathrate crystalline form of silica. ***Science,*** **148, 232-234.**

KAMENETSKY, V. S., KAMENETSKY, M. B., SOBOLEV, A. V., GOLOVIN, A. V., DEMOUCHY, S., FAURE, K., SHARYGIN, V. V. & KUZMIN, D. V. (2008) Olivine in the Udachnaya-East Kimberlite (Yakutia, Russia): Types, Compositions and Origins. ***J. Petrology,*** **49, 823-839.**

KAMENETSKY, V. S., KAMENETSKY, M. B., SOBOLEV, A. V., GOLOVIN, A. V., SHARYGIN, V. V., POKHILENKO, N. P. & SOBOLEV, N. V. (2009) Can pyroxenes be liquidus minerals in the kimberlite magma? ***Lithos,*** **112, Supplement 1, 213-222.**

KAMINSKY, F., WIRTH, R., MATSYUK, S., SCHREIBER, A. & THOMAS, R. (2009) Nyerereite and nahcolite inclusions in diamond: evidence for lower-mantle carbonatitic magmas. ***Mineralogical Magazine,*** **73, 797-816.**

KAWAKAMI, Y., YAMAMOTO, J. & KAGI, H. (2003) Micro-Raman Densimeter for CO2 Inclusions in Mantle-Derived Minerals. ***Applied Spectroscopy,*** **57, 1333-1339.**

KELLER, J. & HOEFS, J. (1995) Stable isotope characteristics of recent natrocarbonatites from Oldoinyo Lengai. IN BELL, K. & KELLER, J. (Eds.) ***Carbonatite Volcanism: Oldoinyo Lengai and the petrogenesis of natrocarbonatites.*** **IAVCEI Proceedings Volcanology.**

KELLER, J., KLAUDIUS, J., KERVYN, M., ERNST, G. & MATTSSON, H. (2010) Fundamental changes in the activity of the natrocarbonatite volcano Oldoinyo Lengai, Tanzania: New magma composition during the 2007-2008 explosive eruptions ***Bulletin of Volcanology,*** **72, 893-912.**

KELLER, J. & KRAFFT, M. (1990) Effusive natrocarbonatite activity of Oldoinyo Lengai, June 1988. ***Bulletin of Volcanology,*** **52, 629-645.**

KELLER, J. & ZAITSEV, A. N. (2006) CALCIOCARBONATITE DYKES AT OLDOINYO LENGAI, TANZANIA: THE FATE OF NATROCARBONATITE. ***Can Mineral,*** **44, 857-876.**

KELLER, J., ZAITSEV, A. N. & WIEDENMANN, D. (2006) Primary magmas at Oldoinyo Lengai: The role of olivine melilitites. ***Lithos,*** **91, 150-172.**

KELLEY, S. P. & WARTHO, J.-A. (2000) Rapid Kimberlite Ascent and the Significance of Ar-Ar Ages in Xenolith Phlogopites. ***Science,*** **289, 609-611.**

KERESZTURY, G. (2006) ***Raman Spectroscopy: Theory*****, John Wiley & Sons, Ltd.**

KERVYN, M., ERNST, G., KELLER, J., VAUGHAN, R., KLAUDIUS, J., PRADAL, E., BELTON, F., MATTSSON, H., MBEDE, E. & JACOBS, P. (2010) Fundamental changes in the activity of the natrocarbonatite volcano Oldoinyo Lengai, Tanzania. ***Bulletin of Volcanology,*** **72, 913-931.**

KERVYN, M., ERNST, G. G. J., KLAUDIUS, J., KELLER, J., MBEDE, E. & JACOBS, P. (2008a) Remote sensing study of sector collapses and debris avalanche deposits at Oldoinyo Lengai and Kerimasi volcanoes, Tanzania. ***Int. J. Remote Sens.,*** **29, 6565-6595.**

KERVYN, M., ERNST, G. J., KLAUDIUS, J., KELLER, J., KERVYN, F., MATTSSON, H. B., BELTON, F., MBEDE, E. & JACOBS, P. (2008b) Voluminous lava flows at Oldoinyo Lengai in 2006: chronology of events and insights into the shallow magmatic system. ***Bull. Volcanol.,*** **70, 1069 - 1086.**

KERVYN, M., HARRIS, A. J. L., BELTON, F. A., MBEDE, E., JACOBS, P. & ERNST, G. J. (2008c) Thermal remote sensing of the low - intensity carbonatite volcanism of Oldoinyo Lengai, Tanzania. ***International Journal of Remote Sensing,*** **29, 6467 - 6499.**

KILBURN, C. R. J. (2007) Giant catastrophic landslides. IN SAMMONDS, P. R. & THOMPSON, J. M. T. (Eds.) ***Advances in Earth Sciences: From earthquakes to global warming.*** **London, Imperial College Press.**

KJARSGAARD, B. (2011) Geochemistry of hypabyssal/coherent kimberlite: a global perspective with insights to mineralogy and volcanology. ***IUGG General Assembly.*** **Melbourne, Australia.**

KJARSGAARD, B. & HAMILTON, D. L. (1988) Liquid immiscibility and the origin of alkali-poor carbonatites. ***Mineral Mag,*** **52, 43 - 55.**

KJARSGAARD, B. & HAMILTON, D. L. (1989) The genesis of carbonatites by immiscibility. IN BELL, K. (Ed.) ***Carbonatites: genesis and evolution.*** **London, Unwin Hyman.**

KJARSGAARD, B. & PETERSON, T. (1991) Nephelinite-carbonatite liquid immiscibility at Shombole volcano, East Africa: Petrographic and experimental evidence. ***Mineralogy and Petrology,*** **43, 293-314.**

KJARSGAARD, B. A., HAMILTON, D. L. & PETERSON, T. D. (1995) Peralkaline Nephelinite/Carbonatite Liquid Immiscibility: Comparison of Phase Compositions in Experiments and Natural Lavas from Oldoinyo Lengai. IN BELL, K. & KELLER, J. (Eds.) ***Carbonatite Volcanism: Oldoinyo Lengai and the Petrogenesis of Natrocarbonatites.*** **Berlin, Springer-Verlag.**

KLAUDIUS, J. & KELLER, J. (2004a) Quaternary debris avalanche deposits at Oldoinyo Lengai (Tanzania). ***IAVCEI General Assembly, ''Volcanism and its Impact on Society''.*** **Pucon, Chile.**

KLAUDIUS, J. & KELLER, J. (2004b) Quaternary debris avalanche deposits at Oldoinyo Lengai, Tanzania. ***IAVCEI General Assembly.*** **Pucon, Chile.**

KLAUDIUS, J. & KELLER, J. (2006) Peralkaline silicate lavas at Oldoinyo Lengai, Tanzania. ***Lithos,*** **91, 173-190.**

KLEMME, S., VAN DER LAAN, S. R., FOLEY, S. F. & GÜNTHER, D. (1995) Experimentally determined trace and minor element partitioning between clinopyroxene and carbonatite melt under upper mantle conditions. ***Earth and Planetary Science Letters,*** **133, 439-448.**

KOEPENICK, K. W., BRANTLEY, S. L., THOMPSON, J. M., ROWE, G. L., NYBLADE, A. A. & MOSHY, C. (1996) Volatile emissions from the crater and flank of Oldoinyo Lengai volcano, Tanzania. ***Journal of Geophysical Research,*** **101, 13819 - 13830.**

KOGARKO, L. N. (1993) ***Geochemical characteristics of oceanic carbonatites from the Cape Verde Islands,*** **Pretoria, AFRIQUE DU SUD, Bureau for Scientific Publications.**

KOLESOV, B. A. & GEIGER, C. A. (2003) Molecules in the SiO_2-clathrate melanophlogite: A single-crystal Raman study. ***American Mineralogist,*** **88, 1364-1368.**

KONNERUP-MADSEN, J., DUBESSY, J. & ROSE-HANSEN, J. (1985) Combined Raman microprobe spectrometry and microthermometry of fluid inclusions in minerals from igneous rocks of the Gardar province (south Greenland). ***Lithos,*** **18, 271-280.**

KOOI, M. E., SCHOUTEN, J. A., VAN DEN KERKHOF, A. M., ISTRATE, G. & ALTHAUS, E. (1998) The system CO2-N2 at high pressure and applications to fluid inclusions. *Geochimica et Cosmochimica Acta,* 62, 2837-2843.

KOORNNEEF, J. M., DAVIES, G. R., DÖPP, S. P., VUKMANOVIC, Z., NIKOGOSIAN, I. K. & MASON, P. R. D. (2009) Nature and timing of multiple metasomatic events in the sub-cratonic lithosphere beneath Labait, Tanzania. *Lithos,* 112, 896-912.

KORENAGA, J. & KELEMEN, P. B. (1998) Melt migration through the oceanic lower crust: a constraint from melt percolation modeling with finite solid diffusion. *Earth and Planetary Science Letters,* 156, 1-11.

KORZHINSKII, D. S. (1957) *Physico-chemical basis of analysis of the paragenesis of minerals,* New York, Consultants Bureau.

KORZHINSKII, D. S. (1968) The theory of metasomatic zoning. *Mineralium Deposita,* 3, 222-231.

KOSTER VAN GROOS, A. F. & WYLLIE, P. J. (1966) Liquid immiscibility in the system Na_2O-Al_2O_3-SiO_2-CO_2 at Pressure to 1 kilobar. *American Journal of Science,* 264, 234 - 255.

KRAMM, U. & SINDERN, S. (1998) Nd and Sr Isotope Signatures of Fenites from Oldoinyo Lengai, Tanzania, and the Genetic Relationships between Nephelinites, Phonolites and Carbonatites. *Journal of Petrology,* 39, 1997-2004.

KRAUSKOPF, K. B. & BIRD, D. K. (1995) *Introduction to Geochemistry,* Singapore, McGraw - Hill International.

KRESTEN, P. & MOROGAN, V. (1986) Fenitization at the Fen complex, southern Norway. *Lithos,* 19, 27-42.

LE BAS, M. (1971) Per-alkaline Volcanism, Crustal Swelling, and Rifting. *Nature Physical Sciene,* 230, 85 - 87.

LE BAS, M. (1977) *Carbonatite - Nephelinite Volcanism: An African Case History,* New York, John Wiley & Sons.

LE BAS, M. (1981) Carbonatite magmas. *Mineralogical Magazine,* 44, 133-140.

LE BAS, M. & ASPDEN, J. (1981) The comparability of carbonatitic fluid inclusions in ijolites with natrocarbonatite lava. *Bulletin of Volcanology,* 44, 429-438.

LE BAS, M. J. (1987) Nephelinites and carbonatites. *Geological Society, London, Special Publications,* 30, 53-83.

LE MAITRE, R. W. (2002) *Igneous Rocks: A Classification and Glossary of Terms*, Cambridge University Press.

LEE, W.-J. & WYLLIE, P. J. (1997) Liquid immiscibility between nephelinite and carbonatite from 1.0 to 2.5 GPa compared with mantle melt compositions. *Contributions to Mineralogy and Petrology,* 127, 1-16.

LEMARCHAND, F., VILLEMANT, B. & CALAS, G. (1987) Trace element distribution coefficients in alkaline series. *Geochimica et Cosmochimica Acta,* 51, 1071-1081.

LEV, O., SHEINTUCH, M., PISEMEN, L. M. & YARNITZKYT, C. (1988) Mantle metasomatism by ephemeral carbonatite melts. *Nature,* 336, 459-462.

LIN, F. (2005) Experimental Study of the PVTX Properties of the System H20 - CH4. Blacksburg, VA, Virginia Polytechnic Institute and State University.

LITHGOW-BERTELLONI, C. & SILVER, P. G. (1998) Dynamic topography, plate driving forces and the African superswell. *Nature,* 395, 269-272.

LIU, S., WELCH, M. D. & KLINOWSKI, J. (1997) NMR study of phase transitions in guest-free silica clathrate melanophlogite. *Journal of Physical Chemistry B,* 101, 2811-2814.

LORENZ, V. (1986) On the growth of maars and diatremes and its relevance to the formation of tuff rings. *Bulletin of Volcanology,* 48, 265-274.

LYSAK, S. V. (1992) Heat flow variations in continental rifts. *Tectonophysics,* 208, 309-323.

MACINTYRE, R. M., MITCHELL, J. G. & DAWSON, J. B. (1974) Age of Fault Movements in Tanzanian Sector of East African Rift System. ***Nature,*** **247, 354-356.**

MANYA, S. & MABOKO, M. A. H. (2008) Geochemistry and geochronology of Neoarchaean volcanic rocks of the Iramba-Sekenke greenstone belt, central Tanzania. ***Precambrian Research,*** **163, 265-278.**

MARTI, J. & GUDMUNDSSON, A. (2000) The Las Cañadas caldera (Tenerife, Canary Islands): an overlapping collapse caldera generated by magma-chamber migration. ***Journal of Volcanology and Geothermal Research,*** **103, 161-173.**

MARTIN, R. F. & MOROGAN, V. (1988) Partial melting of fenitized crustal xenoliths in the Oldoinyo Lengai carbonatitic volcano, Tanzania: Reply. ***American Mineralogist,*** **73, 1468-1471.**

MATTIOLI, G. S., BAKER, M. B., RUTTER, M. J. & STOLPER, E. M. (1989) Upper Mantle Oxygen Fugacity and Its Relationship to Metasomatism. ***The Journal of Geology,*** **97, 521-536.**

MATTSSON, H. & VUORINEN, J. (2009) Emplacement and inflation of natrocarbonatitic lava flows during the March–April 2006 eruption of Oldoinyo Lengai, Tanzania. ***Bulletin of Volcanology,*** **71, 301-311.**

MATTSSON, H. B. & REUSSER, E. (2010) Mineralogical and geochemical characterization of ashes from an early phase of the explosive September 2007 eruption of Oldoinyo Lengai (Tanzania). ***Journal of African Earth Sciences,*** **In Press, Corrected Proof.**

MATVEEV, S. & STACHEL, T. (2009) Evaluation of kimberlite diamond potential using FTIR spectroscopy of xenocrystic olivine. ***Lithos,*** **112, Supplement 1, 36-40.**

MAZZONE, P. & HAGGERTY, S. E. (1989) Peraluminous xenoliths in kimberlite: Metamorphosed restites produced by partial melting of pelites. ***Geochimica et Cosmochimica Acta,*** **53, 1551-1561.**

MCCAMMON, C. (2005) The Paradox of Mantle Redox. ***Science,*** **308, 807-808.**

MCCAMMON, C. & KOPYLOVA, M. G. (2004) A redox profile of the Slave mantle and oxygen fugacity control in the cratonic mantle. ***Contributions to Mineralogy and Petrology,*** **148, 55-68.**

MCCOLLOM, T. M. & SEEWALD, J. S. (2001) A reassessment of the potential for reduction of dissolved CO2 to hydrocarbons during serpentinization of olivine. ***Geochimica et Cosmochimica Acta,*** **65, 3769-3778.**

MCDONOUGH, W. F. & SUN, S. S. (1995) The composition of the Earth. ***Chemical Geology,*** **120, 223-253.**

MCFARLANE, D. A., LUNDBERG, J. & BELTON, F. A. (2004) An unusual lava cave from Ol Doinyo Lengai, Tanzania. ***Journal of Cave and Karst Studies,*** **66, 98 - 101.**

MEEN, J. K. (1987) Mantle metasomatism and carbonatites: An experimental study of a complex relationship. IN MORRIS, E. M. & PASTERIS, J. D. (Eds.) ***Mantle metasomatism and alkaline magmatism.*** **Geological Society of America Special Paper.**

MEEN, J. K., AYERS, J. C. & FREGEAU, E. J. (1989) A model of mantle metasomatism by carbonated alkaline melts: Trace-element and isotopic compositions of mantle source regions of carbonatite and other continental igneous rocks. IN BELL, K. (Ed.) ***Carbonatites: Genesis and Evolution.*** **London, Unwin Hyman.**

MENZIES, M., KEMPTON, P. D. & DUNGAN, M. (1985) Interaction of Continental Lithosphere and Asthenospheric Melts below the Geronimo Volcanic Field, Arizona, U.S.A. ***Journal of Petrology,*** **26, 663-693.**

MENZIES, M. & MURTHY, V. R. (1980) Nd and Sr isotope geochemistry of hydrous mantle nodules and their host alkali basalts: implications for local heterogeneities in metasomatically veined mantle. ***Earth and Planetary Science Letters,*** **46, 323-334.**

MIKHAIL, S. (2011) Stable isotope fractionation during diamond growth and the Earth's deep carbon cycle. *Earth Sciences.* London, University College London.

MITCHELL, R. (2009) Peralkaline nephelinite–natrocarbonatite immiscibility and carbonatite assimilation at Oldoinyo Lengai, Tanzania. *Contributions to Mineralogy and Petrology,* 158, 589-598.

MITCHELL, R. H. (2005) Carbonatites and carbonatites and carbonatites. *Canadian Mineralogist,* 43, 2049-2068.

MITCHELL, R. H. (2006a) An ephemeral pentasodium phosphate carbonate from natrocarbonatite lapilli, Oldoinyo Lengai, Tanzania. *Mineral Mag,* 70, 211-218.

MITCHELL, R. H. (2006b) Mineralogy of stalactites formed by subaerial weathering of natrocarbonatite hornitos at Oldoinyo Lengai, Tanzania. *Mineralogical Magazine,* 70, 437-444.

MITCHELL, R. H. & DAWSON, J. B. (2007) The 24th September 2007 ash eruption of the carbonatite volcano Oldoinyo Lengai, Tanzania: mineralogy of the ash and implications for the formation of a new hybrid magma type. *Mineralogical Magazine,* 71, 483 - 492.

MOHAPATRA, R. K. & HONDA, M. (2006) "Recycled" volatiles in mantle - derived diamonds - Evidence from nitrogen and noble gas isotopic data. *Earth and Planetary Science Letters,* 252, 215 - 219.

MOHAPATRA, R. K. & MURTY, S. V. S. (2000) Origin of air-like noble gases in oceanic basalts. *Geophys. Res. Lett.,* 27, 1583-1586.

MOINE, B. N., GREGOIRE, M., O'REILLY, S. Y., DELPECH, G., SHEPPARD, S. M. F., LORAND, J. P., RENAC, C., GIRET, A. & COTTIN, J. Y. (2004) Carbonatite melt in oceanic upper mantle beneath the Kerguelen Archipelago. *Lithos,* 75, 239-252.

MOORE, K. R. (2012) Experimental study in the Na_2O-CaO-MgO-Al_2O_3-SiO_2-CO_2 system at 3 GPa: the effect of sodium on mantle melting to carbonate-rich liquids and implications for the petrogenesis of silicocarbonatites. *Mineralogical Magazine,* 76, 285-309.

MOROGAN, V. (1994) Ijolite versus carbonatite as sources of fenitization. *Terra Nova,* 6, 166-176.

MOROGAN, V. & MARTIN, R. F. (1985) Mineralogy and partial melting of fenitized crustal xenoliths in the Oldoinyo Lengai carbonatitic volcano, Tanzania. *American Mineralogist,* 70, 1114-1126.

MOROGAN, V. & WOOLLEY, A. R. (1988) Fenitization at the Alno carbonatite complex, Sweden; distribution, mineralogy and genesis. *Contributions to Mineralogy and Petrology,* 100, 169-182.

MULROONEY, D. & RIVERS, T. (2005) REDISTRIBUTION OF THE RARE-EARTH ELEMENTS AMONG COEXISTING MINERALS IN METAMAFIC ROCKS ACROSS THE EPIDOTE-OUT ISOGRAD: AN EXAMPLE FROM THE ST. ANTHONY COMPLEX, NORTHERN NEWFOUNDLAND, CANADA. *The Canadian Mineralogist,* 43, 263-294.

NAKAGAWA, T., KIHARA, K. & FUJINAMI, S. (2005) X-ray studies of structural changes in melanophlogite with varying temperature. *Journal of Mineralogical and Petrological Sciences,* 100, 247-259.

NAKAGAWA, T., KIHARA, K. & HARADA, K. (2001) The crystal structure of low melanophlogite. *American Mineralogist,* 86, 1506-1512.

NAVON, O., HUTCHEON, I. D., ROSSMAN, G. R. & WASSERBURG, G. J. (1988) Mantle-derived fluids in diamond micro-inclusions. *Nature,* 335, 784-789.

NAVON, O. & STOLPER, E. (1987) Geochemical Consequences of Melt Percolation: The Upper Mantle as a Chromatographic Column. *The Journal of Geology,* 95, 285-307.

NAVROTSKY, A., XU, H., MOLOY, E. C. & WELCH, M. D. (2003) Thermochemistry of guest-free melanophlogite. ***American Mineralogist,*** **88, 1612-1614.**

NELSON, D. R., CHIVAS, A. R., CHAPPELL, B. W. & MCCULLOCH, M. T. (1988) Geochemical and isotopic systematics in carbonatites and implications for the evolution of ocean-island sources. ***Geochimica et Cosmochimica Acta,*** **52, 1-17.**

NI, P., RANKIN, A. H. & ZHOU, J. (2003) Fluid inclusion studies on carbonatite dyke and associated quartzite in Bayan Obo, Inner Mongolia, China. ***Acta Petrologica Sinica,*** **19, 297-306.**

NI, S. & HELMBERGER, D. V. (2003) Seismological constraints on the South African superplume; could be the oldest distinct structure on earth. ***Earth and Planetary Science Letters,*** **206, 119-131.**

NIELSEN, R. L., GALLAHAN, W. E. & NEWBERGER, F. (1992) Experimentally determined mineral-melt partition coefficients for Sc, Y and REE for olivine, orthopyroxene, pigeonite, magnetite and ilmenite. ***Contributions to Mineralogy and Petrology,*** **110, 488-499.**

NIELSEN, T. F. & VEKSLER, I. V. (2002) Is natrocarbonatite a cognate fluid condensate? ***Contributions to Mineralogy and Petrology,*** **142, 425-435.**

NIELSEN, T. F. D. & VEKSLER, I. V. (2001) Oldoinyo Lengai natrocarbonatite revisited: a cognate fluid condensate? ***Journal of African Earth Sciences,*** **32, A27-A28.**

NIU, Y. (2004) Bulk-rock Major and Trace Element Compositions of Abyssal Peridotites: Implications for Mantle Melting, Melt Extraction and Post-melting Processes Beneath Mid-Ocean Ridges. ***J. Petrology,*** **45, 2423-2458.**

NORTON, G. & PINKERTON, H. (1997) Rheological properties of natrocarbonatite lavas from Oldoinyo Lengai, Tanzania. ***European Journal of Mineralogy,*** **9, 351-364.**

NYAMAI, C. M., OPIYO-AKECH, N., GACIRI, S. J. & FUJIMAKI, H. (1999) Geochemistry and Tectonomagmatic Affinities of the Mozambique Belt Intrusive Rocks in Matuu-Masinga Area, Central Kenya. ***Gondwana Research,*** **2, 387-399.**

NYAMWERU, C. (1988a) Activity of Ol Doinyo Lengai volcano, Tanzania, 1983-1987. ***Journal of African Earth Sciences,*** **7, 603-610.**

NYAMWERU, C. (1988b) Activity of Oldoinyo Lengai volcano, Tanzania, 1983 - 1987. ***J African Earth Sciences,*** **7, 603 - 610.**

NYAMWERU, C. (1990) Observations on changes in the active crater of Ol Doinyo Lengai from 1960 to 1988. ***Journal of African Earth Sciences,*** **11, 385-390.**

NYBLADE, A. A., OWENS, T. J., GURROLA, H., RITSEMA, J. & LANGSTON, C. A. (2000) Seismic evidence for a deep upper mantle thermal anomaly beneath east Africa. ***Geology,*** **28, 599-602.**

O'NEIL, J. R. & HAY, R. L. (1973) $^{18}O/^{16}O$ **ratios in cherts associated with the saline lake deposits of East Africa.** ***Earth and Planetary Science Letters,*** **19, 257-266.**

OGANOV, A. R., GLASS, C. W. & ONO, S. (2006) High-pressure phases of CaCO3: Crystal structure prediction and experiment. ***Earth and Planetary Science Letters,*** **241, 95-103.**

OGANOV, A. R., ONO, S., MA, Y., GLASS, C. W. & GARCIA, A. (2008) Novel high-pressure structures of MgCO3, CaCO3 and CO2 and their role in Earth's lower mantle. ***Earth and Planetary Science Letters,*** **273, 38-47.**

OLAFSSON, M. & EGGLER, D. H. (1983) Phase relations of amphibole, amphibole-carbonate, and phlogopite-carbonate peridotite: petrologic constraints on the asthenosphere. ***Earth and Planetary Science Letters,*** **64, 305-315.**

OPPENHEIMER, C., BURTON, M. R., DURIEUX, J. & PYLE, D. M. (2002) Open-path Fourier transform spectroscopy of gas emissions from Oldoinyo Lengai volcano, Tanzania. ***Optics and Lasers in Engineering,*** **37, 203-214.**

PAL'YANOV, N., SOKOL, A. G., BORZDOV, M. & KHOKHRYAKOV, A. F. (2002) Fluid-bearing alkaline carbonate melts as the medium for the formation of diamonds in the Earth's mantle: an experimental study. ***Lithos,*** **60, 145-159.**

PATTERSON, M., FRANCIS, D. & MCCANDLESS, T. (2009) Kimberlites: Magmas or mixtures? ***Lithos,*** **112, Supplement 1, 191-200.**

PEARSON, D. G., CANIL, D., SHIREY, S. B., EDITORS-IN-CHIEF:Â Â HEINRICH, D. H. & KARL, K. T. (2003) 2.05 - Mantle Samples Included in Volcanic Rocks: Xenoliths and Diamonds. ***Treatise on Geochemistry.*** **Oxford, Pergamon.**

PETERSON, T. D. (1989) Peralkaline nephelinites. I. Comparative petrology of Shombole and Oldoinyo L'engai, East Africa. ***Contributions to Mineralogy and Petrology,*** **101, 458-478.**

PETERSON, T. D. (1990) Petrology and genesis of natrocarbonatite. ***Contributions to Mineralogy and Petrology,*** **105, 143 - 155.**

PIK, R., MARTY, B. & HILTON, D. R. (2006) How many mantle plumes in Africa? The geochemical point of view. ***Chemical Geology,*** **226, 100-114.**

PINKERTON, H., NORTON, G., DAWSON, J. B. & PYLE, D. M. (1995) Field observations and measurements of the physical properties of Oldoinyo Lengai alkali carbonatite lavas, November 1988. IN BELL, K. & KELLER, J. (Eds.) ***Carbonatite Volcanism.*** **Berlin, Springer.**

PITZER, K. S. & STERNER, S. M. (1994) Equations of state valid continuously from zero to extreme pressures for H_2O and CO_2. ***J. Chem Phys,*** **101, 3111 - 3116.**

PLATT, G. R. & WOOLLEY, A. R. (1990) The Carbonatites and Fenites of Chipman Lake, Ontario. ***Canadian Mineralogist,*** **28, 241 - 250.**

POTTER, J., RANKIN, A. H. & TRELOAR, P. J. (2004) Abiogenic Fischer-Tropsch synthesis of hydrocarbons in alkaline igneous rocks; fluid inclusion, textural and isotopic evidence from the Lovozero complex, N.W. Russia. ***Lithos,*** **75, 311-330.**

POTTER, J., RANKIN, A. H., TRELOAR, P. J., NIVIN, V. A., TING, W. & NI, P. (1998) A preliminary study of methane inclusions in alkaline igneous rocks of the Kola igneous province, Russia: Implications for the origin of methane in igneous rocks. ***European Journal of Mineralogy,*** **10, 1167-1180.**

POWELL, M. & POWELL, R. (1977) A nepheline-alkali feldspar geothermometer. ***Contributions to Mineralogy and Petrology,*** **62, 193-204.**

POWELL, R. (1984) Inversion of the assimilation and fractional crystallization (AFC) equations; characterization of contaminants from isotope and trace element relationships in volcanic suites. ***Journal of the Geological Society,*** **141, 447-452.**

PROCHASKA, W. & POHL, W. (1983) Petrochemistry of some mafic and ultramafic rocks from the Mozambique Belt, northern Tanzania. ***Journal of African Earth Sciences (1983),*** **1, 183-191.**

PUTIRKA, K., JOHNSON, M., KINZLER, R. & WALKER, D. (1996) Thermobarometry of mafic igneous rocks based on clinopyroxene-liquid equilibria, 0-30 kbar. ***Contributions to Mineralogy and Petrology,*** **123, 92 - 108.**

PUTIRKA, K., RYERSON, F. J. & MIKAELIAN, H. (2003) New igneous thermbarometers for mafic and evolved lava compositions, based on clinopyroxene + liquid equilibria. ***American Mineralogist,*** **88, 1542 - 1554.**

PUTIRKA, K. & TEPLEY, F. (2008) Thermometers and barometers for volcanic systems. ***Reviews in Mineralogy and Geochemistry,*** **69, 61 - 120.**

PUTIRKA, K. D., PERFIT, M., RYERSON, F. J. & JACKSON, M. G. (2007) Ambient and excess mantle temperatures, olivine thermometry, and active vs. passive upwelling. ***Chemical Geology,*** **241, 177-206.**

PYLE, D. M., DAWSON, J. B. & IVANOVICH, M. (1991) Short-lived decay series disequilibria in the natrocarbonatite lavas of Oldoinyo Lengai, Tanzania: constraints on the timing of magma genesis. ***Earth and Planetary Science Letters,*** **105, 378-396.**

RANKIN, A. H. (1975) Fluid inclusion studies in apatite from carbonatites of the Wasaki area of western Kenya. ***Lithos,*** **8, 123-136.**

RANKIN, A. H. & LE BAS, M. (1973) A study of fluid inclusions in alkaline rocks with the special reference to critical phenomena. ***Journal of Geological Society London,*** **129, 319.**

RANKIN, A. H. & LE BAS, M. J. (1974) Liquid immiscibility between silicate and carbonate melts in naturally occuring ijolite magma. ***Nature,*** **250, 206-209.**

RECK, H. (1923) Über den Ausbruch des Oldoinyo L'Engai in Deutsch-Ostafrika im Jahre 1917. ***Z Vulk,*** **7, 55 - 56.**

RECK, H. & SCHULZE, G. (1921) Ein Beitrag zur Kenntnis das Baues und der jüngsten Veränderung des L'Engai Vulkanes im nördlichen Deutsch-Ostafrika. ***Z Vulk,*** **6, 47 - 71.**

REGUIR, E. P., CHAKHMOURADIAN, A. R., HALDEN, N. M., MALKOVETS, V. G. & YANG, P. (2009) Major- and trace-element compositional variation of phlogopite from kimberlites and carbonatites as a petrogenetic indicator. ***Lithos,*** **112, 372-384.**

RHODES, J. M. & DAWSON, J. B. (1975) Major and trace element chemistry of peridotite inclusions from the Lashaine volcano, Tanzania. ***Physics and Chemistry of The Earth,*** **9, 545-557.**

RICHARD, J. J. (1942) Volcanological observations in East Africa I. Oldoinyo Lengai. The 1940 - 41 Eruption. ***J East Africa Uganda Nat Hist Soc,*** **16, 89 -108.**

RICHARDSON, D. G. & BIRKETT, T. C. (1996) Carbonatite-associated deposits. IN ECKSTRAND, O. R., SINCLAIR, W. D. & THORPE, R. I. (Eds.) ***Geology of Canadian Mineral Deposit Types.*** **Geological Survey of Canada.**

RIDLEY, W. I. & DAWSON, J. B. (1975) Lithophile trace element data bearing on the origin of peridotite xenoliths, ankaramite and carbonatite from Lashaine volcano, N. Tanzania. ***Physics and Chemistry of The Earth,*** **9, 559-569.**

RITSEMA, J., VAN HEIJST, H. J. & WOODHOUSE, J. H. (1999) Complex Shear Wave Velocity Structure Imaged Beneath Africa and Iceland. ***Science,*** **286, 1925 - 1928.**

ROBINS, B. (1984) Petrography and petrogenesis of nephelinized metagabbros from Finnmark, Northern Norway. ***Contributions to Mineralogy and Petrology,*** **86, 170-177.**

ROBINS, B. & TYSSELAND, M. (1983) The Geology, Geochemistry and Origin of Ultrabasic Fenites Associated with the Pollen Carbonatite (Finnmark, Norway). ***Chemical Geology,*** **40, 65 - 95.**

ROBINSON, J. A. C. & WOOD, B. J. (1998) The depth of the spinel to garnet transition at the peridotite solidus. ***Earth and Planetary Science Letters,*** **164, 277-284.**

RODEN, M. F. & RAMA MURTHY, V. (1985) Mantle Metasomatism. ***Annual Review Earth Planetary Science,*** **13, 269 - 296.**

ROEDDER, E. (1984) FLUID INCLUSIONS. ***Reviews in Mineralogy,*** **12.**

ROEDDER, E. (1992) Fluid inclusion evidence for immiscibility in magmatic differentiation. ***Geochimica et Cosmochimica Acta,*** **56, 5-20.**

ROGERS, N., MACDONALD, R., FITTON, J. G., GEORGE, R., SMITH, M. & BARREIRO, B. (2000) Two mantle plumes beneath the East African rift system: Sr, Nd and Pb isotope evidence from Kenya Rift basalts. ***Earth and Planetary Science Letters,*** **176, 387-400.**

ROHRBACH, A., BALLHAUS, C., GOLLA-SCHINDLER, U., ULMER, P., KAMENETSKY, V. S. & KUZMIN, D. V. (2007) Metal saturation in the upper mantle. ***Nature,*** **449, 456-458.**

ROSATELLI, G., WALL, F. & STOPPA, F. (2007) Calcio-carbonatite melts and metasomatism in the mantle beneath Mt. Vulture (Southern Italy). *Lithos,* 99, 229-248.

RUBIE, D. C. & GUNTER, W. D. (1983) The Role of Speciation in Alkaline Igneous Fluids during Fenite Metasomatism. *Contributions to Mineralogy and Petrology,* 82, 165-175.

RUDNICK, R. L. & GAO, S. (2003) 3.01 - Composition of the Continental Crust. IN HEINRICH, A. A., HOLLAND, D. & TUREKIAN, K. K. (Eds.) *Treatise on Geochemistry.* Oxford, Pergamon.

RUDNICK, R. L., MCDONOUGH, W. F. & CHAPPELL, B. W. (1993) Carbonatite metasomatism in the northern Tanzanian mantle: Petrographic and geochemical characteristics. *Earth and Planetary Science Letters,* 114, 463-475.

RUSSELL, J. K. (2011) Kimberlite Ascent. *IUGG General Assembly.* Melbourne, Australia.

RUSSELL, J. K., PORRITT, L. A., LAVALLEE, Y. & DINGWELL, D. B. (2012) Kimberlite ascent by assimilation-fuelled buoyancy. *Nature,* 481, 352-356.

SAMSON, I. M., LIU, W. & WILLIAMS-JONES, A. E. (1995) The nature of orthomagmatic hydrothermal fluids in the Oka carbonatite, Quebec, Canada: Evidence from fluid inclusions. *Geochimica et Cosmochimica Acta,* 59, 1963-1977.

SAMSON, I. M. & WILLIAMS-JONES, A. E. (1991) C-O-H-N-salt fluids associated with contact metamorphism, McGerrigle Mountains, Quebec: A Raman spectroscopic study. *Geochimica et Cosmochimica Acta,* 55, 169-177.

SCHMID, B. & WEHRLI, C. (1995) Comparison of Sun photometer calibration by use of the Langley technique and the standard lamp. *Applied Optics,* 34, 4500 - 4512.

SCHRAUDER, M. & NAVON, O. (1993) Solid carbon dioxide in a natural diamond. *Nature,* 365, 42 - 44.

SHARMA, T. & CLAYTON, R. N. (1965) Measurement of ratios of total oxygen of carbonates. *Geochimica et Cosmochimica Acta,* 29, 1347-1353.

SHEPHERD, T. J., RANKIN, A. H. & ALDERTON, D. H. M. (1985) *A practical Guide to Fluid Inclusion Studies,* Glasgow, Blackie & Son Ltd.

SHERIDAN, M. F. & WOHLETZ, K. H. (1983) Hydrovolcanism: Basic considerations and review. *Journal of Volcanology and Geothermal Research,* 17, 1-29.

SIEBERT, L. (1984a) Large volcanic debris avalanches: Characteristics of source areas, deposits, and associated eruptions. *Journal of Volcanology and Geothermal Research,* 22, 163-197.

SIEBERT, L. (1984b) Large volcanic debris avalanches: Characteristics of source areas, deposits, and associated eruptions. *J. Volcanol. Geotherm. Res.,* 22, 163 - 197.

SILVA, L. C., LE BAS, M. J. & ROBERTSON, A. H. F. (1981) An oceanic carbonatite volcano on Santiago, Cape Verde Islands. *Nature,* 294, 644 - 645.

SIMONETTI, A., BELL, K. & SHRADY, C. (1997) Trace- and rare-earth-element geochemistry of the June 1993 natrocarbonatite lavas, Oldoinyo Lengai (Tanzania): Implications for the origin of carbonatite magmas. *Journal of Volcanology and Geothermal Research,* 75, 89 - 106.

SKINNER, B. J. & APPLEMAN, D. E. (1963) Melanophlogite, a cubic polymorph of silica. *American Mineralogist,* 48, 845 - 876.

SLUSSER, J., GIBSON, J., BIGELOW, D., KOLINSKI, D., DISTERHOFT, P., LANTZ, K. & BEAUBIEN, A. (2000) Langley method of calibrating UV filter radiometers. *J. Geophys. Res.,* 105, 4841-4849.

SOBOLEV, N. V., LOGVINOVA, A. M., ZEDGENIZOV, D. A., POKHILENKO, N. P., MALYGINA, E. V., KUZMIN, D. V. & SOBOLEV, A. V. Petrogenetic significance of minor elements in olivines from diamonds and peridotite xenoliths from kimberlites of Yakutia. *Lithos,* In Press, Corrected Proof.

SPRAY, J. G. & RAE, D. A. (1995) Quantitative electron-micropbe analysis of alkali silicate glass: A review and user guide. ***The Canadian Mineralogist,*** **33, 323 - 332.**

SRIVASTAVA, R. K. & HALL, R. P. (1995) Tectonic Setting of Indian Carbonatites. IN SRIVASTAVE, R. K. & CHANDRA, R. (Eds.) ***Magmatism in relation to diverse tectonic settings.*** **Taylor & Francis.**

STACEY, J. S. & KRAMERS, J. D. (1975) Approximation of terrestrial lead isotope evolution by a two-stage model. ***Earth and Planetary Science Letters,*** **26, 207-221.**

STACHEL, T., HARRIS, J. W. & BREY, G. P. (1998) Rare and unusual mineral inclusions in diamonds from Mwadui, Tanzania. ***Contributions to Mineralogy and Petrology,*** **132, 34-47.**

STEELE, A., FRIES, M. D., AMUNDSEN, H. E. F., MYSEN, B. O., FOGEL, M. L., SCHWEIZER, M. & BOCTOR, N. Z. (2007) Comprehensive imaging and Raman spectroscopy of carbonate globules from Martian meteorite ALH 84001 and a terrestrial analogue from Svalbard. ***Meteoritics & Planetary Science,*** **42, 1549-1566.**

STOPPA, F., JONES, A. & SHARYGIN, V. (2009) Nyerereite from carbonatite rocks at Vulture volcano: implications for mantle metasomatism and petrogenesis of alkali carbonate melts. ***Central European Journal of Geosciences,*** **1, 131-151.**

STOPPA, F., SHARYGIN, V. V. & JONES, A. P. (2008) Mantle metasomatism and alkali carbonatite silicate phase reaction as inferred by Nyererite inclusion in Vulture volcano carbonatite rocks. ***9th International Kimberlite Conference.*** **Frankfurt, Germany.**

STORMER JR, J. C. (1973) Calcium zoning in olivine and its relationship to silica activity and pressure. ***Geochimica et Cosmochimica Acta,*** **37, 1815-1821.**

STRECKEISEN, A. (1980) Classification and nomenclature of volcanic rocks, lamprophyres, carbonatites and melilitic rocks. IUGS Subcomission on the Systematics of Igneous Rocks. ***Geologische Rundschau,*** **69, 194 - 207.**

SUM, A. K., BURRUSS, R. C. & SLOAN, E. D. (1997) Measurement of Clathrate Hydrates via Raman Spectroscopy. ***The Journal of Physical Chemistry B,*** **101, 7371-7377.**

SUN, D., TAN, E., HELMBERGER, D. & GURNIS, M. (2007) Seismological support for the metastable superplume model, sharp features, and phase changes within the lower mantle. ***Proceedings of the National Academy of Sciences,*** **104, 9151-9155.**

SUN, S.-S. & MCDONOUGH, W. F. (1989) Chemical and isotopic systematics of oceanic basalts: implications for mantle composition and processes. ***Geological Society, London, Special Publications,*** **42, 313-345.**

SUTHERLAND, D. S. (1969) Sodic amphiboles and pyroxenes from fenites in East Africa. ***Contributions to Mineralogy and Petrology,*** **24, 114-135.**

SUWA, B. K., OANA, S., WADA, H. & OSAKI, S. (1975) Isotope geochemistry and petrology of African carbonatites. ***Physics and Chemistry of The Earth,*** **9, 735-745.**

SWEENEY, R. J. (1994) Carbonatite melt compositions in the Earth's mantle. ***Earth and Planetary Science Letters,*** **128, 259-270.**

SWEENEY, R. J., FALLOON, T. J. & GREEN, D. H. (1995) Experimental Constraints on the Possible Mantle Origin of Natrocarbonatite. IN BELL, K. & KELLER, J. (Eds.) ***Carbonatite Volcanism: Oldoinyo Lengai and the Petrogenesis of Natrocarbonatites.*** **Berlin, Springer Verlag.**

SWEENEY, R. J., GREEN, D. H. & SIE, S. H. (1992) Trace and minor element partitioning between garnet and amphibole and carbonatitic melt. ***Earth and Planetary Science Letters,*** **113, 1-14.**

SWEENEY, R. J., THOMPSON, A. B. & ULMER, P. (1993) Phase relations of a natural MARID composition and implications for MARID genesis, lithospheric melting and mantle metasomatism. ***Contributions to Mineralogy and Petrology,*** **115, 225-241.**

TAPPERT, R., STACHEL, T., HARRIS, J. W., MUEHLENBACHS, K., LUDWIG, T. & BREY, G. P. (2005) Subducting oceanic crust: The source of deep diamonds. ***Geology,*** **33, 565-568.**

TAYLOR, H. P., JR (1974) The application of oxygen and hydrogen studies to problems of hydrothermal alteration and ore deposition. ***Econ Geol,*** **69, 843 - 883.**

TEAGUE, A. J., SEWARD, T. M. & HARRISON, D. (2008) Mantle source for Oldoinyo Lengai carbonatites; Evidence from helium isotopes in fumarole gases. ***Journal of Volcanology and Geothermal Research,*** **175, 386 - 390.**

TIEPOLO, M., OBERTI, R. & VANNUCCI, R. (2002) Trace-element incorporation in titanite: constraints from experimentally determined solid/liquid partition coefficients. ***Chemical Geology,*** **191, 105-119.**

TOMLINSON, E., DE SCHRIJVER, I., DE CORTE, K., JONES, A. P., MOENS, L. & VANHAECKE, F. (2005) Trace element compositions of submicroscopic inclusions in coated diamond: A tool for understanding diamond petrogenesis. ***Geochimica et Cosmochimica Acta,*** **69, 4719-4732.**

TOMLINSON, E. L., JONES, A. P. & HARRIS, J. W. (2006) Co-existing fluid and silicate inclusions in mantle diamond. ***Earth and Planetary Science Letters,*** **250, 581-595.**

TOMLINSON, E. L., MULLER, W. & EIMF (2009) A snapshot of mantle metasomatism: Trace element analysis of coexisting fluid (LA-ICP-MS) and silicate (SIMS) inclusions in fibrous diamonds. ***Earth and Planetary Science Letters,*** **279, 362-372.**

TRIBAUDINO, M., ARTONI, A., MAVRIS, C., BERSANI, D., LOTTICI, P. P. & BELLETTI, D. (2008) Single-crystal X-ray and Raman investigation on melanophlogite from Varano Marchesi (Parma, Italy). ***American Mineralogist,*** **93, 88-94.**

TWYMAN, J. D. & GITTINS, J. (1987) Alkalic carbonatite magmas: parental or derivative? ***Geological Society, London, Special Publications,*** **30, 85-94.**

VAN ACHTERBERGH, E., GRIFFIN, W. L., O'REILLY, S. Y., RYAN, C. G., PEARSON, N. J., KIVI, K. & DOYLE, B. J. (2003) Melt inclusions from the deep slave lithosphere: constraints on the origin and evolution of mantle-derived carbonatite and kimberlite. IN MITCHELL, R. H. & GRUTTER, H. S. (Eds.) ***8th International Kimberlite Conference.*** **Victoria, BC, Elsevier.**

VAN ACHTERBERGH, E., GRIFFIN, W. L., RYAN, C. G., O'REILLY, S. Y., PEARSON, N. J., KIVI, K. & DOYLE, B. J. (2002) Subduction signature for quenched carbonatites from the deep lithosphere. ***Geology,*** **30, 743-746.**

VAN DEN KERKHOF, A. M. & HEIN, U. F. (2001) Fluid inclusion petrography. ***Lithos,*** **55, 27-47.**

VAN GROOS, A. F. K. & WYLLIE, P. J. (1963) Experimental data bearing on the role of liquid immiscibility in the Genesis of carbonatites [11]. ***Nature,*** **199, 801-802.**

VASSEUR, G., VERNIERES, J. & BODINIER, J. L. (1991) Modelling of Trace Element Transfer between Mantle Melt and Heterogranular Peridotite Matrix. ***Journal of Petrology*****, 41 - 54.**

VAUGHAN, R. G., KERVYN, M., REALMUTO, V., ABRAMS, M. & HOOK, S. J. (2008) Satellite measurements of recent volcanic activity at Oldoinyo Lengai, Tanzania. ***Journal of Volcanology and Geothermal Research,*** **173, 196-206.**

VEIZER, J. E. A. (1992) Temporal distribution of carbonatites. ***Geology,*** **20, 1147 - 1149.**

VENZKE, E., WUNDERMAN, R. W., MCCLELLAND, L., SIMKIN, T., LUHR, J. F., SIEBERT, L., MAYBERRY, G. & SENNERT, S. (2002-) Global Volcanism, 1968 to the Present. Smithsonian Institution, Global Volcanism Program Digital Information Series

Washington DC.

VISSER, W. & KOSTER VAN GROOS, A. (1977) Liquid immiscibility in K2O-FeO-Al2O 3-SiO2. ***Nature,*** **267, 560.**

WALLACE, M. E. & GREEN, D. H. (1988) An experimental determination of primary carbonatite magma composition. *Nature,* 335, 343 - 346.

WALTER, M. J. & AL, E. (2008) Primary carbonatite melt from deeply subducted oceanic crust. *Nature,* 454, 622 - 626.

WARREN, J. K. (2006) Evaporites: sediments, resources and hydrocarbons. *Lake Natron and Lake Magadi, East Africa.* Berlin, Springer.

WATKINSON, D. H. & WYLLIE, P. J. (1971) Experimental Study of the Composition Join NaAlSiO4-CaCO3-H2O and the Genesis of Alkalic Rock--Carbonatite Complexes. *J. Petrology,* 12, 357-378.

WEDEPOHL, K. H. & MURAMATSU, Y. (1979) The chemical composition of kimberlites compared with the average composition of three basaltic magma types. IN BOYD, F. R. & MEYER, H. O. A. (Eds.) *Kimberlites, diatremes, and diamonds; Their geology, petrology, and geochmistry.* Washington DC, American Geophysical Union.

WEERARATNE, D. S., FORSYTH, D. W., FISCHER, K. M. & NYBLADE, A. A. (2003) Evidence for an upper mantle plume beneath the Tanzanian craton from Rayleigh wave tomography. *J. Geophys. Res.,* 108, 2427.

WEISS, Y., KESSEL, R., GRIFFIN, W. L., KIFLAWI, I., KLEIN-BENDAVID, O., BELL, D. R., HARRIS, J. W. & NAVON, O. (2009) A new model for the evolution of diamond-forming fluids: Evidence from microinclusion-bearing diamonds from Kankan, Guinea. *Lithos,* 112, Supplement 2, 660-674.

WHEILDON, J., MORGAN, P., WILLIAMSON, K. H., EVANS, T. R. & SWANBERG, C. A. (1994) Heat flow in the Kenya rift zone. *Tectonophysics,* 236, 131-149.

WHITE, W. B. (1974) The carbonate minerals. IN FARMER, V. C. (Ed.) *The Infrared Spectra of Minerals.* London, Mineralogical Society.

WILLIAMS-JONES, A. E. & PALMER, D. A. S. (2002) The evolution of aqueous-carbonic fluids in the Amba Dongar carbonatite, India: Implications for fenitisation. *Chemical Geology,* 185, 283-301.

WILLIAMS, S. N., SCHAEFER, S. J., MARTA LUCIA CALVACHE, V. & LOPEZ, D. (1992) Global carbon dioxide emission to the atmosphere by volcanoes. *Geochimica et Cosmochimica Acta,* 56, 1765-1770.

WILSON, M. (1989) Processes which modify the composition of primary magmas. *Igneous Petrogenesis.* London, Chapman & Hall.

WOHLETZ, K. H. & SHERIDAN, M. F. (1983) Hydrovolcanic explosions; II, Evolution of basaltic tuff rings and tuff cones. *Am J Sci,* 283, 385-413.

WOLFF, J. A. (1994) Physical properties of carbonatite magmas inferred from molten salt data, and application to extraction patterns from carbonatite-silicate magma chambers. *Geological Magazine,* 131, 145-153.

WOOD, B. J., BRYNDZIA, L. T. & JOHNSON, K. E. (1990) Mantle Oxidation State and Its Relationship to Tectonic Environment and Fluid Speciation. *Science,* 248, 337-345.

WOODLAND, A. B. & KOCH, M. (2003) Variation in oxygen fugacity with depth in the upper mantle beneath the Kaapvaal craton, Southern Africa. *Earth and Planetary Science Letters,* 214, 295-310.

WOOLLEY, A. R. (1982) A discussion of carbonatite evolution and nomenclature, and the generation of sodic and potassic fenites. *Mineralogical Magazine,* 46, 7-13.

WOOLLEY, A. R. (1987) The spatial and temporal distribution of carbonatites. IN BELL, K. (Ed.) *Carbonatites: genesis and evolution.* London, Unwin Hyman.

WOOLLEY, A. R. (2001) *Alkaline rocks and carbonatites of the World. Part 3:Africa,* London, Geological Society.

WOOLLEY, A. R. (2003) Igneous silicate rocks associated with carbonatites: their diversity, relative abundances and implications for carbonatite genesis. ***Periodico di Mineralogia,*** **72, 9 - 17.**

WOOLLEY, A. R. & BAILEY, D. K. (2012) The crucial role of lithospheric structure in the generation and release of carbonatites: geological evidence. ***Mineralogical Magazine,*** **76, 259-270.**

WOOLLEY, A. R. & CHURCH, A. A. (2005) Extrusive carbonatites: A brief review. ***Lithos,*** **85, 1-14.**

WOOLLEY, A. R. & KEMPE, D. R. C. (1989) Carbonatites: Nomenclature, average chemical compositions and element distrubution. IN BELL, K. (Ed.) ***Carbonatites: Genesis and Evolution.*** **London, Unwin Hyman.**

WOOLLEY, A. R. & KJARSGAARD, B. A. (2008) Carbonatite occurrences of the world: map and database. Natural Resources Canada.

WOPENKA, B., PASTERIS, J. D. & FREEMAN, J. J. (1990) Analysis of individual fluid inclusions by Fourier transform infrared and Raman microspectroscopy. ***Geochimica et Cosmochimica Acta,*** **54, 519-533.**

XU, H., ZHANG, J., ZHAO, Y., GUTHRIE, G. D., HICKMOTT, D. D. & NAVROTSKY, A. (2007) Compressibility and pressure-induced amorphization of guest-free melanophlogite: An in-situ synchrotron X-ray diffraction study. ***American Mineralogist,*** **92, 166-173.**

YAMAMOTO, J. & KAGI, H. (2006) Extended Micro-Raman Densimeter for CO2 Applicable to Mantle-originated Fluid Inclusions. ***Chemistry Letters,*** **35, 610-611.**

YAMAMOTO, J., KAGI, H., KANEOKA, I., LAI, Y., PRIKHOD'KO, V. S. & ARAI, S. (2002) Fossil pressures of fluid inclusions in mantle xenoliths exhibiting rheology of mantle minerals: implications for the geobarometry of mantle minerals using micro-Raman spectroscopy. ***Earth and Planetary Science Letters,*** **198, 511-519.**

YAMAMOTO, J., KAGI, H., KAWAKAMI, Y., HIRANO, N. & NAKAMURA, M. (2007) Paleo-Moho depth determined from the pressure of CO2 fluid inclusions: Raman spectroscopic barometry of mantle- and crust-derived rocks. ***Earth and Planetary Science Letters,*** **253, 369-377.**

YAXLEY, G. & BREY, G. (2004) Phase relations of carbonate-bearing eclogite assemblages from 2.5 to 5.5 GPa: implications for petrogenesis of carbonatites. ***Contributions to Mineralogy and Petrology,*** **146, 606-619.**

YAXLEY, G. M. & GREEN, D. H. (1994) Experimental demonstration of refractory carbonate-bearing eclogite and siliceous melt in the subduction regime. ***Earth and Planetary Science Letters,*** **128, 313-325.**

YAXLEY, G. M., GREEN, D. H. & KAMENETSKY, V. (1998) Carbonatite metasomatism in the southeastern Australian lithosphere. ***Journal of Petrology,*** **39, 1917-1930.**

YOON, J.-H., KAWAMURA, T., YAMAMOTO, Y. & KOMAI, T. (2004) Transformation of Methane Hydrate to Carbon Dioxide Hydrate: In Situ Raman Spectroscopic Observations. ***The Journal of Physical Chemistry A,*** **108, 5057-5059.**

ZAITSEV, A. N. & KELLER, J. (2006) Mineralogical and chemical transformation of Oldoinyo Lengai natrocarbonatites, Tanzania. ***Lithos,*** **91, 191-207.**

ZAITSEV, A. N., KELLER, J. & BILLSTRÖM, K. (2009) Isotopic Composition of Sr, Nd, and Pb in Pirssonite, Shortite and Calcite Carbonatites from Oldoinyo Lengai Volcano, Tanzania. ***Doklady Earth Sciences,*** **425, 302 - 306.**

ZAITSEV, A. N., KELLER, J., SPRATT, J., PEROVA, E. N. & KEARSLEY, A. (2008) Nyerereite - Pirssonite - Calcite - Shortite relationships in altered natrocarbonatites, Oldoinyo Lengai, Tanzania. ***The Canadian Mineralogist,*** **46, 843 - 860.**

ZAK, L. (1972) A Contribution to the Crystal Chemistry of Melanophlogite. ***American Mineralogist,*** **57, 779 - 796.**

ZHARIKOV, V. A., PERTSEV, N. N., RUSINOV, V. L., CALLEGARI, E. & FETTES, D. J. (2007)
Metasomatism and metasomatic rocks. BGS.